# The Digital Dead:

# Virtual Modelling of Human Remains using Photogrammetry for Presentation and Preservation by Record

Heather Marie Tamminen

Thesis submitted in partial fulfilment of the requirements for the degree of

Doctor of Philosophy

Awarded by Bournemouth University

In collaboration with the Dorset Museum

April 2022

# Copyright Statement

Abstract

The Digital Dead: Virtual Modelling of Human Remains using Photogrammetry for Presentation and Preservation by Record

Heather Marie Tamminen

Three-dimensional (3D) modelling techniques have high potential as an active research tool in the study of human remains. The creation of 3D models from overlapping images, Structure-from-Motion Multi-view Stereo photogrammetry, offers a fast, accessible analysis method which reduces risk of damaging the remains. The current study set out to investigate whether photogrammetry can create close-range models of osteological material that are of high metric quality. It looked to develop a method using this technique, explore its applicability in osteological research, and determine what new information could be discovered about a case study collection using photogrammetry.

Sharp force trauma (SFT) to bones was used to test the applicability of this method to the field of trauma analysis. The case study is a collection of Viking remains excavated in 2009 near Weymouth, Dorset, exhibiting extensive SFT. The digitised cutmarks were measured and these measurements compared to conventional manual methods. All the cutmarks were successfully digitised and any differences between the measurement methods were not statistically significant. Therefore, this is thought to be a reliable and accessible method of documenting SFT for both preservation and research purposes.

The ability to study a 3D model of the cutmarks in question allows for a wider range of analytical tools to be used without damaging the original bone. The use of photogrammetry in the detailed study of human remains could have important implications for the way such collections can be studied and displayed. This would make the sharing of collections between institutions both locally and internationally easier whilst providing minimal risk to the collection. Overall, this study has shown that photogrammetry can successfully create 3D models of SFT which augment traditional analysis and allow for additional interpretation of events.

# Table of Contents

# List of Illustrations

# List of Tables

## List of Accompanying Material

Excel Files

- TamminenSupplementary_Assocs and Burials.xlsx
- TamminenSupplementary_PS1 Data Collection.xlsx
- TamminenSupplementary_PS2 Data Collection.xlsx
- TamminenSupplementary_Trauma.xlsx

Illustrator Files (n.b. all saved in legacy format to be compatible with prior versions of Adobe CC)

- TamminenSupplementary_CV1_Compat.ai
- TamminenSupplementary_CV2_Compat.ai
- TamminenSupplementary_CV3_Compat.ai
- TamminenSupplementary_CV4_Compat.ai
- TamminenSupplementary_CV5_Compat.ai
- TamminenSupplementary_CV6_Compat.ai
- TamminenSupplementary_CV7_Compat.ai
- TamminenSupplementary_CVUnk_Compat.ai
- TamminenSupplementary_Skull_Compat.ai
- TamminenSupplementary_Skeleton_Compat.ai
- TamminenSupplementary_Mandible_Compat.ai
- TamminenSupplementary_Shape Analysis_Compat.ai

# Preface and Acknowledgements

This research is dedicated to the individuals who were buried in a mass grave up on the Ridgeway.


Many thanks go out:

To my supervisory team, Dr. Martin Smith, Mr. Andrew Ford, and Prof. Kate Welham, for helping make this piece of work immeasurably better.

To the Dorset Museum and Dr. Jon Murden, for the opportunity to work on such an amazing collection.

To Dr. Samuel Rennie, for the on-going support, friendship, and wonderful statistical advice.

To Miss Gabrielle Delbarre, for being the best laboratory manager there is.

To my [DBR] three and the rest of the AP team, for helping more than they will ever realise, tusind tak.

To my parents, kiitos.

# Author’s Declaration

All work done in this project is original work of the author. The collaborating institution (the Dorset Museum) kindly provided the collection and a portion of the funding.

# 1 Introduction

## 1.1 Digital Technology in Archaeology

The advent of new digital technologies is rapidly changing the way archaeology, osteology, and related disciplines are studied (Thali et al. 2003; Remondino 2011; Beale and Reilly 2017; Mate-Gonzales et al. 2018; Courtenay et al. 2020a, 2020b). One area of development that has impacted these fields greatly is three-dimensional (3D) modelling. Since archaeology is inherently destructive, there is a significant need for accurate and detailed recording throughout the process to avoid the loss of data and detrimental effects to interpretation (De Reu et al. 2014; Dellepiane et al. 2013). The idea of integrating virtual techniques into archaeology to improve recording and interpretation of remains has grown steadily and considerably since the 1990s (Beale and Reilly 2017). The use of 3D techniques can be applied at many scales, from the recording of the overall site to a smaller scale, enabling the recording of objects with complex shapes and the creation of less subjective representations compared to exclusively using two-dimensional (2D) illustrations or photographs (Olson et al. 2013; Sutton et al. 2014; Bleed et al. 2017; Sapirstein 2018). Virtual reproductions of aspects of physical heritage are attractive for several reasons, including their potential to enhance the level of interaction with objects whilst maintaining the integrity of the artefact and even allowing the examination of the artefact remotely (Remondino 2011; Clini et al. 2016; Douglass et al. 2017).

There are a variety of techniques that have been used in the 3D modelling of archaeological sites and artefacts (Thali et al. 2003; Pavlidis et al. 2007; Niven et al. 2009; Remondino 2011; Olson et al. 2013; Villa et al. 2016; Earley et al. 2017). Many of the more popular techniques are considered ‘active’ methods as the respective equipment emits light or radiation at a specific wavelength which is then captured by a sensor (Pavlidis et al. 2007; Opitz, 2013b). Such methods often involve large, expensive, or cumbersome equipment, and also require extensive training or experience to efficiently operate, such as terrestrial laser scanning (TLS) or computed tomography (CT) scanning (Linder 2009; Fonstad et al. 2013; Gallo et al. 2014).

One technique that is becoming increasingly popular in archaeological recording is photogrammetry. This technique creates 3D models from photographs which allow one to capture accurate geometric information about the subject and the surroundings (Konecny 1985; Jebara et al. 1999; Fryer et al. 2007; Lillesand et al. 2015). Distinctive features in overlapping images are matched by software and then placed in 3D space, allowing the creation of a point cloud representing the subject (Wolf and Dewitt 2000). Photogrammetry was originally designed for aerial survey, however with the evolution of computers and the integration of the growing field of computer/machine vision it has been adapted to many different uses, including archaeology and more recently, osteology (Jebara et al. 1999; Snavley et al. 2008; Remondino 2011; Granshaw and Fraser 2015).

## 1.2 Photogrammetry and Osteology

This study explored Structure-from-Motion Multi-View Stereo (SfM-MVS), a type of photogrammetry which involves creating models of an object (structure) by moving the camera (motion) and taking overlapping (stereo) pictures from multiple angles (Micheletti et al. 2015b; Granshaw 2018). This method is fast, cheap, and relatively easy to learn (Olson et al. 2013; Villa et al. 2016; Earley et al. 2017). SfM-MVS is being used more frequently in commercial and research archaeology to create virtual models that provide a record of the appearance of aspects of a site before, during, and after excavations (De Reu et al. 2013; Olson et al. 2013; McCarthy 2014). However, when related to human remains, it is less frequently used to document bone for research purposes at a very close range. In studies where such techniques have been applied to human remains, 3D models are most frequently created for recording *in-situ* burials or to produce aesthetically pleasing models of complete bones (most commonly skulls) for display to the public or for analyses such as facial approximation (see Ducke et al. 2011; Donato et al. 2020 and for a discussion about ethics in such areas, see Squires et al. 2019).

Whilst some osteological SfM-MVS models exist, relatively few have been primarily used for quantitative analytical purposes and metric study (for exceptions, see Maté González et al. 2015; Otárola-Castillo et al. 2018; Morgan et al. 2019). Therefore, they are currently an under-explored resource for research, teaching, and sharing of collections amongst institutions, leaving important questions as to their precision and reliability for such purposes. Over two centuries on from the work of Johann Friedrich Blumenbach (1795) and 150 years after the work of Paul Broca (1861) most osteological analysis and recording continues to be undertaken manually on the bones through measurements or observations (Buikstra and Ubelaker 1994; Boylston 2000; Loe et al. 2014b). When close-range analysis is required, it is often done through microscopy, especially digital microscopy, when available (Bartelink et al. 2001; Tucker et al. 2001; Alunni-Perret et al. 2005, 2010; Freas et al. 2010; Crowder et al. 2013). However, such equipment is not available at many facilities and therefore the investigation of a more accessible technique is important.

The ability to measure bones or aspects of bones is important in osteology as much of biological profiling can be performed via metrics (e.g. Bass 1995; Jantz et al. 1995; Ousley and Jantz 2012). Additionally, metrics can be valuable to analysing the extent of pathologies and injuries. It is commonly used in the latter especially when looking at sharp force trauma (SFT), defined as any osseous injury caused by a bladed object. One exception is recent work by Maté-González et al. (2015, 2018, 2019), Arriaza et al. (2017), Yravedra et al. (2017), and Courtenay et al. (2020a, 2020b), investigating butchery and carnivore damage on both modern experimental and historic samples of animal bone through SfM-MVS. They have demonstrated the potential of using mesh models compared to other digital methods such as confocal microscopy, but they have not yet metrically tested their data against physical measurements from the bone (Maté-González et al. 2018).

Within this study, SFT was chosen to be analysed because it leaves discrete marks with less room for subjective analysis compared to many pathologies and therefore is a good characteristic for testing new methods. Additionally, this is an opportunity to investigate how technology can aid in the reappraisal of trauma in a skeletal collection.

## 1.3 Aims and Objectives

This research aims to explore the extent to which SfM-MVS photogrammetry can create quantitatively accurate 3D models which can be used for research purposes. More specifically, this project is designed to determine what parameters and photographic methods create the most effective models and if these models are of the same or higher standard than current osteological techniques for the analysis of SFT. Thus, the essential question is whether the levels of accuracy achieved in a laboratory can be taken out of the lab and be made more widely accessible and cost-effective. The collection of the Weymouth Ridgeway Vikings (see Loe et al. 2014b for the published osteological report) will be used as a case study to establish and test a methodology and investigate whether photogrammetric models can aid in the interpretation of trauma. In order to achieve this aim, several objectives must be met.

### 1.3.1 Objectives

The methodological objectives are as follows:

1. Critically evaluate the development and use of SfM-MVS and its application in the recording of human remains at close range and the creation of 3D models, and situate this information in the context of current osteoarchaeological approaches/practices to trauma analysis
2. Determine the best practice for creating close range photogrammetric models of incised and shaved SFT (the latter having been made as a result of complete bisection of the bone) by optimising camera parameters and the method and geometry of image capture

The applied methodological objectives are as follows:

3. Measure the lengths and widths of the SFT on the bones manually with callipers and digitally on the 3D models

4. Test the precision of close-range osteological SfM-MVS by comparing the results of digital measurements with the manual measurement methods
5. Investigate the use of shape analysis for the grouping of incised cutmark profiles based on variables such as location on the body
6. Explore the use of geospatial techniques in relation to shaved cutmarks to analyse changes in surface texture across the cutmark

The case study objectives are as follows:

7. Further apply the optimal methods as defined above using the Weymouth Ridgeway Vikings as a case study collection
    - Investigate if it is possible to tell if different wounds were made by the same category of blade (e.g. sword, axe, knife) by examining cutmark profiles
    - Analyse the findings to see if there are any patterns in the trauma that help interpret events, especially regarding the osteological patterns of decapitation trauma seen in the skull, mandible, and vertebrae
8. Reappraise the SFT on the collection to determine if the original information requires any updating since new techniques are now available to use
9. Synthesise and evaluate all findings to determine what conclusions can be drawn
    - What additional knowledge about the deaths of the Weymouth Vikings can be gathered from further study of the SFT?
    - Are there osteological patterns apparent that are specific to decapitation-related injuries?

## 1.4 Contribution to Knowledge

Through the case study collection, the Weymouth Ridgeway Vikings, new and conventional methods of trauma analysis can be evaluated. This study will help design a method of systematically creating high metric quality 3D models of osteological material (through the example of SFT) whilst assessing the benefits and limitations of close-range photogrammetry. This research will also aid in adding details to the narrative surrounding the deaths of the Weymouth Ridgeway Vikings.

### 1.4.1 Exploration of New Modelling Techniques in Osteology

Digital 3D modelling is a growing area and has the potential to be very valuable for osteological study, curation, and display. The use of SfM-MVS for high metric quality models of osteological material is a relatively unexplored area that has great potential for research, education, outreach, historical knowledge, and forensic analysis. Being able to easily create accurate and precise close-range models could open new avenues to more detailed quantitative analysis of SFT and other lesions in the future. This would allow a more comprehensive analysis of life, disease, and warfare. Digital 3D models may help with a more accurate interpretation or reconstruction of possible events. This could have important implications for modern forensic analysis as well. Non-invasive techniques such as SfM-MVS allow interactivity, collaborative research, and sharing of collections whilst maintaining their safety (Earley et al. 2017; Naranjo et al. 2018). The increasing ability to share collections would make it easier for researchers to use larger samples sizes which may also be derived from a wider geographic or chronological span.

Museums would be able to sensitively display remains from distant institutions without risking transport of the bones. Digital 3D models take up much less physical storage space than their original objects, therefore the use of models such as this would allow museums to be able to store more on site. SfM-MVS models can provide an easy and safe method of sharing and presenting specimens with the general population in museums (Ducke et al. 2011). Interactive 3D models that are both attractive to look at and accurate would allow for the public to interact with collections in a manner that is not otherwise possible. This could both increase public interest in the past and help museums increase visitor numbers as well as opening potential for new revenue streams through virtual collections access, a topic that has become very relevant during the COVID-19 pandemic.

SfM-MVS has many characteristics which are optimal for use in places with time and budgetary constraints, such as commercial archaeological units, museums, and research groups. As the use of 3D modelling in cultural heritage and archaeology increases there will be a greater need for people who create and use such models to understand how they are created so that storage and analysis of poorly-created models can be avoided (Bennett 2015). Therefore, the examination of the capabilities and limitations of SfM-MVS will be beneficial for promoting good practice when using it to create models. The metric tests will help establish the level of accuracy achieved with such models and whether it is sufficient to be used for teaching, outreach, and research purposes. It is important to stay abreast of changes in technology and keep testing its capabilities to ensure it is being used appropriately before adopting it widely.

### 1.4.2 Understanding the Significance of the Weymouth Vikings

The case study for this research is a collection of human remains dated to AD 970-1025, within the Viking period in England. A total of approximately 52 individuals were found in a mass grave, all decapitated with their heads placed to one side (Loe et al. 2014b). In addition to the significant trauma seen from the decapitations, there is other evidence of sharp force trauma on the upper bodies and heads (Loe et al. 2014b). Prevailing theory is that these individuals were executed by locals on the Ridgeway shortly after being captured (Chenery et al. 2014; Loe et al. 2014b; Williams 2015; Boyle 2016; Lavelle 2016; Roffey and Lavelle 2016).

An analysis was performed on the Weymouth Vikings when they were first excavated, however the SFT has not been studied since then and therefore has not been investigated using modern technologies. Due to this, there is a high probability that new information would be revealed. A highly detailed evaluation of the trauma also provided additional information about events that surround the deaths of the individuals in this collection. The project undertaken here offers an important opportunity to investigate an event in England's past that has no written record.

The Ridgeway assemblage forms a very rare collection and any additional knowledge that can be determined about their lives and deaths will be beneficial for the understanding of the history of Wessex, England, and the Vikings in general. For collections of significance such as the Weymouth Vikings, these methods will create a digital record of the injuries, allowing easier display of more of the collection and garnering more interest in their history.

## 1.5 Chapter Structure

This document is comprised of ten chapters. Chapter 1 focuses on the aims of the study and its contribution to knowledge. Chapters 2-4 review the literature on photogrammetry and the impact of such technology on archaeology, the historical background of the Vikings in Southern England, and trauma and the conventional osteological methods of analysing SFT, respectively. Chapter 5 describes the materials and methods used in the project. Chapters 6 and 7 present the methodological and osteological results of the study, respectively. Chapter 8 and 9 are discussion chapters which mirror the structure of the results. Chapter 8 addresses the results of SfM-MVS models, their accuracy and use in osteology, and the best methods to create such models, and Chapter 9 presents the findings and interpretation of the trauma analysis on the collection. Lastly, Chapter 10 presents the conclusions that can be drawn from the study as they relate to the three categories of objectives, namely the methodological objectives, the applied methodological objectives, and the case study objectives.

# 2 Photogrammetry

## 2.1 Introduction

Photogrammetry has been defined as "…the science of measuring in photos" (Linder 2009, p.1) and "…the technology to derive measurements of objects from their images" (Konecny 1985, p.922). More specifically, photogrammetry uses photographs to create models, scaled in a relative or absolute sense, to obtain geometric information, spatial measurements, and orientations (Konecny 1985; Jebara et al. 1999; Fryer et al. 2007; Lillesand et al. 2015). In this context the term 'model' (or, in this research, 'photogrammetric model') can relate to a simple plane usually with an orthogonal projection (e.g. a so-called ortho-rectified image), a cloud of points with x, y, and z coordinates, a two-and-half dimensional (2.5D) mesh with no overhangs (such as a Digital Elevation Model, or DEM) or a full three-dimensional (3D) mesh. Photogrammetry uses two or more overlapping photographs of the same object or area taken from different locations (in a relative or absolute sense, as the camera may move relative to the object or vice versa), and therefore perspectives (Figure 1). This chapter discusses the background behind photogrammetry, the important principles involved, and recent developments known as Structure-from-Motion (SfM) and Multi-View Stereo (MVS) which form the basis of the method employed in this doctoral research.

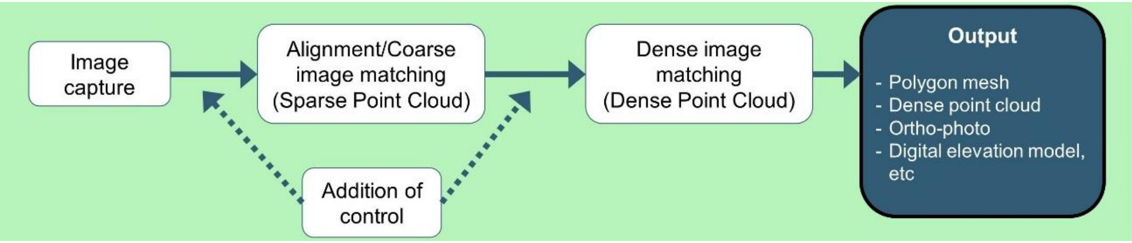


Figure 1: An example of a standard photogrammetric workflow

### 2.1.1 The Output

Before discussing the principles and methods behind photogrammetry, the final output should be outlined to give a clear view as to why this technique is used and what can be done with the outputs. Further discussions about what these outputs can be used for follows in Section 2.5. There are two main types of output: dense point clouds (DPC) and textured (or, less commonly, untextured) polygonal meshes (Figure 1) (Agisoft LLC 2020a). Conventionally, the DPC (Section 2.4.4.2) is a necessary stage before a mesh can be created, however recent software updates allow for the DPC stage to be skipped if desired to allow for faster processing (see Figure 1 and Section 2.4.4.1 for the initial steps that would still be required) (Agisoft LLC 2021).

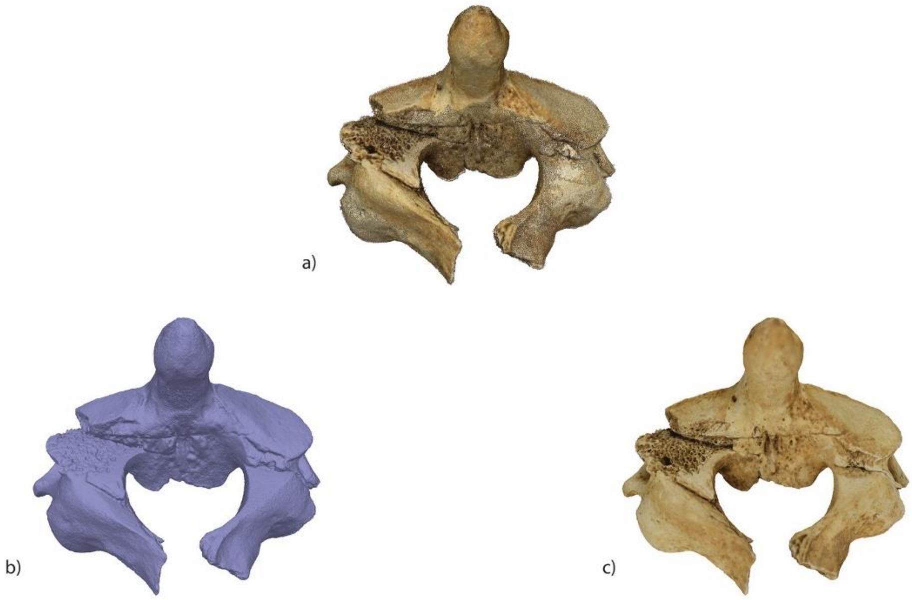


Figure 2: Examples of the types of output from a photogrammetric model: a) a dense point cloud, b) a watertight polygon mesh, and c) a textured polygon mesh

#### *2.1.1.1 Point Clouds*

There is merit to leaving the model as a DPC if performing any metric analysis, as any further process will involve interpolation between the points creating an inherent loss of data (McCarthy 2014). Therefore, the DPC is the metrically purest form of data for 3D models. For objects, the most common process is to turn the DPC into a polygon mesh and then texture it with the images that were taken (Historic England 2017). DPCs are not only a product of photogrammetry; most other 3D modelling techniques also create a DPC before creating a final, textured model. Thus, any metric analysis performed on a photogrammetric DPC, could be performed on a DPC of a difference provenance which allows for the standardisation of analyses across techniques.

#### *2.1.1.2 Textured Polygon Meshes*

A textured mesh can also be created from either the DPC or the pre-cursor, the sparse point cloud (SPC) (see Sections 2.4.3.3 and 2.4.4) (Mallinson and Wings 2014). The mesh is often created through triangles which allows retention of much of the original shape of the point cloud, however it will be less accurate (McCarthy 2014).

For landscapes or scenes, DEMs, digital surface models (DSMs), digital terrain models (DTMs), or ortho-images can be produced. DEMs are raster models that show the height of the terrain throughout the area surveyed on a regularly spaced grid (Opitz 2013b). They provide a numerical representation of the topography of a region (Wolf et al. 2014). When the model has terrain information, including artificial and natural objects, it is a

DSM (Opitz 2013b). DTMs are similar to DSMs, but only contain the information on the terrain, any artificial or natural objects are excluded (Opitz 2013b). Ortho-images, or orthophotographs, are orthorectified photos that remove any perspective distortion from the position of the camera leaving the scale consistent throughout (Wolf et al. 2014; Granshaw 2016). In aerial photogrammetry, this results in an image which has the perspective of a map (Fryer et al. 2007; Lillesand et al. 2015).

## 2.2 Photography

Photogrammetry is tied very closely to the development of photography and different photographic techniques. Photography was presented to the public in 1839 with the disclosure of the processes of three photographers; Nicephore Niepce, William Henry Fox Talbot, Louis Jacques Mande Daguerre (Konecny 1985; Luhmann et al. 2013; Lillesand et al. 2015). Shortly thereafter, photography was used in topographic surveys by Colonel Aimé Laussedat (Konecny 1985; Wolf et al. 2014; Lillesand et al. 2015). Before the roles of images in photogrammetry can be considered, some of the basic principles of photography and cameras must be discussed (Figure 3).

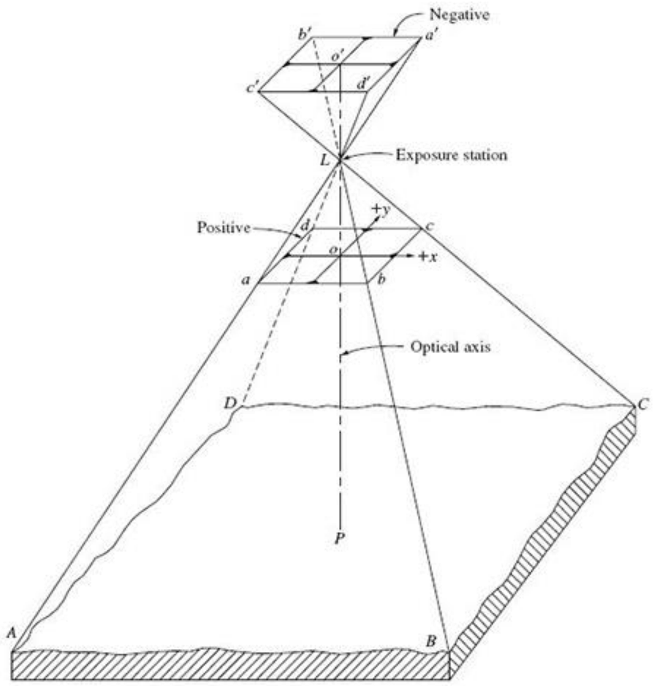


Figure 3: The geometry of a vertical photograph (Wolf et al. 2014, Fig. 6.1)

### 2.2.1 The Camera

For explanations and discussions of photogrammetric principles, pinhole camera diagrams are often used as it is easier to explain the difference in projections and intersecting rays (Figure 4). They assume no lens distortion and therefore collinearity (see Section 2.4.3), so if rays deviate from collinearity, the differences can be used to estimate distortion (Young 1989; Luhmann et al. 2013). Pinhole cameras are not highly practical for photogrammetry as the focus is not uniform and rapidly deteriorates radially. They also require long exposures and therefore camera shake is more likely to occur (Wolf and Dewitt 2000; Wolf et al. 2014; Lillesand et al. 2015). Although the size of the hole the light passes through could be increased, without corrections the light is diffuse and does not result in a clear image. Therefore, the addition of lenses allows for the refraction of the light rays to focus and properly display the image, resulting in the frame cameras traditionally used for photography (Wolf et al. 2014; Lillesand et al. 2015).

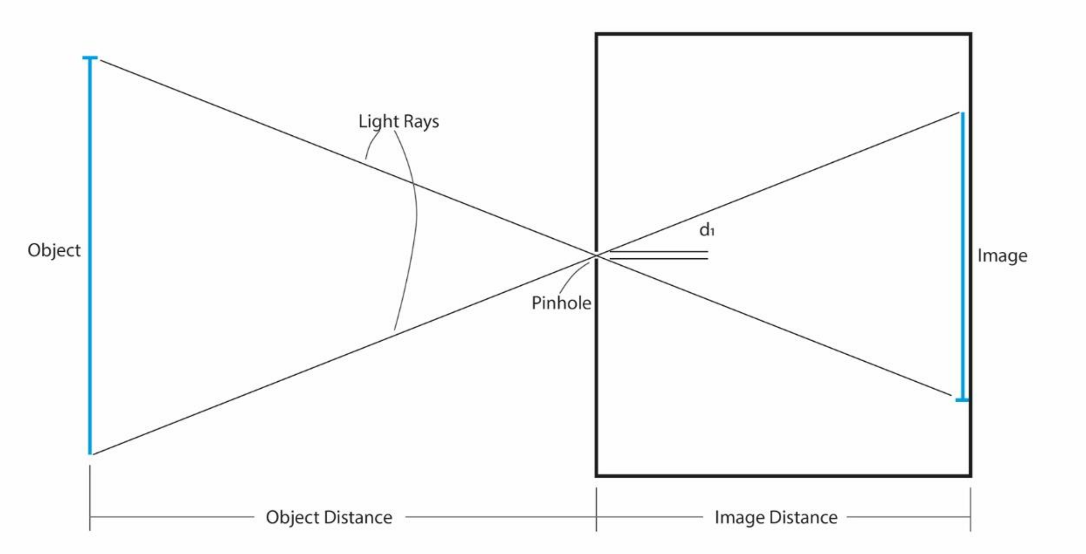


Figure 4: An example of how light enters a camera using a pinhole camera for ease of illustration (amended from Wolf et al. 2014, Fig. 2.1)

Although light can be waves or rays (see Dimitrova and Weis 2008 for a basic discussion of ‘wave-particle duality’), for photogrammetry, it is considered in terms of rays. The basic principles are that light enters the camera through a lens (or series of lenses) and is projected onto the image or focal plane, which is either film or a sensor array, at the back of the camera (Figure 5) (Fryer et al. 2007; Long 2013; Wolf et al. 2014). The point where the longitudinal axis of the lens intersects the image plane at the back of the camera is called the principal point (Fryer et al. 2007). The capture of a digital image is discussed further in Section 2.2.3. The model of light rays using a pinhole camera is known as central perspective projection in which there should be a straight line from the object, or object point, through the optical centre of the camera lens known as the perspective centre to the image point on the plane (Figure 6) (Granshaw 2016). The principal point is found where the normal from the perspective centre intersects with the image plane (Jebara et al. 1999). The importance of this is further explained in Section 2.4.3 on collinearity.

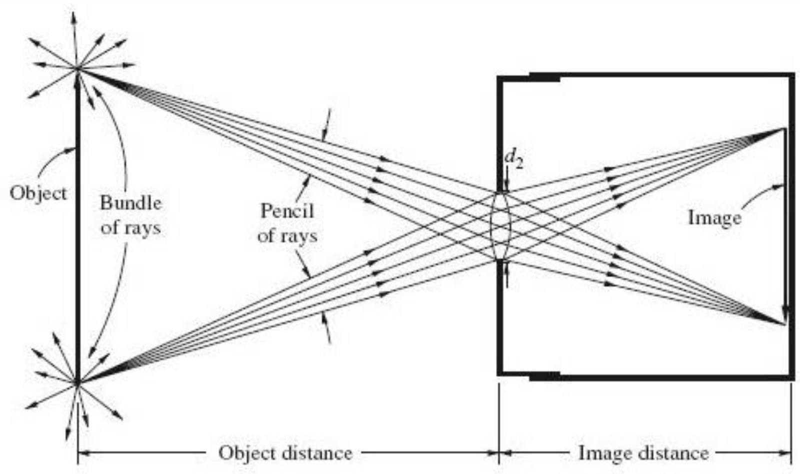


Figure 5: A diagram showing the rays of light in a single-lens camera (Wolf et al. 2014, Fig. 2.6)

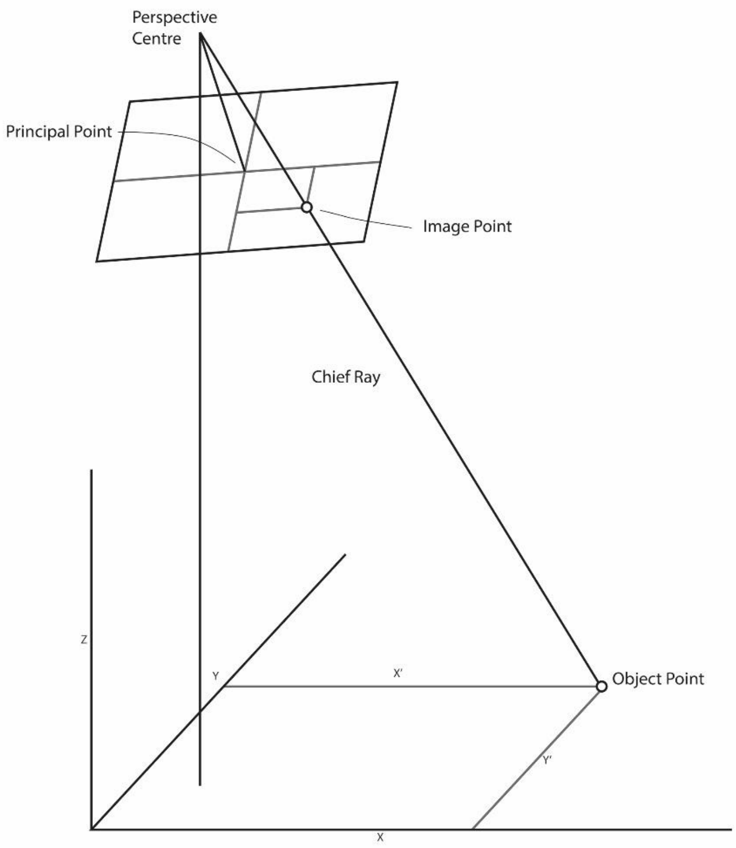


Figure 6: An illustration of a central perspective projection with the positive image plane indicating the image and principal points

In reality, there are many rays that come in through the lens to create an image, but the ray that is a straight line as described in this central projection model is called the chief ray and is often used for simplicity in explanations (Fryer et al. 2007; Historic England 2017). Generally, the chief ray is at a fixed angle compared to the camera but the distance that it is away from the camera is not known. The path of the chief ray from the same object can be found across multiple camera positions the intersection of the lines allows the object to be located and reconstructed (Fryer et al. 2007).

##### 2.2.1.1 Camera Parameters and Properties

In order to select the optimal camera settings for the entire sequence of photogrammetric image capture, it is important to understand these settings because they should be changed as little as possible throughout (McCarthy 2014). There are three parameters of a camera that can be adjusted to change the exposure, which is the amount of light that is captured by an image sensor. It is vital to understand these parameters when capturing images for any type of photogrammetric model to ensure sufficient, but not excess, light.

The first parameter is related to the adjustable diaphragm used in cameras to alter the diameter of the lens which in turn changes the amount of light allowed in, known as the 'aperture' (Figure 7) (Lillesand et al. 2015; Granshaw 2016). This is set through the f-stop (f/) which is the ratio of lens length to aperture size (Long 2013). The f-stop number decreases as the diameter of the lens increases (Wolf et al. 2014; Lillesand et al. 2015).

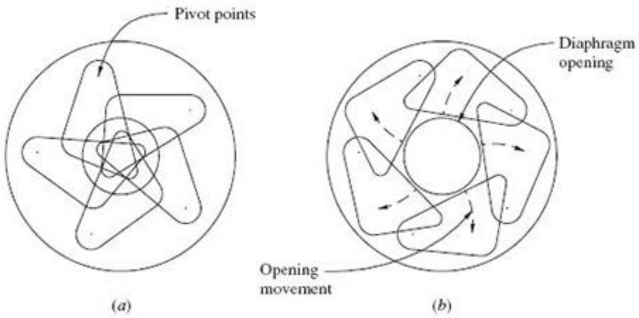


Figure 7: An example of a leaf-type shutter at two different apertures with a) having a larger depth of field than b) (Wolf et al. 2014, Fig. 3.5)

The second parameter is shutter speed. Shutters are important as they control the duration that the film or sensor is exposed to the light (Lillesand et al. 2015). The brightness per unit area of the image plane during exposure is known as the illumination and can be manipulated by aperture and shutter speed (Wolf et al. 2014). These two parameters are inversely proportional; if one is increase by one increment and the other is decreased by the same amount, the total exposure will stay the same (Avery and Berlin 1992; Wolf et al. 2014).

ISO speed is the third parameter than can be manipulated. It is named after the committee that set the standard, the International Standards Organisation. Originally for film cameras, it does not change the amount of light allowed into a camera, rather it dictates how fast the film chemically reacts to the light to form an image. It is still used in digital cameras but instead of changing film speed, it changes the light sensitivity, or signal gain, of the image sensor by amplifying or decreasing the electric signals caused by light hitting the sensor (Long 2013; Granshaw 2016). Increases in sensitivity should cause less light to be required to capture an image. However, a higher ISO also leads to an increase in the noise in the image, because the film or sensor is more sensitive to any small variation, regardless of whether this is associated with the subject or extraneous (Historic England 2017). Noise is described as fluctuations in the intensity value that are unwanted and inaccurate and the amount of noise compared to good data is known as the signal-to-noise ratio. Together, the aperture, shutter speed, and ISO are the main components that needs to be accounted for when dictating the amount of light allowed into the camera (Long 2013).

Focus is an important property for photography and this is dependent on the focal length of the camera (*f*), the distance between the lens and the object that is being photographed (*o,* object distance), and the distance between the lens and the image plane (*i,* image distance) (Figure 8, to demonstrate *f*) (Avery and Berlin 1992; Lillesand et al. 2015). The focal length is the distance from the front of the lens to where the parallel light rays are then focused into a single point near the back of the lens (Lillesand et al. 2015). A longer focal length results in a narrower field of view (Historic England 2017). A wider spread of rays, originating from a smaller focal length, can cause more distortions. However, when the rays are concentrated due to a long local length, any errors can escalate rapidly (Figure 9) (Linder 2009). Camera lenses can either be ‘fixed focal length’, in which the distance that can change is the object-lens, or ‘variable focal length’, in which the length of the lens itself can change. Therefore, it is important to take the type of lens into consideration when photographing so possible distortions and errors can be accounted for. The recommendation for photogrammetry is often fixed focal length lenses, also called ‘prime lenses’ (Fraser 2013; Granshaw 2016).

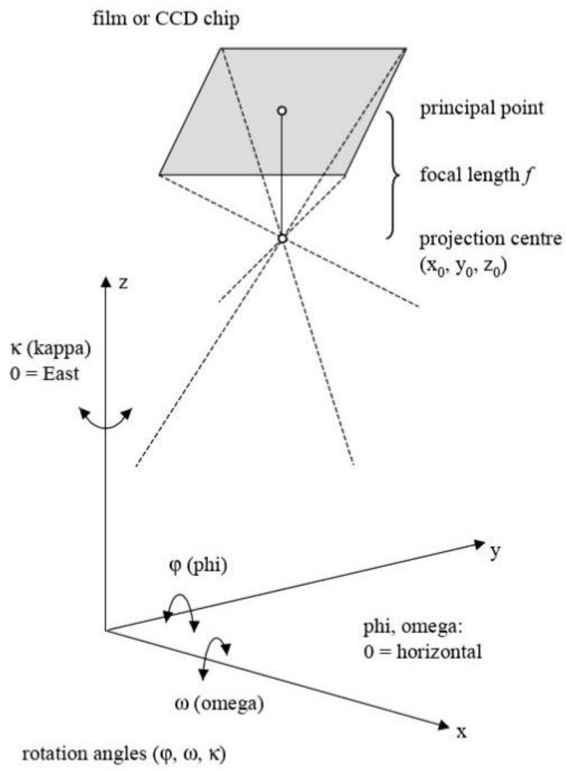


Figure 8: A diagram of the focal length, the coordinates, and the three rotation angles of a projection centre (amended from Linder 2009, Fig. 6, p.12)

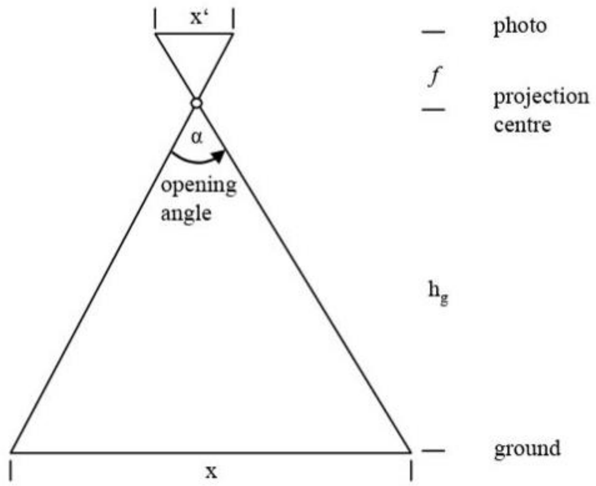


Figure 9: In a camera, the relationship between the focal length (f), height above ground ($h_g$), and the photo scale $f/h_g$ (Linder 2009, Fig. 7, p.13)

The distance over which the image is in focus is important as well. The range over which the camera can properly focus is called the depth of field (DOF) (Wolf et al. 2014; Lillesand et al. 2015). This is influenced by the aperture; the smaller the aperture and therefore the higher the f-stop, the greater the DOF (Wolf et al. 2014). This is extremely important to be aware of when the object is 3D (Mallinson and Wings 2014; Historic

England 2017). The focal length of the lens also impacts the DOF; a shorter *f* has a larger DOF. The field of view (FOV) of a camera is another property to consider and it is necessary when determining the number of pictures and their geometry (external orientation) for photogrammetry. There is a horizontal, vertical, and diagonal FOV which dictate the amount of the object and its surroundings that will be captured in each image (Granshaw 2016). The ground sample distance is the area on the ground that is captured in a single pixel (Lillesand et al. 2015; Historic England 2017). It is affected by the distance the camera is from the object, the focal length of the lens, and the physical size of the pixels (Lillesand et al. 2015). This knowledge can help determine the appropriate amount of distance between images to maintain the required overlap, or side-lap when using parallel aerial images.

#### *2.2.1.2 Types of Cameras*

A frame camera, the type described in the sections above, is the most common type of camera for everyday use. It captures an image simultaneously across the whole image plane (Avery and Berlin 1992; Wolf et al. 2014). The image sensor is small, usually rectangular, but the length and width are similar. Different lenses can often be attached allowing the photographer to change the FOV available (Lillesand et al. 2015). A selection of other types of cameras are listed in Table 1.

Table 1: Common types of non-frame cameras and their descriptions

| Camera | Description |
|---|---|
| Panoramic | - Panning camera<br>- Long rectangular opening for light, controlled by shutter<br>- Film/image sensor on curved platen that rotates, exposing different parts as shutter moves<br>- Either a rotating lens or prism<br>- Designed for aerial photography and surveying<br>- Can capture wider area of view but have significant distortions that need correcting |
| Hemispherical | - Extreme wide-angle cameras<br>- Known as fish-eye lens<br>- Field of view is half a sphere<br>- Are specific hemispherical cameras, regular DSLRs can be turned into with extreme wide-angle lenses<br>- Have been used in scientific studies of forests and clouds |
| 360º | - Essentially two hemispherical cameras attached together<br>- Basically results in two images stitched together<br>- World of virtual reality (VR) gave a lot of impetus behind development |
| Lensless | - Two types: frame camera and panoramic camera<br>- Frame – pinhole camera; light passes through tiny hole, hits image plane capturing entire image at once<br>- Panoramic – only allows a slit of light in as opening sweeps across film |

**Panoramic:** Gao et al. 2010; Wolf et al. 2014; Lillesand et al. 2015; **Hemispherical:** Hale and Edwards 2002; Inoue et al. 2004; Wacker et al. 2015; Beekmans et al. 2016; Ho and Budagavi 2017; **360º:** Ho and Budagavi 2017; Huang et al. 2017; **Lensless:** Young 1989

### 2.2.2 Lens Distortion

Although some simplified models neglect the lens distortion of a camera, it is a factor that must be considered since it affects the geometric quality of an image (Morris 2004; Wolf et al. 2014). Distortions can occur between where an object truly is and where the equivalent point is on the image plane (Clarke and Fryer 1998). These can be quantified and modelled through camera calibration. One method of traditional calibration uses a specialised equipment such as a set of collimator targets with known angles (designed to narrow and direct the light) and the difference residuals between the observed and expected angles help identify the distortions present (Figure 10). Residuals between measured and estimated locations, in terms of both angles and distances, can also be calculated and plotted as vectors (Figure 11). These, together with information on camera parameters such as the focal length and coordinates of any fiducial marks (permanent marks within the camera with known locations) with respect to the principal point, form a conventional camera calibration report/certificate.

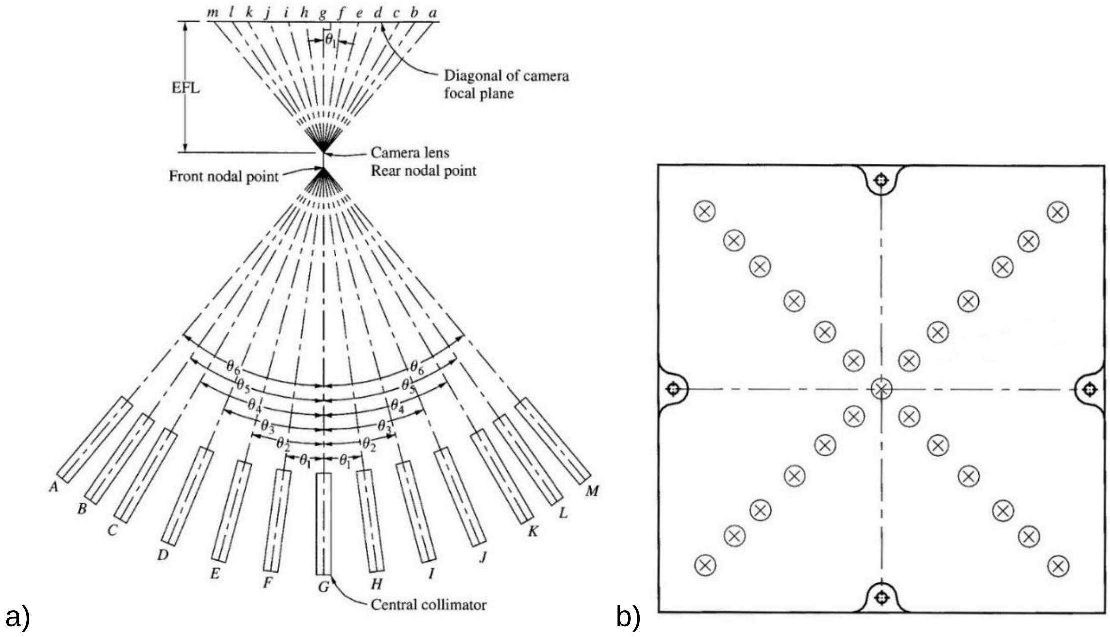


Figure 10: A diagram showing a) a plan and b) an image frame view of collimator targets (in this case in the form of an X), between which the difference in angles is used to measure lens distortions. The intersection (rendered as a dot-dash line) between the four fiducial marks at the edge of the image frame in b) represents the principal point (amended from Wolf et al. 2014, Fig. 3-17 and 3-18)

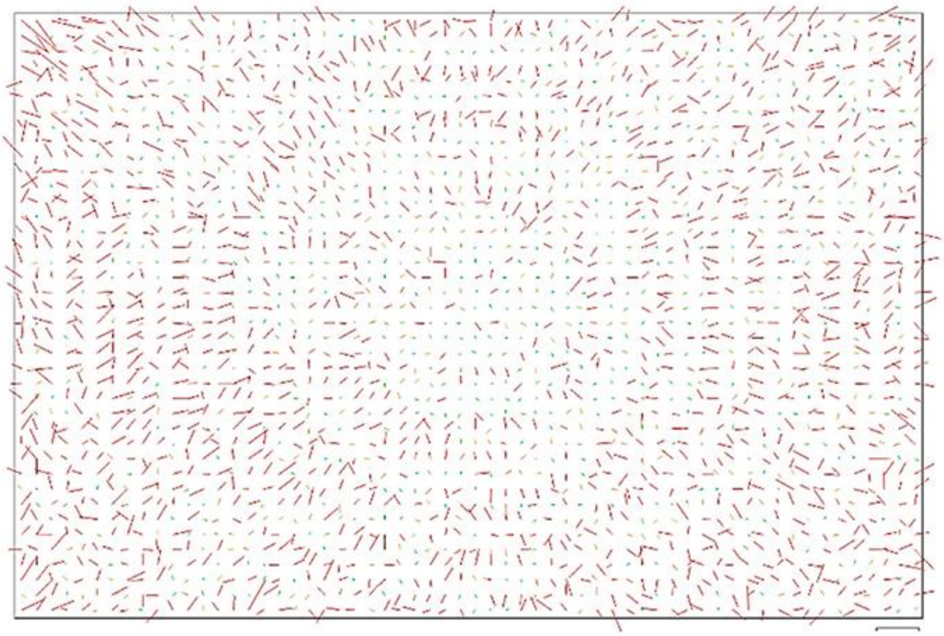

Figure 11: Lens distortions across an image frame (derived from a self-calibrating bundle adjustment, see section 2.2.2 and 2.4.3.3.1) illustrated as vectors. Distortions deemed negligible are shown in green, whilst the remainder are in red. The scale bar at lower right represents a distance of one micron (Sanz-Ablanedo et al. 2018, Fig. 4)

With some types of image-based modelling, the calibration is not done in advance but rather during the process of the bundle adjustment (see Section 2.4.3.3.1). The principal point is the location that all distortions should be symmetric (Clarke and Fryer 1998). There tends to be more distortions around the edge of the lens compared to the middle and they tend to be more significant with a shorter focal length (Morris 2004; Linder 2009). There are three general types of distortion; symmetrical radial distortion (coefficient k), decentring distortion (coefficient p), and in-plane correction parameters (coefficient b) (Figure 12) (Fraser 2013; Wolf et al. 2014; Historic England 2017). Symmetrical radial distortion occurs along radial lines from the optical axis and can either be positive and outward or negative and inward. Decentring distortion has an off-centre pattern and is made up of tangential and asymmetric radial parts (Wolf et al. 2014). In-plane correction parameters address non-orthogonality between the x- and y-axis as well as the possibility of differences in pixel spacing in both directions, however it is not always present (Wolf et al. 2014).

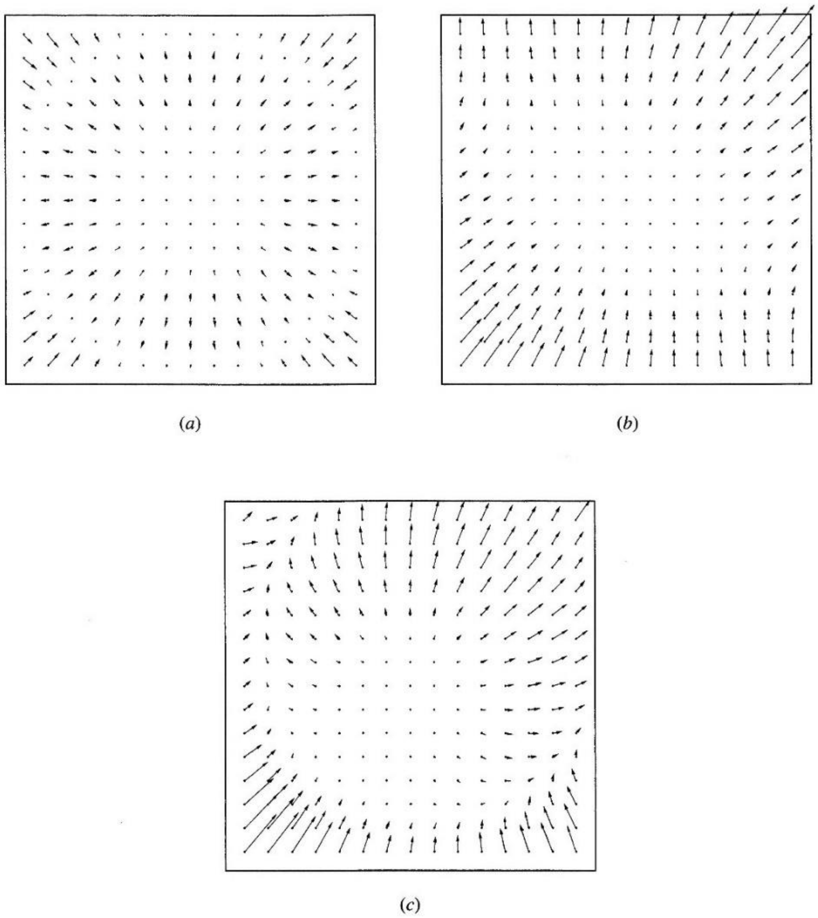


Figure 12: Pre-calibrated lens distortions across an image frame, illustrated as vectors, where a) is symmetric radial, b) is decentring, and c) are the combined distortions (Wolf and Dewitt 2000)

### 2.2.3 The Image

Digital cameras use sensors on the image plane to detect the light that has passed through the lens in order to recreate the image. The light-sensitive picture elements are more commonly known as pixels and are in fixed positions contained within either a charge-coupled device (CCD) or a complementary metal-oxide semiconductor (CMOS) (Figure 13) (Wolf et al. 2014; Lillesand et al. 2015).

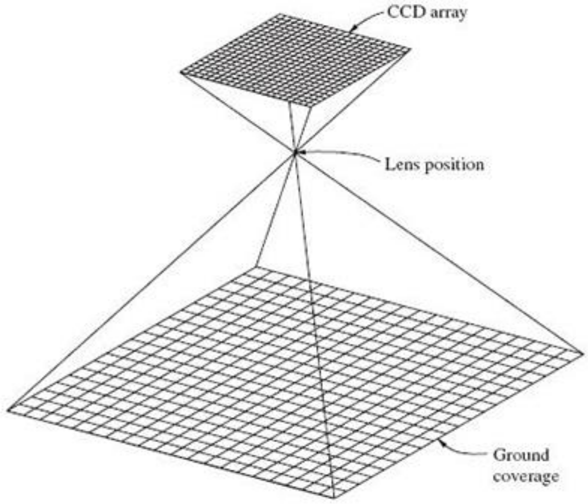


Figure 13: A schematic of a basic digital camera CCD array and where it is in reference to the area of ground coverage (Wolf et al. 2014, Fig. 3.10)

Pixels generate a charge that is based on the amount of light detected by each pixel (Lillesand et al. 2015). This electric charge is measured and digitised, giving each spatial position an intensity value in numerical form (Long 2013). Thus, each pixel is represented by a data number and in its simplest form, it would be represented by a binary value of either 0 or 1, meaning each pixel would have two options, white or black (Figure 14). This is known as a one-bit image (Long 2013). Typically, the information for each colour stored in pictures is of a higher bit depth, usually eight-bits per pixel which appears to the human eye like an unbroken gradient. Eight-bits equates to 256 different variations represented by a binary value between 0 and 255 (Morris 2004; Long 2013; Wolf et al. 2014). Increasing the number of bits does not increase the range of colours or shades that are identified, rather it allows for finer variations within that range.

Figure 14: An example of 1 bit resolution (2 colours)

CCD chips are more common, however CMOS are often in more expensive DSLR cameras as they consume less power and can integrate more functions on the chip (Long 2013). The methods that the light is detected in CCD and CMOS chips are similar, though there are some inherent differences (Mehta et al. 2015). CCD cameras typically use a global shutter design which scans the entire image at once. CMOS tend to have a rolling shutter design which means the image in scanned sequentially from one side to the opposite. The intensities that are recorded have set positions on the sensor. For nearly all cameras, there is a need to filter out the near infrared light (greater than approximately 700nm) and thus have an optically flat filter which only retains the light in the visible spectrum (roughly 400-700nm) without causing distortions (Wolf et al. 2014; Lillesand et al. 2015).

There are two fundamental characteristics involved in the creation of digital image; geometric resolution and radiometric resolution. Geometric resolution involves the size of the pixels (Wolf et al. 2014). For the image to be clearly resolved, a lot of small pixels are needed in order to record all the appropriate variation (Lillesand et al. 2015). There is a trade-off though; when more pixels are fit into a CCD of the same size, there is less space for each to capture the light and therefore the amount of noise can increase compared to the amount of good data (Long 2013; Historic England 2017). Radiometric resolution involves changing of the amplitude of the original signal into discrete numerical levels where more levels result in a more accurate representation with more subtle variations (Wolf et al. 2014).

#### *2.2.3.1 Colour Images*

When the image is colour (RGB), eight-bits are required for each of red, green, and blue, leading to a total of 24-bits of information per pixel. However, CCD and CMOS chips are typically monochromatic and therefore the light must be filtered for the pixels to capture colour (Lillesand et al. 2015). Therefore, colour cameras usually have a filter in them that allow each pixel to ‘see’ a different colour of light; red, blue, or green (Lillesand et al. 2015). The use of a filter means that certain wavelengths of light are restricted from passing through and will not register on the pixel that is covered by that filter (Lillesand et al. 2015). Most commonly, a Bayer filter is used which is arranged in alternative rows and columns of green/red and green/blue with each coloured square overlaying a pixel (Figure 15) (Fraser 2013; Lillesand et al. 2015).

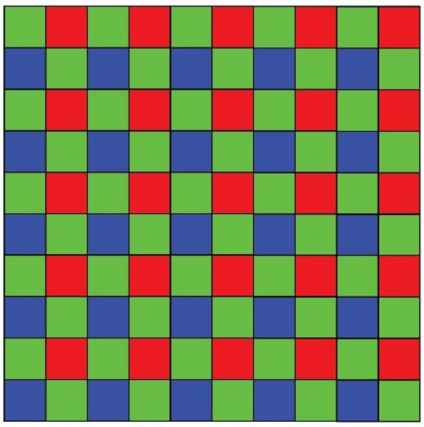

Figure 15: An example of a Bayer filter

The Bayer filter is found to be the most effective method at the moment, however there are inherent problems. For example, one issue is that green is overrepresented. Additionally, when using Bayer filters, it is important to be cognisant of the fact each pixel still requires a value for each colour, even if that colour is filtered out (Fraser 2013). This means that for each pixel, values for the two colours that are filtered out are interpolated from the surrounding ones of the same colour (Long 2013; Lillesand et al. 2015).

## 2.3 Coordinate Systems

Another vital component of image-based modelling is the scaling and orientation of the models, accomplished via coordinate systems. There are four coordinate systems, or spaces, that need to be accounted for in photogrammetry (Figure 16). All of these are Cartesian coordinate systems with the axes x, y, z and the rotation around those axes are denoted by ω, φ, κ (Fryer et al. 2007).

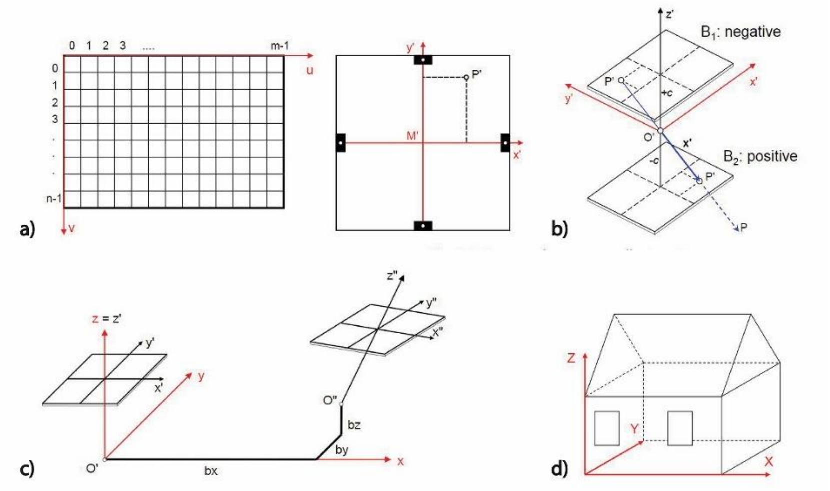


Figure 16: The four coordinate systems involves in photogrammetry a) the pixel or image coordinate system, b) the camera coordinate system, c) the relative object coordinate system, and d) the absolute object coordinate system (amended from Luhmann et al. 2013, Figs. 2.1-2.4, p.28-31)

The first is the image coordinate system (Fryer et al. 2007; Morris 2004). This is the coordinate system related to the image sensor or film in the camera. It is sometimes known as the CCD/CMOS or pixel coordinate system in literature concerning digital cameras. This is a 2D coordinate system with only x- and y- axes. The origin of this system is sometimes considered to be at the top left in a CCD or raster image, however when using a photograph or digital image, this is at the centre of the image. Despite this, some software packages may differ in where the origins of the coordinate systems are (Agisoft LLC 2020a). As described by Wolf et al. (2014) regarding a metric camera, the origin is at the point where lines connecting opposite fiducial marks intersect.

The second coordinate system is the camera coordinate system which is the orientation of the camera itself (Morris 2004). The image coordinate system is usually the same as the camera coordinate system in one dimension. For film cameras, the alignment of the film and the frame of the camera should be the same though are often not and the origins of the image coordinate system should be given through the locations of the fiducial marks and the intersection of lines that join opposite fiducial marks (Heipke 1997). In digital cameras, the principal point is the origin of the camera coordinate system. (Morris 2004). In an ideal camera model, the origin of these two coordinate systems would be the same, however this is not usually the case since the principal point in not typically in the exact centre of the image plane.

The third is the relative object coordinate system. To find the relationship between the camera coordinate system and the relative object coordinate system, it is necessary to determine where the optical centre (also known as the principal point, see Section 2.2.1) of the camera is compared to the origin of the relative object coordinate system which encompasses the object or subject being photographed (Morris 2004). Once the object has been rendered in 3D, its placement in space is arbitrary and not tied to any external coordinate system (Grussenmeyer and Al Khalil 2002).

The final coordinate system is the absolute object coordinate system which is linked to the real world and the coordinate reference system (also widely known as map projections) that the original object is in (Fryer et al. 2007). This is done by using ground control points identified in the individual images, discussed further in Section 2.4.3.3.

## 2.4 Photogrammetry

There are two main branches of 3D image-based modelling; survey/conventional photogrammetry and machine/computer vision (Jebara et al. 1999; Snavley et al. 2008). The two fields have spent much of their history developing separately and thus the terminology and literature is often different despite the overall principles being the same or similar (Granshaw and Fraser 2015). The following section briefly discusses both before detailing the core principles and concepts. Subsequently, the method of image-based modelling used in this study known as SfM-MVS, which combines the two branches, is outlined and discussed.

### 2.4.1 Survey/Conventional Photogrammetry

Survey, or conventional, photogrammetry mostly concerns model creation from aerial images, either acquired during reconnaissance flights or more commonly during aerial survey. It could be argued this is the oldest and original branch of photogrammetry, as it dates from the time of the earliest film cameras and flight (mostly heavier-than-air, but also kites, balloons and airships). There is an emphasis on accuracy, precision, and reliability, with the goal being to create a model with the greatest possible spatial coverage using the least number of images, but the greatest possible accuracy (Barazzetti et al. 2011; Remondino 2011; Granshaw and Fraser 2015). This is reflected in a legacy of more rigid requirements regarding what camera and geometry can be effectively used.

Pre-calibrated film cameras (commonly known as metric cameras, sometimes as mapping or cartographic cameras) were used because the knowledge of internal camera parameters (commonly known as interior orientation) was widely considered a prerequisite to create photogrammetric models (Barazzetti et al. 2011; Wolf et al. 2014; Lillesand et al. 2015). This type of photogrammetry has often been used for a variety of 2D and 3D cartographic products, including everything from site- and cadastral-mapping (i.e. ≤1:1000) to topographic mapping (i.e. ≥1:20000) (Remondino 2011).

The requirements for metric cameras have been largely removed since the advent of digital cameras which are partially or entirely solid-state. This is thanks to the array of detectors remaining static relative to the lens, unlike plate or film cameras, which required either fiducial marks or a reseau plate to be captured during the exposure of each frame (Wolf 1983; Wolf et al. 2014; Granshaw 2020). Both reseau plates and fiducial marks are permanent fixtures within a metric camera; the former is a marked glass grids and the latter are marks around the edge of the camera frame. These would appear in every picture at known points compared to the principal point of the image and remained static relative to the lens to help establish an image coordinate system and determine distortion (Avery and Berlin 1992; Fryer et al. 2007; Lillesand et al. 2015; Granshaw 2020). Calibration to derive interior orientation parameters such as the focal length, location of the principal point and lens distortions (among others) was usually conducted in laboratory conditions prior to any photographs being taken for the purposes of measurement. Initially digital cameras also required pre-calibration. Although still highly desirable, modern algorithms can reduce or eliminate this requirement.

The most efficient geometry for photographing a relatively large, planar area, such as a landscape, is parallel, vertical exposures taken with a single camera, rather than different cameras, a set distance apart with an optimal overlap of 60% along the direction of flight (Figure 17) (Historic England 2017). This overlap, also known as end-lap, is such that the same object can be seen in three photographs. In this case the object can be viewed either by the human eye or, more recently, by a computer algorithm, stereoscopically (hence the terms stereopairs, etc.) (Avery and Berlin 1992; Wolf et al. 2014). In situations where anything other than a strip/corridor survey (such as for roads, rivers etc) was required parallel, adjacent flight tracks were flown in opposite directions (often known as a lawnmower pattern) to create a block, in which case the optimal side-lap between strips of photographs is 30% (Figure 18) (Historic England 2017).

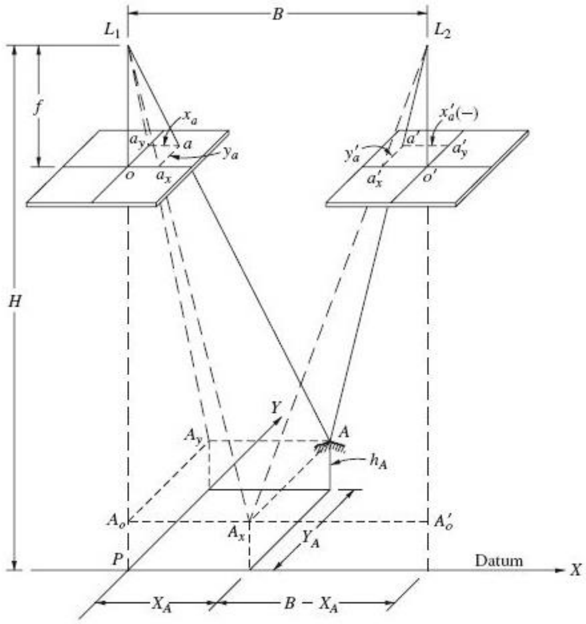


Figure 17: The geometry of two overlapping vertical images (Wolf et al. 2014, Fig. 8.10)

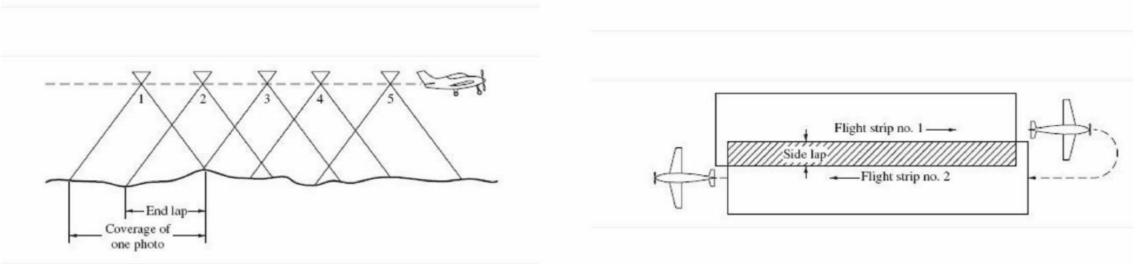


a) b)

Figure 18: An example of a) end-lap during a five-image flight strip and b) side-lap between two flight strips (amended from Wolf et al. 2014, Fig. 1.9-1.10)

In all the aforementioned instances, the photogrammetry was at first entirely analogue, that is to say it used physical devices to make measurement on hard-copy photographs. (Doyle 1964; Konecny 1985; Clarke and Fryer 1998; Linder 2009; Luhmann et al. 2013; Wolf et al. 2014). Numerous refinements were made to the existing equipment during this time through optical instruments, optical-mechanical instruments, and mechanical instruments for aerial photogrammetry, however, there was less focus on close-range or terrestrial photogrammetry (Konecny 1985; Linder 2009). Analogue photogrammetry began to be supplanted and ultimately superseded by analytical photogrammetry from the 1970s, which employed a computer to perform complex geometrical calculations based on measurements originally taken from the hard-copy photographs (Doyle 1964; Konecny 1985; Linder 2009). Analytical photogrammetry itself was superseded by digital photogrammetry in the 1990s, though still designed for the kind of geometry typical of aerial survey (Konecny 1985; Linder 2009). A critical part in the progression of digital photogrammetry is the evolution of digital cameras and digital photography (Lillesand et al. 2015). This phase in the development of photogrammetry can be considered a major catalyst for photogrammetry becoming a viable option for more people to use (McCarthy 2014).

In the past, survey/conventional photogrammetry used discrete objects in successive stereo photographs which could be visually identified by a trained expert as tie points (TP) (Linder 2009; Verhoeven 2011; Historic England 2017; Granshaw 2020). These points had no *a priori* coordinates in any reference frame, but served to reconstruct the location (x, y, z) and orientation (ω, φ, κ) of the camera's centre when each exposure occurred (known as a camera/photo station) relative to each other, thus helping determine the exterior orientation (Figure 19) (Granshaw 2020). Where more than a single stereopair were used (for example with a strip or block of photographs) TPs could be visually identified in three or more photographs and thus a bundle adjustment was used in order to iteratively refine the exterior orientation, often commonly using a least squares approach to minimise residuals in a global sense (Linder 2009; Historic England 2017).

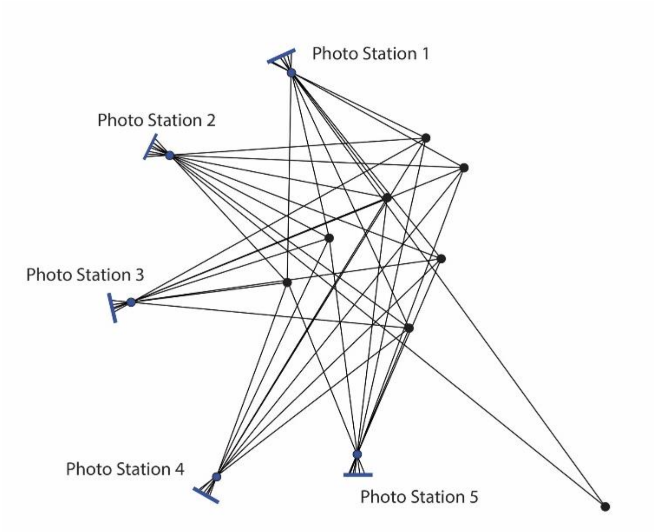


Figure 19: A plan of five photo stations and how they align to eight features

Similarly to TPs, [ground] control points (CP, or more commonly [G]CP) with *a priori* 3D coordinates (either relative or absolute) could be visually identified and used to aid with the reconstruction of exterior orientation, which also provides a scaled model from the outset (Linder 2009; McCarthy 2014). Once exterior orientation, whether in a relative or absolute sense, was optimised measurement could be undertaken using the resulting stereo model. More recently digital photogrammetry was also capable of simultaneously refining the interior and exterior orientation using a self-calibrating bundle adjustment, or SCBA (assuming a single camera was used) (Koutsoudis et al. 2013; Historic England 2017; Granshaw 2020).

### 2.4.2 Machine/Computer Vision

Machine/computer vision, hereon known as computer vision, evolved after the creation of digital computers in the 1940s and 1950s with particularly rapid growth in capability from the 1970s onwards (Snavley et al. 2008; Chiabrando et al. 2015; Beale and Reilly 2017). Computer vision is often considered a science that uses and develops mathematical techniques to find 3D spatial and structural information as well as appearance from images (Morris 2004; Verhoeven 2011; Chiabrando et al. 2015). The focus of computer vision is to automate the processes as much as possible and obtain the level of accuracy and precision that is required based on an object’s location and orientation (Barazzetti et al. 2011; Remondino 2011; García-Gago et al. 2014). The various algorithms that have been created and developed have become instrumental in the performance any computer vision process.

Rapid identification, or quick matching, of the same object in successive frames in order to follow or detect objects or places is another priority of computer vision and it is concerned with its integration into industry and for practical purposes (Granshaw and Fraser 2015). It is often used for things such as object recognition and tracking, shape recognition, robot control, and augmented reality, to name a few (Remondino 2011). There are fewer restrictions on the specifications and type of camera, although much of computer vision was developed since, rather than before, the advent of digital cameras, thus negating the use of fiducial marks or a reseau plate. Unlike survey/conventional photogrammetry, exterior orientation is often known by the camera and is not reliant on the use of [G]CPs (Granshaw 2020). Neither is pre-calibration of the camera or cameras required for interior orientation although it remains desirable. In both cases computer vision also employs self-calibrating bundle adjustment as with later forms of digital methods in survey/conventional photogrammetry (García-Gago et al. 2014; Granshaw and Fraser 2015).

### 2.4.3 Basic Principles and Maths

To more comprehensively understand how models are created through image-based matching, the basic mathematical and geometric principles must be understood. Some of the major principles, such as collinearity, triangulation, epipolar geometry, parallax, disparity, errors, interior orientation, and exterior orientation are outlined here.

Collinearity equations are vital for image orientation and it describes the relationship between the image coordinates, the object coordinates, the exposure/photo station position, and the angular orientation (Barazzetti et al. 2011; Granshaw 2016). In more specific terms, the object point, the optical centre of the camera lens (perspective centre), and the image point will always be in a straight line along the chief ray regardless of the orientation of the photograph with the assumption the sensor is planar (Figure 20) (Fryer et al. 2007; Wolf et al. 2014; Historic England 2017). It is a component of epipolar geometry and it aids in the calculation of exterior orientation in stereopairs or multi-view stereo situations through bundle adjustments (Grussenmeyer and Al Khalil 2002; Granshaw 2016). However, it must be noted that the collinearity equations are based on an ideal camera with no distortion (Historic England 2017).

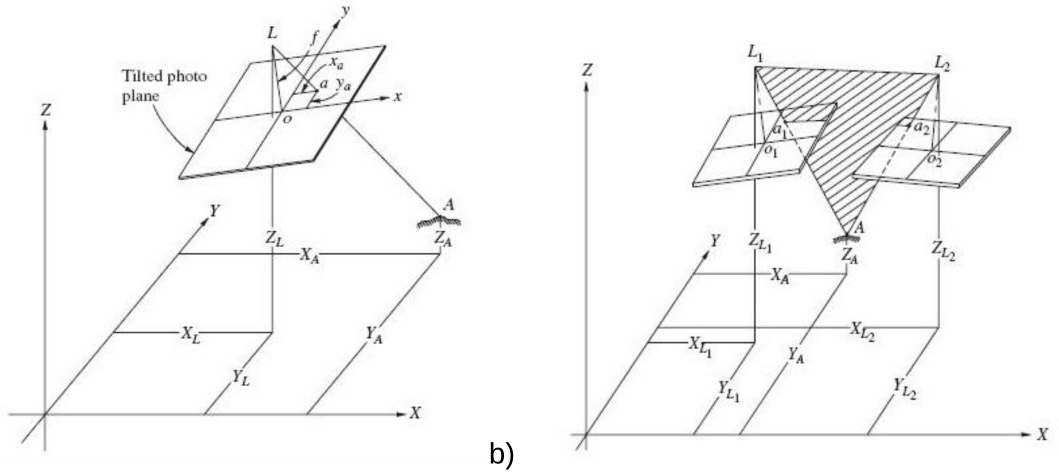


a) b)

Figure 20: An example of a) the collinearity condition with one image and b) the coplanarity condition with two images (Wolf et al. 2014, Fig. 11.1-11.2)

Also important for image orientation is the determination of the ground coordinates of a point using photo-coordinates, a process known as triangulation, analytical triangulation, or aerotriangulation (Barazzetti et al. 2011; Lillesand et al. 2015; Historic England 2017). It is used to estimate the position of a 3D point and the geometry of a scene in a relative object coordinate system (Section 2.3) (Westoby et al. 2012). Before this can be done, knowledge of the tie points or location of the [G]CPs must be known. If using [G]CPs, the relative and absolute exterior orientation can be found, however, if only using tie points, only the relative exterior orientation can be determined. Overall, the assumption of the collinearity equations for the determination of relative exterior orientation can be used to reconstruct 3D points from 2D ones (Historic England 2017).

Epipolar geometry describes the geometric principles behind stereo vision and the relationship between the position of the images captured in image-based modelling. Taking an example with two adjacent cameras, there is a baseline between the perspective centre of each (Jebara et al. 1999). Following the property of collinearity, the perspective centre lies on the same line as the image point and the object point (Granshaw 2016). This is true for both cameras. Those rays and the baseline between them are all coplanar because they lie on the same plane (Grussenmeyer and Al Khalil 2002; Wolf et al. 2014; Granshaw 2016). The intersection of the image plane and the epipolar plane is known as the epipolar line (Heipke 1997; Wolf et al. 2014; Granshaw 2016). All these conditions have to be filled for the geometry to be considered epipolar (Figure 21). With this knowledge, if searching for a conjugate point in an adjacent image, as seen in dense point matching, it should lie along the epipolar line in the search image, therefore reducing the area that needs to be searched from two dimensions to one and making the process more efficient (Barazzetti et al. 2011; Wolf et al. 2014; Granshaw 2016; Kim and Kim 2016).

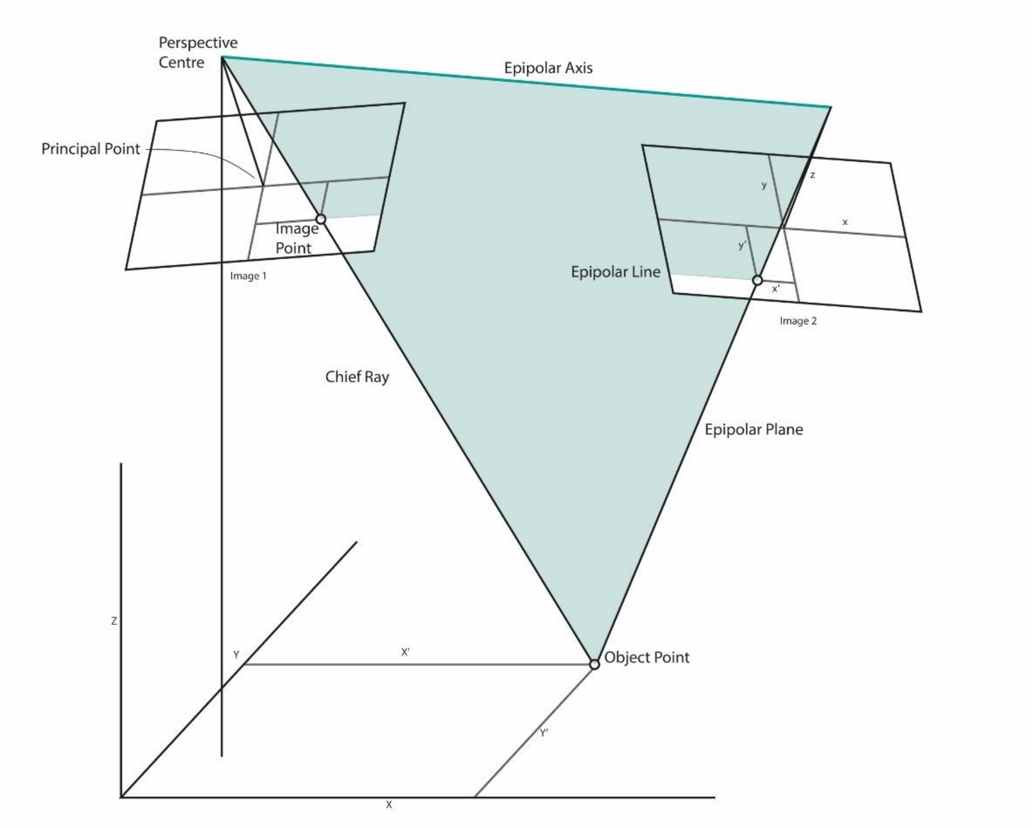


Figure 21: An example of epipolar geometry between two camera stations with the positive image plane represented (amended from Wolf et al. 2014, Fig. 12.16)

Another important factor is parallax, which is the apparent shift in the position of a stationary object due to a change in the location from which it is being viewed (Wolf 1983; Wolf and Dewitt 2000; Lillesand et al. 2015). The ability to match points that are at slightly different locations and orientations is critical in determining camera geometry (Figure 22). This occurs in stereopairs and in sequential images and is a basic tenet of stereovision because the distance between humans' eyes is analogous to the baseline between two cameras, and therefore a stationary object is viewed slightly differently between the left and right eye (Avery and Berlin 1992). There is less apparent displacement when the object is further away compared to when it is near and thus the change is easier to measure when the object is closer. The parallactic angle is the angle where the chief rays from two cameras converge at an object in space (Wolf et al. 2014). In a 'perfect' scenario of a row of pictures, the only parallax that would be present is x-parallax which would be along the axis of the flight path (Wolf and Dewitt 2000). If any of those images were slightly shifted or rotated in any direction, y-parallax would be present as well (Figure 23) (Wolf and Dewitt 2000). When a block of images or an SfM-MVS image capture strategy is used, the proportions of x and y parallax are much more similar.

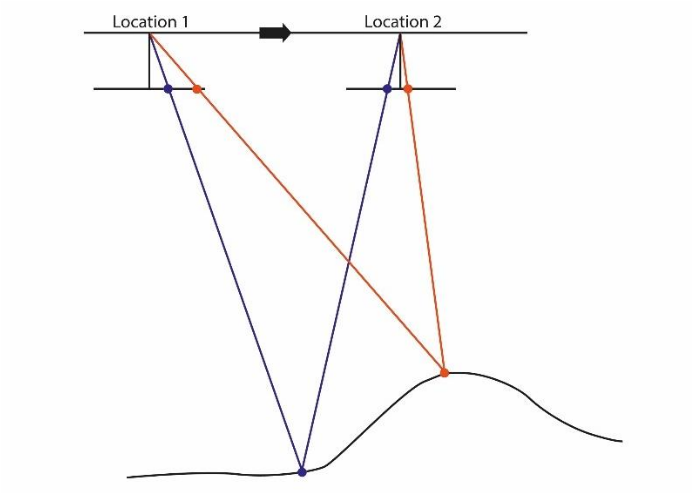


Figure 22: An example of how variation in ground surface height affect the images that are captured (parallax differences) (amended from Wolf et al. 2014, Fig. 8.11)

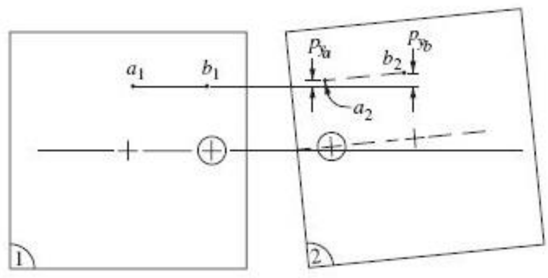

Figure 23: An example of y-parallax that comes from images not being in exact alignment (Wolf et al. 2014, Fig. 7.15)

Disparity is the difference in the two images that is caused by parallax (Barnard and Thompson 1980). For this example, a stereopair with only a horizontal shift will be considered. The images can be examined on a pixel-by-pixel basis and the pixels can be given vectors or a colour value based on the shift between the images (Barnard and Thompson 1980; Mühlmann et al. 2002; Kordelas et al. 2015). This latter is known as a disparity map, though they are sometimes erroneously called depth maps. Depth maps should reflect range whereas disparity does not equate to range, though it can provide a guide to what is relatively close and what is relatively far (Barnard and Thompson 1980; Granshaw 2016). The knowledge of the disparity is important for spatial perception and image matching as it helps determine the relationships of the images to each other (Barnard and Thompson 1980). There are three factors that can influence how effective the disparity of two images would be to aid in matching images; the discreteness and distinctiveness of the points, the similarities of the points, and the consistency of the points compared to other nearby matches (Barnard and Thompson 1980).

#### 2.4.3.1 Accuracy, Precision, Reliability, and Errors

Accuracy, precision, and reliability are all important in scientific studies and therefore it is important to note the distinction between them (Fryer et al. 2007). Accuracy is how close a measured value is to the true value or the result of a gold standard test (Opitz 2013; Wolf et al. 2014; Granshaw 2016). This is often expressed through root mean square error which is the square root of the distance between two measurements of the same point (Oniga et al. 2014). Precision is how much variation there is of the repeated measurement of a value and is commonly measured by standard deviation (Opitz 2013b; Wolf et al. 2014; Granshaw 2016). Being accurate does not inherently means there is a high level of precision and being precise does not mean the measurements are accurate. Reliability is similar to precision but it focuses on whether an instrument is consistently interpreted across different conditions (Field 2009). All of these have been shown to be better when control targets are used when creating the models (Sapirstein 2018).

As defined by Wolf and Dewitt, an error is "…the difference between a particular value and the true or correct value" (2000, p.495). As with every technique, there are sources of error that must be understood and accounted for (Wolf et al. 2014). There are three type of error that can cause inaccurate models; gross, systematic, and random.

Gross error is also known as user error and are genuine mistakes which can be inadvertently introduced by the operator or researcher through carelessness or oversight (Fryer et al. 2007; Wolf et al. 2014; Ferriera et al. 2017). Examples of these would be the incorrect transcription of a value or misreading a measurement (Wolf et al. 2014). These errors should be removed as they represent invalid data (Granshaw 2016). If points in the process at which error could be introduced are known, it is easier to account for and mitigate or reduce them (Lillesand et al. 2015).

Systematic error is due to equipment and follows a mathematical or physical principle (Wolf et al. 2014). Once understood, they are generally straight-forward to correct by mathematical formulae (Lillesand et al. 2015). For example, this type of error can be found in the interior orientation stage of the processing. Things such as uncalibrated or improperly calibrated equipment, non-planar sensors, physical error in pixel geometry of the sensor, incorrect lens distortion estimates, incorrect positioning of the principal point or incorrect alignment of sensor plane and lens axis, and refraction are all problems that could lead to errors (Fryer et al. 2007; Ferriera et al. 2017; Historic England 2017). It is important to be aware of these errors and be able to mitigate for their occurrence through mathematical modelling as effectively as possible (Wolf et al. 2014). Errors in interior orientation parameters can often be corrected during bundle adjustment (Section 2.4.3.3.1) or can be corrected for across the whole procedure once they are identified.

The error that is the hardest to correct for is random, or stochastic, error. This is whatever error remains once the gross and systematic error have been considered; they are unavoidable, cannot be predicted, and can be either negative or positive (Fryer et al. 2007; Wolf et al. 2014; Ferriera et al. 2017). They typically follow a normal distribution and can be estimated through statistics (Granshaw 2016). The method of correcting or mitigating this error is often the use of a least squares adjustment in which transformation equations are used to help correct inaccurate geometry.

Least squares adjustment is a mathematical way to mitigate random error in a set of data as well as find the best fit for a set of data (Wolf 1983; Wolf et al. 2014). This mathematical process has a long history but was only introduced into photogrammetry the 1980s. It is an iterative process that is extremely important in orientation and image matching (Gruen 2012; Wolf et al. 2014). It involves finding residual values, which are the difference between the measured amount and a predicted measurement for said amount. These predicted values are iteratively adjusted until the sum of the squares of the values cannot be any further reduced, in which case the result is the best fit between observed and estimated data (Lowe 2004; Wolf et al. 2014; Granshaw 2016). Generally, more points will help find a more accurate fit with a lower chance of error (Linder 2009). Least squares adjustments work most effectively when there are a large number of observed values being adjusted and when the error follows a Gaussian distribution, however the technique is robust and therefore still provides good results even if these conditions are not met (Wolf et al. 2014)

#### *2.4.3.2 Interior Orientation*

Interior orientation is an important component of photogrammetry as it is needed to obtain spatial information from the camera. It is established through knowledge of the internal geometric parameters of the camera, such as focal length, principal point location and distance, and lens distortion characteristics (Heipke 1997; Grussenmeyer and Al Khalil 2002; Luhmann et al. 2013). Interior orientation establishes the coordinate system in the image by finding the relationship between the camera coordinate system, the origin of which is the principal point, and the image coordinate system (Linder 2009; Luhmann et al. 2013). This relationship is required to be able to orient any images that are taken and ensure that collinearity conditions are met (Historic England 2017).

In order to estimate interior orientation, a camera needs to be calibrated. This is a more extensive process in survey/conventional photogrammetry compared to SfM-MVS, the latter of which does not require advance knowledge of the camera parameters (Westoby et al. 2012). In traditional film camera, camera calibration reports are issued which contain the relevant information. In digital cameras, the information about the camera and each image is contained within a file associated with each image in exchangeable image file (EXIF) format which is a standard that specifies the metadata to be stored with each image (Koutsoudis et al. 2014; Granshaw 2016).

#### *2.4.3.3 Points: Key Points, Tie Points, and [Ground] Control Points*

Algorithms which automatically or semi-automatically identify candidate locations for the same points (conjugate points) across the image, commonly known as key points (KPs). KPs are distinct and identifiable features that algorithms detect in an image, which therefore have the potential to also be distinct and identifiable in other images (Granshaw 2016). Matching algorithms are then used confirm and refine the actual conjugate points (amongst the KPs), which become TPs. Such TPs can then be used to establish the geometric relationship between the images (Figure 24) (Linder 2009; Verhoeven 2011; Granshaw 2016). TPs identified in this way are often more numerous than those which could identified by an operator using labour-intensive analogue, analytical or early digital photogrammetry. This is known as triangulation (Section 2.4.3). Accurate (or precise) coordinates of TPs are not required for this, however they can still form the relative exterior orientation of the object and some software (such as with SfM, described below) can create a sparse point cloud with these TPs (Linder 2009; Historic England 2017).

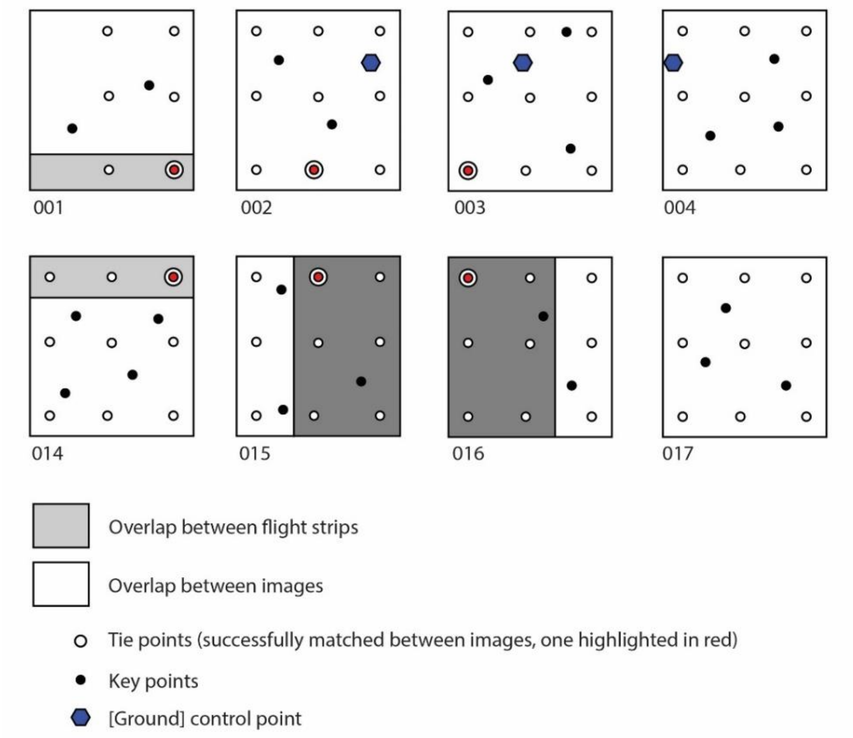


Figure 24: A demonstration of how tie points are identified in multiple images in order to be linked together (amended from Linder 2009, Fig. 32, p.79)

[Ground] control points ([G]CPs) are physical locations on the ground or on a structure with known coordinates and therefore their exact locations can be identified (Linder 2009). Control points (CPs) use an arbitrary coordinate reference system whereas ground control points (GCPs) used a pre-defined coordinate reference system). [G]CPs are required if a model is to be tied to the absolute object coordinate system (McCarthy 2014). They should be clear and unambiguous, and it is more advantageous if they are spread out (Wolf et al. 2014; Historic England 2017). In conventional photogrammetry, these GCPs are placed as regularly as possible around both the periphery and the main area of interest (Ferriera et al. 2017). They can either be placed in advance, or the coordinates can be found retroactively (Fryer et al. 2007). They should generally be selected based on being highly visible from multiple angles. They can be placed markers that are visible from the required object-to-camera distance, or they can be well-delineated natural features (Linder 2009). Sharp changes, such as lines, corners, field boundaries, and crossroads are often good. For smaller objects, a base with markings that are a known distance and angle apart can provide this control.

There are many sources that can provide the numerical data for control. Terrestrial or aerial Global Navigation Satellite System (GNSS), total station theodolite (TST), terrestrial laser scanning (TLS), and light detection and ranging (LiDAR) are all examples of methods of obtaining the required data (Wolf et al. 2014; Historic England 2017). Scale bars can be used, however, they will only provide scale and they will not tie the model into the external coordinate system. Generally, a minimum of two points is required for scale and three for scale and orientation (Linder 2009; Wolf et al. 2014; Historic England 2017). To provide effective control points, these must have data with reference to a known xy system (horizontal) and elevation information (vertical) associated with them (Linder 2009; Lillesand et al. 2015). It is important for the control to be extremely accurate (ADS 2009). The reliability of photogrammetry is dependent on the reliability of the [G]CPs.

##### 2.4.3.3.1 Camera [Pre-] Calibration and Self-Calibrating Bundle Adjustment (SCBA)

Camera calibration helps define the interior orientation, without which, neither the image nor camera could be orientated in space (Morris 2004). Best estimates are made of the lens distortions in order to allow for the determination of parameters such as the calibrated principal distance (the distance between image plane and perspective centre), principal point location and offset, and the location of the fiducial marks (Wolf et al. 2014; Historic England 2017). The knowledge of the internal parameters of the camera helps correct any distortion and set an accurate scale in the photographs (Historic England 2017). There are different methods for traditional calibration, but a camera calibration report should be available regardless of the method (Clarke and Fryer 1998).

Conventionally, as described above, camera calibration would be an entirely separate process, however, with SfM-MVS and digital cameras, this occurs within the photogrammetric process and is often called self-calibration or analytical self-calibration. With the exception of the shutter and adjustable aperture, most digital cameras can be considered solid state. Therefore the pixel dimensions, the location of the CCD or CMOS array (which are fixed) relative to the lens, the focal length and coordinates of the principal point could be said to be pre-determined by the original camera design and many such parameters are written as such into the EXIF image header (Section 2.4.3.2). It may appear that the solid-state nature of digital cameras negates the requirement for not only fiducial and other such metric camera marks, but also for calibration. However, imperfections in manufacture mean each individual as-built camera will have variable parameters, which requires those written into the EXIF header to be considered as estimates only, and these must then be refined through self-calibration (Wolf et al. 2014).

In photogrammetry, a bundle is a conical group of light rays going from object point to image point that pass through the centre of a camera lens at each exposure station/location (Linder 2009; Wolf et al. 2014). A group of images can be referred to as a block, for which the bundle of rays for each exposure can also be considered (Wolf et al. 2014). Space/spatial resection is the trigonometric derivation of exterior orientation for an exposure using known locations identifiable in the image and the bundle of rays which radiate from them. In contrast, the reverse or opposite of this is space/special intersection, which involves the trigonometric derivation of locations in an image using the exterior orientation for the exposure. Using a combination of space/spatial resection and space/spatial intersection, the relative and absolute geometry of all the bundles in the block are based upon the estimated camera parameters (from the EXIF header, for instance) and form the initial conditions (Fryer et al. 2007; Luhmann et al. 2013). If no lens distortion parameters are available for the initial conditions, collinearity can be assumed.

The bundles in a block are then simultaneously adjusted (hence the term bundle adjustment), in terms of both orientation and location, to best fit the TPs and [G]CPs and in exterior orientation (Grussenmeyer and Al Khalil 2002; Wolf et al. 2014; Lillesand et al. 2015), a process which commonly uses a non-linear least square, iterative method (Koutsoudis et al. 2013). In SfM-MVS, self-calibration bundle adjustment (SCBA) is typically performed by SfM (see Section 2.4.4.1). Where TPs and [G]CP are sufficiently numerous it is possible to estimate lens distortions and/or refine other estimated camera parameters (the initial conditions) using the deviation of their locations from those that were based upon the assumption of collinearity. This effectively calibrates the camera and lens *a posteriori*.

#### *2.4.3.4 Exterior Orientation*

The exterior orientation orientates and scale the cameras in relation to one another (and optionally with reference to an arbitrary or pre-defined coordinate reference system) thus also orientating and scaling the object in the process and is a vital photogrammetric property (Grussenmeyer and Al Khalil 2002; Luhmann et al. 2013; García-Gago et al. 2014). As mentioned earlier, there are six geometric parameters used to describe the camera's position in space (x, y, z) and orientation (κ, φ, ω) (Figure 25) (Linder 2009; Historic England 2017).

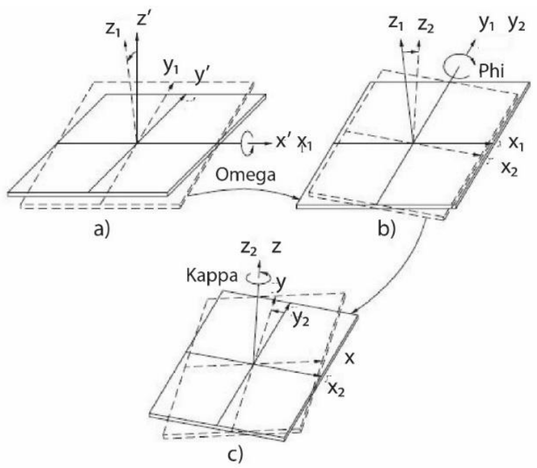


Figure 25: The rotation seen around the a) x-axis (ω) b) y-axis (φ), and c) z-axis (κ) (amended from Wolf et al. 2014, Fig. 10.12)

The entire iterative process involves image matching and plotting the location of those points in space (Green et al. 2014). Collinearity and epipolar geometry are used to determine the location of points and the cameras and the solution results in an associated residual for each point which are the differences between the probable values and measured values. When there are more than three control points, a least squares solution can be used on these residuals to determine alignment. Conventionally, point determination for photogrammetry required both the 3D location and orientation of the camera or the 3D location of a set of control points to be known in advance; SfM-MVS requires neither of these (Westoby et al. 2012). Identifiable features are tracked through the images and a relative object coordinate system is developed. Control points with known 3D locations are required if the model needs to be tied into an absolute object coordinate system, though these can be found after the model is created if necessary (Snavley et al. 2006; Westoby et al. 2012; Green et al. 2014).

There are two types of accuracy that can be present. The first type, relative accuracy, is always desirable regardless of the use for the model. It is the accuracy of the 3D model itself (Historic England 2017). The second type is absolute accuracy, and because it is the accuracy with which the model is set in the appropriate coordinate frame, it is not necessary if the model does not need to be tied in to absolute exterior orientation (Section 2.3) (Historic England 2017). These types of accuracy are reflected in the two types of exterior orientation that exist: relative and absolute exterior orientation.

##### 2.4.3.4.1 Relative and Absolute Exterior Orientation

Relative exterior orientation is concerned with the location of the points compared to the cameras and each other and is associated with a relative object coordinate system. It is a way of describing how the different camera positions relate to each other and is not tied to any external, known coordinate system (Snavley et al. 2006; Fryer et al. 2007; Wolf et al. 2014; Chiabrando et al. 2015). It is found through using TPs and coarse image matching (Linder 2009; Westoby et al. 2012; Historic England 2017). The image matching process that occurs for this component involves the matching of only a portion of the pixels in a photograph because the goal at this stage is to orient the cameras with respect to each other and the image rather than fully reconstruct the model. Through the alignment of the photographs, the location of the camera compared to the object and any other cameras can be found (Historic England 2017). SCBAs are used in this process (Westoby et al. 2012; García-Gago et al. 2014). This process finds the geometry of the object and the relationship between the camera coordinate system and the relative object coordinate system (Verhoeven et al. 2012).

Absolute exterior orientation links the points and the model to a known absolute object coordinate system. GCPs are vital for this and whatever coordinate system they are measured in, whether it be state, government, or international, this will be the coordinate system in which the cameras are orientated (Linder 2009; Remondino 2011). The relative and absolute exterior orientation are related, however, geo-referencing using GCPs helps determine the transformations needed to rectify the orientations (Snavley et al. 2006; Ferriera et al. 2017). Without this information, the orientation and scale of the object within the original context in which it was photographed will be lost. Once this is found, the object will be in the absolute object coordinate system.

##### *2.4.3.5 Image Matching*

Image matching is an important process in computer vision, survey/conventional photogrammetry, and image analysis in general (Gruen 2012). Homologous or conjugate points are image points found in two or more images which represent the same object point (Granshaw 2016). These conjugate points are used in the important process of image matching as they are used to associate stereopairs or multiple images (Granshaw 2016). Image matching is done sparsely at first to establish the relative exterior orientation and the geometry of the object and then it is done more comprehensively to create a full 3D model (Mallinson and Wings 2014; Historic England 2017). In computer vision, image matching is sometimes referred to as the stereo correspondence problem (Granshaw 2016).

### 2.4.4 Structure-from-Motion Multi-View Stereo (SfM-MVS)

SfM-MVS involves taking pictures of a static object by moving the camera around it (Micheletti et al. 2015b; Ferriera et al. 2017; Granshaw 2018). To work to its best potential, it is critical for the object to be stationary because the movement of the camera with respect to the stationary object leads to parallax between the different views which is vital for 3D reconstruction (Mallinson and Wings 2014; McCarthy 2014). Since less details are required to begin, this method can be used with a wider variety of cameras and is considered to be easier and lower cost, but still able to deliver high quality results (Snavley et al. 2006; Fonstad et al. 2013; Granshaw 2018). The only assumption that is required is that the object or area being reconstructed is visible in a minimum of two images (Verhoeven 2011). To more thoroughly reconstruct an area, multiple images have to be used (Historic England 2017). If the photographic strategy is effectively created, all points will be visible in at least two images. This minimises systematic errors that can be caused by inaccurate estimations of factors such as lens distortion (Historic England 2017).

In the SfM-MVS process, algorithms have been developed to allow for a less computationally intensive/costly process, thus permitting the use of more images for a given computer or processing time (in turn allowing a greater overlap between successive images for any given object extent). There is a reference window, or kernel, that is a square subset of pixels within one image, and which has an odd number of pixels (Lillesand et al. 2015; Granshaw 2016). The central pixel is the point that will be searched for in the second image. A larger square search window, or kernel, moves along the second image pixel-by-pixel and row-by-row to find the whatever is specified, such as peak correlation, between the pixels in the reference and search window (Figure 26) (Linder 2009; Wolf et al. 2014; Lillesand et al. 2015).

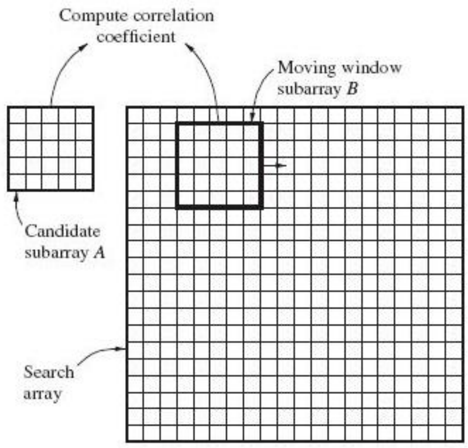


Figure 26: An example of a moving window within a search array computing correlation coefficients (Wolf et al. 2014, Fig. 15.21)

Specifically, in order to digitise the information, SfM is primarily concerned with tracking points across a set of images (Ferriera et al. 2017; Sapirstein 2018). The iterative process, sometimes described as the artificial equivalent of how humans perceive and move through 3D space, involves the both the creation of a 3D point cloud and the determination of the camera's geometry from a set of images (Doneus et al. 2011; Green et al. 2014). A high amount of overlap is vital for the success of this method (Westoby et al. 2012). The mathematical principles discussed above are used throughout this process (Westoby et al. 2012; Ferriera et al. 2017). A point cloud is generated from the information which is representative of the object's surface either in relative or absolute object coordinate systems (Green et al. 2014).

SfM-MVS can be considered a compound acronym of two parts. It originated from the computer vision branch of photogrammetry and developed around two categories of algorithms, SfM algorithms (used for coarse image matching) and MVS algorithms (used for dense image matching) (Snavley et al. 2006; Verhoeven 2011; Plets et al. 2012; Westoby et al. 2012; Micheletti et al. 2015a; Ferriera et al. 2017). There are various SfM and MVS algorithms that can be used for the matching of points between images (Seitz et al. 2006). For both, there are different ways to classify algorithms based on their function and how they operate. Algorithms can be area- or feature-based, in which the former looks for intensity patterns around a pixel of interest and the latter looks for more defined objects like edges and regions (Gruen 2012; Remondino et al. 2014). Image matching algorithms can also be designed for stereopairs or for multi-view stereo camera configurations. A third method of classification is local and global (Remondino et al. 2014). Local algorithms calculate the disparity and/or correlation at a point using intensity values that are within a finite region (Hirschmüller 2005; Remondino et al. 2013). Global methods use the full image to match points and often use energy minimisation approaches (Remondino et al. 2014).

A large portion of the mathematics and geometry used in this 3D imaging method have a basis in photogrammetry, though the automation of the most complex parts of photogrammetry is what makes SfM-MVS attractive and gave rise to the popularity of the acronym in the 2010s (Snavley et al. 2008; McCarthy 2014; Ferriera et al. 2017). The increase in computer processing power over the past decade is a major contributor to the more widespread use of SfM-MVS (Mallinson and Wings 2014).

#### *2.4.4.1 Structure-from-Motion (SfM)*

The term 'structure-from-motion' was first used in the late 1970s by Simon Ullman, however the context in which it was used then does not fully describe what it encompasses now (Granshaw 2018). SfM, as it is known today, developed rapidly through the 1990s (Westoby et al. 2012; Anderson et al 2019). SfM is responsible for rapid exterior orientation estimation using semi- or fully-automated identification of common TPs in stereopairs, strips or blocks. Automatic TP identification removes the need for the trained expert common to survey/conventional photogrammetry, whilst providing a much larger number of points than identifiable by an individual (Verhoeven 2011). A large enough quantity of TP can be identified by SfM that they can be regarded as a cloud, commonly known as a SPC (Koutsoudis et al. 2013; McCarthy 2014). Automatic TP identification is most reliable when large overlaps exist between successive photographs, which makes it most applicable to convergent (as opposed to parallel) photography or discrete objects (rather than landscapes, for instance) (Figure 27).

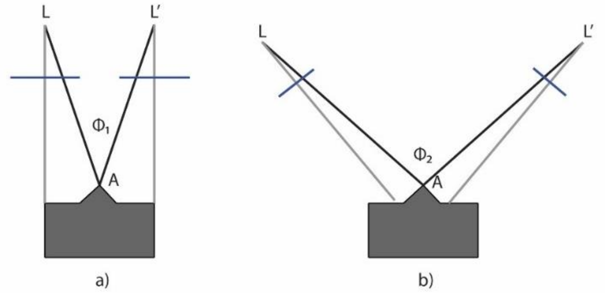


Figure 27: Close-range stereo coverage of Point A with camera axes (light grey lines) in a) parallel and b) convergent arrangements (amended from Wolf et al. 2014, Fig. 19.9)

An SPC containing hundreds or more tie points should result in a robust model, but there are instances where too few points are generated and a solution for the model is not found. In such cases one, some or all photographs may not be matched. In this case some tie points must be manually identified and these act as a guide before automatic tie point generation is attempted once more. This requires some training and extra work (Agisoft LLC 2018a, 2020a).

SfM is greatly aided by, but not dependent on, *a priori* estimates of interior orientation (in terms of focal length and pixel dimensions) stored within the EXIF header of each image from a digital camera. Whether or not *a priori* estimates of interior orientation were available, SfM produces refined interior orientation by means of a SCBA, thus making it less restrictive than methods requiring knowledge of interior orientation (Snavley et al. 2008; Westoby et al. 2012; Chiabrando et al. 2015). Each point will contribute varying amounts of error to the adjusted block, in terms of both orientation and location. Ideally these points are culled according to user-defined thresholds and the SCBA is re-run. This iterative process results in a refined model.

Depending on the settings, application, and digital camera itself, the EXIF headers may also contain estimates of exterior orientation, such as location derived from GNSS within the camera (Cronk et al. 2006; Agisoft LLC 2018a). In such cases absolute rather than relative exterior orientation can be calculated in the SCBA. If such does not exist, but absolute exterior orientation is still desirable, [G]CP can be employed. The coordinates for such can be measured/surveyed before or after image capture, depending on the scenario. [G]CP are given priority over tie points in the SCBA.

The SfM algorithms used by various software packages differ in the details of how they function, but the main premise is the same and they work in the relative object coordinate system. In order to avoid using peak correlation for the coarse image matching process, several methods have been developed that can either work individually or in conjunction. The methods described here are feature-based matching methods (Gruen 2012).

Edge detection is a method of image matching that is less computationally heavy. It is a vital part of computer vision processes (Canny 1986). Edges create boundaries and separate features, or parts of features, and are identified by a local change in intensity (Avery and Berlin 1992; Maini and Aggarwal 2009; Senthilkumaran and Rajesh 2009). It is similar to the image matching technique described in the above section, but what is done in the kernel is different. Rather than looking for peak correlation, it looks for an edge, by way of a local gradient in the intensity values (Morris 2004). For further details, please see papers by Marr and Hildreth (1980), Canny (1986), Morris (2004), Senthilkumaran and Rajesh (2009), Maini and Aggarwal (2009), and Lillesand et al.

(2015). The placement of the edge is then compared between images and a relationship is determined. When there are a lot of edges, the vanishing point can sometimes be used to determine the change in the relative geometry between the images (Grussenmeyer and Al Khalil 2002). The image matching and geometry is found based on vector mathematics. An extension of this method is using edge angles, where two identified edges meet. They are often an efficient feature to find (Morris 2004). Edge angles can be matched between images based on similarity. The location and orientation of the edge angles may have changed a bit between images but the angle should be relatively similar.

One of the more common SfM algorithms is the scale-invariant feature transform (SIFT) which works to identify locations in more than one image and establish the spatial relationship between the locations and the placement of the cameras regardless of changes to the scale or orientation of the images (Lowe 2004; Snavley et al. 2008; McCarthy 2014; Ferriera et al. 2017). These principles are used in the SIFT algorithm which originated from computer vision (Lowe 2004). It has a low computational cost and can therefore use a lot of images. There are four main stages to the algorithm which will briefly be described here; scale-space extrema detection, key point localisation, orientation assignment, and key point descriptor (Lowe 2004). In the first stage, the images are searched over all possible scales and image locations to look for points that are both scale- and rotation-invariant. To do this the images are replicated at different incrementally smaller scales and then at each scale, the images are convoluted by deliberately blurring them using Gaussian blur which has the benefit of removing noise from the images (Lowe 2004). A filter may also be used on the images at this time. This is done multiple times and progressively at each scale, resulting in what is known as a Gaussian pyramid with each size of image known as an octave (Chen and Wang 2018; Yawen and Jinxu 2018). Sequentially blurred images are taken and subtracted to find the difference in Gaussian blur which leads to a Difference of Gaussian pyramid (Figure 28) (Lowe 2004). Taking the difference of the blur makes the edges and details much more apparent and makes the locations of points and features much easier to identify. Subsequently, the algorithm looks to detect edges in the images and looks for points that are consistent across multiple scales and resolutions. This involves finding a model of fit to determine the location and scale at each potential KP to find stable KPs. This is found by comparing the pixel to the eight pixels surrounding it, as well as the nine pixels directly above and below it in the Gaussian pyramid, resulting in comparisons to 26 other local pixels (Lowe 2004; Li and Wang 2018).

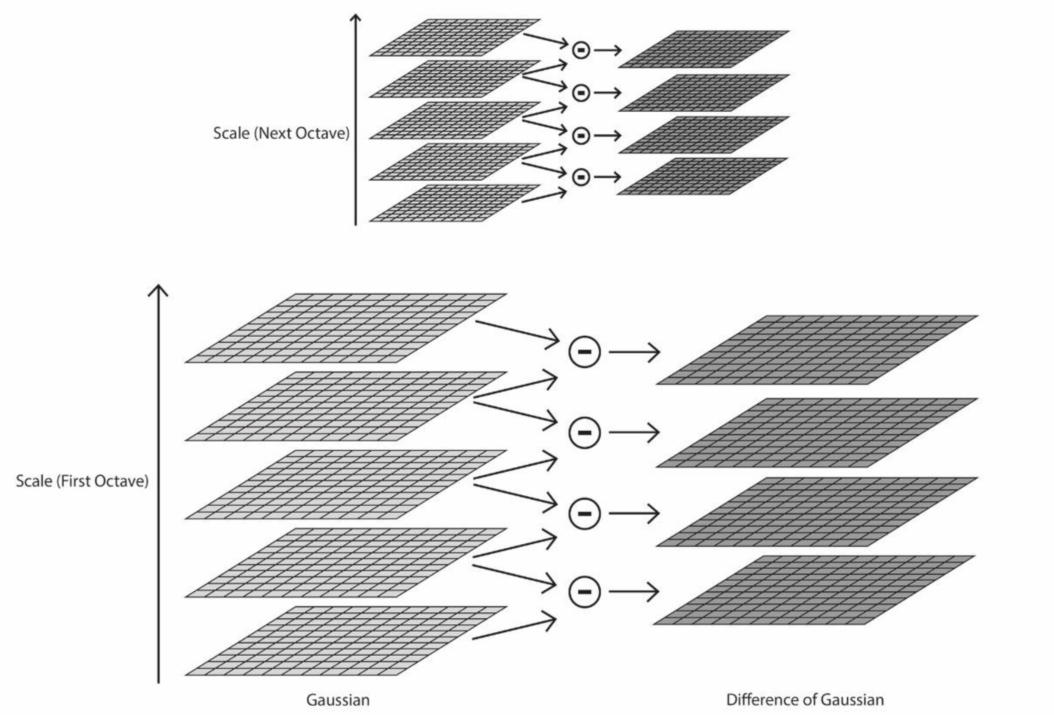


Figure 28: The Difference of Gaussian pyramid used in the SIFT algorithm when searching for matching points (amended from Lowe 2004, Fig. 1, p.95)

The next step is the orientation assessment which includes assigning one or more orientations to each KP based on the local gradient of the image. The orientations of the KP are plotted on a histogram in $10^o$ increments and the mode indicates the orientation to that KP (Lowe 2004). If there is more than one orientation that is close in height and the highest, this can create two KPs with different orientation vectors, though this is less common (Lowe 2004). The final step is the KP descriptor which uses local image gradients at the selected scale around each KP and it is then represented in such a way that distortion and changes in illumination and viewing position will not affect it. To match a KP to a KP in a different image, it uses a proportional threshold based on the distance from the KP to the nearest and next nearest points (Lowe 2004; Guo et al. 2018). The KPs from SIFT are very distinct and that in combination with the lower computational cost make it an appropriate algorithm for the SfM process.

This continues until there are TPs between all the images. Depending on the software, the number of KPs and TPs may be pre-set or set not to exceed a limit. Generally, the more matching images for a point, the more likely that is an accurate point and not just coincidental (Snavley et al. 2008). The overall outcome of these SfM algorithms are a sparse point cloud which shows the geometry of the object, the camera positions and orientations, and the internal calibration parameters of the camera (Verhoeven 2011).

SfM is a prerequisite for the creation of any model or measurements using computer vision, which in recent times (e.g. post-2010) usually concerns the creation of a DPC using a form of MVS. A polygon mesh can also be created directly (using depth maps, an intermediate step in MVS) or from the DPC (Agisoft LLC 2021). This mesh can also be rendered using the original images and model textures exported.

#### *2.4.4.2 Multi-View Stereo (MVS)*

Multi-view stereo is responsible for the automated creation of a model, usually, though not necessarily, in the form of a DPC. The terms pertain to the fact that multiple, and indeed all, overlapping images can be employed for model creation, rather than successive stereopairs in the case of conventional/survey photogrammetry.

The algorithms for the dense MVS reconstruction often use pixel values or intensities rather than being based on feature points and they help generate a high-resolution 3D representation of an object's surface (Doneus et al. 2011; Chiabrando et al. 2015; Sapirstein 2018). Some methods use multi-scale and multi-resolution processes in order to find points that are stable and unaffected by changes in either. This is more computationally intensive than the coarse matching done by the SfM algorithms, however, there are still methods of increasing the efficiency compared to the full peak correlation image matching process (Seitz et al. 2006; Remondino et al. 2014). Through the process of more thorough matching, a DPC is created. An example of a common MVS algorithm is semi-global matching (SGM).

As described in Section 2.4.3.5, the image matching process is integral for MVS and, more recently, survey/conventional photogrammetry. After the SPC is created and the interior and exterior orientation have been optimised, MVS algorithms can be employed. As with SfM, there are various MVS algorithms which can create a DPC, therefore the methods that are described within this section are not exhaustive (Seitz et al. 2006; Remondino et al. 2014). Some reconstruction algorithms are based around cost functions, depth-maps, and pixel intensity (Seitz et al. 2006). During this second round of image matching, all points are used and the values of each pixel are examined by the kernels (Mallinson and Wings 2014).

Based on Hirschmüller (2008), there are four general steps for stereo-matching. The first is cost computations which are often based on differences of intensities or colours which are absolute, squared, or sampling insensitive. Additional methods can be introduced here to speed up computation. The second is cost aggregation which involves summing costs within a kernel at a fixed size with a constant disparity. Pixels may be weighted or areas may be selected based on their intensity or colour properties. Next, disparity computation or optimisation involves local or global algorithms to determine the disparity based on minimised costs. Lastly, disparity refinement can be used to remove peaks, check consistency, interpolate gaps, and to increase the accuracy of subpixel interpolation.

The SGM algorithm is sometimes used to save time and computational power. It is primarily beneficial when the images are more likely to be parallel than convergent and there is *a priori* knowledge that they contain sharp breaks of slope. If one or both are not anticipated, SGM is not required. The assumption is that the images are epipolar and the matching cost is determined from the intensity of the pixel in the reference image and the suspected correspondence in the search image (Hirschmüller 2008; Remondino et al. 2014). SGM decreases computational requirements by narrowing the search area on the assumption that the conjugate point of a point on the scanline of the reference image would be along the same row in the rectified search image (Hirschmüller 2008). In SGM, scanline optimisation is performed at multiple angles and then the overall cost of the vectors is used to determine the disparity (Hirschmüller 2005, 2008).

This produces what is known as the DPC which is a 3D collection of a very large number of x, y, z points (Barazzetti et al. 2011; Opitz 2013b; Granshaw 2016). Unless dictated otherwise, the DPC that results from this will contain colour values for each point (McCarthy 2014).

#### *2.4.4.3 Convergence of Photogrammetric Approaches*

In recent years the term photogrammetry has risen to prominence again, as a result of the two previously disparate approaches of the discipline converging into one. What was previously widely known simply as SfM (a product of computer vision approaches, and often actually SfM-MVS) has now grown to adopt many elements of survey/conventional photogrammetry (at least its digital paradigm), as summarised in Table 2.

Table 2: Colour-coded summary of the generalised differences in elements between the two approaches to photogrammetry, as they existed between approximately 2000-2010, and which have recently converged into one. Elements of survey/conventional [digital] photogrammetry are shown in blue, with computer vision in red. Today the unified practice of photogrammetry (right column) contains many elements of both

| Element | Survey/Conventional [Digital] Photogrammetry c2000-2010 | Computer Vision c2000-2010 | Photogrammetry c2020 |
|---|---|---|---|
| Calibration | Pre-calibrated in a laboratory, resulting in a Camera Calibration Report, which was rarely refined | Commonly self-calibrated, with the additional ability to pre-calibrate using a bespoke target pattern | Commonly self-calibrated, with the additional ability to use Camera Calibration Reports and bespoke pre-calibration for the initial condition |

| Element | Survey/Conventional [Digital] Photogrammetry c2000-2010 | Computer Vision c2000-2010 | Photogrammetry c2020 |
|---|---|---|---|
| Tie point generation | Manual (10s or 100s across a block) | Automatic (100s or 1000s across a block, considered a SPC) | Automatic (100s or 1000s across a block, considered a SPC) |
| Optimum target geometry | Planar surface with little relief and few/no overhangs (2.5D), such as landscapes and building facades | Discrete and 3D objects, potentially with significant relief and/or overhangs | Planar and fully 3D |
| Optimum geometry for acquisition | Parallel stereopairs with minimal overlap (strips and blocks with minimal end- and side-lap) | Convergent stereopairs with maximised overlap | Parallel or convergent with minimal or maximised overlap |
| Model reference | Often absolute (e.g. for a landscape, using GCP with a coordinate reference system) but occasionally relative (e.g. building facades) | Relative | Absolute or Relative (with/without [G]CP) |
| Dense matching sequence | Across/between sequential overlapping stereopairs in a block | Across/between all overlapping frames in a block | Across/between all overlapping frames in a block |

#### *2.4.4.4 SfM-MVS Compared to Other 3D Methods for Close Range Digitisation*

The use of 3D technology when recording objects is a valuable tool as it allows for the capture of all the dimensions the object exists in, rather than just in 2D as is the case with photography, illustrations, or reflectance transformation imaging (RTI) (Miles et al. 2014; Sutton et al. 2014; Newman 2015; Clarke and Christiansen 2016). When deciding what technique to use, it is important to consider factors such as the accuracy and precision, portability, cost, acquisition rate, and flexibility of the technique (Remondino 2011). Not all methods are ideal for all situations and therefore the most appropriate one should be selected. The following sections briefly discuss some other non-destructive 3D methods and compare them to photogrammetry.

The other methods of generating 3D models in archaeology are typically divided into categories; image-based techniques, range-based techniques, and other techniques (Remondino and El-Hakim 2006) (Table 3). Photogrammetry is an image-based method and is considered passive (Evgenikou and Georgopoulos 2015). Techniques like terrestrial laser scanning (TLS), structured light scanning (SLS), and total station theodolite (TST) are range-based and classified as active methods since they emit light of some wavelength (Vosselman and Maas 2010; Granshaw 2020). An example of a method that is considered in the 'other' category is computed tomography (CT) scanning, which would also be an active method (Mamourian 2013).

Table 3: Some of the common methods of data capture for 3D models, excluding photogrammetry

| Method | Description/Uses | Benefits | Limitations |
|---|---|---|---|
| TLS | - Range; active<br>- Ground-based laser system<br>- Emits light, optical detector captures light reflecting off target<br>- Geometry calculated, point cloud created<br>- Typically used on scale of metres/kilometres<br>- Time of flight – measure time taken for emission to return<br>- Phase shift – continuous beam, measures difference in location of emission and return<br>- Triangulation – calculates range and bearing based on geometry | - Accurate<br>- Not dependent on ambient light | - Models lack texture<br>- Expensive<br>- Skill required<br>- Sensitive to field conditions<br>- Excessive light problematic<br>- Cumbersome equipment<br>- High memory requirements for processing |
| TST | - Range; active<br>- Typically used more for GCP capture than full data capture | - Portable<br>- Generally linked to real-world coordinates | - Not always detailed enough on a small-scale |
| SLS | - Range; active<br>- Projects pattern of light<br>- Detector obtains information about geometry from distortions | - Ability to acquire texture<br>- Accurate<br>- Portable<br>- Easy to use once trained | - Expensive<br>- Time required to be proficient<br>- Excessive light problematic |
| CT | - Other; active<br>- 2D x-ray-based scan layered to create 3D model<br>- Can be performed at a smaller scale (µ-CT) | - Able to see internal structures<br>- Detailed | - Time-intensive<br>- Not portable<br>- Training and experience required<br>- No surface colour information |

**TLS:** Remondino and El-Hakim 2006; Pavlidis et al. 2007; Bruno et al. 2010; Remondino 2011; Kuzminsky and Gardiner 2012; Andrews et al. 2013; Opitz and Cowley 2013; Opitz 2013b; Magnani 2014; Shott 2014; Evgenikou and Georgopoulos 2015; Meijer 2015; Obertova et al. 2019; **TST:** Doneus et al. 2011; Oniga et al. 2014; **SLS:** Pavlidis et al. 2007; Niven et al. 2009; Opitz 2013a; Shott 2014; Counts et al. 2016; Obertova et al. 2019; **CT:** Thali et al. 2003; Telmon et al. 2005; Dedouit et al. 2007; Bilfeld et al. 2012; Kuzminsky and Gardiner 2012; Woźniak et al. 2012; Hassett and Lewis-Bale 2017; Uldin 2017; Obertova et al. 2019

All these techniques have some downsides in common. They are typically costly and require a relatively large amount of equipment and training in order to use efficiently (Linder 2009; Fonstad et al. 2013; Gallo et al. 2014). Portability of equipment, especially of CT scanning, is also problematic depending on the remoteness and ease of access of the location under investigation (Remondino 2011; Westoby et al. 2012; Magnani 2014). When modelling techniques are complex and difficult to perform, fewer institutions can employ them. To facilitate growth in the field of 3D modelling within archaeology and heritage it is necessary to find ways of creating models that are accurate, cost-effective, and do not require too much training, all of which result in greater accessibility to a wider variety of people (Bryan and Chandler 2008; Westoby et al. 2012; Fonstad et al. 2013; Khalaf et al. 2018). This has led to more interest in cheaper and easier options and one that has seen increased recommendations and popularity recently is photogrammetry which allows for a wider user-base and cheaper model production (Fonstad et al. 2013; Olson et al. 2013; Green et al. 2014; Cârlan and Dovleac 2017).

###### 2.4.4.4.1 Benefits of Photogrammetry

There are many benefits to SfM-MVS, some of which are the ease of use, the cost, the accessibility, low amounts of training required, and the flexibility of the software (Bryan and Chandler 2008; Olson et al. 2013; Mallinson and Wings 2014; McCarthy 2014; Magnani and Schroder 2015; Bartzis 2017; Douglass et al. 2017; Khalaf et al. 2018). As discussed in Section 2.4.4, one of the major benefits is that the camera locations do not need to be known in advance and the cameras are calibrated by the software in the process (Koutsoudis et al. 2013; Green et al. 2014; Chiabrando et al. 2015).

Despite some initial costs, photogrammetry is a relatively cheap method to create models (Andrews et al. 2013; Marchal et al. 2016; Earley et al. 2017). Cameras that can be used are small, portable, and have their own power supply, all of which are advantageous for documenting objects in the field, especially if sites or items of interest are in remote locations (Luhmann et al. 2013; Evin et al. 2016). These are usually standard digital single-lens reflex (DSLR) cameras and mid-range cameras, costing less than £1000 are effective (Chandler et al. 2005; Linder 2009; Falkingham 2012; Bartzis 2017; Canon 2020; Nikon 2020a). There have even been good results from the use of smartphones for photogrammetric capture (Micheletti et al. 2015a). Provided good quality photographs are taken, the models generated through SfM-MVS can be equally, if not more, accurate than the other methods described here (Sapirstein 2016).

There are various commercial digital photogrammetric software programmes that are capable of processing photographs to make photogrammetric models, and some of which is open-source software or freeware (Bryan and Chandler 2008; Falkingham 2012). These vary in use and cost, though the cost is less than other methods of 3D modelling (Maté González et al. 2015). Importantly, the ease of these methods makes both the process and the output accessible to both experts and non-experts in 3D digitisation (Nicolae et al. 2014; Meijer 2015; Bartzis 2017). With continued technological progress in both camera and software and with increasing automation, models should be able to become both better quality and easier to make (Fonstad et al. 2013; Green et al. 2014).

Data capture is relatively quick, though the speed is dependent on the size of the area or object being photographed. This is especially useful on site as excavations often have constraints on both time and budget as well as large areas that need to be photographed and processed (De Reu et al. 2013). SfM-MVS is capable of creating models from unorganised sets of photos as well, which gives it an advantage, especially when used retrospectively for a site (Snavley et al. 2006). It is a portable method that is useful for documentation in the field; all that is required is a digital camera and the knowledge of the coordinates of GCPs, the latter of which is only necessary if the absolute exterior orientation of the subject is desired. McCarthy (2014) presented a case study in which a group of aged 16 years and under with no prior photogrammetric experience successfully captured images of gravestones that were used to create models.

Although a significant amount of time may be needed to run the software to create the models (e.g. multiple hours for photosets of large areas), there is a benefit that all data acquisition can be done separately from the data processing (Evin et al. 2016). This can be helpful when the location of the data acquisition is not near the requisite computer and software, especially when moving sites or travelling to a location to capture images of an object, because the data processing station does not need to be relocated. The data processing can also be almost entirely automated, and therefore even with the length of processing time on the highest settings or with a lot of pictures, the actual active time for the model creator does not need to be high (Remondino 2011). However, if someone wants a more interactive experience making a model, various software allows for user input at different stages of the process.

Since the actual photographs of the object or area are used to texture and colour the model, photo-realistic models can be obtained (Evin et al. 2016). Recording objects in 3D allows for the retention of more information about the subject and may reveal details which could otherwise be absent or overlooked in a purely 2D photographic record (Garstki 2016; Bartzis 2017). It can be argued it is a more objective method of recording since more of the information about the object is maintained compared to plans or photographs (De Reu et al. 2014). It is a convenient method of looking back at the stages of an excavation, either during or after. Photogrammetric models are also useful to compare objects between parts of an archaeological excavation or to compare something to a reference that is not physically present (De Reu et al. 2014).

##### 2.4.4.4.2 Limitations of Photogrammetry

Like any technique, there are limitations to photogrammetry which the model creator should be aware of in order to mitigate these issues (De Reu et al. 2014). As discussed in Section 2.4.3.1, there are various sources of error that can be introduced into the model (Green et al. 2014). A lot of the success of the photogrammetric model is dependent on the quality of the initial photographs (Meijer 2015; Raimundo et al. 2018). Photographs that are inconsistently lit, blurred, over- or under-exposed, have varying focal lengths (where a zoom lens, or multiple cameras with different lenses, have been used) or have insufficient overlap will create noisy and inaccurate models (Historic England 2017; Granshaw 2018). Items that are strong specular reflectors (as opposed to diffuse reflectors), lack texture, or have repetitive texture often do not create good models (Koutsoudis et al. 2013; Mallinson and Wings 2014; Meijer 2015; Granshaw 2018; Delpiano et al. 2019). In addition, occlusions can result in inaccurate models if objects are not photographed from sufficient angles (Remondino 2011; Green et al. 2014; Granshaw 2018). Very thin objects can also cause problems for digitisation (Mallinson and Wings 2014). Holes in the models can be filled inaccurately by the software and excessive noise can confound the accuracy of models (Garstki 2016). The weather or flight restrictions can pose problems for image capture if working outside or using a drone (Remondino 2011).

There is a potential for models to be less accurate for measurements than the real object, as noted by Remondino (2011), however, if appropriate pictures are taken and the point clouds are edited a model with high accuracy can be created. The scale at which the images are being captured needs to be considered (Barazzetti et al. 2011). If a very small area is needed in detail, taking photographs from very far away could cause the resultant model to be less detailed than desired. This limitation should be mitigated by careful planning in advance.

The length of processing time can be problematic if trying to create models with a lot of images or of a large space, especially if at higher resolutions (Verhoeven 2011; Westoby et al. 2012). The speed at which models can be processed is dependent on the computer specifications, such as size and speed of random-access memory (RAM), the number and speed of processors contained within the Central Processing Unit, and, optionally, the number and speed of processors and size and speed of memory contained within the Graphical Processing Unit (Verhoeven 2011; Koutsoudis et al. 2014; McCarthy 2014). Some data loss is inherent in the processing and interpolation can sometimes decrease the accuracy of the model, though this is also present in other 3D modelling techniques that create point clouds (Westoby et al. 2012). Interpolation occurs when surrounding values are used to estimate a value for an unknown point and is nearly unavoidable in the process of image capture and model creation (Opitz 2013b).

When used to record on-going excavations, one issue that arises is that the model cannot be easily checked whilst being processed and therefore if fault is found that originates from the photographs, it may be impossible to correct if excavation has continued (De Reu et al. 2014). This highlights the importance of understanding the basic processes behind photogrammetry and following standard procedure. Another important aspect to note, commented on by Bennett (2015), is that as the use of 3D modelling in heritage and museum curation increases there will be a greater need for people to understand how the models are created in order to successfully produce and use them. This will be important to avoid storing and analysing poorly-created models. The quality of photogrammetric models can vary greatly, and therefore standard guidelines on how to create good models are required (Magnani 2014). Any measurements taken from models for reconstruction purposes must be done from part of the models that correlate to undamaged, and therefore less interpolated, parts of the original in order for them to be accurate (Bartzis 2017). Similarly, it is important to remember that slight manipulations during the creation of the model can alter the digital record of the subject and therefore digital records will never be complete stand-ins for the original (Garstki 2016). McCarthy (2014) cautions that photogrammetry should be used as a supplement and not a replacement for conventional archaeological recording methods. If working on a model whilst far from the original object, there is a risk of misinterpretation, especially if attempting reconstruction (Bartzis 2017).

As discussed by Beale and Reilly (2017), since archaeology is destructive, the archive and any models created become the beginning point of any analysis and therefore it is incredibly important to make them accurate. It must be noted that most image sensor parameters are dictated by the company that manufactures them and thus this must be taken into consideration if trying to compare models created by different cameras. There are currently no standards in either equipment or the procedures, and therefore these need to be made and followed (Remondino 2011; Green et al. 2014). Historic England (2017) and Mallison and Wings (2014) have recently released documents on guidelines for creating models of certain scales which is a step in the right direction. Overall, despite having some limitations, if they are properly understood and accounted for, the benefits of SfM-MVS outweighs the problems sometimes encountered (De Reu et al. 2014).

## 2.5 The Current Uses of SfM-MVS

SfM-MVS is used in a wide range of subjects at the present, however this section will focus on close-range photogrammetry or projects involving human remains. A more diverse list of such publications, excluding all osteological ones, is presented in Appendix A.

Historical features are known to have immense value to research and the understanding of past cultures and people. The importance of protecting such features has not gone unrecognised (ICOMS 1964; Blake 2000; Yilmaz et al. 2007; McCarthy 2014; Beale and Reilly 2017). Good quality, accurate recording through photogrammetry benefits archaeology as it is inherently destructive; in order to excavate a site, things need to be removed from their original locations, and without proper recording the context and interpretation is lost (Dellepiane et al. 2013; Olson et al. 2013; De Reu et al. 2014). The proactive use of SfM-MVS is seen with the continual monitoring of sites, especially when there is a chance they could be damaged by attrition, conflict, natural disasters, climate change, or human negligence (Yastikli 2007; Yilmaz et al. 2007; Bryan and Chandler 2008; Remondino 2011; Luhmann et al. 2013; Magnani and Schroder 2015; Meijer 2015; Cârlan and Dovleac 2017; Raimundo et al. 2018). Entire areas can be documented, including pre- and post-excavations coverage of a region. This can be beneficial for the holistic analysis of features at a site-wide level and without slowing the excavation down and is starting to be integrated into the commercial sector (e.g. MOLA n.d.; Wessex Archaeology n.d.; Dellepiane et al. 2013; Olson et al. 2013; Green et al. 2014; Giuliano 2014; Oxford Archaeology Ltd. 2019).

Photogrammetry is used for replicating archaeological artefacts as well and has been seen to create very good quality models (Sapirstein 2018). This preserves these objects in a digital form and increases the amount of quality data for analysis and comparison which will be beneficial for research, conservation, and presentation of the objects both now and in the future (Clini et al. 2016; Papworth et al. 2016). This is probably the most common use for close range photogrammetry. Studies attempting to create 3D models of small artefacts often use a turntable to move the object whilst leaving the camera stationary (Gallo et al. 2014; Clini et al. 2016; Douglass et al. 2017; Sapirstein 2018). This does produce models, however since the basis of SfM-MVS is a moving camera, if the object is moving, the background has to be masked out, which removes large areas in which valuable KPs and TPs could be found to give the camera orientations stronger geometry (Jebara et al. 1999; Sapirstein 2018). Therefore, despite this method of image capture being easier, it is not the optimal method of digitising small artefacts.

Museums and heritage sites play a major role in curating and disseminating the culture and history of a region (Earley et al. 2017; Raimundo et al. 2018). In an increasingly digitised, interactive world, they are finding they need to adapt to stay relevant and attract the attention of the public (Hauser et al. 2009). 3D modelling allows visitors to see and interact with more objects as well as providing a multi-dimensional recording of elements of heritage (Pavlidis et al. 2007).

In forensic science, an increasing need for 3D documentation in the analysis and presentation of cases has been noted (Thali et al. 2003, Wong et al. 2008; Buck et al. 2013; Luhmann et al. 2013; Urbanová et al. 2015). SfM-MVS has not been entirely and consistently integrated into the forensic process yet, but there have been studies showing it has use in forensic settings. Generally, the use of 3D technology can help with crime scene reconstruction and interpretation of the events and the ease and speed of

SfM-MVS specifically to document the scene has benefits, especially since the photographs of the scene will be taken regardless. Recently, Berezowski et al. (2020) has published a review on the use of geomatics in forensics which included photogrammetry.

The use of SfM-MVS is seen in geomorphology, ecology, and zooarchaeology as well. It has been used at both large scales and small scales, from large studies of geomorphological features to 3D models of lion tracks (Westoby et al. 2012; Luhmann et al. 2013; Macheridis 2015; Sanger 2015; Marchal et al. 2016; James et al. 2017a, 2017b; Anderson et al 2019). Therefore, the ability to model an environment in-situ and in multiple layers allows for subsequent investigation of the site even if the specialist is not present for the initial data collection (Macheridis 2015). Traditional methods of survey such as TST, TLS, LiDAR, and aerial laser scanning (ALS) can involve high costs and complex logistics (Westoby et al. 2012). Similar to archaeological landscapes, SfM-MVS has shown potential in monitoring changes to the environment, such as erosion and recent progress has even been made in digitising the surface of water at a single point in time (Remondino 2011; James and Robson 2012; Ferriera et al. 2017)

### 2.5.1 Osteology

Presently, most of the photogrammetric work done relating to skeletal remains involves photographing the entire burial to record and model the individual or individuals as they were in-situ (Ducke et al. 2011; Baier and Rando 2016; Trizio et al. 2018). One example of this is the Weymouth Ridgeway Vikings which are the collection under examination in this project and will be fully described in Chapter 5. A photogrammetric model was created from the photographs taken during the excavation in order to preserve a 3D record of how they were placed (Ducke et al. 2011). One major benefit of SfM-MVS use in human osteology, especially if used for individual skeletons, is that it is a non-invasive method of analysing human remains (Maté-González et al. 2017). It does not force an excavation to pause for a long period of time in order to collect the required data. The use of photogrammetry as a supplement to plans of excavations and burials is also beneficial for future researchers as they obtain a more objective view of the situation with less of the inadvertent biases that may come along with conventional survey and recording. Some photogrammetric modelling has been done at the scale of individual bones for record, presentation, or facial reconstruction however the use of photogrammetry with bones on a scale such as this is just beginning to emerge.

In osteology, the use of close-range photogrammetry, as opposed to terrestrial photogrammetry, is required. Close-range photogrammetry (also macro-photogrammetry or small-scale photogrammetry) is a good technique to capture this additional data about an object. There is no specific definition of what is considered ‘close-range’ when discussing human remains, though the majority of studies using that terminology digitise single bones rather than an entire skeleton at a range that would be considered ‘within reach’. The close-range photogrammetry that is of interest in this study is at a range that an entire bone is captured but with sufficient macroscopic detail throughout or in targeted places that fine details and metrics can be recorded. Studying marking on bone at a close scale has been noted as a useful device in analysis as it allows further differences to be seen that would not be noticed with regular human vision or even with a magnification lens. Some studies use technology such as digital microscopes to investigate trauma such as Alunni-Perret et al. (2005) who looked at bone hacking and found that weapon type was more distinguishable at a microscopic level than with the naked eye. They carried out an experiment using fleshed human femora and found differences between knife and hatchet marks in the bone once defleshed (Alunni-Perret et al. 2005). One of the limitations of studies such as this is the cost of the equipment which is not seen to be as great a problem in photogrammetry (Palomeque-González et al. 2017).

In 2020, Lussu and Marini published a review article about close-range photogrammetry in skeletal anthropology. This paper is a good starting point to search for resources, however it is misleading to classify several of the papers they mention as ‘ultra-close range’ since the images in the cited studies encompass entire in-situ burials. Katz and Friess (2014) is one of the first papers published on methods to digitise human skulls via photogrammetry and since then there has been an increase in the number of researchers preserving and/or investigating morphology of single bones using meshes created through photogrammetry (see Bennani et al 2016; Guyomarc’h et al 2017; Buzi et al 2018; Edwards and Rogers 2018; Proficio et al. 2018). Timbrell and Plomp (2019) and Berezowski et al. (2021) have published on using geometric morphometrics (GMM) or shape to explore population affinity and sex, respectively, from models of the skull. Morgan et al. (2019) and Lee and Gerdau-Radonic (2020) both explored craniometrics using meshes of the skull as well, both finding that it was a successful method if the models were created well. Lee and Gerdau-Radonic (2020) called for further investigation into model creation methods as they found the measurements with the most variability were not consistent between manual measurements, photogrammetry, and laser scanning. Overall, all of these studies found that photogrammetry was a useful tool for their respective purposes.

Until recently, when any close-range photogrammetry was used in osteology, it was usually done for display rather than research purposes. Most small-scale recording was done with 2D pictures which inherently creates a loss of data with the loss of a dimension. It is increasingly desirable to make 3D models of things in order to preserve more data.

Some close-range photogrammetry is seen in fields outside of archaeology such as biomedical research and diagnosis (Clini et al. 2018). However, overall few studies have been found that record remains and objects in such a scale. One example involves teeth which are inherently small objects and thus require such a scale for any form of analysis using photogrammetry (Gaboutchain et al. 2008). A growing analysis technique, the accuracy of close-range photogrammetric models is still unknown and multiple studies in photogrammetry have acknowledged that this requires testing (Evin et al. 2016; Macheridis 2015).

A research group in Madrid has been looking at photogrammetry and cutmarks on animal skeletons to investigate butchery and carnivore damage and of studies found, this research design has the greatest similarity to the present study (Maté González et al. 2015; Yravedra et al. 2017). They use macroscopic photographs of the cutmarks and stitch them together using Agisoft Photoscan to create a 3D model of just the cutmark (Maté-González et al. 2018). Their studies are typically focussed on analysis of the cutmark profile seen with various experimental weapons and this is performed in an R-based software, Pandora, specifically developed for this purpose (Palomeque-González et al. 2017; Maté-González et al. 2018). Recently they have shown that photogrammetry-derived blade profiles of experimental knife cuts are statistically comparable to profiles scanned with a digital microscope and profiles generated with 3D laser scanning (Maté-González et al. 2017). The only statistically significant difference they found amongst the three methods was in the opening angle in the digital microscope model compared to the other two models, which was likely due to the larger measurements they generally found with the digital microscopy approach (Maté-González et al. 2017).

Of the methods tried, Maté González and colleagues found the photogrammetry produced very good resolution and the best detail, however this method might be of less use with poorly defined, vague marks (2015). Despite this, Maté-González et al. (2017) highly recommend this method as a low-cost way of producing 3D models. Their work has focused on recent or experimentally derived samples, therefore the extension of this accuracy to archaeological human remains requires testing. Additionally, no metrics were used that were measured directly on the bone therefore comparing the length and width of cutmarks between the bone and the model would have implications for the accuracy of photogrammetric models.

In 2017, Yravedra et al. from the same research group, explored the potential for photogrammetry with carnivore bite and score marks on animal bones. They employed methods used by Maté González et al. (2015) however they used GRAPHOS for the photogrammetric mode creation. They found it was possible to distinguish different carnivore groups to a certain extent based on the photogrammetric model of the score marks, though the sample size was small and the results not entirely conclusive. They have since expanded the study to use GMM to investigate the morphology of these digitised marks (Courtenay et al. 2020a, 2020b).

The use of close-range photogrammetry in osteology is slowly increasing, especially with the increasing accessibility of the required equipment. There are high levels of potential for these techniques, however testing must be done to determine the limitations and accuracy before they can be widely incorporated into analysis.

## 2.6 Summary

Overall, this chapter has discussed the background information necessary to understand photogrammetry. The branches of survey/conventional photogrammetry and machine/computer vision were introduced and the development of each was briefly outlined. Important principles, such as interior and exterior orientation, and the underlying mathematics were discussed. SfM-MVS was discussed in detail and for the remainder of this research, any use of the term 'photogrammetry' refers to SfM-MVS unless otherwise specified. The current uses of photogrammetry in archaeological, cultural heritage, ecological, geomorphological, and forensic science contexts were noted with a focus on the use of photogrammetry in the study of human remains. Lastly, the potential of this technique in research and education, heritage and museums, and forensic science was addressed. With the use of modern digital techniques, it is paramount to test them to explore the benefits and limitations. Within this chapter, Objective 1 was adressed (Section 1.3.1), leading to the following important points:

- The long history of photogrammetry means that there is a large body of literature supporting its use and applications from both conventional photogrammetry and computer vision
- Although photogrammetry is commonly performed at close range, the use of 3D control is not as common as when it is terrestrial scale which could potentially lead to less accurate models
- Further investigation is needed in order to test the metric abilities of close-range photogrammetry and how the geometry of the subject affects the development of the optimal process
- This technique is relatively cheap and accessible and therefore is a good alternative to techniques such as CT or TLS

# 3 Historical Background

A component of the current study involves the re-evaluation of the sharp force trauma found in the case study collection, the Weymouth Ridgeway Vikings (fully discussed in Section 5.1). This collection is historically important within Britain, especially in the south-west as burials from this time period are a relative rarity and mass graves even less common. It has the ability to add to the narrative of early medieval Wessex and the interactions between the Vikings raiders and the local populations. This chapter situates the collection in the historical timeline of Britain and Wessex, beginning briefly with the development of Wessex and running through until the mid-11$^{th}$ century AD (further information can be found in Appendix B). It also discusses the Vikings and their influence in Britain. The final section outlines some of the weaponry which could have caused the injuries to the Weymouth Vikings. All dates noted are AD.

## 3.1 Early Medieval Wessex

The landscape of Dorset preserves a particularly rich archaeological record as far back as the Mesolithic. The two factors that have had the greatest influence on this are firstly the fact that the modern county remains sparsely populated with few urban centres and limited industry, whilst secondly the chalk geology over much of the region has resulted in excellent preservation of human and animal remains. Between the 6$^{th}$ and the 10$^{th}$ centuries, the West Saxon kingdom known as Wessex grew and flourished during an era in which Britain was split into multiple kingdoms (Figure 29) (Cunliffe 1993). However, it was not always a peaceful time; there were animosities between the different polities as well as Scandinavian incursions from across the North Sea, which became increasingly frequent between the 9$^{th}$ and the 11$^{th}$ century. (Yorke 1995; Downham 2008). Before the arrival and impact of the Vikings in Wessex can be effectively discussed, a brief summary of the development of Wessex must be given.


Figure 29: A map of England with the core area of Wessex highlighted (1:2,500,000) (produced by author, amended from Cunliffe 1993, Fig. 9-9, p. 325; basemap credit National Geographic World Map – National Geographic, Esri, Garmin, HERE, UNEP-WCMC, USGS, NASA, ESA, METI, NRCAN, GEBCO, NOAA, increment P Corp.)

### 3.1.1 The Beginnings of Anglo-Saxon Wessex

After the withdrawal of the Roman army in the early 5th century, the Roman systems that had been in place collapsed relatively quickly and the native population, the Britons, were left in charge of their own defence (Cunliffe 1993; Yorke 1995). Towns and villas were still occupied, but the Iron Age hillforts that marked the landscape started to be used again as main regional centres (Yorke 1995; Ward-Perkins 2000). The literacy in Latin vanished, technologies disappeared, and the market economy in place in Roman Britain disintegrated, as evidenced by a low amount of coinage from that time (Cunliffe 1993; Ward-Perkins 2000; Costen and Costen 2016). There was a near-complete severance from the Roman Empire prior to any subsequent invasions (Yorke 1995; Ward-Perkins 2000).

During this time, areas in what are the modern-day Low Countries and Germany were becoming increasingly densely settled which, in turn, increased the stress on that area. They were dealing with rising sea levels, disruption to the trading systems of the Roman empire, and wars to the east of them (Cunliffe 1993). All these factors caused some of the populations in that region to set out to look for new land, and in doing so, they found Britain. Throughout the 5th century, attacks on England by Germanic tribes, such the Saxon, Jutes, and Angles were noted (Cunliffe 1993; Swanton 1996; Underwood 1999; Grimmer 2002). These events are recorded by the Anglo-Saxon Chronicle (*ASC*), however, as discussed in Appendix B, the accuracy of the details of events that occurred this early may be questionable (Cunliffe 1993).

For Wessex, the impact of the Saxons began in 495 when Cerdic and his son Cynric landed somewhere on the central south coast, possibly near Christchurch harbour (Dorset), with a small number of ships (Cunliffe 1993; Yorke 1995). Shortly thereafter, the local Briton population encountered and fought the Jutes near Portsmouth (Hants) (Cunliffe 1993; Yorke 1995; Swanton 1996). Contact with the Germanic tribes was more consistent after that. The original tribe name of the West Saxons, incidentally where the word Wessex originates from, was the *Gewisse* (Yorke 1995; Roffey and Lavelle 2016). They were not known as the West Saxons until later, however that terminology will be used in this document for the Germanic population of Wessex. The term Anglo-Saxon is used here for the larger integrated population of Germanic immigrants and native population subsequently found throughout England.

The Saxons started moving in-land, possibly negotiating as well as fighting for land, though it took them until the mid-6$^{th}$ century to gain control of Dorset (Cunliffe 1993; Yorke 2013). There were likely casualties of the Saxon conquests, however there is evidence a large population of Britons was still living in Wessex under West Saxon control (Yorke 1995; Grimmer 2002). In fact, evidence suggests West Saxons were substantially outnumbered by the native population (Ward-Perkins 2000). The Britons probably saw little initial change to how they lived, though the successful campaign of the West Saxons would have re-introduced some structure and unity to the region (Cunliffe 1993; Yorke 1995). The lineage of Kings of Wessex was recorded at a later date, but is considered to have begun with Cerdic. Some of the genealogical links may be tenuous as the lineage may have been recorded with the purpose of strengthening the claim to the throne. By the 8$^{th}$ century, smaller regions within the kingdom were monitored by ealdorman who would be trusted to report back to the king and carry out his instructions.

The West Saxons retained a fairly separate identity and culture from the Britons and very little of Britonnic culture was reflected in their customs or ways (Ward-Perkins 2000). Ward-Perkins (2000) suggests that is due both to the Britons being very effective at resisting the Saxon invaders and the very rapid and complete de-Romanisation prior to the Saxon arrival. King Ine (688-725/6) created a code of laws that has provided insight into the social status of the different populations in Wessex (Ward-Perkins 2000; Grimmer 2002). Britons were afforded rights, able to own land, and entitled to the king’s protection. However, they were not equal. For example, the amount to be paid to their kin if they were killed (a *wergild*) was less than that of the West Saxons (Yorke 1995; Grimmer 2002). Therefore, it is clear that they were considered a lower class of citizens than the West Saxons but assimilation, the mixing of cultures, and intermarriage were allowed (Grimmer 2002)

Wessex grew into a strong and powerful kingdom, with Mercia, Northumbria, and East Anglia being the other major Kingdoms in England (Richards 2000). The borders of Wessex changed through time, but typically encompassed Dorset, Hampshire, Somerset, Wiltshire, and various times, parts of other surrounding counties (Yorke 1995; Cherryson 2008). There were skirmishes with Mercians along the north border, with various outcomes. At one point, Wessex gained control over all of Mercia, however it did not last long (Yorke 1995).

## 3.2 The Vikings

The term 'Viking' is used to describe raiders from Scandinavian countries (Graham-Campbell 2001). Although the term is originally from the old norse, *víking*, which meant piracy or pirate raid, this does not necessarily accurately reflect the motives of all Scandinavians travelling overseas at this time (Richards 2000; Graham-Campbell 2001). They are sometimes referred to as 'heathens', 'pagans', 'Danes', 'Norse', 'Northmen', or 'Norsemen' though for ease in this study, the word 'Viking' will be used (Richards 2000; Brink 2008; Dumville 2008). From the historic record in England, it seems the Anglo-Saxons did not differentiate between who was from each Scandinavian region except for rare exceptions (Yorke 1995; Graham-Campbell 2001; Dumville 2008; Roffey and Lavelle 2016).

Norway, Sweden, and Denmark were the primary residence of the Vikings (Figure 30). In the Viking Age, part of south-western Sweden was considered Danish, and pockets of Finland were Swedish (Graham-Campbell 2001). Most of the settlements were around the coast or along rivers as the regions they lived in did not provide ample amounts of fertile farming land. Therefore, the sea was the main factor that provided livelihood and because of it, they were very good shipbuilders (Richards 2000; Graham-Campbell 2001). The Vikings were traders both locally and internationally which is evidenced by some raw materials coming from far afield (Graham-Campbell 2001; Baug et al. 2019).

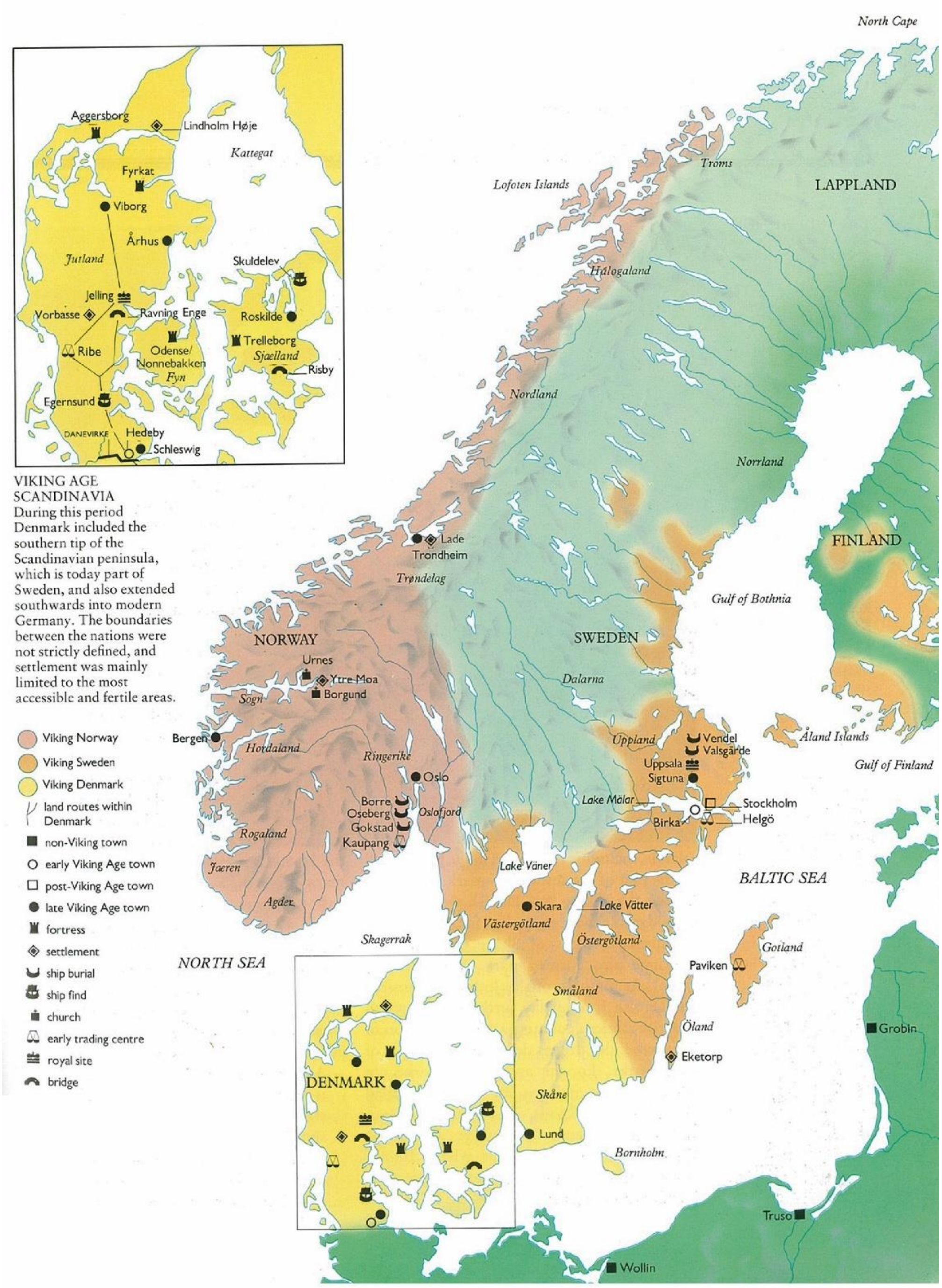


Figure 30: A map of Viking Scandinavia c. 9th-11th C (1:20,000,000) (Graham-Campbell 2001, p.11)

It was mainly the Danish and Norwegian Vikings who travelled west, with their Swedish counterparts setting their sights to the east (Graham-Campbell 2001). From isotope evidence at various sites, it appears that people were mobile within and between the Scandinavian kingdoms and the armies were of mixed composition (Price et al. 2011; Abrams 2012; Chenery et al. 2014; Lavelle and Roffey 2016; Croix et al. 2020). This has been noted during the later raids in England where the Vikings were often of a variety of nationalities (Pollard et al. 2012; Chenery et al. 2014; Loe et al. 2014b; Hadley and Richards 2016).

The king was the highest in the social structure and would have control over chieftains, or *jarls*, who would in turn have a band of warriors from the free men, the *karlar*, in his region (Graham-Campbell 2001). The basic armed group of Vikings which was considered the core part of an army was a *lið* (Raffield et al. 2015). The backgrounds of the individuals could have been diverse, but there would often have been kinship ties or pre-existing links within the group. The size of the *lið* would depend on the power and wealth of the leader (Raffield et al. 2015). The mixed regional background in the groups would lead to the need of a collective identity or cause (Abrams 2012).

Between the 9th and 11th centuries, the Vikings left their homelands to explore, both west and east. By the end of the 11th century, most of the exploration had stopped and they had settled and mixed into the local populations. The motivations for the migrations are thought to be complex and theories such as portable wealth, climatic changes, political factors, population pressures, and the search for *'bridewealth'* have been suggested (Wormald 1982; Richards 2000; Graham-Campbell 2001; Barrett 2008; Brink 2008; Williams 2008; Ashby 2015; Gore 2016) (for further discussions on the motivations behind these migrations, see Appendix B and see Barrett 2008; Abrams 2012; Ashby 2015).

Regardless of the main motivation for the migrations, individuals would have their own personal motivations for going as well (Ashby 2015). Stories of the successes of the preliminary raids would likely have spread, possibly with exaggerations, and become a catalyst for subsequent ventures (Ashby 2015). The increasingly large raids may have been what led to settlement. Although the Vikings are often thought of as being further north in England, their interactions and impact with the south and especially Wessex will be discussed here.

## 3.3 The Viking Invasions of Britain and Wessex

Vikings were present in the south of England, including Wessex at times (Loyn 1977). However, they were mainly known for having settled in the north and east of Britain, in an area that would be termed the *'Danelaw',* thus making the findings of the Weymouth Vikings highly unusual, not only for the amount of trauma present, but for the location as well. Overall, the Viking attacks on England can generally be thought of in two waves; those that occurred prior to 900 and those that occurred after 900 (Lavelle and Roffey 2016). The years following the Vikings' arrival in Britain were tumultuous, with periods of calm interspersed with periods of warfare and raiding (Loyn 1977). The size of the Viking war bands and armies that came to England is debated (see Wormald 1982).

The initial attacks often targeted religious sites because they were both wealthy and poorly defended (Wormald 1982; Richards 2000; Williams 2008). The first recorded raid was at Lindisfarne off the coast of present-day Northumberland in 793 followed by another raid the subsequent year (Swanton 1996; Richards 2000; Graham-Campbell 2001; Downham 2008; Raffield 2020). These events are often considered the start of the Viking Age (Brink 2008). Although not in the form of a raid, it is probable the Vikings were encountered prior to that in the south of England. There are records of three ships appearing near Weymouth or Portland (Dorset) in approximately 789 (Cunliffe 1993; Yorke 1995; Swanton 1996; Richards 2000; Graham-Campbell 2001; Downham 2008; Gore 2016). The crew of these ships killed the reeve from Dorchester (Dorset) who had come to greet them and ask them to come to the town, erroneously thinking they were traders (Cunliffe 1993; Richards 2000; Yorke 2013; Gore 2016; Lavelle 2016). There is also mention of Offa, King of Mercia making arrangements for the defence of Mercia against 'pagan people' though their origins are not mentioned and therefore it cannot be definitively stated that they were Vikings (Richards 2000). For almost half a decade after that, the *ASC* is silent in regards to Viking attacks (Downham 2008).

From about 830, the Viking raids would typically be of a 'hit-and-run' style and were wide-ranging in scale, with anywhere from 30 to 350 ships of Vikings landing (Cunliffe 1993; Downham 2008; Williams 2008). For the better part of the next century, Wessex is mentioned as a location of repeated attacks with both Anglo-Saxon and Viking victories recorded (Swanton 1996). Over time, the nature of the raids would change and larger forces led by earls and kings would arrive (Williams 2008). The Viking Great Army (*se micel here*), landed in East Anglia in 865 and, for the first time, the army itself overwintered on mainland England (Cunliffe 1993; Graham-Campbell 2001; Richards et al. 2004; Downham 2008; Gore 2016). The overwintering of the entire army was an important point as it meant for the first time that the seasonal raids no longer needed to be seasonal and could happen at any point and by 870, the Great Army had set its sights on Wessex leading to several battles and skirmishes in the south-west of England (Williams 2008; Gore 2016; Hadley and Richards 2016).

In the late 9th century, a treaty between King Alfred of Wessex and Viking leader Guthrum, aptly named the Treaty of Alfred and Guthrum or sometimes the Treaty of Wedmore, was created and Guthrum converted to Christianity with Alfred as his sponsor (Cunliffe 1993; Yorke 1995; Richards 2000; Abels 2008; Graham-Campbell 2001; Downham 2008; Hadley and Richards 2016). This treaty also set out the area that was later referred to as the *Danelaw*. This area was under Viking rule and it was the area where most Scandinavians settled (Buckberry et al. 2014; Loe et al. 2014b, Raffield 2020). Although not all was peaceful, a time of comparative calm followed this (Yorke 1995; Swanton 1996; Gore 2016).

Following Alfred's death in 899, the Viking invasions stopped for a while and the Anglo-Saxon kings were able to reclaim control of the Danelaw (Richards 2000; Abels 2008; Downham 2008). However, in the early 10th century, renewed attacks are recorded, increasing the frequency towards the end of the century. These incidents were different in nature to the hit-and-run raids from over a century early; these were conducted by large armies, campaigning to take over kingdoms (Downham 2008). Wessex, especially eastern Wessex, suffered greatly during the last decades of the 10th century (Yorke 1995; Loe et al. 2014b). The Isle of Wight became a favoured base for the Vikings as they pillaged (Cunliffe 1993; Loe et al. 2014b). There were continued attacks on various towns in all shires of Wessex (Cunliffe 1993). It is sometime during this 'second wave' that the Weymouth Ridgeway Vikings were killed (Loe et al. 2014b). All of this culminated around 1016 after years of attacks by Swein Forkbeard of Denmark (also written as Sveinn) and later his son Cnut (also written Knut or Knútr). Cnut was crowned king of all of England in 1016 and divided it into four earldoms; Northumbria, East Anglia, Wessex, and Mercia, keeping Wessex for himself (Yorke 1995; Lund 2008; Williams 2016b) (for further detail about the 9th-11th century Viking raids on England, please see Appendix B).

These events mark the end of the second wave of Viking invasions. The Vikings did play a role in some of the battles of the Norman Conquest later in the 11th century, but most of the Scandinavians who had come to settle new land has successfully integrated into society by that point (Richards 2000; Graham-Campbell 2001). Therefore, 1066 can be said to be the end of the Viking Age in Britain (Brink 2008). Their part in the history of Britain and the regions they settled can be seen in isotope analysis of human remains, in current DNA mixtures, and in place names (Budd et al. 2003; Goodacre et al. 2005; McEvoy and Edwards 2005; Fellows-Jensen 2008).

### 3.3.1 The Impact of the Viking Raids in Wessex

As rightly noted by Lavelle and Roffey (2016), there was no 'Danish Wessex' or 'Viking Wessex', and generally, there is not the same evidence of Viking presence in Wessex as in the *Danelaw*. However, there were Vikings landings and attacks in Wessex and the fact that they were well-recorded suggests they had a major impact (Yorke 1995). So, although the settlement never occurred to any notable extent, the Vikings were a constant presence or threat for almost two centuries (Kershaw 2016). They caused the disruption of local and international trade with their attacks on ports (Yorke 1995).

There are some signs of Scandinavian culture seen in Winchester, such as the burials of Cnut and his family (Biddle et al. 2016). However, Roffey and Lavelle (2016) note there were anti-Viking sentiments in London due to some of the battles in the second wave of Viking attacks. Therefore, it is possible that with Wessex having suffered in the campaigns, it might not have been a particularly inviting place for Scandinavians to settle.

Despite this, there is evidence of Scandinavians, Scandinavian descendants, or people given Scandinavian names being appointed to fairly high positions within Wessex or being significant landowners, the latter especially seen in the Domesday book (Lewis 2016; Roffey and Lavelle 2016; Williams 2016a). Unfortunately, it is usually difficult to definitively distinguish between those three groups. Additionally, Scandinavian influence can be seen in English politics, administration, and society shortly after the Viking Age in England (Williams 2016b). Soon after the Viking raids and settlement, there was another conquest of Britain by the Normans, which could have also masked or obliterated Viking influence (Lewis 2016).

Additionally, Scandinavian influence is seen in some material culture in Wessex (Kershaw 2016). The artefacts do not all look like they were produced in Scandinavia or by Scandinavians, but the fact that the style was adopted does attest to the influence that the Vikings had on Anglo-Saxon culture (Kershaw 2016). Metal finds such as dress accessories, rings, foreign coins, ingots, and weights have been found and reported on through the Portable Antiquities Scheme (Kershaw 2016). Over-interpretation of these finds must be avoided; when they were deposited is not known, and therefore it cannot be said what the motives were for their creation or if they may have been traded with people from the *Danelaw*.  Scandinavian culture may have been associated with honour and military prowess and therefore some of the material culture in Wessex that has Scandinavian influences may have been adopted due to that (Roffey and Lavelle 2016).

### 3.3.2 St Brice's Day Massacre

One notable incident in Anglo-Saxon and Viking relationships is the St Brice's Day Massacre. On the 13$^{th}$ of November 1002, King Æthelred ordered all Danish men in England be killed, presumably as a response to the increasing Viking campaigns and increasing price of the *Danegeld* (Williams 1986; Richards 2000; Durrani 2013). The exact nature of what he meant by this is unclear, but scholars generally interpret this as targeting war bands and mercenaries rather than the Scandinavian population that had integrated itself into the native population living in the *Danelaw* (Richards 2000). There is generally little evidence to the outcome of this proclamation, however, there have been two mass graves found with male Viking remains that date roughly around this time and some speculation is that they were related, though this cannot be known with certainty (Durrani 2013). The former of the two presents a more likely candidate (Chenery et al. 2014; Roffey and Lavelle 2016). It is the St. John's College (Oxon) mass grave dated to 960-1020 and contained 37 people, one of whom was decapitated and many of whom exhibited trauma around the time of death. They appear to have been running away rather than defending themselves (Pollard et al. 2012). The Weymouth mass grave, discussed more fully in Chapter 5, dates to 970-1025 and contains a minimum of 52 systematically decapitated individuals with their heads placed to the side of the pit (Chenery et al. 2014; Loe et al. 2014b). Many of them exhibit defensive sharp force trauma and osteological evidence shows their decapitations were exceedingly brutal in some instances. There are speculations that they may be captured prisoners from a raiding party or a ship's crew rather than the victims of Æthelred's proclamation, though the latter is still a possibility (Chenery et al. 2014; Williams 2015; Lavelle 2016).

## 3.4 Viking and Anglo-Saxon Bladed Weaponry

A variety of weapons were used in the 10th and 11th centuries. These included swords, spears, bows and arrows, seaxes, and axes (Underwood 1999; Pedersen 2008; Williams 2014). Similar equipment was used by both sides at that time (Williams 2014). Although horses may have been used as transport, evidence suggests battles and skirmishes were not fought on horseback (Ayton 1999). Similar to the evidence of the Viking presence in England, the evidence of weaponry in Anglo-Saxon England is from contemporary written sources, from archaeological finds, and from artistic depictions (Williams 2014). Recent studies have been investigating Viking and Anglo-Saxon weaponry through modern techniques, such as radiography and neutron imaging (e.g. Fedrigo et al. 2018; Murasheva et al. 2021). In this study of the Weymouth Ridgeway Vikings, the bladed weapons of each faction, specifically the swords, are of the most interest and therefore will be the focus of the next sections.

### 3.4.1 Swords

The sword was widespread in both Scandinavia and England during the Viking Age (Williams 2014). Over 2000 survive, dating from 800 to 1050 (Figure 31) (Fedrigo et al. 2017). For both communities, having a sword was a sign of prestige (Underwood 1999; Pedersen 2008; Thiele et al. 2014; Hjardar and Vike 2016; Fedrigo et al. 2018). There are a variety of sword typologies and the sword underwent changes throughout this time. Some raw materials might have been locally mined and some imported through wide-reaching trade networks (Fedrigo et al. 2017).

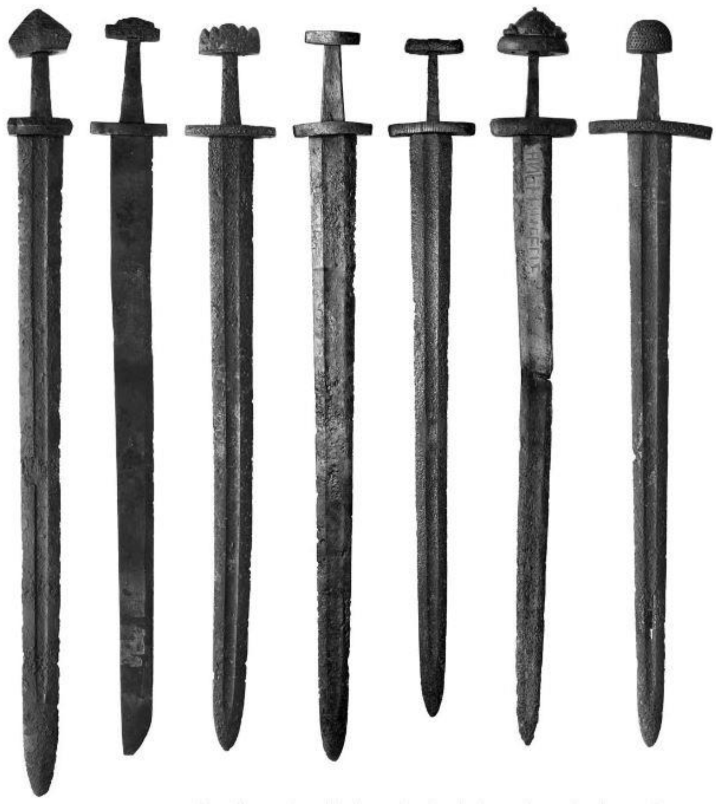

Figure 31: Some examples of Vikings swords that have been found (in chronological order from left to right: Type C, Type F single-edged, Type K, Type M/Q, Type P, Type T, and Type X, from the Scientific Museum in Trondheim and Historical Museum in Oslo; Hjardar and Vike 2016, p.170)

#### 3.4.1.1 Sword Materials

There are many metallurgic studies of iron and steel and their use in swords, but the important characteristics of the main materials in swords are worth noting here (see Lang and Williams 1975; Williams 2007, 2009, 2012; Wadsworth 2015; Fedrigo et al. 2017). The first important differentiation is between iron and steel. Generally, if a ferrous alloy contains over 0.2 wt% of carbon, it is considered a steel (Thiele et al. 2014). Iron is anything less than that though it can contain variable levels of other elements, such as phosphoric iron, which is more than 0.1 wt% phosphorous (Thiele et al. 2014). They all provide different levels of hardness with steel being the hardest.

Steel can also be classified based on the amount of carbon (C) in it. When the C content is around 0.8 wt%, it is called eutectoid steel and when there is over 0.8 wt% C content, it is hypereutectoid steel (Williams 2012). These are both very hard steels able to produce excellent blade edges. Steels of this quality were usually produced through the crucible method and were thought to be beyond the capabilities of many Anglo-Saxon and European smiths of the time.

Bloomery iron and steel are created through heating iron ore in small furnaces with charcoal (Williams 2007, 2009). This was the standard way of producing iron and steel in Europe in the early middle ages with technology becoming more efficient over time (Williams 2009, 2012; Fedrigo et al. 2017). Crucible steel was produced in Asia and it was a better steel with less inclusions (Williams 2007, 2009). It could be created by using sealed crucibles to heat iron and charcoal or cast iron (Williams 2007, 2009) Crucible steel could be moved through trade in the form of ingots (Williams 2009). These could then be forged into blades. Damascus steel begins as crucible steel and is cooled in such a way that the structure of the steel produced patterns, often described as 'watered silk' (Maryon 1960b; Williams 2007, 2009). This pattern looks similar to pattern-welded swords however this steel was not common to Europe at this time (Williams 1977).

Steel could be quenched in cold water which would increase the hardness of the blade (Williams 1977; Underwood 1999). However, this would often increase the brittleness of the metal as well, a characteristic not desirable in swords and not required with high quality steels (Williams 2007, 2009, 2012). If steel is re-heated in a separate process, it is then considered tempered.

#### *3.4.1.2 Sword Characteristics*

The swords that were made were either single- or double-edged, though the latter is more common (Pedersen 2008; Williams 2014). They would need to be the right combination of hard, tough, and flexible (Lang and Williams 1975; Hjardar and Vike 2016; Williams 2012). In some instances, edges were forged on, having been treated separately from the rest of the blade. This would be done in order to make the edges harder (Williams 2012). This sometimes led to blades with sufficiently hard edges, but the edges would not last long once sharpened a few times (Williams 2009; Williams 2012).

Earlier blades were shorter and wider, but by the turn of the first millennium, most swords used by both the Anglo-Saxons and the Vikings would have been thinner, tapered towards the tip, and roughly 90cm long (Underwood 1999; Pedersen 2008; Williams 2014; Fedrigo et al. 2018). There was usually a groove, called a fuller, down the long axis of the blade to lighten it without altering the effectiveness of the weapon (Pedersen 2008). The swords would be balanced in their weight but were typically better designed for cutting than thrusting. They would have been one-handed weapons able to inflict considerable damage (Williams 2014). Whilst not providing the same level of concentrated force as an axe, they would have provided a straighter cut. In Williams' (2014) opinion, a sword from this era would have been capable of beheading someone, though multiple blows may have been necessary.

There were generally two categories of swords; those made with many pieces of metal twisted and forged together and those made with only a few or one piece of metal (Wadsworth 2015). The former was best exemplified by pattern-welding, which was prominent between the 3rd century and the 10th century with a peak in the 7th century (Maryon 1960a; Lang and Ager 1989; Underwood 1999; Williams 2012; Fedrigo et al. 2018). Pattern-welded blades were made up of multiple bars of iron with different levels of carbon or phosphorous (Fedrigo et al. 2017). These would be twisted and hammered together to create a pattern (Maryon 1960a; Lang and Ager 1989; Hjardar and Vike 2016; Fedrigo et al. 2018). Sometimes the entire blade except the edges were pattern-welded, and in other cases, pattern-welded plates would be welded over an iron core (Williams 1977; Lang and Ager 1989; Underwood 1999). This style became less popular as the use of decorative inlay increased and swords started being made out of fewer pieces of metal (Williams 1977). Pattern-welding was originally said to be a functional aspect as it provided the optimal combination of strength and flexibility (Lang and Ager 1989). Whether this provides a stronger blade or not has been debated (Lang and Ager 1989; Williams 2014). There is more evidence now that these blades would have been of lesser quality than those made of fewer pieces of steel and thus were replaced by those of the latter style (Edge and Williams 2003; Williams 2012; Thiele et al. 2014; Fedrigo et al. 2018). Pattern-welded swords may have initially been the best quality blades, but with the progression of time and technology, their use appears to have become more of an aesthetic choice (Thiele et al. 2014; Fedrigo et al. 2018). However, talented smiths should have been able to make pattern-welded swords good regardless (Lang and Ager 1989).

Most of the typology of swords around this era is based on hilt design (Williams 2014). Petersen created a typology in the early 20th century that is still in use today (Figure 32) (Petersen 1919; Pedersen 2008). It provides some indication of the dates of the swords, but only about the last time they were re-hilted and therefore the utility of this typology is debated (Astrup and Martens 2011; Williams 2011). Swords may have been used for a long time if good quality, with their owner changing the hilt when it required replacing or when the style changed. Mostly the decoration on the swords can give an indication of the background, however there are examples that show a mixture of artistic styles.

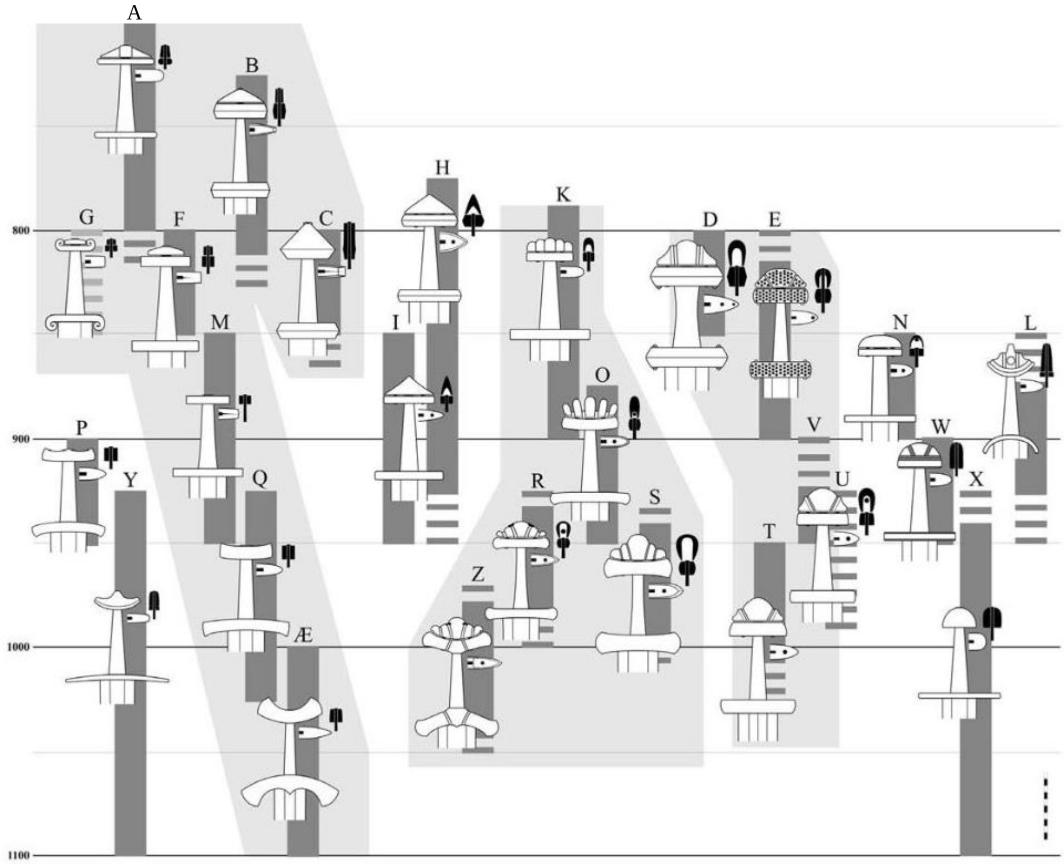


Figure 32: An illustration of Petersen's 1919 sword typology (Hjardar and Vike 2016, p.169)

Differentiating between Anglo-Saxon and Viking swords can be difficult. The guard that protects the hand is one method that some use. Curved guards are common on Anglo-Saxon weaponry whereas continental weapons usually have a straight guard (Wilson 1965). Anglo-Saxon swords are less likely to have a grip encased in metal or with a patterned wire binding compared to Viking swords (Wilson 1965). One other characteristic that seems to geographically differentiate swords is the fuller (Walton 1995). Continentally it was usually ground into the blade whereas on insular examples it was usually created through forging (Walton 1995). From the swords in current collections, it seems the use of crucible steel was a continental trait, though still a rare one (Williams 2012). Inscribed swords can sometimes help with the origin because the inscription may identify the workshop, however imitations of these blades were made in various other locations.

### *3.4.1.3 Ulfberht Swords*

One specific type of sword that must be discussed is the *Ulfberht* swords and contemporary copies. These were originally Viking weaponry and over 100 variants of this type of high-quality sword have been found around the Baltic (Williams 2009;

Williams 2012). They were produced from the 8th to 11th century and their rise and fall coincides with the rise and fall of trade to the Middle East along the Volga (Williams 2009; Hjardar and Vike 2016; Fedrigo et al. 2018). They are all inscribed and the accuracy of the inscription often correlates to the quality of the actual blade (Williams 2012). There appears to have been one main workshop making the highest quality hypereutectoid blades with the same inscription; +VLFBERH+T (Figure 33) (Williams 2009, 2011; Fedrigo et al. 2018).

Figure 33: An example of an Ulfberht sword (sword # A2 from Stuttgart, amended from Williams 2009, Fig. 1, p.146)

A secondary workshop copied the appearance using metal of almost the same high-quality, though all those swords have transposed letters, reading +VLFBERHT+ (Williams 2009). Both these sets of swords, especially the former, were of extremely high quality and would have been expensive (Williams 2012). Due to that, there are many copies of the *Ulfberht* swords, some with steel cores and some with iron cores, but all with the edges welded on. They are of variable quality as well as of variable inscription.

#### *3.4.1.4 Sword Corpuses*

More detail about Early Medieval swords can be found in Lang and Ager (1989), Edge and Williams (2003), Williams (2012), and most recently Brunning (2019). *Ulfberht* swords are discussed in depth in Williams (2007, 2009). For a presentation of the detail around Anglo-Saxon sword finds, Wilson (1965) and Davidson (1998) are recommended.

### 3.4.2 Axes and Seaxes

Axes found in archaeological contexts are not often able to be differentiated between tools and weapons (Williams 2014). There are a range of sizes, from small single-handed axes to large double-handed ones (Figure 34). Axes are seen in both Anglo-Saxon and Viking contexts, though it is unclear if the use of axes in warfare pre-dated the arrival of the Vikings or not (Williams 2014). They are seen in some contemporary art depicting battles, but are not mentioned in the literary sources from some of the battles around that time (Williams 2014). All free Viking men could carry an axe (Pedersen 2008; Hjardar and Vike 2016)

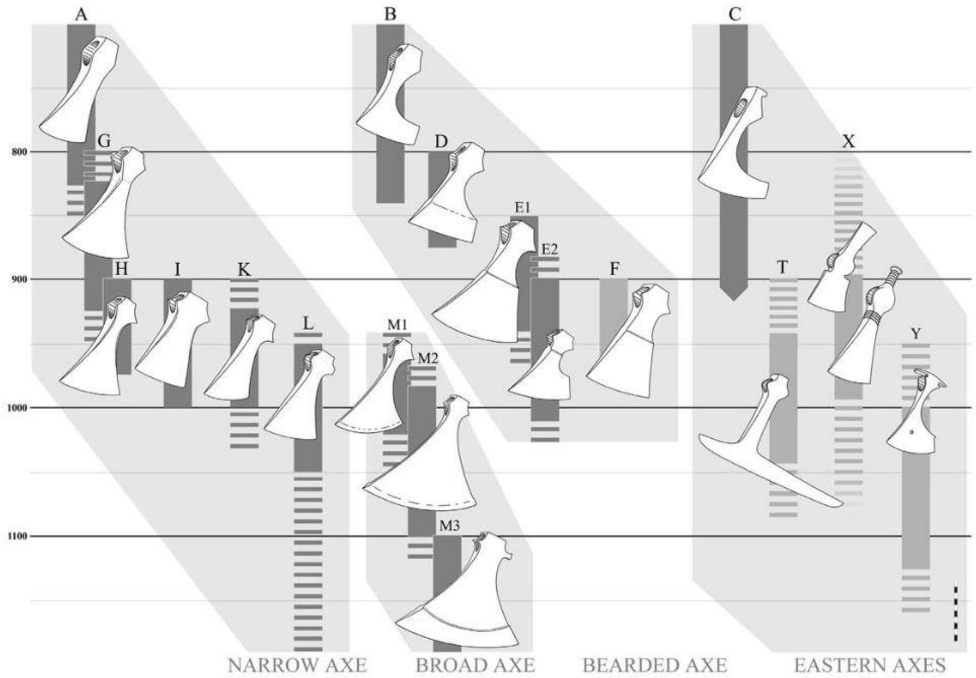


Figure 34: An illustration of Petersen's 1919 axe typology (Hjardar and Vike 2016, p.163)

Seaxes were typically single-edged knives (Williams 2014; Hjardar and Vike 2016). They may have been used for fighting though it is speculated that they may have been tools primarily, going everywhere with their owners, even in to battle (Underwood 1999). Their dimensions are variable and they would not have been the primary fighting weapon though the use of it may have been more flexible in battle situations, especially when in close-quarters (Williams 2014). By the 10th century, it seems likely that these were not being used as battlefield weapons anymore but rather for hunting (Williams 2014).

### 3.4.3 Armour and Shields

Although of less import in this study, brief mention must be made of the armour that would have been seen conventionally. Shields would have been the most common defensive weapon for both Vikings and Anglo-Saxons and were required of any man going on a Viking journey (Underwood 1999; Pedersen 2008; Williams 2014). They would have been circular or kite-shaped, made of wood with a metal shield boss likely with reinforced rims (Figure 35) (Graham-Campbell 2001; Pedersen 2008; Short 2014; Hjardar and Vike 2016). An internal handle would have allowed the shield to be used with one hand whilst a weapon held with the other. Although they were reliable, both information from the sagas and experimental evidence suggests shields could be breached with enough repeated force (Short 2014).

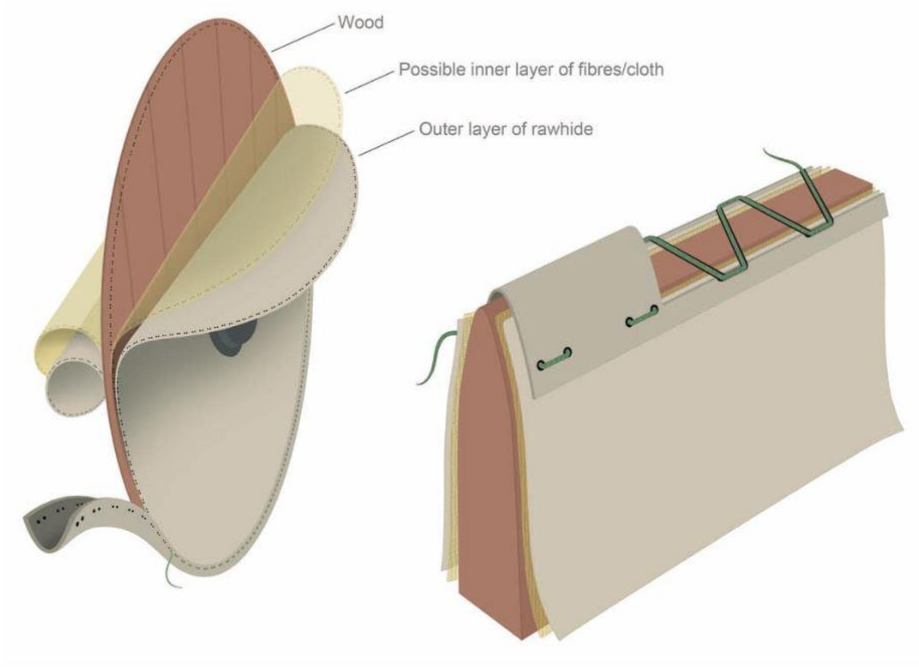


Figure 35: An example of a round Viking shield covered with leather (Hjardar and Vike 2016, p.184)

Helmets are widely seen in artistic representations, but rarely in the archaeological evidence (Pedersen 2008; Williams 2014). They were likely roughly conical with a piece of metal protecting the nose, but little other protection for the face. There is also some speculation they may have been made of boiled leather and therefore not survived in the ground (Williams 2014). The mail shirt was the most common form of body protection though still very expensive (Hjardar and Vike 2016). There was likely a form of padding under the mail shirt to make it able to absorb more force.

The combination of mail, helmets, and shields would have provided a lot of protection to the body though the weapon arm, the lower head and neck, and lower legs were possibly still vulnerable (Williams 2014). In addition, hard blows would have likely still caused trauma to the protected areas (Williams 2014). Additionally, it is unlikely that every Anglo-Saxon warrior would have had this level of protection and there is no artistic representation of the Vikings using any mail shirts (Williams 2014). Helmets and mail are not seen in any Viking codes so the procedure with exactly who would have been able to obtain such armour is unknown.

## 3.5 Summary

Britain was an unsettled place throughout the 8th and 11th century. After large changes following the withdrawal of the Roman military and the invasions of the Germanic tribes, the country was subjected to repeated and unrelenting attacks from Scandinavian Vikings for over two centuries. A first wave of Viking attacks was successfully halted after many battles and skirmishes and many Vikings settled and integrated peacefully in the *Danelaw*. The region was retaken by the Anglo-Saxons only for a second wave of incursions to begin. In the early 11$^{th}$ century, this resulted in England gaining a Viking king in the form of Cnut. The settlement of Vikings in the north and east of England was not reflected in the south despite the latter having been subjected to raids as well. The Vikings and the raids on England were an important period in time as kingdoms grew, fought, changed, flourished, and fell, eventually leading to a country united under one king.

The weaponry at the time for both the Anglo-Saxon and Vikings is fairly well-documented through texts, imagery, and archaeological findings. The swords were sharp and powerful; they were more than capable of causing significant damage. Shields were the most common defensive measure and although they were effective, they were not infallible. This information coupled with the historical background helps set the framework through which any interpretations of the events surrounding the Weymouth Ridgeway Vikings and their trauma must be analysed.

The Weymouth Vikings present a rare opportunity to study Viking remains in Wessex; a region which, despite having several noted Viking incursions, does not have substantial archaeological evidence of a Viking presence, perhaps due to the lack of Scandinavian settlement in the area. Therefore, any additional information that can be gathered about this collection in this study will help add to understanding the region during this period. This is also an opportunity to learn more about the capabilities of Viking weaponry. This chapter, focused on the historical background to the Viking Age in England, primarily addressing Objective 1 (Section 1.3.1) as well as laying a foundation for the synthesis of the findings in later chapters (Objective 9):

- The Vikings had an important impact in parts of England outside of the *Danelaw*
- Although there were times of peace, there were often violent confrontations between factions during this time
- The weaponry in use at the time could be very high-quality and having a collection such as the Weymouth Ridgeway Vikings allows for the exploration of the impact of such weapons
- The discovery of a mass burial of Vikings in Dorset was unexpected and presents the opportunity to learn more about the impact of the Vikings in Wessex (see Chapter 9)

# 4 Trauma Analysis

When the term is used in physiological, or specifically osteological contexts (as opposed to describing psychological phenomena) several definitions of trauma can be found in the literature. According to Lovell (1997, p.1139) trauma is any "…injury to living tissue that is caused by a force or mechanism extrinsic to the body". Roberts (2000, p.337) states trauma can be considered "…any bodily injury or wound and it may affect bone, soft tissue, or both". Overall, these descriptions can be summarised by saying that trauma occurs when there is an injury to living tissues through the transfer of energy from an external force (Cohen et al. 2012). The current chapter focuses on skeletal trauma and starts by examining some of the biomechanical properties of bone and the different categorisations of trauma used in order to effectively research the Weymouth Ridgeway Vikings. Due to the nature of the collection, the primary focus is sharp force trauma, the current types of studies done, and the interpretations that can be made. It then concludes by looking at deviant burials, specifically those with decapitation injuries or sites with mass graves. When regarding trauma analysis in human remains, there are many different terms that are used in various forensic and osteoarchaeological contexts. As noted by Symes et al (2001, p.406), "It is critical that anthropologists are aware of differences between anthropological and medical language and theory and how these differences affect process and outcome in a legal setting". Within this chapter, it is endeavoured to provide a variety of the most common terms, before one is used for consistency in the rest of the thesis.

## 4.1 Skeletal Trauma

As described by Waldron (1996), trauma can be divided in two over-arching categories based on circumstance: accidental trauma and deliberate trauma. Falls and unintentional injuries would be part of the first category, whereas situations like fights, assaults, battles, or judicial punishment would be part of the latter. The difference between them in the osteological record can sometimes be hard to determine though there are certain patterns that osteologists and forensic anthropologists look for in skeletal remains presenting with trauma which can be revealing about the events that occurred (Cunha and Pinheiro 2016).

Some of the most important considerations when analysing trauma are the timing of the trauma, the number of wounds, the location and sequence of them, and their characteristics (Kranioti 2015). The development of trauma analysis in palaeopathology has been shifting from just identifying and describing what is found towards interpreting that trauma in a wider social, cultural, and environmental context as well as looking for temporal and geographic patterns (Lovell 1997). Since then, there has been some recent shift back towards describing individuals and their injuries as detailed case studies, although wider interpretations are still a vital part of these studies (e.g. Appleby et al. 2015; Cohen et al. 2015; Giuffra et al. 2015; Valoriani et al. 2017; Vazzana et al. 2018).

Trauma caused by sharp objects will be the focus for this chapter beginning in Section 4.1.4, however some background information on trauma must be provided for a comprehensive understanding.

### 4.1.1 The Biomechanical Properties of Bone in Relation to Trauma

Overall, living bone is relatively pliable due to its organic components, specifically collagen (Sauer 1998; Pechníková et al. 2011; Symes et al. 2012). This organic structural element provides tensile strength, whilst an inorganic component formed principally of hydroxyapatite crystals gives bone compressive strength (Symes et al. 2012; Loe 2016). Bone is also comprised of moisture, fats, and vasculature, all of which affect how it reacts to force (Figures 36 and 37) (Nawrocki 2016). These properties mean that the bone will react in certain ways and fail in somewhat predictable patterns when force is applied. Bone is considered anisotropic because it can respond differently to different forces (Symes et al. 2012; Loe 2016).

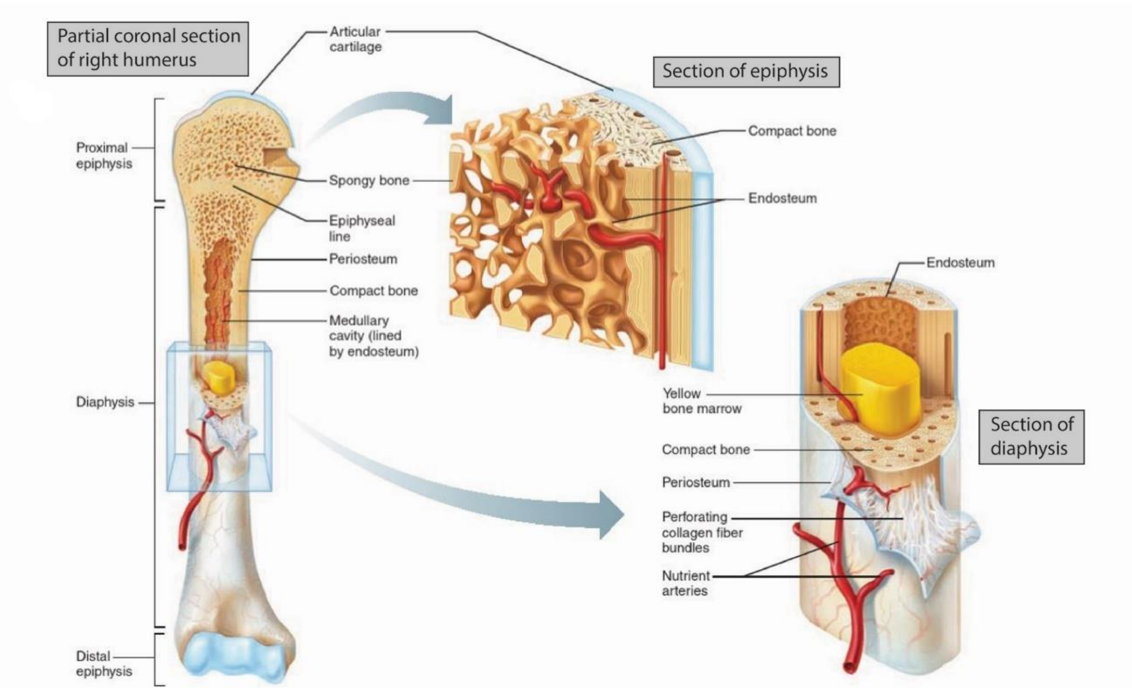


Figure 36: A diagram of the structure of the epiphysis and diaphysis (amended from Marieb et al. 2014, Fig. 4, p.152)

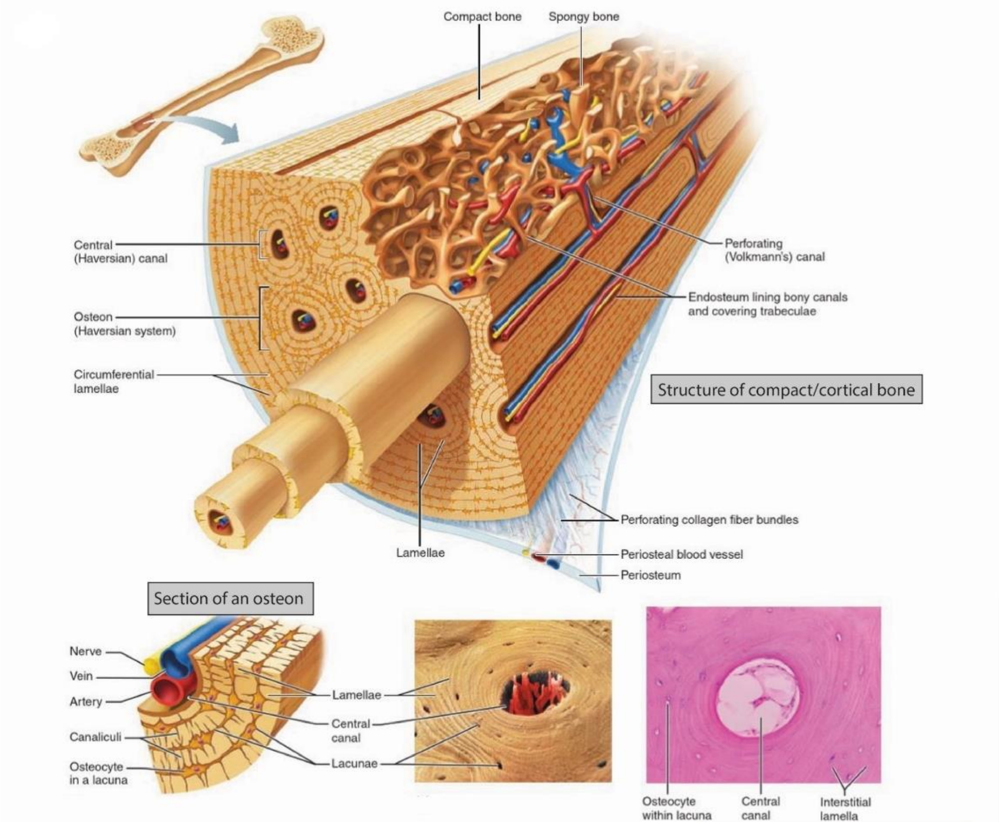


Figure 37: A diagram of the microstructure of a bone (amended from Marieb et al. 2014, Fig. 7, p.156)

The understanding of biomechanical factors can be key in the interpretation of trauma (Ubelaker and Montaperto 2013). In its most basic form, trauma is recognisable on a bone if enough force was applied that its structure yielded (Figures 38 and 39) (Kieser et al. 2013).

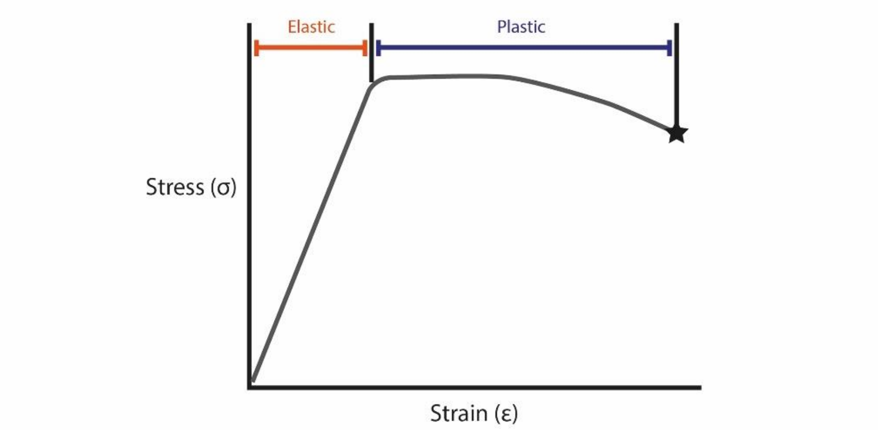


Figure 38: A stress-strain graph of bone showing the elastic and plastic portions before complete failure (amended from Kieser et al. 2013, Fig. 2.4, p.15)

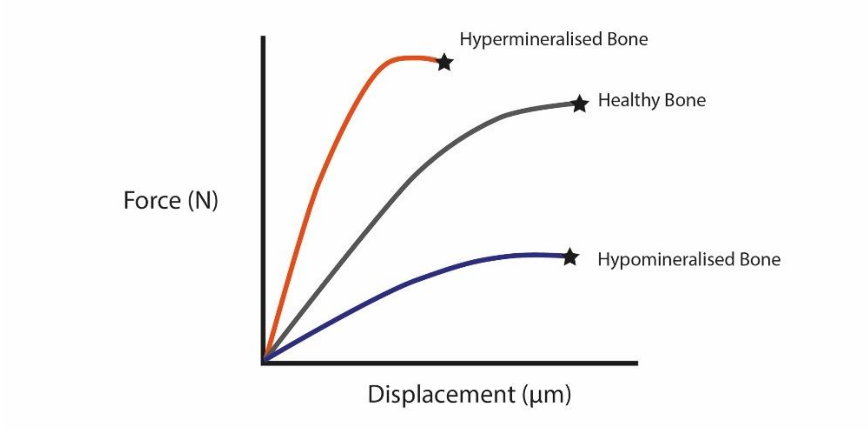


Figure 39: An example of how hypo- and hypermineralised bone effects the force required to cause deformation (amended from Kieser et al. 2013, Fig. 3.2, p.40)

The appearance of skeletal trauma is directly related to the amount of force and the area over which that force is spread (Cohen et al. 2012). There are both intrinsic and extrinsic factors that must be considered when interpreting how bone may have reacted to trauma (Table 4) (Berryman and Jones Haun 1996; Symes et al. 2012). There are five main mechanical loads that can affect bone: compression, tension, shear, torsion, and bending (see Figure 40 for how they can operate alone and in combination) (Martin and Harrod 2015).

Table 4: Factors that impact how trauma affects bone

| Intrinsic Factors | Extrinsic Factors |
|---|---|
| - Age | - Magnitude of the force |
| - Sex | - Type of force |
| - Nutrition and health status | - Speed the force is applied with |
| - Morphology of the bone | - Duration of the force |
| - Thickness of the cortical bone | - Rate of loading of the force onto the bone |
| - Mineral-to-collagen ratios | |
| - Capacity of the bone to absorb energy | |
| Berryman and Jones Haun 1996; Lovell 1997; Wheatley 2008; Ubelaker and Montaperto 2013; Bartelink 2015; Martin and Harrod 2015; Cohen et al. 2017 | |

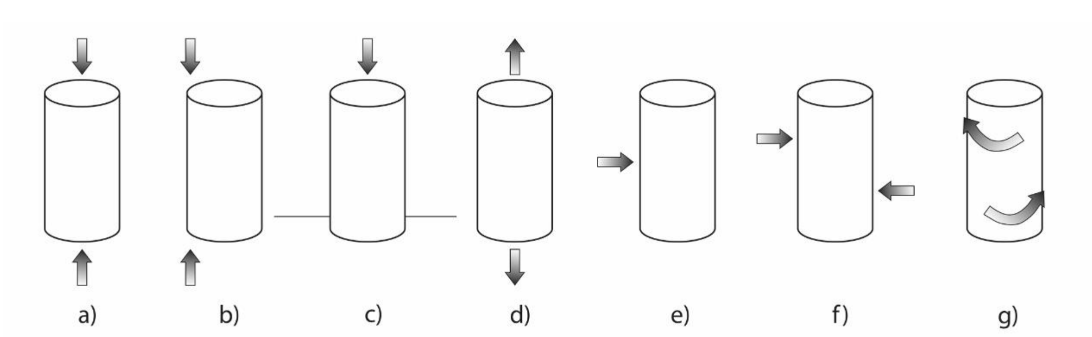


Figure 40: Different types of force that can act on bone to cause fractures a) compression, b) tension/compression: bending, c) compression: impaction, d) tension, e) simple, f) shear, and g) torsion (amended from Kieser et al. 2013, Fig. 3.13, p.53)

These are all factors that can change the appearance of trauma and therefore understanding the effects of each can aid in the interpretation of events related to skeletal damage. For example, a force inflicted by a blade will look different than one inflicted by a baseball bat. Despite this, some caution needs to be exercised because the properties of that specific bone when it was alive are not fully known, thus adding a challenge to the reconstruction of events (Boylston 2000). This does not mean interpretations cannot be made; it simply means that they must be made with caution and over-interpreting the trauma must be avoided (see Section 4.1.7).

#### *4.1.1.1 Fractures*

Fractures occur when forces are exerted on a bone to a degree that it can no longer maintain its functional integrity and it cracks (Roberts 2000; Cunha and Pinheiro 2016). This can either happen with repetitive loading over a long period of time or a large single-impact force (Pechníková et al. 2011). Once the force is greater than can be dealt with by bone's elastic deformation, any deformations that occur are considered plastic and are permanent (Figure 41) (Berryman and Jones Haun 1996; Berryman and Symes 1998; Symes et al. 2012).

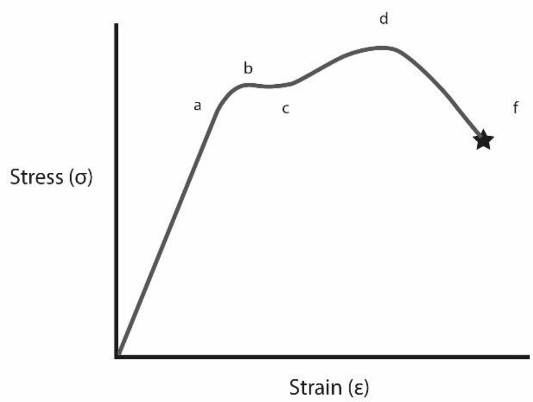


Figure 41: A detailed version of the stress-strain graph for biological materials; a) the proportional limit where the relationship stops being linear, b) the elastic limit where the maximum stress can be applied without permanent deformation, c) the yield point where deformation starts to occur with relatively little extra added stress, d) the point where the material reaches its ultimate strength before failing, and f) the failure point which can be different for each material (amended from Kieser et al. 2013, Fig. 2.5, p.15)

Bone tends to be stronger under compression. Usually, the bone under tension will fracture first, however in some cases the areas under tension and compression will fail simultaneously, especially in cases with multiple forces present (e.g. shear), exemplifying how different mechanical loading can cause different fracture patterns (Figure 42) (Berryman and Jones Haun 1996; Berryman and Symes 1998; L'Abbé et al.

2015). On their own, fractures do not necessarily equate to violence as many causes can be accidental (Martin and Harrod 2015).

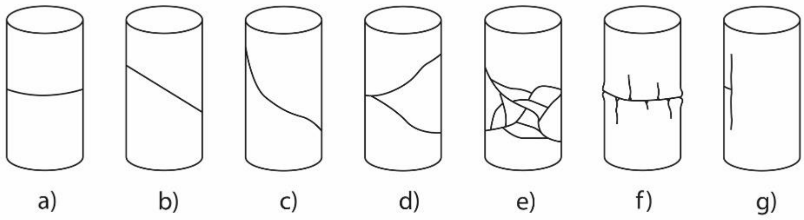


Figure 42: Different fracture patterns that can result using a long bone as an example a) transverse, b) oblique, c) spiral, d) butterfly, e) comminuted, f) impacted, and g) greenstick (amended from Kieser et al. 2013, Fig. 3.13, p.53)

The energy that causes a bone to fracture will radiate until it dissipates (Galloway et al. 1999). Overall, the force that fractures the bone will follow the path of least resistance away from the site of impact often through the thinnest bone of that area. For example, there are areas of buttressing in the skull (midfrontal, midoccipital, posterior temporal, and anterior temporal) that a fracture generally tends to stay between and this often results in the fracture being directed to a fossa (Berryman and Jones Haun 1996; Berryman and Symes 1998; Cohen et al. 2012). This tendency to follow the path of least resistance means fractures will also tend to follow the grain of the bone. Similarly, they will change directions or dissipate at natural points of weakness, for example along the sutures of the skull (Berryman and Symes 1998; Kranioti 2015).

Importantly, fractures will also not cross previously created discontinuities because the energy will dissipate into these pre-existing fractures (Lovell 1997; Berryman and Symes 1998; Loe 2016; Nicklisch et al. 2017). Therefore, fracture patterns and their interpretations can be very important for sequencing the order of multiple weapon strikes (Berryman and Symes 1998; Bartelink 2015; Love 2015). Although usually thought of more for studies of blunt force trauma, sharp force trauma can produce radiating fractures sometimes as well (see Section 9.3 for further discussion). Lovell's (1997) seminal article on trauma analysis in palaeopathology has an extensive description of the variety of fractures that are commonly found in archaeological material and the important information to obtain from them.

#### *4.1.1.2 Mechanisms of Injury*

There are four mechanisms of injury that can cause fracturing of the bone: direct trauma, indirect trauma, stress, and pathology (Lovell 1997). Direct and indirect trauma cannot be differentiated if only skeletal remains are present (e.g. L'Abbé et al. 2019). The fractures that are caused by each are summarised in Figure 43.

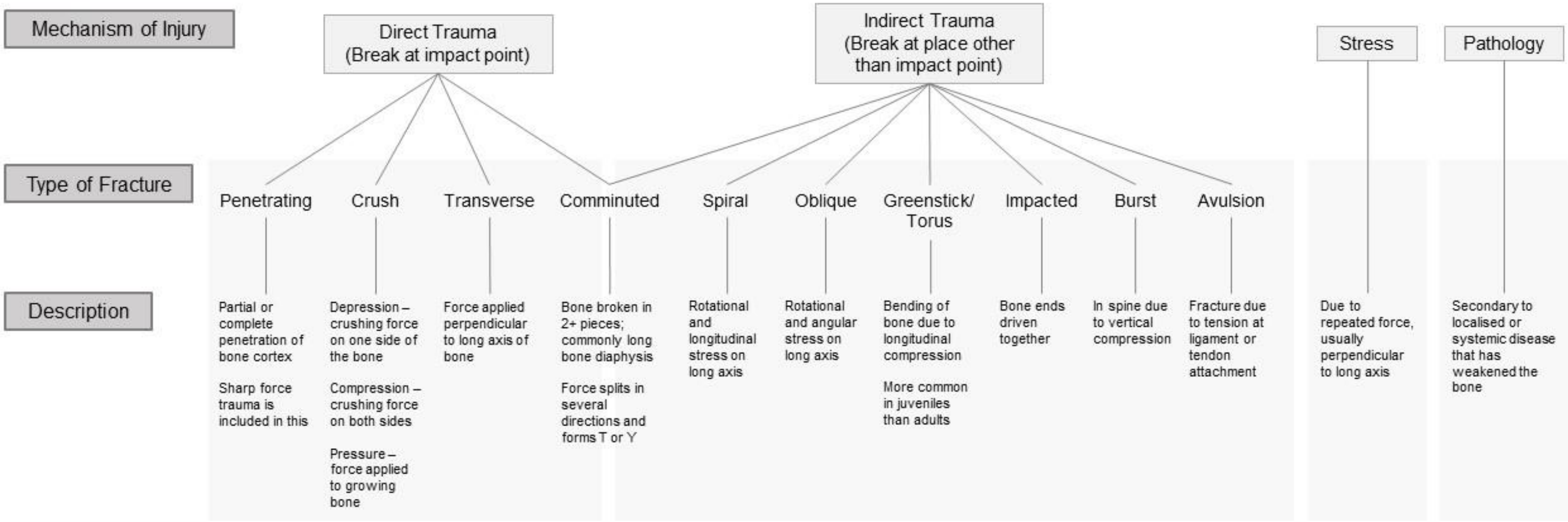


Figure 43: A flowchart showing the four mechanisms of injury (amended from Lovell 1997, Table 2, p.141)

### 4.1.2 Interval of Trauma

The timing of when the trauma occurred is vital to the interpretation of events surrounding the life and death of an individual (Sauer 1998; Coelho and Cardoso 2013). There are three phases: ante-mortem, peri-mortem, and post-mortem (Figure 44) (Galloway et al. 1999; Kranioti 2015; Fleischmann 2019). There is some overlap between these phases, however bone reacts distinctly and differently in each phase (Boylston 2000; Symes et al. 2001). In certain instances such as some forensic contexts, the terms ‘wet’ or fresh’ and ‘dry’ bone is preferred over peri- and post-mortem respectively, however, due to the archaeological nature of the collection in this work, the latter terms are used (e.g. L’Abbé et al. 2015; Fleischmann 2019; Symes et al. 2001, 2014).


Figure 44: Images of fractures: a) healed ante-mortem (femur), b) peri-mortem (femur), and c) post-mortem (tibia)

Ante-mortem trauma happens prior to death and is not connected with the sequence of events leading to death (Cunha and Pinheiro 2016). Often this is differentiated by evidence of healing, remodelling, infection, or necrosis at the site of injury, indicating at least short-term survival (Lovell 1997; Sauer 1998; Galloway et al. 1999; Cohen et al. 2012; Łukasik et al. 2019). The appearance of new bone formation or the rounding and blunting of edges of a traumatic lesion is indicative of healing (Boylston 2000). Healing starts fairly rapidly, however it does not become macroscopically visible for a couple weeks and can vary based on factors such as age, type of injury, and health status, making it difficult to determine the time between death and injury (Lovell 1997; Galloway et al. 1999; Cunha and Pinheiro 2016; Nicklisch et al. 2017). There can be histologic, radiographic, or microscopic evidence of healing within two weeks of the injury (Loe 2016). This uncertainty also results in some overlap in the appearance of ante-mortem and peri-mortem trauma. In such cases, context and historical background may help in the interpretation of the timing of the trauma.

Peri-mortem trauma occurs at the time of death and may have contributed to that death (Sauer 1998; Wheatley 2008). Since not all trauma is reflected on the skeleton, it is not possible to definitively say whether a traumatic lesion was the sole cause of death, but rather that it was involved in the sequence of events leading up to the individual's death. In this type of trauma, no healing will be seen (Cohen et al. 2012). Since fresh or wet bone is pliable, it is able to absorb more stress before yielding and fracture margins tend to be sharp, more irregular, and splintered (Sauer 1998; Wheatley 2008; Nawrocki 2016; Łukasik et al. 2019). Additionally, since bone tends to stain when buried, fractured surfaces that preceded burial are often the same colour as the rest of the bone surface because they too have been directly exposed to the burial environment (Lovell 1997; Sauer 1998).

Post-mortem 'trauma', or post-mortem damage, occurs from after the individual has died and may be because of funerary rituals, disturbance of the burial, taphonomic damage, or excavation and analysis (Sauer 1998; Galloway et al. 1999). Bone tissue starts to die shortly after the death of a person which leads to difference in appearance of fractures that subsequently occur. The loss of organic matter makes bone a lot more brittle in this phase (hence the alternate term 'dry' bone) and alters fracture patterns and the stress-strain graph compared to living bone (Lovell 1997; Roberts 2000; Dirkmaat et al. 2008). The edges of post-mortem fractures are typically rectangular and more regular, though the texture of them is often rough (Lovell 1997; Sauer 1998; Boylston 2000; Wheatley 2008; Łukasik et al. 2019). Often the exposed cortical and trabecular bone of post-mortem fractures is evenly lighter in colour and less stained or dirty because it would not be exposed to the burial environment the same way as surface of the bone would have been, especially if the damage occurred during excavation (Sauer 1998; Boylston 2000; Šlaus et al. 2012).

It is typically the most difficult to distinguish peri- and post-mortem trauma (Figure 44, Table 5) (Cohen et al. 2012; Cappella et al. 2014). The differences in appearance depend on whether the bone has or has not lost its organic component (Coelho and Cardoso 2013; Cappella et al. 2014; L'Abbé et al. 2019). The bone may retain sufficient organic characteristics for a couple weeks after death to cause any fracturing to appear to have occurred on the bone whilst it was living. There have been some attempts to see if there are microscopic differences, such as changes to how the fractures cross osteons, however, no method has met with sufficient success yet (Pechníková et al. 2011).

Similarly, differences in most characteristics that have been examined between living and dry bone are not statistically significant and thus cannot be used as a differentiation method, and considerable variation has been found in how long bones retain their organic components (Wheatley 2008; Coelho and Cardoso 2013).

Table 5: Features of peri- and post-mortem damage (amended from Łukasik et al. 2019, Table 2, p.285)

| Morphological Trait | Peri-Mortem | Post-Mortem |
|---|---|---|
| Plastic deformation | Present | Absent |
| Staining of the bone fracture surface | Similar to the rest of the bone surface | Different in colour than the surrounding bone |
| Fracture surface | Clean and smooth | Jagged/stepped edges |
| Fracture angle | Obtuse/acute | Right |
| Fracture outline | Concentric and radiating | Perpendicular or horizontal |
| Fracture margins | Peeling or lifting | Rough and uneven |
| Loading point | Present | Absent |
| Area adjacent to the fracture site | Small bone fragments adhere to the fracture site | Tendency to break into a number of pieces |
| SFT appearance | Straight lesions with flat, sharp, and polished edges | Straight lesion with rough edges and walls |
| Buikstra and Ubelaker 1994; Anderson 1996; Bennike 2008; Wieberg and Wescott 2008; SWGANTH 2011; Šlaus et al. 2012; Ubelaker and Montaperto 2013; Galloway et al. 2014; Symes et al. 2014; L'Abbé et al. 2019 | | |

### 4.1.3 Types of Trauma

There are five general categories of bone trauma or damage used in forensic sciences: sharp force, blunt force, projectile/ballistic, healing, and burned/thermal (Galloway et al. 1999; Kimmerle and Baraybar 2008; Cunha and Pinheiro 2016). Sharp force trauma is the focus of this project and will be discussed in Section 4.1.4, whereas the blunt and projectile/ballistic trauma will be briefly mentioned in the following sections. Blast trauma is not discussed in this project and healed trauma is described above in ante-mortem trauma. All of these have been studied in both archaeological and modern forensic or experimental contexts as it is important to know how bone reacts to different impacts when it is still living to be able to more effectively understand what traumatic lesions look like compared to post-mortem damage.

#### *4.1.3.1 Projectile/Ballistic Trauma*

Projectile/ballistic trauma occurs when an individual is hit by a propelled object, such as an arrow or a bullet (Sauer 1998; Cohen et al. 2012, 2015, 2016). There is a high amount of energy transfer in this type of injury, much higher than what is seen in other types of trauma. The amount of damage is usually dependent on the type and size of the weapon or projectile and the velocity at which it travels (Dirkmaat et al. 2008; Cohen et al. 2012).

The force usually starts off having a narrow focus and widens after first impact (Kimmerle and Baraybar 2008). The wounds that are created on the bone are often bevelled and fracture patterns radiate from the point of impact, although different types of bone can present different fracture patterns (Figure 45). Depending on the location and the angle of the projectile, both the entrance and exit wounds may be apparent and discernible with the margins being bevelled internally and externally, respectively. Although objects such as spears and lances could be propelled, the velocity they reach is not as high as what is seen in projectile trauma, and therefore they are categorised differently (Section 4.1.4).


Figure 45: An example of projectile trauma (plastic cast skull): a) the anterior view of the exit wound, b) anterior close-up, c) the posterior view of the entry wound, and d) the posterior close-up

#### *4.1.3.2 Blunt Force Trauma*

Blunt force trauma (BFT) is caused by an individual being struck by an object with a wider area of impact (Cohen et al. 2012, 2015; Šlaus et al. 2012). It is usually a lower velocity impact than projectile trauma (Kranioti 2015; L'Abbé et al. 2019). The range of items that cause BFT on the skeleton is important to note; for example, an impact with a vehicle or with the ground would result in BFT (Galloway 1999; Loe 2016; L'Abbé et al. 2015, 2019). These injuries can be challenging to interpret, and the patterning of the fractures is important (Dirkmaat et al. 2008; Cohen et al. 2012, 2015). Depending on the force, the cranium may exhibit characteristic radiating and concentric fractures, allowing the impact point of the object to be determined (Berryman and Symes 1998). BFT can result in small injuries but can still cause a lot of damage, especially if on the cranium (Figure 46). Similar to projectiles, they can create fractures, but the centre will not usually be pierced in the same manner, though it may result in a depressed fracture (Berryman and Symes 1998; Dirkmaat et al. 2008).

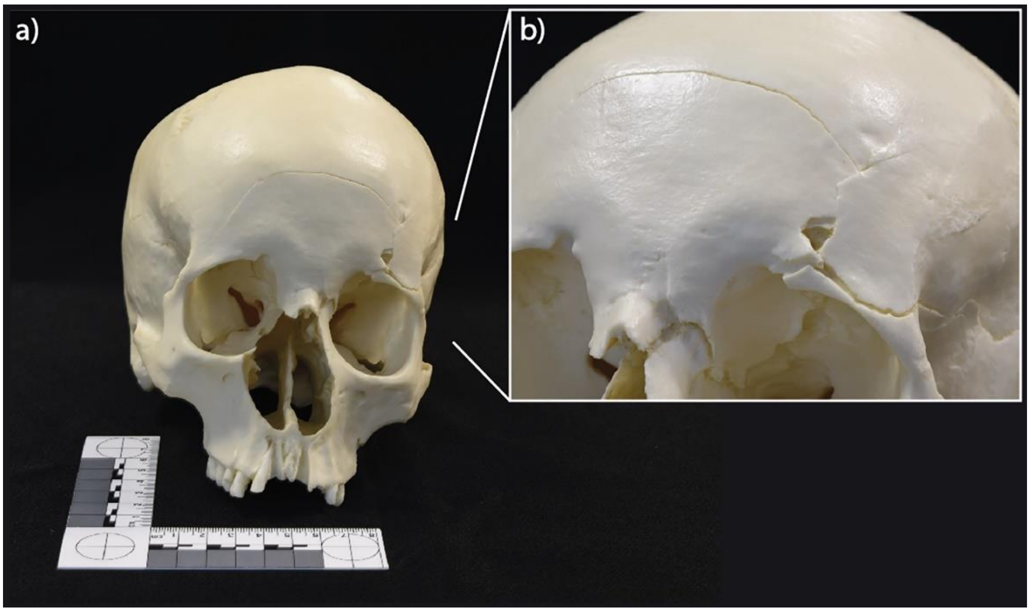


Figure 46: An example of blunt force trauma (plastic cast skull): a) the anterior view and b) the close-up of the anterior view

### 4.1.4 Sharp Force Trauma

Sharp force trauma (SFT) occurs when an individual is hit by a weapon with a fine, sharp edge such as a sword, a knife, or an axe. In these situations, a high amount of force is directed along a thin, sharp surface, creating distinctive marks (Galloway et al. 1999; Symes et al. 2001; Šlaus et al. 2010; Šlaus et al. 2012). Overall, this type of trauma is usually intentional and inflicted by another person, therefore it is a good insight into what types of violent activities may have occurred in society, what factors may have influenced them, and what consequences might have been seen (Cohen et al. 2012; Judd and Redfern 2012).

Due to the nature of SFT, it is good for testing metric or qualitative methods as it is usually clear, well-delineated, and the edges are usually discrete if taphonomically untouched. This project will focus on SFT from this point forth. Dentition is of a different composition than bone and does not heal, therefore it is more difficult to determine when dental trauma occurred compared to the death, however fresh fractures are distinguishable from post-mortem modifications (Buikstra and Ubelaker 1994; White and Folkens 2005;

see Clement 2016 for a discussion of forensic odontology). Due to this, it is not within the remit of this study.

The defects caused by these sharp weapons are typically known as ‘cutmarks’ and they generally have very distinct morphology (Table 6). Two types of morphology will be described here, those that do not fully bisect a bone and those that do. The former was termed ‘incised’ cutmarks or defects and the latter ‘shaved’ cutmarks or defects to aid in differentiating.

Table 6: The description of the different components of a cutmark

| Terminology | Description |
|---|---|
| Cutmark | - Defect left in a bone by a blade<br>- Can be created through hacking, slicing, or stabbing motions<br>- Sometimes called a “kerf” in studies |
| Floor | - Bottom of the incised cutmark<br>- Furthest point the blade travelled into the bone<br>- Sometimes called “apex” in studies |
| Wall | - Sides of the incised cutmark |
| Shoulder | - Area on the surface of the bone that is adjacent to either side of the incised cutmark |
| Edge | - Where the wall meets the surface of the bone |
| Surface | - Exposed, cut surface of shaved cutmarks |
| Boylston 2000; Cohen et al. 2012 | |

Incised cutmarks are produced when a blade traverses only part of the way into the bone and is then removed, leaving a unique linear lesion (Figure 47). The defects made by these sharp weapons usually have a very well-defined, straight edge and a polished, flat surface (Figure 48) (Boylston 2000; Symes et al. 2001; Cohen et al. 2012). The morphology of a cutmark is inherently dependent on nature of the weapon and the way it struck the bone (Maté González et al. 2015). They are typically linear and conventionally have V-shaped profiles, though there are factors that can affect the exact nature of the shape (Sauer 1998; Cohen et al. 2012; Šlaus et al. 2012; Courtenay et al. 2019).

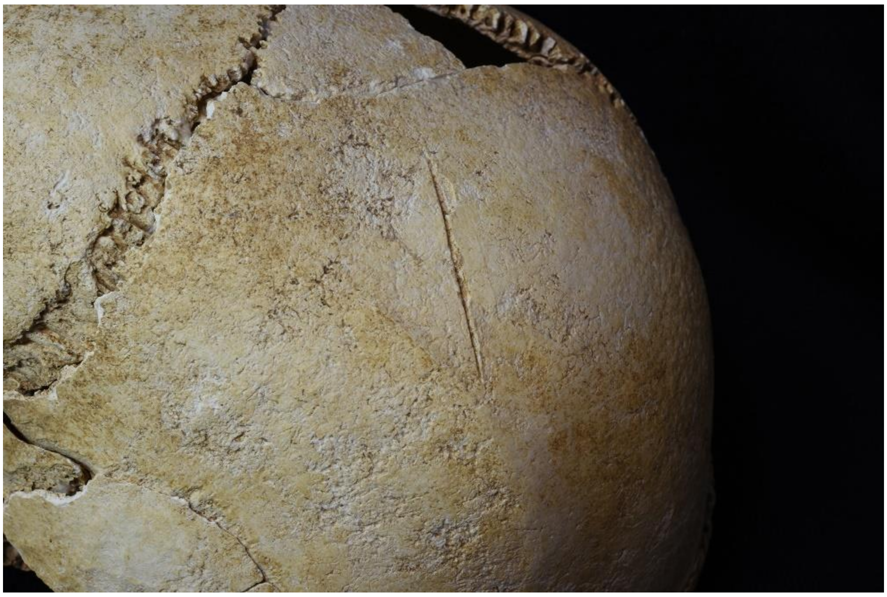

Figure 47: An example of an incised cutmark from the Weymouth Vikings (SK3704)

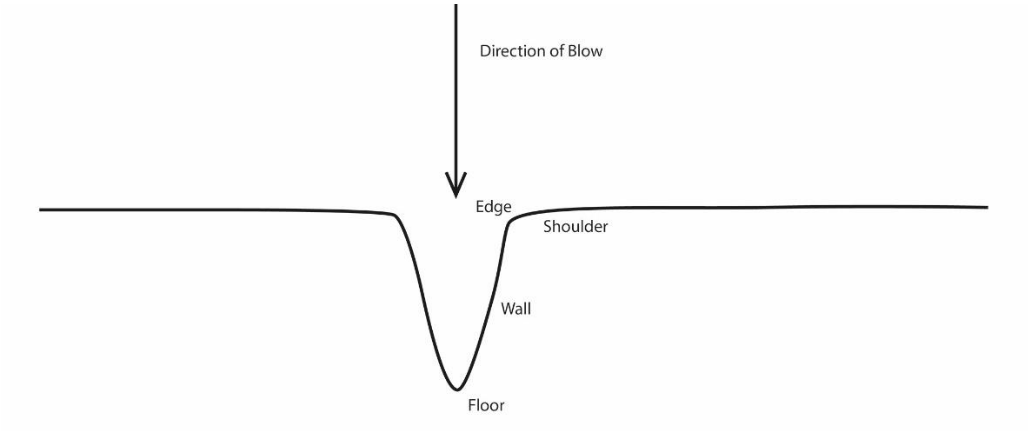


Figure 48: The profile of an incised cutmark with the components labelled (Table 6)

Generally, if a blade enters a bone at an angle, the wall 'under' the blade is smoother and more polished than the other surfaces (Figure 49) (Smith and Brickley 2004; Šlaus et al. 2010). The opposite side is usually more ragged as parts of it may have fractured or splintered from the force and therefore this information can sometimes help determine the direction the blade came from (Smith and Brickley 2004; Šlaus et al. 2010; Cohen et al. 2012). The edges reflect the same pattern, with at least one, the 'entry' edge, nearly always being clean and well-defined. The floor of the cutmark is the deepest point that the blade penetrated and is instrumental in determining the profile of the cutmark and the angle of the cutmark wall.

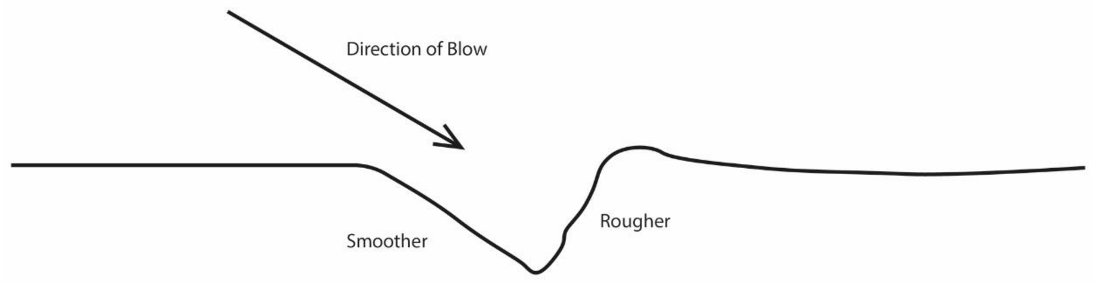


Figure 49: An example of an angled incised cutmark creating a smoother surface ‘under’ the blade

Shaved cutmarks are found when the blow was powerful enough to completely cut the bone in two or cut part of the bone off (Figure 50). These can be created in one of two manners. The first is that the blade can cut right through the bone (Sauer 1998). The second can occur when the blade cuts part way into the bone and the force of either the blow or the withdrawal of the blade causes fractures to propagate, breaking the bone (broken incised cutmark) (see Section 9.3). In this second case, the appearance is not always consistent across the entire bone. Typically, with all shaved cutmarks, the part of the bone closer to the initial point of contact will be smoother with neater edges and sometimes have the polished look of an incised mark if there is compact bone present and therefore can help determine directionality of the blow (Boylston 2000).

As the blade travels further through the bone, the appearance of the SFT may transition to an appearance of fracturing, as described previously. The edges are usually still well-delineated, but the surface loses smoothness and the shine is no longer present. If shaved cutmarks have gone through trabecular bone, it can be more difficult to differentiate which side the blow might have come from because exposed trabecular bone is very delicate and subject to taphonomic damage. Cutmark profiles cannot be easily generated from cuts like this unless all pieces are found undamaged and reconstructed without introducing errors in alignment. Therefore, reconstructing broken incised cutmarks to reform incised cutmarks has not been attempted for this study.

a)

b)

Figure 50: An example of a a) shaved cutmark and b) broken incised cutmark (SK3789 and SK3704)

Microscopic striations can be left on the walls or surface of both incised and shaved cutmarks depending on the blade and these are usually parallel to the direction of the force and thus can sometimes help determine the direction of the blow (Smith and Brickley 2004; Šlaus et al. 2010; Loe 2016). The use of angled lighting, especially in conjunction with a stereomicroscope, is necessary to make such these visible. These striations are produced due to small imperfections in the blade used (Smith and Brickley 2004; Loe 2016; Weber et al. 2021). In rare occurrence, striations are large enough to be seen macroscopically, this usually indicates a large defect in the blade (Loe et al. 2014b).

SFT can result in fractures both around and propagating away from the site of the initial strike (Constantinescu et al. 2017; Nicklisch et al. 2017). In some cases, as discussed above in the context of broken incised cutmarks, the strike decreases with power as it goes deeper into the bone and the result can be a decreased smoothness in the cutmark caused by the bone fracturing along the grain ahead of the blade rather than being cut by it (Galloway et al. 1999; Loe 2016). In other situations, the sharp implement, such as an axe or sword, can cause fracturing that is more typically seen in BFT due to the weight and force of the blow. This is also sometimes called hacking or chopping trauma. Overall, this combination of SFT with BFT fractures is sometimes called 'sharp-blunt force trauma' (SBFT) or "…blunt-force trauma with a sharp object…" (Loe 2016;355) (Alunni-Perret et al. 2005; Downing and Fibiger 2017; Nicklisch et al. 2017). Weaponry such as spears and lances can also create damage that falls within this category. Within this research, the fractures propagating away from the floor of the cutmark, and thus appearing as if an extension of the cutmark, are of particular interest and are addressed as Residual Energy Dispersal (RED) fractures (see Section 9.3; for further information of the fracturing of bone and similar materials, see Lawn 1993, Kieser et al. 2013, and Christensen and Hatch 2019).

Different blades can leave different types of cutmarks which is an area that has been studied in forensic contexts (Reichs 1998; Symes et al. 2001; Cohen et al. 2012; Symes et al. 2012; Loe 2016; Maté-González et al. 2018). For examples, metal blades generally leave a more regular cutmark than other materials, and serrated blades leave different marks with more striations than those with smooth blades (Symes et al. 1998; Freas 2010; Boschin and Crezzini 2012; Cohen et al. 2012). Though some differences are notable macroscopically, such as the size and general depth of the cut, often microscopic analysis, introduced more comprehensively in Section 4.1.6, can be more revealing.

### 4.1.5 Differentially Diagnosing Sharp Force Trauma

Overall, the four diagnostic criteria that are used are based on the distinct morphology and are as follows (Wenham 1989; Houck 1998; Reichs 1998; Symes et al. 1998; Kjellström 2005; Lewis 2008):

1. Linear lesion, well-defined sharp edges (incised) or sharp edges between the surface of the cut and the surface of the bone (shaved)
2. V-shaped cross-section (incised) or flat surface, often transecting a bone (shaved)
3. Flat, smooth, and polished surfaces; possibly flaking on contralateral wall, surface, or edge
4. Signs of parallel striations

Determining which defects on a bone are actually traumatic in origin can also prove surprisingly difficult, especially with archaeological collections that have high levels of fragmentation or poor preservation. Compared to many pathologies, there are fewer questions as to what else could cause SFT, but post-mortem damage and taphonomic alterations can cause confusion (Symes et al. 2001). It is important to be aware of the issues of equifinality created by the decomposition process, to avoid mis-classifying taphonomic damage as trauma (Pinheiro et al. 2015). If not able to be differentiated macroscopically, these can usually be differentially diagnosed with a microscope. Some ante-mortem and post-mortem alterations that can appear similar to SFT are listed in Table 7 (Figure 51).

Table 7: Some examples of ante-mortem and post-mortem alterations that can appear as 'pseudo-SFT' or obscure the aetiology of marks on the bone

| Timing | Cause | Description |
|---|---|---|
| Ante-Mortem | Blood vessel impressions | - Rounded corners; U-shaped<br>- No breakage along edges<br>- Depth can be variable<br>- Often not entirely linear (under magnification)<br>- Can be in places not accessible with a blade |
| | Congenital variations | - Rounded corners; U-shaped<br>- No breakage along edges<br>- Often not entirely linear (under magnification)<br>- Can be in places not accessible with a blade |
| | Partially fused epiphyses | - Found at the joins between epiphyses and diaphyses<br>- Rounded corners<br>- No breakage along edges<br>- Often not entirely linear (under magnification) |
| | Pathologies | - Often not linear<br>- May have undercut edges |
| Post-Mortem | Root etching | - Rounded corners; U-shaped<br>- No breakage along edges<br>- Depth can be variable<br>- Often not entirely linear (under magnification)<br>- Often not entirely continuous (under magnification)<br>- Can be in places not accessible with a blade |
| | Animal damage | - Gnawing, scavenging; both micro and macro fauna<br>- Puncture marks from carnivores' teeth<br>- Can appear linear but usually shallower, less V-shaped<br>- More similar to multiple scrapes across the bone than cutmarks |
| | Excavation/modern equipment damage | - Trowels, surveying equipment, farming equipment<br>- Margins and colouring of the injury usually have distinctive post-mortem features |
| | Taphonomic processes | - Decomposition, weathering, burning<br>- Can obscure edges; create flat surfaces or round originally sharp edges |
| Buikstra and Ubelaker 1994; Anderson 1996; Sauer 1998; Galloway et al. 1999; Boylston 2000; Symes et al. 2001; Ubelaker and Montaperto 2013; Maté González et al. 2015; Cunha and Pinheiro 2016; Loe 2016; Nawrocki 2016; Nicklisch et al. 2017; Yravedra et al. 2017 | | |


Figure 51: Examples of things that are sometimes confused with trauma: a) an epiphyseal line, b) rooting, c) up-close of rooting damage, d) rodent gnawing damage, e) up-close of the rodent gnawing damage with oblique lighting, and f) sampling

To avoid misclassifying variation as trauma, Cunha and Pinheiro (2016) recommend having a solid base in morphological variations. These variations are more problematic for determining ante-mortem trauma because peri-mortem trauma, especially SFT, will have much clearer and sharper edges than would be seen in natural variation.

### 4.1.6 Current Methods of Sharp Force Trauma Analysis

Although recommendations for recording trauma have been proposed by individuals and organisations such as Boylston (2000), the Scientific Working Group for Forensic Anthropology (SWGANTH 2011), and the Chartered Institute for Archaeologists and the British Association of Biological Anthropology and Osteoarchaeology (Brickley and McKinley 2004; Mitchell and Brickley 2018), they are not always followed and descriptions and interpretations can be inconsistent (Lovell 1997; Martin and Harrod 2015). Boylston (2000) suggest diagrams, descriptions, and measurements are all required for a sufficiently detailed analysis. A lot can be learned from careful analysis and therefore it is important to discover as much as possible about the timing of the injury, the trauma itself, and the type of weapon (Dirkmaat et al. 2008; Vazzana et al. 2018). Unfortunately, in some reports, both past and present, trauma is not the focus, and therefore it is noted, briefly described, and there may or may not be speculation as to possible causes. That level of detail may have been sufficient for that publication, but can leave future researchers without vital information, which is especially detrimental if the remains are no longer available to study. As noted by Reichs (1998), the interpretation that results from SFT analysis will only be as good as the observations themselves.

There are several ways that trauma studies can be classified, though these divisions are neither strict nor exclusive. At the present, a mixture of qualitative and quantitative methods used to analyse trauma and this combination of both methods can be beneficial, such as Łukasik et al. (2019) who used descriptive techniques to record the morphology as well as measurements to quantify the size of the cutmarks (also see Bonney 2014; Vazzana et al. 2018). Some studies rely exclusively on one or the other; generally, qualitative analysis has been more common for SFT analysis than its quantitative counterpart (Bartelink et al. 2001; Bello and Soligo 2008; Bonney 2014; Cerutti et al. 2014; Courtenay et al. 2019). The information provided is equally as important, however the general lack of quantitative measurements and inconsistency through guidelines is often notable.

Some studies collect the data solely to present whereas others statistically analyse the data, and such statistics can be a very beneficial tool when applied appropriately. More recently, studies that are more conventionally descriptive are now integrating statistics into their analyses as well, thus adding a level of scientific validity, such as seen in Boschin and Crezzini's (2012) study in which they statistically group cutmarks into different morphological classifications. With respect to SFT, the picture cannot be complete without qualitative, quantitative, and statistical analysis and there is starting to be a greater push to combine all of them in a holistic approach (such as Courtenay et al. 2019; Maté-González et al. 2019).

Along with a transition to the more balanced use of qualitative and quantitative methods, the use of microscopy is becoming more common and can be beneficial depending on the objectives of the study. There are some macroscopically-visible morphological differences seen between general categories of weapon type with SFT, however, some minute differences can only be observed under magnification, therefore if information such as the type of weapon is required, microscopy is recommended, especially with oblique lighting (Bartelink et al. 2001; Alunni-Perret et al. 2010; Weber et al. 2021). Most accessible are light microscopes and it has been shown that they do a sufficiently good job when basic measurements and analysis of the morphology of the cut marks are required (Figure 52) (Crowder et al. 2013).

Figure 52: An example of a light microscope

The partial or full automation of digital microscopes can be seen as more useful as some can create 3D models through sequentially focusing at different levels within a pre-set range (Keyence Corporation 2014). These digital microscopes create very detailed pictures, however the cost of such equipment and training for its use limits how many archaeologists and researchers have access (Bello and Soligo 2008). Even more detailed but less accessible is Scanning Electron Microscopy (SEM) which uses beams of electrons instead of light and is designed to capture highly detailed images (Bell 2008; Freas 2010). When available, SEM is recommended for use in SFT studies especially if examining microscopic characteristics such as striations (Boylston 2000). However, the equipment required is expensive and when trying to create 3D models, it is laborious and time consuming to use (Bello and Soligo 2008).

Experimental studies on proxies for human bone can have great value in interpreting SFT in both a forensic and archaeological situation. They can be used in forensic anthropology to investigate the possible weapons that could have caused injury. Additionally, this type of study is common in investigations of butchery and tool use in the past. In order to differentiate weapon types or characteristics, these studies often involve microscopy. SEM and digital microscopy studies have been used for many topics in experimental toolmark analysis with variable success in differentiating characteristics of the blades. Blade type, handedness, timing and directionality of blow, material of the blade, and whether marks are peri- or post-mortem have all been investigated (e.g. Bromage and Boyde 1984; Sauer 1998; Smith and Brickley 2004; Bello and Soligo 2008; Nagaoka et al 2008; Thompson and Inglis 2009; Alunni-Perret et al. 2010; Freas 2010; Boschin and Crezzini 2012; Ubelaker and Montaperto 2013; Bonney 2014; Nogueira et al. 2017). These experimental studies are often qualitative or analyse the morphology though the patterns of striations are a common focus. There has been some success in distinguishing differences in blade types using striations (Bartelink et al. 2001; Tucker et al. 2001; Alunni-Perret et al. 2005, 2010; Crowder et al. 2013).

Overall, experimental studies using microscopy can help distinguish classes of blade, such as knives compared to hatchets, or serrated compared to non-serrated blades, however there is usually some overlap seen in categories (Bartelink et al. 2001; Thompson and Inglis 2009; Alunni-Perret et al. 2010; Nogueira et al. 2017). They have allowed some other microscopic differences in cutmark appearance to be noted by investigators. Alunni-Perret et al. (2010) found that knives tended to produce two even edges, whereas hatchets tended to produce one even and one irregular edge. Generally serrated knives leave more striations (Reichs 1998; Crowder et al. 2013). These procedures have also been used in forensic toolmark analysis and can help provide more specific results about the weapon if there is a suspected weapon that can be used for comparison.

To appropriately use the results of experimental studies, the many variables used have to be carefully understood and mitigated as they can affect the outcome (Table 8). Both the properties of the blade and bone used in any experimental studies could cause differences as well (Bartelink et al. 2001). Insufficient consideration or explanation of choices can lead to results that may be misleading. For example, Tucker et al. (2001) used blades that were old and worn, thus calling into question whether the differentiating striations that they found were from the category of blade or from defects accumulated through wear.

Table 8: Factors to consider when interpreting experimental SFT studies

| The Blade | The Experimental Sample |
|---|---|
| - Bevel of blade | - Bone density |
| - Serration | - Bone shape |
| - Wear | - Fleshed or defleshed |
| - Defects in blade | - Treatment to deflesh |
| - Angle of blow | - Provenance of the bone |
| - Force of blow | - Freshness of bone |
| - Speed of blow | - How bone is secured for the experiment |
| - Material of blade | - Species used |
| - Thickness of blade | - The location on the cutmark that is analysed |
| - Type/method of strike (stab, slice, etc) | |
| - Extra movement of the knife (wiggled, twisted, withdrawn differently) | - Compact or cancellous bone |
| | - Sample size |
| - Which hand was used | |

Sauer 1998; Bartelink et al. 2001; Bello and Soligo 2008; Dirkmaat et al. 2008; Thompson and Inglis 2009; Alunni-Perret et al. 2010; Freas 2010; Boschin and Crezzini 2012; Crowder et al. 2013; Ubelaker and Montaperto 2013; Bonney 2014; Nogueira et al. 2017

The increasing use of 3D digitisation in archaeology is opening doors to different methods of examining bones, something reflected in the increasing number of studies involving computed tomography (CT), micro-computed tomography (μCT), and terrestrial laser scanning (TLS) for both qualitative and quantitative osteological research. In forensic science, there is a need for methods that are consistent, reliable, and scientifically proven (Dirkmaat et al. 2008). The ability to digitise skeletal remains, specifically those that have traumatic injuries would allow for new methods of analysis that cannot be performed on the original bone itself. This would also allow for analysis and long-distance collaboration without risk of damaging the collection as recommended by Thompson and Inglis (2009), though not in relation to 3D modelling at that time.

As discussed in Sections 2.4.4 and 2.5, Structure-from-Motion Multi-View Stereo photogrammetry (SfM-MVS) is an emerging method that meets the requirements of collection digitisation for preservation and analysis. There have been recent advances in using close range photogrammetry in the analysis of experimental cutmarks, especially in relation to butchery and carnivore activity, however this field is still emerging and therefore it is critical to find out the benefits and limitations of this method for metric studies on human remains (Maté-González et al. 2017, 2018; Palomeque-González et al. 2017; Yravedra et al. 2017). Maté-González et al. (2017) have demonstrated that close range SfM-MVS models produce statistically similar profiles to 3D digital microscopy and laser scanning confocal microscopy. The project Digitised Diseases is an open access resource of examples of pathological human bones that have been digitised using TLS, CT, and radiography, and it has demonstrated the benefits of being able to share models more easily between institutions for research and education (Wilson 2014).

### 4.1.7 The Interpretation of Sharp Force Trauma

Examining trauma can help reveal information about the events that occurred and the society in which they occurred. Interpretations of the causes of trauma must rely on a knowledge of bone biomechanics and how bone will react to different stresses (Ubelaker and Montaperto 2013). There are three type of information that are important to consider (Lovell 1997):

1. The characteristics of the trauma itself and how that might reveal the weaponry
2. The pattern of trauma in both the individual's skeleton and the population
3. The social, cultural, and environmental context surrounding that burial

#### *4.1.7.1 Interpreting the Weapon*

As mentioned, different types of blades can leave different marks and knowing what weapon caused an injury can be useful in both forensic anthropology and osteoarchaeology (Bonney 2014). This knowledge of the weapon can help determine the type of violence that might have been occurring and the nature of the attack. As discussed in Section 4.1.6, there has been some success in differentiating classes of weapon, using both microscopic and macroscopic techniques, though overlap is usually present (Humphrey and Hutchinson 2001; Bonney 2014; Maté-González et al. 2018). Information about the material of the weapon can sometimes be determined as well as whether a metal blade was serrated (Symes et al. 2012). In the world of forensic science, it may be possible to match an exact blade if a reference weapon is available, but this is unlikely in archaeology so the category of blade is usually as specific as an investigator can be (Houck 1998).

Cerutti et al. (2014) cautions about using the size of the cutmark to specify the exact type of weapon used because there are many other factors that can affect morphology, such as angle of entry. Additionally, the compression and subsequent expansion of bone tissue around a cut when it is created could cause the wound to actually be smaller than the width of the blade. This, however, would be a more pressing consideration with incised cutmarks and when a bone was struck perpendicularly. Sometimes the combination of the size of the cutmark, especially the width and depth, and historical context can help give a more accurate indication of what type of weapon was used.

#### *4.1.7.2 Interpreting the Impact and the Sequence of Events*

Details about a cutmark can provide important information about the violent event. From looking at the bone, certain information can be determined about the nature of the blow that caused the injury. The morphology, location, and direction of the cutmark can sometimes help indicate the general angle at which the bone was hit or which side of the person the assailant was placed (Anderson 1996; Bello and Soligo 2008; Thompson and Inglis 2009; Giuffra et al. 2015; Constantinescu et al. 2017). This is very important for forensic analyses and it can also be valuable in osteoarchaeological analysis when trying to interpret as much as possible about the patterns of warfare in use on that occasion (Kjellström 2005; Šlaus et al. 2010; Nicklisch et al. 2017).

There will always be some uncertainties in SFT trauma analysis in archaeological remains, such as details of exact body position when the individual was hit (see L'Abbé et al. 2019 for a discussion about this regarding BFT). As with many parts of osteology, one problem that trauma analysis can encounter is the limit to which interpretations can be made before crossing into speculation, the latter of which is undesirable (Wakely 1996; Pinheiro et al. 2015). Without *a priori* knowledge of what occurred, the amount of information that can be gathered from skeletal remains may not be sufficient to interpret an exact and detailed account of events, therefore drawing too many precise conclusions may further muddle the record rather than clarify it (Symes et al. 2012; Bartelink 2015).

Additionally, incomplete, fragmentary, and commingled remains present an incomplete set of data, limiting what conclusions can be drawn (Roberts 2000; Kjellström 2005; Loe 2016).

Despite the limitations, the information that can be gathered through a detailed examination of the trauma can be sufficient to reconstruct some possibilities of what may have occurred (Loe 2016). For example, cutmarks on radial and ulnar diaphyses are often thought to be defensive, caused when the victim having raised their arms to shield their face (Judd 2008; Valoriani et al. 2017). In such cases, modern forensic and medical literature can aid in the interpretation, despite them not always being specific to SFT (Ambade and Godbole 2006; Racette et al. 2008; Hugar et al. 2012; Mohite et al. 2013). Sometimes the sequence of blows can be determined based on radiating fractures or placement of the cuts and this can help forensically reconstruct what occurred. The context of the skeletal remains is very important for accurate analysis (Pinheiro et al. 2015).

Regardless of the category of trauma, the pattern of the trauma across a skeleton is important to be able to identify what might have happened (Roberts 2000; Cunha and Pinheiro 2016; Loe 2016; for examples, see Cohen et al. 2015 and Lovell et al. 2016). Cohen et al. (2015) provide a good example of the interpretation of trauma on a skeleton without going too far. They outline three possible scenarios of how the trauma could have occurred using information of the historical context and the osteological data. In situations where the skeletal remains are known to be from a battle, the pattern of wounds can give indications about the type of warfare that occurred, what the targets of the blows were, and whether the attack was likely mounted or on foot (Giuffra et al. 2015). In his paper looking at trauma on Early Medieval skeletons in Ireland, Geber (2015) notes that the placement and pattern of some of the trauma present may indicate certain specific acts of violence, such as a cut aimed to sever the vital structures in the anterior neck or the removal of an ear. Something similar is seen in what is thought to be a case of intentional mutilation from Basingstoke, England (Cole et al. 2020).

A comprehensive study of SFT on a skeleton may aid in determining which blows could have been fatal, helping to reveal manner of death, which is important in both modern and archaeological studies, but SFT analysis often cannot provide an exact cause of death or a motive behind the injuries (Sauer 1998; Appleby et al. 2015; Geber 2015; Loe 2016; Łukasik et al. 2019). It is also important to remember that not all trauma that was present will be seen on the skeleton; for example, SFT to the abdomen might be fatal, but might not damage any bone, thus remaining skeletally invisible (Kjellström 2005; Brødholt and Holck 2012; Kemp et al. 2013; Giuffra et al. 2015). A modern study of non-accidental sharp force trauma has shown the outcome of the injuries can be extremely unpredictable and random (Kristoffersen et al. 2016). Regardless of these limitations, when interpreted with the appropriate level of caution and with contextual background, important and compelling arguments for the events that occurred can be made.

#### *4.1.7.3 Interpreting the Trauma in a Broader Context*

In addition to the actual trauma on the bones and the location of the burial, the cultural context is important too (Boylston 2000; Roberts 2000; Nagaoka et al. 2008; Judd and Redfern 2012; Martin and Harrod 2015). Roberts (2000) advocates for a holistic biocultural approach when interpreting trauma. Information such as whether injured individuals were buried together could indicate that they were likely all victims of the same event (Giuffra et al. 2015). Large amounts of healed trauma in addition to peri-mortem trauma could suggest a 'professional' soldier/warrior or an individual having been repeatedly exposed to high levels of interpersonal violence. If there are known historical events that could have led to injuries seen, they may suggest possible causes though care must be taken not to over-interpret the data (Houck 1998; Judd and Redfern 2012; Symes et al. 2012; Martin and Harrod 2015). Sometimes the trauma on a skeleton can be connected to a specific historical event, such as from the Battle of Towton (March 1461) or the Battle of Visby (July 1361), however this is rare and it may be problematic to make such connections if there is a level of uncertainty (Ingelmark 1939; Thoremann 1939; Wakely 1996; Novak 2000a). Events must be interpreted objectively to provide the most accurate assessment possible (Martin and Harrod 2015). Some burial practices such as cremation are not highly conducive to trauma studies and therefore levels of trauma found in populations that used such burial techniques may be under-represented (Boylston 2000; Martin and Harrod 2015).

Trauma studies are often used to try to interpret behaviour in society and the levels of violence that may have been present because skeletal trauma is said to be the most direct evidence of violence (Martin and Harrod 2015; Łukasik et al. 2019). Interpersonal injuries can be identified, but the intent behind the injury is not often possible to determine in the archaeological record though there are some exceptions, such as battles or massacres. In general, SFT has been noted as an indicator of interpersonal violence more consistently than BFT (Šlaus et al. 2012; Krakowka 2017). Trauma can be both between members of the same group or between groups and differential treatment of groups can sometimes be noted through different trauma patterns (Šlaus et al. 2010; Martin and Harrod 2015). The sociocultural implications of interpersonal violence are important to consider both when interpreting the events that may have occurred and the society in which they occurred (Lovell 1997). The levels of violence in a society can be reflective of the stability of that society (Krakowka 2017).

## 4.2 Archaeological Decapitations and Mass Graves

In some cases, the individuals who have met with a violent end have subsequently been buried in methods outside the societal normal for that culture at that time and the Weymouth Ridgeway Vikings could be considered a dramatic example of this. Non-normative burials, sometimes called deviant burials, have been observed amongst geographically and chronologically diverse contexts and may in some form have been common to all cultures (Sledzik and Bellantoni 1994; Aspöck 2008; Murphy 2008; Tsaliki 2008; Reynolds 2009; Harte 2011; Gardeła and Kajkowski 2013; Riisøy 2015; Gregoricka et al. 2017; Miccichè et al. 2019). In post-7th century Anglo-Saxon England, these sites are often on hilltops, near or on prehistoric monuments, and they are often visible from local roadways or waterways (Reynolds 2009). Another distinctive characteristic is that they are often situated near the boundaries of counties, borough, or hundreds (Buckberry 2008; Reynolds 2009; Harte 2011; Williams 2015; Lavelle 2016).

Books by Reynolds (2009) and Murphy (2008) delve further into this world, however the focus in the subsequent sections will be on mass graves and decapitations; both considered non-normative in Anglo-Saxon England and relevant to the Weymouth Ridgeway Vikings. As listed by Reynolds (2009), there are eight factors that may explain the reasons behind deviant burials and are thus important to their interpretation: battle, execution, massacre, murder, plague, sacrifice, suicide, and superstition. Other indicators of deviant burials are variables such as the location, depth of the grave, if the individual was bound, or if the individual was placed in a prone position (Sîrbu 2008; Tsaliki 2008; Reynolds 2009; Kępa et al. 2013; Riisøy 2015; Gregoricka et al. 2017). Sometimes deviant burials are associated with overkill as well, demonstrating more injuries, or more severe injuries, than would have been required to kill the individual. This can be seen in both mass burial related to the battles, such as the Battle of Towton (see Sections 4.2.3 and 9.7), and individual burials (Fiorato et al. 2000; Murphy 2008). There are many speculations as to the reasons why these people viewed as ‘others’ were buried so differently; for example, a mark of shame, superstition, punishment, contempt, or to make them atone (Balter 2005; Aspöck 2008; Taylor 2008; Tsaliki 2008; Reynolds 2009; Harte 2011; Gardeła and Kajkowski 2013; Tucker 2013; Carty 2015).

### 4.2.1 Decapitations

Decapitations are found throughout the burial record and are considered to be deviant of the typical burial pattern (Pitts et al. 2002). They have been found as single burials all the way through to mass burials (Pitts et al. 2002; Taylor 2008; Caffell and Holst 2012; Loe et al. 2014b). Decapitation burials can usually be identified through the displacement of the head or characteristic damage (Waldron 1996). Any displacement must be carefully considered to exclude the possibility of movement during taphonomic processes. This starts to appear in the burial record in England in Roman and Anglo-Saxon times (Boylston 2000; Mattison 2016).

There are differences in the types of decapitations that are found and they are not always easy to distinguish. There are burials found where the individual was decapitated post-mortem, likely after skeletonisation, and in cases like this, it is rare that any vertebrae will be with the skull and there may not be any evidence of toolmarks. As appears to be the case with the Weymouth Vikings, there are also burials where the individual was either killed by the decapitation or was decapitated shortly after death with the decapitation directly related to the burial rite. These two are often more difficult to differentiate because in both cases sharp force trauma may be present (Section 4.1.4) (McKinley et al. 1993; Buckberry 2008; Taylor 2008). Additionally, the upper vertebrae and mandible will often be with the skull, articulated (McKinley et al. 1993; Buckberry and Hadley 2007; Taylor 2008). Heavy, chopping blows, often multiple, tend to be seen more in burials where decapitation was the manner of death (Tucker 2013). Decapitations with many blows to the head or excessive violence could be an indication of a formalised or judicial execution (Reynolds 2009). If the only cuts that are found are small, incised cuts it is possible that the head was removed after death for ritual purposes (Tucker 2013).

The sharp force trauma that is present in decapitation can change based on variables such as the position the individual was in, the weapon used, and whether done peri- or post-mortem (Waldron 1996; Buckerry and Hadley 2007; Carty 2015). Many osteological reports of decapitated skeletons describe the trauma present on each, but a pattern of trauma on each bone has not been firmly established (see McKinley et al. 1993; Waldron 1996; Buckerry and Hadley 2007; Buckberry 2008; Taylor 2008; Loe et al. 2014b; Geber 2015). In this study, there is the potential to investigate decapitation-specific trauma patterns since the collection has a large number of individuals who were decapitated in the same event (Section 5.1 and 9.6).

The locations that trauma is commonly found on decapitated skeletons is the cervical vertebrae, the mandible, and the base of the cranium (McKinley et al. 1993; Waldron 1996; Buckerry and Hadley 2007; Cessford et al. 2007; Buckberry 2008; Taylor 2008; Tucker 2013). What was done with the head itself varies; there are individuals whose heads were not buried with them and have not been found, there are heads that have been placed back in anatomical position, and there are heads that have been placed in various locations around or on the body. Sometimes the head is ‘replaced’ with something like a stone (Taylor 2008). Overall, it seems like the removal of the heads is important enough that if they were not completely successful in one strike, they would continue until the head was fully severed (Tucker 2013).

### 4.2.2 Mass Burials

Mass graves are considered an exception in burial practice which goes against conventional burial practice in European societies (Kjellström 2013). The number of individuals that comprises a mass grave can vary considerably (Figure 53) (e.g. Loe et al. 2014a, 2014b; Constantinescu et al. 2017). It could indicate that the deaths were a public spectacle (Kjellström 2013). Judicial executions have been a public spectacle throughout history, both as punishment and a deterrent (for a more comprehensive discussion of executions in early medieval England, see Mattison 2016).

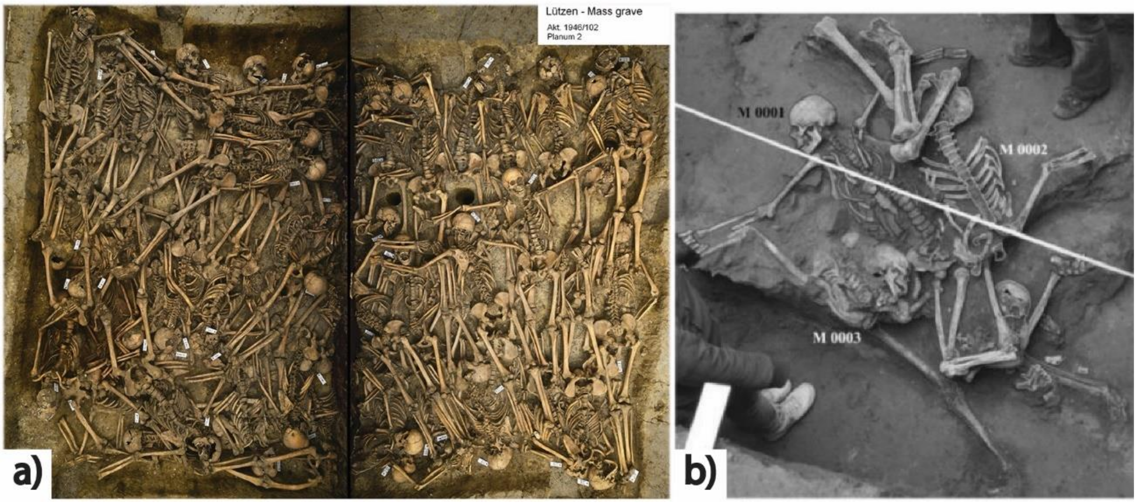


Figure 53: Two examples of mass graves from a) Lützen and b) Bucharest (Nicklisch et al. 2017, Fig. 2, p.11 and Constantinescu et al. 2017, Fig. 2, p.109)

However, with mass burials, it is important to remember that the circumstances of the burial could seriously affect the way in which the individuals were interred. Mass graves can be a result of a number of different circumstances such as a battle, a massacre, a natural disaster, a mass casualty accident, or a disease. Additionally, the individuals who buried the dead are important because it can make a difference to how they were buried; whether it was compatriots, kinsmen, perpetrators, opponents, or locals who may never have interacted with those dead whilst they were living (Reynolds 2009; Šlaus et al. 2010; Loe et al. 2014a; Nicklisch et al. 2017). All these factors can be reflected in the amount of care that appears to have been used when burying the bodies; some demonstrate organised alignment whereas other sites appear chaotic and uncaring (Section 9.7.8). A high level of organisation might indicate compatriots or neutral parties buried the bodies, or if they were buried by an enemy, that was with respect. It might also suggest the need to systematically bury the dead after a disaster. A chaotic burial might demonstrate burial by a disrespectful enemy or the need for a fast burial due to a large number of dead, or the presence of disease, which could create unsanitary conditions if left.

### 4.2.3 Selected Comparative Sites

Although the type of burial found on the Weymouth Ridgeway is rare, there are multiple instances of mass graves and cemeteries being found containing an unusually high number of individuals with evidence of SFT or violent deaths. Table 9 contains a select list of some such examples.

Table 9: A list of selected sites that were mass burials, had high levels of trauma, or both. The time period ranges from the 1st C to 17th C and is primarily focused on Europe (amended from Constantinescu et al. 2017, Table S4)

| Location | Type of burial | Number of Individuals | Time Period | Publication |
|---|---|---|---|---|
| Aljubarrota, Portugal | Ossuary | 400 | 1385 Battle of Aljubarrota | Cunha and Silva 1997 |
| Bucharest, Romania | Mass grave | 3 | $16^{th}$-$17^{th}$ C | Constantinescu et al. 2017 |
| Čepin, Croatia | Cemetery | 147 | 1441 | Šlaus et al. 2010 |
| Driffield Terrace, England | Cemetery | 82 | $1^{st}$ to $4^{th}$ C | Caffell and Holst 2012 |
| Fishergate, England | Cemetery | ~48 | Late $10^{th}$ – $12^{th}$ | Stroud and Kemp 1993 |
| Gołańcz, Poland | Mass grave | 25 | 1656 Battle of Gołańcz | Łukasik et al. 2019 |
| Krakow, Poland | Mass grave | 4 | Mid-$17^{th}$ C (possibly 1657) | Kępa et al. 2013 |
| Lützen, Germany | Mass grave | 47 | 1632 Battle of Lützen | Nicklisch et al. 2017 |
| Mohács, Hungary | Mass grave | 353 | 1526 | Zoffmann 1982 |
| Niesulice, Poland | Mass grave | 3 | $14^{th}$ C | Dziedzic et al. 2011 |
| Öland, Sweden | Shipwreck | 150-200 | 1676 Man-of-war *Kronan* | During 1997 |
| Oslo, Norway | Cemetery | 337 | 1050-1540 | Brødholt and Holck 2012 |
| Sandbjerg, Denmark | Mass grave | 60 | 1300-1350 | Bennike 2006; Boucherie et al. 2017 |
| Sidon, Lebanon | Mass grave | 25 | $13^{th}$ C (possibly 1253 or 1260) | Mikulski et al. 2021 |
| St John's, England | Mass grave | ~35 | Late $10^{th}$ C | Pollard et al. 2012 |
| Towton, England | Mass grave | 38 | 1461 Battle of Towton | Fiorato et al. 2000 |
| Turin, Italy | Cemetery | 113 | $10^{th}$-$11^{th}$, $15^{th}$ C | Giuffra et al. 2015 |
| Uppsala, Sweden | Mass grave | 60 | 1440-1650 Battle of Good Friday (1520) | Kjellström 2005 |
| Vadum Iacob | Mass grave | >5 | 1096 | Mitchell 2013 |
| Visby, Sweden | Mass grave | 1185 | 1361 Battle of Visby | Ingelmark 1939 |
| Weymouth Ridgeway, England | Mass grave | 50 | 970-1025 | Loe et al. 2014b; This study |

| Location | Type of burial | Number of Individuals | Time Period | Publication |
|---|---|---|---|---|
| Wittstock, Germany | Mass grave | 125 | 1636 | Eickhoff et al. 2012 |
| York, England | Mass grave | 113 | 17$^{th}$ C (possibly 1644) | McIntyre 2017 |

A select number of sites of comparative importance will be discussed here, specifically Walkington Wold (E Yorks), Driffield Terrace (N Yorks), Towton (N Yorks), and Visby (Sweden). Unfortunately, due to the COVID-19 pandemic, the full osteological report for St John's was unable to be obtained.

Although not a mass burial, Walkington Wold contains burials from 640 to 1030 which have evidence of decapitation (Buckberry and Hadley 2007; Buckberry 2008). Thirteen individuals were analysed, all of whom were either male or indeterminate, and a majority of whom were young to prime adult. Some of the skulls were left with, presumably, their skeletons, but some were moved around and are missing. The possibility of the use of heads as trophies or head-stakes is discussed due to the mismatch in the number of mandibles and individuals present, though there is no evidence of osteological to suggest it (Buckberry and Hadley 2007; Buckberry 2008). Decapitation trauma was seen on mandibles and vertebrae, some individuals presenting with multiple cutmarks. It has been interpreted as an Anglo-Saxon execution cemetery (Buckberry and Hadley 2007; Buckberry 2008; Reynolds 2009).

Driffield Terrace is of earlier date than the time period of interest in this study because it dates to Roman Britain, however it has such a high number of decapitated burials, it needed to be considered as well (Caffell and Holst 2012). Of the 72 skeletons (commingled excluded), 70.8% show either osteological or contextual evidence for decapitation. The contextual evidence typically relates to the head being placed in a position that is not possible anatomically. In cases where the mandible and some cervical vertebrae are still attached, it becomes unlikely this placement would be due to any factor such as animal activity or burial disturbance (Caffell and Holst 2012). Osteologically, many had cuts to the cervical vertebrae, mandible, or both, however the majority were decapitated with one blow. In a couple instances, cutmarks were seen on the cranium, likely from blows intended to decapitate but not accurately aimed (Caffell and Holst 2012). Demographically, the majority of the burials were young males and there were some cases of previously healed trauma, typically BFT. Caffell and Holst (2012) have said it is likely these individuals were some form of military or engaged in fighting, but the exact details cannot be known.

In contrast to the Driffield Terrace collection, Towton and Visby have no decapitation, but high amounts of battle-related trauma. The Battle of Towton took place in March 1461 with the Lancastrian army being routed. In 1996, a mass burial of 37-38 male skeletons, mainly from ages 16-45, was found, many with severe trauma (Fiorato et al. 2000). There are good examples of the extent of damage a sword can do as well as the types of marks left by penetrating weapons, such as halberds or lances. From the patterns of trauma, it appears all the individuals were killed during the battle and the healed injuries found suggest they were likely professional soldiers (Fiorato et al. 2000).

Visby was also a battle (Battle of Visby, July 1361), however the compositions of individuals was different as it was a professional army against locals (Ingelmark 1939). Approximately 1185 individuals were found across three mass graves. The bones examined were mainly as disarticulated as the magnitude of the task of reassociating skeletons across multiple years of excavations was likely deemed too great relative to the data that would have been provided (Ingelmark 1939). This unfortunately means that there is no individual patterning for the site, however there are overall patterns that were examined. The majority are males, though many os coxae were not in a condition for sex to be determined. A small number of possibly female os coxae were found. The ages of the individuals spanned from adolescent to older adult and the three graves each had a different composition of ages. Ingelmark (1939) suggests this indicates the local army was comprised of nearly the entire male population, both old and young, in many states of health. The SFT injuries (N=456) that are seen are consistent with a brutal battle, with many deep cutmarks on limbs and crania indicating close-combat (Ingelmark 1939).

The remains found at St. John's, Oxford, are also useful for comparative purposes (Also noted in Section 3.3.2 in relation to the St Brice's Day Massacre) (Pollard et al. 2012). Dating to the late 10$^{th}$ century, isotopic signature and aDNA analysis suggest the individuals (33 males, 2 juveniles) found in a chaotic mass grave were Vikings. They suffered from SFT and many had evidence of ante-mortem trauma. These men were generally young or prime adults, between 16 and 35 and possibly professional soldiers (Pollard et al. 2012). There was some evidence they might have been exposed to burning around the time of death. There was no evidence of decapitation in these cases, but the event that caused their deaths was clearly violent and likely a mass execution (Pollard et al. 2012).

All of these sites provide interesting comparisons for the site being researched here as they are generally from a similar time period, when metal, bladed weapons were primarily used, and show comparable trauma and/or burial patterns. These sites will be discussed alongside the osteological findings (Chapter 7) in Chapter 9.

## 4.3 Summary

A good knowledge of bone properties and biomechanics is vital to the successful interpretation of trauma. SFT is typically considered a less equivocal indicator of inter-personal violence than the other types of trauma as it is less likely to be accidental. There are many methods used to analyse and report trauma; macroscopically and microscopically, qualitatively and quantitatively, statistically, or through a combination of these. Studies that investigate trauma are usually either focused on experimental trials or reporting the trauma from a site or individual. Either of these categories could benefit from a fast, accessible, and accurate method of digitising cutmarks, such as SfM-MVS photogrammetry (Chapter 3). The analysis of SFT on skeletons can be revealing about societies and the violence that was present within them. Sometimes these wounded skeletons can be linked back to historical events, and having an osteological record of those occurrences can augment knowledge about what occurred. The interpretations that are made about the weapons, sequences of events, and the trauma in a broader context must all be made with appropriate caution as the over-interpretation of SFT can lead to erroneous conclusions. This chapter addressed Objective 1 (Section 1.3.1) by providing background to the field of osteological trauma analysis and discussing methods and collections that have been examined in later chapters (Objectives 8 and 9):

- Sharp force trauma, the focus of this project, tends to present as thin linear cutmarks (incised) or cutmarks that have transected the bone (shaved)
- There are many factors to consider when interpreting trauma regarding things such as the cutmark itself, how it was caused, and the contextual or historical evidence
- SFT analysis typically relies on manual measurements and microscopy is sometimes used, however 3D techniques have recently been shown to be an asset to this type of analysis and should be further investigated in order to be made more accessible
- Mass burials and sharp force trauma are found together in the archaeological record and indicate a burial outside of societal conventions, leading to implications about the events that occurred, such as seen with the Weymouth Ridgeway Vikings
- By further exploring the SFT from a mass burial in relation to other similar collections, further interpretations can be made about the event

# 5 Materials and Methods

Within this chapter, the collection that was used and its background will be presented. The prior work will be outlined, with a focus on the elements that are pertinent to this study. This is followed by a discussion of the methods used to create the models and how the models are further analysed. This portion begins with the pilot studies where the workflow was developed and then progresses to the full collection methodology.

## 5.1 The Collection

The collection used in this study were the ‘Weymouth Vikings’ (site code WEY08). They were discovered and excavated in 2009 during the building of the Ridgeway Hill Relief Road near Weymouth, Dorset. Monographs about the site and the skeletons were published in 2014 (Brown et al. 2014; Loe et al. 2014b). They have not been studied since the initial report, apart from an aDNA study and an on-going PhD project regarding dental wear by K. Faillace (Cardiff University) (Margaryan et al. 2020).

### 5.1.1 Site Background

The site was on the top of Ridgeway Hill along the South Dorset Ridgeway at NGR SY 672 859 (Figure 54) (Tamminen et al. 2019). It was immediately east of the A354, near the Roman road running from Dorchester (*Durnovaria* at the time) to Radipole, Weymouth, within the boundaries of the Domesday Cullifordtree Hundred. The geology in that area is Upper Chalk of the Cretaceous period which had roughly 0.3m of ploughsoil over the top (BGS 2021). The grave itself was 7.m by 6.8m, slightly longer in the north-south direction. The maximum depth of the pit was 1.66m, however it had been partially infilled when the remains were deposited and therefore the maximum depth of the human remains was about 0.75m. The pit is thought to have originally been a small-scale Roman quarry pit, one of a number found throughout the excavated area.

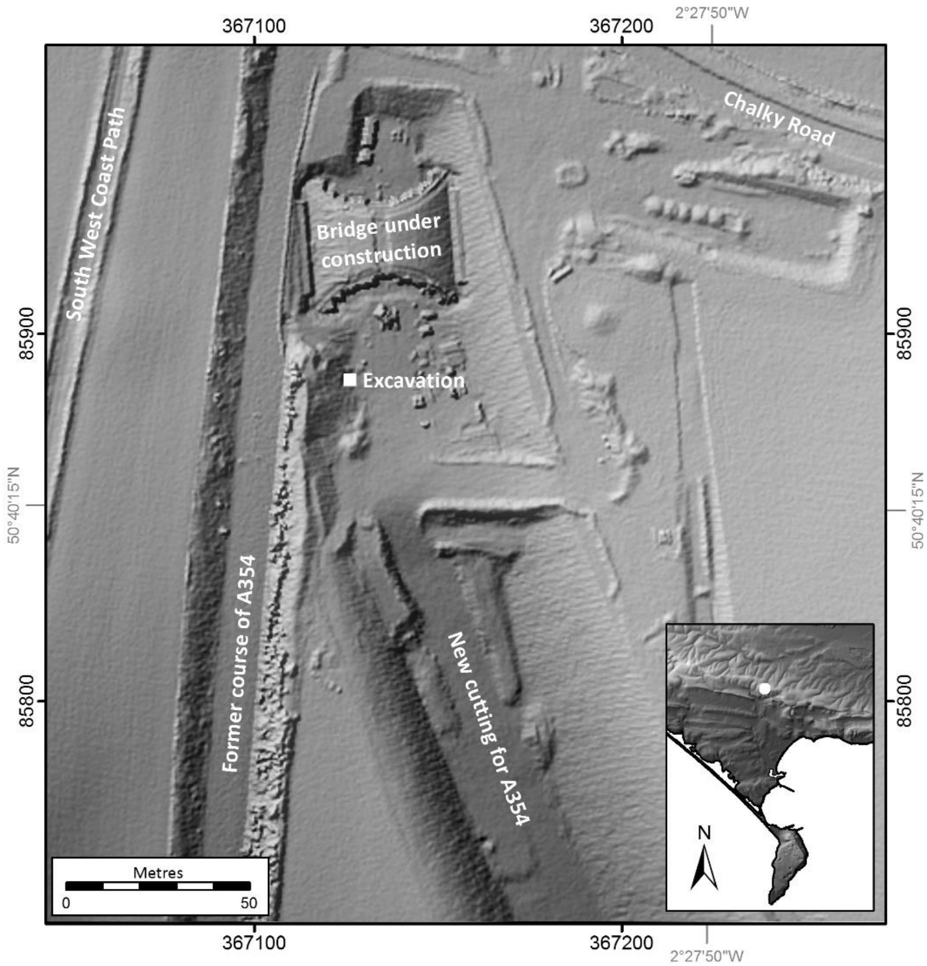


Figure 54: Location of the excavation as seen in Airborne Laser Scanning (ALS) data (via the Environment Agency for England & Wales) acquired December 2009 & January 2010 during the construction of the Weymouth Relief Road (A354). Contains OS data © Crown copyright and database right (2019). British National Grid (BNG) projection, Airy 1830 ellipsoid, Ordnance Survey 1936 datum (Tamminen et al. 2019, Fig. 1, p.81)

### 5.1.2 Demography

The demographics for the collection will be treated in two discrete parts: cranial remains and postcranial remains (Table 10).

Table 10: Number and preservation of individuals (information from Loe et al. 2014b)

| Characteristic | Cranial | Postcranial |
|---|---|---|
| Most Likely Number of Individuals (MLNI) | 47 | 52<br>17 complete skeletons<br>23 partial skeletons<br>25 isolated extremities* |
| Preservation | Good | Good |
| Completeness | 51-75% | 26-100% |
| Fragmentation | High (machine damage from excavation) | Moderate to high |

*Associations with the partial skeletons and other isolated extremities unknown

For this study, both 47 and 52 are used as the most likely number of individuals (MLNI), however, 52 is given priority because it is highly probable there were an equal number of bodies and heads when the individuals were decapitated. The calculation of MLNI was performed since it can be considered more statistically accurate than minimum number of individuals (MNI) (equation from Adams and Konigsberg 2004, 2008; calculations done by Loe et al. 2014b).

$$MLNI = \frac{(left + 1)(right + 1)}{(paired + 1)} - 1$$

All demographic information was obtained by Loe et al. (2014b) and is presented in Tables 11 and 12. Wherever possible, sex and age were determined and are presented in their respective cranial or postcranial sections.

Table 11: The results of the sex determination of the cranial and postcranial remains (information from Loe et al. 2014b)

| Category | Number | |
|---|---|---|
| | Cranial | Postcranial |
| Male | 43 | 31 |
| ?Male (and ??Male) | 4 | 5 |
| Indeterminate | 0 | 0 |
| ?Female (and ??Female) | 0 | 0 |
| Female | 0 | 0 |
| Unable to sex – preservation | 3 | 4 |
| Total | | |
| *Contexts analysed* | 50 | |
| *Discrete skeletons* | | 40 |

Table 12: The results of the age determination of the cranial and postcranial remains (information from Loe et al. 2014b)

| Category | Number | |
|---|---|---|
| | Cranial | Postcranial |
| Adolescent (13-17) | 0 | 8 |
| Young Adult (18-25) | 21 | 10 |
| Prime Adult (26-35) | 10 | 9 |
| Mature Adult (36-45) | 9 | 6 |
| Older Adult (>45) | 2 | 3 |
| Adult (>18, unable to further determine) | 8 | 4 |
| Sub-Adult (<18, unable to further determine) | 0 | 0 |
| Total | | |
| *Contexts analysed* | 50 | |
| *Discrete skeletons* | | 40 |

#### *5.1.2.1 The Cranial Remains*

From the cranial remains, the temporal bones were used to calculate the number of individuals. A total of 45 right, 40 left and five disarticulated (three right and two left) were found resulting in an MNI of 48. The MLNI that was established for the skulls was 47 (Loe et al. 2014b). No individuals presented as female and the largest group represented was young adults, followed by the prime adults (Table 12). Metric and non-metric trait assessments and data on dental and cranial pathology was collected as well and can be found in the monograph. Peri-mortem trauma was also recorded (see Section 7.1 for updated tables).

#### *5.1.2.2 The Postcranial Remains*

For the postcranial remains, a MNI was calculated based on the distal right femur. A total of 46 right were found, 31 of which were pairs. In the disarticulated remains, a total of five highly likely pairs were found, leading to an overall MLNI of 52 (Loe et al. 2014b). No remains were identified as female, however several did not have sufficient elements to determine sex (Table 11). Young adults, prime adults, and adolescents were the largest categories (Table 12). Stature, robusticity, handedness, non-metric traits, and ante-mortem pathology and trauma were all investigated as part of the monograph however are not the focus of this study. Peri-mortem trauma was investigated as well (see Section 7.1 for updated tables).

### 5.1.3 Geographic Origin and Health Status

#### *5.1.3.1 Dating and Geographic Origin*

During the original analysis, radiocarbon dating was performed and the results are presented in Table 13. From the isotopic analysis, it was seen that the individuals consumed some marine protein, however, it was argued that the amount they ate would not have significantly altered the radiocarbon dates, a theory which is reflected in the consistency of the three values. Additionally, because of the Vikings' mobility, it is unlikely they would have maintained the same diet over their whole lives.

Table 13: The radiocarbon dating from WEY08 performed at the Scottish Universities Environmental Research Centre (SUERC) using OxCal 1.4.7 and atmospheric data from IntCal13 (Reimer et al. 2013)

| SK Number | SUERC Number | Bone | Dates BP* | Calibrated Dates* |
|---|---|---|---|---|
| 3689 | 24206 | Right Tibia | 1055 +/- 40 | 890-1020 |
| 3763 | 27339 | Left Fibula | 1090 +/- 30 | 890-1040 |
| 3804 | 27335 | Left Fibula | 1005 +/- 30 | 970-1160 |
| Weighted mean | | | 1045 +/- 19 | 970-1025 |

*A probability of 95.4% is noted

Isotopic analysis was performed using both bones and teeth. The former was performed on a total of 40 individuals and the latter on 31 individuals using only one tooth from each skeleton, typically the most distal molar present. The isotopes that were investigated were oxygen ($\delta^{18}O$), strontium ($^{87}Sr/^{86}Sr$), carbon ($\delta^{13}C$), and nitrogen ($\delta^{15}N$). Full techniques can be found in Chenery et al. (2014) and Loe et al. (2014b). General findings are presented in Tables 14 and 15. Overall, the majority of the individuals were most likely originally from outside the British Isles and many appear to have lived in various locations in Northern Europe and Scandinavia before their deaths (Section 5.1.3.2 and Appendix C).

Table 14: The results of the isotopic analysis of the origins of WEY08 (information from Loe et al. 2014b) with italicised SK numbers indicating aDNA analysis

| Birth Region | Number (N=31) | Potential Locations | Skeleton Numbers |
|---|---|---|---|
| Potentially local | 5 | Weymouth area, England/United Kingdom, Denmark | 3725; 3726; 3729; 3752; 3757 |
| *Potentially local but not around Weymouth* | 3 | Devon, Cornwall, west coast of the Lake District, Denmark, north east Scotland, southern Norway | 3726; 3729; 3757 |
| Outside the British Isles | 26 | Scandinavia (not Denmark), Baltic States, Northern Germany and Poland, Belarus, Russia | |
| *Very cold regions* | 5 | Arctic Norway, Sub-arctic Scandinavia, very high altitudes in Europe | 3694; 3711; 3712; 3747; 3759 |
| | 1 | South of Baltic, Western Russia, coastal Northern Scandinavia | 3759 |
| | 1 | Sub-Arctic Scandinavia, parts of Russia or Ukraine | 3747 |
| | 1 | Northern Scandinavia, Iceland, parts of Russia | 3694 |
| *Cold regions* | 21 | Baltic Shield of Norway, Sweden, Finland, some areas of Denmark, south of the Baltic Sea | |
| Younger geological terrain | 11 | Southern and western Baltic, eastern Russian, Belarus, coastal north-eastern and eastern Denmark, southern Sweden | 3696; 3706; 3710; *3722*; 3730; *3733*; 3738; *3739*; *3744*; *3746*; 3758 |
| | 5 | Coastal Eastern Denmark, Southern Sweden, Western Baltic | 3706; 3710; *3733*; 3738; 3758 |
| | 6 | Baltic east of River Vistula | 3696; *3722*; 3730; *3739*; *3744*; *3746* |
| Older geological terrain | 10 | Mid-latitude Scandinavia, some areas in eastern Germany and the Czech Republic/Slovakia | 3704; 3705; 3707; 3720; 3724; 3743; 3749; 3751; 3760; 3761 |
| | 2 | Not specified further | 3705; 3743 |
| | 3 | Not specified further | 3707; 3720; 3749 |
| | 1 | Not specified further | 3724 |
| | 1 | Not specified further | 3760 |

Table 15: The results of the isotopic analysis of the mobility of WEY08 (information from Loe et al. 2014b)

| | Number (N=38*) | Potential Locations | SKs |
|---|---|---|---|
| Habitation up to 15 years prior to death | | | |
| *Very cold climates* | 26 | Scandinavia, north-eastern Russia | 3687; 3689; 3716; 3719*; 3763; 3764; 3768*; 3775; 3777; 3778; 3781; 3784*; 3786; 3791; 3792*; 3794; 3795; 3796; 3798; 3800; 3801; 3804; 3806; 3809; 3810; 3811 |
| Extremely cold climates | 6 | Arctic, high altitudes | 3687; 3763; 3786; 3791; 3804; 3806 |
| *Cold climates* | 12 | Mid-south Scandinavia (not southern-most Norway, Sweden, not Denmark), eastern Russia, Belarus | Not specified |
| Habitation within 2-5 years prior to death | | | |
| *Cold climates* | 13 | Sub-arctic regions of Scandinavia | 3688; 3689; 3762; 3770; 3775; 3778; 3781; 3790; 3796; 3800; 3806; 3809; 3810 |
| *Less cold climates* | 25 | Mid-south Scandinavia (not southern-most Norway, Sweden, not Denmark), western Russian, Belarus, northern Iceland | Not specified |
| Migrated prior to arrival at Weymouth | 6 | Generally moving from colder to less cold / cold to warmer<br>Mid-south Scandinavia (not southern-most Norway, Sweden, not Denmark), Belarus, western Russia, northern Iceland | 3687; 3764; 3786; 3791; 3804; 3806 |

*38 total, 31 paired rib and femur samples; denotes unpaired samples

### *5.1.3.2 Ancient DNA (aDNA)*

Since the publication of the monograph, ten of the skulls have been tested as part of a large Viking aDNA study (Margaryan et al. 2020). Of those that were tested, only five also had isotopes analysed and all of these were ones with average values within the group and all were from within the same grouping of likely origin (Italicised in Table 14). All of the oxygen values suggested an origin of outside of the UK and most of the nitrogen values for these five had similar results, with values above the upper limits for the UK and below the upper limits for Denmark. All were within the range of values for 'Cold Regions'. All ten successfully had DNA extracted and details from Margaryan et al. (2020) on those individuals are in Appendix C. When looking at the regional contributions to the DNA, all the individuals present with a mixture of geographical affinities which supports the idea of gene flow throughout Scandinavia for generations prior (Margaryan et al. 2020). In general, the three highest components are 'North-Atlantic type', 'Danish type', and 'Norwegian type' which generally aligns with what is expected. 'Swedish type', 'Polish type' and 'Finnish type' have the lowest contributions across the ten individuals.

#### *5.1.3.3 Physical Health and Attributes*

The Vikings were generally taller in stature than contemporary British populations, but similar to contemporary Scandinavian populations (Loe et al. 2014b). Overall, they are a very robust group of individuals, many with notable muscle attachments. They have an interesting phenomenon commonly in their clavicles at the costoclavicular ligament attachment and in the humerus at the bicipital groove where the muscle attachments there are notable but have a lytic appearance. This is seen in some other populations housed at Bournemouth University, specifically on a collection of royal navy sailors. Generally, they were found to be more notably robust in their upper bodies, perhaps suggesting that the activities they did required upper body strength or movement. Additionally, some of the joints of the upper body had pathologies that can be associated with activity, such as osteoarthritis or osteochondritis dissecans. Their overall young age profile and the relative dearth of healed ante-mortem trauma may suggest that they were either a relatively newly assembled force or they were not professionals.

Skeletal collections, such as this one, that are classified as having 'catastrophic' rather than 'attritional' profiles provide opportunities to study the health of individuals who died when they were still in their prime. The pathologies that are found on these individuals are more likely to be related to occupation and general health status than related to aging. The vertebrae of many individuals reflect they likely had a hard life of work; Schmorl's nodes and osteoarthritis are commonplace and Scheuermann's disease is seen. There is evidence of non-specific infection in the form of periostitis and a case of osteomyelitis. Loe et al. (2014b) re-iterates that this does not mean these individuals were of "…weak constitution…" (p.214). On the contrary, the opposite argument could be made as they were all still alive; whatever hard life they might have endured prior to this had not killed them. Additionally, there are few indicators associated with the cessation of growth during childhood, suggesting they were adequately nourished, or at least never malnourished to an extent that it affected their skeletons.

## 5.2 Stage One: Initial Analogue Analysis of the Collection

To begin the discussion of the current research project, the definition of 'cutmark' compared to 'blow' must be discussed first. Here, a cutmark is any defect made by the blade, whereas a blow is all cutmarks made by a single strike of the weapon (Section 4.1.4). Therefore, in this study, a cutmark will not extend beyond one bone, but a blow will.

The initial step of this study was to look through the collection manually to make sure all the cutmarks were identified (Figure 55, Figure 115 in Appendix D). This was done by examining each bone for each skeleton and noting any trauma before comparing the findings with the osteological report (Loe et al. 2014b). Any discrepancies were re-checked with magnification (Section 4.1.6) and a second opinion was obtained if required. During this time, the cutmarks were classified. Please see Table 16 for the working definitions of the categories of cutmarks found in this study. For this research, the cutmarks were only classified into two main groups, one with a subgroup. These categories were used for ease with the development of the photogrammetric process; regardless of the unique properties of each cutmark, the geometry required for image capture within each group was the same.

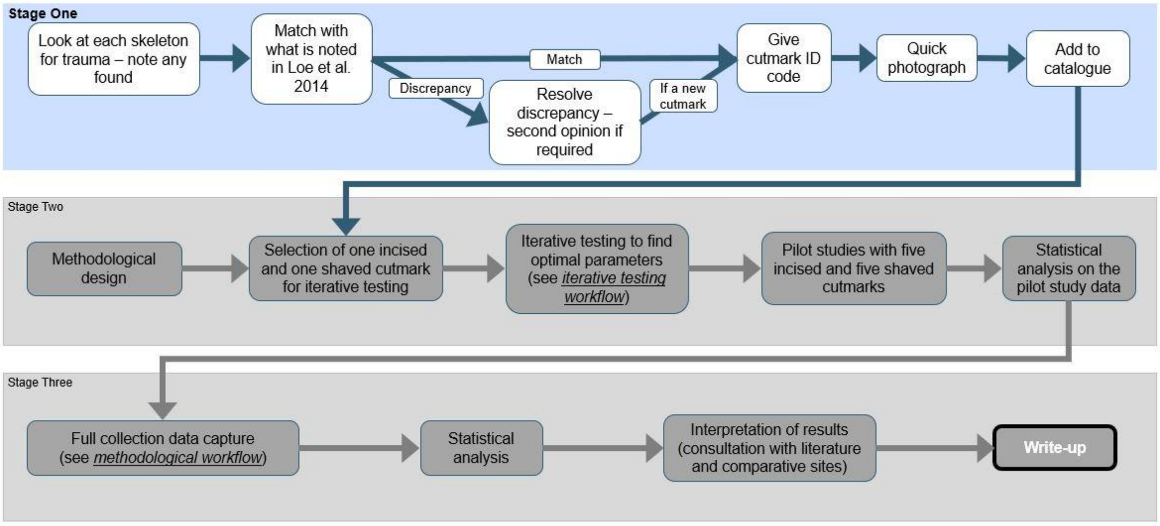


Figure 55: The workflow for the study with Stage One highlighted (Appendix D Figure 115 for the full workflow without highlights)

Table 16: The definitions for different types of cutmarks found in the collection

| Term | Characteristics |
|---|---|
| Incised Cutmark (I) | - V-shaped profile<br>- Did not bisect the bone<br>- Force did not cause the bone to break |
| Shaved Cutmark (S) | - No distinct profile<br>- Bone fully bisected by the blow |
| *Broken Incised Cutmark (BI)* | - Originally V-shaped profile<br>- Cut did not bisect the bone, but post-mortem damage or residual energy dispersal fracturing (Sections 4.1.4 and 9.3) caused the two halves of the cutmark to be separate<br>- Both halves may be present, however reuniting could introduce error and therefore has not been performed<br>- Processed the same as S |

After classification, observations were written about the cutmarks and a photograph taken. An identification code was given to each to ensure the image and observations could be matched and then later the digital models could be connected as well.

### 5.2.1 Cutmark Coding

Each cutmark was given a unique identification code, based on the skeleton and bone it was on. The code system works as follows:

Articulated Components
**0000_A0**

Skeleton Number
Cutmark ID
Segment of cutmark, if applicable

Disarticulated Components
**0000.00_A0**

Context Number
Discrete piece of bone
Cutmark ID
Segment of cutmark, if applicable

Some initially identified ‘cutmarks’ were re-diagnosed as fracturing or deemed to have too much uncertainty due to taphonomy after the initial codes were given, thus the final numbers and letters are not always sequential. In cases where a cutmark runs across multiple bones, it was given a new cutmark ID (letter) on each bone to avoid erroneously attributing segments of cutmarks to the same blow because the coding was completed early in the analysis process.

## 5.3 Stage Two: Developing the Photogrammetric Workflow

The overall workflow used is outlined in Figure 56. A more specific workflow regarding the model creation is introduced further in the chapter. The software that was used for this project is outlined in Appendix D (Figure 115).

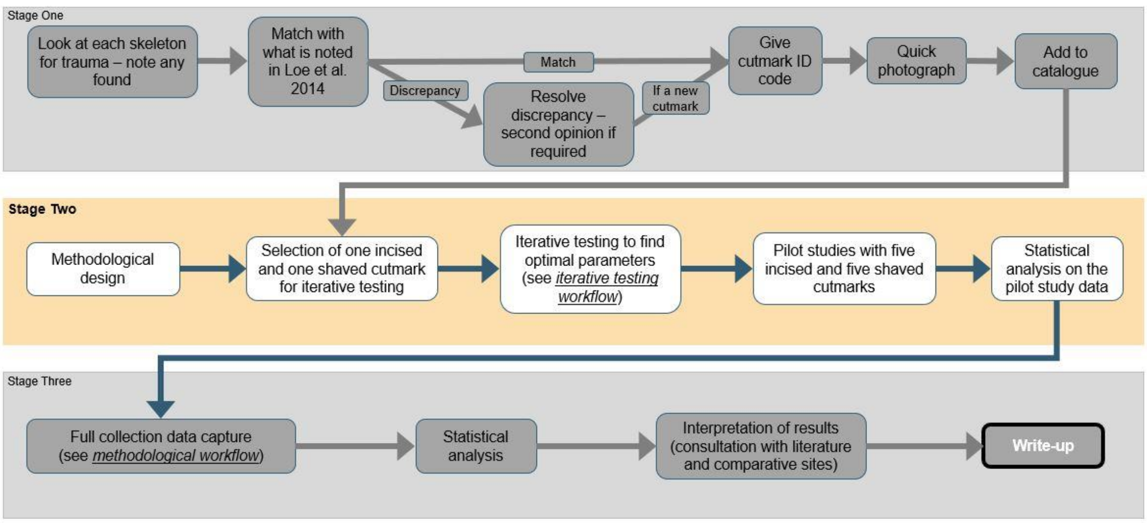


Figure 56: The workflow for the study with Stage Two highlighted (Appendix D Figure 115 for the full workflow without highlights)

### 5.3.1 The Photography

Nikon cameras with standard SD cards were used for the image capture (Figure 57). Two types of Nikons were chosen because they are different camera ranges, with the ‘DX’ being a mid-range camera and the ‘FX’ being higher-end. The latter is considered a ‘full-frame’ camera whereas the former has a 1.5x crop factor due to a smaller sensor size (Nikon USA 2019a, 2019b). The DX camera that was used was the D5300 and the FX cameras was the D810 (Appendix D). Other brands of cameras with similar specifications should produce similar results.


Figure 57: The camera equipment used in the main part of the study (Nikon D810 and FX AF-S Micro NIKKOR 60mm f/2.8G ED lens)

The lens was an FX AF-S Micro NIKKOR 60mm f/2.8G ED lens (Appendix D). This allowed for close-up photographs whilst maintaining the focal length of the camera, thus eliminating any confounding effects from a change in focal length. The FX lens was compatible with both the DX and FX cameras and did not reduce the quality or size of the array in either camera.

#### *5.3.1.1 File Format*

Photographs were captured in fine Joint Photographic Experts Group (JPEG) format and 14-bit RAW. The RAW files (.NEF for Nikon) were converted to Tag Image File Format (TIFF) files using Adobe Photoshop 2018. Since the number of images required is small and TIFFs are a lossless image format, they were chosen as superior to JPEGs. This was confirmed in the initial trials (Section 5.3.4 and Appendix E). JPEGs were also used to quickly test the alignment of the models to ensure no images had been missed.

High Dynamic Range (HDR) photography was considered as it allows for a larger range of exposures to be captured in one photograph. This is done by bracketing the 'optimal' image with an over- and under-exposed image from the same location taken sequentially. These can then be combined using Photoshop. The results from HDR tests were inconclusive as to whether the models appeared better. However, the process of creating HDR photographs was inconsistent as not all images would combine as they were meant to, therefore either delaying model creation significantly or requiring an entirely new set of images. Thus, other methods of creating optimal images were considered.

### 5.3.2 3D Control

In order to create a model that is scaled properly in all dimensions, 3D control was needed (Section 2.4.3.3) (Linder 2009, 2016; Wolf et al. 2014; Lillesand et al. 2015; Historic England 2017). Due to the size of the subject, conventional photogrammetric methods of surveying-in control (e.g. a total station theodolite [TST] or Global Navigation Satellite System [GNSS]) were not possible (For larger-scale studies, see Chandler et al. 2007, Verhoeven et al. 2012; Olson et al. 2013, Sapirstein 2016). Several options for how to add 3D control into the models were considered and it was decided that the best method for this project was to use a bespoke design created by additive printing, more widely known as 3D printing. It could be scaled to different sizes for different requirements and could also be replicable. The impact of this decision on accessibility was thoroughly considered, especially around the issue of obtaining access to the 3D printer. Fortunately, fused deposition modelling desktop 3D printers, designed for use with a variety of plastic filaments (most often polylactide, PLA, or polyethylene terephthalate glycol, PETG) in the home or office, can be relatively inexpensive (~£200) and are widely available (3DSourced 2021; Hsueh et al. 2021). There are also many businesses that will 3D print objects for individuals. The cost of printing such an object is highly dependent on its size and the material one wishes to print it with. The design will be published for other researchers to use.

The 3D printed control was named the 'Control Cradle'. This device was made to hold small bones securely whilst taking up the entire camera frame. This allowed for the Control Cradle-Object complex (CC-O) to be moved rather than the camera, since the objects and control points would always be in the same place with respect to each other. Although conventionally, Structure-from-Motion Multi-View Stereo photogrammetry (SfM-MVS, or simply 'photogrammetry' within this research) requires the object to be stationary and the camera moving, the same effect can be created when all control points move with the object and therefore stay in constant relative position (Section 2.4.4) (Micheletti et al. 2015b; Ferreira et al. 2017; Granshaw 2018). It was also important to assure that the small amount of background seen outside the Control Cradle had no identifying features or defects that the software might consider to be Key Points (KP) since these would not move with the CC-O.

The original Control Cradle (OG) was symmetric with five control points (CPs) in each quadrant. These points were at four different heights to allow for multiple z-values to be input and seen in each image. An arrow was added after printing to keep track of the rotations during photography. The initial cradle designed for the pilot study is pictured in Figure 58a. It was designed using Sketchup, sliced using Cura, and printed on an Ender-3 (courtesy of A. Ford). The coordinates and file are found in a supplemental data file. The control points were created at multiple levels by making cylindrical voids with a diameter of 1mm. After printing, these were filled with a dark putty in order to make them visible in images. In more recent iterations (MK2 and PH), a narrow gauge (1mm) black rubber gasket was used instead as it created a cleaner CP. For the pilot studies, OG was used for all samples. Due to the differences in geometry of the bones in the general collection, an additional set of 3D control needed to be designed. It was based on the 3D control used for the pilot study with modifications to make it more universal (Section 5.4.1.2).

OG and MK2 were of similar design, created to hold smaller irregular bones (central inset) and long bones (V-shaped cut-outs) (Figure 58a and c). The original design used a series of small hooks and elastics to hold the bone in place on the rubberised black stickers. In the later iteration (MK2), the Vs were deepened, the height of the towers raised, and screws inserted as braces in order to accommodate taller bones without the surface being too far away from the CPs. One side of the base was made unique so it could be used as a starting and ending point for each rotation of photographs, thus not requiring the drawn arrow that was seen on OG. A stand was also created for MK2 because some of the bones, such as mandibles, were overhanging the cradle and thus made it impossible to lie flat without additional height (Figure 58d). The rectangular-shaped cut-outs in the base of MK2 were similarly designed to accommodate such bones. Not bones would naturally lie so that the cutmark was level in the transverse plane, thus the wedges were created for both OG and MK2 to help give them support and level them for photography (Section 5.4.1.2).

PH was designed specifically for bones that were too large to fit in the cradle, such as skulls (Figure 58b). In this case the cradle would sit on the bone, the opposite method compared to the other two cradles. It would encircle the cutmark whilst not overlying any of it. It was designed to be secured using thin string, such as thread, as opposed to elastics, due to the fragility of the bones. Since PH needed to be larger to surround the defects, an extra CP was added to each side to avoid clustering of the control.

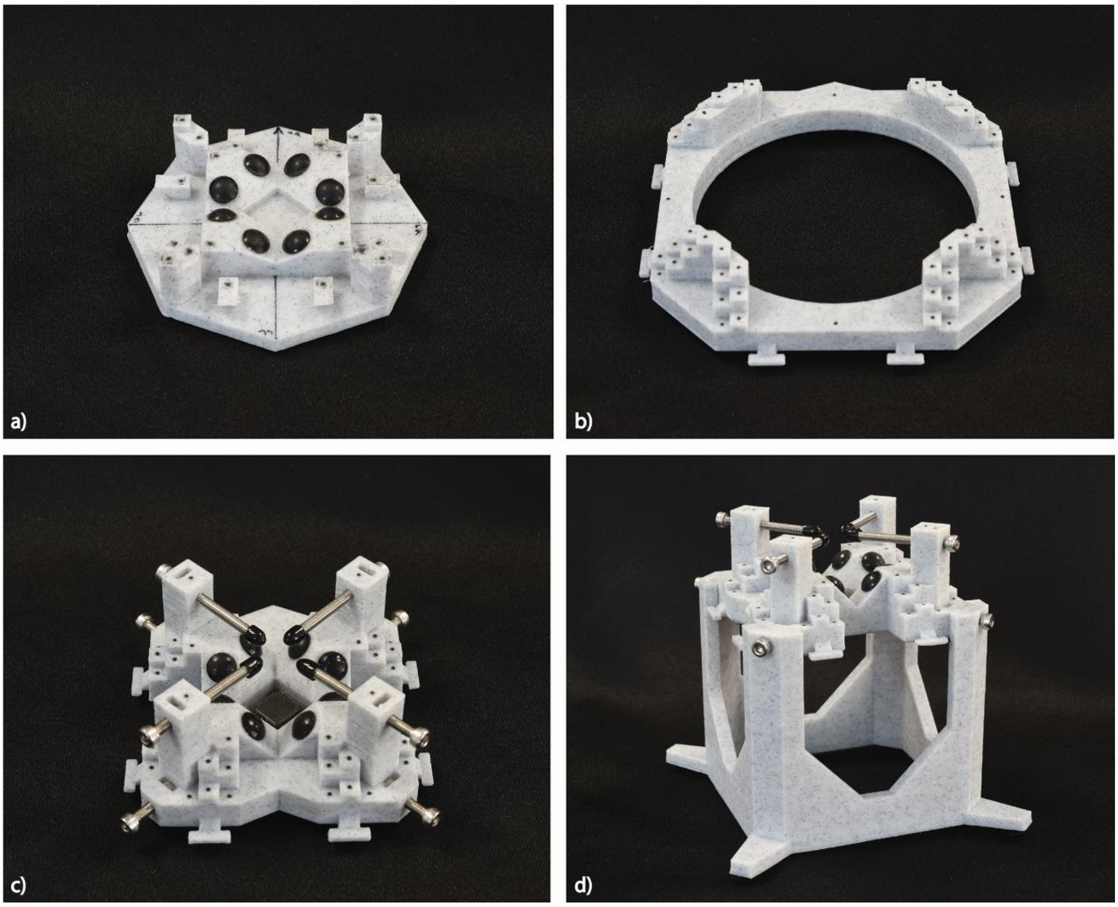


Figure 58: The control cradles used in the project: a) the original cradle (OG), b) the party hat (PH), c) MK2, and d) MK2 on its stand

### 5.3.3 The Image Capture

#### *5.3.3.1 Camera Parameters*

The following protocol was developed through the pilot study and found to be effective to digitise the remaining collection as well. In order to vary as few parameters as possible, an aperture was chosen that allowed the entirety of the longest pilot study cutmark to be in focus when viewed obliquely. This was found to be *f*22 in the incised cutmark pilot study and *f*25 in the shaved cutmark pilot study. The majority of the light used was natural light, with some overhead artificial lighting, and therefore varied at times. Due to this, the shutter speed changed between captures to compensate (Section 2.2.1). The only requirement was that the shutter speed be kept the same with both the DX and FX camera for each bone in the pilot studies. The ISO was set to 100 since the camera would always be on a tripod. No camera remote was available at this point, so the two-second self-timer setting was used to ensure that the camera would not shift in the middle of capturing a photograph due to the pressing of the shutter release.

### 5.3.3.2 Photographic Strategy

For both pilot studies, the following photographic strategy described below was repeated twice; first with the DX camera and second with the FX. This order was chosen because the DX was a more restrictive field of view and therefore it was important to make sure the placement of the camera and the parameters were sufficient to capture the required amount of data.

To begin, the Control Cradle was set up on a white piece of paper with a white backdrop to both avoid confounding non-moving points and allow some illumination from the reflected light. The set-up was illuminated with natural and artificial light. It was placed near the edge of a table to allow the tripod to stand on the floor beside (Figure 59). The distance from the object was set to be approximately the minimum focusing distance of the lens (18.5cm) which allowed the Control Cradle to fill the majority of the frame whilst retaining as many control points as possible to be in each image.

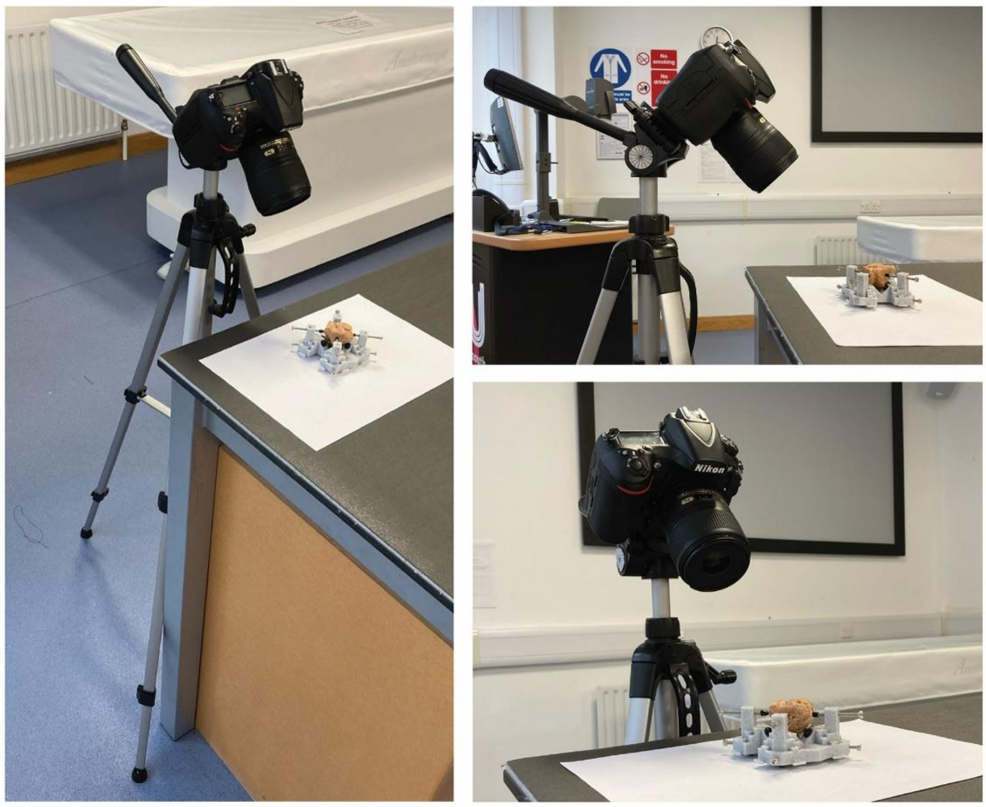

Figure 59: The control cradle holding a bone (cuboid) set up for the lower orbit of images in the image capture strategy used in this study (n.b. the white paper backdrop has been removed for the purposes of capturing these three images)

Images were taken in a pattern than would form a ‘Union Jack’ (Figure 60). To avoid moving the camera as much as possible, all eight ‘low-angle’ pictures were photographed first whilst rotating the CC-O 45° after each image, followed by all eight ‘high-angle’ pictures using the same strategy. The final picture was taken from directly above in landscape with the longitudinal axis of the cutmark aligned horizontally whenever possible.

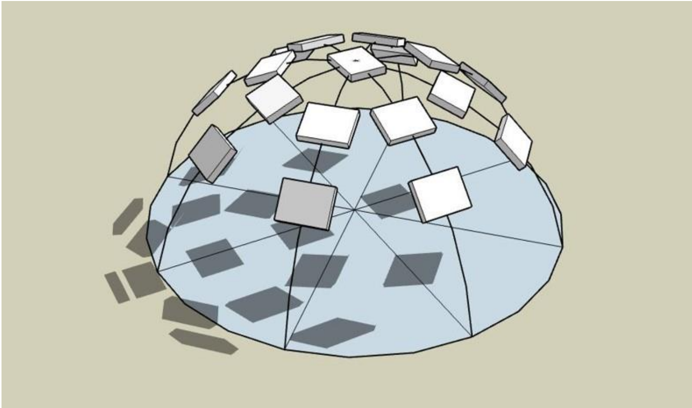

Figure 60: The ‘Union Jack’ image capture strategy

The low-angle pictures were taken at 45° to the vertical axis of the tripod and the high-angle pictures were taken after the tripod was raised slightly and the angle changed to 22.5° to the vertical axis of the tripod (Figure 61). A total of 17 images were taken per capture.

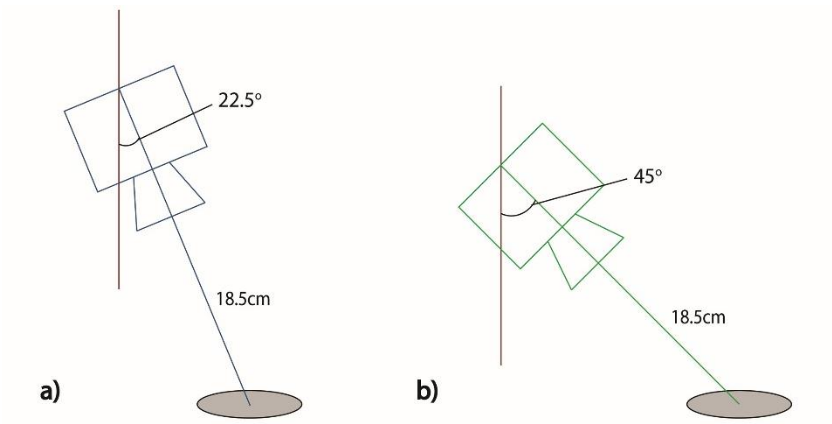


Figure 61: The camera angles used for the image capture strategy, a) 22.5° and b) 45° (final vertical image not pictured)

### 5.3.4 Initial Iterative Photogrammetric Trials

Several iterative tests were designed to find the ideal processing parameters for this collection and were done twice as there were two major categories of geometry in the cutmarks which required separate testing (Sections 4.1.4 and 5.2). One sample was chosen from each pilot study to create the methodology. The cut that was picked for each was chosen based on both being representative of the others in the pilot study and likely being the most restrictive due to geometry (e.g. the longest). The final workflow was determined to be the best procedure for this project. All initial tests and pilot studies were performed on Agisoft Photoscan 1.4, before the release and update to Agisoft Metashape 1.6. This change did not subsequently cause any changes to workflow or model quality.

For the incised cutmark test, pilot study sample 3685.10_K was used. It was a second cervical vertebrae with a cutmark running horizontally across the posterior aspect where the odontoid process joins the body. For the shaved cutmark test, pilot study sample 3734_C2 was used. It was a fragment of skull, left parietal, that was originally thought to be extraneous to SK3735 and therefore the models are coded as 3735_X. It was later found to reassociate with the cranial fragments of SK3734. The cut has penetrated the outer table of the skull and exposed the diploë (Figure 62). The total number of points in the dense point cloud (DPC) and the number of points surrounding the cutmark in the DPC were both measured (Figure 63). Errors were also examined (pixel and mm), however, errors were found to be more dependent on the precision of placing the points compared to the quality of the model. Additional tables and figures associated with the iterative tests are found in Appendix E (workflow Figure 116). Overall, the models all appeared robust to changes and very few were unusable.

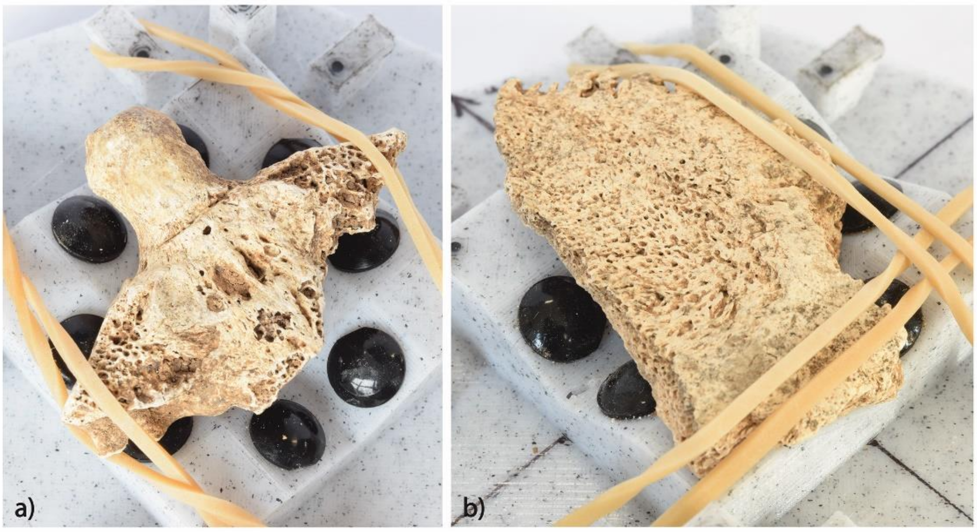


Figure 62: The cutmarks used for a) the first pilot study (3685.10_K) and b) second pilot study (3734_C2; originally numbered as 3735_X)

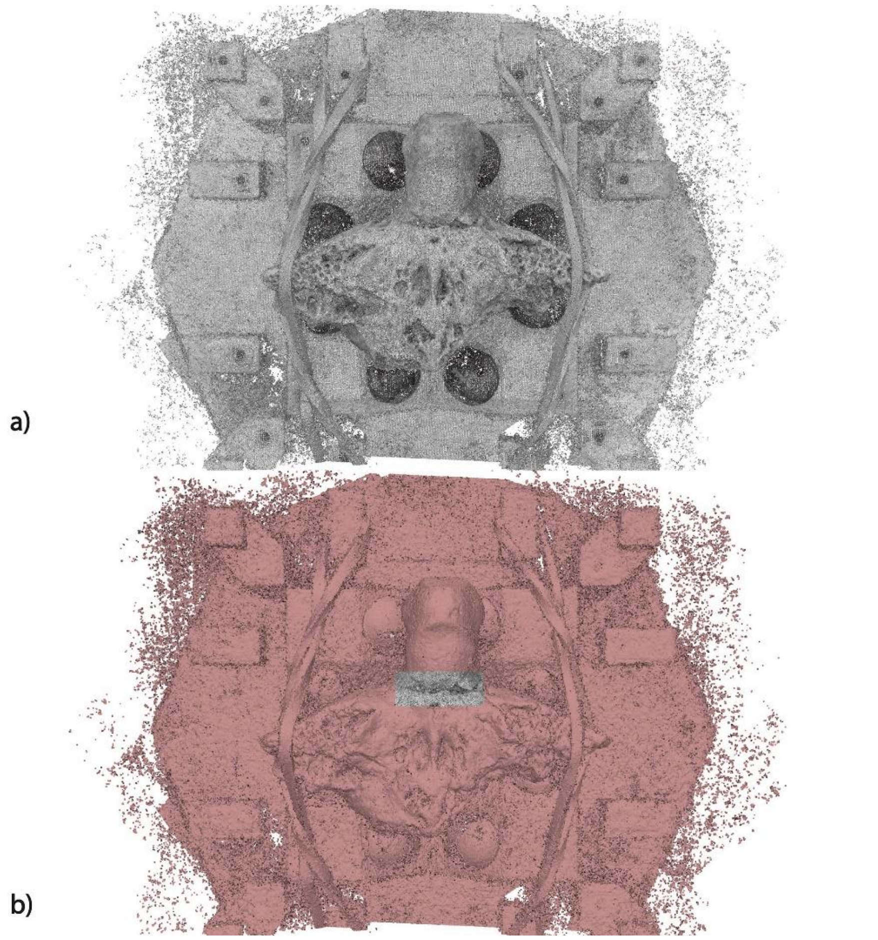


Figure 63: The a) full DPC and b) cutmark DPC (when the highlighted section is deleted) of cutmark 3685.10_K used during the iterative tests

The DX Nikon camera (D5300) was chosen for the iterative tests because the field of view was more restrictive and therefore it would likely be the limiting factor for what the best settings were. The image capture strategy, detailed in Section 5.3.3.2, was the same for both categories of cutmark. All 17 images were used for each model and these sets of images were used for all the iterative trials to avoid confounding the results. Camera parameters are found in Table E-1 (Appendix E). The aperture was increased for the shaved cutmarks because 3735_X was overall larger than the incised cutmarks and therefore an increased depth of field was needed to capture the entire cut in focus.

When examining the percentage difference, ±5% was used as a delineator. Any differences less than that were considered to be likely due to chance. Figure 116 details the iterative process used for this testing and the final settings can be found in Table D-4.

#### *5.3.4.1 File Format, Bit Depth, and Editing*

The first variable examined in the iterative testing process was bit-depth. Additionally, models created from edited and unedited images were compared at each bit-depth to determine which were superior. During image capture, the images were saved as both RAW and large, fine JPEGs. This set of JPEGs were used throughout this aspect of the trials as a baseline for the number of points generated and the file size of the images.

The RAW images, in Nikon's NEF format, were converted into TIFFs using Adobe Photoshop 2018. They were converted at both 8-bits/channel (24-bit depth) and 16-bits/channel (48-bit depth). These were then duplicated and turned into greyscale. This resulted in four bit depths to test: 8-bit (greyscale), 16-bit (greyscale), 24-bit (colour), and 48-bit (colour).

Initially, high dynamic range (HDR) photographs were going to be tested and therefore each image was bracketed at an exposure that was one higher and one lower than the set exposure. However, there was significant inconsistency when trying to get the photographs to merge into one HDR image in Photoshop. Due to this, it was decided that editing the image to achieve similar results was superior. The same RAW images as above were taken and the contrast was fully decreased and the shadows fully increased before converting into a TIFF. They visually appear more faded, however this was done to try to augment the area in shadow, specifically within the cutmark. The images were then saved in the same manner as the unedited images, resulting in the same four bit depths.

The JPEGs were not edited nor converted to greyscale. The model they created was used as 'control' and the relative number of points and relative file size compared to the JPEG model were examined for all bit depths and levels of editing in order to determine if there was a place at which the exponentially increasing file size would outweigh the benefits of extra points obtained from an increased bit depth (Appendix E, Tables E-2 to E-4). Visually, the point clouds were examined to see if it appeared as if many points were 'jumping off' the surface which would be indicative of a noisy model.

All nine models for each cutmark were aligned on High with the default settings of 40,000 key points (KP) and 4,000 tie points (TP). After the initial sparse point cloud (SPC) was created, the values for the control points were input and the points were placed on all images. An accuracy of 1.5mm was used for the control points in order to mitigate for human error in point placement. Camera optimisation was performed following that to allow for the software to perform a bundle adjustment using the control coordinates. The values that were used for the optimisation were the default values of: f, cx, cy, k1, k2, k3, p1, p2. The number of points was recorded (Table E-2). There are notable pixel error differences between the two pilot studies and this is due to user experience rather than the first pilot study being less precise. The iterative trials for the second pilot study were done after the entire first pilot study had been finished and therefore the tester had significantly more experience placing the markers consistently on the control points by the beginning of the second pilot study. This is not thought to affect the outcomes of the iterative tests or the first pilot study.

Gradual selection was used to edit the SPC to reduce erroneous points and noise. The value of 0.2 was used for the reprojection error (RE). Reproduction uncertainty (RU) and projection accuracy (PA) were below what would be considered acceptable for that RE (roughly 2xRE, therefore 200), however, they were further reduced to approximately 12 and 60 based on the visual appearance of the number of deleted points at those selected levels. The shaved cutmark sample was found to always have an RU of under 10 and therefore it was left unchanged. The cameras were then optimised again using the same values. The number of points in the SPC after the editing was recorded.

The dense point cloud (DPC) was then created on High with Disabled depth filtering to get the most recreation accurate of the cutmark possible, avoiding any artificial smoothing. The number of points for the entire model (fDPC) was recorded as well as for just the cutmark itself (cDPC). To measure the points in and around the cutmark, markers were placed on the photographs of each model at distinct features. These were used as boundaries for the rectangular selection tool. The model not rotated as inconsistencies in rotation could lead to erroneous differences in point cloud numbers. The area that was measured was approximately 10 mm by 4 mm for the incised cutmark and 30 mm by 40 mm for the shaved cutmark. Since the two types of cutmarks were not compared to each other, this difference in area measured was inconsequential.

The results are shown in Tables E-3 and E-4. For the file format and bit depth, the most important parameters were the file size and the number of points in the fDPC because that was an indication of the quality of the model overall, since the SPC had been rigorously edited to mitigate noise. The magnitude of the errors was also noted to see how that changed. When examining the merits of editing the point cloud prior to running the model, the number of points in the cDPC was the focus because that was the region the editing was intended to influence. The numbers of points in the in the overall model and just the cutmark were both transformed into additional variables with values relative to the JPEG model (assigned the value of 0). The values of the relative number of points and relative file size for both the edited and unedited images were plotted on a scatter plot to see if it could be visually determined where the extra points became more of a limitation than a benefit.

When examining the fDPC in the incised cutmark iterative tests, the three highest variables compared to the JPEG were the 48-bit edited TIFF, the 16-bit edited TIFF, and the 48-bit unedited TIFF (21.5%, 20.7%, and 20.6%, respectively). For both the 48-bit

TIFFs, the file size was 193% greater than that of the 16-bit TIFF with less than a 1% increase in points in both instances. Therefore, it was decided that the 16-bit TIFF would be the optimal bit depth. This would only create a greyscale model; however, the lack of colour would not affect the measurements, only the aesthetics of the model.

In the shaved cutmark iterative test, difference higher than 5% were only seen in the fDPC. Compared to the JPEG values, the unedited 48-bit TIFF, edited 48-bit TIFF, and the unedited 16-bit TIFF had the highest differences and the only differences over 5% (6.8%, 6.7%, and 5.4%, respectively). Similar to the incised cutmark pilot study, the increase in file size was exponentially higher than the increase in points when going from the 16-bit TIFF to the 48-bit TIFF. Therefore, greyscale was again considered to be the superior option. The smaller differences were interesting to note. This may be due in part to the points in the shaved cutmark being much greater and therefore the differences less notable, however, part of the difference may be due to the geometry of the cutmarks.

In the iterative tests if both types of cutmarks, the fDPC and the cDPC were examined to determine whether the edited or unedited point clouds were superior. Here the two pilot studies diverged (Table E-5). In general, for the incised cutmark pilot study, the edited point clouds produced more points. The results for the cutmark were given priority as the editing was designed to increase the visibility into the cut. This comparison supported the earlier result that the edited version of the 16-bit TIFF would be the optimal format to use for this pilot study. Conversely, the unedited point cloud for the fDPC were all superior to the edited ones in the shaved cutmark pilot study. The differences seen when just looking at the cDPC were minimal and therefore they could be due to chance. Overall, the shaved cutmark inherently has less deviation in the profile than the incised cutmark and therefore, since the editing was designed to augment the cutmark, as expected, the impact of editing was lower for the shaved cutmarks.

In both pilot studies, the chosen format had low errors for both mm and pixels. Although they were not necessarily the lowest, the differences between the errors in the chosen file format and the file format with the lowest error was small. Overall, the findings suggested that the process is fairly robust to changes and all combinations produced a usable point cloud.

#### *5.3.4.2 Tie Points and Key Points*

The number of TPs and KPs were manipulated to determine what the optimal number would be. For each value tested, the difference in number of points in the fDPC and cDPC were examined in comparison to the points found using the default value. As a result of the bit depth trials, the 16-bit edited images were used for this trial when exploring the incised cutmarks. For the shaved cutmarks the 16-bit unedited images were used.

At the time this was completed, the default setting for Agisoft Photoscan 1.4 were 40,000 KP and 4,000 TP and thus were used as a baseline for these trials. The default KP was left unchanged and five levels of TP were chosen to be investigated: 4,000, 8,000, 12,000, 16,000, and 20,000. These variables and the following process was the same for both the incised and shaved cutmark pilot studies.

Other than varying the TP numbers, the method of SfM-MVS model creation was the same as for the bit depth trials. Once the SPC was created and the control was input and the cameras optimised, the model was duplicated so the RE could be edited differently. One set of models was edited using the values of 0.2 (RE), 11 (RU), and 50 (PA) and the other was edited using 0.1 (RE), 11 (RU), and 50 (PA). RU and PA numbers were based on visual gradual selection and were pushed as far as they could be without losing a significant number of points. DPCs were then created and the number of points in the fDPC and cDPC were recorded. The overview of variables tested are in Table 17 and the full numerical results are in Appendix E (Tables E-5 to E-11).

Table 17: The Tie Point and Key Point variables evaluated in the iterative testing process (default values in bold)

| Variable | Reprojection Error | Values Tested | Selected Value? |
|---|---|---|---|
| Tie Points | 0.1 | **4000** | Yes |
| | | 8000 | |
| | | 12000 | |
| | | 16000 | |
| | | 20000 | |
| | 0.2 | **4000** | |
| | | 8000 | |
| | | 12000 | |
| | | 16000 | |
| | | 20000 | |
| Key Points | 0.1 | 10000 | |
| | | 20000 | |
| | | 30000 | |
| | | **40000** | Yes |
| | | 50000 | |
| | 0.2 | 10000 | |
| | | 20000 | |
| | | 30000 | |
| | | **40000** | |
| | | 50000 | |

The errors were examined for each trial model. It was found that the error values that were recorded were more dependent on the precision of placing the points compared to the actual changes in the quality of the model. For example, the 40,000/4,000 (KP/TP) combination in the first pilot study was executed twice; once in each of the TP and KP trials. The difference in error between the two in both mm and pixels was large (9% and

30% respectively) despite containing the same parameters and generally improved with user experience. Differences in errors between the editing levels for each trial were either non-existent or less than a fraction of a mm or px and thus were not considered important in the decision process. Therefore, unless an error value appeared large enough to be anomalous, it was not heavily weighted in the consideration of the best method.

The results for the fDPC were initially examined as it was thought that would give a better indication of the quality of the model overall at each level of TPs. No differences of a magnitude greater than 5% were seen for either level of RE or between the levels of RE, therefore the results for just the cutmark were looked at as well (Tables E-6 to E-8).

In the incised cutmark tests, the only the TP of 16,000 had an increase of points in the cutmark compared to the default settings. This percentage was not greater than 5%, therefore any differences could have been due only to chance and therefore the default value was chosen for this pilot study. The difference between each trial with and RE of 0.2 and an RE of 0.1 demonstrated that 0.1 was superior in all cases, though only the cDPC showed any improvements that were over 5%. There was a 6% increase in the default trial when using 0.1. Therefore, pending confirmation through the KP trials, an RE of 0.1 was decided to be best in combination with 4,000 TPs.

In the shaved cutmark tests, in both the fDPC and the cDPC, there were minimal differences between the different levels of TPs. There were small increases seen between the higher TP levels and the default value, however, none of the differences were over 5%. The RE of 0.1 had no values over 0.6% for either the fDPC or the cDPC and the RE of 0.2 has one difference of 1.4% and no other values over 0.7%. Therefore, the default value was chosen because it would reduce computational time compared to using higher numbers of TPs.

There were minimal differences between the number of points found in the RE of 0.2 and of 0.1 and any differences that were seen were likely to have been through change and random error. Therefore, because editing the point cloud to an RE of 0.1 should allow for a better bundle adjustment without creating any negative effects on the point cloud, this was chosen in combination with 4,000 TPs. In both cases, the hope was the increase in the strictness of the editing parameters would lead to a decrease in, or removal of, any extra noise.

The same images were used for this trial as were used for the KP trials. From the previous trials, 4,000 had been established as the optimal TP number and therefore this was used throughout these trials. Five KP values were chosen; 10,000, 20,000, 30,000, 40,000, and 50,000. 40,000 was typically the default value.

The same procedure was followed for these trials as for the TP trials. The fDPC was looked at first in both tests to determine if there were any differences in the quality of the model for each number of KPs. All differences that were seen were less than 5%, therefore the values from the cDPC were investigated as well (Tables E-9 to E-11). When analysing the incised cutmarks, the number of points that was produced by 10,000 KPs was very similar to the number produced by the default of 40,000. However, when editing the 10,000 KP SPC, the model started to lose its distinctiveness and identifiability. Due to this, 40,000 was decided to be superior.

In the shaved cutmark trials, the differences that were found were minimal, the majority did not have a magnitude of greater than 1%. Overall, the models with more KPs had more points in the DPC. As this parameter does not seem to make a major difference in the total point or the cutmark points, the default value of 40,000 was chosen since this value was superior in the incised cutmark trials and therefore would be standardised between all geometries of cutmarks.

Although no large changes were seen when comparing 0.1 and 0.2 RE in the full point cloud, there was seen to be a 5% increase in cutmark points when using 0.1. Therefore, this supported the findings from the TP trials that 0.1 RE would be better in this study. Overall, TP and KP values were left at default and the RE used was 0.1. This was able to be used for both types of cutmarks which aided in standardising and speeding up the data capture.

#### *5.3.4.3 Control Point Accuracy*

Lastly, the accuracy of the control points was varied. A SPC of one model was created, using 40,000 KP and 4,000 TP. Control was imported through the reference pane and the points were placed. This model was not optimised, instead it was duplicated multiple times and different accuracies were entered for the control in each model. The CP accuracy was never varied within a model. This was done to avoid any changes in error due to difference in placing the control points or in the alignment of the photographs. After these accuracy values were input, each model was optimised.

From there, the procedure was the same as the TP and KP tests. The errors in mm and pixels were recorded both before and after editing to see what the effect of the accuracy changes was. The number of points in the fDPC and the cDPC were recorded.

Overall, the models were very robust and did not break until an accuracy likely unachievable by human placement. The errors in the model did not change over a wide range of values; from 0.1mm to 1000mm (Tables E-12 and E-13). The accuracy of 1.5mm was used as the default value as that was initially used for the prior tests. This value was determined through the size of the control points (approximately 1mm in diameter) and the possibility of human error in the placement (0.5mm). The number of points in the fDPC did not increase by more than 0.3% from the default in any of the tests. Similarly, when focusing on the cutmark, no increases were greater than 2.3% from the default, therefore none of the differences in DPC values was thought to be due to the changes in accuracy. The number of points in the SPC starts declining at 0.1mm however. The model was taken until ‘breaking point’ where the error (mm) would start to increase again. This corresponded with a decrease in the number of points as well. However, when trying to apply this level of accuracy to a different cutmark, the model was found to be unusably noisy regardless of what amount of gradual selection was used. Therefore, despite the increased number of points, this was discarded as a method of improvement.

Initially, the shaved cutmark trial yielded similar results with a wide range of accuracies resulting in the same errors. The number of points in the fDPC remained consistent until the accuracy of 0.001mm where there was an 3.5% increase. An increase of over 5% was seen at the accuracy of 0.0005, however, due to what occurred with the incised cutmark pilot study, this was suspected to primarily be an increase in noise. Therefore, the accuracy at which the error started to increase is thought to be an appropriate cut-off point because the accuracies smaller than that would risk not accounting for the prospect of human error in the placement of the control points.

Therefore, for both trials, since the size of the control points is 1mm in diameter, an accuracy of 0.5mm was decided to be the minimum that should be used due to the possibility of human error. It appeared that pixel and mm error work slightly reciprocally in these models and balancing between the two was optimal. Therefore, even though neither error was minimised at 0.5mm, that was thought to be an optimal point as it would also account for the possibility of human error in placing the control points and reduce the noise whilst maintaining a high level of accuracy. Despite being able to push the accuracy further, it was deemed ‘safer’ to avoid that as it did not automatically equate to a better model.

Overall, the final processes are reflected within this chapter and are deemed to be the best for use in these situations. However, it is recommended to perform iterative trials such as this with any different types of subjects and differences in geometry and material could affect these results. The method overall appears to be robust. Very few of the models apart from those in the accuracy trial were unusable.

### 5.3.5 Workflow Design through Pilot Studies

The following workflow was performed on Photoscan 1.4 before being updated to Metashape 1.6 (Figure 64, Appendix D). For ease, both will be called Agisoft as the workflow was unchanged (Agisoft LLC 2018a, 2020a).

#### *5.3.5.1 Importing Photographs*

Each cutmark was designated its own project in Agisoft. Within that, stages of each model were duplicated and kept as separate ‘chunks’. This was done to allow for records of the earlier stages of processing, especially the pre-edited versions so they could be referred to in case there was a problem with the final model. The chunks were renamed to reflect their contents after the importing of the images. In this project, the background was generally not masked because anything beyond the control cradle was uniform in colour and texture to avoid causing erroneous feature matches. In some photographs, a small corner of the table was seen. In these situations, just that part was masked before alignment to prevent it affecting the model.

#### *5.3.5.2 Alignment and Sparse Point Cloud Generation*

All parameters used for this stage of processing are found in Appendix D. If not discussed, a setting was left at its default value. The first stage after the importation was the creation of the SPC (Section 2.4.4.1).

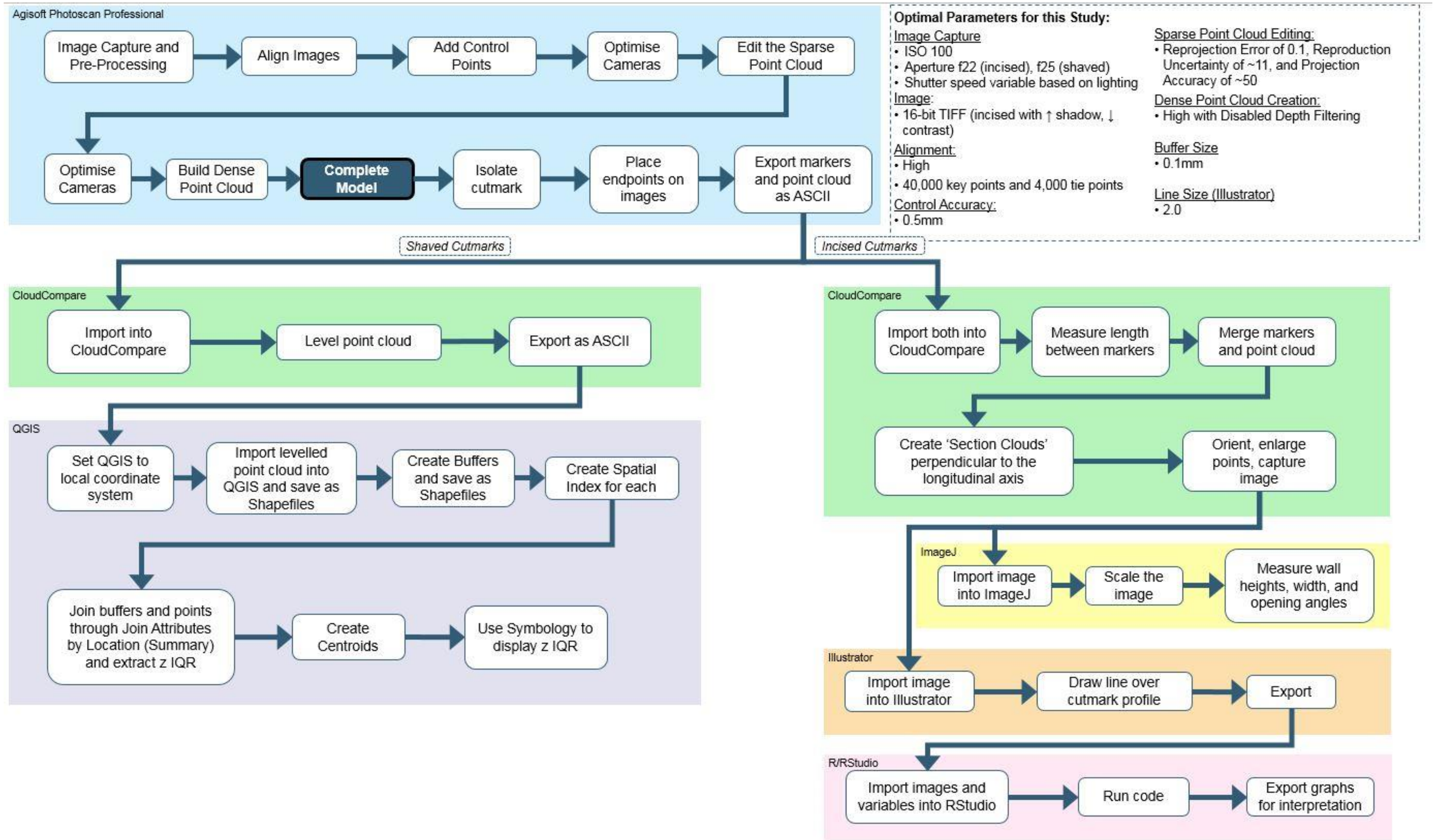


Figure 64: The detailed methodological workflow used for creating and processing the models

#### 5.3.5.3 Adding Control Points

Control can either be added before or after the creation of the SPC. In this situation, control was added after as it sped up the process of placing control because the software would project the CP once two were placed and then the researcher could confirm or adjust the point rather than placing them without a guide. The control values were imported into the software and markers were placed on CPs with known x, y, z-coordinates in an arbitrary (local) coordinate system. Markers must be placed in at least two images, however, it was often beneficial to place them in the majority of images to give them a higher likelihood of being in the correct position in all three planes. In this project, all visible control points were marked in all images. The accuracy was set to 0.5mm based on the accuracy trials. Once all control was input, the cameras were optimised using the default variables (Appendix D, Table D-4) (Figure 64). The errors in both metres and pixels were examined and if they were anomalously high, whichever points were the cause would be located and checked to see if those points had been misidentified or misplaced. If they were, they would be fixed and re-optimised. Since the average errors that appeared initially were usually between 0.5 and 1.6 pixels, it was decided that ideally the pixel error for each marker should be under 1.5 pixels. If the error was too high, the markers would be moved to their correct location and the cameras would be optimised again. The m error was more dependent on the point placement and is further discussed in the Section 6.2 and 8.2.

#### 5.3.5.4 Sparse Point Cloud Editing

The next stage was to edit the SPC to remove points that were of lower quality (Figure 64). Using the ‘Gradual Selection’ tool, four different parameters of point quality were examined. The parameter of ‘Image Count’, which says the number of images that a point is found in, was not used due to the small sets of photographs in this project. This Gradual Selection tool can be used as a sliding scale and there is generally no consensus on the optimal values as it is often highly influenced by the subject and the images. As established in the initial trials, 0.1 was the preferable RE. Since, both RU and PA are on a sliding scale, a value for each was looked for which would remove some points without culling them unnecessarily (Section 5.3.4, Appendix E, Table E-5 to E11). Following that, the cameras were finely adjusted through Optimise Cameras using the same variables as previous optimisations.

#### 5.3.5.5 Creation of the Dense Point Cloud

The DPC was created using the parameters in Appendix D and E (Table D-4, Figure 64) (Section 2.4.4.2). For the incised cutmarks, some area around the cut was maintained to properly determine the profile, whereas for the shaved cutmarks, the point cloud was trimmed to the edge of the cut so the unaffected surface would not impact any surface roughness calculations. The point cloud was then exported to be used in different software (see Section 5.4.4 for the incised cutmarks and Section 5.4.3 for the shaved cutmarks).

### 5.3.6 Testing the Control Cradles

The cradles needed to be tested to ensure they were not introducing systematic errors to the models. To do this, initially one models for each cradle was chosen at random. The two types of cutmarks, shaved and incised, were not separated for this aspect because the cradle was the focus of this component of the analysis, not the cut. Any models that were aligned on Highest, not High, were excluded. Markers were placed on all the CPs following standard procedure and optimised. Subsequently, the other half of the points present on the cradle that had not been used as CPs, were designated as check points (ChPs) and placed on the model. These ChPs were then deselected and a secondary optimisation was run before all the error values for the CPs and ChPs were exported and statistically compared for differences (Section 5.3.8.3 for more detail on the statistical tests used). Ideally, there would be no statistical difference between the CP and ChP errors.

Following this, five random models were chosen for each cradle and the three types of cradle were analysed both separately and together. The x, y, and z-values were extracted along with the x, y, and z-errors for each CP. Any correlation between value and error would indicate if a systematic error was being inadvertently introduced (Section 5.3.8.3).

### 5.3.7 Pilot Study Cutmark Measurement and Comparison

The follow section details how the measurements were taken and compared. Originally, digital microscopy was going to be used as a ‘gold standard’ for comparison with the photogrammetric measurements in order to test metric accuracy (Section 4.1.6). Due to the microscope itself (Keyence VHX-5000) there was low confidence in the accuracy of the measurements taken, and due to COVID-19, this could not be further explored to rectify or mitigate the problems. This is discussed in Section 8.3.1. Instead, since callipers are the most commonly used method of measuring cutmarks, this was deemed as an acceptable amount of reference for this study. Measurements were converted to millimetres at two decimal places. All measurements were taken three times and the mean calculated. If one measurement of three measurements was 25% greater or less than the mean of the other two, it was considered a potential outlier and an additional measurement was taken to confirm or reject this idea. If confirmed, the outlier would be omitted, however none were found. Additionally, approximately a week after the round of three measurements was completed, a single set of measurements was taken. These were used to test for intra-observer error. For the pilot studies, both manual and SfM-

MVS measurements were used in order to determine the applicability of the models. Subsequently, any full population analysis that occurred was performed solely on the digital 3D models.

The measurements that were compared between manual and photogrammetric models from both cameras were length (measurement from end-to-end of the cutmark along the longitudinal axis) and width (measured from the upper break of slope on each side at 50%, and of the length).

#### 5.3.7.1 Conventional Measurements

The manual measurements were taken using a Mitutoyo Digimatic Calliper (CD-6” ASX; 500-196-30) (Figure 65). This specific calliper was chosen because it was easier to use on small targets compared to some of the larger callipers and it contained the certificate of inspection. The sample and the callipers were held under an illuminated magnifying glass in order to aid in data capture.


Figure 65: The calliper used for the manual measurements

#### 5.3.7.2 SfM-MVS Model Measurements

It was easier to identify the edges of the cutmark on the photograph compared to the full point cloud as the size of the points could not be increased in Agisoft when zoomed in to the necessary magnification. Therefore, after the DPC was completed, markers were added to each end of the incised cutmark on the images. For the shaved cutmark pilot study, markers were placed across the longest part (length) and then at the maximum distance perpendicular to the length was found (width). For both types of cutmarks, the points were added in three images each. Once completed, the markers were made to appear on the DPC (Figure 66a). The point cloud was imported into CloudCompare (ClCo) as a .LAS file and the markers as an ASCII file. This could be done with the point cloud also as an ASCII and retrospectively it would be recommended. The markers identifying the ends of the cutmark were marked as point and then the markers and point cloud were merged. The length, and width in the case of the shaved cutmarks, was then measured.

For the shaved cutmarks, both length and width were measured in ClCo. For the incised cutmarks, the only measurement captured in ClCo was length. With both types of cutmark, the 'Point Selector' tool was used and the imported markers were selected and the distance between them measured. ClCo was used for the lengths because it accounts for all three dimensions present in the model, allowing an accurate measurement since any vertical displacement is also accounted for, which is especially important if the model is not completely level.

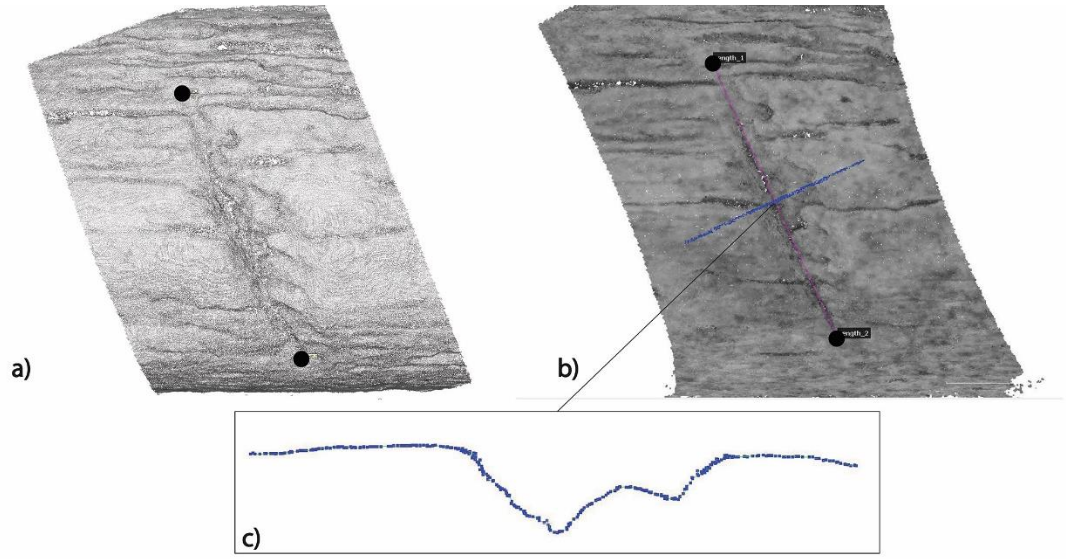


Figure 66: An example of the placement of the points denoting the ends of the cutmark 3789_B with markers highlighted in black a) in Agisoft, b) in CloudCompare with the extracted 50% section highlighted, and c) a side-view of the profile of the cutmark at 50%

For the incised cutmarks only, the segmentation tool was used to get the profile at 50% (Figure 66). In cases where there was taphonomy or other obscuring factors at the relevant location, the incised cutmark was sectioned at 5% intervals and the closest section to 50% with a useable profile was used. The profiles were taken from the same place for both the FX and DX models.

Using the ability to fix rotation around an axis (z-axis in this case), the section cloud of interest was rotated so it could be viewed perpendicularly to the longitudinal axis of the cutmark. This was captured as an image to analyse in ImageJ. The image of the profile was imported into ImageJ and scaled using the scale bar that was captured in the corner of the image. Due to the maximum number of decimal points that ImageJ can use, the units were converted from metres (as is found in ClCo) to mm. Wall heights, opening angles, and widths were measured to compare the DX and FX models. Although the above procedure was only performed on the incised cutmarks, the shaved cutmarks were further investigated in the population-level analysis as described in Section 5.4.3.

## 5.3.8 Pilot Study Statistical Analysis

Overall, non-parametric statistical tests were used for the pilot studies because of the small number of samples (McCrum-Gardener 2008). A significance level of p=0.05 was used for all tests unless otherwise mentioned (McCrum-Gardener 2008). Work by Field (2009) provided guidance for choosing statistical tests throughout the following sections.

Since the pilot studies were non-parametric due to sample size, the values that were explored for the descriptive statistics were primarily the median and range, however the standard deviation and standard error were also examined.

### *5.3.8.1 Intra-Observer Error*

Intra-observer error was calculated for each of the measurements from the SfM-MVS models. The mean of the initial three measurements were used as the ‘test’ (Test 1) and the later measurements that were taken as the ‘re-test’ (Test 2) and therefore non-parametric repeated measures tests were applicable (Field 2009).

In this case, typically a Wilcoxon Signed Rank test would be used (Wilcoxon 1945; McCrum-Gardener 2008). The basis of this test is that differences are calculated between the two measurements and then ranked and the sign of the difference is given to the rank (Wilcoxon 1945; Field 2009). However, there are some issues with this test when running it in either R or SPSS. R ignores any tied values which becomes problematic if a substantial portion of the tests fall within this category; it can skew the statistic by omitting a large number of samples. SPSS does use any tied values in the analysis, however, it seemingly arbitrarily assigns them to be within the negative or positive category; this can also alter the significance level. Due to the small sample size, either of these can be an issue that alters significance. In order to combat these potential problems, a Sign test was also run. This is similar to a Wilcoxon but only looks at the sign of the difference and not the magnitude and is not as affected by differences of zero, however it is less sensitive to differences because of this (Field 2009). The descriptive statistics were also examined for similarities, differences, and patterns between the first and second test. This was also visually examined using box plots.

### *5.3.8.2 Comparing Measurements*

To compare the same type of measurement taken using each combination of methods, paired-sampled statistics were appropriate since the same object was being measured multiple times at different points in time using different methods. There are two types of tests that are most appropriate for these parameters. For the comparison of two measurements, a Wilcoxon Signed Rank test is used and for three or more measurements, a Friedman's test is used (Friedman 1937, 1939, 1940; McCrum-Gardener 2008). The Friedman's test works on the same principles as the Wilcoxon Signed Rank test and is often considered an extension of that test.

The comparison of the manual values to both types of SfM-MVS models was analysed using a Friedman's test. An additional comparison between the two SfM-MVS models and between each and the manual measurement was done using a Wilcoxon Signed Rank with a Bonferroni correction (Dunn 1961; Field 2009).

#### *5.3.8.3 Control Cradle Analysis*

For each cradle, the errors (m) for the control and check points were exported and analysed, both overall and in the constituent x, y, z-components. Descriptive statistics were calculated and the normality was examined in order to appropriately compare the control and check point errors (Shapiro and Wilk 1965). The Mann-Whitney U test was used for consistency as the normality tests indicated a mixture of parametric and non-parametric data (Mann and Whitney 1947). The x, y, z-values were also compared to their respective errors to determine if there were systematic errors. These were visually examined using scatterplots and correlation analysis was run; a Spearman's Rho was used (Spearman 1904).

## 5.4 Stage Three: Application to the Full Collection

### 5.4.1 Procedural Modifications for the Full Collection Analysis

Various small changes were made to the procedures for the full data collection based on the pilot studies in order to increase the efficiency of the process and decrease the time required. The final full workflow from image capture to data output is seen in Figure 64. The workflow for Stage Three is seen in Figure 67.

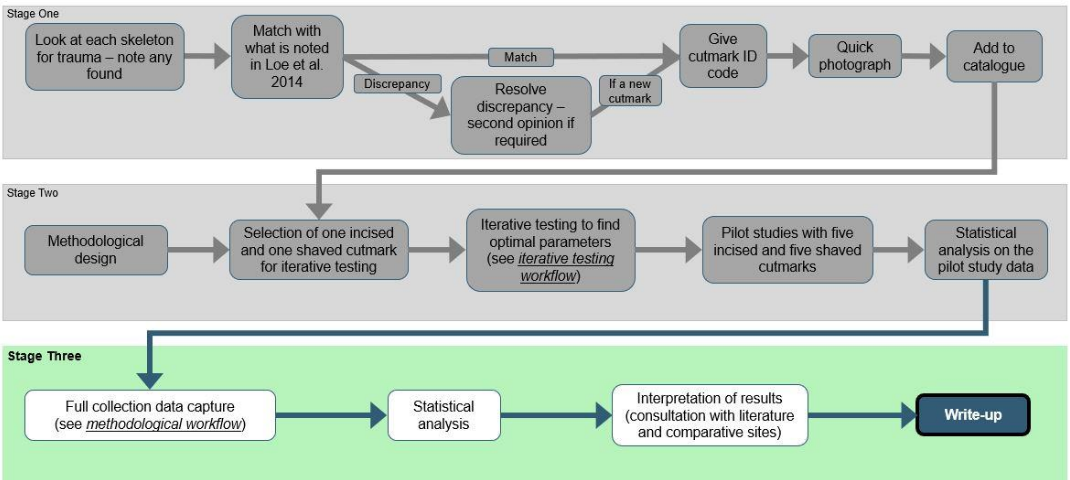


Figure 67: The full workflow for the study with Stage Three highlighted (Appendix D Figure 115 for the full workflow without highlights)

##### *5.4.1.1 Prioritisation*

All cutmarks that were found before 18 December 2020 were photographed and processed. Any that were subsequently found (N=14 new cutmarks or extra segments of known cutmarks) were added into the patterning up until 25 August 2021 but could not be modelled. These were not all used for analysis due to the sheer number of cutmarks or cutmark segments that were present (For example, when accounting only for those modelled, there were 535 segments and 454 models). As discussed further in Section 5.4.3, ten shaved cutmarks were chosen for analysis as this portion of the study was testing a method not previously applied to bone, thus a smaller number of examples with the greatest potential to provide useful results about the method were chosen. For the incised cutmarks, nearly all (N=107/115) were used in order to perform a more comprehensive shape analysis. Any incised cutmarks with substantial taphonomy or any other factor that may have confounded their shape were excluded.

###### 5.4.1.1.1 COVID-19 Impact

The plans for full population data collection were changed when the university closed twice in alignment with government regulations in the face of the COVID-19 pandemic. Progress was delayed during the first closure (20 March 2020 to 10 August 2020) since data collection and image capture was on-going. Prior to the second closure (6 January 2021 to 15 March 2021), all photography was completed and models were created. Due to the closures and the subsequent limited access (March 2021 to September 2021), the Keyence Digital Microscope and SEM could not be fully investigated.

##### *5.4.1.2 Control Cradle Modifications*

The shape of some bones required adaptations to the control cradle to allow the bone to be held in such a position that the cutmark was facing up and level horizontally, whilst being kept secure and stationary. A selection of optional support wedges was made to keep the bone steady if it needed to be tilted. In addition to the wedges, a raised base was created so bones that required overhang could be accommodated (Figure 68).

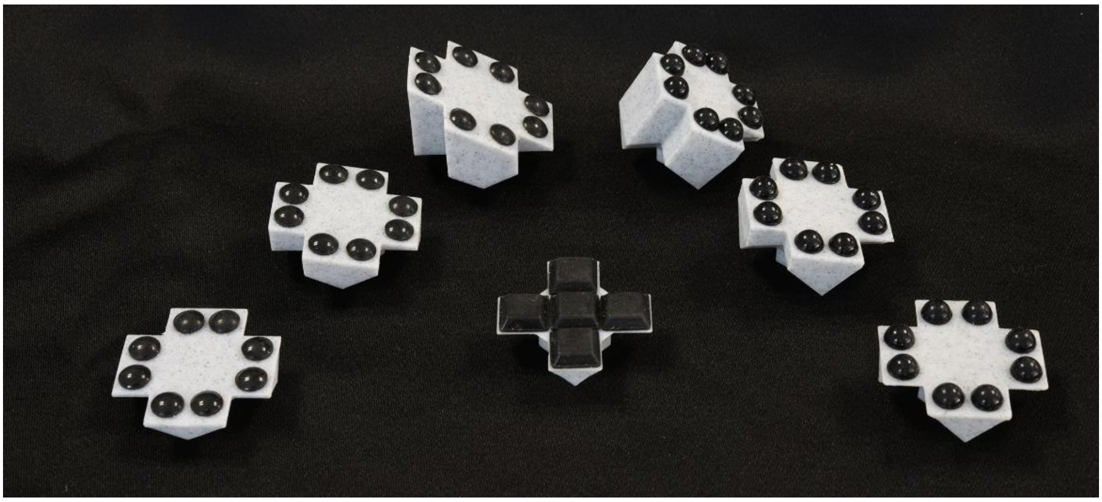

Figure 68: The various wedges used in the project with the ones for OG on the left and MK2 on the right. Wedges were angled at (back to front) 30°, 10°, and 0°

As initially introduced in Section 5.3.2, various iterations of the control cradle were developed, trying to use the initial one (OG) as a base as much as possible. The second control cradle (MK2) contained a deep V through the middle and higher control points for bones which were too tall for the original cradle. It also included a system to brace the bone with nuts and bolts rather than with elastic bands to avoid occluding the surface of the bone (Figure 58c and d). A total of 52 CPs were used in this version so some could be reserved as ChPs and more were likely to be visible if the subject is either large or oddly-shaped. One further control cradle (PH) was developed for use with bones that would not rest nicely in the cradle, such as skulls. As in the case of MK2, extra CPs were added to PH (up to 60) (Figure 58b). Like the original cradle, both new cradles were designed to be symmetrical and easy to rotate, though the symmetry was now confined to one axis rather than two.

#### *5.4.1.3 Image Capture Strategy Modifications*

The first modification of the image capture strategy was that only one camera was used. The statistically non-significant differences between measurements from each type of model meant that the camera used should not affect the quality of the results. This choice was made for pragmatic purposes; first, the D810 was not available to as many individuals as the D5300 and therefore was more likely to be available for use during periods of intense image capture, and second, the lens in use was a FX lens, thus the lens is designed to work best with the FX camera, therefore the FX camera (the D810) was used. The use of a photographic tent was considered in order to extend the hours during the day that image capture could be performed, however the geometry of the available tent proved to be a hinderance so the idea was discounted.

For all cutmarks, the aperture was set to be *f*25 since that was the maximum used for either pilot studies. Having additional depth of field was expected to enhance model creation for the incised cutmarks and therefore it was decided that standardising the aperture for all image capture would speed up the process. Overall, slower shutter speeds tended to be used during full data collection because in the pilot studies several of the models were slightly darker than desired once changed to greyscale and because the image capture began in the winter with poorer lighting conditions. In general, for the shaved cutmarks, the slightly over-exposed images created models that were easier to analyse. The incised cutmarks were more robust to variation in the light between days because they were edited, which generally resulted in a lighter image.

#### *5.4.1.4 Processing Modifications*

If any models did not align on High or Highest, the images were re-taken. This was an issue in less than 2% of the models (N=9/454) and all were successfully created with a new set of images. Only two models failed at the DPC stage but were successful using a new photoset.

### 5.4.2 Further Data Collection from the Skeletons

Frequencies of blows, cutmarks, and affected bones were examined along with the patterning of each bone and the overall patterns in the side of the body and location (Appendix F, G, and H; Supplementary Adobe Illustrator [.ai] files). Demography and burial were also examined in regards to the number of blows. Further analysis was performed on the point clouds as they are a resource that allows for a variety of digital examinations that cannot be done on the actual bone. The direction of decapitation-related blows was also investigated through frequencies.

### 5.4.3 Surface Roughness

In the earth and environmental sciences, rugosity is typically a term used only when a continuous surface is analysed and since the point cloud was analysed in this study, the term 'surface roughness' is used instead (Smith 2014). Typically, in osteology, surface roughness is used to look at muscle markers and it is a relatively subjective, nominal scale (Mariotti et al. 2004, 2007; Henderson et al. 2013). It was proposed that looking at surface roughness of bones through an earth science lens could be a good way of quantifying the roughness of the shaved cutmarks. This could be beneficial for learning about directionality since the entrance is usually the smoothest area since it has encountered the least resistance by that point. This is further discussed in Sections 6.3, 7.3, 8.4, and 9.5 and the principles of fracture propagation and Residual Energy Dispersal (RED) fractures, which denote the opposite side to entry, are discussed in Sections 4.1.1 and 9.3.

There are several methods by which roughness could be calculated and they are further outlined in Section 8.5.4. For this project, it was decided that surface roughness would be analysed on the point cloud itself rather than on a triangulated irregular network (TIN) or mesh of the point cloud. This decision was made because the rest of the analysis was on the point cloud itself and therefore this would remain consistent and avoid interpolation. Additionally, there are many methods of surface reconstruction and in order to properly investigate the roughness of a cutmark rendered as a mesh surface, these methods and their variables would need to be explored to ensure the optimal one was selected which was beyond the remit of this project.

In order to investigate surface roughness, ten shaved cutmarks that had a visible difference between exit and entrance were used as a pilot to create the method (Figure 64). In order to create an initial methodology, the trabecular bone was ignored and only the outer, compact bone was analysed. This was done because the added surface area of the trabeculae raised questions about differential rates of taphonomic damage across the surface as well as inherently increasing roughness. This meant that some shaved cutmarks would be excluded because they did not have sufficient compact bone, however, since this was a pilot study to see if this technique would be able to produce helpful results, it was deemed an acceptable limitation.

The cutmarks with known directions were trimmed and extracted as ASCII files, levelled in ClCo, exported, and imported as XY files into a QGIS project which was set in local coordinates. They were then saved as a Shapefile and it was ensured that the project and the file were in a local coordinate system. All subsequent outputs were saved as shapefiles. Buffers were created around each point (radius=1mm) and a spatial index was created for both the points and the buffers. The tool ‘Join Attributes by Location (Summary)’ was used in order to calculate the statistics for the points that fell within each buffer and the z-statistics were extracted (specifically interquartile range [IQR] and mean). The output was polygons that were identical to the buffers but with added columns in the attribute table. This was then converted to centroids in order to plot the zIQR value in the location of the original point. IQR was chosen in order to examine the variability in the height of the surrounding points whilst attempting to exclude points that were potentially noise. The areas of lower variability were smoother and likely to be closer to the entry of the blade because that is the region where the most force is transmitted to the bone and propagating fractures will not have arisen yet.

In order to get as close as possible to a continuous colour ramp when visualising the data, 256 classes were initially used (comparable to an 8-bit image; Section 2.2.3.1) and the output was compared to 128 classes. No differences were seen so 128 classes were used in order to make the classification easier: running from dark blue (smoothest) to yellow (roughest) using the ‘Viridis’ colour ramp. The classes were made in two ways; linear (equal intervals), and equal counts (the default). The outlines were removed from each point in order to avoid adding any artificial grid-like patterns that sometimes occur visually.

The differences in roughness are easier to see with equal counts, however images of both have been included in Appendix I. Standard deviation was considered and appeared visually similar to equal counts, but the software would automatically change the number of classes to a bespoke setting for each cutmark, therefore it was not used. In this study, the classes were not standardised between cutmarks as the cutmarks were being compared.

These were processed blind with respect to the direction of the blow and the orientation of the cutmark as the points were given a solid colour when imported to QGIS. Since the orientation of the cutmark on the screen was arbitrary, the suspected direction of each was identified using a 1-8 system rather than anatomically-based directions (Figure 69). In this case, 1 indicated the top of the screen, with numbers increasing clockwise every 45°. The number that was closest to the smoothest part of the cutmark was assigned as the blow direction. The original images of the cutmark were orientated to the same direction as the QGIS image and compared.

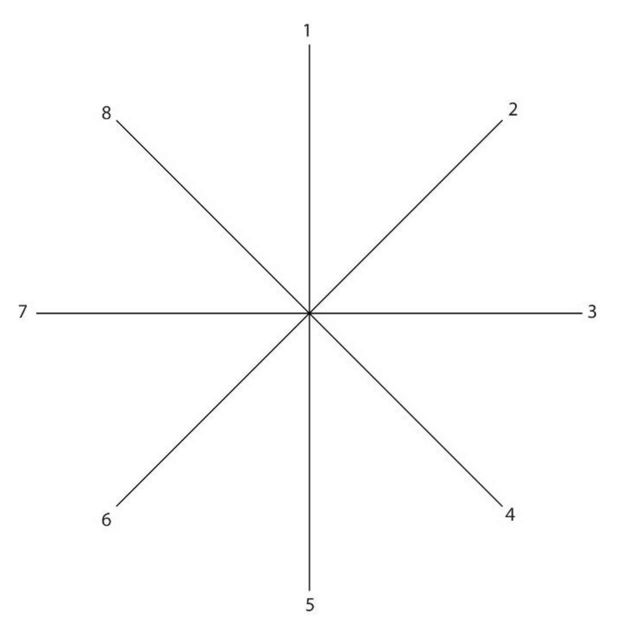


Figure 69: The direction system used to assign a location to the smoothest part of the shaved cutmarks under analysis

### 5.4.4 Shape Analysis

Shape analysis was performed on the incised cutmarks in order to examine any patterns or groupings in their shape (Figure 58, Appendix I). The incised cutmarks were segmented into profiles perpendicular to the longitudinal axis at every 5% using ClCo. Initially, the profiles from only 50% were extracted unless there was a large gap in the profile in which an adjacent profile (45%, 55%) was chosen in its place. These profiles were manually turned into a black line on a white background in Illustrator as binary images are required for shape analysis. It was decided to initially test the 50% profiles and then try combining the 25% and 50% profiles to see if there is any separation based on distance along the length of the cutmark, however none was found. This is further outlined in Section 7.2 and the final decision was to focus on the 50% profiles to test how effective the method would be for analysis of the collection. Each profile was given a set of attributes to see if the factors that influenced the shape of the cut most significantly could be determined. These can be seen in Appendix I. The attributes examined were angle, location, width, and side. The suspected throat cut marks were also noted and an exploratory analysis was run in order to see whether they would cluster when the shapes of the profiles were analysed.

This analysis was done in R/RStudio using Momocs, Here, and Tidyverse (Bonhomme et al. 2014; Müller 2017; Wickham et al. 2019). All code for this was adapted from a workshop by Dr. C. Hoggard as the code is graciously provided on GitHub (Hoggard 2020). The adapted code is in Appendix D. The images were digitised into coordinates within RStudio. Since the initial procedure involves the equivalent of a General Procrustes Analysis (GPA) which scales and shifts all the imported outlines to be the same size, cutmark width was added to the attributes (very small, small, medium, large) so it would still be accounted for. If the results clearly showed that all separation was due to size, a separate set of un-scaled outlines would have been used and the R-based scaling would be skipped, however this was not the case.

For the attributes that were entirely or mostly known, such as location or side of the body, Principal Components Analyses (PCA; using Elliptical Fourier Analysis) were run. As further exploratory analysis, Discriminant Function Analyses (DFA; using Linear Discriminant Functions, terms used interchangeably in this study) were used and hierarchical clustering were performed whether the chosen variables may have influenced the shape and whether cutmarks on this collection could be categorised based on said shape (Pearson 1901; Hotelling 1933, 1936; Martinez and Kak 2001). For some attributes, a secondary analysis was run omitting any cutmarks with ‘unknown’ for that category.

Overall, since these are exploratory statistics, a nearly infinite number of combinations of factors and ‘what if’s’ could be examined. However, that was not feasible and therefore the number of avenues chosen to explore were limited. Future work could look at other combinations of factors as well as investigate the covariance of factors.

### 5.4.5 Full Collection Statistical Analysis

Non-parametric statistical tests (Pearson's Chi-Squared and Kruskal Wallis) were used to explore any relationships between the number of cutmarks per individual and aspects such as demography and burial differences (Pearson 1900; Kruskal and Wallis 1952). Age (five categories), burial orientation (eight directions) and stratigraphic layer (three and five layer) were examined. Sex was not investigated as all were suspected to be male. The Chi-Squared tests were used for checking the binary value of Affected/Not in each variable group and the Kruskal Wallis test was used to look at the number of blows.

## 5.5 Summary

This chapter discussed the collection under investigation (the Weymouth Ridgeway Vikings) and the three stages used in research methods (Initial Analogue Analysis, Development of the Workflow, and Application to the Full Collection). Within the creation of the workflow, the iterative tests, pilot studies, and control development have all been detailed before subsequent discussions in Sections 6.1 and 6.2 as well as Chapter 8. The osteological results from the analogue analysis have been combined with the results from the digital analysis of the 3D models in Chapters 7 and 9. Overall, a method was successfully created which produced photogrammetric models of high metric quality with measurements that were statistically similar to manual calliper measurements. The 3D models were subsequently investigated for profile shape and surface roughness. The location of the trauma on the collection was noted and illustrated. It was also statistically analysed to look for differences in demography or burial pattern. Within this chapter, Objective 2 was addressed (Section 1.3.1).

# 6 Methodological Results

This chapters touches on the results of the iterative tests (Section 5.3.4, Appendix E), before detailing the development of the workflow and outcome of the pilot studies, the testing of the control cradles, and the technical use of surface roughness analysis. Due to the osteological results being dependent on the development of the photogrammetric methodology, the results from Stage Two of the methods are presented first (Section 5.3). The osteological results, encompassing the both the analogue analysis of Stage One and the digital outputs from Stage Three are presented the subsequent chapter (Chapter 7).

## 6.1 Methodological Development through the Pilot Studies

The first steps of the development of the methods were to determine the best file format and pre-processing. These steps are described more fully in Section 5.3.4 and Appendix E. Once it was established that a greyscale 16-bit TIFF would be best (edited for incised, unedited for shaved), the basic parameters such as Tie Point (TP) and Key Point (KP) numbers were analysed with the results suggesting keeping the default values (4,000 and 40,000, respectively) was optimal (Section 5.3.4.2).

The full workflow was then established during the two pilot studies (Figure 64, Section 5.3.5). Throughout the studies, approximate timings of each stage were noted and Table 18 presents the results for one model from set-up to completion. Further discussed in upcoming Section 8.1, it is possible to work on multiple models simultaneously depending on the specification of the computer being used.

Table 18: The timings for each stage of the process to create one model

| Stage | Time (min) | Included in stage |
|---|---|---|
| Photography | 15 | Retrieving and setting up sample<br>Photography<br>Packing sample away |
| Pre-processing | 10 | Transferring images<br>Converting to TIFF<br>Converting to Greyscale<br>Organising files |
| Sparse Point Cloud | 2-4 | Agisoft file creation<br>Sparse Point Cloud creation |
| Control and Editing | 30-60 | Addition of markers on control points<br>Optimisation (x2+)<br>Gradual selection and editing of Sparse Point Cloud (SPC) |
| Dense Point Cloud | 5-8 | Dense Point Cloud (DPC) creation |
| Total | 62-97 | |

After the ten pilot study models were complete, measurements were taken manually and with both DX and FX camera (Section 5.3.7).

### 6.1.1 Descriptive Statistics

Similar procedures were conducted with both pilot studies (Section 5.3.8). Descriptive statistics were found for each measurement obtained by each method. Boxplots were created to visualise the data by comparing the median and interquartile range (IQR) of each measurement taken (e.g. length, width, etc) amongst different methods of model creation (Figures 70 to 73, Appendix E Figures 117 to 119). All descriptive statistics were run, but the median and IQR were the most closely examined because they are better for smaller data sets where outliers could cause a large effect on the results (Field 2009).

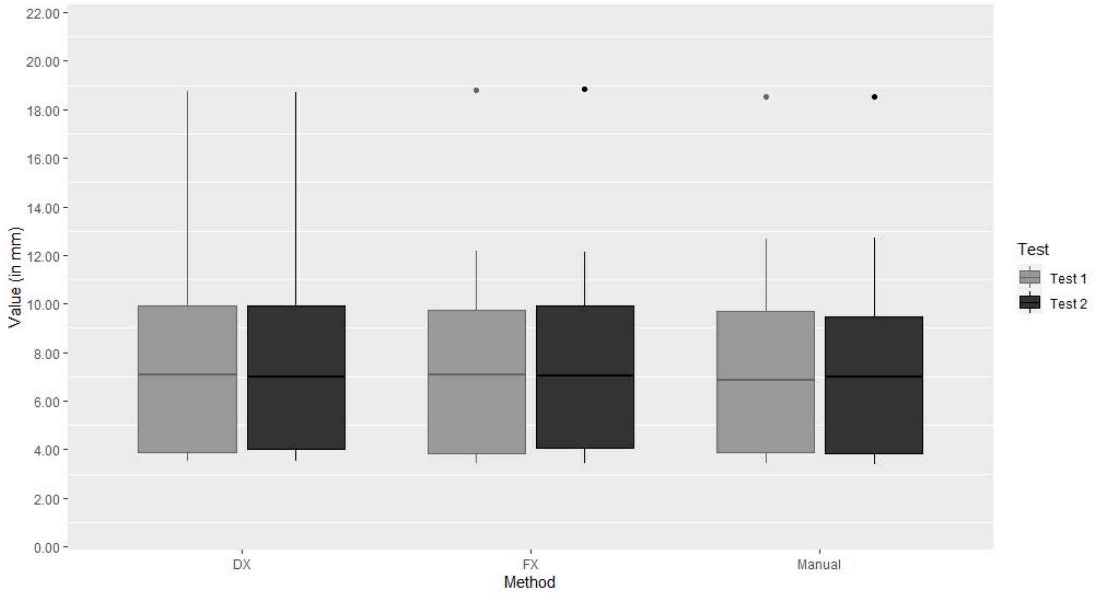


Figure 70: Boxplots of the manual, DX, and FX length measurements for inter-method and intra-observer comparisons of pilot study 1

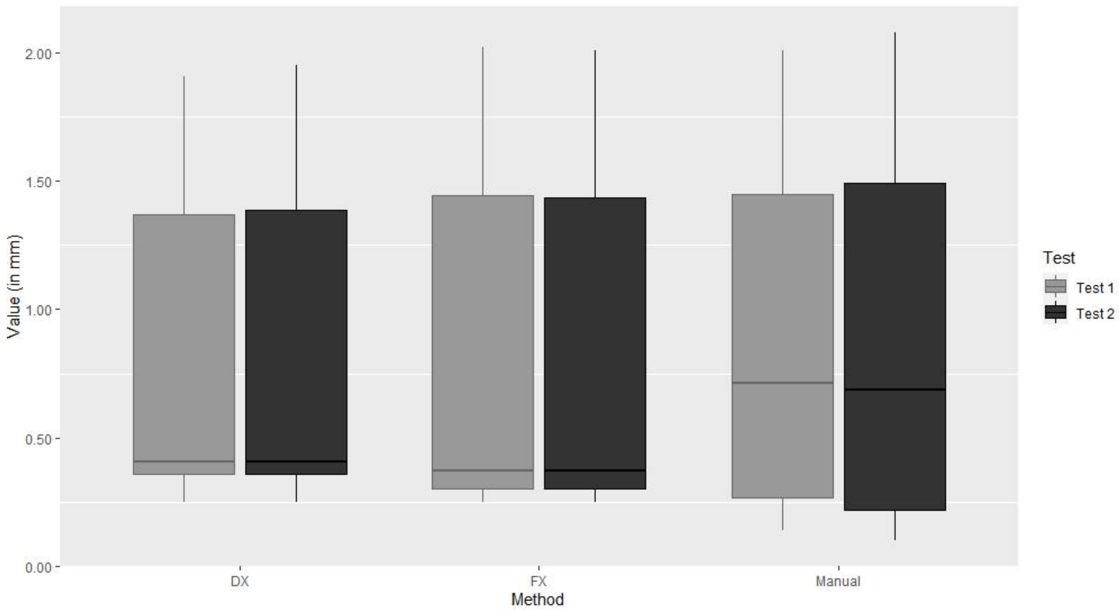


Figure 71: Boxplots of the manual, DX, and FX width measurements for inter-method and intra-observer comparisons of pilot study 1

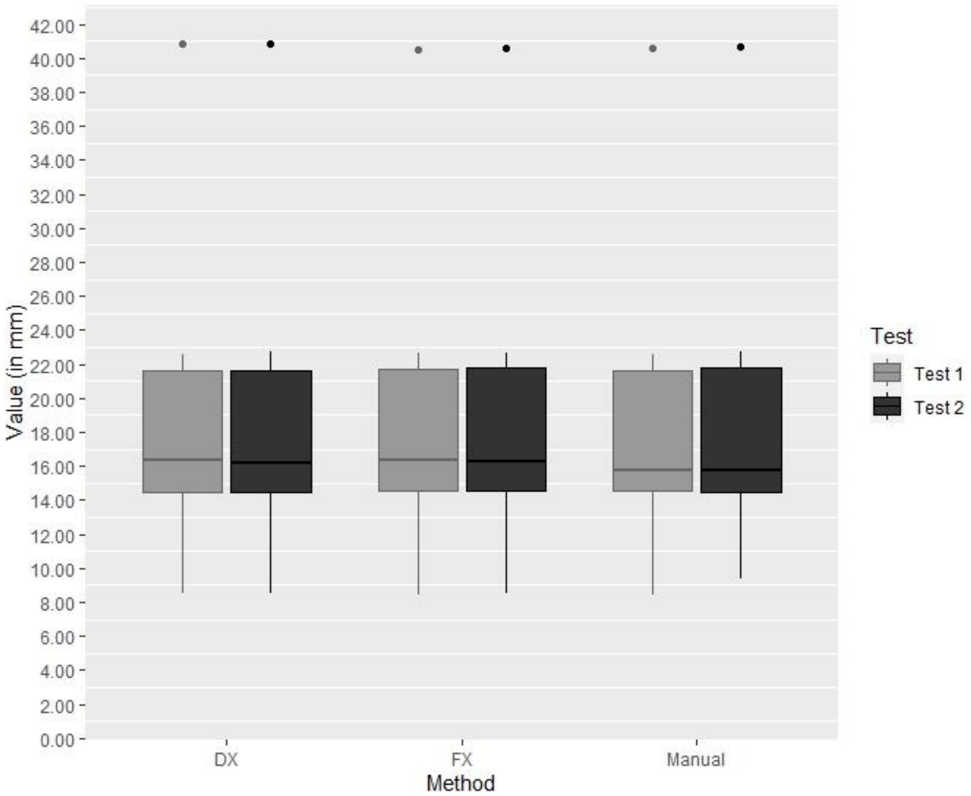


Figure 72: Boxplots of the manual, DX, and FX length measurements for inter-method and intra-observer comparisons of pilot study 2

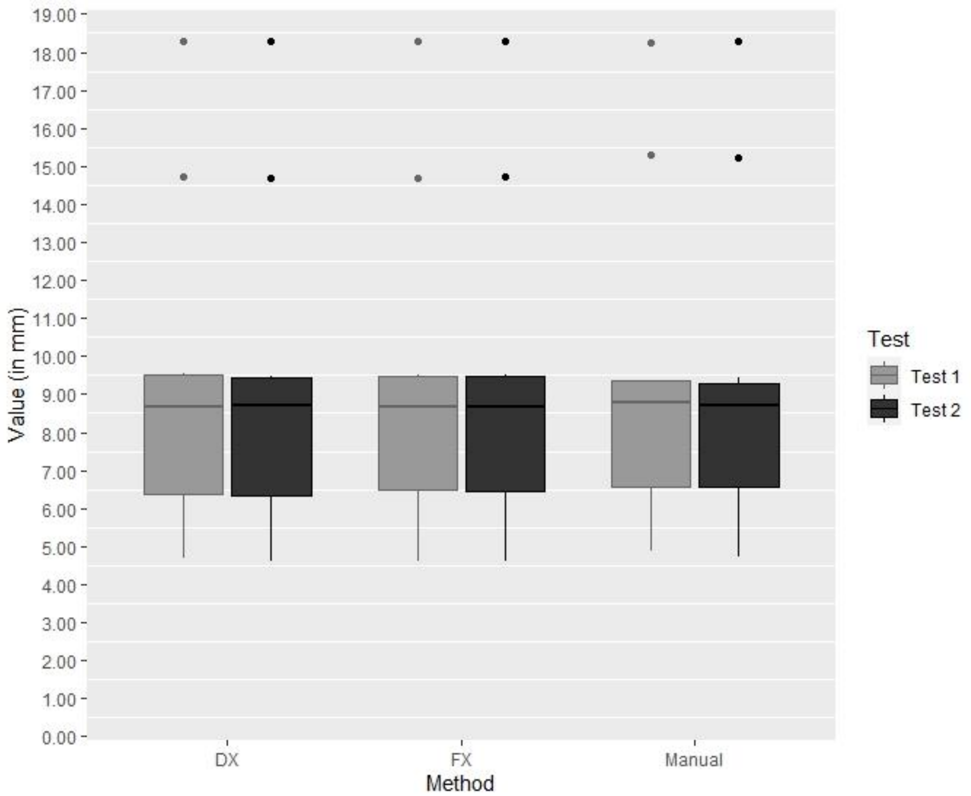


Figure 73: Boxplots of the manual, DX, and FX width measurements for inter-method and intra-observer comparisons of pilot study 2

The test (Test 1) and re-test (Test 2) values were also plotted side-by-side to investigate intra-observer error. Subsequently, statistical tests were run for intra-observer error, however, the small sample size of the pilot studies meant that some of the tests were thought to be less reliable based on how tied values were handled differently in different software (Section 5.3.8) (Field 2009). Additionally, the methods of measurement were compared to determine if they produced statistically similar results. The descriptive statistics of each of the measurements found through each method is presented in Tables 19 and 20.

Table 19: The descriptive statistics for Tests 1 and 2 from pilot study 1 with measurements in mm unless otherwise specified

| | | DX | | FX | | Manual | |
|---|---|---|---|---|---|---|---|
| Measurement | Statistic | Test 1 | Test 2 | Test 1 | Test 2 | Test 1 | Test 2 |
| | N | 10 | 10 | 10 | 10 | 10 | 10 |
| Length | Mean | 7.993 | 8.001 | 7.952 | 7.985 | 7.911 | 7.867 |
| | SE of Mean | 1.536 | 1.529 | 1.544 | 1.538 | 1.542 | 1.547 |
| | Median | 7.069 | 7.014 | 7.097 | 7.011 | 6.855 | 6.980 |
| | 25%ile | 3.758 | 3.882 | 3.713 | 3.903 | 3.754 | 3.738 |
| | 75%ile | 10.575 | 10.588 | 10.417 | 10.590 | 10.495 | 10.285 |
| | IQR | 6.817 | 6.706 | 6.704 | 6.687 | 6.741 | 6.548 |
| Width | Mean | 0.815 | 0.818 | 0.818 | 0.815 | 0.880 | 0.874 |
| | SE of Mean | 0.199 | 0.201 | 0.215 | 0.213 | 0.262 | 0.276 |
| | Median | 0.407 | 0.405 | 0.370 | 0.371 | 0.713 | 0.685 |
| | 25%ile | 0.333 | 0.334 | 0.290 | 0.290 | 0.201 | 0.153 |
| | 75%ile | 1.448 | 1.465 | 1.536 | 1.526 | 1.552 | 1.578 |
| | IQR | 1.116 | 1.130 | 1.246 | 1.236 | 1.351 | 1.425 |
| Wall Height 1 | Mean | 0.533 | 0.540 | 0.549 | 0.555 | | |
| | SE of Mean | 0.145 | 0.146 | 0.159 | 0.162 | | |
| | Median | 0.273 | 0.278 | 0.226 | 0.229 | | |
| | 25%ile | 0.189 | 0.192 | 0.166 | 0.167 | | |
| | 75%ile | 0.879 | 0.884 | 0.954 | 0.947 | | |
| | IQR | 0.691 | 0.692 | 0.788 | 0.780 | | |
| Wall Height 2 | Mean | 0.386 | 0.391 | 0.425 | 0.427 | | |
| | SE of Mean | 0.128 | 0.129 | 0.142 | 0.142 | | |
| | Median | 0.164 | 0.166 | 0.192 | 0.195 | | |
| | 25%ile | 0.123 | 0.130 | 0.094 | 0.092 | | |
| | 75%ile | 0.582 | 0.593 | 0.670 | 0.670 | | |
| | IQR | 0.459 | 0.463 | 0.576 | 0.578 | | |
| Opening Angle (°) | Mean | 87.528 | 87.501 | 90.171 | 90.620 | | |
| | SE of Mean | 7.328 | 7.174 | 7.519 | 7.276 | | |
| | Median | 84.414 | 84.706 | 88.884 | 88.910 | | |
| | 25%ile | 75.879 | 75.467 | 77.466 | 79.703 | | |
| | 75%ile | 104.648 | 103.347 | 103.371 | 103.879 | | |
| | IQR | 28.769 | 27.880 | 25.905 | 24.176 | | |

Table 20: The descriptive statistics for Tests 1 and 2 from pilot study 2 with measurements in mm

| Measurement | Statistic | DX | | FX | | Manual | |
|---|---|---|---|---|---|---|---|
| | | Test 1 | Test 2 | Test 1 | Test 2 | Test 1 | Test 2 |
| | N | 10 | 10 | 10 | 10 | 10 | 10 |
| Length | Mean | 18.680 | 18.677 | 18.737 | 18.745 | 18.549 | 18.691 |
| | SE of Mean | 2.836 | 2.838 | 2.803 | 2.813 | 2.831 | 2.802 |
| | Median | 16.365 | 16.205 | 16.380 | 16.245 | 15.775 | 15.755 |
| | 25%ile | 13.480 | 13.525 | 13.613 | 13.630 | 13.618 | 13.608 |
| | 75%ile | 22.450 | 22.470 | 22.448 | 22.565 | 22.473 | 22.575 |
| | IQR | 8.970 | 8.945 | 8.835 | 8.935 | 8.855 | 8.968 |
| Width | Mean | 9.319 | 9.287 | 9.337 | 9.334 | 9.444 | 9.360 |
| | SE of Mean | 1.328 | 1.331 | 1.317 | 1.322 | 1.333 | 1.339 |
| | Median | 8.675 | 8.715 | 8.655 | 8.680 | 8.770 | 8.695 |
| | 25%ile | 6.043 | 5.983 | 6.195 | 6.158 | 6.138 | 6.175 |
| | 75%ile | 10.853 | 10.785 | 10.815 | 10.828 | 10.860 | 10.883 |
| | IQR | 4.810 | 4.803 | 4.620 | 4.670 | 4.723 | 4.708 |

### 6.1.2 Intra-Observer Error

Intra-observer error was evaluated for the manual reference measurements and the photogrammetric measurements (Section 5.8.3.1). It was visually considered using boxplot and was also statistically analysed. When examining the descriptive statistics of each method in both pilot studies, good agreement was shown between the first and second test, indicating that these methods have good intra-observer reliability. Visually, the similarity between the repeated measurements can be seen in the boxplots in Figures 70 and 71 and Appendix E. This was further statistically underlined by the use of the Wilcoxon Signed-Rank test and the Sign test as discussed in Section 5.8.3 (Table 21).

Table 21: The Intra-observer error results for the Wilcoxon Signed Rank and the Sign Test for the pilot study 1

| Measurement | Statistic | DX | FX | Manual |
|---|---|---|---|---|
| Length | Z | $-0.153^{c}$ | $-0.255^{c}$ | $-0.561^{b}$ |
| | Wilx Sig.* | 0.878 | 0.799 | 0.575 |
| | Sign Exact Sig. | 0.754^ | 1.000^ | 1.000^ |
| Width | Z | $-0.051^{b}$ | $-1.588^{b}$ | $-0.210^{b}$ |
| | Wilx Sig.* | 0.959 | 0.112 | 0.833 |
| | Sign Exact Sig. | 0.754^ | 0.109^ | 0.727^ |
| WH1 | Z | $-1.785^{c}$ | $-1.071^{c}$ | -- |
| | Wilx Sig.* | 0.074 | 0.284 | -- |
| | Sign Exact Sig. | 0.754^ | 0.754^ | -- |
| WH2 | Z | $-0.652^{c}$ | $-1.009^{c}$ | -- |
| | Wilx Sig.* | 0.514 | 0.313 | -- |
| | Sign Exact Sig. | 1.000^ | 0.508^ | -- |
| OA | Z | $-0.051^{b}$ | $-1.478^{c}$ | -- |
| | Wilx Sig.* | 0.959 | 0.139 | -- |
| | Sign Exact Sig. | 1.000^ | 0.109^ | -- |

a. Wilcoxon Signed Ranks Test, b. Based on positive ranks., c. Based on negative ranks; Test 2 - Test 1
*Asymp. Sig. (2-tailed)
^ Binomial distribution used

The same procedure was completed for the second pilot study as for the first. The visual depiction is show in Figures 72 and 73. Further analysis was performed using the Wilcoxon Signed Rank and Sign test to check the intra-observer error. All results were non-significant except for one Wilcoxon Signed Rank test which is thought to be due to how the software handles ties (Table 22).

Table 22: Intra-observer error results from the Wilcoxon Signed Rank and Sign test for the pilot study 2

| Measurement | Statistic | DX | FX | Manual |
|---|---|---|---|---|
| Length | Z | -0.102[c] | -0.474[c] | -1.888[c] |
| | Wilx Sig.* | 0.919 | 0.635 | 0.059 |
| | Sign Exact Sig. | 1.000^ | 1.000^ | 0.109^ |
| Width | Z | -2.094[b] | -2.094[b] | -0.255[b] |
| | Wilx Sig.* | 0.036 | 0.779 | 0.799 |
| | Sign Exact Sig. | 0.180^ | 1.000^ | 0.754^ |

a. Wilcoxon Signed Ranks Test, b. Based on positive ranks., c. Based on negative ranks; Test 2 - Test 1
*Asymp. Sig. (2-tailed)
^ Binomial distribution used

Overall, all the methods used show non-significant differences when both statistically and visually comparing test and re-test values. Therefore, all methods have sufficient intra-observer reliability to use in studies (Section 8.1.2). The method designed for this study has similar intra-observer error to the established methods, such as manual measurements which were also tested here, thus indicating it is appropriately reliable.

### 6.1.3 Statistical Comparison of Methods

For both pilot studies, the photogrammetric models were compared to the manual method through multiple methods (Sections 5.3.7 and 5.3.8.2). Overall, the descriptive statistics and boxplots of the measurements showed that the measurements were similar (Figures 70 to 73, Appendix E). Additionally, all methods of measurement were compared using a Friedman test, which showed non-significance (Table 23). The different combinations were also compared pair-wise with a Wilcoxon Signed Rank test and a Sign test. For these results, a Bonferroni correction was required and therefore the p-value for significance was p=0.017 for both pilot studies. All of these resulted in non-significant values as well (Tables 24 and 25).

Table 23: Results of the Friedman Test for both pilot studies

| Pilot Study | Measurement | Chi-Square | Degrees of Freedom | Asymp. Sig |
|---|---|---|---|---|
| PS 1 | Length | 2.400 | 2 | 0.301 |
| | Width | 1.000 | 2 | 0.607 |
| PS 2 | Length | 0.649 | 2 | 0.723 |
| | Width | 0.667 | 2 | 0.717 |

Table 24: Comparisons using the Wilcoxon Signed Ranks Test and Sign Tests of measurements that have a manual equivalent for pilot study 1 (those without a manual equivalent are in Table 26)

| | Length | | | Width | | |
|---|---|---|---|---|---|---|
| | Z | Asymp. Sig. (2-tailed) | Sign* | Z | Asymp. Sig. (2-tailed) | Sign* |
| FX-DX | -1.478[c] | 0.139 | 0.109 | -0.764[b] | 0.445 | 0.754 |
| DX-Manual | -0.968[b] | 0.333 | 0.754 | -0.980[b] | 0.327 | 0.727 |
| FX-Manual | -0.561[b] | 0.575 | 0.754 | -0.980[b] | 0.327 | 0.727 |

a. Wilcoxon Signed Ranks Test, b. Based on negative ranks., c. Based on positive ranks.
*Binomial distribution

Table 25: Comparisons using the Wilcoxon Signed Ranks and Sign Tests for length and widths for pilot study 2

| | Length | | | Width | | |
|---|---|---|---|---|---|---|
| | Z | Asymp. Sig. (2-tailed) | Sign* | Z | Asymp. Sig. (2-tailed) | Sign* |
| FX-DX | -1.187[d] | 0.235 | 0.508 | -0.119[c] | 0.906 | 1.000 |
| DX-Manual | -0.119[c] | 0.906 | 1.000 | -1.428[b] | 0.153 | 0.344 |
| FX-Manual | -1.011[c] | 0.312 | 1.000 | -0.919[b] | 0.358 | 1.000 |

a. Wilcoxon Signed Ranks Test, b. Based on negative ranks., c. Based on positive ranks.
*Binomial distribution

In summary, the results of the comparisons in both pilot studies reveal that the measurements obtained from photogrammetric models are statistically similar to currently used methods (manual measurements), and therefore they are valid means to obtain measurements. When comparing multiple methods, the Friedman test produced results indicating non-significant differences between the methods for each measurement.

### 6.1.4 FX and DX Comparison

In both pilot studies, the models created from the two types of cameras needed to be compared to determine if the specifications of the camera had altered the results (Appendix D). Even without any Bonferroni correction, these were deemed non-significant, demonstrating that the specifications of the camera do not impact the models created or the measurements derived from either shaved or incised cutmarks (Table 26).

Table 26: Comparisons of DX and FX cameras in both pilot studies

| | PS 1 | | | PS 2 | | |
|---|---|---|---|---|---|---|
| | Z | Wilx Sig.* | Sign Exact Sig. | Z | Wilx Sig.* | Sign Exact Sig. |
| Length | -1.478$^{c}$ | 0.139 | 0.109 | -1.187$^{c}$ | 0.235 | 0.508$^{\wedge}$ |
| Width | -0.764$^{b}$ | 0.445 | 0.754 | -0.119$^{b}$ | 0.906 | 1.000$^{\wedge}$ |
| WH 1 | -0.561$^{b}$ | 0.575 | 1.000 | - | - | - |
| WH 2 | -1.580$^{b}$ | 0.114 | 0.344 | - | - | - |
| OA | -1.274$^{b}$ | 0.203 | 0.109 | - | - | - |

## 6.2 The Control Cradle

Another methodological component of this study was to examine the control cradle itself to decide whether the design was appropriate to use to create scaled models of small objects (Sections 2.4.3.3, 5.3.6, and 5.3.8.3). Overall, all models were successfully created using a combination of three control cradles and associated wedges.

Tables 27 and 28 contain the descriptive statistics and the normality tests that were performed on the errors from the control and check points for each of the three control cradles (Figure 74). The errors were analysed as a whole using Mann-Whitney U tests and also broken down into constituent x, y, and z-components. No statistically significant differences were found between the control point error and check point error.

Table 27: The summary statistics and Shapiro-Wilk results for the overall error (in mm) in the check and control points with significant values in bold and the p values in parentheses

| | OG ($N_{CP}$=12, $N_{ChP}$=8) | | MK2 ($N_{CP}$=26,$N_{ChP}$=26) | | PH ($N_{CP}$=30, $N_{ChP}$=30) | |
|---|---|---|---|---|---|---|
| | Control | Check | Control | Check | Control | Check |
| Mean | 0.081 | 0.078 | 0.157 | 0.158 | 0.328 | 0.306 |
| SD | 0.036 | 0.040 | 0.084 | 0.105 | 0.123 | 0.102 |
| SE of Mean | 0.010 | 0.014 | 0.017 | 0.021 | 0.022 | 0.019 |
| Median | 0.073 | 0.092 | 0.138 | 0.137 | 0.355 | 0.313 |
| IQR | 0.024 | 0.068 | 0.064 | 0.086 | 0.175 | 0.089 |
| Range | 0.114 | 0.109 | 0.394 | 0.458 | 0.560 | 0.490 |
| Shapiro-Wilk | **0.810 (0.012)** | 0.895 (0.261) | **0.833 (0.001)** | **0.784 (<0.001)** | 0.963 (0.360) | 0.931 (0.053) |
| Mann-Whitney U | | 48.000 (1.000) | | 319.000 (0.728) | | 378.500 (0.290) |

Table 28: The summary statistics and Shapiro-Wilk results for the error (in mm) in the check and control points with significant values in bold and the p values in parentheses broken down into x, y, and z components for each cradle

| | | x | | y | | z | |
|---|---|---|---|---|---|---|---|
| | | Control | Check | Control | Check | Control | Check |
| OG ($N_{CP}$=12 $N_{ChP}$=8) | Mean | 0.039 | 0.028 | 0.038 | 0.039 | 0.050 | 0.051 |
| | SD | 0.023 | 0.021 | 0.030 | 0.031 | 0.031 | 0.039 |
| | SE of Mean | 0.007 | 0.007 | 0.009 | 0.011 | 0.009 | 0.014 |
| | Median | 0.037 | 0.024 | 0.029 | 0.039 | 0.047 | 0.038 |
| | IQR | 0.039 | 0.019 | 0.038 | 0.061 | 0.038 | 0.062 |
| | Range | 0.072 | 0.071 | 0.107 | 0.072 | 0.114 | 0.114 |
| | Shapiro-Wilk | 0.957 (0.746) | 0.863 (0.130) | 0.894 (0.132) | 0.853 (0.103) | 0.915 (0.246) | 0.903 (0.309) |
| | Mann-Whitney U | | 32.000 (0.217) | | 46.000 (0.877) | | 44.500 (0.787) |
| MK2 ($N_{CP}$=26 $N_{ChP}$=26) | Mean | 0.062 | 0.092 | 0.069 | 0.066 | 0.109 | 0.081 |
| | SD | 0.046 | 0.082 | 0.050 | 0.052 | 0.081 | 0.085 |
| | SE of Mean | 0.009 | 0.016 | 0.010 | 0.010 | 0.016 | 0.017 |
| | Median | 0.042 | 0.063 | 0.053 | 0.055 | 0.108 | 0.056 |
| | IQR | 0.065 | 0.087 | 0.080 | 0.056 | 0.082 | 0.069 |
| | Range | 0.174 | 0.343 | 0.175 | 0.221 | 0.353 | 0.368 |
| | Shapiro-Wilk (W) | **0.907 (0.022)** | **0.834 (0.001)** | 0.942 (0.151) | **0.834 (0.001)** | **0.847 (0.001)** | **0.770 (<0.001)** |
| | Mann-Whitney U | | 273.000 (0.234) | | 310.500 (0.615) | | 232.000 (0.052) |
| PH ($N_{CP}$=30 $N_{ChP}$=30) | Mean | 0.195 | 0.195 | 0.166 | 0.134 | 0.138 | 0.120 |
| | SD | 0.114 | 0.116 | 0.130 | 0.116 | 0.095 | 0.094 |
| | SE of Mean | 0.021 | 0.021 | 0.024 | 0.021 | 0.017 | 0.017 |
| | Median | 0.181 | 0.161 | 0.132 | 0.102 | 0.130 | 0.103 |
| | IQR | 0.195 | 0.172 | 0.186 | 0.158 | 0.118 | 0.139 |
| | Range | 0.444 | 0.435 | 0.447 | 0.472 | 0.415 | 0.396 |
| | Shapiro-Wilk | 0.975 (0.681) | 0.955 (0.236) | **0.880 (0.003)** | **0.892 (0.005)** | 0.935 (0.068) | **0.925 (0.037)** |
| | Mann-Whitney U | | 433.500 (0.807) | | 386.500 (0.348) | | 397.000 (0.433) |

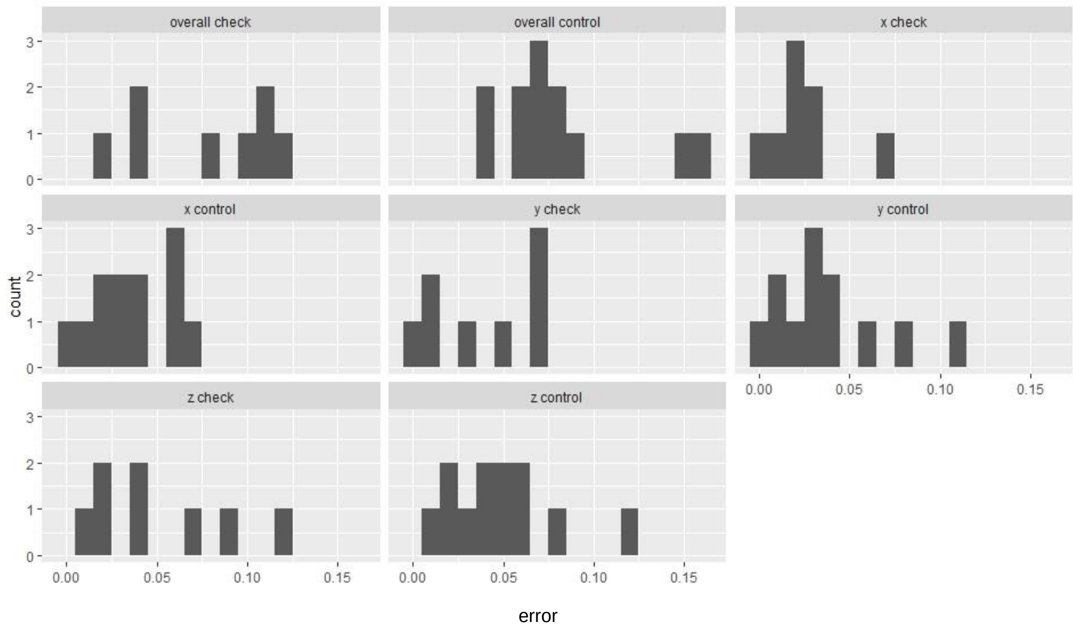


Figure 74: Normality histograms of the errors (in mm) seen for OG (other graphs found in Appendix E Figure 120 and 121)

For each of the three cradles, five different models were randomly selected and the coordinates exported along with the errors (Sections 5.3.6 and 5.3.8.3). The values of each x, y, and z were graphed against the absolute x, y, and z errors in order to determine whether any of the error was systematic as opposed to purely random (Figure 75, Appendix E Figures 122 to 132).

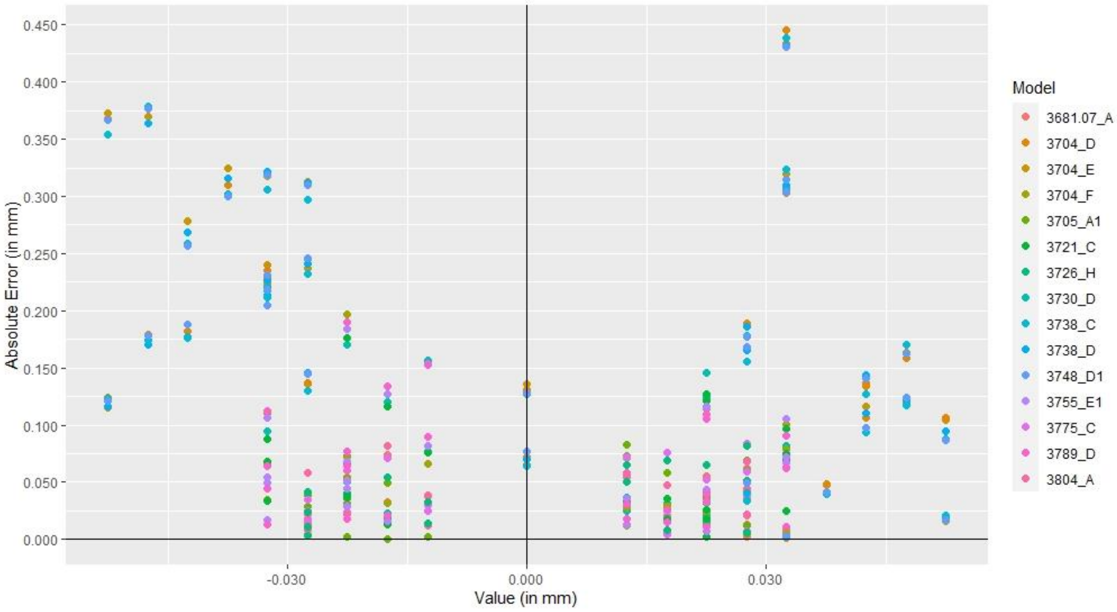


Figure 75: A scatterplot of the values and errors along the x-axis of all control cradles (see Appendix E for the scatterplots that are split by cradle)

The only error that had visual evidence of systematic issues when plotted was the z errors, though this was not statistically significant for any cradle other than OG when analysed using the Spearman's rho ($r_s$). Additionally, the relationship was weak and therefore it was considered acceptable and not confounding for this study. There was statistical significance in some correlations involving x and y, however, when examining the $r_s$ and $R^2$ value of each, these relationships were not seen to be strong. They were therefore not of concern for this study but should be examined for any control cradle in use.

Despite the non-significance, it appears there might be a relationship between the height of the control point and the error magnitude likely due to the printing process. This is discussed further in Section 8.2. The error, both z and overall, was considered small enough to be fit for purpose for this study (Table 29).

Table 29: The correlations on the x, y, and z-values and x, y, and z error for each control cradle with significant values in bold using non-parametric tests as established by the normality tests also included in the table. For each cradle, five models are in use

| | | N/df | Kolmogorov-Smirnov* | | Shapiro-Wilks* | | $r_s$ | Sig (two tailed) | $R^2$ Linear |
|---|---|---|---|---|---|---|---|---|---|
| | | | Value | Sig | Value | Sig | | | |
| OG | x | 100 | 0.105 | **0.009** | 0.945 | **0.000** | 0.202 | 0.044 | 0.068 |
| | y | 100 | 0.083 | 0.083 | 0.944 | **0.000** | -0.260 | **0.009** | 0.029 |
| | z | 100 | 0.152 | **0.000** | 0.871 | **0.000** | 0.666 | **0.000** | 0.423 |
| MK2 | x | 130 | 0.137 | **0.000** | 0.910 | **0.000** | -0.106 | 0.229 | 0.032 |
| | y | 130 | 0.129 | **0.000** | 0.925 | **0.000** | 0.404 | **0.000** | 0.218 |
| | z | 130 | 0.143 | **0.000** | 0.849 | **0.000** | -0.057 | 0.518 | 0.314 |
| PH | x | 150 | 0.091 | **0.004** | 0.970 | **0.002** | -0.501 | **0.000** | 0.201 |
| | y | 150 | 0.150 | **0.000** | 0.876 | **0.000** | -0.420 | **0.000** | 0.276 |
| | z | 150 | 0.073 | 0.050 | 0.946 | **0.000** | 0.114 | 0.166 | 2.627e-5 |
| Overall | x | 380 | 0.175 | **0.000** | 0.842 | **0.000** | -0.213 | **0.000** | 0.063 |
| | y | 380 | 0.169 | **0.000** | 0.783 | **0.000** | -0.072 | 0.159 | 0.078 |
| | z | 380 | 0.121 | **0.000** | 0.886 | **0.000** | 0.030 | 0.561 | 0.034 |

*Only the normality for the error data is presented here, this is due to the locations of the CP and ChP (values) being known and systematically set-up, therefore they will inherently have a non-normal distribution

## 6.3 Surface Roughness

The final methodological aspect of this study was the creation of a workflow to analyse surface roughness on bones (Table 30) (Sections 4.1.1, 4.1.4, and 5.4.3). The workflow that was designed successfully created images that could be visually analysed for directionality, with the entry corresponding to the smoother portion. In this study, the output Z_IQR was not further mathematically or statistically analysed, though potentially could be. An example of the image captured, both alone and superimposed on the bone itself, are seen in Figure 76. The remainder are found in Appendix E. Overall, the bones and 3D models all showed a clear bias towards one side when the smoothest areas were examined. All were found to match or nearly match.

Table 30: The ten cutmarks used for the surface roughness analysis with the minimum and maximum zIQR values (in m)

| Cutmark Code | Location | Digital Direction | Manual Direction | Minimum zIQR | Maximum zIQR |
|---|---|---|---|---|---|
| 3708_F2 | Mandibular corpus | 5 | 5 | 0.000029 | 0.008277 |
| 3711_F | Mandibular corpus | 6 | 6 | 0.000034 | 0.000525 |
| 3720_B2 | Mandibular corpus | 2 | 2 | 0.000030 | 0.000752 |
| 3730_D | Mandibular corpus | 5 | 5 | 0.000026 | 0.001105 |
| 3735_A1 | Mandibular corpus | 7 | 7 | 0.000016 | 0.000897 |
| 3748_B | Mandibular corpus | 5 | 5 | 0.000010 | 0.000492 |
| 3750_C2 | Mandibular corpus | 7 | 7 | 0.000012 | 0.000967 |
| 3752_D1 | Mandibular corpus | 7 | 7 | 0.000017 | 0.000576 |
| 3752_E | Mandibular neck | 2/3 | 2 | 0.000016 | 0.000718 |
| 3763_D | Clavicle | 1 | 1 | 0.000015 | 0.000797 |

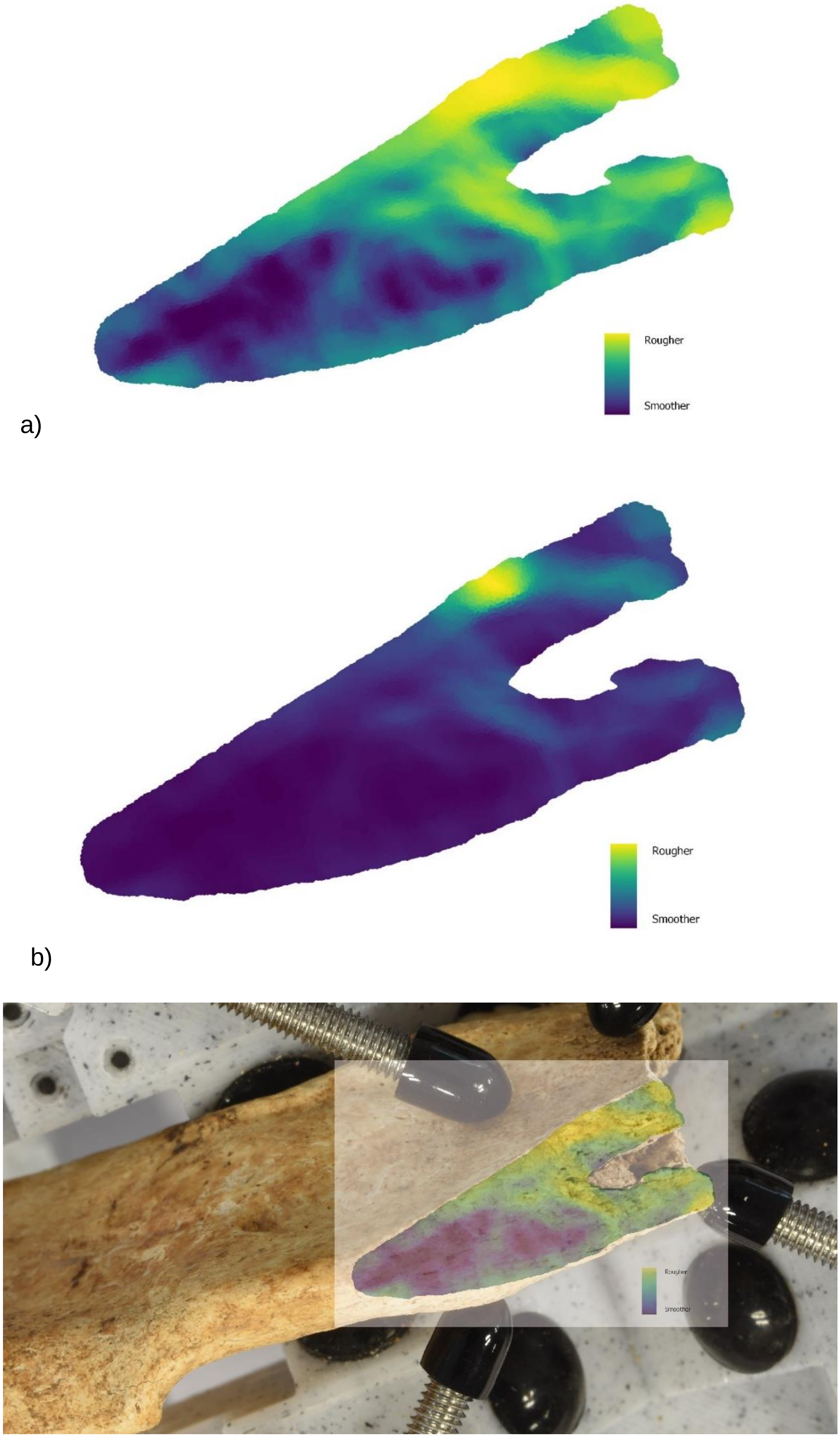


Figure 76: An example of the output of 3748_B seen using a) 128 classes of equal counts, b) 128 classes of equal intervals, and c) the overlayed version. The smoothest value is 0.00001m and the roughest 0.000492m (remaining images are in Appendix I)

## 6.4 Summary

This chapter presented the results of the methodological aspect of this project. Overall, it was shown that the methodology designed was successful and the control cradle was beneficial for creating models which were of high metric quality. These findings all supported the use of close-range photogrammetry in the digitisation of human remains. The implications of these results and further work that could be explored are discussed in Chapter 8. This chapter addressed Objectives 2 to 4, and 6 (Section 1.3.1):

- Photogrammetric models allow for the lengths and widths of SFT to be measured on bone with high levels of precision
- The statistical results found from these measurements are comparable to those taken manually and there was no difference between models made from DX and FX cameras
- Intra-observer error was low for each measurement from the photogrammetric models and it was comparable to the manual intra-observer error
- The 3D control cradle was successful and there were no differences in error between the control and the check points, however it is important to test the control cradle before use to ensure there are no systematic errors in the x, y, and z-components
- The use of QGIS for exploring surface roughness of cutmarks shows great promise and requires further examination

# 7 Osteological Results

This chapter covers the osteological results from Stage One and Three and encompasses the initial analogue investigation and the data from the 3D models (Sections 5.1 and 5.3). It focuses on the Weymouth Ridgeway Vikings and presents the number and distribution of injuries and the statistical results analysing these injuries in relation to assorted demographic and burial variables. It also discusses the outcome of the shape analysis and surface roughness analysis (Sections 5.4.3, 5.4.4, 8.4, and 9.4). The full catalogues of sharp force trauma (SFT) found in the articulated and disarticulated remains are found in Appendix F and G, respectively (also see supplementary Adobe Illustrator [.ai] files).

## 7.1 Trauma throughout the Collection

It was not within the remit of this study to look at re-associating the individuals and therefore it is possible that some of the cutmarks found on the cranial and postcranial remains were caused by the same blow. Due to this, the cranial and postcranial remains are mainly examined separately to evaluate frequencies. The cervical vertebrae (CV) are an exception to this as the full number of affected vertebrae was required to compare to other sites (Section 9.6). The disarticulated remains are also discussed separately to the articulated ones. Any affected fragments from within the articulated collection that were noted as ‘commingled’ are discussed within the disarticulated section. No bones labelled as commingled in the postcranial remains were found to have trauma. Tables 31 and 32 show the total number of individuals that received each number of blows; both the minimum and maximum number of blows, based purely on osteological evidence, are presented (Figures 77 and 78). In this instance, ‘maximum’ refers to the total number of blows if the tentative associations between cutmarks on different bones (e.g. a vertebrae and mandible) are disregarded due to the level of uncertainty. It is not the maximum possible number of blows the individual received as that number cannot be determined with only skeletal remains. Both numbers are presented here to avoid the over-interpretation of which cutmarks may have been related.

Table 31: The number of individuals with each maximum and minimum number of blows seen based on osteological evidence in the articulated cranial remains

| | | Number of Blows | | | | | | | | | | | | | | |
|---|---|---|---|---|---|---|---|---|---|---|---|---|---|---|---|---|
| Number of Individuals Affected (Min./Max.) | Total Number Affected (N=49) | 0 | 1 | 2 | 3 | 4 | 5 | 6 | 7 | 8 | 9 | 10 | 11 | 12 | 13 | 14 |
| Min. Blows | 38 | 9 | 6 | 9 | 4 | 9 | 3 | 2 | 1 | 2 | 2 | 2 | 0 | 0 | 0 | 0 |
| Max. Blows | 38 | 9 | 6 | 8 | 4 | 8 | 3 | 2 | 3 | 0 | 2 | 2 | 2 | 0 | 0 | 0 |

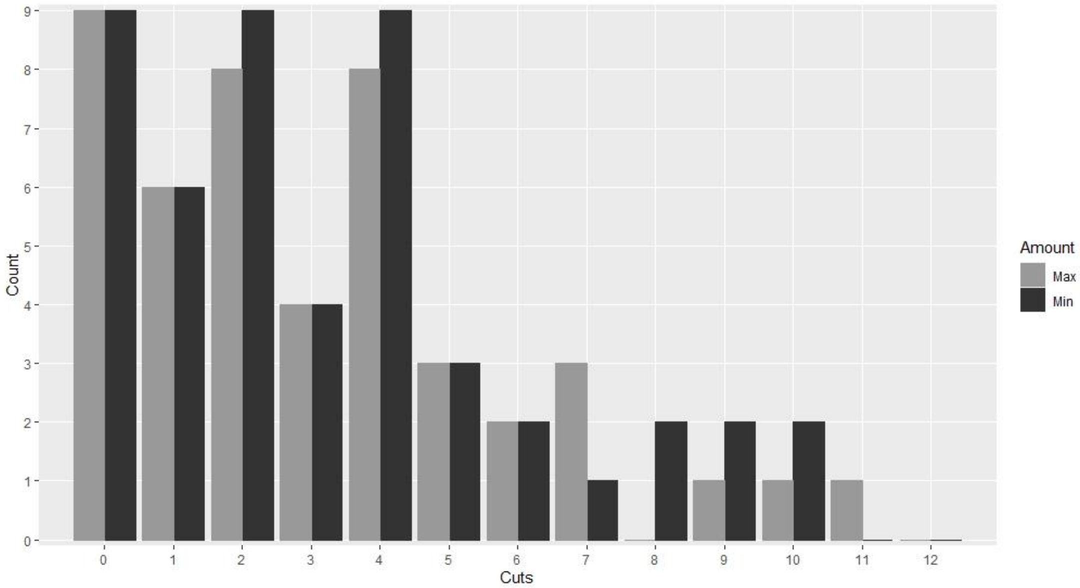


Figure 77: A grouped bar chart of the minimum and maximum number of blows found on the cranial remains

Table 32: The number of individuals with each maximum and minimum number of blows seen based on osteological evidence in the articulated postcranial remains

| | | Number of Blows | | | | | | | | | | | | | | |
|---|---|---|---|---|---|---|---|---|---|---|---|---|---|---|---|---|
| Number of Individuals Affected (Min./Max.) | Total Number Affected (N=61) | 0 | 1 | 2 | 3 | 4 | 5 | 6 | 7 | 8 | 9 | 10 | 11 | 12 | 13 | 14 |
| Min. Blows | 27 | 34 | 7 | 5 | 8 | 0 | 2 | 1 | 1 | 0 | 1 | 0 | 1 | 1 | 0 | 0 |
| Max. Blows | 27 | 34 | 7 | 5 | 8 | 0 | 2 | 1 | 1 | 0 | 0 | 0 | 1 | 2 | 0 | 0 |

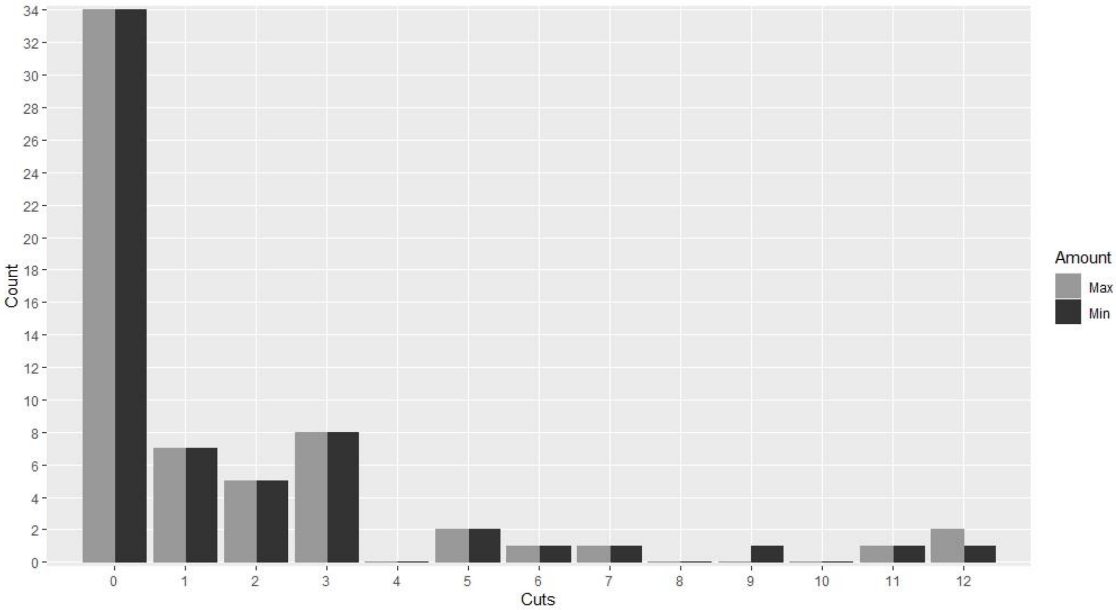


Figure 78: A grouped bar chart of the minimum and maximum number of blows found on the postcranial remains

Table 33 presents the total number of blows found and rates of blows per person. The majority of individuals with cutmarks were affected by three or less blows (postcranial) or four or less blows (cranial). Although the use of mean is not entirely appropriate, as it is impossible to have a fraction of a cutmark present, the postcranial median is not entirely representative since over half the postcranial individuals do not have trauma. The six most highly affected individuals are presented in Table 34 and further discussed in Section 9.1.

Table 33: The number of blows per individual seen across the collection

| | | Number of Individuals | | | Per Person | | Per Affected Person | |
|---|---|---|---|---|---|---|---|---|
| | Discrete Blows | Total | Affected | Not Affected | Mean | Median | Mean | Median |
| Articulated | 257-274 | *52 | | | | | | |
| *Cranial* | 161-175 | 49 | 38 | 9 | 3.29-3.57 | 3 | 4.24-4.61 | 4 |
| *Postcranial* | 69-99 | 61 | 27 | 34 | 1.13-1.62 | 0 | 2.55-3.67 | 3 |
| Disarticulated | 39-40 | | | | | | | |

*The highest MNLI was chosen here as it is highly probable all postcranial remains did initially have a skull despite the lower cranial MNLI currently

Table 34: The individuals with the highest blows and their age category (YA=young adult, PA=prime adult, MA=mature adult)

| Cranial/Postcranial | SK | Minimum Blows | Maximum Blows | Age Group |
|---|---|---|---|---|
| Cranial | 3704 | 10 | 11 | YA |
| | 3707 | 10 | 10 | PA |
| | 3722 | 9 | 11 | YA |
| Postcranial | 3715 | 11 | 12 | PA |
| | 3777 | 12 | 12 | MA |
| | 3778 | 9 | 11 | MA |

### 7.1.1 Neurocrania

The skulls suffered extensive post-mortem damage (Section 4.1.2). Despite this, amongst what remains of the skulls, it is thought that most of the SFT has been able to be identified. However, quick reconstructions were done of the skulls and it is thought at least 16 have indications of blunt force trauma (BFT). Further reconstructions would be required to confirm and refine this number, as well as potentially find further SFT currently obscured by fracturing. Table 35 contains the number of neurocranial blows found in the cranial remains (Figure 79).

Table 35: The number of individuals with each number of blows seen in the neurocranium and its components based on osteological evidence in the articulated cranial remains

| | Side | Total Number of Individuals Affected | Number of Blows 1 | 2 | 3 | 4 |
|---|---|---|---|---|---|---|
| Neurocranium | Left | 10 | 8 | 1 | 0 | 0 |
| | Right | 12 | 7 | 2 | 1 | 0 |
| | Central | 2 | 2 | 0 | 0 | 0 |
| | Bilateral | *1 | 1 | 0 | 0 | 0 |
| | Total | 18 | 10 | 6 | 1 | 1 |
| Parietal | Left | 3 | 3 | 0 | 0 | 0 |
| | Right | 4 | 2 | 1 | 1 | 0 |
| | Bilateral | 0 | 0 | 0 | 0 | 0 |
| | Total | 5 | 2 | 2 | 0 | 1 |
| Frontal | Left | 2 | 1 | 1 | 0 | 0 |
| | Right | 1 | 1 | 0 | 0 | 0 |
| | Central | 0 | 0 | 0 | 0 | 0 |
| | Total | 3 | 2 | 1 | 0 | 0 |
| Occipital | Left | 3 | 2 | 0 | 0 | 0 |
| | Right | 6 | 4 | 1 | 0 | 0 |
| | Central | 2 | 2 | 0 | 0 | 0 |
| | Bilateral | *1 | 1 | 0 | 0 | 0 |
| | Total | 8 | 7 | 2 | 0 | 0 |
| Temporal | Left | 4 | 3 | 0 | 0 | 0 |
| | Right | 4 | 3 | 0 | 0 | 0 |
| | Bilateral | *1 | 1 | 0 | 0 | 0 |
| | Total | 7 | 7 | 0 | 0 | 0 |

*Also represented individually for each side

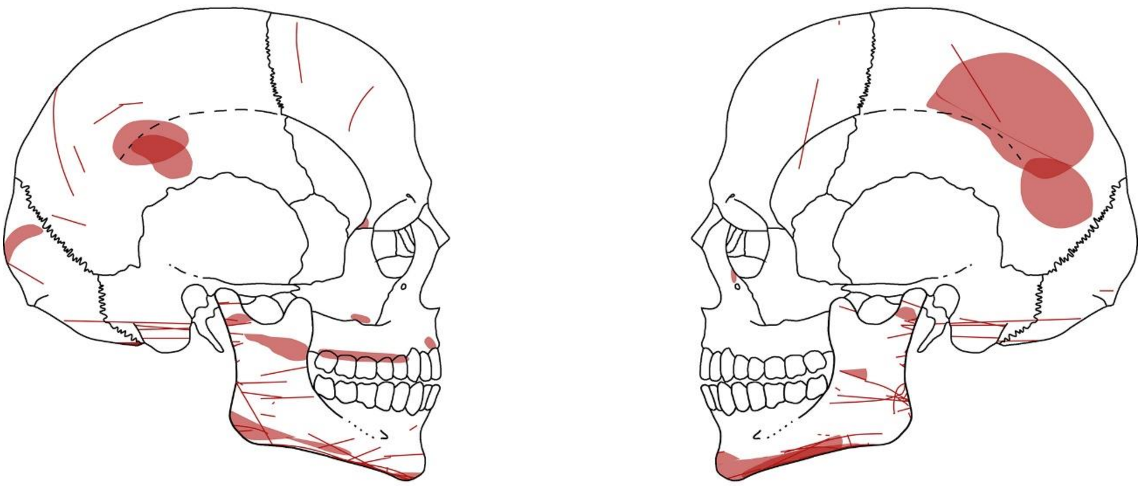

a) b)

Figure 79: The patterned cutmarks showing the distribution on the a) right and b) left cranium of the full collection (Other orientations can be found in Appendix H)

In total, 18 of the 49 cranial remains showed some indication of SFT on the neurocranium. Of these, eight had multiple cuts on them leading to an average of 1.61

blow per affected neurocranium (median=1.00) throughout the whole collection and 0.59 blows per skull (crude prevalence rate; CPR).  These cuts were all peri-mortem and most of the cuts on the cranial vault would not have been immediately fatal. The cuts that were found at the base of the skull were associated with the decapitation attempts and are often related to cuts found either on the mandible or the upper cervical vertebrae (Sections 9.6 and 9.7.7).

The occipitals were the most affected of the neurocranial bones. In some cases, such as SK3748, the damage to the occipital was bilateral and extensive, removing a substantial basilar portion (Figure 80). These were thought to be decapitation attempts. There were other individuals, such as SK3707, with injuries to the squama of the occipital which were at angles that do not correspond to missed decapitation attempts. The temporal bones and the mastoid processes were the second most affected component with seven individuals affected (seven cutmarks). There were minimal differences seen between sides in the overall collection, though there was only one in which the mastoids are definitely bilaterally affected on the same person (SK3748). However, this number could be affected by the aDNA sampling; petrous portions from the temporal bones were removed but the exact amount of bone taken and the appearance of the temporal bones before the extraction is unknown (Appendix C and H). In some instances, the trauma on the occipital and temporals can be linked to the same blow.

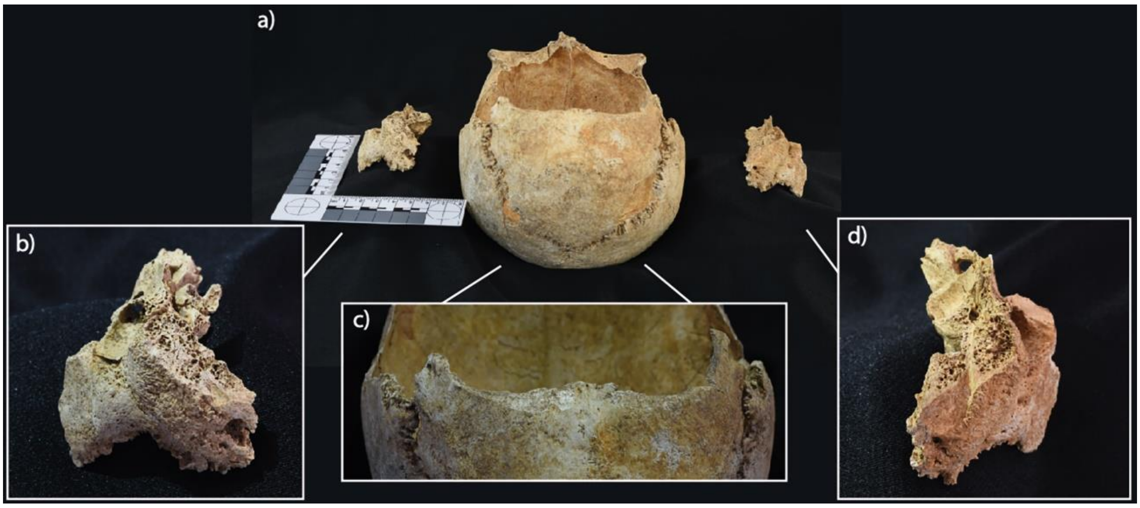


Figure 80: An example of the trauma seen on a) the neurocranium of SK3748, and close-up images of the trauma seen on each component; b) the right temporal, c) the occipital, and d) the left temporal

The frontal bone was the least affected of the cranial vault bones with only three individuals having cuts. The posterior parts of the parietal squama were more impacted than the anterior portions. Many of the blows likely came from the sides, though the exact location of where the assailant was placed compared to the victim is unknown. There were more cuts on the right parietal (N=4 with eight cuts) compared to the left (N=3 with three cuts).

#### *7.1.1.1 Disarticulated/Commingled Skulls*

No disarticulated cranial remains from contexts 3681 and 3685 had trauma.

### 7.1.2 Facial Bones and Mandibles

The mandibles had large amounts of trauma on them, especially the inferior and posterior parts, and were the most affected skull component (Figure 80) (N=28 with 65 blows; 2.32 blows per affected; 1.33 CPR). Additionally, many mandibles were significantly fractured (Sections 4.1.1.1 and 9.3). Although a lot of this could be PM fracturing due to the weight of the excavator on top of them, some appeared to have extensive fracturing that resulted from the cuts, directly or indirectly. Some of these were Residual Energy Dispersal (RED) fractures and are discussed further in Section 9.3. Other fractures were indirectly related to the cutmarks and were often on parts of the mandible away from the location of the cut. Despite the blow being with a sharp weapon, it still struck the individual with a force which led to some of the fracturing seen on remote parts of the mandible (Appendix H). Table 36 contains the number of blows sustained to the mandibles and maxillae in the cranial remains.

Table 36: The number of individuals with each number of blows seen in the maxilla, mandible, and hyoid based on osteological evidence in the articulated cranial remains

| | | | Number of Blows | | | | |
|---|---|---|---|---|---|---|---|
| | Side | Total Number of Individuals Affected | 1 | 2 | 3 | 4 | 5 |
| Maxilla | Left | 1 | 1 | 0 | 0 | 0 | 0 |
| | Right | 3 | 3 | 0 | 0 | 0 | 0 |
| | Bilateral | 0 | 0 | 0 | 0 | 0 | 0 |
| | Total | 4 | 4 | 0 | 0 | 0 | 0 |
| Mandible | Left | 20 | 8 | 3 | 3 | 1 | 1 |
| | Right | 21 | 10 | 7 | 1 | 0 | 0 |
| | Central | 0 | 0 | 0 | 0 | 0 | 0 |
| | Bilateral | *6 | 6 | 0 | 0 | 0 | 0 |
| | Total | 28 | 9 | 10 | 3 | 3 | 3 |
| Hyoid | | 2 | 2 | 0 | 0 | 0 | 0 |

*Also represented individually for each side

There were no major differences in the number of blows or the number of affected mandibles on either side. The cuts on the mandibles were mainly found on the ascending ramus, especially posterior, and on the inferior border of the corpus. There were some cuts that are anterior, but these were only along the border of the corpus.

The majority of the cuts on the inferior of the corpus were angled in the transverse plane or very near to it. The right side had more cuts that are angled to some degree compared to the left side. Generally, there was more variability in the angle of the cuts on the posterior portion of the ascending ramus compared to the rest of the mandible. The RED fracturing on the mandible commonly resulted in sweeping, curved fractures that ran along similar paths, often running from cuts that impacted from the posterior (Figure 81) (Sections 9.3 and 9.6).

a)

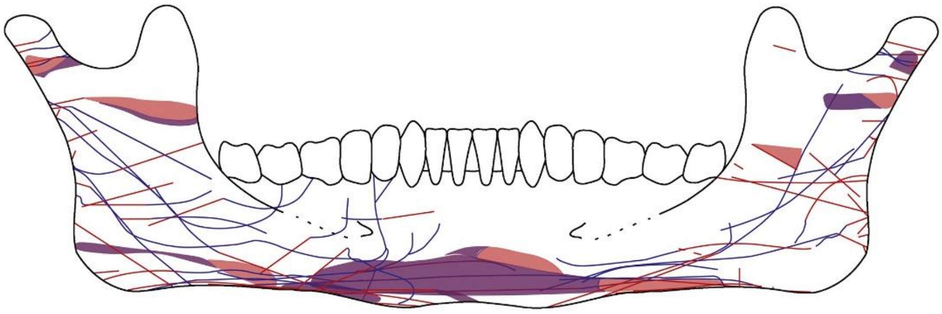

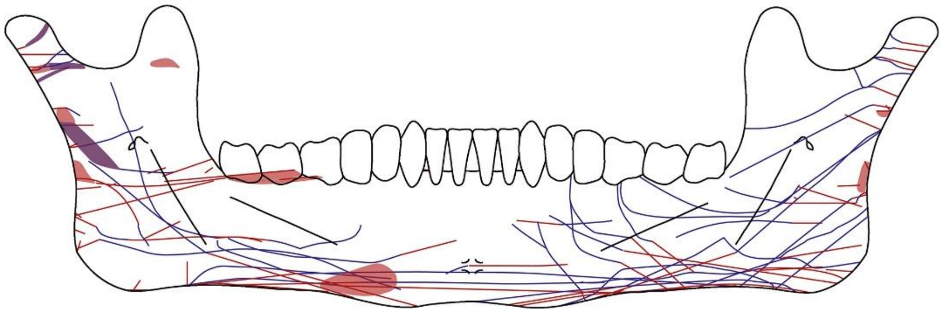

b)

Figure 81: The patterned cutmarks including the RED fractures (purple/blue) showing the distribution on the a) buccal and b) lingual mandible of the full collection (Other orientations can be found in Appendix H)

There were clusters of cuts on the posterior of the condyles or the condylar necks. All of these blows were struck from the back, often transitioning to RED towards the front. Some were bilateral and there were some examples which potentially were bilateral however, due to either taphonomy or bone loss, the opposite side could not be properly examined.

The maxillae were relatively unaffected. There was a total of four maxillae that had been cut, in some instances in association with mandibular cuts (such as SK3723). The rest of the facial bones were not found to be impacted, however there were large amounts of fragmentation in many cases. One right zygomatic bone had indications of SFT along the inferior margin, however this also had taphonomic damage.

#### 7.1.2.1 Disarticulated/Commingled Mandibles

There were eight disarticulated mandibular fragments that presented with cutmarks (Table 37). Two were within the general collection labelled as commingled (3724_X, 3730_X). Four of the eight were small finds. Two of them (SF 10420 and 10421) are approximately 50% of a mandible. Both present with multiple cuts (N=4 and 2, respectively) and one had extensive RED fracturing. Most of these blows were close to the transverse plane and from the right. The other two small finds were condyles which were hit from a posterior direction. Although they were of opposite side, it is unknown if they were related.

In context 3685, there were two mandibular fragments which have cutmarks on them. One was a probable left condyle, cut from the posterior side and the other was a portion of right ascending ramus which had four discrete cuts. Three of the cuts were in close proximity below the lingula but come from various directions; one posterior, one left, and one unknown. The final cut was above the lingula and quickly progresses to a long RED fracture and therefore likely was from the posterior.

Table 37: The number of individuals with each number of blows seen in the mandible based on osteological evidence in the disarticulated cranial remains

| | | Number of Blows | | | |
|---|---|---|---|---|---|
| | Side | 1 | 2 | 3 | 4 |
| Mandible | Left | 4 | 0 | 0 | 1 |
| | Right | 3 | 0 | 0 | 1 |
| | Central | 0 | 0 | 0 | 0 |
| | Bilateral | 0 | 0 | 0 | 0 |
| | Total | 5 | 1 | 0 | 2 |

### 7.1.3 Vertebrae

The vertebrae associated with the skulls were the most affected component. Less of the vertebrae associated with the postcranial skeletons had trauma because the vertebrae that were present were generally lower down on the neck. Relatively few vertebrae superior to CV4 were present in the postcranial remains; the opposite to what was seen in the cranial remains. Vertebrae below CV6 are typically covered by the main belly of the trapezius muscle, making them less likely to have been a primary target to aim for as they would no longer be at the narrowest and 'easiest' part of the neck to cut through (Marieb et al. 2014).

Overall, CV2 and CV3 were the most affected (N=29 and 25, respectively) with the CV7 the least affected (N=3). For CV2 and CV3, this represented approximately 50% of total individuals. The majority of the cuts were in or near the transverse plane though overall, the inferior vertebrae had cuts that were most consistently in the transverse plane (Figure 82).

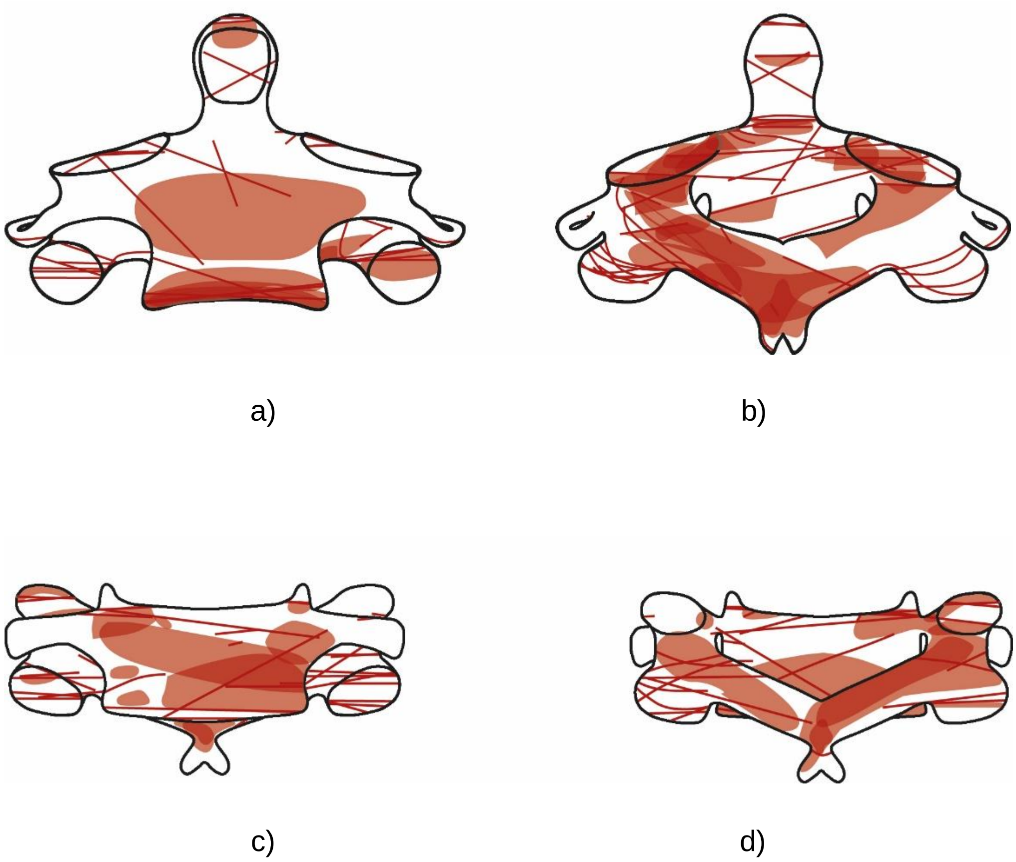


Figure 82: The patterned cutmarks showing the distribution on the a) anterior CV2, b) posterior CV2, c) anterior CV3, and d) posterior CV3 (Other orientations and CVs can be found in Appendix H)

Amongst the vertebrae, there was no overriding common location that was most impacted, although articular facets are typically affected. The bodies of the vertebrae were more affected from CV2 through CV5, however the differences between these and CV6 and CV7 could primarily be related to the overall number of cutmarks. Patterns that were seen between the vertebrae and with the mandible will be discussed in Section 9.6. Any patterns seen with each vertebra are noted in Table 38. The unknown CV (CV Unk) showed no bias towards any specific part of the bone. There were a mix of angles, however the majority were in the transverse plane or level between right and left. The total number of blows to each vertebrae follow, in Tables 39 to 43.

Table 38: The patterns seen amongst the cutmarks on the vertebrae with the regions of higher frequency highlighted

| CV | How affected | Anterior/ Posterior preference | Left/ Right preference | Superior/ Inferior preference | Transverse / Oblique preference | Notes |
|---|---|---|---|---|---|---|
| 1 | Low-Moderate | Posterior | Left | Inferior | Transverse | IAF > SAF, aligns with goal of decapitation |
| 2 | High | Posterior | Left (arch) | -- | Transverse | No clear patterns<br>Base of odontoid commonly affected |
| 3 | High | -- | -- | Inferior | | No clear patterns |
| 4 | Moderate | -- | -- | Superior | Transverse | IAF > SAF |
| 5 | Moderate | -- | Left (AFs) | Superior | Transverse | Body > AFs and arch |
| 6 | Low-Moderate | -- | Right (superior)<br>Left (inferior) | -- | Transverse | S/I highly affected, less in middle |
| 7 | Low | N/A | N/A | N/A | N/A | Unable to draw patterns due to low number |

Table 39: The number of individuals with each number of blows seen in the cervical vertebrae based on osteological evidence in the full collection of articulated remains

| | Number of Blows | | | | | | | |
|---|---|---|---|---|---|---|---|---|
| CV | 1 | 2 | 3 | 4 | 5 | 6 | 7 | Total Cut |
| CV1 | 9 | 0 | 0 | 1 | 1 | 0 | 0 | 11 |
| CV2 | 19 | 4 | 4 | 1 | 0 | 1 | 0 | 29 |
| CV3 | 20 | 5 | 1 | 0 | 0 | 0 | 0 | 26 |
| CV4 | 9 | 5 | 2 | 1 | 0 | 0 | 0 | 17 |
| CV5 | 11 | 2 | 0 | 0 | 0 | 0 | 0 | 13 |
| CV6 | 4 | 2 | 1 | 0 | 0 | 0 | 0 | 7 |
| CV7 | 3 | 0 | 0 | 0 | 0 | 0 | 0 | 3 |
| CV Unk | 6 | 3 | 1 | 0 | 0 | 0 | 0 | 10 |

Table 40: The number of individuals with each number of blows seen in the cervical vertebrae based on osteological evidence in the articulated cranial remains

| | Number of Blows | | | | | | | | |
|---|---|---|---|---|---|---|---|---|---|
| CV | 0/Not present | 1 | 2 | 3 | 4 | 5 | 6 | 7 | Total Cut |
| CV1 | 39 | 9 | 0 | 0 | 0 | 1 | 0 | 0 | 10 |
| CV2 | 23 | 17 | 4 | 4 | 1 | 0 | 0 | 0 | 26 |
| CV3 | 31 | 15 | 2 | 1 | 0 | 0 | 0 | 0 | 18 |
| CV4 | 39 | 6 | 2 | 1 | 1 | 0 | 0 | 0 | 10 |
| CV5 | 46 | 2 | 1 | 0 | 0 | 0 | 0 | 0 | 3 |
| CV6 | 47 | 1 | 1 | 0 | 0 | 0 | 0 | 0 | 2 |
| CV7 | 49 | 0 | 0 | 0 | 0 | 0 | 0 | 0 | 0 |
| CV Unk | 43 | 5 | 1 | 0 | 0 | 0 | 0 | 0 | 6 |

Table 41: The number of individuals with each number of blows seen in the cervical vertebrae based on osteological evidence in the articulated postcranial remains

| | Number of Blows | | | | | | | | |
|---|---|---|---|---|---|---|---|---|---|
| CV | 0/Not present | 1 | 2 | 3 | 4 | 5 | 6 | 7 | Total Cut |
| CV1 | 60 | 0 | 0 | 0 | 1 | 0 | 0 | 0 | 1 |
| CV2 | 58 | 2 | 0 | 0 | 0 | 0 | 1 | 0 | 3 |
| CV3 | 53 | 5 | 3 | 0 | 0 | 0 | 0 | 0 | 8 |
| CV4 | 54 | 3 | 3 | 1 | 0 | 0 | 0 | 0 | 7 |
| CV5 | 51 | 9 | 1 | 0 | 0 | 0 | 0 | 0 | 10 |
| CV6 | 56 | 4 | 1 | 0 | 0 | 0 | 0 | 0 | 5 |
| CV7 | 58 | 3 | 0 | 0 | 0 | 0 | 0 | 0 | 3 |
| CV Unk | 57 | 1 | 2 | 1 | 0 | 0 | 0 | 0 | 4 |

Table 42: The number of individuals with each number of articulated cervical vertebrae affected by at least one blow

| | Number Affected | | | | | | | |
|---|---|---|---|---|---|---|---|---|
| | CV1 | CV2 | CV3 | CV4 | CV5 | CV6 | CV7 | CV Unk |
| Cranial | 10 | 26 | 18 | 10 | 3 | 2 | 0 | 5 |
| Postcranial | 1 | 3 | 8 | 7 | 10 | 5 | 3 | 4 |
| Total | 11 | 29 | 26 | 17 | 13 | 7 | 3 | 9 |

Table 43: The prevalence rates of blows in the present articulated cervical vertebrae and the entirety of the collection. MLNI of 47 and 52 correspond to cranial and postcranial MNLIs, respectively. Numbers 49 and 61 correspond to the number of contexts for cranial and postcranial, respectively.

| | | CV1 | CV2 | CV3 | CV4 | CV5 | CV6 | CV7 |
|---|---|---|---|---|---|---|---|---|
| Number Present (Loe et al. 2014b) | Cranial | 42 | 41 | 30 | 16 | 8 | 3 | 0 |
| | Postcranial | 1 | 5 | 11 | 20 | 25 | 32 | 34 |
| | Total Present | 43 | 46 | 41 | 36 | 33 | 35 | 34 |
| Number Affected (This study) | | 11 | 29 | 26 | 17 | 13 | 7 | 3 |
| Prevalence Rates | TPR% (Loe et al. 2014b) | 25.6 | 63.0 | 63.4 | 47.2 | 39.4 | 20.0 | 8.8 |
| | CPR% MLNI 52 | 21.2 | 55.8 | 50.0 | 32.7 | 25.0 | 13.5 | 5.8 |
| | CPR% MLNI 47 | 23.4 | 61.7 | 55.3 | 36.2 | 27.7 | 14.9 | 6.4 |
| | CPR% Cranial (49 contexts) | 20.4 | 53.1 | 36.7 | 20.4 | 6.1 | 4.1 | N/A |
| | CPR% Postcranial (61 contexts) | 1.6 | 4.9 | 13.1 | 11.5 | 16.4 | 8.2 | 4.9 |

#### *7.1.3.1 Disarticulated/Commingled Vertebrae*

There were seven vertebrae with nine cuts from the disarticulated material (Table 44). One CV1 was found missing the left SAF. Three CV2 were damaged; one missing the tip of the odontoid process, one with a combined incised/shaved cut to the posterior neck of the odontoid and SAFs, and the third with both an incised cut to the posterior neck of the odontoid and a shaved cut to the inferior body. Three unknown CV had cutmarks on them; one of which had both a superior and inferior cutmark affecting the entire body and sole-existing AF.

Table 44: The number of individuals with each number of blows seen in the cervical vertebrae based on osteological evidence in the disarticulated remains

| | Number of Blows | | | | | | | |
|---|---|---|---|---|---|---|---|---|
| CV | 1 | 2 | 3 | 4 | 5 | 6 | 7 | Total Cut |
| CV1 | 2 | 0 | 0 | 0 | 0 | 0 | 0 | 2 |
| CV2 | 2 | 1 | 0 | 0 | 0 | 0 | 0 | 3 |
| CV Unk | 2 | 0 | 0 | 0 | 0 | 0 | 0 | 2 |

### 7.1.4 Hyoids

There were several individuals who had a portion of a hyoid associated with the body. Of these, there were two with cuts on the internal aspect of the greater horn of the hyoid (SK3708 and SK3760). Since only isolated fragments of the greater horn remain, it was difficult to determine the side or direction of the cut. It was thought that these could relate to the anterior cuts that were found on some of the vertebrae, discussed further in Section 9.2.

### 7.1.5 Pectoral Girdles

Overall, there were a much lower number of appendicular injuries compared to axial ones (Figure 83).

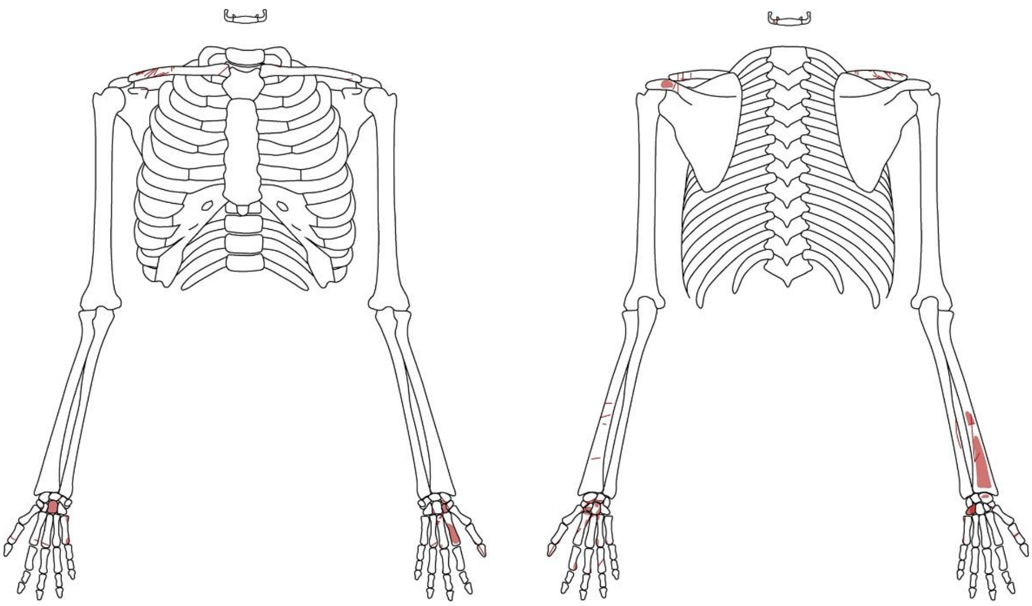

Figure 83: The patterned cutmarks showing the distribution on the a) anterior and b) posterior postcranial remains (enlarged figure in Appendix H)

The number of blows for each aspect of the pectoral girdle are found in Table 45 at the end of this section. The clavicle was the most commonly affected of these. The cuts on the clavicles were slightly more predominantly on the right, although both sides were affected. There were many more anterior and superior cuts compared to the left side. These tended to be at a shallow angle to the transverse plane, running from superior/medial to inferior/lateral, possibly from an attacker facing the victim and swinging a sword downwards from right to left. Some of the cuts were at angles such that they could have occurred in the same blow as the decapitation.

The cuts that were found on the left clavicle are mostly on the posterior aspect of bone. Interestingly, there were some cuts found on the inferior portion of the clavicle on one individual. These cuts came from the inferior/lateral direction, which would be a hard location to impact on the clavicle without involving the ribs as well which do not appear to be injured in this individual (Sections 4.1.7 and 9.7). One likely possibility is that the arm was not in the anatomical position. For example, when the arm is extended and abducted, the clavicle is rotated to the inferior aspect and is more exposed.

On the scapulae, cuts appeared linked to clavicular damage on those individuals. These seemed to be hard strikes as many went deep into the bone, mainly from above but some were angled.

Table 45: The number of blows seen in the pectoral girdle and forearms based on osteological evidence in the articulated postcranial remains

| | | | Number of Blows | | | | | |
|---|---|---|---|---|---|---|---|---|
| | Side | Total Number of Individuals Affected | 1 | 2 | 3 | 4 | 5 | 6 |
| Clavicle | Left | 4 | 3 | 1 | 0 | 0 | 0 | 0 |
| | Right | 5 | 2 | 2 | 0 | 1 | 0 | 0 |
| | Total | *7 | 2 | 4 | 0 | 0 | 1 | 0 |
| Scapula | Left | 1 | 1 | 0 | 0 | 0 | 0 | 0 |
| | Right | 1 | 1 | 0 | 0 | 0 | 0 | 0 |
| | Total | *2 | 2 | 0 | 0 | 0 | 0 | 0 |
| Ulna | Left | 0 | 0 | 0 | 0 | 0 | 0 | 0 |
| | Right | 1 | 1 | 0 | 0 | 0 | 0 | 0 |
| | Total | *1 | 1 | 0 | 0 | 0 | 0 | 0 |
| Radius | Left | 2 | 1 | 1 | 0 | 0 | 0 | 0 |
| | Right | 2 | 1 | 2 | 0 | 0 | 0 | 0 |
| | Total | *4 | 2 | 2 | 0 | 0 | 0 | 0 |

*Also represented individually for each side; unknown sides also included

#### *7.1.5.1 Disarticulated/Commingled Pectoral Girdle*

In context 3685, a disarticulated left scapular spine was found which has two cutmarks, one incised nearly in the sagittal plane and one shaved nearly in the coronal plane with a slight superior tilt anteriorly. The blow that led to the incised cut came from superior/right. From context 3681, a clavicle was found with two widely angled incised cutmarks on the lateral end. Both blows were hit from the superior/left.

### 7.1.6 Upper Extremities

There are four individuals that had trauma on their forearms which appear to be defensive trauma (See 7.1.6.1 for an example of defensive forearm trauma). The numbers for the upper limb were listed in Table 45 in the prior section. The number of cutmarks found on the hands are seen in Table 46. No forearms were bilaterally affected in the remains that were present. There was one example (SK3778) of an ulna and radius both affected, possibly by the same blow. In the cases in which the positioning of the cut on the bone can be determined, they were generally on the posterior or posterior/lateral sides. Excluding disarticulated material, there were seven individuals with injuries to the hands; four were affected on their left, two on their right, and one bilaterally. Two of the unilaterally affected skeletons had SFT on unsided phalanges as well. The cuts were significant and are suggestive of defensive wounds since a high amount of force would have been needed to cause such dramatic cuts (Sections 4.1.7 and 9.7).

Table 46: The number of cutmarks seen in the hands based on osteological evidence in the articulated postcranial remains

| | Number of Cutmarks | | | | | | | | | | | | | | | | |
|---|---|---|---|---|---|---|---|---|---|---|---|---|---|---|---|---|---|
| | 1 | 2 | 3 | 4 | 5 | 6 | 7 | 8 | 9 | 10 | 11 | 12 | 13 | 14 | 15 | 16 | 17 |
| Left | 0 | 0 | 1 | 1 | 0 | 1 | 1 | 0 | 0 | 0 | 0 | 0 | 0 | 1 | 0 | 0 | 0 |
| Right | 0 | 2 | 1 | 0 | 0 | 0 | 0 | 0 | 0 | 0 | 0 | 0 | 0 | 0 | 0 | 0 | 0 |
| Unsided | 0 | 1 | 1 | 0 | 0 | 0 | 0 | 0 | 0 | 0 | 0 | 0 | 0 | 0 | 0 | 0 | 0 |
| Total | 0 | 1 | 2 | 1 | 0 | 0 | 2 | 0 | 0 | 0 | 0 | 0 | 0 | 0 | 0 | 0 | 1 |

There were slightly more cuts on the left hand and this was more notable on the posterior side. There were several phalanges that were unable to be sided due to either being disarticulated or too fragmented for re-association and therefore the true bilateral distribution of cuts may be different. A fairly good recovery of manual bones revealed that a relatively small proportion of individuals had their hands affected. However, in those that were affected, there was a pattern of multiple blows having been afflicted. In many cases, multiple bones in each hand were affected by the same blow due to the size of the bones and their close proximity to each other. Due to their mobility and the number of separately moveable joints, hands have a high complexity when attempting to determine the number of blows (Marieb et al. 2014).

All the trauma found on the long bones was on the posterior aspect. Compared to the left radii, the right radii were found to have more cuts that were either shaved or at a very wide angle though the overall numbers of blows were approximately the same between sides (N=4 and N=3, respectively). An unexpected pattern was that the radii were more affected than the ulnae. Typically, defensive trauma occurring from someone raising their arms to shield from a blow to the head or face region primarily affect the ulna because when the shoulder and elbow are both flexed, it is the bone that would be facing anterior/superior, such as seen in parry fractures (Section 4.1.7.2) (Bohnert et al. 2006; Judd 2008; Geldenhuys et al. 2016). This is further discussed in Section 9.7.4. There is also the possibility that not all of those blows were inflicted in a situation in which the victim had free movement.

#### *7.1.6.1 Disarticulated/Commingled Upper Extremities*

One right radius was found in context 3681 which has two incised and very angled cutmarks. Due to the close proximity, it is possible that the much smaller cut is associated with the larger one, possibly to do with withdrawing the blade, however this cannot be confirmed. A left radius in context 3681 was found in two pieces and reassociated (Figure 84). Only one of the pieces had a cut on it, but they physically reassociated very well and were a very good example of resultant fracturing from a cutmark, likely from a twist of the blade, possibly when withdrawing.

Figure 84: The posterior aspect of the left radius from context 3681 that was found in two pieces and subsequently reassociated

There were some disarticulated fragments of upper extremities in which the positioning of blows cannot be determined. For two fragments, the identity of the bone could not be established due to their size and taphonomic damage; however one was likely humerus and the other was either radius or ulna. Both of these were incised cutmarks. A first proximal phalanx with a cut to the dorsal aspect of the head was found in context 3681.

The side of this phalanx was unknown. From context 3685, there were two proximal phalanges that had shaved cutmarks nearly in the sagittal plane. No further information is known about side or position in the hand. A left, second metacarpal (MC2) with a longitudinal cut though the shaft was also present.

## 7.2 Incised Cutmark Focus: Shape Analysis

Shape analysis was used to look at the profiles of the incised cutmarks to see what, if any, patterns could be found (Sections 5.4.4 and 9.4). The profiles of the incised cutmarks at 50% were examined using R. Several variables were included in order to see if there was any separation in the shapes found (Appendix I, Supplementary File). The goal was to discover if there was any clear indicator of what affected the shape the most significantly, and if none was found, to test whether it was possible different weaponry was used, as represented by unexplained clustering. For this study, the variables that were focused on were the angle of impact, the side of the body, and the location on the body (Sections 4.1.1 and 4.1.7). There are further variables that could be examined but some were excluded from this analysis because the focus was on variables that might shed light on differences caused by weaponry or execution methods.

Initially, only the 50% profiles were used in order to minimise confounding factors. The results of those analyses are presented here. The 50% were subsequently run with the 25% in order to check if there were any differences. No differences were found between the two groups (linear discriminant analysis [LDA] correction percentage 0.7461905) and no differences in the patterns were seen in the harmonics or the general running of the principal component analysis (PCA) (PC1 62.58%, $6.275887^{-01}$; PC2 16.9%, $1.689680^{-01}$; PC3 8.13%, $8.129485^{-02}$). Due to this, it was decided to focus on the 50%. Although this led to a smaller sample size, some of the group sizes are very small so the addition of multiple profiles of the same cut was thought to potentially be more confounding than revealing. Since there are already possible unknown factors that could affect the shape of the cutmarks, it was decided that using the 50% would be sufficient to see how appropriate the methodology is.

Once it was established that there was no separation of the 25 and 50% profiles, a PCA was performed on the 50% profiles of the cutmarks. A total of 107 profiles were used for the analysis. Elliptic Fourier Transforms were used to obtain the required harmonics. During normalisation, the PCA with the outlines both rotated to be aligned and not rotated were checked to see if there were any differences (Figure 85). None were found and therefore the rotated ones were used since the cutmarks were not guaranteed to be in anatomical position to begin with. A total of 16 harmonics were able to account for 99.9% of the variation in the collection, with five and nine accounting for 95% and 99%, respectively. Based on this, nine harmonics were used and this was found to be appropriate for all the PCAs run in this study (Figure 86).

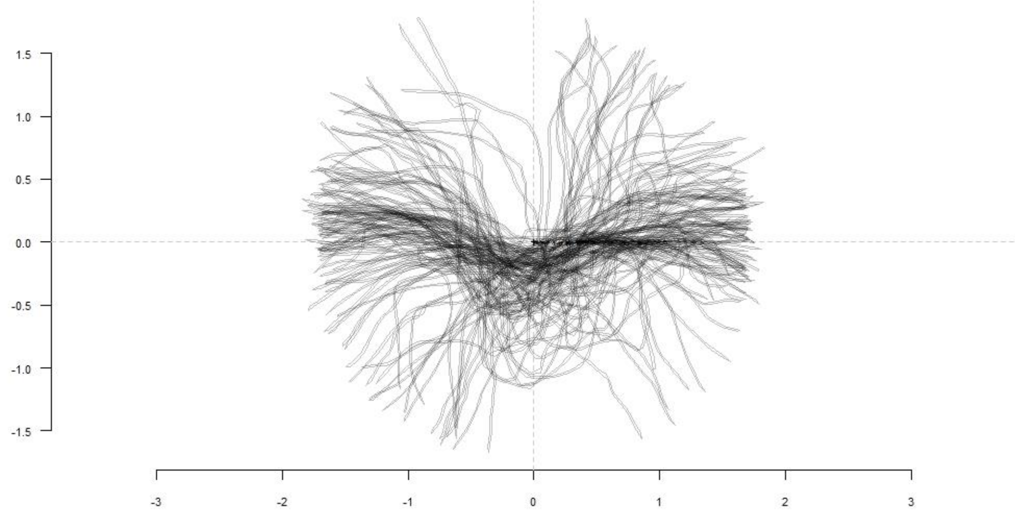


Figure 85: An example of the normalised and stacked outlines with 'coo_slidedirection()' used for the shape analysis of the full incised cutmark collection

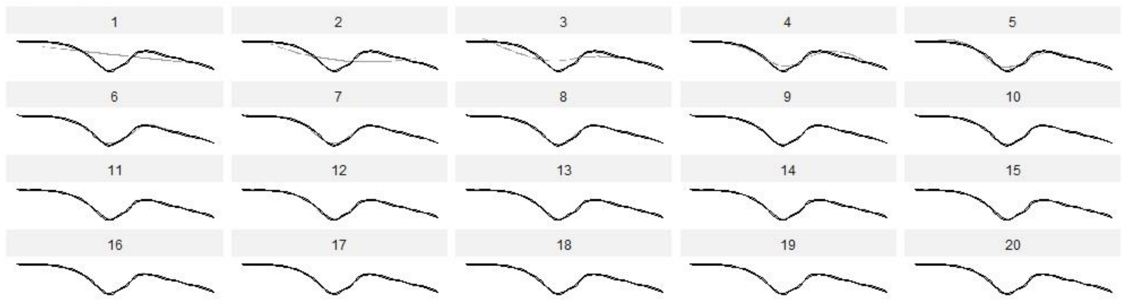


Figure 86: An example of the profile at 50% of cutmark 3753_D with up to 20 harmonics

The proportions of variation accounted for by each of the first ten principal components (PCs) is seen in Table 47. The first three PCs were all plotted in conjunction with one another for the different factors that were under analysis. PC1 accounted for 60.9% ($6.086319^{-01}$), PC2 accounted for 18.8% ($1.882055^{-01}$), and PC3 accounted for 9.2% ($9.180827^{-02}$). This number of PC values was chosen because it was the second inflection on the scree plot and the proportion of variance that was accounted for was over 5% for each (Appendix I, Supplementary File). The amount of additional information that would be gathered from using further PCs was thought to be negligible. These PCs roughly equate to: depth of the cut, the difference between the angles of the cutmark walls (visually, whether the cut appears upright or leaning), and whether the base of the cut is offset to the left or right of the extracted profile (Figure 87) (Section 9.4).

Table 47: The PCs, proportion, and cumulative sum from the shape analysis of the incised cutmarks

| PC | Proportion | Cumulative Sum |
|---|---|---|
| 1 | 0.60900 | 60.9 |
| 2 | 0.18800 | 79.7 |
| 3 | 0.09180 | 88.9 |
| 4 | 0.04540 | 93.4 |
| 5 | 0.02160 | 95.6 |
| 6 | 0.01280 | 96.8 |
| 7 | 0.00755 | 97.6 |
| 8 | 0.00665 | 98.3 |
| 9 | 0.00551 | 98.8 |
| 10 | 0.00328 | 99.1 |

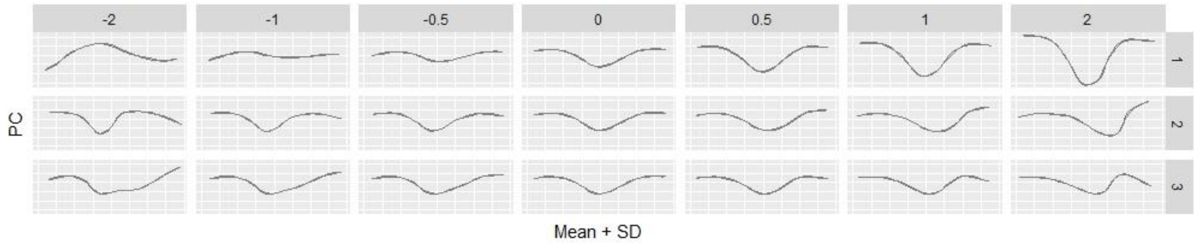


Figure 87: An example of the first three PC for the full collection

Overall, there was a tighter cluster and a larger number of profiles that fall on the shallower side of PC1 up to approximately -0.25 SD, however there was greater variation along the deeper side of PC2 which has points beyond 0.50 SD (Appendix I). Along PC2, a high number of points fall relatively centrally. The upright side of PC2 was more clustered towards the centre, with a few outliers beyond -0.125 SD. The more sloped side of PC2 was slightly more spread out. The profiles were relatively centred on the mean along PC3 and those that were outliers tend to be, but were not always, outliers along another PC as well. The PC descriptions and results can be found in Tables 48 to 51.

Table 48: The PC descriptions of the three PCs used for the shape analysis of the incised cutmarks

| | PC1 | PC2 | PC3 |
|---|---|---|---|
| Full Collection | Depth (deep to shallow) | Difference between angles/“leaning” (upright to sloped) | Base offset (left to right) |
| Angled Only | Depth (deep to shallow) | “Leaning” and inflection of the shoulder (upright/downwards to sloped/upwards) | Width/overall size (narrow to wide) |
| Non-Angled Only | Depth (deep to shallow) | Difference between angles/“leaning” (upright to sloped) | Base offset (left to right) |

Table 49: The results of the shape analysis for each variable when using the full dataset

| Main | Subdivision | N | PC1 | PC2 | PC3 | Notes |
|---|---|---|---|---|---|---|
| Impact angle | No | 67 | Deeper Spread | Moderate | Moderate Clustered | Overall wider variety than Yes |
| | Yes | 40 | Shallower Clustered | Slightly sloped | Moderate Clustered | Overall more clustered<br>Overlap with No |
| | Moderate | 20 | Shallower Clustered | Upright | Slightly right Clustered | |
| | Big | 20 | Shallower Clustered | Sloped | Moderate Clustered | |
| Location | Cranium | 8 | Deeper Spread | Upright | Right Spread | Most variation Visually different than others but overlap present Obliquely orientated ellipse |
| | Postcranial | 27 | Moderate | Moderate | Moderate Clustered | Low variation |
| | Neck* | 48 | Slightly flatter | Slightly sloped | Moderate | Obliquely orientated ellipse |
| | Mandible | 24 | Moderate | Slightly upright | Moderate | Obliquely orientated ellipse |
| Width | Large | 4 | Moderate Clustered | Slightly upright Clustered | Right Clustered | Least variation |
| | Medium | 19 | Deeper Spread | Sloped Spread | Slightly left | |
| | Small | 48 | Moderate | Moderate | Moderate | |
| | Very small | 36 | Shallower | Upright Clustered | Moderate | |
| Side | Central | 18 | Slightly shallower | Slightly upright | Slightly right Clustered | |
| | Right | 41 | Moderate | Slightly upright | Moderate Clustered | |
| | Left | 46 | Slightly deeper | Slightly sloped | Slightly left Clustered | Greatest difference from the others |
| | Unknown | 2 | -- | -- | -- | Excluded |

*vertebrae + hyoid

Table 50: The results of the shape analysis for each variable when using only the angled cutmarks

| Main | Subdivision | N | PC1 | PC2 | PC3 | Notes |
|---|---|---|---|---|---|---|
| Location | Cranium | 1 | -- | -- | -- | Excluded |
| | Postcranial | 15 | Slightly deeper | Slightly upright | Narrower Clustered | |
| | Neck* | 13 | Shallower Spread | Slightly sloped/ upwards inflection Spread | Slightly narrower Spread | Most variation |
| | Mandible | 11 | Deeper Clustered | Moderate | Slightly wider Clustered | Nearly within Neck variation |
| Width | Large | 4 | Deeper | Sloped/ upwards inflection | Narrower Clustered | |
| | Medium | 11 | Slightly shallower | Upright/ downwards inflection Spread | Slightly wider Clustered | Overlap with other groups |
| | Small | 15 | Deeper Spread | Sloped/ upwards inflection Spread | Narrower Spread | |
| | Very small | 10 | Shallower | Upright/ downwards infection | Narrower Clustered | Greatest difference from the others |
| Side | Central | | Shallower Spread | Sloped/ upward inflection | Wider | |
| | Right | | Moderate | Slightly upright/ downwards infection | Slightly narrower Clustered | |
| | Left | | Moderate | Slightly sloped/ upwards inflection | Moderate Clustered | |
| | Unknown | | -- | -- | -- | Excluded |

*vertebrae + hyoid

Table 51: The results of the shape analysis for each variable when using only the non-angled cutmarks

| Main | Subdivision | N | PC1 | PC2 | PC3 | Notes |
|---|---|---|---|---|---|---|
| Location | Cranium | 7 | Deeper Spread | Moderate | Right Spread | Most variation Visually different than others but overlap present |
| | Postcranial | 12 | Slightly deeper | Moderate | Slightly left | |
| | Neck* | 35 | Moderate | Slightly upright Spread | Slightly left | |
| | Mandible | 13 | Slightly shallower Spread | Slightly sloped Spread | Moderate | |
| Width | Large | 0 | -- | -- | -- | Excluded |
| | Medium | 8 | Deeper | Slightly sloped Spread | Left | No overlap with Very Small along PC2 |
| | Small | 33 | Moderate | Slightly sloped | Moderate | |
| | Very small | 26 | Shallower | Upright Clustered | Right Clustered | No overlap with Medium along PC2 |
| Side | Central | 15 | Shallower | Upright Clustered | Moderate Clustered | |
| | Right | 22 | Moderate | Slightly upright | Left | |
| | Left | 29 | Slightly deeper | Sloped | Slightly right | Most different |
| | Unknown | 0 | -- | -- | -- | Excluded |

*vertebrae + hyoid

LDAs were run on the PCA output whilst retaining 95% of the variation. The correct classification percentage was not high enough in any case to be considered truly discriminatory. MANOVAs were run despite this, all of which were non-significant when appropriate Bonferroni corrections were implemented. These are all found in Section 7.2.2. Chi-Square tests were also performed to compare the number of each group that were angled and non-angled. They were run on the full collection of 107 profiles.

When first exploring entry angles and how they affected the analysis, no significance was found, but there was some difference in how the categories were grouping, therefore the cutmarks that were perpendicular to the surface of the bone and those that were oblique were separated for each analysis was well. The separate PCAs for the full collection are described below, with the findings of the full angle analysis immediately following (also see Section 9.4).

#### 7.2.1.1 Angled and Non-Angled PCAs

The number of harmonics for the angled cutmarks was found to be the same as for the entire collection, with a similar inflection point in the scree plot. The PCA for the angled cutmarks included 40 samples in total and PC1 accounted for 47.2% ($4.722100^{-01}$), PC2 accounted for 30.4% ($3.036181^{-01}$), and PC3 accounted for 7.9% ($7.901322^{-02}$).

For the non-angled PCAs, the values were similar to that of the full collection. The required harmonics and the contribution of variance was nearly the same and the inflection on the scree plot was similar. The PCA for the non-angled cutmarks included 67 samples and PC1 accounted for 62.9% ($6.290811^{-01}$), PC2 accounted for 18.4% ($1.842463^{-01}$), and PC3 accounted for 8.52% ($8.522720^{-02}$).

For both cases, the descriptions of the PCs are found in Table 48. These separated PCAs were used for width, location, and side. However, the latter two all required a second running with modifications as there were some groups with N=1 which required exclusion. The PC values for those will be presented in their respective sections.

### 7.2.2 Impact Angle of the Blow

The angles were checked in two different ways; once binary and once with three categories. A total of 107 samples were used for each (Figure 88).

For the binary angle PCA, there was a much wider distribution of non-angled cutmarks. Angled cutmarks were more tightly clustered, however, because of the wide spread of the non-angled cutmarks, it might be possible to say a cutmark was potentially non-angled, but it would not be possible to state a cutmark was angled.

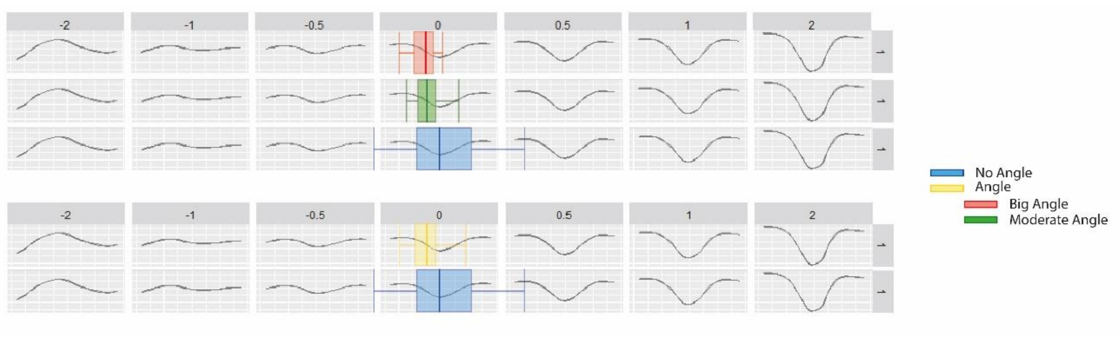


Figure 88: The distribution of each category overlaid on PC1 for the angle of the cutmarks when using the full collection (The remainder are found in a Supplementary .ai file)

In the PCA with three categories, the tighter clusters of ‘moderate’ and ‘big’ profiles were likely due to the number of each being substantially smaller than for ‘no’ profiles (Table 49, Figure 89) (Section 9.4). In all instances, ‘moderate’ has the tightest cluster. The separation between ‘big’ and ‘moderate’ along PC2 was easily explained; all cutmarks were oriented in the same direction so that the ‘entry’ wall would be on the left. A larger angle would mean that the cutmark profile would be more sloped as opposed to upright which is the aspect of the shape reflected in PC2. Therefore ‘big’ profiles would shift towards the more sloped profiles whereas the ‘moderate’ profiles would shift towards the more upright ones.

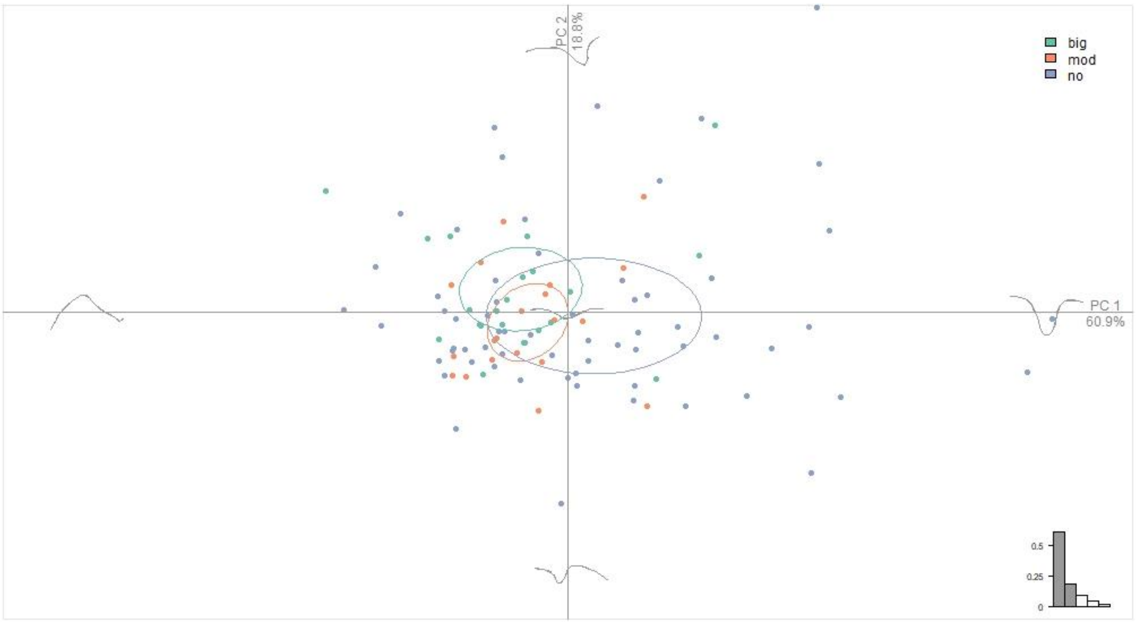


Figure 89: The plot showing PC1 and PC2 of Angled/Not for the full collection. (The remainder are found in Appendix I)

An LDA was performed for both binary and non-binary angle of impact, retaining 95%, and no significance was found. No clear clusters were created along any axes of the LDA and classification percentage is low (Table 52). Therefore, despite any visual differences, it cannot be said that they were due to the angle of the blade (Non-binary LD1 75.5%, LD2 24.2%; Binary LD1 >99%)

When examining the full collection with three levels of angle, despite no differences in the MANOVA, a significant difference was found in the pairwise MANOVA (95% retained, PCA Scores) between the big and moderate angled cutmarks with a Bonferroni correction implemented (required p=0.01667) (F=2.745, 10, 29, p=0.01642) (Table 53). No other significant differences were found.

Neither the binary nor categorical variables of angle separated out in the hierarchical cluster; they are heavily interleaved.

Table 52: The results of the LDAs run on the full collection with 95% retention using the PCA scores

| Variable | | Correction Percentage | Category | Classification Error |
|---|---|---|---|---|
| Binary Angle | | 0.5700935 | No Angle | 0.88059700 |
| | | | Angle Present | 0.05000000 |
| Non-Binary Angle | | 0.5887850 | No Angle | 0.94029850 |
| | | | Moderate Angle | 0.00000000 |
| | | | Big Angle | 0.00000000 |
| Location | | 0.3738318 | Cranium | 0.00000000 |
| | | | Mandible | 0.00000000 |
| | | | Postcranial | 0.07407407 |
| | | | Neck | 0.79166667 |
| | *Angled* | 0.1794872 | Mandible | 0.18181818 |
| | | | Postcranial | 0.26666667 |
| | | | Neck | 0.07692308 |
| | *Non-Angled* | 0.4477612 | Cranium | 0.00000000 |
| | | | Mandible | 0.00000000 |
| | | | Postcranial | 0.08333333 |
| | | | Neck | 0.82857143 |
| Width | | 0.4299065 | Large | 0.00000000 |
| | | | Medium | 0.10526320 |
| | | | Small | 0.62500000 |
| | | | Very Small | 0.38888890 |
| | *Angled* | 0.3500000 | Large | 0.00000000 |
| | | | Medium | 0.36363640 |
| | | | Small | 0.40000000 |
| | | | Very Small | 0.40000000 |
| | *Non-Angled* | 0.5671642 | Medium | 0.12500000 |
| | | | Small | 0.63636360 |
| | | | Very Small | 0.61538460 |
| Side | | 0.4857143 | Central | 0.00000000 |
| | | | Left | 0.65217390 |
| | | | Right | 0.51219510 |
| | *Angled* | 0.4615385 | Central | 0.00000000 |
| | | | Left | 0.35294120 |
| | | | Right | 0.63157890 |
| | *Non-Angled* | 0.4696970 | Central | 0.00000000 |
| | | | Left | 0.79310340 |
| | | | Right | 0.36363640 |

Table 53: The results of the MANOVAs run on the full collection as a follow-up to the LDAs with significant values in bold (if still significant after a Bonferroni correction) and bold italics (if not still significant after a Bonferroni correction)

| Variable | | Df | Hotelling-Lawley | Approx F | Num Df | Den Df | Pr(>F) |
|---|---|---|---|---|---|---|---|
| FC Binary Angle | Fac | 1 | 0.083023 | 1.67700 | 5 | 101 | 0.14690 |
| | Resid | 105 | | | | | |
| FC Angle | Fac | 2 | 0.113360 | 1.12230 | 10 | 198 | 0.34710 |
| | Resid | 104 | | | | | |
| Location | Fac | 3 | 0.124630 | 0.81147 | 15 | 293 | 0.66470 |
| | Resid | 103 | | | | | |
| *Angled* | Fac | 2 | 0.168020 | 0.52085 | 10 | 62 | 0.86900 |
| | Resid | 36 | | | | | |
| *Non-Angled* | Fac | 3 | 0.212250 | 0.81597 | 15 | 173 | 0.65890 |
| | Resid | 63 | | | | | |
| Width | Fac | 3 | 0.224390 | 1.46100 | 15 | 293 | 0.11880 |
| | Resid | 103 | | | | | |
| *Angled* | Fac | 3 | 0.574550 | 1.17460 | 15 | 92 | 0.30550 |
| | Resid | 36 | | | | | |
| *Non-Angled* | Fac | 2 | 0.431200 | 2.54400 | 10 | 118 | **0.00815** |
| | Resid | 64 | | | | | |
| Side | Fac | 2 | 0.107370 | 1.04140 | 10 | 194 | 0.41020 |
| | Resid | 102 | | | | | |
| *Angled* | Fac | 2 | 0.649400 | 2.01310 | 10 | 62 | ***0.04687*** |
| | Resid | 36 | | | | | |
| *Non-Angled* | Fac | 2 | 0.201340 | 1.16780 | 10 | 116 | 0.31960 |
| | Resid | 63 | | | | | |

Even though there was no statistical significance, because there was an indication that the angled and non-angled cutmarks are shaped differently, additional analysis was run on those two groups separately to see if any further differences were seen. In the split cases, any variables that caused issues in the full analysis due to low sample size were omitted. Chi-Square analyses were also run on the angled and non-angled samples to see if the distribution was different.

### 7.2.3 Location on the Body

For location, when the entire sample was pooled, a total of 107 samples were used (cranium=8, postcranial=27, neck [vertebrae and hyoid]=48, mandible=24). Visually, when plotting the location of the cutmarks, there appears to be no significant separation of the categories (Table 49, Section 9.4, Appendix I).

The results from the LDA for classification percentages and error show low correct classification and high error (Table 52). No significance was found in the MANOVAs or the pairwise MANOVAs with a Bonferroni correction (range of p found 0.05775-0.85301, required p=0.008333) (LD1 74.8%, LD2 18.7%, LD3 6.53%) (Table 53). A hierarchical cluster was run, both with and without setting the number of branches expected. In both cases, it was evident that the groups do not separate out into four discrete groups. There are large amounts of intermixing in branches of the cluster that 'should' be separate, if able to be delineated by location.

Therefore, the differences in shape that were seen in the cutmarks does not separate out by location on the body when the collection is analysed as a whole. There was some evidence that the cranial cutmarks are slightly different, but this was not statistically significant. Since some separation was seen between the cuts that were angled and those that were not, the collection was split and the tests re-run to see whether any difference would be present.

The collection was not separated based on location for further analysis because the sample sizes for each location would start to become too small to find meaningful differences, especially if subsequently examining non-binary variables. However, a 4x4 Chi-Square test was performed on the location and width of the cutmarks in order to examine any patterns that did show significant differences in those expected and observed, notably with the neck having more very small cutmarks than expected and the postcranial had more large cutmarks than expected ($\chi^2$ (9)=25.947, p=0.002084) (Table 54).

Table 54: The expected and observed values of cutmark location and cutmark width

| Location | | Large | Medium | Small | Very Small |
|---|---|---|---|---|---|
| Cranium | Observed | 0 | 1 | 5 | 2 |
| | Expected | 0.3 | 1.42 | 3.59 | 2.69 |
| | Residuals | -0.547 | -0.353 | 0.745 | -0.422 |
| Mandible | Observed | 0 | 9 | 11 | 4 |
| | Expected | 0.9 | 4.26 | 10.77 | 8.07 |
| | Residuals | -0.947 | 2.295 | 0.071 | -1.434 |
| Neck | Observed | 0 | 4 | 21 | 23 |
| | Expected | 1.79 | 8.52 | 21.53 | 16.15 |
| | Residuals | -1.340 | -1.549 | -0.115 | 1.705 |
| PC | Observed | 4 | 5 | 11 | 7 |
| | Expected | 1.01 | 4.79 | 12.11 | 9.08 |
| | Residuals | 2.977 | 0.094 | -0.320 | -0.691 |

Additionally, the Chi Square analysis revealed a significant difference between the distributions of the angled and non-angled cutmarks ($\chi^2$ (3)=8.8327, p=0.0316) with more angled cutmarks than expected seen in the mandible and postcranial regions (Table 55).

Table 55: The expected and observed values of cutmark location and cutmark angle

| Angle | | Cranium | Mandible | Neck | PC |
|---|---|---|---|---|---|
| No Angle | Observed | 7 | 13 | 35 | 12 |
| | Expected | 5.01 | 15.03 | 30.06 | 16.91 |
| | Residuals | 0.889 | -0.523 | 0.902 | -1.193 |
| Angle | Observed | 1 | 11 | 13 | 15 |
| | Expected | 2.99 | 8.97 | 17.94 | 10.09 |
| | Residuals | -1.15 | 0.677 | -1.167 | 1.544 |

#### 7.2.3.1 Location Divided by Angle

Additionally, the sample was split by whether the cut was angled or not. For these analyses, 40 samples were used for angled (cranium=1, postcranial=15, vertebra=13, mandible=11) (Table 50). The different distribution of location for angled compared to non-angled is notable, especially for neck and cranium (Supplementary File). Cranium had to be excluded from the angled analysis due to sample size, thus leaving N=39. The variation was primarily accounted for by PC1 with 47.3% ($4.734716^{-01}$), PC2 with 30.3% ($3.031377^{-01}$), and PC3 with 7.91% ($7.911872^{-02}$).

When performing an LDA, no separation was noted (LD1 71.3%, LD2 28.7) (Table 52). When using a MANOVA or when using pairwise MANOVAs with a Bonferroni correction (range of p found 0.2192-0.8090, required p=0.0166667) no significant differences were found, therefore despite some visual differences, no statistical significance was seen (Table 53). As in the case of the full collection, the hierarchical cluster analysis did not separate the groups (Section 9.4).

A total of 67 samples were used for non-angled (cranium=7, postcranial=12, vertebra=35, mandible=13) (Table 51). When examining the non-angled, an overall similar pattern is seen to the full collection; cranium is slightly visually different, especially when plotting PC2 and 3, but it does not have statistical significance. There is no statistical significance when analysed using a DFA and the MANOVAs do not produce significant results (95 LD1 69.3%, LD2 17.4%, LD3 13.3%) (Tables 52 and 53). In the pairwise analysis, the required p=0.00833 and the range of p found was 0.03463-0.92120. Hierarchical clustering did not delineate the groups properly.

### 7.2.4 Width of the Cutmark

Four levels of width were examined, looking at a total of 107 profiles; large (N=4), medium (N=19), small (N=48), and very small (N=36) (Table 49). When visually examining the PCA plots for width, there was some visual separation of the group centroids along the PC1 axis when plotted against PC2 and PC3, the latter to a lesser extent (Appendix I). There was still substantial overlap between the groups, however. The different sizes had different patterns to them and show some separation, however none of the groups are discrete along any axis (Section 9.4).

Overall, there was no clear evidence that the profiles can be separated by width despite there being some significant or near-significant differences when examining the pairwise MANOVAs (Tables 52 and 53). Pairwise analyses were run on the full collection which resulted in no significant differences when a Bonferroni correction was implemented (range of p found 0.04326-0.80683, required p=0.00833). There was no clear clustering amongst the plotted LDA results (95 LD1 69.2%, LD2 27.7%, LD3 3.06%). The hierarchical cluster analysis did not properly separate the groups.

The Chi Square analysis performed indicated a significant difference between the angled and non-angled frequencies for each width category ($\chi^2$ (3)=12.305, p=0.006407) which was not surprising as a more oblique cutmark will inherently be wider (Table 56).

Table 56: The expected and observed values of cutmark angle and cutmark width

| Angle | | Large | Medium | Small | Very Small |
|---|---|---|---|---|---|
| No Angle | Observed | 0 | 8 | 33 | 26 |
| | Expected | 2.5 | 11.9 | 30.06 | 22.54 |
| | Residuals | -1.583 | -1.130 | 0.537 | 0.728 |
| Angle | Observed | 4 | 11 | 15 | 10 |
| | Expected | 1.5 | 7.1 | 17.94 | 13.46 |
| | Residuals | 2.048 | 1.462 | -0.695 | -0.943 |

#### *7.2.4.1 Width Divided by Angle*

The angled cutmarks contained representation from each of the groups (large=4, med=11, small=15, very small=10) (Table 50). It is notable that this includes the entire collection of large cutmarks. There are some visual differences between the groups when examining the PCA plots (Supplementary File). In general, the largest variation was along PC1 and the smallest along PC3. The LDA did not show any clustering, (LD1 67.8%, LD2 23.6%, LD3 8.58%). There were no statistical differences between groups (Tables 52 and 53, Section 9.4). Pairwise analysis also did not yield any significance when a Bonferroni correction was implemented (range of p found 0.05808-0.70165, required p=0.0083). Hierarchical clustering did not appropriately separate the groups.

In the non-angled group, there were 67 cutmarks used (large=0, medium=8, small=33, very small=26) (Table 51). There were notable differences in the patterns of the PCA plots. The LDA did not show any clustering (LD1 87.1%, LD2 12.9). The MANOVA shows statistically significant differences and the pairwise with Bonferroni correction indicates that this was between the medium and very small cutmarks (F=3.765, 8, 25, p=0.005081) (Tables 52 and 53). There was a difference between medium and small, however when a Bonferroni correction was added, it was not statistically significant (p=0.046417, required p=0.00167). Small and very small showed no differences. Despite this, the hierarchical cluster analysis did not separate the groups.

### 7.2.5 Side of the Body

The full collection of profiles was examined to look at side (total=107, central=18, right=41, left=46, unknown=2) (Table 49). The unknown cutmarks were excluded because it could not be verified that they have the same side. The patterns seen in the PCA plots were unchanged with the results of the analysis being N=105, PC1=60.8%

($6.077744^{-01}$), PC2=18.9% ($1.887888^{-01}$), and PC3=9.22% ($9.223966^{-02}$). Generally, the central and left cutmarks were the most separate, with the right in between, however all ellipses overlap (Appendix I). Central and right seemed to be closer in proximity to each other than either is to left. As was seen with some of the other factors examined, there were visible differences but there were still substantial overlaps in the groups (Section 9.4).

There were no clear clusters present when examining the LDA plots (LD1 97.1%, LD2 2.92%). The differences were not seen statistically either in the full or pairwise MANOVAs with a Bonferroni correction in the latter (Tables 52 and 53). The hierarchical cluster analysis did not result in appropriately differentiated groups.

The Chi-Square test did not show any statistical significance between the frequencies of angled and non-angled cutmarks in each of the side categories ($\chi^2$ (2)=4.7191, p=0.09446) (Table 57).

Table 57: The expected and observed values of cutmark side and cutmark angle

| Angle | | Central | Left | Right |
|---|---|---|---|---|
| No Angle | Observed | 15 | 29 | 22 |
| | Expected | 11.31 | 28.91 | 25.77 |
| | Residuals | 1.096 | 0.016 | -0.734 |
| Angle | Observed | 3 | 17 | 19 |
| | Expected | 6.69 | 17.09 | 15.23 |
| | Residuals | -1.425 | -0.021 | 0.966 |

#### *7.2.5.1 Side Divided by Angle*

The angled set of cutmarks was run with a total of 40 variables initially, however the unknown cutmark was excluded because it was the only variable in that group and the lack of information about the side might have confounded the analysis since the overall sample size was relatively low. This exclusion led to a total N=39. The variation was accounted for by PC1 (48.0%, $4.797469^{-01}$), PC2 (29.6%, $2.957997^{-01}$), and PC3 (7.76%, $7.764212^{-02}$) (Table 50, Supplementary File).

In the LDA analysis, there was no clustering of groups (LD1 85.7%, LD2 14.3%). This group produces a significant difference in the MANOVA (Tables 52 and 53). When the pairwise analyses were run to see where the differences are found, a significant difference was seen between central and left, however, it was not significant once an appropriate Bonferroni correction was implemented (p=0.03072, required p=0.0167). Right was not significantly different to either group. This may partially be related to the unequal sample sizes. The hierarchical cluster analysis did not separate the groups.

The non-angled group contained 67 samples in groups central (N=15), left (N=29), right (N=22), and unknown (N=1) (Table 51). The unknown sample was also excluded and no differences were noted in the patterns, therefore the latter analysis with N=66 is described here. Three PCs were used to examine the majority of the variation and these described the same components of variation as the general non-angled PCA. PC1 accounted for 62.8% ($6.281566^{-01}$) of the variation, with PC2 accounting for 18.5% ($1.850341^{-01}$), and PC3 making up 8.54% ($8.537590^{-02}$).

The non-angled cutmark profiles were examined and some visual differences were seen, though no statistically significant ones. All three groups show low variation along the PC3 axis when plotted against PC1 but more differences could be seen against PC2.

The LDA analysis shows no distinct clustering (LD1 81%, LD2 19%). No significant differences were seen through the MANOVAs or pairwise MANOVAs (range of p found 0.6357-0.8994, required p=0.0166667) and hierarchical clustering did not resolve the directions into their correct classes (Tables 52 and 53).

### 7.2.6 General Shape of Weaponry Types and Implications

This section is entirely exploratory (Sections 3.4, 4.1.7, and 9.4). A column of data was added to the table used for the analyses described above denoting the cuts that were thought to relate to throat-cutting so it would be possible to see if they clustered on the PCA plots. Clustering would not necessarily indicate a different weapon; however, it might suggest there is a signature to the shape of these cuts. This was first explored with the entire collection (with the PCA that was run earlier on the entire collection), and since all but two of the potential throat cuts were non-angled, with just the non-angled cutmarks (with the PCA run on the entire non-angled collection).

These analyses were run twice; once as a binary variable, and once with levels of certainty (no, possible, definite).

#### *7.2.6.1 Full Collection*

For the full collection, there were a total of 107 profiles, 93 of which were not potential throat cuts (NPTC) and 14 which were potential throat cuts (PTC) (possible=4, definite=10). One of the more definite PTC could not be digitised and therefore was not included in this component of the study. No statistical significance was found when running MANOVAs (either Tables 58 and 59), however, there were some patterns and separation seen in the PCA plots which is the focus of this section (Figure 90).

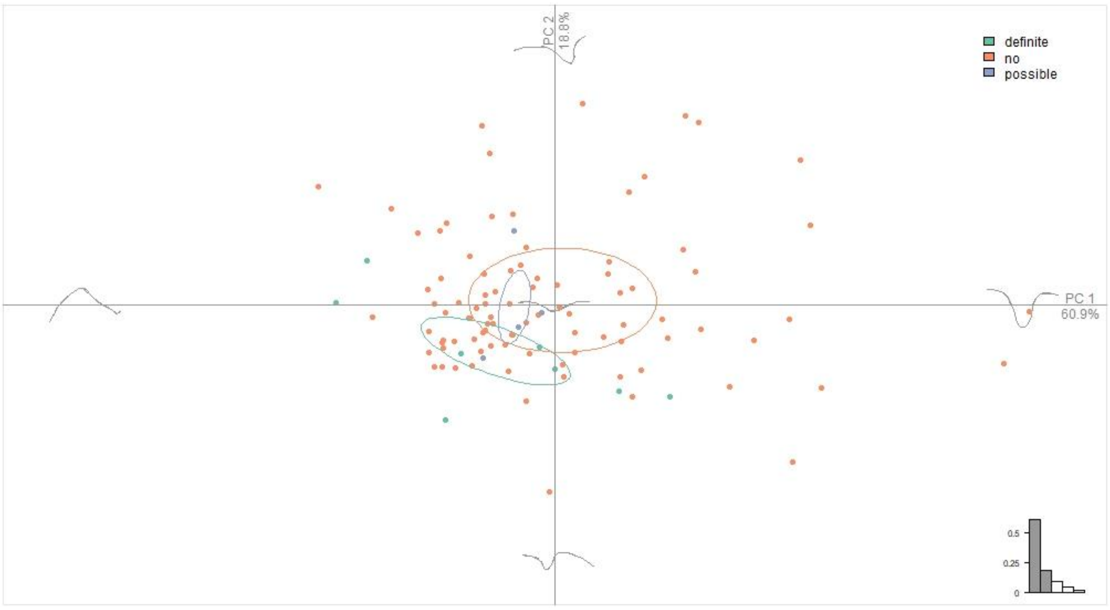

Figure 90: The plot showing PC1 and PC2 of the weaponry analysis when using the full collection

The PTC were seen to be relatively shallower and more upright than the general collection with the definite cuts presenting a more significant shift with little overlap to the ellipse of the general collection. The possible cuts were within the NPTC but show a distinct shift towards the shallower end. Overall, there was no separation along PC3 (LD1 93.1%, LD2 6.9%).

Table 58: The correction percentage and classification error from the LDA when using the full collection to explore PTC

| Variable | Correction Percentage | Category | Classification Error |
|---|---|---|---|
| Binary Weapon | 0.8785047 | NPTC | 1.0 |
| | | PTC | 0.0 |
| Weapon | 0.8785047 | NTPC | 1.0 |
| | | Definite PTC | 0.0 |
| | | Potential PTC | 0.0 |

Table 59: The results of the MANOVAs when using the full collection to explore PTC

| | | Df | Hotelling-Lawley | Approx F | Num Df | Den Df | Pr(>F) |
|---|---|---|---|---|---|---|---|
| Binary Weapon | Fac | 1 | 0.058017 | 1.17190 | 5 | 101 | 0.3282 |
| | Resid | 105 | | | | | |
| Weapon | Fac | 2 | 0.078831 | 0.78042 | 10 | 198 | 0.6476 |
| | Resid | 104 | | | | | |

### *7.2.6.2 Non-Angled Collection*

The non-angled PCA was used for this exploration since none needed to be excluded. A total of 67 profiles were analysed with 56 NPTC and 11 PTC (possible=3, definite=9).

When looking at the plots, there was a clear tendency for the PTC to be shallower and smaller with less variation than the NTPC. In addition, less overlap was seen than when using the full collection. Both PTC and NPTC were fairly neutral along the PC3 (skew of base), though the PTC show a slight indication of more commonly being offset to the right.

No distinct clusters were seen on the LDA plot and no statistical differences were found (LD1 98.2%, LD2 1.8%). Both the LDA showed a large majority of the proportion of variation along LD1 (Tables 60 and 61).

Table 60: The correction percentage and classification error from the LDA when using the non-angled cutmarks to explore PTC

| Variable | Correction Percentage | Category | Classification Error |
|---|---|---|---|
| Non-Angled Binary Weapon | 0.8208955 | NPTC | 0.9821429 |
| | | PTC | 0.0000000 |
| Non-Angled Weapon | 0.8208955 | NTPC | 0.9821429 |
| | | Definite PTC | 0.0000000 |
| | | Potential PTC | 0.0000000 |

Table 61: The results of the MANOVAs when using the non-angled cutmarks to explore PTC

| | | Df | Hotelling-Lawley | Approx F | Num Df | Den Df | Pr(>F) |
|---|---|---|---|---|---|---|---|
| Non-Angled Binary Weapon | Fac | 1 | 0.15082 | 1.83990 | 5 | 61 | 0.1184 |
| | Resid | 65 | | | | | |
| Non-Angled Weapon | Fac | 2 | 0.15432 | 0.91048 | 10 | 118 | 0.5261 |
| | Resid | 64 | | | | | |

### 7.2.7 Shape Analysis Conclusion

Overall, with the attributes that were checked here, there was little in the way of statistically significant separation in the shapes of the cutmarks. All the variables had overlaps between them, though there were cases where certain groups separated slightly away from other groups. The possible reasons for this and implications are discussed in Section 9.4.

## 7.3 Shaved Cutmark Focus: Surface Roughness

The main intention with the surface roughness analysis was to test if it worked on those cutmarks with known direction (Section 5.4.3). This was also discussed in Section 6.3. A further two cutmarks with blade defects were examined to see how distinctly the defects would be evident (Figure 91). In the latter, both showed clear evidence of the blade defects though it was not easy to discern the direction from which blade entered. This may be because of the magnitude of the defect, in which case this should be tested by removing the part of the point cloud with the defects and re-running the analysis. There was no evidence in this collection of identical blade defects on more than one shaved cutmark, therefore the idea of testing which defects could be matched could not be explored.

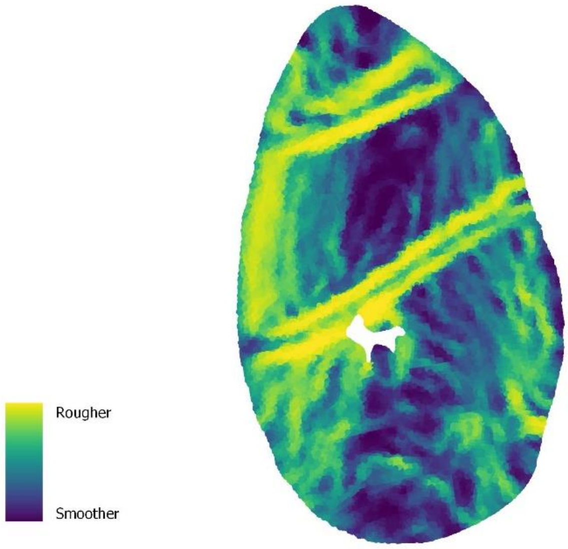


Figure 91: An example of two blade defects seen on the shaved cutmark 3738_D using equal counts to visualise (zIQR 0.000013-0.000367m)

## 7.4 Demographic and Burial Patterns

The number of blows found on the individuals were examined to see if there were any patterns in relation to the demography or the burial position (Sections 4.1.7 and 5.4). These results were all run twice; once with the minimum number of blows counted, and once with the 'maximum' number of blows counted. The latter is not the true maximum each individual had because the soft tissue injuries are not known, but this category does not include any 'Possible' (or tenuous) cutmark associations. For all these categories, a Chi-Square test was initially run using binary (cut/not cut) data. It was further analysed using a Kruskal-Wallis test to investigate if the quantity of blows altered the pattern that was seen compared to what was expected.

### 7.4.1 Age and Number of Blows

For the results from comparing age and number of blows, the cranial remains and postcranial remains were examined separately since they do not represent isolated but also cannot be reassociated to give a full number of injuries to each person (Section 5.4.5). For the postcranial remains, five age categories were examined for the 2x5 Chi-Square test and Kruskal-Wallis test (Adolescent=9, Young Adult=10, Prime Adult=9, Mature Adult=6, Older Adult=4). Those individuals who were not classified more specifically than “Adult” (N=23) were excluded from the statistical analysis to avoid confounding effects. The variable responsible for whether there were cuts present for the Chi-Square test had N=24 and 14 (Cut and Not Cut, respectively). No significant differences were found for either test ($\chi^2$ (4)=0.802, p=0.938; Min: *H*(4)=1.435, p=0.838; Max: *H*(4)=1.411, p=0.842), suggesting the level of violence seen was not related to the age of the individual. The same process was done with the cranial remains and the same result was found when excluding Adult (Cut=35, Not Cut=4; Adolescent=0, Young Adult=20, Prime Adult=9, Mature Adult=9, Older Adult=1, Adult [excluded]=10) ($\chi^2$ (3)=1.639, p=0.651; Min: *H*(3)=5.568, p=0.135 ; Max: *H*(3)=4.116, p=0.249).

Sex was not examined as a variable as all the individuals who could have their sex determined were male which was also supported by the aDNA results of ten individuals (Margaryan et al. 2020).

### 7.4.2 Burial Level and Number of Blows

The burial levels that were indicated in the original osteological report were used for this portion of the analysis (Section 5.4.5). They were grouped in five (lowest=5, lower=10, middle=23, upper=7, uppermost=4) and three (low=15, middle=23, upper=11); those who were the first deposited, those with no skeletons under them, those with skeletons above and below, those with no skeletons above them, and those that were last deposited. The skeletons that could not be rectified were not included (N=12). Similarly, the skulls were not included in the analysis because they were not easily grouped into layers. The 2x3 and 2x5 Chi Square ‘Cut/Not’ variable had 26 with cuts and 23 without cuts

No significance was found when using five groups ($\chi^2$ (4)=5.008, p=0.287; Min: *H*(4)=5.188, p=0.269; Max: *H*(4)=5.189, p=0.268) or three groups ($\chi^2$ (2)=3.790, p=0.150; Min: *H*(2)=3.116, p=0.211; Max: *H*(2)=3.117, p=0.210).

### 7.4.3 Burial Orientation and Number of Blows

Only postcranial remains were examined for this section (Section 5.4.5). Individuals with unknown burial orientation were excluded (N-S=4, NE-SW=1, E-W=4, SE-NW=2, S-N=6, SW-NE=6, W-E=9, NW-SE=5, Unknown[excluded]=24). The number of cutmarks and the compass direction upon which the body was aligned showed no significant differences ($\chi^2$ (7)=9.552, p=0.215; Min: *H*(7)=5.915, p=0.550; Max: *H*(7)=5.923, p=0.549), suggesting no differential treatment of individuals based on injuries when placing them in the grave. Similarly, no significant differences were seen when looking at number of cutmarks and whether the body was prone, supine, or on its side (Prone=26, Side=3, Supine=14, Unknown=18) ($\chi^2$ (2)=4.297, p=0.117; Min: *H*(2)=2.428, p=0.297; Max: *H*(2)=2.390, p=0.303).

## 7.5 Decapitating Blows

The direction of the blows that were thought to have either caused decapitation or been an attempt at decapitation were examined for direction prior to the investigation of surface roughness (Sections 4.2, 5.4, 9.7, and 9.7.7) (also see Appendix H). Both in the cranial and postcranial remains, there was a high number where the direction could not be determined by eye, either because of damage or because of a visually consistent surface (Sections 8.4, 9.3, and 9.5). Of the directions that could be determined, posterior was the most frequent with left and posterior-left also showing slightly higher than median numbers (Tables 62 to 65). In the cranial remains, all directions were represented. The postcranial remains had less decapitation-related blows overall therefore not all directions are present, but the patterns seen were similar. Most individuals had one or two blows in the represented directions with some notable exceptions, mainly in the posterior direction, with the most blows from a single direction on an individual being five (cranial) and six (postcranial). When looking at the full collection of articulated remains, some individuals had blows coming from opposite sides (N=13) and of those, eight were from directly opposite (Sections 9.6 and 9.7.7). These numbers could simultaneously be an over- or under-estimate because some of the cranial remains with blows in opposite directions could be the same as the postcranial remains with blows in opposite directions. However, the full reassociation of all individuals was not possible, so it is conceivable that some of the unidirectional decapitating blows in each group might actually be on the same individual and in opposite directions. The disarticulated remains also showed similar tendencies to the articulated ones, however they are low in number overall (N=12) making it difficult to draw conclusions about the observed patterns in the direction of blows.

Table 62: The directions of the successful or attempted decapitating blows in the articulated full collection (Ant=Anterior, Post=Posterior)

| | Number of Blows | | | | | | | | | | |
|---|---|---|---|---|---|---|---|---|---|---|---|
| Direction | 1 | 2 | 3 | 4 | 5 | 6 | 7 | 8 | 9 | 10 | Total Blows |
| Ant-Left | 5 | 0 | 0 | 0 | 0 | 0 | 0 | 0 | 0 | 0 | 5 |
| Ant | 5 | 2 | 0 | 0 | 0 | 0 | 0 | 0 | 0 | 0 | 7 |
| Ant-Right | 5 | 0 | 0 | 0 | 0 | 0 | 0 | 0 | 0 | 0 | 4 |
| Right | 4 | 3 | 0 | 0 | 0 | 0 | 0 | 0 | 0 | 0 | 7 |
| Post-Right | 7 | 0 | 0 | 0 | 0 | 0 | 0 | 0 | 0 | 0 | 7 |
| Post | 18 | 6 | 4 | 1 | 1 | 1 | 0 | 0 | 0 | 0 | 31 |
| Post-Left | 6 | 1 | 1 | 0 | 0 | 0 | 0 | 0 | 0 | 0 | 8 |
| Left | 7 | 3 | 2 | 0 | 0 | 0 | 0 | 0 | 0 | 0 | 12 |
| Unk | 22 | 17 | 2 | 1 | 0 | 0 | 0 | 0 | 0 | 0 | 42 |
| Total Blows | 17 | 16 | 10 | 9 | 3 | 1 | 1 | 1 | 2 | 1 | |

Table 63: The directions of the successful or attempted decapitating blows in the articulated cranial remains (Ant=Anterior, Post=Posterior)

| | Number of Blows | | | | | | | | | | |
|---|---|---|---|---|---|---|---|---|---|---|---|
| Direction | 1 | 2 | 3 | 4 | 5 | 6 | 7 | 8 | 9 | 10 | Total Blows |
| Ant-Left | 5 | 0 | 0 | 0 | 0 | 0 | 0 | 0 | 0 | 0 | 5 |
| Ant | 4 | 1 | 0 | 0 | 0 | 0 | 0 | 0 | 0 | 0 | 5 |
| Ant-Right | 4 | 0 | 0 | 0 | 0 | 0 | 0 | 0 | 0 | 0 | 4 |
| Right | 3 | 3 | 0 | 0 | 0 | 0 | 0 | 0 | 0 | 0 | 6 |
| Post-Right | 6 | 0 | 0 | 0 | 0 | 0 | 0 | 0 | 0 | 0 | 6 |
| Post | 13 | 6 | 3 | 1 | 1 | 0 | 0 | 0 | 0 | 0 | 24 |
| Post-Left | 6 | 1 | 1 | 0 | 0 | 0 | 0 | 0 | 0 | 0 | 8 |
| Left | 5 | 3 | 2 | 0 | 0 | 0 | 0 | 0 | 0 | 0 | 10 |
| Unk | 13 | 10 | 1 | 1 | 0 | 0 | 0 | 0 | 0 | 0 | 25 |
| Total Blows | 7 | 7 | 7 | 8 | 3 | 1 | 1 | 1 | 2 | 1 | |

Table 64: The directions of the successful or attempted decapitating blows in the articulated postcranial remains (Ant=Anterior, Post=Posterior)

| | Number of Blows | | | | | | | | | | |
|---|---|---|---|---|---|---|---|---|---|---|---|
| Direction | 1 | 2 | 3 | 4 | 5 | 6 | 7 | 8 | 9 | 10 | Total Blows |
| Ant-Left | 0 | 0 | 0 | 0 | 0 | 0 | 0 | 0 | 0 | 0 | 0 |
| Ant | 1 | 1 | 0 | 0 | 0 | 0 | 0 | 0 | 0 | 0 | 2 |
| Ant-Right | 1 | 0 | 0 | 0 | 0 | 0 | 0 | 0 | 0 | 0 | 1 |
| Right | 1 | 0 | 0 | 0 | 0 | 0 | 0 | 0 | 0 | 0 | 1 |
| Post-Right | 1 | 0 | 0 | 0 | 0 | 0 | 0 | 0 | 0 | 0 | 1 |
| Post | 5 | 0 | 1 | 0 | 0 | 1 | 0 | 0 | 0 | 0 | 7 |
| Post-Left | 0 | 0 | 0 | 0 | 0 | 0 | 0 | 0 | 0 | 0 | 0 |
| Left | 2 | 0 | 0 | 0 | 0 | 0 | 0 | 0 | 0 | 0 | 2 |
| Unk | 9 | 7 | 1 | 0 | 0 | 0 | 0 | 0 | 0 | 0 | 17 |
| Total Blows | 10 | 9 | 3 | 1 | 0 | 0 | 0 | 0 | 1 | 0 | |

Table 65: The directions of the successful or attempted decapitating blows in the disarticulated remains (Ant=Anterior, Post=Posterior)

| | Number of Blows | | | | | | | | | | |
|---|---|---|---|---|---|---|---|---|---|---|---|
| Direction | 1 | 2 | 3 | 4 | 5 | 6 | 7 | 8 | 9 | 10 | Total Blows |
| Ant-Left | 0 | 0 | 0 | 0 | 0 | 0 | 0 | 0 | 0 | 0 | 0 |
| Ant | 0 | 0 | 0 | 0 | 0 | 0 | 0 | 0 | 0 | 0 | 0 |
| Ant-Right | 0 | 0 | 0 | 0 | 0 | 0 | 0 | 0 | 0 | 0 | 0 |
| Right | 0 | 0 | 1 | 0 | 0 | 0 | 0 | 0 | 0 | 0 | 1 |
| Post-Right | 1 | 0 | 0 | 0 | 0 | 0 | 0 | 0 | 0 | 0 | 1 |
| Post | 3 | 1 | 0 | 0 | 0 | 0 | 0 | 0 | 0 | 0 | 4 |
| Post-Left | 2 | 0 | 0 | 0 | 0 | 0 | 0 | 0 | 0 | 0 | 2 |
| Left | 2 | 0 | 0 | 0 | 0 | 0 | 0 | 0 | 0 | 0 | 2 |
| Unk | 9 | 1 | 0 | 0 | 0 | 0 | 0 | 0 | 0 | 0 | 10 |
| Total Blows | 10 | 4 | 0 | 2 | 0 | 0 | 0 | 0 | 0 | 0 | |

## 7.6 Summary

This chapter presented the osteological results gathered through Stages One and Three of the methods. The frequencies and locations of trauma in the Weymouth Ridgeway Viking collection were discussed, with the cervical vertebrae and mandibles being the most highly affected elements. The number of blows was examined with regards to demographic and burial patterns and no significant differences were found between any variables. Further details about the trauma were gathered using shape analysis for the profiles of the incised cutmarks which demonstrated there was no clear separation of shape based on the variables tested or by potential weapon used. Surface roughness analysis of the shaved cutmarks was only briefly discussed here as it was mainly a methodological aspect of the study (Sections 6.3 and 8.4). This chapter related to Objectives 5-8 (Section 1.3.1) and the discussion of these findings follows in Chapter 9. Overall, the reappraisal of the SFT using more modern technology has allowed for the following major conclusions:

- From the articulated remains, 38 of 49 cranial contexts were affected and 27 of 61 postcranial contexts were affected with CV2 and CV3 most affected and no clear bilateral differences
- Only the upper body was affected, consistent with the findings from Loe et al. (2014b)
- The decapitating blows came from multiple directions though most were from the posterior direction
- Shape analysis and the exploration of surface roughness showed promise for exploring incised and shaved cutmarks, respectively, and should be experimentally investigated

# 8 Methodological Discussion

This chapter discusses the findings related to the methodological component of this project; the results of the workflow development designed on the Weymouth Vikings have been presented in Chapter 6. This project was designed to thoroughly investigate photogrammetric (specifically Structure-from-Motion Multi-View Stereo, SfM-MVS) models of cutmarks in order to determine what information they can provide and to establish if and when photogrammetry is applicable for both answering research questions and as a recording technique (Sections 2.4.4, 2.5, 5.3, and 5.4). Several of the objectives first described in Chapter 1 are discussed in this chapter, such as the undertaking of a critical analysis of the use of photogrammetry and its application to human remains, the establishment of best practices for the creation of metrically viable models, the comparison of precision to other methods of measurements, and the use of techniques found in geographical research to analyse the surface of shaved cutmarks. This chapter discusses if there is an accessible way to get more information from cutmarks than can currently be obtained by the most common method of analysis, namely callipers, and the potential for further analysis which is not possible without a 3D representation.

## 8.1 The Utility of SfM-MVS and the Optimal Procedure

Overall, the most complex and time-consuming part of the model creation process was designing the optimal strategy and iteratively testing the variables (Sections 5.3.4 and 5.3.5). Both of these are reliant on the size and geometry of the sample so if the sample is varied, it is optimal to create subgroups that have similar geometry. This will help ensure that the best method is used for the geometry present. The length of the iterative testing process depends on how many variables are examined and at what level of detail, but only needs to be once for each sample. The different parameters under investigation can affect the number of points and errors obtained. In general, there are essentially infinite combinations of variables that can be iteratively tested and therefore the ones that are thought to be most important for the project should be prioritised. In this study, the goal was to achieve the 'best' quality structure for the model as possible. Therefore, the focus was on the variables involved in the sparse point cloud (SPC) because it is the basis for the model, and without a good SPC providing adjusted/optimised exterior (and interior) orientation, a dense point cloud (DPC) of good metric quality cannot be achieved (Section 2.4.4) (Falkingham 2012).

Once the strategy is set, data collection progresses faster. In this project, image capture for each bone took approximately 10-15 minutes (Table 18, Section 5.3.5). Depending on the processing power of the computer in use, some of these stages can be concurrent when working on different models; for example, whilst the DPC is run for Model A, the points can be placed for Model B. The editing and placement of control points was the longest process as it required the most user input. The time varies substantially in this stage because it is dependent on the number of control points in total and the number of points that are visible in each image (Section 2.4.3.3). User experience increases the speed of this stage (for research on experience and point placing in Geometric Morphometrics (GMM, see Giacomini et al. 2019). It may be possible to use fewer control points (CPs) for each model and maintain the quality; this could be investigated in the future.

### 8.1.1 Workflow Design

The workflow that was designed follows similar steps to those seen in the United States Geological Survey's (USGS) Agisoft guidance though with a slightly different order (USGS 2016, since updated in 2021). This workflow was designed for use with uninhabited aerial vehicle (UAV) photogrammetry and therefore it is not specifically tailored to small objects. It is not thought that this impacts the quality of the model, however this is something that could be investigated in the future.

Several methods of image capture were discussed in order to determine what would likely be the most effective (Section 2.4.1). Not all of them were tested due to time constraints, but the 'Union Jack' image capture strategy was considered to be the best option as it would allow full coverage without a large number of images, therefore keeping processing time and file size reasonable (Section 5.3.5). The Union Jack is technically a two-tiered orbital pattern with a single vertical image (Figure 60). This helps maintain consistency with the location of the photographs both between orbits and between samples. Given the size of the cutmarks, this approach allowed sufficient overlap of the images (Historic England 2017). Therefore, this was the first method trialled and since it created sufficiently high-quality models with less than 20 images captured quickly, it was determined to be an efficient technique for this study. For larger or longer objects, the image capture protocol might need to be extended with some parallel overlapping images along the sides if the goal is to capture the full object. Further methods of image capture could be tested, but due to the successful results of the pilot studies, this was not deemed necessary for this study.

In this project, the outcomes of iterative tests studied were the number of points in both the full DPC (fDPC) and the cutmark DPC (cDPC) (Section 5.3.4, Appendix E). Depending on the purpose of the project, other researchers may find they have other methods of defining the 'best' model, but for this study, determining what provided the most detail in the area of interest was paramount. Hassett and Lewis-Bale (2017) have shown that having a dense DPC aids in studies where point or coordinate identification is important, such as GMM in their study. The percentage difference was also important because it would give a better indication if the differences seen were within the realm of normal variation or were large enough to be caused by the change in settings. In general, most changes did not cause differences of more than 5% in the number of points in the DPC, and therefore the default values were maintained for variables such as key and tie points (KP and TP, respectively).

Another consideration that was initially tested in the iterative tests was the file format and size. When determining these variables, the JPEG taken with the camera was considered the baseline for both the file size of all the images and the total number of dense points. It was important to consider the benefits of using difference file types (more points) compared to the limitations (more storage space). A balancing point was therefore targeted where the number of points that were found would be substantially more than from a JPEG but the file size would not be increased to the point where creating multiple models would cause storage problems. A major finding from this was that 16-bit greyscale images were optimal without making the file size unmanageable, and the models were able to be edited to a reprojection error (RE) of 0.1, helping reduce the number of potentially extraneous points at the initial stage (Section 5.3.4.1, Appendix E).

Additionally, the model was visually inspected to determine if the extra points in some of the DPCs were additional noise, as sometimes this is readily apparent (Sections 2.2 and 2.4.4). Since this cannot always be determined, the error in both pixels and metres for the control points were examined. They were generally found to have an inverse relationship and therefore a balancing point was found where neither was at its maximum, however neither were completely minimised either. To help mitigate any impact of error, when the markers were being placed on the models, the error was continually checked and iteratively optimised (Section 5.3.5.4). If the error was above a cradle-specific threshold and could not be reduced without clearly being in the wrong position on the image, the model was restarted or the images retaken. Therefore, it is thought that the level to which the errors were reduced is acceptable for the level of detail required for the study.

Throughout the pilot studies and the digitisation of the entire collection, it was found that in most cases the levels of error that were obtained tended to be impacted more by the researcher's placement of the markers than any other parameter (Section 5.3.5.3). As the researcher refined and practiced the method, the placement of the points became more precise, with levels of error for the OG cradle consistently under 0.1mm and 1.5 px. The levels of error are slightly higher with the other cradles due to their larger size (see Section 6.2). It is important to note that this might lead to higher levels of inter-observer error if two observers have very different levels of experience with placing points (Siapno et al. 2020; Omari et al. 2021). Within this study, the effect of different levels of error on the quality of the measurements was not investigated.

### 8.1.2 Precision Studies and Comparisons

Multiple studies have compared photogrammetric models to other methods of modelling and found high levels of accuracy (Koppel 2015; Robleda Prieto and Perez Ramos 2015; Bertsatos et al. 2019; Morgan et al. 2019). Similarly, through the intra-observer error analysis performed in this study, it is seen that this method is precise when using both the DX and FX cameras (Section 6.1). The intra-observer error is similar for the manual measurements as well, however the photogrammetric methods have the benefit that the point cloud can be sectioned and manipulated repeatedly without damage to the original bone and without causing permanent alterations which is beneficial in any studies of human remains (Sections 2.5.1 and 4.1.6) (Ducke et al 2011; Maté González et al. 2015; Errickson et al. 2017; Harten-Buga et al. 2018, 2021; Omari et al. 2021). When comparing the intra-observer error between the DX and FX at each measurement the median and range are very similar, typically with less than a tenth of a mm of difference between the two (Section 6.1.2). All FX values have a slightly larger range than their DX counterparts, possibly due to the difference in the frame sizes.

Inter-observer error analysis was not able to be performed due to the timing of the COVID-19 pandemic during the research process. However, the main step that would vary by individual was the point placing process of the markers. Point identification has been previously studied and found to have an acceptable inter-observer error, therefore for this study, it was deemed sufficient to demonstrate prior testing of the underlying principles by others, but this is something that would need further exploration (Raoult et al. 2017; Siapno et al. 2020; Omari et al. 2021). In their paper on the photogrammetric models of skin wounds, Villa (2017) found that inter- and intra-observer differences were minimal and showed no statistical significance. Some studies like Alsop et al. (2021) and Colman et al. (2019) have shown low inter-observer error when identifying points on 3D models created using other methods. The latter found some higher errors with a few of their measurements, however these were all linked to one poorly-placed point having a knock-on effect on multiple measurements. These various studies of 3D digital models are similar to the work done in this research with the Weymouth Vikings, which suggests that although inter-observer error needs investigation, the general techniques used to measure in this study have been proven to be valid.

When looking at the pilot studies, the differences in measurement between the DX and FX cameras were non-significant (Section 6.1.4). In the majority of cases, the profiles that were created by the FX camera were smoother and visually ‘nicer’ to work. Despite this, the measurements that were taken were statistically similar, therefore both were deemed to be suitable cameras. Additionally, this underscores the ability of photogrammetry to be a reliable procedure since two different cameras created models that yielded the same measurements (Section 2.4).

Since the two cameras provided no statistical difference in measurements for either category of cutmarks and both were easy to use, the decision to use the FX camera was partly pragmatic because there was greater access to this camera relative to the DX camera. The FX camera was also newer and the lens was specifically designed for them. The larger frame was helpful for capturing the full background of the cradle, especially with larger bones. In the field, the DX may be superior as it has the benefit of costing less and being lighter weight than the FX as well. The lenses specifically for the DX camera are also less expensive, but the range of fixed focal length lenses can be smaller. However, the study was all in the laboratories, therefore the FX's added size and weight were not an issue. The FX camera is of higher-specification and arguably the better camera with less noise inherent in the pixels and a larger dynamic range (Nikon 2020a, 2020b).

Overall, the current and prior research indicates that the photogrammetric process can be performed accurately even without a camera that is considered top-of-the-line. This has implications for smaller museums, research groups, or forensic companies that may not have the budget to purchase an FX camera, or equivalent, in addition to whichever photogrammetric software they require (Sections 2.5 and 6.1.4). This is also important for commercial archaeology where the cameras are taken on site and undergo a lot of wear-and-tear in a variety of weather. Commercial archaeological units might be less inclined to buy expensive cameras that could only be used for photogrammetry but the similarities between the DX and FX measurements show that the site cameras would be sufficient. However, a separate lens that is only kept indoors might be recommended for photogrammetry in such situations.

One aspect that could be either an advantage or limitation is that the size of the FX frame allows for a wider field-of-view and therefore more CPs are captured in a single image. This is beneficial if the object being digitised is of a size or shape that it obscures a substantial number of CPs in some images. However, if essentially all CPs are visible in all images, that does increase the amount of time spent processing the model because all the CPs need to be manually placed in each image.

### 8.1.3 Challenges of SfM-MVS

As with every method, there are certain challenges present with SfM-MVS. One challenge experienced was the need to ensure that a computer with sufficient specifications could be obtained. In order to proceed with a software like Agisoft, as of 2020, the minimum requirements for a computer are Windows 7 SP 1 (64 bit), Mac OS X High Sierra, Debian/Ubuntu with GLIBC 2.13+ (64 bit), Intel Core 2 Duo processor/equivalent and 4 GB of RAM, with the recommendations being Windows 7 SP 1 or later (64 bit), Mac OS X Mojave or later, Debian/Ubuntu with GLIBC 2.13+ (64 bit), Intel Core i7 or AMD Ryzen 7 processor, a discrete NVIDIA or AMD graphical processing unit, and 32 GB of random access memory (RAM) (Agisoft 2020a). Higher specifications for aspects like RAM and graphics cards would result in faster processing time, but sometimes that can be prohibitive due to cost or money. This might be a challenge for some smaller commercial archaeological or research units, police forces or forensic laboratories, and museums. In situations like this, it could be beneficial to test some of the freeware that is designed for SfM-MVS that is available either to download or use online (e.g. VisualSFM, Regard3D). Additionally, with the rapid development of computer hardware, it is likely that computers with sufficient processing power will become more affordable in the foreseeable future.

An additional challenge was found during the shape analysis when examining the profiles (Sections 5.4.4 and 9.4). In some instances, there was obvious noise within the base of the cutmark at the desired profile location. For this study, the nearest clean profile was used instead, usually less than 1mm away from the original location. However, if it is necessary to use a very specific location, ways of avoiding this would have to be further studied. For example, capturing more images per orbit or an additional orbit could potentially mitigate this.

### 8.1.4 General Conclusions Regarding the Utility and Optimisation of SfM-MVS

The visual quality of the models of the cutmarks on the Weymouth Vikings was generally high for the area around the cutmark itself (Figure 92). The further from the area that was in-focus in images, the poorer the visual quality became, though for the purposes of this study, that was not a problem. If a model with uniformly high visual quality is desired, placing the camera further from the object to create a larger depth of field would help. The dense point clouds in this study could be turned into meshes, however, depending on the purpose of these meshes, alternate settings for depth filtering might be recommended to make it as visually pleasing as possible.

Figure 92: A cropped DPC of two incised and one shaved cutmark with blade defects on a parietal (3738_D, E, and F) (Figure 91 for the surface roughness output of 3738_D)

Plenty of research has been done in the world of photogrammetry and archaeological modelling however there is still much to explore in regard to close-range photogrammetric modelling (e.g. Snavley et al. 2006; Remondino 2011; Maté González et al. 2015; Sapirstein 2016; Sapirstein and Murray 2017). It is important to determine the full capabilities and limitations of current methods to avoid creating poor models that then are not fit for purpose in the future (Sections 1.4.1 and 2.4.4.4). Given the speed at which technology advances, it is also vital to get into the habit of exploring methods to ensure they work to the best of their ability before integrating into analyses. This research contributes to the growing body of literature surrounding photogrammetry, helping other researchers to be able to make informed choices about what methods are best for their studies.

Although comparison to a ‘true’ value would be ideal, the comparisons done within this study are deemed to be sufficient to demonstrate this methodology and the 3D control cradle work (see Section 8.3 for a discussion of ‘gold standards’). With respect to the initial pilot study samples, manual measurements are commonly used when analysing cutmarks and therefore would be the most likely method to be replaced by photogrammetry, and the statistic similarities between the manual and photogrammetric measurements show that this would be a valid replacement. Overall, these results show the SfM-MVS models are precise enough to be considered for use and do not have any greater inconsistency than other methods. The workflow designed in this study was found to be very effective for this project and would be recommended for other research requiring metric analysis of small objects (Figure 64, Appendix D). This, however, comes with the caveat that the process and the parameters may need to be tailored to the specific sample and objectives of the project.

Importantly, the SfM-MVS measurements allow for the cutmarks to be analysed in ways that cannot be done manually in a more accessible manner than many other methods, such as µCT (e.g. Harten-Buga et al. 2018, 2021). The profile can be examined in different places along the cut for incised cutmarks and it can be investigated repeatedly and superimposed on other cutmarks without the bone undergoing damage (Sections 4.1.6, 5.4.4, and 7.2). This is invaluable when studying human remains as it is important to be able to protect the remains themselves from damage whilst conducting research or teaching. The ability to create precise 3D models at a relatively low-cost can help with research and collaboration between institutions (Section 2.4.4.4). Studies of the digital copy of the bone can be repeated, even if the study involves sectioning the model, which is beneficial for independent validation of techniques. Additionally, with just the images and the control coordinates, the bone can be re-created by a different individual, allowing for independent testing of results. These models can also be used for teaching, both as supplements for in-person lab sessions, or as primary material if learning has to be performed online, such as during the COVID-19 pandemic.

## 8.2 3D Control

The addition of control points into the model is a critical step in order to make the models scaled and measurable (Sections 2.3, 2.4.3.3, and 5.3.2) (Linder 2009; Wolf et al. 2014; Historic England 2017). Overall, 2D control can easily be added in the form of a static ruler or other similar device (e.g. Falkingham 2012; Maté González et al. 2015; Mallinson and Wings 2014; Historic England 2017; Sapirstein 2018). However, when creating 3D models that are going to be measured, z-control is required. To be most effective, control points should be referenced to an x, y (horizontal), and z (vertical) origin or datum, preferably well-distributed along each axis (Wolf 1983; Linder 2009; Wolf et al. 2014; Lillesand et al. 2015). Additionally, when the accuracy of the control points is not known, this can be mitigated through using a sufficient number of well-distributed [ground] control points ([G]CPs) and if the errors are random rather than systematic (Section 2.4.3.1). In their recent article on SfM repeatability and reproducibility in geomorphology, De Marco et al. (2021) highlight the importance of using [G]CPs and independent check points (ChPs) to create high quality models. Without sufficient control, or with inadequately placed control, it is more likely that erroneous image matches may go uncorrected and height differences may not properly reflect the true elevation (Barrand et al. 2009). For example, Silvester and Hillson (2020) found that their dental SfM-MVS models lacked some detail, however they did not have well-distributed z-control, a common issue in studies using flat targets or scale bars.

As discussed in Section 5.3.2, for this study, the use of 3D printing was chosen as the best way to add 3D control into the models (see George et al. 2017 for a discussion of accuracy and reproducibility in 3D printing). In order to create control that would have the optimal qualities described above, the ‘Control Cradle’ was designed (Section 6.2). It was designed using a freeware (Sketchup) and the design can be scaled because it was meant to be shared with other researchers and institutions so they can print their own if required for digitising. It was specifically designed with the samples for the pilot study and then modifications and extra components were added to make the cradle more universal. It was made out of non-reflective, randomly-speckled material which could provide unique points for the software without a glare being created from the light (Section 2.4.4.4.2) (Schaich 2013; Nicolae et al. 2014; Micheletti et al. 2015b; Sapirstein 2018).

The additional benefit of this type of control was that it filled the entire frame of the camera and therefore, once the object was secured, the cradle and object could be rotated whilst the camera remained stationary. Although this initially appears to be opposite to SfM-MVS principles of having a static object and moving camera, it does not result in any differences in the images taken provided any visible background is entirely neutral (Section 2.4.4) (Micheletti et al. 2015b; Ferreira et al. 2017; Granshaw 2018). This works because the only visibly different background seen in the images remains in the same place relative to the object regardless of any transformation of the control cradle-object (CC-O) complex. This has the benefit of decreasing data capture time because the camera can be set to the angle for the lower pictures for each traverse, followed by the upper ones, and eight images can be captured at each position without moving the camera.

The cradle was very useful and easy to use. It increased the ability to use a consistent photographic strategy. The design is lightweight and easily transportable. As attachments were created to be added, it increased the number of bones that could be digitised. The OG cradle with two wedges was able to digitise roughly 70% of the collection. Once the two additional cradles were added, 100% of the bones were able to be housed. Out of 454 total models made, a small number (approx. 2%) did not align on High or Highest and thus were retaken. Since a second set aligned without issues, these failures were thought to be to do with the lighting or photography rather than with the cradle itself (Figure 93). Two failed at the DPC stage but were successfully rephotographed and run, so these are also not thought to be a systemic issue with the cradle.


Figure 93: An example of a failed SPC where all images aligned but did not align properly

Although there may be an initial investment of time and cost to produce an appropriate cradle, the cradles are very versatile and can be used for a wide breadth of objects; in this study, everything from a fragment of a vertebrae to a cutmark on an intact skull was successfully digitised. This method of photogrammetry and 3D control create good quality models that are statistically comparable to manual measurements, the most common method of cutmark analysis (Sections 4.1.6 and 5.3.7). Similar results were found by Maté-González et al. (2017). The benefit of having appropriate control measures makes the investment worthwhile. The cradles are easy to use and versatile and are considered an asset in close range photogrammetry.

Ideally, the number of check points and control points used to test the cradles would be equal to allow for the most robust statistically analysis, although the test used here (Mann-Whitney U) does accommodate difference sample sizes (Sections 5.3.8.3 and 6.2) (Mann and Whitney 1947; Field 2009). This was possible with the MK2 and PH cradles as they were designed with the use of check points in mind. For the OG cradle, splitting the points into two equal halves would result in large gaps in control and thus an unequal split of twelve CP to eight ChP were used. Symmetrical patterns were used in all cases to choose CPs. The errors were examined as a whole and broken into x, y, and z-components. In all cases, the errors that were found were all statistically similar and therefore the findings that the model was of good photogrammetric quality were supported. The errors for all the CPs were considered acceptably low for this study; ~0.07-0.1mm for the OG cradle, ~0.17-0.19mm for MK2, and ~0.3mm for PH. Part of the reason for this difference in acceptable and typically seen errors is because of the size of the cradle; the larger cradles require a wider FOV leading to an increased error in mm and a decreased pixel error. Future research could investigate how to reduce errors when using a larger control cradle, though often when the subject is larger, the acceptable level of error is as well.

As noted by Baier et al. (2021), different 3D printers or printing methods can produce slightly different results so it is important to be cognisant of this and it is advisable to test the cradle rather than assuming it is accurate. A subsample of models using each cradle were chosen to analyse the component error against the corresponding value to see if there was any systematic error or if it was random (Sections 5.3.8.3 and 6.2, Appendix E). The errors were found to be random for all three cradles in all directions, however some statistically significant relationships were found, though none of the relationships were strong enough to show any design flaw. When visually plotting error and value, MK2 did appear to have a systematic error in the z-direction, albeit this was not statistically significant. There was a moderate positive relationship between the height of the point and the error, a relationship also seen in OG cradle, and it was suggested that overall there might be a minor systematic error with the z-value with the printing, resulting in a minute cumulative error (Baumann and Roller 2016; Choi et al. 2016). This aligns with the fact that this error is most notable in MK2 because the highest z-value is approximately 20mm higher than in either of the other cradles.

This potential z-relationship needs further exploration using more than five sample models to determine if this error either reduces with more data, or starts to present a clearer trend because even the statistically significant relationships were weak (Section 6.2). Although this was not rectified within the remit of this study as the errors produced were still considered acceptable it was noted as something for further investigation. Best practice should be determined to avoid this in other studies, especially if larger cradles are required. In retrospect, the accuracy of the z-values should have been set differently to see if this affected any error values. This is something for researchers to be aware of if they use a larger 3D printed cradle as the printer used could have a similar systematic error that is more problematic at that scale. However, if unable to correct the error in the printing, there should be ways to mitigate it, such as altering the accuracy for z or finding a regression equation that fits the systematic error and implementing a mathematical correction. This underlines the importance of testing equipment before launching into data collection and being prepared to find and mitigate errors.

In summary, the control cradle provided a useful method of implementing 3D control into the SfM-MVS of small objects. In its current state, it would not be suitable for all studies, but it can be adapted with relative ease. This is an extremely useful piece of equipment when trying to create photogrammetric models of objects that are too small to be tied to real-world coordinates through something like a total station theodolite (TST). These cradles can be adapted as required and used for objects other than just bone. For example, the third cradle design, PH, has successfully been used to digitise the surface of a carved rock. Having this type of control allows for confidence in the measurements that are taken from the 3D models and helps new avenues of analysis, such as surface roughness, be possible.

## 8.3 SfM-MVS Compared to Other Methods

The intention behind comparing the SfM-MVS models to other methods was to determine the accuracy, however, this is inherently a problem because a method needs to be deemed ‘better’ than the others and designated as the reference method (Sections 5.3.7 and 6.1.3) (see Walsh 2018 for a discussion in the context of dentistry). Many studies chose different methods of measurement as a ‘best’ comparative method based on what they have available (e.g. Andronoswki et al. 2018; Carew et al. 2019). Any time a measurement is taken, it is an approximation of the measurement and thus no measurement will ever be ‘reality’, however Versi (1992) argues that the ‘gold standard’ is not what is perfect, but rather what is the best available and will be ever-evolving with new technology and procedures; thus, the perfect standard will never be achieved. Despite this, an attempt was made to compare the SfM-MVS model to other common ways of measuring cutmarks. Most commonly, measurements are taken with digital callipers, and therefore it is arguable that it was most important for the SfM-MVS measurements to align with the manual measurements as that is what they might be replacing in many cases (e.g. Fiorato et al. 2000; Loe et al. 2014b; Giuffra et al. 2015). Additionally, a measurement using digital microscopy was sought as being closer to a ‘gold standard’ than manual measurements (Sections 5.3.7 and 8.3) (e.g. Alunni-Perret et al. 2005; Bonney 2014; Nogueira et al. 2017).

Additionally, the findings demonstrate that neither the DX or FX camera showed any significant difference in length or width measurements when compared to the manual measurements (Section 6.1.4). This suggests the results obtained with the SfM-MVS models are consistent with those obtained conventionally and therefore are just as valuable to use. Compared to measuring manually, the ability to zoom in on and move the point cloud as required has additional benefits as it allows for the more precise placement of markers which note the edges of the cut.

Overall, the measurements taken from the bone with the digital callipers and the measurements from the SfM-MVS models were statistically similar, suggesting that any analysis done on the models would result in the same measurements as those from the real bone which was the outcome hoped for in the methodological testing (Section 6.1.3). Only one of the pilot studies was analysed with the digital microscope due to COVID-19, however, there were issues raised about the use of the digital microscope as a ‘gold standard’ and therefore the results were omitted, regardless (further discussed in the following section).

### 8.3.1 Limitations of '3D' Digital Microscopy

Initially, a digital microscope, the Keyence VHX-5000, was to be used for reference data as mentioned in Chapter 5 (Keyence Corporation 2014). Two major problems were encountered in using this method. First, it appears any measurements that are taken from the 2D viewer assume the object is level, thus negating any displacement in the z-direction between the start and end of the measurement and therefore is akin to taking measurements off a scaled image. This causes issues if the sample is not perfectly aligned in parallel with the lens of the microscope as this neglects any vertical displacement. Due to this, length measurements performed in this method will be erroneously shorter than they should be. There were plans to investigate this curvature further in order to see how this affects measurements taken or if this was an error in the set up on the day the images were originally taken. However, because of the COVID-19 pandemic, the laboratories were closed for an extended period of time and this aspect had to be eliminated. This is an avenue that should be further investigated along with SEM in the future. The digital measurements that were discarded did not show any significant differences and therefore may not have been erroneous in this study, however this could be problematic if the curvature is more significant and the uncertainty of the effect led to omission of such measurements (Section 5.3.7). More importantly, it means that this particular digital microscope cannot be considered an appropriate reference for length measurements.

A second limitation encountered with the use of the digital microscope was related not to the instrument itself but to the requirement for sufficient training in its use. This was found to be critical in terms of establishing efficient workflow and optimal results. For example, when creating the profiles, there is a method of altering the scale on the image, which changes the ratio of x:y axis, thus stretching or compressing the image. However, this information was not included in two initial training sessions. As a result, the setting that was toggled when the initial images were captured was not known, so measurements like the opening angle may have been highly affected. Due to the COVID-19 closures, this could not be rectified or investigated. Therefore, the researcher decided to omit measurements as the impact of this was not known (Sections 5.3.7 and 6.1.3). This experience leads to the recommendations are that all staff or post-graduate researchers who require the use of the equipment should be trained by the company liaison at the earliest possible opportunity.

### 8.3.2 Conclusion on Comparative Analyses

Overall, the comparative analysis has shown that the measurements obtained from the SfM-MVS models are statistically similar to the most commonly used method, namely manual measurements (Section 6.1.3). A 'gold standard' could not be thoroughly tested due to availability, but since callipers are the most frequently used method of obtaining metrics, this was not deemed to be an insurmountable issue in this study. The similarities between manual and SfM-MVS measurements indicate that the photogrammetric method can be used for metric studies which opens up opportunities to share models and collaborate with other researchers. It also allows the re-analysis of the models without damage to the collection. Compared to manual measurements, there is the major additional benefit of being able to analyse metrics such as depth of the cut of the opening angle. Without a digital version of the cutmarks, the analyses that were done using shape analysis and surface roughness would not have been possible.

## 8.4 Surface Roughness in Osteology

Surface roughness is used very differently in different fields. In osteology, surface roughness tends to be applied to areas such as muscle attachments and the roughness of the surface there. It is done through visual inspection using nominal scales and much work has been done to create scales for muscle entheses (e.g. Mariotti et al. 2004, 2007; Henderson et al. 2013). The surface texture of bone is noted in several other contexts, often aging, but it is either qualitative or through a relative scoring system (e.g. Brooks and Suchey 1990; Lovejoy et al. 1985; Buikstra and Ubelaker 1994).

In earth and environmental science, rugosity is a calculated measurement of ground surface roughness and can be used as a metric by itself or to infer other things, such as water flow (Smith 2014). By considering the shaved cutmarks to be small landscapes and analysing them as such, it allows surface roughness to become a much less subjective measurement in osteology (Section 5.4.3). This is useful for shaved cutmarks because they are currently under-interrogated in the data (Sections 4.1.4 to 4.1.7). They can be measured, but those length and width measurements actually provide more information about the bone than they do about the cut or the events leading to it. Due to the properties of bone and the propagation of forces (Sections 4.1.1, 9.3, and 9.5), the entry of a shaved cutmark is usually smoother than the exit or opposing side and this can provide information about the direction of the blow which is of much greater benefit when trying to interpret an event than information about the size of the bone (Galloway et al. 1999; Loe 2016; Boylston 2000). This can sometimes be visually determined, but sometimes visual determination is not possible. In the situations directionality cannot be easily determined, it was speculated that quantitatively analysing the surface could help establish the directionality of the impact (Section 4.1.4 to 4.1.7).

There are multiple ways to calculate surface roughness and they have varying complexities. For example, analysis can be performed in 2D, using a profile and calculating the length of a line compared to the distance it covers and it can be determined using raster information in digital elevation models (DEMs), however a DEM is not fully 3D either (e.g. Riley et al. 1999; Bhushan 2000; Du Preez 2014; Lazarus and Belmaker 2021). Other possibilities include using surface reconstruction on the point cloud and then calculating the ratio of total surface area to planar surface area. For methods using raster data or a mesh instead of a point cloud, decisions have to be made about what type of interpolation or surface reconstruction to use (Section 2.1.1). There are several common interpolation methods for raster files such as Inverse Distance Weighting, Kriging, and Spline, each of which have variations (Shepard 1968; Schoenberg 1969; Krige 1976). Surface reconstruction methods are similarly diverse, and commonly performed through Poisson Reconstruction and Delaunay Triangulation (Lee and Schachter 1980; Kazhdan et al. 2006; Kazhdan and Hoppe 2013). In all cases, different methods have been found to be superior in different situations.

Once the decision was made to analyse the surface roughness in the point clouds of the trauma on the Weymouth Vikings, an appropriate method had to be determined to investigate it. One way would be to use the root mean square error or standard deviation from a plane of best fit (representing the cutmark). This would be an acceptable method on the compact bone, however, on trabecular bone, the natural dips in the exposed trabeculae would artificially increase the magnitude of the surface roughness (Section 4.1.1). The decision was made to exclude the trabeculae as there was the possibility of confounding effects on the initial development of the methodology. Primarily, the differing amount of exposed surface area in the compact surfaces compared to the trabecular surface could lead to differing rates of taphonomic damage which may obscure the surface texture of the original cutmark.

The trimming of the point cloud is important because if extraneous points are left or the edges of the cutmark are incorrectly identified, it can cause the subsequent IQR calculations to be erroneous around the edges. This is usually fairly obvious visually once the analysis is run and can subsequently be re-trimmed and re-analysed. Of similar importance is the levelling of the point cloud before importation into QGIS to avoid any skewing of the height data. In this study, the levelling was performed in CloudCompare (ClCo) by fitting a plane to three points (Section 5.4.3). The model was then rotated around the z-axis to ensure it was as level as possible. Not all cutmarks will level nicely as some of them may have an inherently curved surface, either due to Residual Energy Dispersal (RED) fracturing (see Section 9.3) or the movement of the blade itself (often called a ‘scoop lesion’, Appleby et al. 2015; Mikulski et al. 2021). Whether some type of mathematical correction should be input to flatten out this type of cutmark is something that could be explored in future research.

The workflow that was designed was made to mimic the Terrain Ruggedness Index (TRI) tool found in SAGA, except using a point cloud and thus called the Point Ruggedness

Index (PRI) (Riley et al. 1999; Conrad et al. 2015). TRI works through searching a DEM with a set radius or kernel to find the change in elevation between a cell in the kernel and the other within the search area and results in a positive value without any set units. Different buffer sizes were tested and it was found that anything over 1.5mm was not sensitive enough to differences and involved a very long processing time, therefore a 1mm buffer was used in order to really retain local differences. The interquartile range (IQR) of the z-values were calculated within the buffer of each point. This measurement was chosen as it negates the highest and lowest values (those outside of the 25th to 75th quartiles) which will minimise the influence of noise. Once the procedure was established, it was relatively straightforward to turn the workflow into a model using the Graphic Modeller of QGIS (Figure 94) (Appendix D). This can then be output in Python or continue to be used within the QGIS environment.

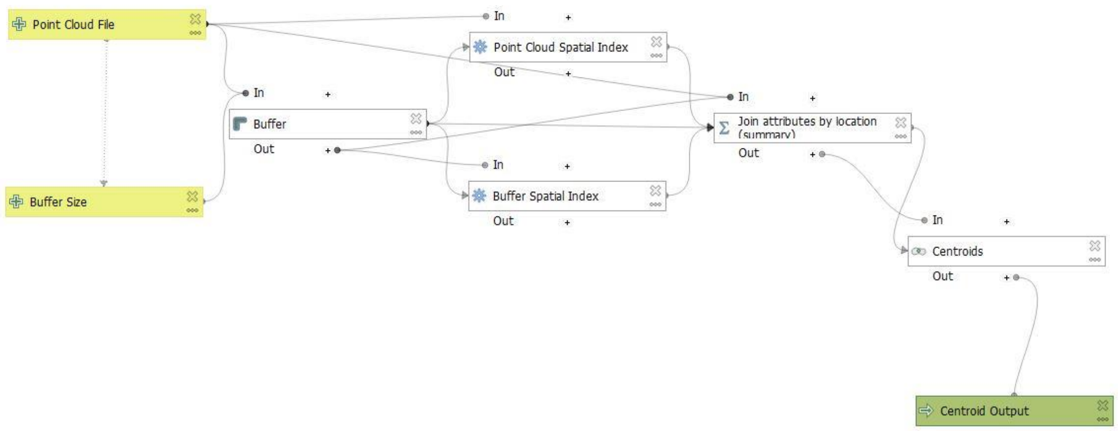


Figure 94: An image of the graphic modeller in QGIS with the surface roughness workflow (Python code for the modeller can be found in Appendix D)

The symbological choices were found to be important for visualisation. For this project, only two symbologies were compared, as described in Section 5.4.3. Future studies could explore how the differences in number of classes and separation of classes could affect the interpretation of results. From what was seen here, using equal counts provides a more evident difference than does equal intervals. The use of standard deviation appears not to be possible with a high number of classes because the different number of maximum classes allowed for each point cloud would make it impossible to standardise if a near-continuous scale would be required.

Ideally, a completely continuous graduated colour ramp would have been used, however this did not appear to be possible at the time of analysis and therefore the number of classes was increased instead, in order to mimic a continuous scale (Section 5.4.3). One limitation of this portion of the study was that the majority of the cutmarks analysed were from the mandible as it tended to have the largest area of compact bone. Many vertebrae had shaved cutmarks, but their bodies are primarily trabecular bone and thus would only leave a small ring of compact bone to analyse so they were not considered optimal for the initial testing of this method.

### 8.4.1 Implications for the Study of Human Remains

Studying the shaved cutmarks in the collection of Weymouth Vikings has allowed for the discovery that the surface roughness of a bone can be quantified at a very small scale. This is very important and opens the doors for further research, especially regarding directionality of cutmarks and fracture patterns. This may also aid with the creation of less subjective methods for essential procedures outside of trauma analysis, such as in age determination. New methods such as this may also allow for the refinement of previously-made interpretations. More research needs to be performed in this area and some related ideas are outlined in Section 8.5.4.

## 8.5 Further Methodological Work

There are many aspects of the use of 3D digitisation through photogrammetry that are still unexplored; a few avenues for future research have been noted throughout this chapter, but some of the major points are discussed here.

### 8.5.1 Changing the Camera and Software

One important aspect that can be investigated are the levels of accessibility (Section 2.4.4.4). In this study, the equipment that has been used is typical equipment that might be found in a university or a commercial archaeological unit. However, it would be good to know how much the quality of equipment can be altered until the models produced are no longer of sufficient metric quality. This could be done by trying different levels of camera; a basic point-and-shoot, a phone camera, a microscope, and a digital viewer. There are papers using different levels of camera which have found they are able to create successful models, however only recently have studies started to comprehensively compare metric results (e.g. Snavely et al. 2008; Micheletti et al. 2015a; Nocerino et al. 2017; Liba et al. 2019; Omari et al. 2021). Different software could also be used. There are many types of SfM-MVS freeware as well as different licenced versions (see Vacca 2019; Bartos et al. 2014; Forsmoo et al. 2019; Kingsland 2020). It would be interesting to test the effectiveness of different methods of 3D control, such as using scaled and printed slot cards, or LEGO®, since it is designed to a very high metric specification (LEGO 2010; Villa 2017; Larsen et al. 2021).

### 8.5.2 Increasing the Number of Comparative Measures

It would also be ideal to compare SfM-MVS to a wide variety of reference measurements (Sections 6.1.3 and 8.3). This way, the full range of benefits of limitations of each method would be known and thus people could make educated decisions on which method they use. Harten-Buga et al. (2018, 2021) have created excellent 3D visualisations of SFT using micro-CT scanning. However, such equipment is often inaccessible to researchers so it would be valuable to know how the quality of photogrammetric models are compared to models like this (Sections 2.4.4.4 and 4.1.6). Methods of microscopy are likely to be more accessible to people than medical scanners, therefore testing SEM, confocal microscopy, and other digital microscopes would be optimal. In this project, there was the intention of comparing the SfM-MVS models to primarily digital microscopy and potentially SEM, however, as explained in Section 8.3, this still remains to be investigated.

### 8.5.3 Inter-observer Error

Inter-observer error is also something that should be investigated, both for measurements off a base model and for measurements off models created independently from the same set of images. It is important to compare the inter-observer error compared to other methods of cutmark analysis because the most critical thing with using 3D digital visualisations instead of the actual bone for analysis is that the method is as good as or better than conventional methods. This was not within the remit of this study as discussed in Section 8.1, however it should be investigated in order to learn more about the advantages and limitations of this technique especially with users of difference levels of experience.

### 8.5.4 Surface Roughness Methods

Other methods of analysing surface roughness could be explored. The method used in this study is one way of analysing surface roughness and was chosen as the best method here, however there are many other types of surface roughness analysis in the earth sciences (Smith 2014). The point clouds can be turned into digital elevation models or meshes and can be analysed through software such as QGIS. Other methods of levelling the point clouds would be good to investigate, especially if it is possible to incorporate in the PRI script, either to run in QGIS or through Python. The current method is more subjective than the rest of the methods because it involves determining the three levelling points by eye (Section 5.4.3). This would inherently be problematic on rougher surfaces as slightly different placements of points could drastically alter the plane to which the point cloud is aligned. In this study, the point cloud was checked from every angle to try to ensure it was as level as possible, but this would be improved if the process was automated. There are currently further tests being performed on this analysis, however they were not in the remit of this project and therefore the results are not included here, however, they are detailed in the following paragraphs.

#### 8.5.4.1 Surface Roughness: Further Exploration of the PRI

The first area of exploration is the testing the values from the PRI compared to the equivalent, and already present, method of analysing surface roughness on meshes. It would be useful to compare the surface roughness from the method used in this project to the equivalent TRI on a mesh developed from the same point cloud. If it could be applied to both types of 3D model and provide the same results, it would increase its use. Testing this with something like the auricular surface could potentially open doors to using this method on a living population (CT through meshes) to determine age categories based on quantitative surface roughness and then apply that method to dry bone when applicable, such as in forensic cases which could use either photogrammetry or CT data. Either selected archaeological individuals of known age and sex or teaching casts will be used for this as a viability study. This would also be an opportunity to test Metashape v1.7's new feature that allows meshes to be created directly from the depth maps, rather than via a dense point cloud (Agisoft LLC, 2021). As this feature has only been released recently, it is not yet known how different the two meshes would be in this type of study.

#### 8.5.4.2 Surface Roughness: Cutmarks of No Known Direction

The second area to further explore the utility of this method with cutmarks that have no visibly known direction (Sections 4.1.1, 4.1.4, and 6.3). Ideally, this would be done with experimentally performed cutmarks with the individual analysing the surface roughness blind to the cutmarks so a larger dataset can be created and the influences of confounding factors such as taphonomy would not be present. At the moment, some tests can be done on cutmarks of unknown direction, however it is unknown if any subtleties are lost due to taphonomic damage. It would therefore be better to further explore this to see if it can successfully determine directionality on bones where it is not visibly obvious before implementing such analysis on archaeological remains. This might also allow for exploration of how the analysis of trabecular bone could be performed as well.

#### 8.5.4.3 Surface Roughness: Blade Defects

Other aspect of shaved cutmarks that could be analysed with surface roughness is the appearance of blade defects (Sections 6.3 and 7.3). There are two obvious ones in this collection and, as discussed earlier, both were analysed to see how clearly the defects would be to see (Figure 91). In both cases, they were obvious in the surface roughness images. Interestingly, neither showed a clear bias towards one side being smoother than the other so the impact of blade defects on the overall surface roughness symbology needs to be further investigated (Section 9.5). It is possible that the magnitude of the defects means that the current symbology is not showing the same level of detail in the general cutmark surface. It would be worth running the analysis again with the defects removed in order to determine what type of impact they might have.

#### *8.5.4.4 Surface Roughness: Intrinsic Bone Properties*

A final area worth exploring is whether there are underlying differences in roughness in the non-entry areas that are related to the properties of the bone itself (Section 4.1.1). For example, it is known that buttressing in the skull affects how fracture propagate. Postcranial bones have lines of stress through them that tend to build more bone (see Ruff et al. 2006 for a discussion of Wolff's Law) and whether these areas would cause differences in the RED fractures when cut may need exploration. This would not largely impact the investigation of cutmark directionality, but it might provide more information about the structure of the bone itself.

## 8.6 Summary

Overall, through the study of the trauma on the Weymouth Ridgeway Vikings, it was found that photogrammetry was a useful method for creating 3D models to both visualise and analyse cutmarks on bones. This chapter was based on the results from Chapter 6, and primarily focused on Stage Two of the project methods. It addressed Objectives 2-4, 6, and 9 (Section 1.3.1). The photogrammetric method created here was easy and relative quick, resulting in measurements that were statistically similar to the most common method of analysis, namely manual measurement. The ability to analyse and manipulate the cutmark in many ways without damaging the original specimen was found to be invaluable (Sections 2.5.1, 4.1.6, and 4.1.7). The use of digital technology also opens the doors to new types of analysis that would not be possible to perform on just the bone itself, such as surface roughness analysis. These techniques can be applied to more than just SFT and therefore are useful for multiple avenues of research involving the study of human remains.

Exploring surface roughness was found to be a useful tool when investigating the typically under-analysed shaved cutmarks as it was possible to quantify the change in roughness across the surface and successfully identify the direction of the blade in all known-direction cases that were examined which is more than has been accomplished metrically in the past with these types of cutmarks. Surface roughness still has many avenues that need to be explored in relation to human bone in order to fully understand its benefits, limitations, and uses. There are several that can be investigated in relation to photogrammetric capabilities and cutmarks as well as other forms of trauma to continue to test the capabilities and limitations of this type of technology. This chapter has addressed Objectives 2, 4, 6, and 9 (Section 1.3.1) and shown:

- SfM-MVS creates models of cutmarks which are good metric quality when using 3D control on a macro-scale
- Testing camera parameters, software settings, and using 3D control is highly recommended as the different geometry of objects can impact the optimal procedure
- Methods considered 'gold-standards' must still be approached cautiously as they may not be as 'perfect' as they initially seem and therefore could impact study results
- Models of bones can be repeatedly and destructively analysed without damaging the original and new techniques from other fields can be used on such models, allowing for more information
- There is much left to explore regarding the use of photogrammetry in the study of human remains as there are many possibilities for future quantitative work

# 9 Osteological Interpretation

Within this chapter, the analogue and digital findings (from Stage One and Three, reported in Chapter 7) related to the sharp force trauma found on the Weymouth Vikings are discussed and the effects of said results on the interpretation of events are analysed. A detailed analysis will be presented regarding the patterning of the trauma specifically relating to the decapitations (Section 4.1.4). As with any analysis of trauma on skeletal remains, the full extent of the injuries will never be known as only the trauma that caused osseous damage is visible. Therefore, all events must be discussed with this caveat. Subsequently, interpretations of the events are presented, addressing different possibilities that the osteological findings support. Finally, the impact on the historical knowledge of this region in this time are discussed (Sections 3.1 to 3.3).

## 9.1 Demographic Differences

Overall, there was no evidence that the age of the individuals was related to the number of wounds that are osteologically visible on the Weymouth Vikings (Section 7.1). Both the osteological minimum and maximum were examined; the osteological maximum in these circumstances a result of the exclusion of the cutmark associations that were considered tentative (further explanation in Section 7.1). The three most highly affected skulls (SK3704, 3707, and 3722) are young and prime adults (two and one, respectively) and the three most affected skeletons (SK3715, 3777, and 3778) are prime and mature adults (one, and two, respectively) (Section 7.1). However, those individuals with a high number of blows are a mix of ages and although there is a slightly higher proportion of relatively older individuals, this is not statistically significant. Therefore, it does not seem likely that individuals were targeted specifically based on their ages, however the level of violence on some is severe and it is possible they were targeted for other reasons. One potential reason could be that these individuals either fought back the hardest, or were symbolically important to the group of Vikings. Conversely, this could be to do with that particular attacker, possibly their confidence or emotions, rather than the victim (Solarino et al. 2019).

The orientation the bodies were placed in has no relation to the number of blows per person either (Section 7.4). Similar results were seen with whether the bodies were prone, supine, or on their side. Although the sample size was low because many were of unknown position, the results do align with the bodies being placed in the grave haphazardly with no organisation. Further discussions about the deposition as a whole and how the placement of the bodies may reflect the attitudes of those who buried them are found in Section 9.7.3.

Due to the complexity of the stratigraphy, the layers that the postcranial remains were buried in could only be separated into either three or five layers (Section 5.4.5 and 7.4.2). No significant difference was found with three or five layers, though it is notable that the lowest individuals had a lot of trauma on them proportionally (N=4/5), though due to the unequal group sizes and small sizes of some of the groups, this did not cause significance. Also interestingly, the opposite was true of the uppermost layer where only one had evidence of trauma (N=1/4). This might indicate that the first individuals placed in the grave were attacked very violently, possibly as a show of force to prevent the others from struggling or to 'open the show' if there was an aspect of spectacle to the executions (Section 4.2; see Mattison 2016 for a discussion of execution as a spectacle in Early Medieval England). This could also suggest that the efficiency with which the individuals were decapitated increased with practice, something that is reported to have occurred during the Rwandan genocide, although not in specific relation to decapitation (Ferllini 2013). However, because the results of this are non-significant, it is interesting to note but cannot firmly be said that this is anything other than pure chance. This is a prime example of a case in which having only hard tissue trauma is a limitation as it is impossible to tell what soft-tissue injuries may have also been present, and which could potentially support or refute these suggestions.

## 9.2 The Anterior Throat Cuts

In the process of re-examining the trauma, both traditionally and digitally, some small, thin cutmarks on the anterior cervical vertebrae were noticed that were not evident when the collection was first analysed for the monograph (Figure 95) (Loe et al. 2014b). The majority were found with the use of more modern technology compared to when they were first analysed nearly a decade ago. Although not on every individual, there are enough of these cutmarks to indicate that at least some individuals had their throats cut prior to being beheaded (Sections 7.1.3 and 7.2.6) (Milella et al. 2021). These cuts looked different than the blows that were designed to decapitate the individuals. The latter were found on vertebrae, mandibles, and basilar occipitals and had the appearance of heavy, chopping blows which cut deep into the bone. Some had cut through the entirety of the bone. Conversely, the small, incised cuts suspected to be related to throat-cutting were very shallow and thin.

a) 


b ) 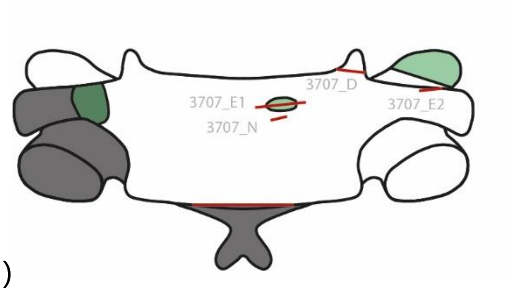


Figure 95: An example of the thin anterior cervical cutmarks, interpreted as throat cuts (SK3707) with a) the image and b) the illustrator patterning of the anterior of the CV (green representing taphonomic damage and grey representing missing areas). For comparison, see Fig. 102 for an example of the decapitation-related blows.

It was considered that these fine blade marks could relate to 'defleshing' or removing flesh that was not allowing the head to be entirely removed (Section 4.1.7). These are sometimes discussed in the literature as disarticulation or filleting marks, though those two terms have a slightly different definition in the typical situations in which they are found (Galán and Domínguez-Rodrigo 2013; Bello et al. 2016). Such marks are often seen on anatomical or teaching collections that were never buried. Additionally, they can be seen on animal bones as a result of butchery. However, defleshing marks are typically even smaller than the ones found here and are often in clusters, running parallel to each other (Galán and Domínguez-Rodrigo 2013). Within the collection at Bournemouth University, there are some skeletons (former anatomical teaching collection) which present with defleshing marks and clear differences in the sizes are seen, with defleshing marks being even smaller and fainter than the anterior throat cuts seen in this collection (Figure 96). Additionally, given the quantity and severity of trauma on the rest of the collection, it would seem out of place for the attackers to pause and carefully remove the remaining muscles and ligaments, rather than just striking another heavy blow (Section 7.1). If these cutmarks were related to defleshing, it would be uncharacteristically controlled and meticulous compared to the rest of the attack, therefore, this is thought not to be the cause.


Figure 96: An example of defleshing marks on a maxilla; characterised by very fine cutmarks commonly found in clusters as seen here and magnified in the in-set (CSR99 Sp2)

Of all individuals amongst the Weymouth Vikings, nine of the MLNI of 52 had possible indications of throat cutting; five of which were considered definite, though one of those was only available in an image (Section 7.1.3). Some of the cuts, especially those on SK3712, are slightly offset to the right, with cuts that are around the transverse process or pedicle which are where the carotid arteries run, potentially suggesting some of the cuts were aims for those arteries (Marieb et al. 2014). This suggests they could fit a pattern of throat-cutting rather than decapitation. There are two cases of vertebrae that are noted to have cuts in the initial osteological report, however these were not received at Bournemouth University. Since the CV2 with said cut on SK3743 has been photographed in the original osteological report, it has been included solely in this part of the analysis (not in the statistics in Results) as the image clearly matches with what is seen with the rest of the anterior cuts. Conversely, the additional missing vertebra (CV3 of SK3794) has no figures and therefore the nature of the cut cannot be determined, and it has been excluded (Table 66).

Two hyoid bones were found with small incised marks on the ventral side of the greater horn that did not appear to correspond to any vertebral trauma from decapitating blows (Section 7.1.4). Additionally, there was one cut on a mandible that appears to be made from a blow in an inferior to superior direction. It is possible this was made in the course of the decapitations if the neck was hyperflexed to the point where the base of the anterior mandible was touching the neck, though none of the vertebral trauma appears to relate to that cut. Therefore, there is a possibility this could have been caused by a small blade being drawn across the neck, tilted in an upwards direction, though this cannot be definitely stated.

Table 66: The individuals with potential throat injuries

| SK | N | Location | Age | Number of Blows (Min/Max) | Status |
|---|---|---|---|---|---|
| 3707 | 3 | CV3 | Prime | 10/10 | Definite |
| 3708 | 1 | Hyoid | Mature | 7/7 | Possible |
| 3712 | 3 | CV4 | Mature | 6/7 | Definite |
| 3722 | 1 | CV Unk | Young | 9/11 | Definite |
| 3743 | 1 | CV2 | Prime | *1 | Definite |
| 3748 | 1 | Mandible | Mature | 4/4 | Possible |
| 3760 | 1 | Hyoid | Young | 2/2 | Possible |
| 3764 | 2 | CV4 | Prime | 2/2 | Definite |
| 3810 | 1 | CV5 | Young | 7/7 | Possible |

*only present as an image in Loe et al. 2014b

There are some similar osteoarchaeological findings at Anglo-Saxon execution cemeteries (Sections 4.2 and 9.7.6) (Buckberry and Hadley 2007; for a full discussion on execution cemeteries, see Reynolds 2009). Such findings are typically noted, but due to the low numbers at each site or the age of the site report, they are often not thoroughly investigated and have not been compiled into a meta-analysis. The descriptions and images of CV4 of Skull 8 from Walkington Wold (E Yorks) (mid-to-late Anglo-Saxon period; Section 9.7.6) appeared to be similar to what was seen in this collection, and it was speculated that it could be to do with blood-letting or throat slitting with a different type of blade, likely much thinner than those used to decapitate (Buckberry and Hadley 2007; Buckberry 2008; Ubelaker et al. 2020; Milella et al. 2021). As discussed in Section 4.2.3, there were several skulls at Walkington Wold that were not articulated with a skeleton and there was evidence of decapitation. There was additionally potential evidence of a similar anterior cut on the CV of skull 8, however it was difficult to tell through the images whether the 'thin cutmark' would be consistent with what was considered a throat-cut injury in The Weymouth Ridgeway Vikings.

Current medical literature was consulted in order to see how many cases of SFT left marks on the bone itself. Cappella et al. (2014) examined the skeletal remains of an individual on which an autopsy had been performed on 20 years earlier. They found that of the 30 SFT lesions recorded at the autopsy, only four were visible on the bone both at the time of the autopsy and upon re-examination. Brunel et al. (2010) found a higher presence of cartilaginous and osseous trauma in the 118 SFT autopsies they studied, however they did not limit the anatomical region of their analysis and included locations with less soft tissues than the anterior neck (such as the ribs) and therefore the amount of osseous trauma found would be expected to be higher than what is seen on the Vikings. For further discussion, Quatrehomme and Alunni detail the connections seen between injuries in the hard and soft tissue in forensic cases in their 2019 article. This is important to remember as it is very possible the Weymouth Vikings also had more injuries prior to death than it appears skeletally.

There are a lot of soft tissue structures that sit in front of the vertebrae in the neck, many of which would lead to death if punctured in advance of getting to the vertebrae (Marieb et al. 2014). However, it is not unheard of for there to be marks left on the neck. In a modern study based in Turkey looking at throat cutting and honour killings, it was found that only 33% had any mark on the vertebrae (Ozdemir et al. 2013). A study in Jamaica showed that 8.12% of victims had visible cutmarks (Rao 2015).

In this research project looking at the Weymouth Vikings (using MNLI=52), five had definite anterior cutmarks that looked like they could be associated with throat-cutting which was 9.6% of the population if including the ‘definite only’ classification and the cutmark that was only present in an image (7.7% with the latter excluded). If all possible associated cutmarks were included, that percentage increased to 17.3%. These fell within the numbers found in the modern literature and aligned with the idea that osteological evidence of such activities would not be present on all of the collection (Quatrehomme and Alunni 2019). These numbers supported the finding that some individuals, possibly a larger number than are directly reflected in the osteological record, had their throats cut, and also underscore that it is possible to get marks on the anterior vertebrae from events other than an anterior beheading. Logic would dictate that these cuts would have preceded any beheading as it would both be unnecessary and impractical to cut someone’s throat after beheading them.

When examining the demography of the individuals, there does not appear to be any pattern to the ages. Statistics were not run as it was too small a sample to produce any meaningful significance. The number of blows on each of the individuals was also looked at and the majority of them have multiple blows. The means for the general collection are 1.13-1.62 and 3.29-3.57 cuts per person (postcranial and cranial, respectively) and the mean for the individuals with anterior throat cuts is 6.75-7.50 cuts per person (if considering only the definite ones and excluding SK3743; the mean for all eight individuals is 5.88-6.25) (Section 7.1). This is interesting to note, but this variance may be a result of the anterior cuts rather than a reason behind them; at least three of the individuals with definite anterior cuts have multiple cuts close together that appear to be from multiple attempts to slit the throat or drawing the blade back and forth. This is a very interesting new addition to the story of the events that may have occurred as it could suggest that the decapitations were done more for spectacle than as a method of killing or as a way to denigrate the dead by treating them with a lack of respect (Sections 4.2 and 9.7.8) (Reynolds 2009).

## 9.3 Residual Energy Dispersal (RED) Fracturing

This study of the SFT on the Weymouth Ridgway Vikings was performed nearly ten years after the original analysis had taken place, and in the intervening time, the development of technology has increased the ability to analyse trauma on bones. During the reappraisal with more technologically advanced methods, it was noted that there were examples of the length of cutmarks being overstated in the original osteological report because a fracture that propagated from them was considered part of the cut due to their similar appearances (Sections 4.1.1, 4.1.4, 7.3, and 8.4).

Injuries with cutmarks and associated fractures can be called sharp-blunt force trauma (SBFT), chopping trauma, or hacking trauma which generally refers to SFT that is performed with a heavy weapon, such as an axe, because the weight of the weapon can cause some crushing characteristics of BFT as well as SFT (Loe 2016; Nicklisch et al. 2017; see initial discussion in Section 4.1.4). Mikulski et al. (2021) brought attention to fractures radiating various directions from SFT in their study of remains from Sidon, using the term 'SFT/BFT'. In these situations, there can be fractures radiating specifically from the floor of the cutmark. It is important to differentiate these fractures from the actual cutmark itself or it can lead to misestimates of the extent of damage present, which could lead to erroneous conclusions about potential weaponry used. Therefore, in this project, a new term has been proposed for these fractures that appear as a continuation of a cut: Residual Energy Dispersion Fractures (RED fractures or RED) (Section 4.1.1). This is the focus of a forthcoming publication. In addition, due to the different mechanisms of trauma between pure BFT and SBFT, RED fractures are of slightly different aetiologies to the radiating and concentric fractures of BFT so are important to consider in the context of SFT (Figures 97 and 98) (Section 4.1.7).

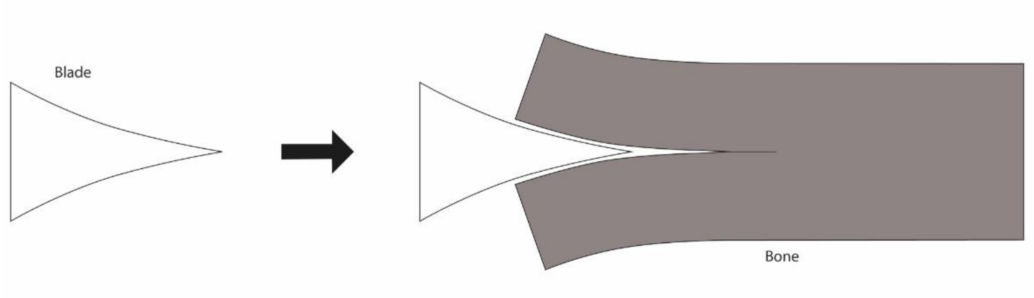


Figure 97: An example of a blade acting as a wedge and 'prying' apart a bone, resulting in the fracture propagating ahead of the blade itself

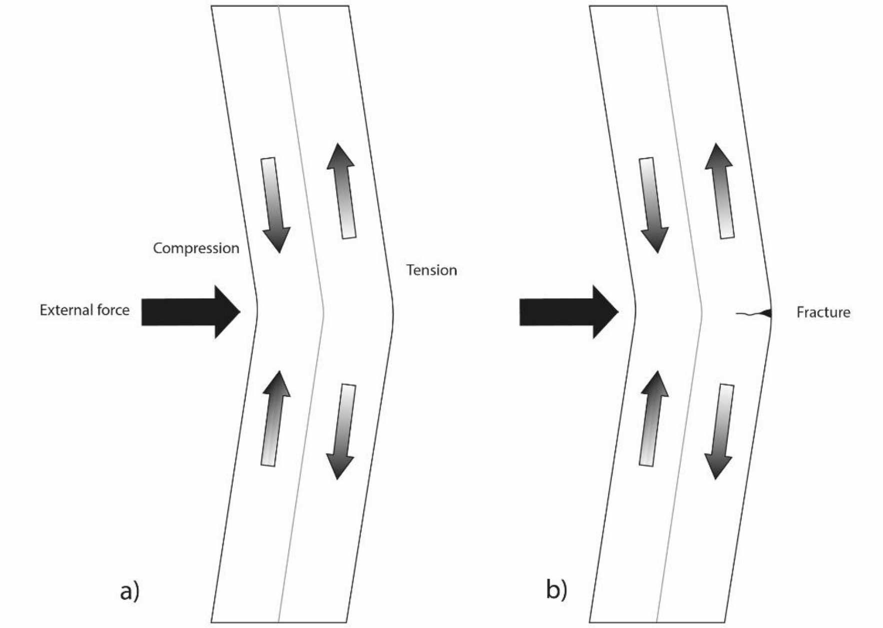


Figure 98: An example of a) how a blunt force subsequently b) causes a fracture on the opposite side to the impact, a feature not seen in sharp force trauma due to the differences in characteristics of the force (amended from Kieser et al. 2013, Fig 2.8, p.20)

There are multiple potential causes of RED fractures (Section 4.1.1.1). They may occur when a bone is cut initially and the energy from the blow then propagates ahead of the blade, creating a fracture ahead of the cut, similar to how wood fractures when hit by an axe. This typically occurs along the ‘grain’ of the bone as it is easier for cortical bone to fracture longitudinally along the osteons (Figure 99) (Pope and Outwater 1972; Galloway et al. 1999; Kieser et al. 2013; Li et al. 2013; Loe et al. 2016). A second potential cause could be through the removal of the blade, especially if it is twisted as this can pry the bone apart. Additionally, the fractures may be extended through post-mortem modification, such as dehydration. Lastly, they may be a combination of the afore mentioned factors in various, unique proportions.

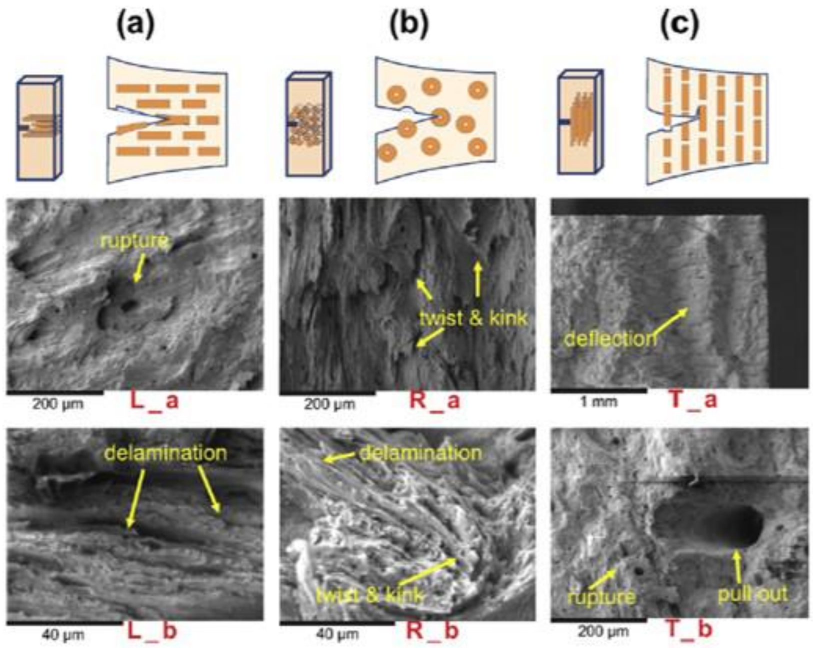


Figure 99: The characteristics of different microfractures based on the direction of initiation compared to the osteons with a) longitudinal, b) radial, and c) transverse. The upper row shows the diagram whereas the lower two rows show scanning electron microscope (SEM) images at two different magnifications with features highlighted by Li et al. in yellow text (Li et al. 2013, Fig. 6, p.456)

When conducting the in-depth analysis of the cutmarks on the Weymouth Vikings, differences in the surface texture of the bone between actual cut and the resultant fracture was notable (Sections 6.3 and 7.3). Table 67 contains some of the major visible differences that aid in delineating where a cutmarks turns to a fracture, focusing on cortical bone. RED fractures do not have the characteristic smoothness or polished surfaces that are seen in SFT (Section 4.1.4). The edges can still be relatively straight, but there is usually some raggedness or unevenness in them and they appear more similar to a fracture than a cutmark. It may be difficult to find the exact delineation between SFT and RED, but it will usually be where the surface loses the polished appearance or there might be a slight change in angle or topography of the surface (Figure 100, end of section). In some cases, the change is very evident, whereas in others it is much more subtle but still present. In trabecular bone, the surface is inherently different, so it is often easier to find by looking at the cutmark from side-on. In other cases, the changes in direction or surface texture can be easier to find via touch (Section 4.1.1.1). These are still considered part of the injury process, but because they are created indirectly by the blade unlike cutmarks, they were coloured differently in the trauma patterning illustrations in this study (Section 7.1, Appendix H).

Table 67: The proposed characteristics commonly seen in RED fractures on cortical bone that help differentially diagnose them

| Characteristics | Description |
|---|---|
| Surface Texture | Macroscopically: relatively smooth with some unevenness, no shine<br>Microscopically: rougher than macroscopically, small undulations, appearance of delamination (see Figure 99) |
| Edges | Macroscopically: relatively smooth with potential undulations<br>Microscopically: more irregularities are noticeable |
| Angle | Often a slight change from the angle of the cutmark<br>Similar 'fracture paths' are often seen between multiple bones if they are struck in similar locations |
| Shape | Rectilinear or slightly curvilinear |

Amongst the Weymouth Vikings, some patterns were noticed in the RED fracturing. For example, when impacted from behind, cuts on the lower portion of the inferior mandibular ramus would usually have a propagating fracture that had a fairly smooth curve to it, running anteriorly and slightly inferiorly towards the lower part of the corpus. Less consistent patterns are seen where there was RED fracturing across trabecular bone because the arrangement of the osteons is correspondingly less consistent.

It is important to consider these RED fractures when analysing trauma because it does change the patterning and magnitude of the trauma which can alter interpretations of the events that may have occurred (Section 4.1.7). It also underlined the importance of re-examining collections, especially with modern technology as it can reveal additional information (Sections 1.4 and 2.5.1). It is also possible that some of the RED fractures were even further exacerbated in the post-excavation period between the initial examination and this study, making the fracturing more obvious now. This type of fracturing has been described in some osteological reports, although not specifically named:

> "The mandible is in two halves; a radiating fracture runs through the corpus of the jaw. It may be an old post-mortem fracture and result from the pressure of the overlying stratigraphy, but it could be a peri-mortem fracture, secondary to and a result of the blade trauma to the jaw and neck." (Cessford et al. 2007, p.209)

The fracture in the images published by Cessford et al. (2007) look very similar to what was seen in the Weymouth Vikings, both in appearance and pattern. Further research needs to be conducted on this type of fracturing to determine if there are any distinct signatures seen in the different possible causations. Primarily, is there a difference between fractures caused solely by either the blow or the removal of the blade (RED fractures) compared to fractures resulting from or exacerbated by PM drying? The rate of the propagation of PM extension to such fractures would be useful to explore with experimental studies.


Figure 100: An example of a cutmark on a gonial angle turning into RED fracturing (3721_C) with inset a) showing a medial view and inset b) highlighting the cutmark in red and the fracturing in blue

## 9.4 Shape Analysis

In general, when performing shape analysis on the incised cutmarks from the Weymouth Vikings, very few significant differences were seen in the groups examined when appropriate Bonferroni corrections were implemented (Sections 5.4.4 and 7.2). None of the hierarchical cluster analyses properly classified the groups although there were some interesting separations that were noted in the principal component analysis (PCA) plots (Section 7.2, Appendix I). It could be that there were real differences that the method used was not sensitive enough to distinguish or the differences may not be discrete enough to result in significant test results. It is also possible that the differences were not that large or taphonomy may have impacted them. This may also have been influenced by methodological decisions such as how much of the non-affected bone surface to include on either side or other grouping decisions. For example, the hyoids were included in the same category as the vertebrae because they are in the same anatomical region, though arguments could be made to put them in the category of mandibles instead as they are also in proximity. Other choices such as more categories of angle could be explored. All choices made during this type of exploratory analysis affect the outcome but there were too many possible factors to investigate every possible combination. Not all the chosen factors that were selected were expected to separate out. However, since these factors were known, unlike the information about the weaponry, it was deemed beneficial to explore them regardless as they could then be ruled out as a source of the variation.

Generally, there is a lot of variation within the maxima found along each principal component (PC), however the maxima themselves were never found to be more than +/- 1 standard deviation (SD) from the mean shape. Thus, despite the variation, overall the shapes were relatively similar which was understandable because incised cutmarks generally have a very distinct, unique shape (Section 7.2, Appendix I). The first PC had the most influence and it was the depth of the cutmark, ranging from 47.2% to 62.9% of the variance seen. PC1 was more influential with the non-angled (62.9%) compared to the angled (47.2%) which is logical considering the nature of the angled cutmarks as further discussed below. The depth was understandably the most influential factor, especially on this collection since the weaponry was suspected to be similar or at least within the same class of weapons (swords) in all cases. This would lead to relatively low variation in other aspects, such as width, in the non-angled categories.

There was larger variety of shapes, specifically depth, in non-angled cutmarks compared to angled ones and the latter were typically shallower. From observations in this collection, it appears that cuts that enter the bone at an angle are generally shallower because when they get a certain distance into the bone, they are more likely to break the bone fully, becoming shaved/broken incised cutmarks instead. When the blade is removed, it is easier to turn the blade into a lever when it is situated in the bone at an angle, causing a RED fracture that extends across the bone and dividing the bone in multiple pieces (Figure 101) (Section 4.1.1). Therefore, in this collection, there were fewer deep angled cutmarks compared to deep non-angled cutmarks. The big angle and moderate angle showed some difference in signatures when the angled sample was sub-divided; the larger angles tended towards the more sloped shape whereas the moderate ones tended towards the more upright shape. This suggested that PC accounts for variation due to differences in angle between the two walls (Section 7.2.2, Appendix I).

Figure 101: An example of an angled incised cutmark on a medial clavicle that has become a broken incised cutmark due to the level and directionality of RED fracturing and subsequent post-mortem fracturing (3763_D)

There were some slight differences in the PCA plots when looking at location. Cranial cutmarks separated out the most from the other groups which may have been related to the geometry of a cranium (sphere) compared to the other groups (cylinders or irregularly-shaped) (Section 4.1.1). There were also different types of cuts on the crania; both related and unrelated to the decapitations which may have accounted for some of the variation seen in the shapes. Conversely, the postcranial remains were generally unrelated to the decapitations and most likely related to defensive or subduing action and therefore the low variation seen might reflect this. Interestingly, only one of the cranial cutmarks was considered angled compared to seven that were non-angled. This may be reflective of the shape of a cranium because an angled blow would be likely to create a shaved cutmark rather than an incised one. The incised cuts on the mandibles were often on the ascending ramus and generally were nearly in the transverse plane which may be why they had the tendency to be more upright.

The incised cutmarks around the neck also had a fairly tight, central distribution, though not as condensed as postcranial. There were thought to be two causes of these cuts: the probable throat-cut injuries and the decapitation-related injuries (Sections 7.5, 9.2, and 9.6). Many of the cuts that were related to decapitation resulted in shaved cutmarks so although they were the predominant action behind the cuts seen on the vertebrae of the entire collection, this was not the case in this portion of the study. Some of the cutmarks around the neck were slightly shallower than average, which was likely due to the very fine marks possibly related to throat-cut wounds. Most of their variation was along the component that describes depth, which may reflect the two motivations behind the cuts. When examining the angled cutmarks only, neck had the most variation, which may have been influenced by the inherently irregular shape of vertebrae. Had the collection been larger, it would have been interesting to divide the locations and examine the other factors, especially angle and width, for each group.

Width is often influenced by angle, so more differences were seen when the angled/non-angled were separated (Section 7.2.4, Appendix I). The images were scaled so all the cutmarks appeared roughly the same size; they were then subsequently scaled by the R script as well, so any differences seen should not be because of the size of the original image but rather the shapes themselves. All the ‘large’ cutmarks were within the angled category, therefore suggesting the covariance of variables should be explored in the future. The ‘medium’ cutmarks had the most variation to them whereas ‘large’ overall have the least. Both ‘medium’ and ‘large’ cutmarks included angled ones (often shallower) and non-angled ones (often deeper) likely leading to the variety seen. Similar patterns were seen within the ‘small’ cutmarks but with less variation. The ‘very small’ ones tended to be shallower and more upright which aligned with what was seen macroscopically; these were often the very small, fine cuts that did not penetrate far into the cortical bone. All the ‘large’ cutmarks were within the angled category. These cutmarks showed the most differences in this category: their ellipse did not overlap with the ‘large’ cutmarks at all and they tended to be the smallest overall, not just the smallest width.

In the non-angled category, there was a statistical difference found between the ‘medium’ and ‘very small’ cutmarks which suggested a true difference in shape, not just that the ‘medium’ cutmarks were expanded versions of the ‘very small’ ones. The ‘medium’ and ‘small’ were close to being significant but not once a Bonferroni correction was applied. This may support the idea that the ‘very small’ cutmarks were created by either a different weapon or a different action (see discussion on weaponry below and Sections 9.7.6 and 9.7.7). This was an example in which the possibility of covariance made things more challenging as the suspected throat cuts were within the ‘very small’ category and mostly within the non-angled category, but since the weaponry is unknown, this cannot be firmly established.

As a parameter, the side the cutmark was on did not show many differences (Section 7.2.5, Appendix I). It was interesting to note the differences in the side when split by angled or non-angled. Central cutmarks had a wide variation and were much more likely to be non-angled. This might be related to some of the centrally placed vertebral cuts because they tended to be non-angled, whereas more lateral cuts had more tendency to be angled. The angled group should be interpreted with caution because of the very different sample sizes, especially because central was so low.

Since there was no major separation along any of the variables and the PCA plot did not have any large separation, it did lend support to the idea that similar weaponry was used in all injuries, which aligns with what the archaeological and osteological evidence suggests. Visually, there were very few cuts that had an appearance that might indicate a different weapon. In those cases, they may have been outliers on the plots or possibly were the same weaponry, but other factors might have caused the visible differences, such as whether the victim was moving at the time of impact.

An additional column was added to the analysis with the cutmarks that are thought to be throat cuts. When run through shape analysis, it was found that they did tend to cluster towards the shallower and narrower side (Section 7.2.6, Appendix I). This was also seen when just the non-angled cutmarks were run. As only two of the possible throat cuts were angled, this analysis was not performed. This aligns with what was visually seen with these cutmarks and was originally why they were noticed and thought to be different. It was suspected they were created either with a very thin, fine blade, or just the initial edge of a sword, either being drawn across the neck rather than swung (Sections 3.4 and 4.1.7). Therefore, the fact that there were a much higher number of them in the non-angled category compared to the angled followed what would be expected.

### 9.4.1 Shape Analysis Conclusions

Although there were no statistically significant differences amongst the profiles of the incised cutmarks in the Weymouth Vikings, these patterns were interesting to note and also led to some thoughts about the technique itself (Sections 5.4.4 and 7.2, Appendix I).

First, this showed that the models created through SfM-MVS found the same differences that were seen by eye, thus supporting the conclusion that this method is applicable for studying cutmarks. This type of analysis would be an avenue to investigate in conjunction with other 3D methodologies that allow a view into the bone, such as μCT, in order to see whether the profiles are statistically similar and if more or less subtle differences are noticed. Though the latter point would raise the question as to whether any subtle differences were true differences or purely noise.

Second, it indicated that the use of shape analysis has potential in investigating cutmark profiles. Further investigation with more controls would hopefully provide a better indication of what information can be accurately gathered from profiles with known and unknown characteristics (Section 4.1.6). To properly investigate the use of shape analysis for cutmark profiles, this should be done experimentally with known weapons that are substantially different (e.g. knife, axe, sword) because then the weaponry will be defined and the taphonomic processes can be recorded and controlled to an extent. The Weymouth Vikings, as a collection, also have many variables for each cut and it would be easier to examine the quality of shape analysis as a tool for looking at weapon differences with less variables to confound possible results.

Thirdly, one question that arose from this collection was whether the differences in 'weaponry' were actually differences in blade category or whether it could be the same category used in different manners, such as swinging a sword compared to drawing it across a surface. This could also be further explored through experimental studies, where the exact weapon, type of blow, and force are known.

A fourth discovery of note was that when analysing the cutmark profiles from the locations 50% and 25% along the cutmarks, no separation was seen in the PCA and DFA plots. In their paper, Maté González et al. (2015) found that cutmark profiles from locations between 30% and 70% of total length were statistically similar in measurements. The profiles chosen here were outside of that range purposefully. However, because some of the bones had damage or were broken, the true midpoint (50%) of the original cutmark may not be the location that was digitised. As outlined in Section 5.4.4 and 7.2, profiles from different locations along the same cutmark were not combined despite the fact it would raise the sample size. It was thought that doing this could impact the groups with very small sample sizes severely and unpredictably. This could have led to erroneous differences or similarities and therefore it has been left as an avenue to investigate in the future.

Overall, shape analysis has supported the findings of potential throat cuts in the Weymouth Viking collection and did not suggest multiple categories of blade were used; therefore, it is likely the majority of the injuries were inflicted with the same type of weapon (Section 3.4 and 7.2). It revealed that the shapes of the profiles of angled and non-angled cutmarks was not statistically different but did indicate better results might be obtained if analysed separately. The slight separations in some of the PCA scatter plots were thought to often be attributed to the shape and nature of the bone or the differences in type of blow or force that was used.

## 9.5 Surface Roughness

The initial tests regarding surface roughness in cutmarks were designed to check the method with cutmarks where the direction was clear, either with the ending point of the blade evident in another part of the bone, or significant RED fracturing on the opposite side of entry (Sections 6.3 and 7.3). The analysis of these cutmarks confirmed that the method picked up surface variation and therefore it must be tested on cutmarks with no known direction. If this method also works on cutmarks where the direction is not visibly apparent, this could add to the body of knowledge around what occurred to these individuals. Additionally, two cutmarks with blade defects were tested and the resulting images clearly showed the defects on the surface (Figure 91, Section 7.3) (also see Section 3.4). Unfortunately, these defects were not made with the same blade so it was not possible to test whether the point clouds could be used to match defects successfully.

If this method is able to effectively match blade defects, it could have implications for trying to match weapons to injuries in forensic cases.

## 9.6 Patterns of Decapitation

In the Weymouth Viking collection, the patterning of the decapitation was of particular interest as it was a significant aspect of their deaths and depositions (Section 4.2.1 and 7.5). The cuts addressed here are the ones thought to be directly related to decapitation or decapitation attempts. Overall, there were some patterns seen within the decapitation-related injuries (Section 7.1 and 7.5, Appendix H and Supplementary Adobe Illustrator [.ai] files). The majority of the cuts were in or nearly in the transverse plane with some in an oblique plane. This was similar to what was seen with other evidence of decapitation such as that found at Driffield Terrace (N Yorks) and Walkington Wold (E Yorks) (both discussed in Sections 4.2.1 and 4.2.3) (Buckberry and Hadley 2007; Buckberry 2008; Caffell and Holst 2012). In these sites, heavy blows were seen on the vertebrae and mandibles. Like what was seen with the Weymouth Vikings, there were some cuts on the crania of the Walkington Wold skeletons which have been interpreted as somewhat mis-hit decapitation attempts (Buckberry and Hadley 2007). The decapitations at Driffield Terrace appear to have been more efficient than those at Walkington Wold or Weymouth based on the number of blows needed to be successful (Caffell and Holst 2012).

In the Weymouth Vikings, many of the cuts completely bisected the vertebrae, but some did not, which means multiple blows would have been needed in order to finish severing the soft tissue even if the rest of the vertebrae itself broke due to RED fracturing (Figure 102). This was supported by several cases in which there were multiple catastrophic blows in close proximity; any of the blows on their own would have been fatal, however may not have fully removed the head from the body. The number of cuts on the vertebrae may actually be an underrepresentation because not all vertebrae were recovered and small fragments that might have been damaged by a blade would be more likely to be affected by bioturbation and lost compared to larger bones (Mays et al. 2012; Robb 2016).


Figure 102: A CV2 with at least three blows that were decapitation attempts from the posterior (SK3742)

CV2 and CV3 were the most affected vertebrae and the most likely to have multiple cuts (Sections 7.1.3 and 7.5). When looking an individual's neck, on a living human it generally appears to extend from the base of the skull, around the inferior nuchal line, to the top of the trapezius, which, depending on the person, could appear to be around CV6, where the body of the muscles 'ends' by tapering closer to the vertebrae (Marieb et al. 2014). Thus, this puts CV2 and CV3 roughly in the centre of the 'visible' neck. The vertebrae superior and inferior to that had less damage to them and the CV7 was the least damaged of the vertebrae, supporting the thought that the blows were aimed at a specific part of the neck. There are individual differences, but the distance between the spinous process of CV7 and nuchal crest on a 50$^{th}$ percentile modern American adult male in anatomical position is approximately 10.8cm, which is not a large target and includes more than what would be considered the visible neck when aiming a blow (Vasavada et al. 2008; Roos et al. 2020).

The cuts on the upper CV were found in association with cuts to the mandible, similar to what was seen at Driffield Terrace where nine individuals had evidence of cuts to both their vertebrae and mandibles (discussed in Section 4.2.3) (Caffell and Holst 2012). The inferior corpus of the mandible seemed to mainly be injured in conjunction with the inferior portion of CV2 to the superior portion of CV4 (Sections 7.1.2, 7.1.3, and 7.5). Whereas the cuts on the posterior ascending ramus were variable, many were at some type of angle, and seemed to also have impacted bones ranging from the occipital bone to CV3. The cuts on the lateral side of the ascending rami did not necessarily impact the vertebrae since the mandible is substantially wider than the vertebrae (Marieb et al.

2014). However, these can be complex to resolve because if the neck is flexed/extended or the mandible open, the alignment of the CV, mandible, and skull could be very different. The CV2 cuts also were mainly from the posterior (or adjacent) as seen by the higher amounts of RED fractures anteriorly. This was anatomically logical because when observing the anterior aspect of a head and neck, the CV2 would be behind the mandible and thus not easily accessible or a natural location to aim for from the front (Marieb et al. 2014). In those circumstances, it was more likely vertebrae from CV3 on would be affected.

Similarly, amongst the Weymouth Vikings, cuts on the temporal bone were often found to have damaged the CV1 or CV2 and sometimes the superior portion of the mandibular ascending ramus depending on the angle (Sections 7.2 and 7.5). The majority of the cuts on the CV1 were from the posterior side which aligns with what was found on the temporal and occipital bones. These cuts would be right at the base of the skull which does not seem like an optimal place to target when trying to decapitate a body because it would not be very efficient for quickly removing the head entirely. However, since it did appear that the aim was inconsistent at times, these might have been slightly mis-hit.

CV1 and the odontoid process of CV2 were often found to be damaged by the same blow, usually from the posterior direction. The left IAF was more affected than the right on the CV1 and a matching pattern was seen on the CV2 with the left side of the superior arch and SAF more affected than the right. It is difficult to suggest if this was because of a certain position and handedness of the assailant as the weapon could have been held with two hands or missing material could prevent the cut being identified bilaterally (Section 3.4.1).

There were some anterior shaved cuts to the inferior corpus of the mandible as well. These appear to have been created with much force and therefore it seems likely they were also intended to decapitate. It is interesting, however, that the mandible would be affected in this way as it would be a fairly prominent feature to try to avoid when attempting to severe the neck. This might suggest some of the individuals were in awkward positions when their heads were removed or it might suggest a level of carelessness from the attackers (Section 4.1.7).

There were some decapitation injures that affected the skull. Those that affected the occipital or temporals were predominantly from the back or the back and side (Figure 79) (Sections 7.1.1 and 7.5). These seem likely to be ‘misses’ since that would not be the easiest place to remove the head. The reasons for the misses, both high and low, can be speculated but cannot definitively be known. It is possible the individual was struggling, though if some of the individuals were killed in advance of the beheadings, that may not be the case. It is also possible the individuals, either alive or dead, were in a prone position, possibly with their head on a chopping block; this latter possibility is discussed further later (Section 9.7.7). The individual or individuals who were performing the beheadings may have had different levels of skill in regards to both beheading and aiming. They also may have become more tired as the event proceeded, or conversely, become more efficient. Due to how the heads were placed in a group but off to the side of the bodies, the sequence of decapitation and order of placement is unknown.

If the perpetrator was tired or inexperienced, the placement of the blow could have been an accident (Sections 4.1.7 and 9.7.3). Additionally, if the neck was extended, that would narrow the space that one was aiming for if aiming at the posterior of the neck. The opposite would be true if aiming at the anterior as a flexing of the neck or opening of the jaw could cover a portion of the neck. This is one major problem when trying to connect which cutmarks could be linked to the same blow because the positioning of the mandible in relation to the vertebrae is changeable and it cannot be known exactly how they were at the time of the strike. Similarly, if the head was turned or the neck tilted, it is possible that some associations were missed because when regarded in anatomical position, it is not clear that they are associated.

There have been studies into decapitation-related injuries in the osteological record (such as Tucker 2013), however, there is a gap in the literature regarding which vertebrae is most commonly affected at each site. The initial hope had been to compare contemporary sites, however that would result in a very narrow body of literature so the search was expanded and some are presented here to compare to the findings of the Weymouth Vikings. Unfortunately, due to differences in detail and availabilities of these publications, the number of each vertebra available for examination in said studies is not always known. Additionally, due to the COVID-19 pandemic, this search was limited to those publications that were available online and not all osteological reports are published in such a manner. This would be useful to extend further across regions and time periods to find if there are patterns to decapitations as an overall act (Sections 4.1.7 and 4.2.3).

Overall, the patterns were fairly similar with CV2-4 showing the highest number affected (Section 7.5, Appendix H). There were slight differences seen though; for example, the Vikings were the only group that were most highly affected at CV2. There was a slight shift in distribution towards the superior portion of the neck compared to other sites, however these numbers did not account for the number of each vertebrae found at each site (Table 68). Conversely, five 13$^{th}$ to 16$^{th}$ century burials from Znojmo, Czech Republic had decapitation-related cutmarks on their lower CV (Pechníková et al. 2009). These four men and one woman were interpreted as judicial execution victims and the placement of the cutmarks was thought to be due to the position of the individual at the time they were executed (Pechníková et al. 2009). The cuts appear very similar to the trauma seem in the Vikings, with clean cuts all the way through multiple vertebrae (Sections 7.1 and 7.5). Additionally, the individuals from Driffield Terrace, the most comparable site in numbers, had a slightly lower distribution of cutmarks on the neck than the Weymouth Vikings and they were more centred around the mid-neck (CV4) (Caffell and Holst 2012). Another notable difference between that collection and the present one was the number of mandibles affected (DT=8, WEY08=28) which was likely connected to the difference in the distribution of the affected vertebrae. It is possible that the executioners at Driffield were purposefully trying to avoid the jaw area as it would be more material to have to cut through, or it could be unintentional simply related to differences in head position during the decapitations.

Table 68: Number of each type of vertebrae affected by decapitation-related SFT at various sites

| | | CV | | | | | | | | | |
|---|---|---|---|---|---|---|---|---|---|---|---|
| Site | Date (C) | 1 | 2 | 3 | 4 | 5 | 6 | 7 | Unk | TV | Ref |
| Weymouth Ridgeway | 10$^{th}$-11$^{th}$ | 11 | 29 | 26 | 17 | 13 | 7 | 3 | 10 | | This project (articulated only) |
| Walkington Wold | 7$^{th}$-10$^{th}$ | | 1(?) | 1 | 1 | | | | | 1 | Buckberry and Hadley (2007) |
| Chesterton Lane Corner | 7$^{th}$-9$^{th}$ | 1 | 2 | 3 | 3 | 2 | 2 | 2 | | 1 | Cessford et al. (2007) |
| Meon Hill | Anglo-Saxon | 1(?) | 1 | 1 | 2 | 3 | 2 | 1 | | | Liddell (1933) |
| 42-54 London Rd, Staines | 8$^{th}$-12$^{th}$ | | 1 | | | 1 | | | | | Haymen et al. (2005) |
| Stockbridge Down | c. 11$^{th}$ | | 2 | 3 | | | | | | | Hill (1937) |
| Bran Ditch | Anglo-Saxon | | 2 | 2 | 3 | | 1 | | 1 | | Duckworth (1929), Hill (1976) |
| Lith | 14$^{th}$-17$^{th}$ | | 1 | 1 | 2 | 2 | | 1 | | 1 | Kozakaité et al. (2018) |
| Med Czechia | 13$^{th}$-16$^{th}$ | | | | | 2 | 3 | 1 | | | Pechníková et al. (2009) |
| Driffield Terrace | 1$^{st}$-4$^{th}$ | 4 | 10 | 13 | 17 | 13 | 15 | 7 | | 2 | Caffell and Holst (2012) |
| Beds | | | 1 | 2 | 3 | 3 | 1 | 1 | 1 | | Boylston (2000) |
| Owenbristy | 6$^{th}$-11$^{th}$ | | | 2 | 4 | 4 | | | | | Geber (2015) |
| Total | | 17 | 50 | 54 | 52 | 43 | 31 | 16 | 11 | 5 | |

## 9.7 Possible Interpretations of the Events that Occurred

Within this section, some possibilities of how the Weymouth Vikings came to be buried in a former Roman quarry pit on the ridgeway will be discussed (see specifically Sections 3.3, 4.2, 5.1, and Chapter 7). The basis of many of these theories was presented in Loe et al. (2014b) and Boyle (2016) and have been added to or adjusted based on the osteological findings from this project. The full extent of injuries can never be known because only the ones that affect the bone are visible, which is an ever-present challenge in trauma analysis. Additionally, with archaeological collections, there is always the chance that there is either preservation or recovery bias which has led to fragments or bone being lost either whilst in the ground or whilst being excavated. As with any attempt at the reconstruction of events from archaeological material and historical literature, the present writes the past more than it should. The actual occurrences and their sequence will never be fully understood therefore the suggestions discussed here are only presented as possibilities, fitting as closely as possible with the current evidence. With future research, it is hoped that these possibilities can be further supported or discounted.

### 9.7.1 Location of the Grave

The location of the grave placement generally conforms to what is seen with Anglo-Saxon deviant burials and execution cemeteries (As discussed in Section 4.2 and Reynolds 2009). Although the focus of this project has not been to analyse the landscape in relation to the grave, some questions have emerged throughout the project. One of these is in relation to the ‘empty graves’ that are north of the mass grave (Brown et al. 2014; Loe et al. 2014b). With no way of concretely dating these graves, their original purpose remains unknown, but one must wonder if they were originally dug for the Vikings but abandoned because of the number of graves that would be needed. If that was the case, it would suggest some planning and time between the capture of the Vikings and their murder.

The location of the grave itself is of interest (Figure 54 and 103). It is at a high point, overlooking multiple prehistoric monuments in present-day Dorset, most notably Maiden Castle in Dorset (Section 5.1.1). Chalbury hillfort also lies nearby, as well as a Bronze Age cremation cemetery of Rimbury Unrfield. Other prehistoric monuments and barrows can be seen in the landscape, especially along the ridgeway. Throughout the surrounding area and the rest of the excavation site, there was evidence of burial activity in the area ranging from prehistoric through to medieval, suggesting it might have been an important area to the past people of Wessex.

Figure 103: A view from the site towards Weymouth and Portland

Although the current ground level in that area may be slightly different than it was at the time of the deaths, the views from the ridgeway would be similar now as they were then; multiple barrows are visible along the top of the ridgeway and the settlements that evolved into present-day Weymouth and Portland to the south, and Dorchester to the north, would have been clearly visible, to the north Dorchester sits a bit to the east of Maiden Castle (Sections 4.2 and 5.1.1). Based on the barrows and the land height of the burial, this point on the ridgeway is slightly lower than some of the adjacent hills, and is likely part of the reason why it was selected as a path between the two towns. The site is close to said road as well as hundred boundaries, a common feature associated with execution cemeteries or deviant burials in Anglo-Saxon times (Reynolds 2009; Loe et al. 2014b). Additionally, pre-Christian barrows were sometimes seen as the opposite of consecrated ground and thus the 'worst' location to bury offenders (Semple 1998)

Therefore, the question must be raised about why that specific Roman quarry pit was chosen. It appears there were other possibilities along that stretch of the ridgeway, of various sizes and at various heights. With that information, did the captors pick that quarry pit randomly? Or was it chosen for specific reasons, such as its location compared to other nearby monuments and landmarks, its size, or some other reason unknown to modern day investigators? The pit that was chosen is roughly equidistant between the highly-visible Bronze Age barrows W415 and B24 (Brown et al. 2014; Loe et al. 2014b). Today these barrows are labelled as being part of two different groups, but would they have been notably different in the past and, if so, is this another example of choosing a location that has liminal characteristics? (see Reynolds 2009 for a discussion on liminality in burials).

These characteristics of burial location are often seen in deviant burials/execution cemeteries such as Walkington Wold (Section 4.2, specifically Section 4.2.3) (Reynolds 2009). Since these characteristics seem to be present in the case of the Weymouth Vikings' burial site, it could be speculated that the executioners were Anglo-Saxons rather than mercenary Vikings because the latter would have had no reason to conform to this pattern unless it was requested. Thus, the burial location potentially strengthens the idea that the Vikings were killed and deposited by Anglo-Saxons. Alternatively, the choice of the burial location may have been entirely arbitrary and held no significance to the identity of the attackers.

One question that has been raised in the investigation is whether it is possible that the pit was actually a doline originally rather than a man-made feature (Sperling et al. 1977). Dolines are essentially sinkholes that are commonly found in certain chalk or limestone-based landscapes and are found along the South Dorset Ridgeway. Regardless, the same questions regarding the specific choice of pit still remain regardless of whether the pit was from Roman quarrying, naturally formed, or a combination of both.

### 9.7.2 The Vikings

As fully discussed in Section 5.1.3.3, the group of approximately 52 Vikings skeletally appear to be of strong disposition. However, there are two individuals that are interesting to consider in the context of this collection. One of these has a well-healed but slightly malaligned fracture of the proximal femur, at the trochanters. However, it does not appear to present with osteoarthritis on the available joint surfaces, potentially suggesting that if the individual did walk with a limp due to one leg being shorter than the other, it was not severe enough or not for long enough to result in compensatory joint alterations. Also notable in a second individual is a disarticulated femur with severe and long-standing osteomyelitis (Figure 104). This likely would have caused pain, swelling, and difficulties with mobility. The cloacae in the femur suggest the wound was partly open to drain pus, however the healed appearance of much of the new bone formation suggest the infection was long-standing. The proximal articulation appears unaffected by any joint deterioration and the distal articulation is absent. A heavily fragmented second femur also presents with infection to a lesser but still significant extent, however, due to the high PM damage and low completeness, they cannot definitively be associated. Neither of these individuals were in peak health but they were joining the rest of this band of Vikings regardless and the question of why could be raised. A plausible argument could be made that they were invaluable to whatever the group of Vikings were hoping to achieve and were therefore brought along despite potentially having hindered mobility. This may support the theory that it was a relatively inexperienced band of Vikings, as they potentially could not do without these two individuals, despite their possible physical shortcomings (Section 3.3).


Figure 104: Two of three cloacae seen in a disarticulated femur in the Weymouth Vikings collection

Something similar is seen in some of the burials at Visby related to the Battle of Visby (Section 4.2.3) where an individual with a severe knee ankylosis was present as well as some evidence of malaligned healed fractures and severe osteoarthritis or joint disease (Ingelmark 1939). It is likely all individuals from the location population who were present when the battle began were needed to fight, thus leading to a mixed group of individuals in different states of health. Although from a different time period than the Weymouth Vikings, this does support the idea of calling upon those who might not be in peak physical condition when required, either for war or for something vital such as navigating.

### 9.7.3 The Assailants and Timing of Events

The question of how many people were responsible for the executions of the Weymouth Vikings will likely never be solved, however it seems that it was a fairly substantial number as they would have to keep control of the Vikings or they would have needed to relocate the bodies from wherever they were killed to the top of the Ridgeway (Section 4.2). The simplest explanation might be that the Vikings were on or near the ridgeway under their own power, whether forced up there by the attackers or captured there. Additionally, the beheadings and deposition of the bodies into the pit likely would have been physically tiring, supporting the thought that there were probably a fairly large number of captors. It appears as if the bodies were either all buried at the same time or deposited within a relatively small span of time because weathering damage is minimal or absent and there is no evidence of carnivore or scavenging activity (Loe et al. 2014b) (Section 4.1.5).

There is evidence of non-decapitation related injuries amongst the Weymouth Vikings as well (primarily Sections 7.1.1, 7.1.5, and 7.1.6). There are individuals with cutmarks to their neurocranium which were not in locations that would link them to decapitation attempts, even if missed. There are multiple blows to SK3704, 3707, 3759, and 3738. Individuals SK3686, 3693, 3708, 3710, 3734, 3736, and 3750 also have a cut to their neurocrania (Figure 105). These injuries might have been inflicted whilst capturing or subduing the Vikings or may have occurred immediately prior to the executions if the captors needed to prevent the Vikings from struggling.

Figure 105: SK3738 presenting with one of the most significant cranial injuries amongst the collection

Some of these individuals (SK3693, 3704, 3708, 3734, 3738) had wounds that did not penetrate into the brain and therefore, although painful, they would not have been incapacitated other than potentially being concussed (Section 7.1.1) (Langlois et al. 2006; Churchill et al. 2017; Jha et al. 2019). Other individuals, however, have much more significant injuries. The blows to the occipital of SK3707, the frontal of SK3736, the parietal of SK3759, and the parietal of SK3686 were substantial enough to produce RED fractures that removed a portion of bone (the preservation of the removed portion/roundel is variable). These would have exposed the brain but potentially could have been survivable, although not without some sort of attention (Voormolen et al. 2019). Without the full length of the cut in some cases, it is challenging to estimate their depth. Of the cranial injuries, SK3738 has three less severe injuries as well as arguably the most severe one, and would likely have been incapacitated due to the size of the roundel that was removed on the left parietal. Based on how far the cut goes before it turns into RED, the blade almost definitely would have impacted the brain, specifically around the junction of the parietal, frontal, and temporal lobes. This potentially could have affected the primary motor cortex and the integration of various sensory information (Marieb et al. 2014).

### 9.7.4 The Defensive Trauma

Unlike what is sometimes seen in conflict-related violence, there are a fairly small proportion of skeletal remains in the collection that exhibit defensive trauma; however, it is not absent (Sections 4.1.7 and 7.1.6). If compared to clinical literature, Loe et al. (2014b) it is noted that the patterns are more similar to defence than they are to offence. However, the relatively low number of defensive wounds compared to what might be expected for such a situation then raises questions about why they did not fight back to a greater extent. Naturally, there is a possibility that the Vikings were significantly wounded but the wounds may not have been deep enough or in places that would leave marks on the bone, therefore it is hard to determine the level of violence or injury that may have been inflicted on them or what violence they might have inflicted on their eventual killers. As first discussed in Section 4.1.7, interpreting the events surrounding trauma can be challenging, however the following interpretation of the defensive injuries aligns with both osteological data and the broader historical context.

Defensive injuries are commonly located on the upper extremities, including the hand, due to an attempt to shield oneself from a blow; this is seen both in archaeological and forensic cases (e.g. Ambade and Godbole 2006; Judd 2008; Racette et al. 2008; Hugar et al. 2012; Ferllini 2013; Mohite et al. 2013). The majority of research on defensive injuries in this field are focused on BFT, however the location of the defensive injuries should theoretically be the same whether BFT or SFT (for an example of SFT, see Constantinescu et al. 2017). Although there are some cutmarks on the arms that appear defensive, they are not in the exact pattern that was expected. Typically, the medial aspect of the ulnae is impacted first when the arms are raised, palms out, to shield oneself; often resulting in parry or ‘nightstick’ fractures (Judd 2008; Geldenhuys et al. 2016). In this collection, when examining the articulated remains, only one ulna has trauma whereas injuries can be seen on four radii and two disarticulated radii (Figure 106) (Section 7.1.6). It is thought there are two main possibilities for why this is the case; first, a passive rather than active defence, and second, the use of shields.


Figure 106: An example of a cutmark, possibly defensive in origin, on the posterior aspect of a radius and ulna (SK3778)

In their study of domestic violence victims, Thomas and colleagues found the radius was more affected than the ulna (2021). The authors did not delve into why this might be the case other than stating this possibly meant the blows were not caused by the standard parry fracture mechanism. Some of these wounds could still be defensive in nature, but the angle required to hit the posterior radius without impacting the ulna (as seen in cases like SK3796) would likely mean the palms were facing in, possibly with the arms protecting the head (Section 7.1.6). In this area, the medical and osteoarchaeological literature is lacking because there is no standard method of presenting such injuries. Studies looking at defensive trauma, typically BFT, often combined the radius and ulna into 'forearm' so do not specify the aspect of the arm that was hit, or they combine various regions in the body (e.g. Raclette et al. 2008; Brunel et al. 2010; Curca et al. 2012; Geldenhuys et al. 2016; Redfern 2017). The standardisation of reporting trauma would be beneficial if trying to explore patterns of trauma both nationally and internationally and it both archaeological and medicolegal settings. The difference between defensive positions is not typically considered either, though it would be useful to study the differences in trauma patterns when 'actively' defending, such as in the cases resulting in parry fractures, compared to 'passively' defending, such as the cases of purely radial involvement (Bohnert et al. 2006).

An alternative possibility with the Weymouth Vikings is that a shield or sword was being held in the affected hand, likely leading to an arm positioning in which the hand would be partially pronated, placing the radius superior to the ulna (Sections 3.4, 4.1.7, and 7.1.6). In this configuration, the radius would be more likely to be hit by a downward or oblique blow than the ulna would. As described by the archaeological and historical records, Viking shields were typically wooden, round and between 80-90cm in diameter (Section 3.4.3) (Graham-Campbell 2001; Pedersen 2008; Short 2014). There are some discrepancies about type of wood used, but there is general agreement that iron was used as a central shield boss and, in some situations, for re-enforcement (Short 2014). The handle for the shield would result in the arm being held in the position described earlier in this paragraph. In their book on Viking weaponry, Short experimentally tested replica Viking shields against weaponry of the time and found that the shields could be breached, a fact also mentioned in various sagas (2014). Therefore, it is entirely possible that the injuries seen on the arms and hands are the result of a skirmish that involved shields, possibly indicating there was a small battle, or the Vikings at least had enough knowledge of the attack that some were able to get to their shields before it occurred (Sections 3.4 and 4.1.7).

However, since it will never be known exactly what position the individual was in when they were struck, it is possible that their arms were hit from behind as well. There are a few radii in both the articulated and disarticulated remains that show evidence of glancing, or very oblique, blows as well.

What happened to affected hands is arguably more difficult to reconstruct as there are many joints that have relatively large ranges of motion, and since hands have a high number of joints, it is easy for them to be in a position other than anatomical and this should be kept in mind when interpreting results (Karray et al. 2021). With two of the skeletons that had high numbers of blows, there were repeated cuts to their hands (Figure 107) (Section 7.1.6). It is possible that in some cases, multiple cuts may have been made by the same blow, leading to less total blows, but the bone were not able to be reassociated in a way that supported that in this study. These injuries could be related to using a hand to shield oneself as hands are a common location of defensive injuries, and those observed in the Vikings appear similar to some of the hand trauma seen at Towton and in victims of the Rwandan genocide, where some phalanges, metacarpals, and carpals are affected (Rouse 1994; Novak 2000a, 2000b; Ambade and Godbole 2006, Bohnert et al. 2006; Ferllini 2013).

Figure 107: An example of some of the trauma seen on the hands of one of the Vikings (SK3778)

It is also possible that some injuries to the Vikings were sustained when the victim was holding a weapon with an unprotected hand or holding a shield that was penetrated. Those individuals with hand injuries often appear to have multiple blows and often more than one of the blows would have been severe enough to render parts of the hand inoperable. None of the cuts appear to be the result of blows designed to remove the hand because those at the wrist were not in the transverse plane. Osteological findings of Roman burials at Driffield Terrace (N Yorks), first discussed in Section 4.2.3, found two individuals with a total of eight of cuts to metacarpal 4, metacarpal 5, and proximal phalanges (Caffell and Holst 2012). Some similar cuts are also seen on the skeletons from the Battle of Townton as well (N Yorks). All cuts are consistent with the blade hitting the back of the hand and are interpreted as defensive injuries, similar to some of the cuts seen here. There they also saw a similar phenomenon of multiple blows to the same hand, but to a lesser extent.

There is one articulated case of a clavicle and scapula being cut from the posterior in a blow that was clearly not related to decapitation (SK3755) (Section 7.1.5). This may have been some type of subduing blow, either when the Vikings were first captured or prior to execution. The resultant fracturing from the blow severed the clavicle and scapular spine and would have likely rendered that arm functionally impaired at the time (Marieb et al. 2014). There is a similar injury seen amongst the disarticulated remains though to a lesser extent. This one appears similar to an injury seen on skeleton 23 from Towton (Section 4.2.3) who has a large incised wound to the scapular spine which appears very similar to 3685.01_A of the Weymouth Vikings (Novak 2000b).

On the Vikings, there are other clavicular injuries and some of them appear unrelated to any decapitation attempts (SK3763, 3778, 3786, 3789) (Section 7.1.5). However, there are others that have entered the superior surface from the medial direction at a very shallow angle and therefore may have been related to the decapitations, especially if the shoulder was elevated or the arm raised (SK3715, 3810). Unfortunately, the number of vertebrae associated with the postcranial remains with clavicular trauma is not substantial enough to be able to thoroughly investigate. Although this is seen at Driffield Terrace, due to the separation of skulls and skeletons in the Weymouth Vikings it is not possible to establish what vertebral trauma might be linked to which clavicular trauma (Caffell and Holst 2012). If reassociations were possible, it might be more possible for this to be explored.

This evidence, coupled with the findings that many of the Vikings likely had BFT to their skulls, lends support to the idea that the Vikings were a weakened force by the time that the executions actually began. Exactly when these injuries took place in the chronology is unknown, although the most likely times would have been at the point of capture or initial overwhelming, during transportation up to the Ridgeway (if applicable), or just prior to execution.

### 9.7.5 The Attackers

The other question that is raised by Loe et al. (2014b) and continues here; who were the attackers? It seems likely that is would have been local people from Wessex as they might have been able to take the Vikings by surprise due to local knowledge, thus the need for equal numbers might not have been as great. However, it could have also been a different band of Vikings since there is evidence of Vikings sometimes turning into mercenaries for the Anglo-Saxon kings (Williams 1986; Yorke 1995; Graham-Campbell 2001; Williams 2016b). If this were the situation, it is unknown whether the attackers or the victims would have been the mercenaries. The lack of any entry about such a large massacre in the ASC is noteworthy, however, this is not an impossibility and similarly, the specific detail of the attack at St John's Oxford, likely linked with the St Brice's Day Massacre, is not recorded (see Sections 3.3.2 and 4.2) (Swanton 1996; Pollard et al. 2012).

With all available evidence weighed, it does seem slightly more likely that the attackers were familiar with the area as the burial location seems purposeful and there are some added elements to the executions that appear like a spectacle. Additionally, the franticness of some of the injuries does suggest a very mixed level of confidence or experience, which one might expect from a group that does not regularly perform such activities.

Who the attackers were also has implications about what weaponry might have been used. If locals, would they have had access to the weapons required for such clean blows? Or might they have used the Vikings' own weapons against them for the decapitations? Overall, it seems that the Viking and Anglo-Saxon swords used at the time, especially the very high-quality ones, would have been effective (see Section 4.3.1). Another possibility of weapon other than a sword could be the 'Dane axe' or Viking broad axe, or any thin Anglo-Saxon equivalent (Underwood 1999; Short 2014). Initially, axes of the Viking Age were relatively small, but by the end of this time period, the edges of the battle axes could be up to 45cm (Short 2014). Some of the axes of the time had edges that were too thick to cause the injuries seen here (e.g. those with diamond edges), however others were much thinner, potentially able to create cutmarks similar to the decapitation-related ones here (Underwood 1999; Short 2014). This would be a fascinating line of enquiry to pursue with experimental archaeology as it could have implications about the perpetrators or the movement and transfer of weaponry at that time. Clearly the blades that were used had to be very sharp and heavy enough to cause injuries that would cleanly go through vertebral bodies, thus also having gone through all the soft tissue structures up to that point and likely the ones beyond as well.

### 9.7.6 The Possible Throat Cutting

Arguably the most impactful new addition of information to the event surrounding this collection are the cutmarks on the anterior vertebrae. This is a new dimension that was not considered before. Prior to this, there was no evidence of a manner of death other than the decapitations. However, now it suggests that at least some of the individuals were killed before their heads were removed. This lends weight to the idea that there were some significant ritual or spectacle aspects to the event as the decapitations then become superfluous. Although no specific evidence for such practices has been found, there are cases where individuals' head have been removed after death (see Tucker 2013; Mattison 2016) though they do not appear to have had their throats cut. There are many papers discussion the symbolic role of decapitation in Anglo-Saxon, Iron Age, and Viking contexts (Godfrey 1993; Gardela 2013; Eriksen 2020). That body of literature is not deeply discussed within this project as the anonymity of the attackers leads to many different possible theories that would require much further analysis of primary sources (For a comprehensive discussion of the idea of the 'cult of the head', please see Clarke 1998). Regardless, it is clear that the heads were important in this instance, whether as an assurance of death, as a dramatic display of power, or for other symbolic reasons.

It is possible that more of the individuals had their throats cut, but because of the amount of strong soft tissue structures anterior to the vertebrae, not all of them may have osteological evidence of such an event. If trying to kill someone by cutting their throat, there are structures in front of the vertebrae, such as the trachea and various cartilaginous structures, that could result in a fairly quick death if cut, thus making it unnecessary to cut with enough force to hit the bones (Marieb et al. 2014). If such throat-cutting did occur in a large number of cases, it would make it seem more likely that the decapitations were possibly done as a ritual, as a show of force, or as a spectacle. The cuts to the throat would have been deep in the soft tissue and in some instances, there are multiple cuts on the front of the same vertebrae suggesting this was done. Some of these may have been from drawing the blade back and forth rather than completely discrete cuts. Exploring this further using a scanning electron microscope (SEM) would be interesting as there might be striations that would indicate the direction the blade was drawn.

There are other indications that the heads of the Weymouth Ridgeway Vikings might have been an important component, for example, compared to the bodies, the heads were placed with more organisation and care. Additionally, another new finding that has come to light in this study is evidence suggesting that at least two of the heads were placed on spikes, spears, or something similarly sharp and square, possibly to display. Both of these individuals have peri-mortem damage that is unnaturally square and too close to the foramen magnum to have occurred when the head was still attached to the body. In these cases, the skulls are also damaged post-mortem, but this penetrating trauma does not appear to be caused by that. The damage appears similar in shape to what is seen on skeletons from the Battle of Towton (e.g. 9 or 41) though in different locations on the skull (see Section 4.2.3; Fiorato et al. 2000). For example, Towton 9 was a mature male found with a near-perfect square hole along the anterior right squamous suture (Novak 2000b). These traumatic lesions are also unnaturally square and have bevelled surfaces and are thought to be due to weapons such as poleaxes. Although that is not weaponry used during the time the Vikings were killed, there were other square-shaped spears in use (see Underwood 1999).

There are two other individuals amongst the Vikings who have trauma that might also be from the placing of the head on a spike, but these have more significant damage. These skulls displayed small (approx. 1cm) holes with squared edges with bevelling. This appearance was consistent with an injury that occurred to wet bone (e.g. Mikulski et al. 2021). The location of these lesions was on the nuchal planum of the occipital in close proximity to the foramen magnum, a location that would be inaccessible if the head was attached to the neck in anatomical position. The use of head-stakes or heads as trophies was considered at Walkington Wold, however unlike this site, there was no osteological damage that would support that (Buckberry and Hadley 2007; Buckberry 2008). There was already speculation that some of the heads may have been taken due to the unequal number of skulls and postcranial remains and this finding potentially adds weight to both that theory and the idea that heads were an important part of the spectacle (Loe et al. 2014b).

### 9.7.7 The Decapitations

This section explores some of the possibilities that may have occurred in the decapitations of the Vikings. If some of the Vikings were dead prior to the removal of their heads, that might explain the contrast of the cleanness of some of the cuts and the relative franticness of others (Sections 7.5 and 9.6). Interestingly, SK3707, which has the most blows amongst the cranial remains, also has evidence of anterior cuts to the neck. This suggests that his death it took multiple attempts to decapitate him, likely after his throat was already cut. It could be speculated that the multiple attempts were not due to his struggling but perhaps due to anger or inexperience of the attacker, or a struggle to position the body in such a way that the head could be successfully removed, however, those details are beyond what can be interpreted from the skeletal record.

If the chopping blows were designed to remove the head rather than to kill the victim, then the accuracy would have been less critical and missing the neck or not successfully removing the head in a single blow would not have been a major issue. Additionally, if some were already dead when their heads were removed, the head and neck might not be in an optimal position for decapitation. This could also suggest that multiple people performed the beheadings which would account for the inconsistency.

The majority of the decapitation-related blows amongst the Weymouth Vikings were from the posterior or adjacent to posterior, a similar pattern seen at Driffield Terrace (Caffell and Holst 2012) (Section 7.5). The variety of directions as well as multiple differing directions on one individual does also support the narrative that the execution of the Vikings was a chaotic event that was not particularly consistent or methodical (Section 9.6). Additionally, it seems unlikely that all were beheaded on a chopping block or similar because there are several that have decapitation-related blows from multiple directions. This type of positioning seems improbable as it would involve rotating a nearly-decapitated body since some of these blows nearly or entirely bisected the vertebrae from different directions. Therefore, it might be speculated that these individuals were upright, possibly sat or kneeling, which would make it both easier to access opposite sides of the neck and slightly reposition an objecting or deadweight individual. This also lends support to the idea that there were a fair number of attackers.

Unfortunately, it is not possible to sequence a lot of the blows and the lack of reassociations of cranial and postcranial make it challenging build a clearer picture of the events. It is possible that there was a system in place that is not reflected in the osseous remains or, conversely, that it was even a less organised procedure than speculated here. It will never be known for certain but based on the inconsistency of many aspects of the injuries and burial, it seems more likely that there was no methodical plan for the decapitations themselves.

Interesting parallels can be draw to the crania examined from the Cambodia killing fields (Choeung Ek). Although the trauma seen there is blunt, the location of many of the injuries and the extent of the damage is similar to what is seen amongst the Weymouth Vikings. Both Ta'ala et al. (2006) and Fleischmann (2019) noted basilar skull fractures, affecting the occipital primarily around the foremen magnum and nuchal planum. From the osteological and historic evidence, this trauma was caused by a blunt force to the back of the skull to execute the individual. It is thought that typically weapons of convenience were used, such as cart axels (Fleischmann 2019). The executions appear to have been systematic.

Amongst the Weymouth Vikings, there are several individuals with high numbers of blows to the neck, such as SK3707, 3715, and 3810 (Sections 7.1, 7.6, and 9.1). Any of these blows would have severed the spinal cord and caused death (Marieb et al. 2014). Therefore, from the quantity of trauma, it is clear that more blows were inflicted than required. The exact definition of 'overkill' can be debated, but it tends to include the use of more force, blows, or numbers of weapons than required to kill (Solarino et al. 2019; Tumler et al. 2019; Karakasi et al. 2021, see Trojan et al. 2019 for further discussion of definitions). Solarino and colleagues use the phrase "…will to annihilate…" in their modern-day Italian study of overkill (2019, p. 402).

In addition to the quantity of the blows amongst the Weymouth Vikings, the severity of blows is also noteworthy. Blows of this magnitude have been seen on other collections, as noted in Section 4.2.3, at Visby, 456 cases of bladed injuries are found (Ingelmark 1939). Some of the cuts have clearly been performed with large heavy blades, having completely severed part of limbs, mainly the lower extremity. As described by Ingelmark, "…it is almost incomprehensible that such blows could be struck" (1939, p.165) which is similar to sentiments regarding the severity of some of the blows seen on the vertebrae and mandibles of the Weymouth Vikings.

Though the number of injuries on some of the Weymouth Vikings would indicate overkill, the motive behind them is not known and cannot be determined; they may have been performed in order to remove the head rather than kill the individual. Similar amounts of overkill trauma are found on some individuals from St. John's and Towton, however the latter was part of a battle rather than an execution and therefore may be interpreted as being due to a chaotic battle (Fiorato et al. 2000; Pollard et al. 2012). The skeletons from the Battle of Visby (Section 4.2, especially Section 4.2.3) also show some levels of overkill, though more typically in magnitude of injuries rather than quantity of injuries (Ingelmark 1939). There are examples of entire limbs being cut off demonstrating "…the berserker rage which overcame the warriors in the heat of battle" (Ingelmark 1939, p.164).

### 9.7.8 Deposition and Burial

#### *9.7.8.1 General Deposition*

There are generally no post-mortem alterations that would be consistent with the bodies having been exposed for a long period of time, unlike Fromelles where the presence of fly pupae suggested burial 5-10 days after death (Loe et al. 2014a; see Section 4.2.3 for a list of mass graves for comparative purposes). There is no clear evidence of scavenging; many of the small bones of the body which usually disappear first with scavenging activity are still present. There is some potential water damage on some of the skeletons, but that could occur after the bodies were buried. There was no indication of clothing, therefore either they were wearing clothing that would not survive 1000 years underground, or they were stripped of their clothing (similar to what is seen in McIntyre 2017). If they were stripped of clothing, it would likely have been done before they were decapitated as the act of de-clothing a recently decapitated body would not be practical. Although much more recent, a similar phenomenon was seen at Fromelles where the dead were stripped of their boots except for those that had grievous lower leg injuries (Loe et al. 2014a). The deposition of the bodies at St. John's (Oxon) (Sections 3.3.2 and 4.2), appears to have been similar to that of the Ridgeway Vikings, however in the former case, the heads were not removed. The individuals at St. John's may also have been stripped of clothing and possessions as well since minimal finds were associated with the mass grave there (Pollard et al. 2012). Unlike what was seen with the Weymouth Vikings, some of the bodies at Visby still had armour associated with them (Ingelmark 1939). In that case, it is thought that armour and individuals from both sides represented and were buried together. There were no related artefacts that were buried with the Weymouth Vikings, such as brooches or weaponry, so it can be speculated that anything valuable or useful may have been taken by the attackers.

Additionally, there is no indication the Weymouth Vikings were bound. It is possible that bindings were used but did not survive burial, though the hand placement would be expected to be more consistently close together if this were the case (*c.f.* Definis Gojanović and Sutlović 2007). This does not exclude the possibility that they were bound but untied before burial, however. The Vikings may have been tied to help control them prior to their death, though it is unlikely this possibility will ever be able to be proven or disproven.

#### *9.7.8.2 The Placement of the Bodies in the Grave*

The placement of the bodies in the grave itself is interesting beyond just the separation of heads and bodies. The heads were all tightly grouped whereas the bodies appear to have been thrown in with less care. The heads are placed in a pile on the south side of the pit. That could either suggest that the intended backdrop was Weymouth or towards Maiden Castle, depending on whether the head were at the 'back' or 'front' of the it (Section 5.1.1). It could be purely random but given that the new findings are supporting that an element of ritual or spectacle was involved in the beheadings, it might indicate that the placement of the heads in the grave was not randomly chosen. The archaeological record contains other instances of heads being placed in unusual positions either with or away from the skeleton from which they were removed, but there is nothing in the published literature on this scale (see Taylor 2008; Reynolds 2009; Tucker 2013). There is some evidence of the skeletons from St. John's (Oxon) having been burned which possibly could indicate their deaths were also part of a spectacle, however, without the availability of the full osteological report, interpretations cannot be fully drawn (Pollard et al. 2012). Conversely, the burials at Towton and Visby (see earlier in Section 9.7 and Section 4.2.3) have no evidence that they were any type of event other than the necessary burial of war dead (Ingelmark 1939; Fiorato et al. 2000).

The Weymouth skeletons were not aligned to any particular position relative to any cardinal direction or to each other, and the bodies were intermingled and, in some places, even intertwined (Figure 108). They do not appear to have any type of organisational pattern, such as seen at Fromelles, where evidence suggests that the bodies were placed typically head-to-head or head-to-toe in a row in two layers (Loe et al. 2014a, for other examples, see Definis Gojanović and Sutlović 2007; McIntyre 2017; Willmott et al. 2020). There are some sites, like Towton, that are a mix of chaotic and organised placement; in general, most individuals are orientated the same direction, but they have not been placed in the grave in an orderly fashion (Fiorato et al. 2000).

Figure 108: An example of the relatively chaotic deposition seen at Weymouth (Loe et al. 2014 cover image)

The mass graves at Visby are a mixture; in some, the lower layers of skeletons are neatly arranged, head-to-toe, whereas the upper layers are chaotic (Figure 109, Section 4.2) (Ingelmark 1939). There is some suggestion that the burials in the different graves were performed differently based on the layout and the armour or lack thereof. Not all the graves had the same proportion of each age group (Ingelmark 1939). As in the case of the graves at Towton and those at Fromelles, it is clear these individuals died in battle, whereas the Weymouth Vikings and even the site at St. John’s do not fully fit the pattern one would expect from post-battle burials (Fiorato et al. 2000; Pollard et al. 2012; Loe et al. 2014a).

Figure 109: Common Grave 3, Burial I at Visby where the lower layers of individuals were buried in a more organised fashion (Thordeman et al. 1939, Fig. 41, p.61)

It is most likely the Weymouth Vikings were deposited individually or a small number at a time rather than *en masse*. This is supported by the statistical analysis of the number of cutmarks and the orientation of the bodies (Sections 7.4 and 9.1). If there was a reason the different individuals were placed in the direction they were, it is not currently known, however, given the general disorganisation in which the bodies appear, it is thought likely that they were placed due to convenience of burial rather than any other reason (see Section 4.2.2).

The pit that was used for the deposition was fairly wide so the bodies were able to be spread over the base of the pit without creating a large number of distinct layers (see Section 5.1.1) (Loe et al. 2014b). Unfortunately, this means that the stratigraphic relationships of all the skeletons is not entirely clear in many cases so it is not possible to determine the deposition sequence with accuracy. Based on the placement of most of the individuals in an extended position, it seems likely at least two people deposited each body as it would be challenging to place a dead-weight body in such a position alone, especially approximately 50 times. From the placement of the lowest five individuals, it is clear that the deposition was haphazard from the beginning rather than becoming that way as time went on.

## 9.8 Summary

Overall, the patterns of trauma seen in this collection support the narrative of a very violent end for these individuals and these findings add to the story that surrounded these Vikings (Chapter 7). New evidence suggests at least some of the individuals were killed before their heads were removed furthering the idea that the event was a spectacle (Sections 7.1.3 and 9.2). It is unknown how many may have been affected in this way as throat cuts are not always visible osteologically. Additionally, there is potentially more support for the idea that the Vikings had shields and possibly weapons when they were attacked due to the location of the postcranial trauma; the defensive injuries are not what would initially be expected for raising one's arms to protect oneself (Sections 7.1.6 and 9.7).

Though the Vikings may have been armed, this does not necessarily mean a battle occurred. They might have been taken by surprise but some had enough time to get their shields before being overwhelmed. There is evidence a portion of them may have been injured, either through SFT or BFT, not long before their deaths. This could add weight to the idea of some type of ambush occurring (Section 9.7). Since there are instances of Vikings landing on the Dorset coast and travelling through Wessex, it is possible that these individuals were either moving away from their ship or back towards it when they were captured and killed. One could speculate that they were attacked by locals who either did not want them on their land or did not want them to make it back to their ship, or they were set upon by Viking mercenaries in the employ of the Anglo-Saxon king (Section 3.3).

Although the attackers could have been mercenaries, the location of the grave in the landscape makes it seem more likely that the attackers were of local origin as it could be argued that the location has significance in proximity to hundred boundaries and prehistoric monuments, something that is said to be common amongst Anglo-Saxon execution cemeteries and deviant burials. Although decapitations were used by the Vikings as well, it seems less likely that these individuals were killed by mercenary Vikings than by Anglo-Saxons.

The amount of violence present in the deaths as well as the location points towards the event having involved executions as a spectacle. Whether it was witnessed purely by the attackers or by the local community from the region is not known. Additionally, the indication that two or more of the heads may have been placed on spikes adds to this theory of creating drama around the deaths. This could have been as a celebration of victory or as a warning to others, but it is clear these heads were not left for long as they were buried at the same time as the other skulls (Section 5.1). However, there are less skulls present than skeletons so it is possible other skulls were not buried in the mass grave.

The events that occurred on the South Dorset Ridgeway are a unique insight into the mass execution of individuals in the late 10th or early 11th century England. It was a violent event which, in this study, has been further investigated through the use of modern technology, namely photogrammetry. The following chapter addresses the final conclusions about both the methodological and osteological findings of this work. This chapter discussed the osteological findings from the analogue and digital analysis and interpreted them in the historical context, thus addressing Objectives 7-9 (Section 1.3.1). The following are some of the most important findings relating to the osteoarchaeological analysis and the events surrounding these deaths:

- Some individuals likely had their throats cut; the full number cannot be known because of the lack of soft tissue
- It appears to have been a chaotic event but may have been built around ritualistic or symbolic elements, as opposed to being purely utilitarian executions
- There was likely a fair number of attackers in order to subdue or transport the Vikings
- Some of the defensive trauma suggests the possibility of shield use though the overall lack of defensive trauma may suggest they were taken by surprise
- There is evidence that at least two of the skulls may have been placed on spikes, however were likely still buried at the same time as the rest of the skulls and skeletons

# 10 Conclusion

This research set out to examine the use of Structure-from-Motion Multi-View Stereo (SfM-MVS) photogrammetry for the creation of high metric quality 3D models of human skeletal material for research and preservation. The Weymouth Ridgeway Vikings were used as the case study collection for this research in order to both develop the methodology and discover more about the trauma on the collection in order to refine the information about the events surrounding their deaths.

This study has demonstrated this method successfully makes models which are precise enough to allow for traditional metrics to be taken as well as other modern analytical techniques to be involved. This chapter summarises what has been discovered in this project and ties together the methodological and osteological results. It starts by addressing the objectives that were first discussed in Chapter 1 before going on to briefly discuss some of the more major conclusions in the thesis. The final section will draw together some of the key avenues identified for further research.

## 10.1 Aims and Objectives Reconsidered

This study has successfully answered the essential questions posed at the outset of this work and summarised in Section 1.1. Overall, the levels of accuracy obtained in a laboratory can be made more widely accessible through SfM-MVS, with the caveat that effective 3D control and iterative testing must be implemented to ensure the best possible model is created. This allows for the preservation of collections whist still being able to conduct repeatable research on them. It also means that techniques that cannot be performed on the physical remains could become possible and techniques from other disciplines can be integrated into the field.

Objective 1 (evaluation of photogrammetry and its potential for use with human remains, especially trauma analysis) was discussed in Chapters 2-4, with the conclusion that the techniques used in trauma analysis could benefit from further advancing and photogrammetry is an appropriate tool for this.

Objective 2 (determination of methodology for close range photogrammetry of two geometries of cutmarks) was primarily addressed in Chapter 5 where the three major stages of the methodology were presented: the initial analogue analysis of the trauma (Section 5.2), the development of the photogrammetric method (Section 5.3), and the application of the photogrammetric method to the full collection (Section 5.4). The camera parameters and geometry of image capture were explored as well as the use of a 3D printed control cradle. A very quick and efficient strategy was developed for digitising cutmarks which resulted in all being successfully digitised to a standard that is sufficient for analysis to take place in the absence of the physical remains.

Objective 3 (measurements of the lengths and widths of the cutmarks on the bones and 3D models) was discussed in the pilot study results (Chapter 6 and 8). The cutmarks were measured from both FX and DX 3D models and also manually where applicable. All measurements were found to be statistically similar to each other (Section 6.1)

Objective 4 (investigation of the precision of close-range photogrammetry through intra-observer error and comparing measurement methods) was also incorporated in the pilot study results (Chapter 6 and 8). Intra-observer error was acceptably low and there were no significant differences between methods. As manual calliper measurements are one of the most common methods of examining cutmarks, especially where resources are limited, it was decided this was the most important metric to use for comparison (see Appendix J for a list of osteoarchaeological studies of various aspects of human remains which have relied on manual measurements with callipers, published in the last two years).

Objective 5 (investigation of 2D shape analysis as a method of further research incised cutmarks) was presented in the osteoarchaeological results and methods chapters (7 and 9, respectively). This analysis was performed with known variables to see if there was any pattern that correlated with the shape of the incised cutmark profiles. The overall spread of the points was examined to see if there were any distinct separations in the data that could not be explained by any of the test variables, because this might have indicated a difference in the categories of blade that were used (e.g. sword, axe, knife) (Section 7.2). In this study of the Weymouth Vikings, no clear distinctions were found. Interestingly, there were a few groups that appeared to cluster, though they were not clearly delineated. Most notably, the potential throat cut injuries seemed to have a tight grouping compared to the other cutmarks. This may indicate that shape analysis could be used to either determine if different categories of weapon or different methods of striking were used but this would need to be explored in a situation where more variables could be controlled.

Objective 6 (exploration of geospatial techniques in the analysis of shaved cutmarks) was primarily incorporated into Chapters 6 and 8 (methodological results and analysis) but was also mentioned in Chapter 7 (osteological results). These chapters showed that 3D digital models of cutmarks allow for analysis of aspects that were previously unable to be analysed, such as the surface roughness.

Objective 7 (application of the methodology to the Weymouth Vikings) is addressed in Chapters 7 and 9 to explore how modern technology may provide further information about the cutmarks and how they might have arisen. These chapters focus on the osteological findings and implications where originally-noted and newly-noted cutmarks were found. Some of the newly-noted sharp force trauma (SFT) appeared to be related to throat cutting and some of the originally-noted SFT being reinterpreted as propagating fracture, now labelled as Residual Energy Dispersal (RED) fractures (Sections 9.2, 9.3, 9.6, and 9.7).

Objective 8 (reappraisal of the SFT with modern technology) was discussed in Chapters 7 and 9 as well. The cutmarks that were found were catalogued into Appendix F and G and visually patterned so the characteristics of the decapitations of the Weymouth Vikings could be more thoroughly analysed. This helped underscore the importance of reanalysing skeletal remains with new technology, as these patterns and characteristics would not have been found without a reappraisal with a macro-lens.

Objective 9 (synthesis and evaluation of the findings) is the primary focus of the latter half of Chapter 9 with detailed discussions about the impact of the findings with respect to the Weymouth Vikings. For example, there was a tendency for the second and third cervical vertebrae (CV) to be the most impacted, a trend that is slightly different than that seen at other archaeological sites with decapitation burials which have more trauma in the mid-cervical region. The patterns seen support the idea that this group of Vikings were the victims of a chaotic event with no systematic procedure.

## 10.2 Benefits of 3D Analysis and Recording

The use of 3D technology for investigating human remains is currently a growing field, and metric analyses on 3D models have been starting to be more commonly used (Maté González et al. 2015; Morgan et al. 2019; Courtenay et al. 2020a, 2020b). Due to this, it is important that the methods used are tested thoroughly to ensure that inaccurate or imprecise data are not being unknowingly preserved. The strength and limitations of each method need to be investigated, which is what was done in this study in relation to SfM-MVS.

The 3D models created in this project can be repeatedly sectioned, manipulated, and analysed in ways that only become possible using virtual tools. This opens the door to borrowing methods of analysis from other fields, such as has been done here with surface roughness (for examples, see QGIS toolboxes for further possibilities of tools QGIS.org 2021a). Photogrammetry should also be able to help with the reassembly of items. Although this was outside the scope of the current project, the refitting of fragments has potential to be useful beyond just osteology, and especially in the conservation of artefacts for both preservation and presentation (see Delpiano et al. 2019 and Collings and Brown 2020 for examples of different digitisation methods).

This research has designed a workflow that is straightforward and consistently successful using a camera, tripod, and three 3D printed wedges. Any instances where models did not successfully align were due to human error in the photography conditions and were quickly rectified. The ability to use photogrammetry in the field as well as in the lab in a short amount of time helps make it a useful method of quick and precise documentation. It is important to note, however, basic training should be given regarding image capture as the models produced are only as good as the images captured.

## 10.3 Osteological Insights Obtained during the Current Study

The study of sharp force injuries to the skeleton has generated considerable interest in recent years, whilst also arguably reaching a point of stagnation both regarding macroscopic and microscopic observations. The current research involving the Weymouth Ridgeway Vikings has demonstrated new ways that trauma analysis can be augmented and advanced. Discussed more in depth in Chapters 8 and 9, this section will briefly highlight three of the more important findings: the ability to analyse surface roughness, the potential for shape analysis as a tool, and the importance of radiating fractures from SFT.

The analysis of the surface roughness enabled quantification of aspects that have only been qualitatively discussed before. This point is particularly important with regard to the study of shaved cutmarks. The latter are frequently less explored than incised cutmarks, as they cannot produce a profile of the cut for examination in weapon-related studies and, in this respect, have been an understudied form of sharp force injury. The ability to investigate directionality of cutmarks in more detail could have both osteoarchaeological and forensic implications. This study has showed that this type of analysis also has potential beyond trauma analysis, such as adult age estimation (e.g. using the pubic symphysis and auricular surface) and requires more investigation both with point clouds and meshes (Section 8.5.4). Geometric morphometrics (GMM) and shape analysis are becoming more commonly used in archaeology, but have only recently started to be used in human osteology, with 3D GMM being more common (e.g. Courtenay et al. 2019, 2020b). The use of shape analysis avoids the requirement of landmarks, but only operates in 2D space. In the case of cutmarks, the length of the cut is often determined more by the size and geometry of the bone than by the blade itself, therefore the analysis of just the profile in 2D is still sufficiently data-rich to provide information about the cut (Section 9.4).

The importance of identifying the fractures that propagate from SFT was also addressed (Section 9.3). Radiating fractures from blunt force trauma and projectile/penetrating trauma are commonly discussed in various studies, but less so those from SFT. In this study, it was seen that such RED fractures were sometimes originally mistaken for SFT due to their similar appearance. This sometimes led to incorrect length and impact angles being noted before they were reappraised. This is not a flaw in the initial report, but rather a limitation of the technology being used and the time pressure the authors were working under.

## 10.4 Insights Regarding the Study Collection

In the course of this project, new information was also discovered about the Weymouth Ridgeway Vikings (Section 9.7). The placement of the defensive trauma on the forearms is not consistent with the type of parry trauma that is commonly seen on the ulna (Judd 2008). However, the locations that are injured could correspond with injuries to an arm that is holding a shield or sword, exposing the radius more predominantly than the ulna. This would suggest that there was possibly some type of skirmish before the Vikings were captured, or that they had at least enough time for some of them to gather shields.

With the ability to examine the bones with magnification (through a camera's macro lens in this research), some small cutmarks were found on the anterior surfaces of the cervical vertebrae. This has led to the conclusion that at least some of the Vikings had their throats cut prior to their decapitation. This may add weight to the theory that the executions were a spectacle, as the decapitation of an individual whose throat has been cut is superfluous. This new detail, coupled with the decapitations, location, and burial positions of the individuals, makes it appear as if this was an event put on for spectators, not just a utilitarian method of disposing of the enemy.

In a preliminary look, several of the skulls present with evidence of blunt force trauma and some with possible penetrating trauma. There are two instances of penetrating trauma that are in locations that only would have been accessible if the head was no long attached in anatomical position. This could indicate that those heads were placed on spikes. Although this specific possibility was not suggested before, the unequal number of head and bodies did lead to Loe et al. discussing that heads may have been taken as trophies (2014b). One thing can be stated with certainty, if these two heads were placed on spikes, they were not left there for long as they were buried with the rest of the heads shortly after the decapitations.

## 10.5 Future Research

There is much potential for further research regarding the methodology designed here, the application of these digital methods to osteological analysis, and the Weymouth Ridgeway Vikings themselves. As highlighted in Chapters 6 and 8, methodologically, the inter-observer error needs to be examined for measurements taken from a 3D model one individual has created and from measurements from models of the same subject that were created by different observers. It would also be beneficial to compare results generated by individuals of different skill level in both trauma analysis and photogrammetry.

Another area that requires further study is surface roughness as it has potential for the analysis of cutmarks as well as other aspects of osteology. There are several types of analysis in osteology that qualitatively use surface roughness. These staples for biological profiling are unfortunately subjective at times and the use of surface roughness may allow for a more objective, quantitative look as these aspects. Current techniques struggle to provide a narrow age range for individuals over about 50 years of age. It is possible that using digital techniques such as surface roughness as defined by photogrammetry might allow for finer changes to be identified which could lead to more accurate methods of age estimation, something that would be especially helpful in forensic anthropology. Evaluation of this would need to be performed with collections of known age and sex.

As demonstrated in the osteology-focused Chapters 7 and 9, the use of shape analysis for the study of cutmarks profiles has also shown promise. Experimental studies in which more variables are controlled would be ideal to determine the extent to which the type of blade, force, or type of strike affect the shape of the profile. If able to distinguish categories of blade, it might help determine if multiple weapons were used in a situation where several blows have been struck.

One inevitable issue that arises with the use of digital technology is the storage and accessibility of the data that is created. The benefits of being able to share data are outweighed if it cannot be accessed. In order for most accessibility, storing the models in a non-proprietary format with metadata is recommended. There are also ethical implications that need to be considered when storing images or models of human remains since they must be treated respectfully and following any local laws or guidance. It is important to ensure that proper permissions are received before other researchers can use the data. For this project, the data will be provided to the Dorset Museum since the collection is curated by them. The specific details of what data is stored at the academic institution and how it is stored are still under discussion.

# References

3DSourced, 2021. *The 11 best FDM 3D printers 2021 (in every price range).* Available from: https://www.3dsourced.com/rankings/best-fdm-3d-printer/ [Accessed 15 October 2021].

Abels, R., 2008. France, J. and De Souza, P., eds. *War and peace in ancient and medieval history* [online]. Cambridge: Cambridge University Press, 173-192.

Abrams, L. 2012. Diaspora and identity in the Viking age. *Early Medieval Europe,* 20 (1), 17-38.

Adobe, 2018. *Adobe Photoshop CC*. Version 19 [computer programme]. Berkeley: Peachpit Press.

Adobe, 2020. *Adobe Illustrator CS*. Version 24.0 [computer programme]. Berkeley: Peachpit Press.

Agisoft LLC, 2018a. *Agisoft PhotoScan User Manual, Professional Edition, Version 1.4.*

Agisoft LLC, 2018b. *Agisoft PhotoScan*, Version 1.4 [computer programme].

Agisoft LLC, 2020a. *Agisoft Metashape User Manual, Professional Edition, Version 1.6.*

Agisoft LLC, 2020b. *Agisoft Metashape*, Version 1.6 [computer programme].

Agisoft LLC, 2021. *Agisoft Metashape User Manual, Professional Edition, Version 1.7.*

Alberto-Barroso, V., Delgado-Darias, T., Ordóñez, A.C., Serrano, J.G., Fregel, R., and Velasco-Vázquez, J., 2021. Perinatal burials at pre-hispanic noncemetery sites in gran canaria: Tophet, infanticide, or natural mortality?. *International Journal of Osteoarchaeology,* 1-11.

Alsop, K., Baier, W., Norman, D., Burnett, B., and Williams, M.A. 2021. Accurate prediction of saw blade thickness from false start measurements. *Forensic Science International* 318, 110602.

Alunni-Perret, V., Borg, C., Laugier, J-P., Bertrand, M-F., Staccini, P., Bolla, M., Quatrehomme, G., and Muller-Bolla, M., 2010. Scanning electron microscopy analysis of experimental bone hacking trauma of the mandible. *The American Journal of Forensic Medicine and Pathology,* 31 (4), 326-329.

Alunni-Perret, V., Muller-Bolla, M., Laugier, J.-P., Lupi-Pégurier, L., Bertrand, M.-F., Staccini, P., Bolla, M., and Quatrehomme, G., 2005., Scanning electron microscopy analysis of experimental bone hacking trauma. *Journal of Forensic Science*, 50 (4), 1-6.

Ambade, V.N. and Godbole, H.V., 2006. Comparison of wound patterns in homicide by sharp and blunt force. *Forensic Science International*, 156, 166-170.

Anastopoulou, I., Karakostis, F.A., Eliopoulos, C., and Moraitis, K., 2020. Technical note: Development of regression equations to reassociate upper limb bones from commingled contexts. *Forensic Science International*, 315, 110439.

Anderson, K., Westoby, M.J., and James, M.R., 2019. Low-budget topographic surveying comes of age: Structure from motion photogrammetry in geography and the geosciences. *Progress in Physical Geography*, 43 (2), 163-173.

Anderson, T., 1996. Cranial weapon injuries from Anglo-Saxon Dover. *International Journal of Osteoarchaeology*, 6, 10-14.

Andrews, D.P., Bedford, J., and Bryan, P.G., 2013. A comparison of laser scanning and structure from motion as applied to the Great Barn at Harmondsworth, UK. *In:* Grussenmeyer, P., ed. *International archives of the photogrammetry, remote sensing and spatial information sciences volume XL-5/W2, 2013 international CIPA symposium.* Strasbourg 2-6 September 2013. 31-36.

Andronoswki, J.M., Crowder, C., and Soto Martinez, M. 2018. Recent advancements in the analysis of bone microstructure: New dimensions in forensic anthropology. *Forensic Sciences Research*, 3 (4), 294-309.

Ansbacher, T., 1998. John Dewey's experience and education: Lesson for museums. *Curator: The Museum Journal*, 41 (1), 36-50.

Anzellini, A. and Toyne, J.M., 2020. Estimating the stature of ancient high-altitude Andean populations from skeletal remains of the Chachapoya of Peru. *American Journal of Physical Anthropology*, 171 (3), 539-549.

Appleby, J., Rutty, G.N., Hainsworth, S.V., Woosnam-Savage, R.C., Morgan, B., Earp, R.W., Robinson, C., King, T.E., Morris, M., and Buckley, R., 2015. Perimortem trauma in King Richards III: A skeletal analysis. *The Lancet*, 385, 253-259.

Archaeological Data Service (ADS), 2009. *Close-range photogrammetry: A guide to good practice* [online]. Available from: https://guides.archaeologydataservice.ac.uk/g2gp/Photogram_Toc [Accessed 28 March 2019].

Arriaza, M.C., Yravedra, J., Domínguez-Rodrigo, M., Mate-González, M.A., García Vargas, E., Palomeque-González, J.F., Aramendi, J., González-Aguilera, D., and Baquedano, E., 2017. On applications of micro-photogrammetry and geometric morphometrics to studies of tooth mark morphology: The modern Olduvai

Carnivore Site (Tanzania). *Palaeogeography, Palaeoclimatology, Palaeoecology,* 488*,* 103-112.

Ashby, S.P., 2015. What really caused the Viking age? The social content of raiding and exploration. *Archaeological Dialogues,* 22 (1), 89-106.

Ashton, N., Lewis, S.G., De Groote, I., Duffy, S.M., Bates, M., Bates, R., Hoare, P., Lewis, M., Parfitt, S.A., Peglar, S., Williams, C., and Stringer, C., 2014. Hominin footprints from Early Pleistocene deposits at Happisburgh, UK. *PLoS ONE,* 9 (2), e88329, 1-13.

Aspöck, E., 2008. What actually is a ‘deviant burial’? Comparing German-language and anglophone research on ‘deviant burials’. *In:* Murphy, E.M., ed. *Deviant burial in the archaeological record.* Oxford: Oxbow Books, 17-34.

Astrup, E.E. and Martens, I., 2011. Studies of Viking age swords: Metallography and archaeology. *Gladius*, 31, 203-206.

Attia, M.H., Badr El-Dine, F.M.M., Attia, M.H., and El-Sekily, N.M.A., 2020. Sample specific sex estimation method using parameters around dominant nutrient foramina in unknown femur bones collection of contemporary Egyptians. *International Journal of Osteoarchaeology*, 30 (5), 583-593.

Avery, T.E. and Berlin, G.L., 1992. *Fundamentals of remote sensing and airphoto interpretation*. 5th edition. Upper Saddle River: Prentice-Hall Inc.

Ayton, A. 1999. Arms, armour, and horses. *In:* Keen, M., ed. *Medieval warfare: A history* [online]. Oxford: Oxford University Press, 186-208.

Baier, W. and Rando, C., 2016. Developing the use of structure-from-motion in mass grave documentation. *Forensic Science International*, 261, 19-25.

Baier, W., Norman, D.G., Donnelly, M.J., and Williams, M.A., 2021. Forensic 3D printing from micro-CT for court use: Process validation. *Forensic Science International*, 318, 110560.

Baier, W., Norman, D.G., Warnett, J.M., Payne, M., Harrison, N.P., Hunt, N.C.A., Burnett, B.A., and Williams, M.A., 2017. Novel application of the three-dimensional technologies in a case of dismemberment. *Forensic Science International*, 270, 139-145.

Balter, M., 2005. ‘Deviant’ burials reveal death on the fringe in ancient societies. *Science*, 310 (5748), 613.

Barazzetti, L., Binda, L., Scaioni, M., and Taranto, P., 2011. Photogrammetric survey of complex geometries with low-cost software: Applications to the ‘G1’ temple in Myson, Vietnam. *Journal of Cultural Heritage,* 12, 253-262.

Barnard, S. T. and Thompson, W. B. 1980. Disparity analysis of images. *IEEE Transactions on Pattern Analysis and Machine Intelligence,* PAMI-2 (4), 333-340.

Barrand, N.E., Murrey, T., James, T.D., Barr, S.L., and Mills, J.P. 2009. Optimising photogrammetric DEMs for glacier volume change assessment using laser-scanning derived ground-control points. *Journal of Glaciology*, 55 (189), 106-116.

Barrett, J.H., 2008. What caused the Viking age?. Antiquity, 82 (317), 671-685.

Bartelink, E.J., 2015. Blunt force trauma patterns in the human skull and thorax: A case study from northern California. *In:* Passalacqua, N.V. and Rainwater, C.W., eds. *Skeletal trauma analysis: case studies in context* [online]. Chichester: John Wiley & Sons, Ltd., 56-73.

Bartelink, E.J., Wiersema, J.M., and Demaree, R.S., 2001. Quantitative analysis of sharp-force trauma: An application of scanning electron microscopy in forensic anthropology. *Journal of Forensic Science*, 46 (6), 1288-1293.

Bartoš, K., Pukanská, K., and Sabová, J. 2014. Overview of available open-source photogrammetric software, its use and analysis. *International Journal for Innovation Education and Research*, 2 (04), 62-70.

Bartzis, D., 2017. Towards reconstructing a Doric column in a virtual construction site. *The International Archives of Photogrammetry, Remote Sensing and Spatial Information Sciences*, 42, 91-96.

Bass, W.M. III, *Human osteology: A laboratory and field manual.* 4th Edition. Columbia: Missouri Archaeological Society.

Baug, I., Skre, D., Heldal, T., and Jansen, Ø.J., 2019. The beginning of the viking age in the west. *Journal of Maritime Archaeology*, 14, 43-80.

Baumann, F., and Roller, D., 2016. Vision based error detection for 3D printing processes. *In:* Abdul Amir, H.F., Korsunsky, A.M., and Guo, Z., eds. *2016 international conference on frontiers of sensor technologies (ICFST 2016)*, Hong Kong 12-14 March 2016. Les Ulis: edp Sciences. 06003.

Beale, G. and Reilly, P., 2017. After virtual archaeology: Rethinking archaeological approaches to the adoption of digital technology. *Internet Archaeology* [online], 44. Available from: http://intarch.ac.uk/journal/issue44/1/index.html [19 November 2018].

Beekmans, C., Schneider, J., Läbe, T., Lennefer, M., Stachniss, C., and Simmer, C., 2016. Cloud photogrammetry with dense stereo for fish-eye cameras. *Atmospheric Chemistry and Physics*, 16, 14231-14248.

Bell, S., 2008. *Encyclopedia of forensic sciences* [online]. New York: Facts on File.

Bello, S.M. and Soligo, C., 2008. A new method for the quantitative analysis of cutmark micromorphology. *Journal of Archaeological Science*, 35, 1542-1552.

Bello, S.M., Wallduck, R., Dimitrijević, V., Živaljević, I., and Stringer, C.B. 2016. Cannibalism versus funerary defleshing and disarticulation after a period of decay: Comparisons of bone modifications from prehistoric sites. *American Journal of Physical Anthropology*, 161, 722-743.

Bennani, H., McCane, B., and Cornwall, J., 2016. Three dimensional (3D) lumbar vertebrae data set. *Data Science Journal*, 15 (9), 1-15.

Bennett, M.J., 2015. Evaluating the creation and preservation challenges of photogrammetry-based 3D models. *In:* Society for Imaging Science and Technology, ed. *Archiving 2015 final program and proceedings*. Los Angeles 19-22 May 2015. Springfield: Society for Imaging Science and Technology, 78-82

Bennike, P., 2006. Rebellion, combat and massacre: A medieval mass grave at Sandjberg near Næstved, Denmark. *In:* Otto, T., Thrane, H., and Vandkilde, H., eds. *Warfare and society*. Aarhus: Aarhus University Press, 305-318.

Bennike, P., 2008. Trauma. *In:* Pinhasi, R. and Mays, S., eds. Advances in human palaeopatholgy. Chichester: John Wilesy & Sons, Ltd., 309-328.

Berezowski, V., Mallett, X., and Moffat, I. 2020. Geomatic techniques in forensic science: A review. *Science & Justice*, 60, 99-107.

Berezowski, V., Rogers, T., and Liscio, E., 2021. Evaluating the morphological and metric sex of human crania using 3-dimensional (3D) technology. *International Journal of Legal Medicine*, 135, 1079-1085.

Berryman, H.E. and Jones Haun, S., 1996. Applying forensic techniques to interpret cranial fracture patterns in an archaeological specimen. *International Journal of Osteoarchaeology*, 6, 2-9.

Berryman, H.E. and Symes, S.A., 1998. Recognising gunshot and blunt cranial trauma through fracture interpretation. *In:* Reichs, K.J., ed. *Forensic osteology: Advances in the identification of human remains*. 2nd edition. Springfield: Charles C Thomas Publisher, Ltd., 333-352.

Bertsatos, A., Athanasopoulou, K., and, Chovalopoulou, M.-E., 2019. Estimating sex using discriminant analysis of mandibular measurements from a modern Greek sample. *Egyptian Journal of Forensic Sciences*, 9 (25), 1-12.

Bettey, J.H., 1986. *Wessex from AD1000.* Harlow: Longman Group Limited.

Bhushan, B., 2000. Surface roughness analysis and measurement techniques. *In:* Bhushan, B., ed. *Modern tribology handbook, two volume set*. Boca Raton: CRC press, 79-150.

Biddle, M. and Kjølbye-Biddle, B., 1992. Repton and the Vikings. *Antiquity*, 66, 36-51.

Biddle, M. and Kjølbye-Biddle, B., 2001. Repton and the 'great heathen army', 873-4. *In:* Graham-Campbell, J., Hall, R., Jesch, J., and Parsons, D.N., eds. *Vikings and the Danelaw*. Oxford: Oxbow Books, 45-96.

Biddle, M. and Kjølbye-Biddle, B., 2016. Danish royal burials in Winchester: Cnut and his family. *In:* Lavelle, R. and Roffey, S., eds. *Danes in Wessex: The Scandinavian impact on southern England, c.800-c.1100.* Oxford: Oxbow Books, 212-249.

Bilfeld, M.F., Dedouit, F., Rousseau, H., Sans, N., Braga, J., Rougé, D. and Telmon, N., 2012. Human coxal bone sexual dimorphism and multislice computed tomography: Geometric morphometric analysis of 65 adults. *Journal of Forensic Sciences*, 57 (3), 578-588.

Blake, J., 2000. On defining cultural heritage. *International and Comparative Law Quarterly*, 49 (1), 61-85.

Bleed, P., Douglass, M., Sumner, A., Behrendt, M., and Mackay, A., 2017. Photogrammetrical assessment of procedural patterns and sequential structure in "handaxe" manufacture: A case study along the Doring River of South Africa. *Lithic Technology*, 42 (1), 3-12.

Blumenbach, J.F., and Banks, J., 1795. *De generis humani varietate nativa*. Gottingae: Vandenhoek et Ruprecht

Bohnert, M., Hüttemann, H., and Schmidt, U. 2006. Homicide by sharp force. *In:* Tsokos, M., ed. *Forensic pathology reviews, vol 4*. Totowa, New Jersey.

Bonfield, W., and Datta, P.K., 1976. Fracture toughness of compact bone. *Journal of Biomechanics*, 9, 131-134.

Bonhomme, V., Picq, S., Gaucherel, C., and Claude, J., 2014. Momocs: Outline analysis using R. *Journal of Statistical Software*, 56 (13), 1–24.

Bonney, H., 2014. An investigation of the use of discriminant analysis for the classification of blade edge type from cut marks made by metal and bamboo blades. *American Journal of Physical Anthropology*, 154, 575-584.

Boschin, F. Crezzini, J., 2012. Morphometrical analysis on cut marks using a 3D digital microscope. *International Journal of Osteoarchaeology*, 22, 549-562.

Boucherie, A., Jørkov, M.L.S., and Smith, M., 2017. Wounded to the bone: Digital microscopic analysis of trauma in a medieval mass grave assemblage (Sandbjerget, Denmark, AD 1300-1350). *International Journal of Paleopathology*, 19, 66-79.

Boyle, A., 2016. Death on the Dorset Ridgeway: The discovery and excavation of an early medieval mass burial. *In:* Lavelle, R. and Roffey, S., eds. *Danes in Wessex: The Scandinavian impact on southern England, c.800-c.1100.* Oxford: Oxbow Books, 109-121.

Boylston, A., 2000. Evidence for weapon-related trauma in British archaeological samples. *In:* Cox, M., and Mays, S., eds. *Human osteology in archaeology for forensic science*. London: Greenwich Medical Media Ltd., 357-380.

Boylston, A., Knüsel, C.J. Roberts, C.A., and Dawson, M., 2000. Investigation of a Romano-British rural ritual in Bedford, England. *Journal of Archaeological Science,* 27, 241-254.

Brickley, M. and McKinley, J., 2004. *Guidelines to the standards for recording human remains* [online]. Southampton and Reading: BABAO and IFA. IFA paper no. 7.

Brink, S., 2008. Introduction. *In:* Brink, S. and Price, N.S., eds. *The Viking world*. Abingdon: Routledge, 1-3.

British Geological Survey (BGS), 2021. *Geology of Britain viewer.* Available from: https://mapapps.bgs.ac.uk/geologyofbritain/home.html?&_ga=2.93666141.1374205390.1634408334-1517739267.1634408334 [Accessed 16 October 2021]

Broca, P., 1861. *Sur le volume et al forme du cerveau suivant les individus et suivant les races*. Paris: Hennuyer.

Brødholt, E.T. and Holck, P., 2012. Skeletal trauma in the burials from the royal church of St. Mary in medieval Oslo. *International Journal of Osteoarchaeology*, 22, 201-218.

Bromage, T.G. and Boyde, A., 1984. Microscopic criteria for the determination of directionality of cutmarks on bone. *American Journal of Physical Anthropology*, 65, 359-366.

Brooks, S. and Suchey, J.M. 1990. Skeletal age determination based on the os pubis: A comparison of the Acsádi-Nemeskéri and Suchey-Brooks methods. *Human Evolution,* 5 (3), 227-238

Brown, L., Hayden, C., and Score, D., 2014. *'Down to Weymouth town from ridgeway': Prehistoric, roman and later sites along the Weymouth relief road.* Dorset natural history and archaeological society monograph series no. 23. Dorset Natural History and Archaeological Society, Dorchester.

Brunel, C., Fermanian, C., Durigon, M., Lorin de la Grandmaison, G. 2010. Homicidal and suicidal sharp force fatalities: Autopsy parameters in relation to the manner of death. *Forensic Science International*, 198, 150-154.

Brunning, S., 2019. *The sword in early medieval northern Europe: Experience, identity, representation.* Woodbridge: Boydell Press.

Bruno, F., Bruno, S., De Sensi, G., Luchi, M-L., Mancuso, S., and Muzzupappa, M. 2010. From 3D reconstruction to virtual reality: A complete methodology for digital archaeological exhibition. *Journal of Cultural Heritage,* 11, 42-49.

Bryan, P., and Chandler, J.H., 2008. Cost-effective rock-art recording within a non-specialist environment. *In:* Chen, J., Jiang, J., and Maas, H.-G. eds. *International Archives of the Photogrammetry, Remote Sensing and Spatial Information Sciences XXIst ISPRS congress technical commission V*. Beijing 3-11 July 2008. 259-264.

Buck, U., Buße, K., Campana, L., Gummel, F., Schyma, C., and Jackowski, C., 2020. What happened before the run over? Morphometric 3D reconstruction. *Forensic Science International*, 306, 1-9.

Buck, U., Naether, S., Rass, B., Jackowski, C., and Thali, M.J., 2013. Accident or homicide – virtual crime scene reconstruction using 3D methods. *Forensic Science International*, 225, 75-84.

Buckberry, J., 2008. Off with their heads: The Anglo-Saxon execution cemetery at Walkington Wold. *In:* Murphy, E.M., ed. *Deviant burial in the archaeological record.* Oxford: Oxbow Books, 148-168.

Buckberry, J., Montgomery, J., Towers, J., Müldner, G., Holst, M., Evans, J., Gledhill, A., Neale, N., and Lee-Thorp, J., 2014. Finding Vikings in the Danelaw. *Oxford Journal of Archaeology,* 33 (4), 413-434.

Buckberry, J.L. and Hadley, D.M., 2007. An anglo-saxon execution cemetery at Walkington Wold, Yorkshire. *Oxford Journal of Archaeology*, 26 (3), 309-329.

Budd, P., Millard, A., Chenery, C., Lucy, S., and Roberts, C., 2004. Investigating population movement by stable isotope analysis: A report from Britain. *Antiquity*, 78 (299), 127-141.

Buikstra, J. and Ubelaker, D., 1994. *Standards for data collection from human skeletal remains*. *Archaeological survey research series no. 44.* Fayetteville: Arkansas.

Buzi, C., Micarelli, I., Profico, A., Conti, J., Grassetti, R., Cristiano, W., Di Vincenzo, F., Tafuri, M.A., Manzi, G., 2018. Measuring the shape: Performance evaluation of photogrammetry improvement applied to the neanderthal skull Saccopastore 1. *Acta Imeko,* 7 (3), 79-85

Caffell, A. and Holst, M. 2012. *Osteological Analysis 3 and 6 Driffield Terrace, York, North Yorkshire*. York: York Archaeological Trust.

Canny, J. 1986. A computation approach to edge detection. *In:* Institute of Electrical and Electronics Engineering (IEEE), ed. *IEEE transactions on pattern analysis and machine intelligence,* PAMI-8 (6), 679-698.

Canon, 2020. DSLR cameras [online]. Available from: https://store.canon.co.uk/dslr-cameras/ [Accessed 23 March 2020].

Cappella, A., Amadasi, A., Castoldi, E., Mazzarelli, D., Gaudio, D., and Cattaneo, C., 2014. The difficult task of assessing perimortem and postmortem fractures on the skeleton: A blind text on 210 fractures of known origin. *Journal of Forensic Sciences*, 59 (6), 1598-1601.

Carew, R.M., Morgan, R.M., and Rando, C. 2019. A Preliminary investigation into the accuracy of 3D modelling and 3D printing in forensic anthropology evidence reconstruction. *Journal of Forensic Science*, 64 (2), 342-352

Cârlan, I. and Dovleac, B., 2017. 3D modelling of Arutela Roman Castrum using close-range photogrammetry. *International Journal of Conservation Science*, 8 (1), 35-42.

Carty, N., 2015. ‘The halved heads’: osteological evidence for decapitation in medieval Ireland. *Papers from the Institute of Archaeology*, 25 (1), 1-20.

Cerutti, E., Magli, F., Porta, D., Cibelli, D., and Cattaneo, C., 2014. Metrical assessment of cutmarks on bone: Is size important?. *Legal Medicine*, 16, 208-213.

Cessford, C., Dickens, A., Dodwell, N., and Reynolds, A., 2007. Middle Anglo-Saxon justice: The Chesterton Lane Corner execution cemetery and related sequence, Cambridge. *Archaeological Journal*, 164 (1), 197-226.

Chandler J.H., Fryer, J.G., and Jack, A., 2005. Metric capabilities of low-cost digital cameras for close range surface measurement. *The Photogrammetric Record*, 20 (109), 12-27.

Chandler, J.H., Bryan, P. and Fryer, J.G., 2007. The development and application of a simple methodology for recording rock art using consumer-grade digital cameras. *The Photogrammetric Record*, 22 (117), 10-21.

Chen, Z. and Wang, X. 2018. Trademark image retrieval system based on SIFT algorithm. *In:* Institute of Electrical and Electronics Engineering (IEEE) ed. *Proceedings 2018 IEEE/ACIS 17th international conference on computer and information science (ICIS)*. Singapore 6-8 June 2018. 740-743.

Chenery, C.A., Evans, J.A., Score, D., Boyle, A., and Chenery, S.R. 2014. A boat load of Vikings? *Journal of the North Atlantic.* Special volume 7, 43-53.

Cherryson, A.K., 2008. Normal, deviant and atypical: Burial variation in late saxon Wessex. *In:* Murphy, E.M., ed. *Deviant burial in the archaeological record.* Oxford: Oxbow Books, 115-130.

Chevalier, T. and Tignères, M., 2020. Age-related site-specific modifications in diaphyseal structural properties of the human fibula: Furrows and cross-sectional geometry. *American Journal of Physical Anthropology,* 173 (3), 535-555.

Chiabrando, F., Donadio, E., and Rinaudo, F., 2015. SfM for orthophoto generation: A winning approach for cultural heritage knowledge. *The International Archives of Photogrammetry, Remote Sensing and Spatial Information Sciences*, 40 (5), 91-98.

Chibunichev, A.G., Knyaz, V.A., Zhuravlev, D.V., and Kurkov, V.M., 2018. Photogrammetry for archaeology: Collection pieces together. *In:* Remondino, F., Toschi, I., and Fuse, T. eds. *International Archives of the Photogrammetry, Remote Sensing & Spatial Information Sciences volume XLII-2, 2018, ISPRS II mid-term symposium "towards photogrammetry 2020"*. Riva del Garda, 4-7 June 2018. 235-240.

Choi, Y.-H., Kim, C.-M., Jeong, H.-S., and Youn, J.-H., 2016. Influence of bed temperature on heat shrinkage shape error in FDM additive manufacturing of the ABS-engineering plastic. *World Journal of Engineering and Technology*, 4, 186-192.

Christensen, A.M., and Hatch, G.M., 2019. Forensic fractography of bone using computed tomography (CT) scans. *Journal of Forensic Radiology and Imaging*, 18, 37-39.

Churchill, N.W., Hutchison, M.G., Graham, S.J., and Schweizer, T.A. 2017. Symptom correlates of cerebral blood flow following acute concussion. *NeuroImage: Clinical*, 16, 234-239.

Clarke, D., 1998. *The head cult: Tradition and folklore surrounding the symbol of the severed human head in the British Isles* [online]. PhD thesis. The University of Sheffield. Available from: https://etheses.whiterose.ac.uk/3472/ [Accessed 18 June 2021].

Clarke, S. and Christensen, A.M., 2016. Reflectance transformation imaging (RTI) of saw marks on bones. *Journal of Forensic Radiology and Imaging*, 7, 33-37.

Clarke, T.A., and Fryer, J.G., 1998. The development of camera calibration methods and models. *The Photogrammetric Record*, 16 (91), 51-66.

Clement, J., 2016. Forensic odontology. *In:* Blau, S. and Ubelaker, D.H., eds. *Handbook of forensic anthropology and archaeology.* 2nd edition. New York: Routledge, 430-444.

Clini, P., Frapiccini, N., Mengoni, M., Nespeca, R., and Ruggeri, L., 2016. SfM technique and focus stacking for digital documentation of archaeological artifacts. *In:* Halounova, L., Šafář, V., Remondino F., Hodač, J., Pavelka, K., Shortis, M., Rinaudo, F., Scaioni, M., Boehm, J., and Rieke-Zapp, D., eds. *The international archives of the photogrammetry, remote sensing & spatial information sciences, volume XLI-B5, 2016 XXIII ISPRS congress*. Prague, 12-19 July 2016. 229-236.

CloudCompare, 2019. *CloudCompare*. Version 2.10.0 [computer programme].

Coelho, L., Cardoso, H.F.V., 2013. Timing of blunt force injuries in long bones: The effects of the environment, PMI length and human surrogate model. *Forensic Science International*, 233, 230-237.

Cohen, H., Kugel, C., May, H., Medlej, B., Stein, D., Slon, V., Brosh, T., and Hershkovitz, I., 2016. The impact velocity and bone fracture pattern: Forensic perspective. *Forensic Science International*, 266, 54-62.

Cohen, H., Kugel, C., May, H., Medlej, B., Stein, D., Slon, V., Brosh, T., and Hershkovitz, I., 2017. The influence of impact direction and axial loading on the bone fracture pattern. *Forensic Science International*, 277, 197-206.

Cohen, H., Sarie, I., Medlej, B., Bocquentin, F., Toledano, T., Hershkovitz, I., and Slon, V., 2012. Trauma to the skull: A historical perspective from the southern Levant (4300BCE-1917CE). *International Journal of Osteoarchaeology*, 24, 722-736.

Cohen, H., Slon, V., Barash, A., May, H., Medlej, B., and Hershkovitz, I., 2015. Assyrian attitude towards captive enemies: A 2700-year-old paleo-forensic study. *International Journal of Osteoarchaeology*, 25, 265-280.

Cole, G., Ditchfield, P.W., Dulias, K., Edwards, C.J., Reynolds, A., and Waldron, T., 2020. Summary justice or the king's will? The first case of formal facial mutilation from Anglo-Saxon England. *Antiquity*, 94 (377), 1263-1277.

Collings, A.J. and Brown, K., 2020. Reconstruction and physical fit analysis of fragmented skeletal remains using 3D imaging and printing. *Forensic Science International: Reports*, 2, 100114.

Colman, K.L., de Boer, H.H., Dobbe, J.G.G., Liberton, N.P.T.J., Stull, K.E., van Eijnatten, M., Streekstra, G.J., Oostram R.-J., van Rijn, R.R., and van der Merwe, A., 2019. Virtual forensic anthropology: The accuracy of osteometric analysis of 3D bone models derived from clinical computed tomography (CT) scans. *Forensic Science International*, 304, 109963.

Condorelli, F., and Rinaudo, F., 2018. Cultural heritage reconstruction from historical photographs and videos. *In:* Remondino, F., Toschi, I., and Fuse, T. eds. *International Archives of the Photogrammetry, Remote Sensing & Spatial Information Sciences volume XLII-2, 2018, ISPRS II mid-term symposium "towards photogrammetry 2020"*. Riva del Garda, 4-7 June 2018. 259-265.

Conrad, O., Bechtel, B., Bock, M., Dietrich, H., Fischer, E., Gerlitz, L., Wehberg, J., Wichmann, V., and Böhner, J., 2015. System for Automated Geoscientific Analyses (SAGA) v. 2.1.4. *Geoscientific Model Development*, 8, 1991-2007.

Constantinescu, M., Gavrilă, E., Greer, S., Soficaru, A., and Ungureanu, D., 2017. Fighting to the death: Weapon injuries in a mass grave ($16^{th}$-$17^{th}$ century) from Bucharest, Romania. *International Journal of Osteoarchaeology*, 27, 106-118.

Costen, M.D. and Costen, N.P., 2016. Trade and exchange in Anglo-Saxon Wessex, c AD 600-780. *Medieval Archaeology*, 60 (1), 1-27.

Counts, D.B., Averett, E.W., and Garstki, K., 2016. A fragmented past: (Re)constructing antiquity through 3D artefact modelling and customised structured light scanning at Athienou-Malloura, Cyprus. *Antiquity*, 90 (349), 206-218.

Courtenay, L.A., Herranz-Rodrigo, D., Huguet, R., Mate-González, M.Á., González-Aguilera, D., and Yravedra, J., 2020a. Obtaining new resolutions in carnivore tooth pit morphological analyses: A methodological update for digital taphonomy. *PLoS ONE*, 15 (10), e0240328.

Courtenay, L.A., Huguet, R., González-Aguilera, D., and Yravedra, J., 2020b. A hybrid geometric morphometric deep learning approach for cut and trampling mark classification. *Applied Sciences,* 10 (150), 1-16.

Courtenay, L.A., Yravedra, J., Mate-González, M.Á., Aramendi, J., and González-Aguilera, D., 2019. 3D analysis of cut marks using a new geometric morphometric methodological approach. *Archaeological and Anthropological Sciences,* 11, 651-665.

Croix, S., Frei, K.M., Sindbæk, S., and Søvsø, M., 2020. Individual geographic mobility in a viking-age emporium: Burial practices and strontium isotope analyses of Ribe's earliest inhabitants. *PLoS ONE*, 15 (8), e0237850.

Cronk, S., Fraser, C., Hanley, H., 2006. Automated metric calibration of colour digital cameras. *The Photogrammetric Record*, 21 (116), 355-372.

Crowder, C., Rainwater, C.W., and Fridie, J.S., 2013. Microscopic analysis of sharp force trauma in bone and cartilage: A validation study. *Journal of Forensic Sciences*, 58 (5), 1119-1126.

Cunha, E. and Pinheiro, J., 2016. Antemortem trauma. *In:* Blau, S. and Ubelaker, D.H., eds. *Handbook of forensic anthropology and archaeology.* 2nd edition. New York: Routledge, 322-345.

Cunha, E., and Silva, A.M., 1997. War lesions from the famous Portuguese medieval battle of Aljubarrota. *International Journal of Osteoarchaeology,* 7 (6), 595-599.

Cunliffe, B., 1993. *Wessex to A.D. 1000.* Harlow: Longman Group UK Ltd.

Curca, G.C., Dermengiu, D., Hostiuc, S., 2012. Patterns of injuries in domestic violence in Romanian population. *Journal of Interpersonal Violence*, 27 (14), 2889-2902.

Davidson, H. E., 1998. *The sword in Anglo-Saxon England: Its archaeology and literature.* Woodbridge: The Boydell Press.

De Marco, J., Maset, E., Cucchiaro, S., Beinat, A., Cazorzi, F. 2021. Assessing repeatability and reproducibility of structure-from-motion photogrammetry for 3D terrain mapping of riverbeds. *Remote Sensing*, 13, 2572.

De Reu, J., De Smedt, P., Herremans, D., Van Meirvenne, M., Laloo, P., and De Clercq, W., 2014. On introducing an image-based 3D reconstruction method in archaeological excavation practice. *Journal of Archaeological Science*, 41, 251-262.

De Reu, J., Plets, G., De Smedt, P., Bats, M., Cherretté, B., De Maeyer, W., Deconynck, J., Herremans, D., Laloo, P., Van Meirvenne, M., and De Clercq, W., 2013.

Towards a three-dimensional cost-effective registration of the archaeological heritage. *Journal of Archaeological Science*, 40 (2), 1108-1121.

Dedouit, F., Telmon, N., Costagliola, R., Otal, P., Joffre, F., and Rougé, D., 2007. Virtual anthropology and forensic identification: Report of one case. *Forensic Science International*, 173, 182-187.

Definis Gojanović, M. and Sutlović, D., 2007. Skeletal remains from world war II mass grave: From discovery to identification. *Croatian Medical Journal*, 48 (4), 520-527.

Dellepaine, M., Dell'Unto, N., Callieri, M., Lindgren, S., and Scopigno, R., 2013. Archaeological excavation monitoring using dense stereo matching techniques. *Journal of Cultural Heritage*, 14, 201-210.

Delpiano, D., Cocilova, A., Zangrossi, F., and Peresani, M., 2019. Potentialities of the virtual analysis of lithic refitting: Case studies from the middle and upper paleolithic. *Archaeological and Anthropological Sciences*, 11, 4467-4489.

Díaz-Navarro, S., 2021. A new case of prehistoric trepanation and scalping in the Iberian peninsula: The tomb of la saga (Cáseda, Navarre). *International Journal of Osteoarchaeology*, 31 (1), 88-98.

Dimitrova, T.L. and Weis, A., 2008. The wave-particle duality of light: A demonstration experiment. *American Journal of Physics*, 76 (2), 137-142.

Dirkmaat, D.C., Cabo, L.L., Ousley, S.D., and Symes, S.A., 2008. New perspectives in forensic anthropology. *Yearbook of Physical Anthropology*, 51, 33-52.

Donato, L., Cecchi, R., Goldoni, M., and Ubelaker, D.H., 2020. Photogrammetry vs CT scan: Evaluation of accuracy of a low-cost three-dimensional acquisition method for forensic facial approximation. *Journal of Forensic Sciences*, 65 (4), 1260-1265.

Doneus, M., Verhoeven, G., Fera, M., Briese, C., Kucera, M., and Neubauer, W., 2011. From deposit to point cloud – a study of low-cost computer vision approaches for the straightforward documentation of archaeological excavations. *Geoinformatics FCE CTU*, 6, 81-88.

Dorado, E., Herrerín, J., Ramírez, I., Parro, L., Carrillo, M.F., and Murillo, J., 2021. A case of brachymetacarpia in a skeleton from a Mudejar cemetery from Spain ($13^{th}$-$14^{th}$ century AD). *International Journal of Osteoarchaeology,* 31 (4), 621-627.

Douglass, M., Kuhnel, D., Magnani, M., Hittner, L., Chodoronek, M., and Porter, S., 2017. Community outreach, digital heritage and private collections: a case study from the North American Great Plains. *World Archaeology*, 49 (5), 623-638.

Downham, C., 2008. Vikings in England. *In:* Brink, S. and Price, N.S., eds. *The Viking world*. Abingdon: Routledge, 341-349.

Downing, M. and Fibiger, L., 2017. An experimental investigation of sharp force skeletal trauma with replica bronze age weapons. *Journal of Archaeological Science: Reports,* 11, 546-554.

Doyle. F.J. 1964. The historical development of analytical photogrammetry. *Photogrammetric Engineering,* 30 (2), 259-265.

Du Preez, C. 2014. A new arc-chord ratio (ACR) rugosity index for quantifying three-dimensional landscape structural complexity. *Landscape Ecology*, 30, 181-192.

Ducke, B., Score, D., and Reeves, J., 2011. Multiview 3D reconstruction of the archaeological site at Weymouth from image series. *Computers & Graphics*, 35, 375-382.

Duckworth, W.L.H. 1929. Notes on the human remains from Mr. Lethbridge's excavations of the Bran Ditch in 1927. *Proceedings of the Cambridge Antiquarian Society with Communications made to the Society,* 30, 94-97.

Dumville, D.N., 2008. Vikings in insular chronicling. *In:* Brink, S. and Price, N.S., eds. *The Viking world*. Abingdon: Routledge, 350-367.

Dunn, O.J., 1961. Multiple comparisons among means. *Journal of the American Statistical Association*, 56(293), 52-64.

During, E., 1997. Specific skeletal injuries observed on the human skeletal remains from the Swedish seventeenth century man-of-war, Kronan. *International Journal of Osteoarchaeology*, 7, 591-594.

Durrani, N., 2013. Vengeance: on the Vikings. *Archaeology*, 66 (6), 47-51.

Dziedzic, P., Michalak, A., and Szczepanek, A., 2011. Co kości mówią nam o wojnie? Uwagi na marginesie odkryć urazów na czaszkach z Masowej mogiły z grodziska w Niesulicach koło Swiebodzina. *Acta militaria mediaevalia*, 7, 49-78.

Earley, K., Livingstone, D., and Rea, P.M., 2017. Digital curation and online resources: Digital scanning of surgical tools at the royal college of surgeons of Glasgow for an open university learning resource. *Journal of Visual Communication in Medicine*, 40 (1), 2-12.

Edge, D. and Williams, A., 2003. Some early medieval swords in the Wallace Collection and elsewhere. *Gladius,* 23, 191-210.

Edwards, J. and Rogers, T., 2018. The accuracy and applicability of 3D modeling and printing blunt force cranial injuries. *Journal of Forensic Sciences*, 63(3), 683-691.

Eickhoff, S. Grothe, A., and Jungklaus, B. 2012. *1636. Ihre letzte Schlacht. Leben im Dreißigjährigen Krieg*. Darmstadt: Theiss Verlag.

Ellis, C., 2021. Remembering the Vikings: Violence, institutional memory and the instruments of history. *History Compass*, 19, e12644.

Eriksen, M.H. 2020. 'Body-objects' and personhood in the iron and viking ages: Processing, curating, and depositing skulls in domestic space. *World Archaeology*, 52(1), 103-119

Errickson, D., Grueso, I., Griffith, S.J., Setchell, J.M., Thompson, T.J.U., Thompson, C.E.L., and Gowland, R.L. 2017. Towards a best practice for the use of active non-contact surface scanning to record human skeletal remains from archaeological contexts. *International Journal of Osteoarchaeology*, 27, 650-661.

Errickson, D., Thompson, T.J.U., and Rankin, B.W.J., 2014. The application of 3D visualization of osteological trauma for the courtroom: A critical review. *Journal of Forensic Radiology and Imaging*, 2, 132-137.

Evgenikou, V., and Georgopoulos, A., 2015. Investigating 3D reconstruction methods for small artefacts. *In:* González-Aguilera, D., Remondino, F., Boehm, J., Kersten, T., and Fuse, T. *International archives of the photogrammetry, remote sensing & spatial information sciences XL-5/W4, 2015 3D virtual reconstruction and visualisation of complex architectures*, Avila 25-27 February 2015, 101-108.

Evin, A., Souter, T., Hulme-Beaman, A., Ameen, C., Allen, R., Viacava, P., Larson, G., Cucchi, T., and Dobney, K., 2016. The use of close-range photogrammetry in zooarchaeology: Creating accurate 3D models of wolf crania to study dog domestication. *Journal of Archaeological Science: Reports*, 9, 87-93.

Fahlke, J.M. and Autenrieth, M., 2016. Photogrammetry vs. micro-CT scanning for 3D surface generation of a typical vertebrate fossil – A case study. *Journal of Paleontological Techniques*, 14, 1-18.

Falkingham, P.L., 2012. Acquisition of high resolution 3D models using free, open-source, photogrammetric software. *Palaeontologia Electronica,* 15 (1), 1-15.

Fedrigo, A., Grazzi, F., Williams, A.R., Panzner, T., Lefmann, K., Lindelof, P.E., Jørgensen, L., Pentz, P., Scherillo, A., Porcher, F., and Strobl, M., 2017.

Extraction of archaeological information from metallic artefacts – A neutron diffraction study on Viking swords. *Journal of Archaeological Science: Reports*, 12,425-436.

Fedrigo, A., Strobl, M., Williams, A.R., Lefmann, K., Lindelof, P.E., Jørgensen, L., Pentz, P., Bausenwein, D., Schillinger, B., Kovyakh, A., and Grazzi, F., 2018. Neutron imaging study of ‘pattern-welded swords from the Viking age. *Archaeological and Anthropological Sciences,* 10, 1249-1263.

Fellows-Jensen, G., 2008. Scandinavian place names in the British Isles. *In:* Brink, S. and Price, N.S., eds. *The Viking world*. Abingdon: Routledge, 391-400.

Ferllini, R., 2013. Recent conflicts, deaths and simple technologies: The Rwandan case. *In:* Knüsel, C. and Smith, M.J., eds. *The routledge handbook of the bioarchaeology of human conflict* [online]. Abingdon: Routledge, 641-655.

Ferrari, R., Lachs, L., Pygas, D.R., Humanes, A., Sommer, B., Figueira, W.F., Edwards, A.J., Bythell, J.C., and Guest, J.R. [in press], 2021. Photogrammetry as a tool to improve ecosystem restoration. *Trends in Ecology & Evolution*, 1-9.

Ferreira, E., Chandler, J., Wackrow, R., and Shiono, K., 2017. Automated extraction of free surface topography using SfM-MVS photogrammetry. *Flow Measurement and Instrumentation*, 54, 243-249.

Field, A., 2009. *Discovering statistics using SPSS*. 3rd Edition. London: Sage Publications Ltd.

Fiorato, V., Boylston, A., and Knüsel, C. 2000. *Blood red roses*. 2nd Edition. Oxford: Oxbow Books.

Fjalldal, M. 2015. The last Viking battle. *Scandinavian Studies,* 87 (3), 317-331.

Fleischmann, J.M., 2019. Analysis of the skeletal demographics and traumatic injuries from the Khmer Rouge-period mass gravesite of Choeung Ek, Cambodia. *Forensic Anthropology*, 2(4), 347-365.

Foard, G., 2003. *Maldon battle and campaign*. Battlefields Trust, UK Battlefields Resource Centre.

Fonstad, M.A., Dietrich, J.T., Courville, B.C., Jensen, J.L., and Carbonneau, P.E., 2013. Topographic structure from motion: A new development in photogrammetric measurement. *Earth Surface Processes and Landforms*, 38, 421-430.

Forsmoo, J., Anderson, K., Macleod, C.J.A., Wilkinson, M.E., DeBell, L., and Braier, R.E. 2019. Structure from motion photogrammetry in ecology: Does the choice of software matter? *Ecology and Evolution*, 9, 12964-12979.

Fraser, C.S., 2013. Automatic camera calibration in close range photogrammetry. *Photogrammetric Engineering & Remote Sensing,* 79 (4), 381-388.

Freas, L.E., 2010. Assessment of wear-related features of the kerf wall from saw marks in bone. *Journal of Forensic Sciences*, 55 (6), 1561-1569.

Friedman, M., 1937. The use and ranks to avoid the assumption of normality implicit in the analysis of variance. *Journal of the American Statistical Association*, 32 (200), 675-701.

Friedman, M., 1939. A correction. *Journal of the American Statistical Association*, 34 (205), 109.

Friedman, M., 1940. A comparison of alternative tests of significance for the problem of m rankings. *The Annals of Mathematical Statistics*, 11(1), 86-92.

Fryer, J.G., Mitchell, H.L., and Chandler, J.H. 2007. *Applications of 3D measurement from images*. Dunbeath: Whittles Publishing.

Gaboutchian, A., Simonyan, H., Knyaz, V., Petrosyan, G., Ter-Vardanyan, L., Leybova, N.A. and Apresyan, S.V., 2018. Automated shape analysis of teeth from the archaeological site of Nerqin Naver. *In:* Remondino, F., Toschi, I., and Fuse, T. eds. *International Archives of the Photogrammetry, Remote Sensing & Spatial Information Sciences, volume XLII-2, 2018, ISPRS II mid-term symposium "towards photogrammetry 2020"*. Riva del Garda, 4-7 June 2018. 339-345.

Galán, A.B. and Domínguez-Rodrigo, M., 2013. Distribution of cut marks created by filleting and disarticulation on long bone ends. *Archaeometry*, 55 (6), 1132-1149.

Gallo, A., Muzzupappa, M., and Bruno, F., 2014. 3D reconstruction of small sized objects from a sequence of multi-focused images. *Journal of Cultural Heritage*, 15, 173-182.

Galloway, A., Symes, S.A., Haglund, W.D., and France, D.L., 1999. *In:* Galloway, A., ed. *Broken bones: Anthropological analysis of blunt force trauma.* Springfield: Charles C. Thomas, Publisher Ltd., 5-31.

Gao, C., Hua, H., and Ahuja, N., 2010. A hemispherical imaging camera. *Computer vision and Image Understanding*, 114, 168-178.

García-Gago, J., González-Aguilera, D., Gómez-Lahoz, J., and San José-Alonso, J.I., 2014. A photogrammetric and computer vision-based approach for automated 3D architectural modelling and its typological analysis. *Remote Sensing*, 6, 5671-5691.

Gardeła, L. 2013. The headless norsemen: Decapitation in viking age Scandinavia. *In:* Gardeła, L. and Kajkowski, K., eds. *The head motif in past societies in a comparative perspective*. Bytów:Muzeum Zachodniokaszubskie w Bytowie, 88-155.

Gardeła, L. and Kajkowski, K., 2013. Vampires, criminals or slaves? Reinterpreting 'deviant burials' in early medieval Poland. *World Archaeology*, 45 (5), 780-796.

Garstki, K., 2017. Virtual representation: The production of 3D digital artifacts. *Journal of Archaeological Method and Theory*, 24 (3), 726-750.

Gattet, E., Devogelaere, J., Raffin, R., Bergerot, L., Daniel, M., Jockey, P. and De Luca, L., 2015. A versatile and low-cost 3D acquisition and processing pipeline for collecting mass of archaeological findings on the field. *The International Archives of Photogrammetry, Remote Sensing and Spatial Information Sciences*, 40 (5), 299-305.

Gauthier, R., 2017. *Crack propagation mechanisms in human cortical bone on different paired anatomical locations: Biomechanical, tomographic and biochemical approaches* [online]. Thesis (PhD). Université de Lyon. Available from: https://tel.archives-ouvertes.fr/tel-01636213/document [Accessed 20 February 2021].

Geber, J., 2015. Comparative study of perimortem weapon trauma in two early medieval skeletal populations (AD 400-1200) from Ireland. *International Journal of Osteoarchaeology.* 25 (3), 253-264.

Geldenhuys, E-M., Burger, E.H., Alblas, A., Greyling, L.M., and Kotzé, S.H. 2016. The association between healed skeletal fractures indicative of interpersonal violence and alcoholic liver disease in a cadaver cohort from the Western Cape, South Africa. *Alcohol*, 52, 41-48.

George, E., Liacouras, P., Rybicki, F.J., and Mitsouras, D., 2017. Measuring and establishing the accuracy and reproducibility of 3D printed medical models. *Radiographics*, 37 (5), 1424-1450.

Giacomini, G., Scaravelli D., Herrel, A., Veneziano, A., Russo, D., Brown, R.P., and Meloro, C., 2019. 3D photogrammetry of bat skulls: Perspectives for macro-evolutionary analysis. *Evolutionary Biology*, 46, 249-259.

Giuffra, V., Pejrani Baricco, L., Subbrizio, M., and Fornaciari, G., 2015. Weapon-related cranial lesions from medieval and renaissance Turin, Italy. *International Journal of Osteoarchaeology*, 25, 690-700.

Giuliano, M.G., 2014. Cultural heritage: An example of graphical documentation with automated photogrammetric systems. *The International Archives of Photogrammetry, Remote Sensing and Spatial Information Sciences*, 40 (5), 251-255.

Godfrey, M.F. 1993. Beowulf and Judith: Thematizing decapitation in Old English poetry. *Texas Studies in Literature and Language*, 35 (1), 1-43.

Goodacre, S., Helgason, A., Nicholson, J., Southam, L., Ferguson, L., Hickey, E., Vega, E., Stefánsson, K., Ward, R., and Sykes, B., 2005. Genetic evidence for a family-based Scandinavian settlement of Shetland and Orkney during the Viking periods. *Heredity*, 95, 129-135.

Gore, D., 2016. A review of Viking attacks in western England to the early tenth century: Their motives and responses. *In:* Lavelle, R. and Roffey, S., eds. *Danes in Wessex: The Scandinavian impact on southern England, c.800-c.1100.* Oxford: Oxbow Books, 56-69.

Gower, J.C., 1975. Generalized procrustes analysis. *Psychometrika*, 40, 33-51.

Graham-Campbell, J., 2001. *The Viking world.* London: Frances Lincoln Limited.

Granshaw, S.I., 2016. Photogrammetric terminology: Third edition. *The Photogrammetric Record,* 31 (154), 210-251.

Granshaw, S.I., 2018. Editorial – Structure from motion: Origins and originality. *The Photogrammetric Record,* 33 (161), 6-10.

Granshaw, S.I., 2020. Photogrammetric terminology: Fourth edition. *The Photogrammetric Record,* 35 (170), 143-288.

Granshaw, S.I., and Fraser, C.S., 2015. Editorial – Computer vision and photogrammetry: Interaction or introspection?. *The Photogrammetric Record,* 30 (149), 3-7.

Green, S., Bevan, A., and Shapland, M., 2014. A comparative assessment of structure from motion methods for archaeological research. *Journal of Archaeological Science*, 46, 173-181.

Gregoricka, L.A., Scott, A.B., Betsinger, T.K., and Polcyn, M., 2017. Deviant burials and social identity in a postmedieval Polish cemetery; An analysis of stable oxygen and carbon isotopes from the “vampires” of Drawsko. *American Journal of Physical Anthropology*, 163, 741-758.

Grimmer, M., 2002. Britons and Saxons in Pre-Viking Wessex: Reflections on the Law 77 of King Ine. *Parergon,* 19 (1), 1-17.

Gruen, A., 2012. Development and status of image matching in photogrammetry. *The Photogrammetric Record,* 2 (137), 36-57.

Grussenmeyer, P. and Al Khalil, O. 2002. Solutions for exterior orientation in photogrammetry: A review. *The Photogrammetric Record,* 17 (100), 615-634.

Guo, F., Yang, J., Chen, Y., and Yao, B. 2018. Research on image detection and matching based on SIFT features. *In:* Institute of Electrical and Electronics Engineering (IEEE), eds. *3rd international conference on control and robotics engineering (ICCRE),* Nagoya 20-23 April 2018. 130-134.

Guyomarc'h, P., Samsel, M., Courtaud, P., Mora, P., Dutailly, B., and Villotte, S. 2017. New data on the paleobiology of the Gravettian individual L2A from Cussac cave (Dordogne, France) through a virtual approach. *Journal of Archaeological Science: Reports*, 14, 365-373.

Hadley, D.M. and Richards, J.D., 2000. Introduction: Interdisciplinary approaches to the Scandinavian settlement. *In:* Hadley, D.M. and Richards, J.D., eds. *Cultures in contact: Scandinavian settlement in England in the ninth and tenth centuries.* Turnhout: Brepols Publishers, 3-16.

Hadley, D.M. and Richards, J.D., 2016. The winter camp of the Viking great army, AD 872-3, Torksey, Lincolnshire. *The Antiquaries Journal*, 96, 23-67.

Hadley, D.M., 2008. The creation of the Danelaw. *In:* Brink, S. and Price, N.S., eds. *The Viking world*. Abingdon: Routledge, 375-378.

Hale, S.E., and Edwards, C., 2002. Comparison of film and digital hemispherical photography across a wide range of canopy densities. *Agricultural and Forest Meteorology*, 112, 51-56.

Harrison, K., 1971. Early Wessex Annals in the Anglo-Saxon Chronicle. *The English Historical Review*, 86 (340), 527-533.

Harte, J., 2011. Maimed rites: Suicide burials in the English landscape. *Time and Mind,* 4 (3), 263-282.

Harten-Buga, H., Brinker, U., Schramm, A., Jantzen, D., Nikulka, F., and Orschiedt, J., 2021. Digital trauma analysis and the mechanism of weapon related injuried: The bronze age human bones from the Tollense Valley. *In:* Shvedchikova, T., Moghaddam, N., and Barone, P.M. eds. Crimes in the past: Archaeological and anthropological evidence. Oxford: Archaeopress Publishing Ltd., 100-120.

Harten-Buga, H., Schwinning, M., Brinker, U., Lidke, G., Terberger, T., Jantzen, D., Nikulka, F., and Orschiedt, J., 2018. Micro-traces of a major bronze age conflict:

Digital trauma analysis in the Tollense valley, Germany. *PAST: The Newsletter of the Prehistoric Society*, 90, 1-4.

Hassett, B.R., and Lewis-Bale, T., 2017. Comparison of 3D landmark and 3D dense cloud approaches to hominin mandible morphometrics using structure-from-motion. *Archaeometry*, 59 (1), 191-203.

Hauser, W., Noschka-Roos, A., Reussner, E., and Zahn, C., 2009. Design-based research on digital media in a museum environment. *Visitor Studies*, 12 (2), 182-198.

Haymen, G., Reynolds, A., Coward, F., Robb, J., and Scottish Universities Research and Reactor Centre. 2005. A Saxon and Saxo-Norman execution cemetery at 42-54 London Road, Staines. *Archaeological Journal*, 162 (1), 215-255.

Heipke, C., 1997. Automation of interior, relative, and absolute orientation. *ISPRS Journal of Photogrammetry & Remote Sensing*, 52, 1-19.

Helgason, A., Hickley, E., Goodacre, S., Bosnes, V., Stefánsson, K., Ward, R., and Sykes, B., 2001. mtDNA and the islands of the north atlantic: Estimating the proportions of norse and gaelic ancestry. *American Journal of Human Genetics,* 68, 723-737.

Henderson, C.Y., Mariotti, V., Pany-Kucera, D., Villotte, S., and Wilczak, C. 2013. Fibrocartilaginous entheses: Initial tests using the Coimbra Method. *International Journal of Osteoarchaeology*, 23, 152-162.

Hill, D., 1976. Il Bran Ditch: The burials reconsidered. *Proceedings of the Cambridge Antiquarian Society*, 66, 126-129.

Hill, N.G., 1937. Excavations on Stockbridge Down, 1935-36. *Hampshire field club: Papers and proceedings*, 13 (3), 247-259.

Hirschmüller, H., 2005. Stereo processing by semiglobal matching and mutual information. *IEEE Transactions on Pattern Analysis and Machine Learning*, 30 (2), 328-341.

Hirschmüller, H., 2008. Accurate and efficient stereo processing by semi-global matching and mutual information. *In:* Institute of Electrical and Electronics Engineering (IEEE), ed. *IEEE Conference on Computer Vision and Pattern Recognition (CVPR),* San Diego 20-26 June 2005. 807-814.

Historic England, 2017. *Photogrammetric applications for cultural heritage. Guidance for good practice* [online]. Swindon: Historic England.

Hjardar, K. and Vike, V., 2016. *Vikings at war*. Oxford: Casemate Publishers.

Hlad, M., Veselka, B., Wolfe Steadman, D., Herrgods, B., Elskens, M., Annaert, R., Boudin, M., Capuzzo, G., Dalle, S., De Mulder, G., Sabaux, C., Salesse, K., Sengeløv, A., Stamataki, E., Vercauteren, M., Warmenbol, E., Tys, D., and Snoeck, C., 2021. Revisiting metric sex estimation of burnt human remains via supervised learning using a reference collection of modern identified cremated individuals (Knoxville, USA). *American Journal of Physical Anthropology*, 175 (5), 777-793.

Ho, T. and Budagavi, M., 2017. Dual-fisheye lens stitching for 360-degree imaging. *In:* Institute of Electrical and Electronics Engineering (IEEE), ed. *IEEE 2017 International conference on acoustics, speech, and signal processing,* New Orleans 5-9 March 2017. 2172-2176.

Hoggard, C.S., 2020. *Geometric morphometrics (GMM) and archaeology workshop (July 2020)* [online]. Available from: https://github.com/CSHoggard/-gmm_liverpool_2020 [Accessed 21 July 2020].

Hotelling, H., 1933. Analysis of a complex statistical variables into principle components. *Journal of Educational Psychology*, 24, 417-441.

Hotelling, H., 1936. Relations between two sets of variates. *Biometrika*, 28 (3/4), 321-377.

Houck, M.H., 1998. Skeletal trauma and the individualization of knife marks in bones. *In:* Reichs, K.J., ed. *Forensic osteology: Advances in the identification of human remains*. 2nd edition. Springfield: Charles C Thomas Publisher, Ltd., 410-424.

Hsueh, M.-H., Lai, C.-J., Wang, A.-H., Zeng, Y.-S., Hsieh, C.-H., Pan, C.-Y., and Huang, W.-C., 2021. Effect of printing parameters on the thermal and mechanical properties of 3D-printed PLA and PETG, using fused deposition modeling. *Polymers,* 13 (11), 1758.

Huang, J., Chen, Z., Ceylan, D., and Jin, H., 2017.  6-DOF VR videos with a single 360-camera. *In:* Institute of Electrical and Electronics Engineering (IEEE) ed. *2017 IEEE virtual reality (VR),* Los Angeles 18-22 March 2017. 37-44

Hugar, B.S., Harish, S., Girish Chandra, Y.P., Praveen, S., and Jayanth, S.H., 2012. Study of defence injuries in homicidal deaths: An autopsy study. *Journal of Forensic and Legal Medicine*, 19, 207-210

Humphrey, J.H. and Hutchinson, D.L., 2001. Macroscopic characteristics of hacking trauma. *Journal of Forensic Sciences*, 46 (2), 228-233.

IBM, 2019. *IBM SPSS statistics – gradpack.* Version 26 [computer programme]. Portsmouth: IBM.

Ingelmark, B.E., 1939. The skeletons. *In:* Thordeman, B., Nörlund, P., and Ingelmark, B.E., eds. *Armour from the Battle of Wisby, 1361*. Stockholm: Almqvist and Wiksell, 149-209.

Inoue, A., Yamamoto, K., Mizoue, N., and Kawahara, Y., 2004. Effects of image quality, size and camera type on forest light environment estimates using digital hemispherical photography. *Agricultural and Forest Meteorology*, 126, 89-97.

International Council on Monuments and Sites (ICOMS), 1964. *International charter for the conservation and restoration of monuments and sites (The Venice Charter 1964)*. Venice: ICOMS.

James, M.R., and Robson, S., 2012. Straightforward reconstruction of 3D surfaces and topography with a camera: Accuracy and geoscience application. *Journal of Geophysical Research,* 117, 1-17

James, M.R., Robson, S., and Smith, M.W., 2017a. 3-D uncertainty-based topographic change detection with structure-from-motion photogrammetry: Precision maps for ground control and directly georeferenced surveys. *Earth Surface Processes and Landforms*, 42, 1769-1788.

James, M.R., Robson, S., d'Oleire-Oltmanns, S., and Niethammer, U., 2017b. Optimising UAV topographic surveys processed with structure-from-motion: Ground control quality, quantity and bundle adjustment. *Geomorphology*, 280, 51-66.

Jantz, R.L., Hunt, D.R., and Meadows, L., 1995. The measure and mismeasure of the tibia: Implications for stature estimation. *Journal of Forensic Sciences*, 40 (5), 758-761.

Jarman, C. L., Biddle, M., Higham, T., and Bronk Ramsey, C., 2018. The Viking great army in England: New dates from the Repton charnel. *Antiquity,* 92 (361), 183-199.

Jebara, T., Azarbayejani, A., and Pentland, A., 1999. 3D structure from 2D motion. *IEEE Signal Processing Magazine*, 16 (3), 66-84.

Jha, R.M., Kochanek, P.M., and Simard, J.M. 2019. Pathophysiology and treatment of cerebral edema in traumatic brain injury. *Neuropharmacology*, 145, 230-246.

Jocks, I., Livingstone, D., Rea, P.M., 2015. An investigation to examine the most appropriate methodology to capture historical and modern preserved anatomical specimens for use in the digital age to improve access – A pilot study. *9th international technology, education and development conference, Madrid, Spain, 2-4 March 2015.* 6377-6386.

Judd, M.A. and Redfern, R., 2012. Trauma. *In:* Grauer, A., ed. *A companion to paleopathology*. Chichester: Blackwell Publishing Ltd., 357-379.

Judd, M.A., 2008. The parry problem. *Journal of Archaeological Science*, 35 (6), 1658-1666.

Karakasi, M.-V., Nastoulis, E., Zisopoulos, K., Markopoulou, M., Alexandri, M., Bakirtzis, C., Douzenis, A., Zaggelidou, E., and Pavlidis, P., 2021. *Journal of Forensic and Legal Medicine*, 81, 102184.

Karray, N., Dedouit, F., Dubois, C., Savall, F., and Telmon, N., 2021. Homicide by unusual-edged weapons: Forensic considerations of two cases. *Journal of Forensic Sciences*, 66, 398-402.

Katz, D. and Friess, M., 2014. Technical note: 3D from standard digital photography of human crania – A preliminary assessment. *American Journal of Physical Anthropology*, 154, 152-158.

Kazhdan, M. and Hoppe, H. 2013. Screened poisson surface reconstruction. *ACM Transactions on Graphics*, 32 (3), 29:1-13.

Kazhdan, M., Bolitho, M., and Hoppe, H. 2006. Poisson surface reconstruction. *In:* Polthier, K. and Sheffer, A., eds. *Proceedings of the fourth eurographics symposium on geometry processing Volume 7,* Cagliari 26-28 June 2006. Goslar: Eurographics Association, Postfach 2926, 61-70.

Kemp, W., McKeown, A., Symes, S., and Skelton, R., 2013. Identification of skeletal fractures before and after removal of soft tissue: A case report. *The American Journal of Forensic Medicine and Pathology*, 34, 18-22.

Kępa, M., Szostek, K., Wrębiak, A., Gląb, H., Buśko, C., Glowa, W., and Dryja, S., 2013. A case of the execution of Swedish soldiers at the market square in Cracow (17$^{th}$ c.). *International Journal of Osteoarchaeology*, 23, 730-736.

Kershaw, J., 2016. Scandinavian-style metalwork from southern England: New light on the ‘first Viking age’ in Wessex. *In:* Lavelle, R. and Roffey, S., eds. *Danes in Wessex: The Scandinavian impact on southern England, c.800-c.1100.* Oxford: Oxbow Books, 87-108.

Kershaw, P., 2000. The Alfred-Guthrum treaty: Scripting accommodation and interaction in Viking age England. *In:* Hadley, D.M. and Richards, J.D., eds. *Cultures in contact: Scandinavian settlement in England in the ninth and tenth centuries.* Turnhout: Brepols Publishers n.v., 43-64.

Keyence Corporation, 2014. *Digital microscope VHX-5000 user's manual* [online]. Japan: Keyence Corporation.

Khalaf, A., Ataiwe, T., Mohammed, I., and Kareem, A., 2018. 3D digital modelling for archaeology using close range photogrammetry. *In:* Al-Attar, T.S., Al-Neami, M.A., and AbdulSahib, W.S., eds. *The 3rd international conference on buildings, construction and environmental engineering, BCEE3-2017.* Sharm el-Shiekh 23-25 October 2017, EDP Sciences, Vol 162.

Kieser, J., Taylor, M., and Carr, D., 2013. *Forensic biomechanics.* Chichester: John Wiley & Sons, Ltd.

Kim, J.-I. and Kim, T. 2016. Comparison of computer vision and photogrammetric approaches for epipolar resampling of image sequence. *Sensors,* 16 (412), 1-12.

Kimmerle, E.H. and Baraybar, J.P. 2008. *Skeletal trauma: Identification of injuries resulting from human rights abuse and armed conflict.* Boca Raton: Taylor & Francis Group, LLC.

Kingsland, K. 2020. Comparative analysis of digital photogrammetry software for cultural heritage. *Digital Applications in Archaeology and Cultural Heritage*, 18, e00157.

Kjellström, A., 2005. A sixteenth-century warrior grave from Uppsala, Sweden: The battle of good Friday. *International Journal of Osteoarchaeology*, 15, 23-50.

Kjellström, A., 2013. Interpreting violence: A bioarchaeological perspective of violence from medieval central Sweden. *In:* Knüsel, C. and Smith, M.J., eds. *The routledge handbook of the bioarchaeology of human conflict* [online]. Abingdon: Routledge, 237-250.

Knüsel, C., 2013. Courteous knights and cruel avengers: A consideration of medieval warfare from the perspective of human remains. *In:* Knüsel, C. and Smith, M.J., eds. *The routledge handbook of the bioarchaeology of human conflict* [online]. Abingdon: Routledge, 263-281.

Konecny, G., 1985. The international society for photogrammetry and remote sensing – 75 years old, or 75 years young. *Photogrammetric Engineering and Remote Sensing*, 51 (7), 919-933.

Koppel, P. 2015. Agisoft photoscan: Point cloud accuracy in close range configuration. Koppel Engineering Messdienstleistungen.

Kordelas, G.A., Alexiadis, D.S., Daras, P., and Izquierdo, E., 2015. Enhanced disparity estimation in stereo images. *Image and Vision Computing,* 35, 31-49.

Koutsoudis, A., Vidmar, B., and Arnaoutoglou, F., 2013. Performance evaluation of a multi-image 3D reconstruction software on a low-feature artefact. *Journal of Archaeological Science*, 40, 4450-4456.

Koutsoudis, A., Vidmar, B., Ioannakis, G., Arnaoutoglou, F., Pavlidis, G., and Chamzas, C., 2014. Multi-image 3D reconstruction data evaluation. *Journal of Cultural Heritage*, 15, 73-79.

Kozakaitė, J., Girčius, R., Dementavičienė, J., Jankauskas, R., and Riobino-Mascali, D. 2018. Four cases of beheading from 14th-17th century Lithuania. *Anthropolischer Anzeiger: Journal of Biological and Clinical Anthropology*, 75 (3), 243-249.

Krakowka, K., 2017. Violence-related trauma from the Cistercian abbey of St Mary Graces and the late black death cemetery. *International Journal of Osteoarchaeology*, 27, 56-66.

Kranioti, E.F. 2015. Forensic investigation of cranial injuries due to blunt force trauma: Current best practice. *Research and Reports in Forensic Medical Science*, 5, 25-37.

Krige, D. G. 1976. A review of the development of geostatistics in South Africa. *In:* Guarascio, M., David., M., and Huijbregts, C., eds.. *Advanced geostatistics in the mining industry*. Dordrecht: Reidel, 279-93.

Kristoffersen, S., Normann, S-A., Morild, I., Lilleng, P.K., and Heltne, J-K., 2016. The hazard of sharp force injuries: Factors influencing outcome. *Journal of Forensic and Legal Medicine*, 37, 71-77.

Kruskal, W.H., and Wallis, W.A., 1952. Use of ranks in one-criterion variance analysis. *Journal of the American Statistical Association*, 47(260), 583-621.

Kuzminsky, S.C., and Gardiner, M.S., 2012. Three-dimensional laser scanning: Potential uses for museum conservation and scientific research. *Journal of Archaeological Science*, 39, 2744-2751.

L'Abbé, E.N., Symes, S.A., Pokines, J.T., Cabo, L.L., Stull K.E., Kuo, S., Raymond, D.E., Randolph-Quinney, P.S., and Berger, L.R., 2015. Evidence of fatal skeletal injuries on Malapa Hominins 1 and 2. *Scientific Reports*, 5(15120), 1-11.

L'Abbé, E.N., Symes, S.A., Raymond, D.E., and Ubelaker, D.H., 2019. The Rorschach butterfly, understanding bone biomechanics prior to using nomenclature in bone trauma interpretations. *Forensic Science International*, 299, 187-194.

Laffranchi, Z., Mazzucchi, A., Thompson, S., Delgado-Huertas, A., Granados-Torres, A., and Milella, M., 2020. Funerary reuse of a roman amphitheatre: Palaeodietary and osteological study of early middle ages burials (8th and 9th centuries AD) discovered in the arena of Verona (northeastern Italy). *International Journal of Osteoarchaeology,* 30 (4), 435-448.

Lang, J. and Ager, B., 1989. Swords of the Anglo-Saxon and Viking Periods in the British Museum: A Radiographic Study. *In:* Hawkes, S. C., ed. *Weapons and Warfare in Anglo-Saxon England*. Oxford: Oxford University Committee for Archaeology, 85-122.

Lang, J. and Williams, A.R., 1975, The hardening of iron swords. *Journal of Archaeological Science,* 2, 199-207.

Langlois, J.A., Rutland-Brown, W., and Wald, M.M. 2006. The epidemiology and impact of trauma brain injury: An overview. *Journal of Head Trauma Rehabilitation,* 21 (5), 375-378.

Larsen, H., Budka, M., and Bennett, M.R., 2021. Technological innovation in the recovery and analysis of 3D forensic footwear evidence: Structure from motion (SfM) photogrammetry. *Science & Justice*, 61, 356-368.

Lavelle, R. and Roffey, S., 2016. Introduction: Danes in Wessex. *In:* Lavelle, R. and Roffey, S., eds. *Danes in Wessex: The Scandinavian impact on southern England, c.800-c.1100.* Oxford: Oxbow Books, 1-6.

Lavelle, R., 2016. Law, death and peacemaking in the ‘second viking age’: An ealdorman, his king, and some ‘Danes’ in Wessex. *In:* Lavelle, R. and Roffey, S., eds. *Danes in Wessex: The Scandinavian impact on southern England, c.800-c.1100.* Oxford: Oxbow Books, 122-143.

Lawn, B. 1993. *Fracture of brittle solids*. 2nd edition. Cambridge: Cambridge University Press.

Lazarus, M. and Belmaker, J., 2021. A review of seascape complexity indices and their performance in coral and rocky reefs. *Methods in Ecology and Evolution*, 12, 681-695.

Leahy, K. and Paterson, C., 2001. New light on the viking presence in Lincolnshire: The artefactual evidence. *In:* Graham-Campbell, J., Hall, R., Jesch, J., and Parsons, D.N., eds. *Vikings and the Danelaw*. Oxford: Oxbow Books, 181-202.

Lee, D.T. and Schachter, B.J. 1980. Two algorithms for constructing a Delaunay triangulation. *International Journal of Computer and Information* Sciences, 9 (3), 219-242.

Lee, M. and Gerdau-Radonic, K., 2020. Variation within physical and digital craniometrics. *Forensic Science International*, 306, 110092.

LEGO, 2010. *Company profile: An introduction to the LEGO® Group* [online]. The LEGO Group.

Lewis, C.P., 2016. Danish landowners in Wessex. *In:* Lavelle, R. and Roffey, S., eds. *Danes in Wessex: The Scandinavian impact on southern England, c.800-c.1100.* Oxford: Oxbow Books, 172-211.

Lewis, J.E., 2008. Identifying sword marks on bone: Criteria for distinguishing between cut marks made by different classes of bladed weapons. *Journal of Archaeological Science*, 35, 2001-2008.

Li, Q. and Wang, X. 2018. Image classification based on SIFT and SVM. *In:* Institute of Electrical and Electronics Engineering (IEEE), ed. *2018 IEEE/ACIS 17th international conference on computer and information science*. Singapore 6-8 June 2018. 762-765

Li, S., Abdel-Wahab, A., and Silberschmidt, V.V., 2013. Analysis of fracture processes in cortical bone tissue. *Engineering Fracture Mechanics*, 110, 448-458.

Liba, N., Metsoja, K., Järve, I., and Miljan, J., 2019. Making 3D models using close-range photogrammetry: Comparison of cameras and software. *In:* SGEM Conferences, ed. *Proceedings of the international multidisciplinary scientific geoconference SGEM 19,* Albena 28 June-7 July 2019. Curran Associates, Inc., 561-568.

Liba, N., Metsoja, K., Järve, I., and Miljan, J., 2019. Making 3D models using close-range photogrammetry: Comparison of cameras and software. *In:* no eds. *19th international multidisciplinary scientific geoconference SGEM 2019*. Albena 30 June-6 July 2019. Sofia: SGEM Conferences. 561-568.

Liddell, D.M. 1933. Excavations at Meon Hill. *Hampshire field club: Papers and proceedings,* 12 (2), 127-162.

Liebenberg, L., and Krüger, G.C., 2020. Standardization and quality assurance in skeletal landmark placement and osteometry. *Forensic Science International*, 308, 110168.

Lillesand, T., Kiefer, R.W., and Chipman, J. 2015. *Remote sensing and image interpretation*. 7th edition. Hoboken: John Wiley & Sons.

Linder, W., 2009. *Digital photogrammetry: A practical course*. 3rd edition. Berlin: Springer.

Linder, W., 2016. *Digital photogrammetry: A practical course*. 4th edition. Berlin: Springer.

Loe, L., 2016. Perimortem trauma. *In:* Blau, S. and Ubelaker, D.H., eds. *Handbook of forensic anthropology and archaeology.* 2nd edition. New York: Routledge, 346-372.

Loe, L., Barker, C., Brady, K., Cox, M., and Webb, H., 2014a. *'Remember me to all': The archaeological recovery and identification of soldiers who fought and died in the battle of Fromelles, 1916.* Oxford Archaeology Monograph No. 23. Eynsham: Berforts Information Press.

Loe, L., Boyle, A., Webb, H., and Score, D. 2014b. *'Given to the Ground': A Viking age mass grave on Ridgeway Hill, Weymouth.* Dorset natural history and archaeological society monograph series no. 22. Dorset Natural History and Archaeological Society, Dorchester.

Long, B. 2013. *Complete digital photography* [online]. 7th edition. Boston: Course Technology.

Lorentz, K.O., and Casa, B., 2020. First metacarpal fractures from chalcolithic cyprus: A fall or a fist?. *International Journal of Osteoarchaeology*, 30 (5), 712-735.

Love, J.C., 2015. Neurocranial fractures. *In:* Passalacqua, N.V. and Rainwater, C.W., eds. *Skeletal trauma analysis: case studies in context* [online]. Chichester: John Wiley & Sons, Ltd., 130-146.

Lovejoy, C.O., Meindl, R.S., Pryzbeck, T.R., and Mensforth, R.P., 1985. Chronological metamorphosis of the auricular surface of the ilium: A new method for the determination of adult skeletal age at death. *American Journal of Physical Anthropology*, 68 (1), 15-28.

Lovell, N.C., 1997. Trauma analysis in paleopathology. *Yearbook of Physical Anthropology*, 40, 139-170.

Lowe, D.G. 2004. Distinctive image features from scale-invariant keypoints. *International Journal of Computer Vision*, 60 (2), 91-110.

Loyn, H.R., 1977. *The Vikings in Britain*. London: Batsford.

Luhmann, T., Robson, S., Kyle, S., and Boehm, J., 2013. *Close-range photogrammetry and 3D imaging.* Berlin: De Gruyters.

Łukasik, S., Krenz-Niedbała, M., Zdanowicz, M., Różański, A., and Olszacki, T., 2019. Victims of a 17th century massacre in central Europe: Perimortem trauma of castle defenders. *International Journal of Osteoarchaeology*, 19, 281-293.

Lund, N., 2008. Cnut the great and his empire. *In:* Brink, S. and Price, N.S., eds. *The Viking world*. Abingdon: Routledge, 665-667.

Lussu, P., and Marini, E., 2020. Ultra close-range digital photogrammetry in skeletal anthropology: A systematic review. *PLoS ONE*, 15 (4), e0230948.

Macheridis, S., 2015. Image-based 3D modeling as documentation method for zooarchaeological remains in waste-related contexts. *Ethnobiology Letters*, 6 (2), 242-248.

Magnani, M., 2014. Three-dimensional alternatives to lithic illustration. *Advances in Archaeological Practice*, 2 (4), 285-297.

Magnani, M., and Schroder, W., 2015. New approaches to modeling the volume of earthen archaeological features: A case-study from the Hopewell culture mounds. *Journal of Archaeological Science*, 64, 12-21.

Maijanen, H., Junno, J.-A., Mannermaa, K., Niskanen, M., and Wessman, A., 2021. Re-analysis of the Levänluhta skeletal material: Sex and stature estimation of individuals in an iron age water curial in Finland. *International Journal of Osteoarchaeology,* 31 (3), 347-357.

Maini, R. and Aggarwal, H. 2009. Study and comparison of various image edge detection techniques. *International Journal of Image Processing*, 3 (1), 1-12.

Majid, Z., Ariff, M.F.M., Idris, K.M, Yusoff, A.R., Idris, K.M., Aspuri, A., Abbas, M.A., Zainuddin, K, Ghani, A.R.A, and Ardi. 2017. Three-dimensional mapping of an ancient cave paintings using close-range photogrammetry and terrestrial laser scanning technologies. *In:* Aguilera, D., Georgopoulos, A., Kersten, T., Remondino, F., and Stathopoulou, E. eds. *The international archives of the photogrammetry, remote sensing and spatial information sciences volume XLII-2/W3, 2017, TC II & CIPA 3D virtual reconstruction and visualization of complex architectures.* Nafplio 1-3 March 2017. 453-457.

Mallison, H. and Wings, O., 2014. Photogrammetry in paleontology: A practical guide. *Journal of Paleontological Techniques,* 12, 1-31.

Mamourian, A.C. 2013. *CT imaging: Practical physics, artifacts, and pitfalls*. New York: Oxford University Press.

Mann, H. B., and Whitney, D. R. 1947. On a test of whether one of 2 random variables is stochastically larger than the other. *Annals of Mathematical Statistics*, 18, 50-60.

Manna, R., and Palumbo, R., 2018. What makes a museum attractive to your people? Evidence from Italy. *International Journal of Tourism Research,* 20, 508-517.

Marchal, A.F.J., Lejeune, P., and de Bruyn, P.J.N., 2016. Virtual poster cast: Digital 3D modelling of lion paws tracks using close range photogrammetry. *Journal of Zoology*, 300 (2), 111-119.

Margaryan, A., Lawson, D.J., Sikora, M., Racimo, F., Rasmussen, S., Moltke, I., Cassidy, L.M., Jørsboe, E., Ingason, A., Pedersen, M.W., Korneliussen, T., Wilhelmson, H., Buś, M.M., de Barros Damgaard, P., Martiniano, R., Renaud, G., Bhérer, C., Moreno-Mayar, J.V., Fotakis, A.K. Allen, M., Allmäe, R., Molak, M., Cappellini, E., Scorrano, G., McColl, H., Buzhilova, A., Fox, A., Albrechtsen, A., Schütz, B., Skar, B., Arcini, C., Falys, C., Jonson, C.H., Błaszczyk, D., Pezhemsky, D., Turner-Walker, G., Gestsdóttir, H., Lundstrøm, I., Gustin, I., Mainland, I., Potekhina, I., Muntoni, I.M., Cheng, J., Stenderup, J., Ma, J., Gibson, J., Peets, J., Gustafsson, J., Iversen K.H., Simpson, L., Strand, L., Loe, L., Sikora, M., Florek, M., Vretemark, M., Redknap, M., Bajka, M., Pushkina, T., Søvsø, M., Grigoreva, N., Christensen, T., Kastholm, O., Uldum, O., Favia, P., Holck, P., Sten, S., Arge, S.V., Ellingvåg, S., Moiseyev, V., Bogdanowicz,W., Magnusson, Y., Orlando, L., Pentz, P., Dengsø Jessen, M., Pedersen, A., Collard, M., Bradley, D.G., Jørkov, M.L., Arneborg, J., Lynnerup, N., Price, N., Gilbert, M.T.P., Allentoft, M.E., Bill, J., Sindbæk, S.M., Hedeager, L., Kristiansen, K., Nielsen, R., Werge, T., and Eske Willerslev, E., 2020. Population genomics of the viking world. *Nature*, 585, 390-413.

Marieb, E.N., Mallatt, J., and Brady, P., 2014. *Human anatomy*, 7th Edition. Harlow: Pearson.

Mariotti V., Facchini F., and Belcastro M.G. 2004. Enthesopathies: Proposal of a standardized scoring method and applications. *Collegium Anthropologicum,* 28, 145-159.

Mariotti V., Facchini F., and Belcastro M.G. 2007. The study of entheses: Proposal of a standardised scoring method for twenty-three entheses of the postcranial skeleton. *Collegium Antropologicum,* 31, 291-313.

Marr, D. and Hildreth, E., 1980. Theory of edge detection. *Proceedings of the Royal Society of London B,* 207, 187-217.

Martin, D.L. and Harrod, R.P., 2015. Bioarchaeological contributions to the study of violence. *Yearbook of Physical Anthropology*, 156, 116-145.

Martinez, A.M. and Kak, A.C., 2001. PCA versus LDA. *IEEE transactions on pattern analysis and machine intelligence*, 23(2), 228-233.

Maryon, H., 1960a. Pattern-welding and damascening of sword-blades: Part 1 pattern-welding. *Studies in Conservation*, 5 (1), 25-37.

Maryon, H., 1960b. Pattern-welding and damascening of sword-blades: Part 2. The damascene process. *Studies in Conservation*, 5 (2), 52-60.

Maté González, M.Á., Yravedra, J., González-Aguilara, D., Palomeque-González, J.F., and Domínguez-Rodrigo, M., 2015. Micro-photogrammetry characterization of cut marks on bones. *Journal of Archaeological Science*, 62, 128-142.

Maté-González, M.Á., Aramendi, J., Yravedra, J., Blasco, R., Rosell, J., González-Aguilara, D., and Domínguez-Rodrigo, M., 2017. Assessment of statistical agreement of three techniques for the study of cut marks: 3D digital microscopy, laser scanning confocal microscopy and micro-photogrammetry. *Journal of Microscopy*, 267 (3), 356-370.

Maté-González, M.Á., González-Aguilara, D., Linares-Matás, G., and Yravedra, J., 2019. New technologies applied to modelling taphonomic alterations. *Quaternary International*, 517, 4-15.

Maté-González, M.Á., Palomeque-González, J.F., Yravedra, J., González-Aguilara, D., and Domínguez-Rodrigo, M., 2018. Micro-photogrammetric and morphometric differentiation of cut marks on bone using metal knives, quartzite, and flint flakes. *Archaeological and Anthropological Sciences*, 10 (4), 805-816.

Mattison, A., 2016. *The execution and burial of criminals in early medieval England, c. 850-1150: An examination of changes in judicial punishment across the Norman conquest* [online]. PhD thesis. The University of Sheffield. Available from: https://etheses.whiterose.ac.uk/17173/ [Accessed 18 June 2021].

Mays, S. and Steele, J. 1996. A mutilated human skull from Roman St Albans, Hertfordshire, England. *Antiquity*, 70, 155-61.

Mays, S., Vincent, S., and Campbell, G. 2012. The value of sieving of grave soil in the recovery of human remains: An experimental study of poorly preserved archaeological inhumations. *Journal of Archaeological Science,* 39, 3248-3254.

McCarthy, J. 2014. Multi-image photogrammetry as a practical tool for cultural heritage survey and community engagement. *Journal of Archaeological* Science, 43, 175-185.

McCrum-Gardener, E., 2008. Which is the correct statistical test to use? *British Journal of Oral and Maxillofacial Surgery,* 46, 38-41.

McEvoy, B. and Edwards, C.J., 2005. Reappraising the Viking image. *Heredity*, 95, 111-112.

McFarlane, G., Floyd, B., Smith, C., and Mahoney, P., 2021. Technical note: Estimating original crown height in worn mandibular canines using aspects if dentin morphology. *American Journal of Physical Anthropology,* 176 (4), 692-702.

McIntyre, L.J., 2017. The York 113: Osteological analysis of 10 mass graves from Fishergate, York. *Journal of Conflict Archaeology*, 11 (2-3), 115-134.

McKinley, J.I., 1993., A decapitation from the Romano-British cemetery at Baldock, Hertfordshire. *International Journal of Osteoarchaeology*, 3, 41-44.

Mehta, S., Patel, A., and Mehta, J., 2015. CCD or CMOS image sensor for photography. *In: In:* Institute of Electrical and Electronics Engineering (IEEE), ed. *2015 international conference on communications and signal processing (ICCSP)*. Melmaruvathur 2-4 April 2015. 291-294.

Meijer, E., 2015. Structure from motion as documentation technique for rock art. *Adoranten*, 1-8.

Miccichè, R., Carotenuto, G., and Sìneo, L., 2019. An execution in medieval Sicily: Computerised tomography scan analysis and 3D reconstruction of an ancient forensic context. *International Journal of Osteoarchaeology,* 29, 350-355.

Micheletti, N., Chandler, J.H., and Lane, S.N., 2015a. Investigating the geomorphological potential of freely available and accessible structure-from-motion photogrammetry using a smartphone. *Earth Surface Processes and Landforms,* 40 (4), 473-486.

Micheletti, N., Chandler, J.H., and Lane, S.N., 2015b. Structure from motion (SFM) photogrammetry. *In:* Clarke, L.E. and Nield, J.M., eds. *Geomorphological techniques* [online]. London: British Society for Geomorphology, 1-12.

Mikulski, R.N.R., Schutkowski, H., Smith, M.J., Doumet-Serhal, C., and Mitchell, P.D., 2021. Weapon injuries in the crusader mass graves from a 13$^{th}$ century attack on the port city of Sidon (Lebanon). *PLoS ONE* 16(8), e0256517.

Milella, M., Caspari, G., Kapinus, Y., Sadykov, T., Blochin, J., Malyutina, A., Keller, M., Schlager, S., Szidat, S., Alterauge, A., and Lösch, S., 2021. Trouble in Tuva: Patterns of perimortem trauma in a nomadic community from southern Siberia (second to fourth c. CE). *American Journal of Physical Anthropology,* 174, 3-19.

Miles, J., Pitts, M., Pagi, H., and Earl, G., 2014. New applications of photogrammetry and reflectance transformation imaging to an Easter Island statue. *Antiquity*, 88, 596-605.

Mitchell, P.D. and Brickley, M., 2018. *Updated guidelines to the standards for recording human remains* [online]. CIfA/BABAO

Mitchell, P.D., 2013. Violence and the crusades: Warfare, injuries and torture in the medieval middle east. *In:* Knüsel, C. and Smith, M.J., eds. *The routledge handbook of the bioarchaeology of human conflict* [online]. Abingdon: Routledge, 251-262.

Mohite, P.M., Mohite, D.P., Dixit, P.G., Anjankar, A.J., and Keche, A.S., 2013. Autopsy evaluation of defence wounds in homicidal death in central India. *Journal of Forensic Research*, 4 (5), 1000205.

Morgan, B., Ford, A.L.J., and Smith, M.J., 2019. Standard methods for creating digital skeletal models using structure-from-motion photogrammetry. *American Journal of Physical Anthropology*, 169 (1), 152-160.

Morris, T., 2004. *Computer vision and image processing.* Basingstoke: Palgrave Macmillan.

Mühlmann, K., Maier, D., Hesser, J., and Männer, R., 2002. Calculating dense disparity maps from color stereo images, an efficient implementation. *International Journal of Computer Vision*, 47 (1/2/3), 79-88.

Müller, K., 2017. *Here: A Simpler Way to Find Your Files* [online]. Available from: https://CRAN.R-project.org/package=here [Accessed 20 January 2021].

Murasheva, V.V., Kainov, S.Y., Kovalenko, E.S., Podurets, K.M., Glazkov, V.P., Murashev, M.M., Chichaev, I.A., Presniakova, N.N., Tereschenko, E.Y., Retivov, V.M., and Yatsishina, E.B., 2021. 'Barbarian scepters' of the viking age from Chernaya Mogila burial mound at Chernigov (present-day Ukraine). *Journal of Archaeological Science: Reports*, 37, 102946.

Murphy, E.M., 2008. *Deviant burial in the archaeological record.* Oxford: Oxbow Books.

Museum of London Archaeology (MOLA), n.d. *Historic building recording* [online]. Available from: https://www.mola.org.uk/commercial/archaeological-fieldwork/historic-building-recording [Accessed 10 July 2019].

Nagaoka, T., and Uzawa, K., and Hirata, K., 2008. Weapon-related trauma of human skeletons from Yuigahama Chusei Shudan Bochi, Japan. *Anatomical Science International*, 84, 170-181.

Naranjo, J.M., Parrilla, Á., and de Sanjosé, J.J., 2018. Geometric characterization and interactive 3D visualization of historical and cultural heritage in the provinces of Cáceres (Spain). *Virtual Archaeology Review*, 9 (18), 1-11.

Navitainuck, D.U., Vach, W., Alt, K.W., and Schibler, J., 2021. Best practice for osteological sexing in forensics and bioarchaeology: The utility of combining metric and morphological traits from different anatomical regions. *International Journal of Osteoarchaeology*, 1-14.

Nawrocki, S.P.,2016. Forensic taphonomy. *In:* Blau, S. and Ubelaker, D.H., eds. *Handbook of forensic anthropology and archaeology.* 2nd edition. New York: Routledge, 373-390.

Newman, S.E., 2015. Applications of reflectance transformation imaging (RTI) to study of bone surface modifications. *Journal of Archaeological Science*, 53, 536-549

Nicklisch, N., Ramsthaler, F., Meller, H., Friederich, S., and Alt, K.W., 2017. The face of war: Trauma analysis of a mass grave from the battle of Lützen (1632). *PLoS ONE,* 12 (5), e01 178252, 1-30.

Nicolae, C., Nocerino, E., Menna, F., and Remondino, F., 2014. Photogrammetry applied to problematic artefacts. *The International Photogrammetry, Remote Sensing and Spatial Information Sciences,* XL-5, 451-456.

Nikon USA, 2019a. *DX series* [online]. Available from: https://www.nikonusa.com/en/nikon-products/dslr-cameras/dx.page [Accessed 16 July 2019].

Nikon USA, 2019b. *FX series full frame DSLR cameras* [online]. Available from: https://www.nikonusa.com/en/nikon-products/dslr-cameras/fx.page [Accessed 16 July 2019].

Nikon, 2020a. *DSLR Cameras* [online]. Available from: https://www.nikon.co.uk/en_GB/products/category_pages/digital_cameras/category_slr.page [Accessed 23 March 2020].

Nikon, 2020b. *AF-S Micro NIKKOR 60mm f/2.8G ED* [online]. Available from: https://www.nikon.co.uk/en_GB/product/nikkor-lenses/auto-focus-lenses/fx/single-focal-length/af-s-micro-nikkor-60mm-f-2-8g-ed [Accessed 23 March 2020].

Nikon, 2021a. *D5300* [online]. Available from: https://www.nikon.co.uk/en_GB/product/discontinued/digital-cameras/2020/d5300-red [Accessed 14 October 2021].

Nikon, 2021b. *D810* [online]. Available from https://www.nikon.co.uk/en_GB/product/discontinued/digital-cameras/2020/d810 [Accessed 14 October 2021].

Niven, L., Steele, T.E., Finke, H., Gernat, T., and Hublin, J.-J., 2009. Virtual skeletons: Using a structured light scanner to create a 3D faunal comparative collection. *Journal of Archaeological Science*, 36, 2018-2023.

Nocerino, E., Menna, F., and Remondino, F., 2014. Accuracy of typical photogrammetric networks in cultural heritage 3D modeling projects. *In:* Remondino, F. and Menna, F. eds. *The international archives of the photogrammetry, remote sensing and special information sciences volume XL-5, 2014 ISPRS technical commission V symposium*. Riva del Garda 23-25 June 2014. 465-472.

Nogueira, L., Quatrehomme, G., Bertrand, M-F., Rallon, C., Ceinos, R., du Jardin, P., Adalian, P., and Alunni, V., 2017. Comparison of macroscopic and microscopic (stereomicroscopy and scanning electron microscopy) features of bone lesions due to hatchet hacking trauma. *International Journal of Legal Medicine*, 131, 465-472.

Novak, S. 2000a. Battle-related trauma. *In:* Fiorato, V., Boylston, A., and Knüsel, C., eds. *Blood red roses*. 2nd edition. Oxford: Oxbow Books. 90-102.

Novak, S. 2000b. Case studies. *In:* Fiorato, V., Boylston, A., and Knüsel, C., eds. *Blood red roses*. 2nd edition. Oxford: Oxbow Books. 240-268.

Núñez, M.A., Buill, F., and Edo, M., 2013. 3D model of the Can Sadurní cave. *Journal of Archaeological Science,* 40, 4420-4428.

Obertová, Z., Leipner, A., Messina, C., Vanzulli, A., Fliss, B., Cattaneo, C., and Sconfienza, L.M., 2019. Postmortem imaging of perimortem skeletal trauma. *Forensic Science International*, 302, 109921.

Olson, B.R., Placchetti, R.A., Quartermaine, J., and Killebrew, A.E., 2013. The Tel Akko Total Archaeology Project (Akko, Israel): Assessing the suitability of multi-scale 3D field recording in archaeology. *Journal of Field Archaeology*, 38 (3), 244-262.

Omari, R., Hunt, C., Coumbaros, J., and Champman, B., 2021. Virtual anthropology? Reliability of three-dimensional photogrammetry as a forensic anthropology measurement and documentation technique. *International Journal of Legal Medicine*, 135, 939-950.

Oniga, E., Chirila, C., and Şutu, M., 2012. Terrestrial laser scanner surveying versus total station surveying for 3D building model generation. *Mathematical Modelling in Civil Engineering,* 4, 168-177.

Oniga, V.-E., Breaban, A.-I., and Statescu, F., 2018. Determining the optimum number of ground control points for obtaining high precision results based on UAS images. *Proceedings*, 2 (7), 352-362.

Opitz, R.S. 2013a. An overview of airborne and terrestrial laser scanning in archaeology. *In:* Opitz, R.S. and Cowley, D.C., eds. *Interpreting archaeological topography: Airborne laser scanning, 3D data and ground observation.* Oxford: Oxbow Books, 13-31.

Opitz, R.S. 2013b. Appendix: Key technical terms. *In:* Opitz, R.S. and Cowley, D.C., eds. *Interpreting archaeological topography: Airborne laser scanning, 3D data and ground observation.* Oxford: Oxbow Books, 266-268.

Opitz, R.S. and Cowley, D.C., 2013. Interpreting archaeological topography: lasers, 3D data, observation, visualisation and applications. *In:* Opitz, R.S. and Cowley, D.C., eds. *Interpreting archaeological topography: Airborne laser scanning, 3D data and ground observation.* Oxford: Oxbow Books, 1-12.

Osipov, B., Alaica, A.K., Pickard, C., Garcia-Donas, J.G., Márquez-Grant, N., and Kranioti, E.F., 2020. The effect of diet and socio-political change on physiological stress and behaviour in late roman-early byzantine (300-700 AD) and Islamic (902-1,235 AD) populations from Ibiza, Spain. *American Journal of Physical Anthropology,* 172 (2), 189-213.

Otárola-Castillo, E., Torquato, M.G., Hawkins, H.C., James, E., Harris, J.A., Marean, C.W., McPherron, S.P., and Thompson, J.C., 2018. Differentiating between cutting actions on bone using 3D geometric morphometrics and Bayesian analyses with implication to human evolution. *Journal of Archaeological Science*, 89, 56-67.

Ousley, S.D. and Jantz, R.L. 2012. Fordisc 3 and statistical methods for estimating sex and ancestry. *In:* Dirkmaat, D.C. ed. *A companion to forensic anthropology*. Malden: Wiley-Blackwell, 311-329.

Over, J.R., Ritchie, A.C., Kranenburg, C.J., Brown, J.A., Buscombe, D., Noble, T., Sherwood, C.R., Warrick, J.A., and Wernette, P.A., 2021. *Processing coastal imagery with Agisoft Metashape Professional Edition, version 1.6— Structure from motion workflow documentation*. Reston: U.S. Geological Survey (USGS). 2021–1039.

Oxford Archaeology Ltd., 2019. *Archaeological survey* [online]. Available from: https://www.oxfordarchaeology.com/archaeology-and-heritage/fieldwork/survey [Accessed 10 July 2019].

Ozdemir, H., Sampson, C.C., de Almeida, G.A.M. and Bates, P.D., 2013. Evaluating scale and roughness effects in urban flood modelling using terrestrial LIDAR data. *Hydrology and Earth System Sciences*, 17, 4015-4030.

Palamenghi, A., Cinti, A., Mann, R.W., Viano, G., Girotti, M., Garanzini, F., Fulcheri, E., and Boano, R., 2020. The supracondylar process in subadult skeletal remains from northern Italy ($15^{th}$-$18^{th}$ century A.D.). *International Journal of Osteoarchaeology,* 30 (4), 575-579.

Palomeque-González, J.F., Maté-González, M.Á., Yravedra, J., Juan-Blazquez, M.S., García Vargas, E., Martín-Perea, D.M., Estaca-Gómez, V., González-Aguilara, D., and Domínguez-Rodrigo, M., 2017. Pandora: A new morphometric and statistical software for analysing and distinguishing cut marks on bones. *Journal of Archaeological Science: Reports*, 13, 60-66.

Papworth, H., Ford, A., Welham, K., and Thackray, D. 2016. Assessing 3D metric data of digital surface models for extracting archaeological data from Archive stereo-aerial photographs. *Journal of Archaeological Science*, 72, 85-104.

Pavlidis, G., Koutsoudis, A., Arnaoutoglou, F., Tsioukas, V., Chamzas, C., 2007. Methods for 3D digitization of cultural heritage. *Journal of Cultural Heritage*, 8, 93-98.

Pearson, K., 1900. X. On the criterion that a given system of deviations from the probable case of a correlated system of variables is such that it can be reasonably supposed to have arisen from random sampling. *The London, Edinburgh, and Dublin Philosophical Magazine and Journal of Science*, 50 (302), 157-175.

Pearson, K., 1901. LIII On lines and planes of closest fit to systems of points in space. *The London, Edinburgh, and Dublin Philosophical Magazine and Journal of Science,* 2 (11), 559-572.

Pechníková, M, Drozdová, E, and Čižmář, Z. 2009. Decapitations in the medieval hospital cemetery from Znojmo, Czech Republic. *Anthropologie*, 47 (3), 265-271.

Pechníková, M., Porta, D., and Cattaneo, C., 2011. Distinguishing between perimortem and postmortem fractures: are osteons of any help?. *International Journal of Legal Medicine*, 125, 591-595.

Pedersen, A., 2008 Viking weaponry. *In:* Brink, S. and Price, N.S., eds. *The Viking world*. Abingdon: Routledge, 204-211.

Peng, F., Lin, S.C., Guo, J., Wang, H., and Gao, X., 2017. The application of SfM photogrammetry software for extracting artefact provenience from palaeolithic excavation surfaces. *Journal of Field Archaeology*, 42 (2), 326-336.

Petersen, J., 1919. *De norske vikingesverd, en typologisk-kronologisk studier over vikingetidens vaaben*. Kristiania: I kommission hos J Dybwad.

Pinheiro, J., Cunha, E., and Symes, S., 2015. Over-interpretation of bone injuries and implications for cause and manner of death. *In:* Passalacqua, N.V. and Rainwater, C.W., eds. *Skeletal trauma analysis: case studies in context* [online]. Chichester: John Wiley & Sons, Ltd., 27-41.

Pitts, M., Bayliss, A., McKinley, J., Boylston, A., Budd, P., Evans, J., Chenery, C., Reynolds, A., and Semple, S., 2002. An Anglo-Saxon decapitation and burial at Stonehenge. *Wiltshire Archaeological & Natural History Magazine,* 95, 131-146.

Plets, G., Verhoeven, G., Cheremisin, D., Plets, R., Bourgeois, J., Stichelbaut, B., Gheyle, W., and De Reu, J., 2012. The deteriorating preservation of the Altai rock art: Assessing the three-dimensional image-based modelling in rock art research and management. *Rock Art Research*, 29 (2), 139-156.

Pollard, A.M., Ditchfield, P., Piva, E., Wallis, S., Falys, C., and Ford, S., 2012. 'Sprouting like cockles amongst the wheat': The St Brice's Day massacre and the isotopic analysis of the human bones from St John's College, Oxford. *Oxford Journal of Archaeology,* 31 (1), 83-102.

Pope, M.H., and Outwater, J.O. 1972. The fracture characteristics of bone substance. *Journal of biomechanics*, 5, 457-465.

Praxmarer, E.-M., Tutkuviene, J., and Kirchengast, S., 2020. Metric and morphological analysis of pelvic scars in a historical sample from Lithuania: Associations with sex, age, body size and pelvic dimensions. *International Journal of Osteoarchaeology*, 30 (5), 629-641.

Price, N., 2008. Dying and the dead: Viking age mortuary behaviour. *In:* Brink, S. and Price, N.S., eds. *The Viking world*. Abingdon: Routledge, 257-274.

Price, T.D., Frei, K.M., Dobat, A.S., Lynnerup, N., and Bennike, P., 2011. Who was in Harold Bluetooth's army? Strontium isotope investigation of the cemetery at the Viking age fortress at Trelleborg, Denmark. *Antiquity,* 85, 476-489.

Proficio, A., Bellucci, L., Buzi, C., Di Vincenzo, F., Micarelli, I., Strani, F., Tafuri, M.A., and Manzi, G., 2018. Virtual anthropology and its application in cultural heritage studies. *Studies in Conservation*, 64 (6), 323-336.

QGIS.org, 2021a. *QGIS geographic information systems*. Version 3.16 [ computer programme]. QGIS Association.

QGIS.org, 2021b. QGIS 3.16. Geographic Information System User Guide. QGIS Association. Electronic document: https://docs.qgis.org/3.16/en/docs/user_manual/index.html [Accessed on 2 May 2021].

Quatrehomme, G. and Alunni, V. 2019. The link between traumatic injury in soft and hard tissue. *Forensic science* international, 301, 118-128.

R Core Team, 2020. *R: A language and environment for statistical computing*. Version 3.6.3 [computer programme]. Vienna: R Foundation for Statistical Computing.

Racette, S., Kremer, C., Desjarlais, A., and Sauvageau, A., 2008. Suicidal and homicidal sharp force injury: A 5-year retrospective comparative study of hesitation marks and defense wounds. *Forensic Science, Medicine, aAnd Pathology*, 4, 221-227.

Raffield, B., 2020. The Danelaw reconsidered: Colonization and conflict in Viking-age England. *Viking and Medieval Scandinavia*, 16, 181-220.

Raffield, B., Greenlow, C., Price, N., and Collard, M., 2015. Ingroup identification, identity fusion and the formation of Viking war bands. *World Archaeology*, 48 (1), 35-50.

Raimundo, P.O., Apaza-Agüero, K., and Apolinário Jr, A.L., 2018. Low-cost 3D reconstruction of cultural heritage artifacts. *Revista Brasileria de Computação Aplicada*, 10 (1), 66-75.

Rao, D., 2015. An autopsy study of 74 cases of cut throat injuries. *Egyptian Journal of Forensic Sciences,* 5, 144-149.

Raoult, V., Reid-Anderson, S., Ferri, A., and Williamson, J.E. 2017. How reliable is structure from motion (SfM) over time and between observers? A case study using coral reef bommies. *Remote Sensing*, 9 (7), 1-15.

Rasband, W.S., 2015. *ImageJ*. 2.0.0 [computer programme]. Bethesda: U.S. National Institutes of Health.

Rathmann, H., Stoyanov, R., and Posamentir, R., 2021. Comparing individuals burial in flexed and extended positions at the Greek colony of chersonesos (crimea) using cranial metric, dental metric, and dental nonmetric traits. *International Journal of Osteoarchaeology*, 1-15.

Redfern, R.C., 2017. Identifying and interpreting domestic violence in archaeological human remains: A critical review of the evidence. *International Journal of Osteoarchaeology*, 27, 13-34.

Reichs, K.J., 1998. *Forensic osteology: Advances in the identification of human remains*. 2nd edition. Springfield: Charles C Thomas Publisher, Ltd

Reimer, P.J., Bard, E., Bayliss, A., Beck, J.W., Blackwell, P.G., Bronk Ramsey, C., Brown, D.M., Buck, C.E., Edwards, R.L., Friedrich, M., Grootes, P.M., Guilderson, T.P., Haflidason, H., Hajdas, I., Hatté, C., Heaton, T.J., Hogg, A.G., Hughen, K.A., Kaiser, K.F., Kromer, B., Manning, S.M., Reimer, R.W., Richards, D.A., Scott, E.M., Southon, J.R., Turney, C.S.M., van der Plicht, J., 2013. Selection and treatment of data for radiocarbon calibration: An update to the international calibration (IntCal) criteria. *Radiocarbon*, 55 (4), 1923-1945.

Remondino, F. and El-Hakim, S., 2006. Image-based 3D modelling: A review. *The Photogrammetric Record*, 21 (115), 269-291.

Remondino, F., 2011. Heritage recording and 3D modelling with photogrammetry and 3D scanning. *Remote Sensing*, 3, 1104-1138.

Remondino, F., Spera, M.G., Nocerino, E., Menna, F., and Nex, F., 2014. State of the art in high density image matching. *The Photogrammetric Record,* 29 (146), 144-166.

Remondino, F., Spera, M.G., Nocerino, E., Menna, F., Nex, F., and Gonizzi-Barsanti, S., 2013. Dense image matching: Comparison and analyses. *In: In:* Institute of Electrical and Electronics Engineering (IEEE) ed. *2013 digital heritage international congress (DigitalHeritage)*. Marseille 28 October-1 November 2013. 47-54.

Reynolds, A., 2009. Anglo-Saxon deviant burial customs. Oxford: Oxford University Press.

Richards, J.D., 2000. *Viking age England.* Stroud: Tempus Publishing Ltd.

Richards, J.D., 2002. The case of the missing Vikings: Scandinavian burial in the Danelaw. *In:* Lucy, S. and Reynolds, A. eds. *Burial in early medieval England and Wales. Society of medieval archaeology monograph, vol 17.* London: Society for Medieval Archaeology, 156-170.

Richards, J.D., 2008. Viking settlement in England. *In:* Brink, S. and Price, N.S., eds. *The Viking world*. Abingdon: Routledge, 368-374.

Richards, J.D., Beswick, P., Jecock, M., McKinley, J., Rowland, S., and Worley, F., 2004. Excavations at the Viking barrow cemetery at Heath Wood, Ingleby, Derbyshire. *The Antiquaries Journal*, 23-116.

Riisøy, A.I., 2015. Deviant burials: Societal exclusion of dead outlaws in medieval Norway. *In:* Korpiola, M. and Lahtinen, A., eds. *Cultures of death and dying in medieval and early modern Europe. Studies across disciplines in the humanities* *and social sciences 18*. Helsinki: Helsinki Collegium for Advanced Studies, 49-81.

Riley, S.J., DeGloria, S.D., and Elliot, R., 1999. A terrain ruggedness index that quantifies topographic heterogeneity. *Intermountain Journal of Sciences*, 5 (1-4), 23-27.

Robb, J. 2016. What can we really say about skeletal part representation, MNI and funerary ritual: A simulation approach. *Journal of Archaeological Science: Reports*, 10, 684-692.

Roberts, C. 2000. Trauma in biocultural perspective: Past, present and future works in Britain. *In:* Cox, M., and Mays, S., eds. *Human osteology in archaeology for forensic science*. London: Greenwich Medical Media Ltd., 337-356.

Robleda Prieto, G. and Perez Ramos, A., 2015. Modeling and accuracy assessment for 3D-virtual reconstruction in cultural heritage using low-cost photogrammetry: Surveying of the “Santa María Azogue” church’s front. *In:* González-Aguilera, D., Remondino, F., Boehm, J., Kersten, T., and Fuse, T. *International archives of the photogrammetry, remote sensing & spatial information sciences XL-5/W4, 2015 3D virtual reconstruction and visualisation of complex architectures*, Avila 25-27 February 2015. 263-270.

Rodríguez-Martín, M., Rodríguez-Gonzálvez, P., Lagüela, S., and Gonzálvez-Alguilera, D., 2016. Macro-photogrammetry as a tool for the accurate measurement of three-dimensional misalignment in welding. *Automation in Construction*, 71, 189-197.

Roffey, S. and Lavelle, R., 2016. West Saxons and Danes: Negotiating early medieval identities. *In:* Lavelle, R. and Roffey, S., eds. *Danes in Wessex: The Scandinavian impact on southern England, c.800-c.1100.* Oxford: Oxbow Books, 7-34.

Roos, P.E., Vasavada, A., Zheng, L., and Zhou, X. 2020. Neck musculoskeletal model generation through anthropometric scaling. *PLoS ONE*, 15(1), e0219954.

Rouse, D.A., 1994. Pattern of stab wounds: A six year study. *Medicine, Science, and the Law,* 34 (1), 67-71.

Rozendaal, A.S., Scott, S., Peckmann, T.R., and Meek, S., 2020. Estimating sex from the seven cervical vertebrae: An analysis of two European skeletal populations. *Forensic Science International*, 306, 110072.

RStudio Team, 2021. *RStudio: Integrated development for R*. 1.4.1103 [computer programme]. Boston: RStudio, PBC.

Ruff, C., Holt, B., and Trinkaus, E., 2006. Who's afraid of the big bad Wolff?: "Wolff's law" and bone functional adaptations. *American Journal of Physical Anthropology*, 129 (4), 484-498.

Sanger, M.C., 2015. Determining depositional events within shell deposits using computer vision and photogrammetry. *Journal of Archaeological Science*, 53, 482-491.

Sanz-Ablanedo, E., Chandler, J.H., Rodríguez-Pérez, J.R., and Ordóñez, C., 2018. Accuracy of unmanned aerial vehicle (UAV) and SfM photogrammetry survey as a function of the number and location of ground control points used. *Remote Sensing*, 10 (10), 1606.

Sapirstein, P. and Murray, S., 2017. Establishing best practices for photogrammetric recording during archaeological fieldwork. *Journal of Field Archaeology*, 42 (4), 337-350.

Sapirstein, P., 2016. Accurate measurements with photogrammetry at large sites. *Journal of Archaeological Science*, 66, 137-145.

Sapirstein, P., 2018. A high-precision photogrammetric recording system for small artifacts. *Journal of Cultural Heritage,* 31, 33-45.

Sauer, N.J., 1998. The timing of injuries and the manner of death: Distinguishing among antemortem, perimortem, and postmortem trauma. *In:* Reichs, K.J., ed. *Forensic osteology: Advances in the identification of human remains*. 2nd edition. Springfield: Charles C Thomas Publisher, Ltd., 321-332.

Schaich, M. 2013. Combined 3D Scanning and Photogrammetry Surveys with 3D Database Support for Archaeology & Cultural Heritage. A Practice Report on ArcTron's Information System aSPECT3D*. In:* Fritsch, D., ed. *Photogrammetric week '13*. Stuttgart 9-13 September 2013. Berlin und Offenbach: Wichmann Verlag, VDE Verlag GmbH, 233-246.

Schoenberg, I.J., 1969. Cardinal interpolation and spline functions. *Journal of Approximation Theory*, 2, 167-206.

Scientific Working Group for Forensic Anthropology (SWGANTH), 2011. *Trauma analysis* [online]. Available from: https://www.nist.gov/system/files/documents/2018/03/13/swganth_trauma.pdf [Accessed 26 November 2018].

Šedina, J., Pavelka, K., and Housarová, E., 2016. Archaeological documentation of a defunct Iraqi town. *The International Archives of Photogrammetry, Remote Sensing and Spatial Information Sciences*, 41, 1031-1035.

Seitz, S.M., Curless, B., Diebel, J., Scharstein, D., and Szeliski, R., 2006. A comparison and evaluation of multi-view stereo reconstruction algorithms. *In:* Institute of Electrical and Electronics Engineering (IEEE) ed. *2006 IEEE computer society conference on computer vision and pattern recognition (CVPR'06)*, New York 17-22 June 2006. 519-528.

Semple, S., 1998. A fear of the past: The place of the prehistoric burial mound in the ideology of middle and later Anglo-Saxon England. *World Archaeology*, 30 (1), 109-126.

Senthilkumaran, N. and Rajesh, R., 2009. Edge detection techniques for image segmentation – A survey of soft computing approaches. *International Journal of Recent Trends in Engineering,* 1 (2), 250-254.

Shapiro, S.S. and Wilk, M.B., 1965. An analysis of variance test for normality (complete samples). *Biometrika*, 52 (3-4), 591-611.

Shepard, A. 1968. Two-dimensional interpolation function for irregularly-spaced data. *In:* Blue, R.B. and Rosenberg, R.M., eds. *Proceedings of the 1968 ACM national conference*, 27-29 August 1968. New York: Association for Computing Machinery. 517–524.

Short, W.R. 2014. *Viking weapons and combat techniques*. Yardley: Westhome Publishing

Shott, M., 2014. Digitizing archaeology: A subtle revolution in analysis. *World Archaeology*, 46 (1), 1-9.

Siapno, A.E.D., Yim B.C., Daniels, D., Bolagani, A., Kwan, L., Walker, D., Aninwene, G.E. II, Eleswarapu, S., Joshi, S.H., and Sturm, R.M., 2020. Measuring accuracy of 3-dimensional mapping technologies versus standard goniometry for angle assessment. *Journal of Pediatric Urology*, 16, 547-554.

Silvester, C.M. and Hillson, S. 2020. A critical assessment of the potential for Structure-from Motion photogrammetry to produce high fidelity 3D dental models. *American Journal of Physical Anthropology*, 173, 381-392.

Sîrbu, V., Ritual inhumations and 'deposits' of children among the Geto-Dacians. *In:* Murphy, E.M., ed. *Deviant burial in the archaeological record.* Oxford: Oxbow Books, 71-90.

Šlaus, M., Novak, M., Bedić, Ž., and Strinović, D., 2012. Bone fractures as indicators of intentional violence in the eastern Adriatic from the antique to the late medieval period (2$^{nd}$-16$^{th}$ century AD). *American Journal of Physical Anthropology*, 149, 26-38.

Šlaus, M., Novak, M., Vyroubal, V., and Bedić, Ž., 2010. The harsh life on the 15th century Croatia-ottoman empire military border: Analysing and identifying the reasons for the massacre in Čepin. *American Journal of Physical Anthropology*, 141, 358-372.

Sledzik, P.S. and Bellantoni, N., 1994. Brief communication: Bioarchaeological and biocultural evidence for the New England vampire folk belief. *American Journal of Physical Anthropology*, 94, 269-274.

Smith, D.E.M., Humphrey, L.T., and Cardoso, H.F.V., 2021. Age estimation of immature human skeletal remains from mandibular and cranial bone dimensions in the post-natal period. *Forensic Science International*, 327, 110943.

Smith, M.J. and Brickley, M.B., 2004. Analysis and interpretation of flint toolmarks found in bones from West Tump Long Barrow, Gloucestershire. *International Journal of Osteoarchaeology*, 14, 18-33.

Smith, M.W., 2014. Roughness in the earth sciences. *Earth-Science Reviews*, 136, 202-225.

Snavely, N., Seitz, S.M., and Szeliski, R., 2006. Photo tourism: exploring photo collections in 3D. *ACM Transactions on Graphics (TOG)*, 25 (3) 835-846.

Snavely, N., Seitz, S.M., and Szeliski, R., 2008. Modeling the world from internet photo collections. *International Journal of Computer Vision*, 80 (2), 189-210.

Solarino, B., Punzi, G., Di Vella, G., Carabellese, F., and Catanesi, R. 2019. A multidisciplinary approach in overkill: Analysis of 13 cases and review of the literature. *Forensic Science International*, 298, 402-407.

Spearman, C., 1904. The proof and measurement of association between two things. *The American Journal of Psychology*, 15 (1), 72-101.

Speed, G. and Walton Rogers, P., 2004. A burial of a Viking woman at Adwick-le-Street, South Yorkshire. *Medieval Archaeology,* 48 (1), 51-90.

Sperling, C.H.B., Goudie, A.S., Stoddart, D.R., and Poole, G.G. 1977. Dolines of the Dorset chalklands and other areas in southern Britain. *Transactions of the Institute of British Geographers,* 2 (2), 205-223.

Squires, K., Errickson, D., and Marquez-Grant, N., 2019. *Ethical approaches to human remains: A global challenge in bioarchaeology and forensic anthropology*. Cham: Springer.

Stroud, G., and Kemp, R.L., 1993. *Cemeteries of St. Andrew, Fishergate. In:* Addyman, P.V. and Kinsler, V., eds. The archaeology of York 12(2). York: Council for British Archaeology, 121-294.

Sutton, M.D., Rahman, I.A., and Garwood, R.J., 2014. *Techniques for virtual palaeontology.* Chichester: John Wiley & Sons, Ltd.

Swanton, M. 1996. *The anglo-saxon chronicle.* London: J.M. Dent.

Symes, S.A., Berryman, H.E., and Smith, O.C., 1998. Saw marks in bone: Introduction and examination of residual kerf contour. *In:* Reichs, K.J., ed. *Forensic osteology: Advances in the identification of human remains*. 2nd edition. Springfield: Charles C Thomas Publisher, Ltd., 389-409.

Symes, S.A., L'Abbé, E.N., Chapman, E.N., and Dirkmaat, D.C., 2012. Interpreting traumatic injury to bone in medicolegal investigations. *In:* Dirkmaat, D.C. ed. *A companion to forensic anthropology*. Malden: Wiley-Blackwell, 340-389.

Symes, S.A., L'Abbé, E.N., Stull, K.E., LaCroix, M., and Pokines, J.T., 2014. Taphonomy and the timing of bone fractures in trauma analysis. *In:* Pokines, J.T. and Symes, S.A., eds. *Manual of forensic taphonomy*. Boca Raton: CRC Press

Symes, S.A., Williams, J.A., Murray, E.A., Hoffman, J.M., Holland, T.D., Saul, J.M., Saul, F.P., and Pope, E.J., 2001. Taphonomic context of sharp-force trauma in suspected cases of human mutilation and dismemberment. *In:* Haglund, W.D. and Sorg, M.H., eds. *Advances in forensic taphonomy: Method, theory, and archaeological perspective*. Boca Raton: Taylor & Francis Group.

Ta'ala, S.C., Berg, G.E., and Haden, K., 2006. Blunt force cranial trauma in the Cambodian killing fields. *Journal of Forensic Sciences*, 51(5), 996-1001.

Tamminen, H.M., Ford, A., Welham, K., and Smith, M.J., 2019. Vikings go digital: Using the Ridgeway mass burial to investigate skeletal injuries in three dimensions. *Proceedings of the Dorset Natural History & Archaeology Society*, 140, 81-84

Taylor, A., Aspects of deviant burial in roman Britain. *In:* Murphy, E.M., ed. *Deviant burial in the archaeological record.* Oxford: Oxbow Books, 91-114.

Telmon, N., Gaston, A., Chemla, P., Blanc, A., Joffre, F., and Rougé, D., 2005. Application of the Suchey-Brooks method to three-dimensional imaging of the pubic symphysis. *Journal of Forensic Science*, 50 (3), 1-6.

Thali, M.J., Taubenreuther, U., Karolczak, M., Braun, M., Brueschweiler, W., Kalender, W.A., and Dirnhofer, R., 2003. Forensic microradiology: Micro-computed tomography (Micro-CT) and analysis of patterned injuries inside of bone. *Journal of Forensic Sciences*, 48 (6), 1336-1342.

Thiele, A., Hošek, J., Kucypera, P., and Dévényi, L., 2015. The role of pattern-welding in historical swords – Mechanical testing of materials used in their manufacture. *Archaeometry*, 57 (4), 720-739.

Thomas, R., Dyer, G.S.M., Tornetta III, P., Park, H., Gujrathi, R., Gosangi, B., Lebovic, J., Hassan, N., Seltzer, S.E., Rexrode, K.M., Boland, G.W., Harris, M.B., and Khurana, B., 2021. Upper extremity injuries in the victims of intimate partner violence. *European Radiology*, 31, 5713-5720.

Thompson, T.J.U. and Inglis, J., 2009. Differentiation of serrated and non-serrated blades from stab marks in bone. *International Journal of Legal Medicine,* 123, 129-135.

Thordeman, B., Nörlund, P., and Ingelmark, B.E., 1939. *Armour from the Battle of Wisby, 1361*. Stockholm: Almqvist and Wiksell.

Timbrell, L. and Plomp, K.A., 2019. Using the shape of the basicranial portion of the temporal bones to distinguish between relatively closely-related human populations. *Journal of Archaeological Science: Reports*, 26, 101885.

Trizio, I, Savini, F., and Giannangeli, A., 2018. Integration of three-dimensional digital models and 3D GIS: The documentation of the medieval burials of amiternum (L'Aquila, Italy). *In:* Remondino, F., Toschi, I., and Fuse, T. eds. *International Archives of the Photogrammetry, Remote Sensing & Spatial Information Sciences volume XLII-2, 2018, ISPRS II mid-term symposium "towards photogrammetry 2020"*. Riva del Garda, 4-7 June 2018. 1121-1128.

Trojan, C., Salfati, C.G., and Schanz, K., 2019. Overkill, we known it when we see it: Examining definitions of excessive injury in homicide research. *Journal of Criminal Psychology*, 9 (2), 61-74.

Tsaliki, A., 2008. Unusual burials and necrophobia: An insight into the burial archaeology of fear. *In:* Murphy, E.M., ed. *Deviant burial in the archaeological record.* Oxford: Oxbow Books, 1-16.

Tucker, B.K., Hutchinson, D.L., Gilliland, M.F.G., Charles, T.M., Daniel, H.J., and Wolfe, L.D., 2001. Microscopic characteristics of hacking trauma. *Journal of Forensic Sciences,* 46 (2), 234-240.

Tucker, K., 2013. The osteology of decapitation burials from roman Britain: A post-mortem burial rite?. *In:* Knüsel, C. and Smith, M.J., eds. *The routledge handbook of the bioarchaeology of human conflict*. London: Routledge, 213-236.

Tumler, D., Paladin, A., and Zink, A., 2019. Perimortem sharp force trauma in an individual from the early medieval cemetery of Säben-Sabiona in South Tyrol, Italy. *International Journal of Paleopathology,* 27, 46-55.

U.S. Geological Survey (USGS), 2016. *Unmanned aircraft systems data post-processing* [online]. Available from: https://training.fws.gov/courses/references/tutorials/geospatial/CSP7304/2016documents/HandsOn_Afternoon/UAS/UAS%20II%20Post%20Processing/PhotoScan%20Processing%20Procedures%20DSLR%20Feb%202016.pdf [Accessed 16 October 2018]. (N.B. information tabulated at https://edisciplinas.usp.br/pluginfile.php/5729272/mod_resource/content/0/USGS%20PhotoScan%20Workflow%20-%20advanced.pdf)

Ubelaker, D.H. and Montaperto, K.M., 2013. Trauma interpretation in the context of biological anthropology. *In:* Knüsel, C. and Smith, M.J., eds. *The routledge handbook of the bioarchaeology of human conflict*. London: Routledge, 25-38.

Ubelaker, D.H., Cordero, Q.R., Wu, Y., and Linton, N.F., 2020. Anthropological analysis of trauma in throat bone and cartilage: A review. *Forensic Science International: Synergy*, 2, 224-229.

Uldin, T., 2017. Virtual anthropology – A brief review of the literature and history of computed tomography. *Forensic Sciences Research*, 2 (4), 165-173.

Underwood, R., 1999. *Anglo-Saxon weapons & warfare.* Stroud: Tempus Publishing Limited.

Urbanová, P., Hejna, P., Jurda, M., 2015. Testing photogrammetry-based techniques for three-dimensional surface documentation in forensic pathology. *Forensic Science International*, 250, 77-86.

Vacca G. 2019. Overview of open source software for close range photogrammetry. *In:* Brovelli, M.A. and Marin, A.F. eds. *The international archives of the photogrammetry, remote sensing and spatial information sciences volume XLII-4/W14, FOSS4G 2019 academic track.* Bucharest 26-30 August 2019. 239-245.

Valoriani, S., Eliopoulos, C., and Borrini, M., 2017. Sharp force trauma death in a young individual from medieval Gloucester. *American Journal of Forensic Medicine and Pathology,* 38, 111-114.

Vasavada, A.N., Danaraj, J., and Siegmund, G.P. 2008. Head and neck anthropometry, vertebral geometry and neck strength in height-matched men and women. *Journal of Biomechanics,* 41, 114-121.

Vazzana, A., Scalise, L.M., Traversari, M., Figus, C., Apicella, S.A., Buti, L., Oxilia, G., Sorrentino, R., Pellegrini, S., Matteucci, C., Calcagnile, L., Savigni, R., Feeney, R.N.M., Gruppioni, G., and Benazzi, S., 2018. A multianalytic investigation of weapon-related injuries in a late antiquity necropolis, Mutina, Italy. *Journal of Archaeological Science: Reports,* 17, 550-559.

Verhoeven, G., 2011. Taking computer vision aloft – Archaeological three-dimensional reconstructions from aerial photographs with PhotoScan. *Archaeological Prospection*, 18, 67-73.

Verhoeven, G., Taelman, D., and Vermeulen, F., 2012. Computer vision-based orthophoto mapping of complex archaeological sites: The ancient quarry of Pitaranha (Portugal-Spain). *Archaeometry*, 54 (6), 1114-1129.

Versi, E. 1992. "Gold standard" is an appropriate term. *The British Medical Journal (BMJ)*, 305, 187.

Viciano, J., Tanga, C., D'Anastasio, R., Belcastro, M.G., and Capasso, L., 2021. Sex estimation by odontometrics of nonadult human remains from a contemporary Italian sample. *American Journal of Physical Anthropology*, 175 (1), 59-80.

Villa, C., 2017. Forensic 3D documentation of skin injuries. *International Journal of Legal Medicine*, 131, 751-759

Villa, C., Buckberry, J., and Lynnerup, N., 2016. Evaluating osteological ageing from digital data. *Journal of Anatomy*, 235 (2), 386-395.

Voormolen, D.C., Polinder, S., von Steinbuechel, N., Vos, P.E., Cnossen, M.C., and Haagsma, J.A. 2019. The association between post-concussion symptoms and health-related quality of life in patients with mild traumatic brain injury. *Injury*, 50, 1068-1074.

Vosselman, G., and Maas, H.-G., 2010. *Airborne and terrestrial laser scanning*. Dunbeath: Whittles Publishing.

Wacker, S., Gröbner, J., Zysset, C., Diener, L., Tzoumanikas, P., Kazantzidis, A., Vuilleumier, L., Stöckli, R., Nyeki, S. and Kämpfer, N., 2015. Cloud observations in Switzerland using hemispherical sky cameras. *Journal of Geophysical Research: Atmospheres*, 120 (2), 695-707.

Wadsworth, J., 2015. Archeometallurgy related to swords. *Materials Characterization*, 99, 1-7.

Wakely, J., Limits to interpretation of skeletal trauma – Two case studies from medieval Abingdon, England. *International Journal of Osteoarchaeology,* 6, 76-83.

Waldron, T., Legalized trauma. *International Journal of Osteoarchaeology*, 6, 114-118.

Walsh, T. 2018. Fuzzy gold standards: Approaches to handling an imperfect reference standard. *Journal of Dentistry*, 74, S47-S49.

Walton, S., 1995. Words of technological virtue: “The battle of Brunanburh” and Anglo-Saxon sword manufacture. *Technology and Culture,* 36 (4), 987-999.

Ward-Perkins, B., 2000. Why did the Anglo-Saxons not become more British?. *The English Historical Review*, 155 (462), 513-533.

Weber, M., Banaschak, S., and Rothschild, M.A., 2021. Sharp force trauma with two katana swords: Identifying the murder weapon by comparing tool marks on the skull bone. *International Journal of Legal Medicine*, 135, 313-322.

Wenham 1989. Anatomical interpretations of Anglo-Saxon weapon injuries. *In:* Hawkes, S.C. ed. *Weapons and warfare in Anglo-Saxon England*. Oxford: Oxford University

Wessex Archaeology, n.d. *Photogrammetry* [online]. Available from: https://www.wessexarch.co.uk/archaeological-services/photogrammetry [Accessed 10 July 2019]

Westoby, M.J., Brasington, J., Glasser, N.F., Hambrey, M.J., and Reynolds, J.M., 2012. ‘Structure-from-motion’ photogrammetry: A low-cost, effective tool for geoscience applications. *Geomorphology*, 179, 300-314.

Wheatley, B.P., 2008. Perimortem or postmortem bone fractures? An experimental study of fracture patterns in deer femora. *Journal of Forensic Sciences*, 53 (1), 69-72.

White, T.D. and Folkens, P.A., 2005.*The human bone manual*. Burlington Elsevier Academic Press.

Wickham, H., Averick, M., Bryan, J., Chang, W., McGowan, L.D., François, R., Grolemund, G., Hayes, A., Henry, L., Hester, J., Kuhn, M., Pedersen, T.L., Miller, E., Bache, S.M., Müller, K., Ooms, J., Robinson, D., Seidel, D.P., Spinu, V., Takahashi, K., Vaughan, D., Wilke, C., Woo, K., and Yutani, H., 2019. Welcome to the tidyverse. *Journal of Open Source Software*, 4 (43), 1686.

Wieburg, D.A.M. and Wescott, D.J., 2008. Estimating the timing of long bone fractures: Correlation between the postmortem interval, bone moisture content, and blunt force trauma fracture characteristics. *Journal of Forensic Sciences,* 53 (5), 1028-1034.

Wilcoxon, F., 1945. Individual comparisons by ranking methods. *Biometrics Bulletin,* 1 (6), 80-83.

Williams, A., 1986. ‘Cockles amongst the wheat’: Danes and English in the western midlands in the first half of the eleventh century. *Midland History,* 11 (1), 1-22.

Williams, A., 2007. Crucible steel in medieval swords. *In:* La Niece, S., Hook, D.R., and Craddock, P.T., eds. *Metals and mines: Studies in archaeometallurgy*. London: Archetype Publications.

Williams, A., 2009. A metallurgical study if some Viking swords. *Gladius*, 29, 121-184.

Williams, A., 2011. A note on the analysis of Viking swords. *Gladius*, 31, 207-210.

Williams, A., 2012. *The sword and the crucible: A history of the metallurgy of European swords up to the 16th century.* Leiden: Koninklijke Brill NV.

Williams, A., 2016a. A place in the country: Orc of Abbotsbury and Tole of Tolepuddle, Dorset. *In:* Lavelle, R. and Roffey, S., eds. *Danes in Wessex: The Scandinavian impact on southern England, c.800-c.1100.* Oxford: Oxbow Books, 158-171.

Williams, A., 2016b. Thorkell the tall and the bubble reputation: The vicissitudes of fame. *In:* Lavelle, R. and Roffey, S., eds. *Danes in Wessex: The Scandinavian impact on southern England, c.800-c.1100.* Oxford: Oxbow Books, 144-157.

Williams, A.R., 1977. Methods of manufacture of swords in medieval Europe: Illustrated by the metallography of some examples. *Gladius*, 13, 75-101.

Williams, G., 2008. Raiding and warfare. *In:* Brink, S. and Price, N.S., eds. *The Viking world*. Abingdon: Routledge, 193-204.

Williams, G., 2014. Weapons and armour. *In:* Loe, L., Boyle, A., Webb, H., and Score, D., eds. *‘Given to the Ground’: A Viking age mass grave on Ridgeway Hill, Weymouth.* Dorset natural history and archaeological society monograph series no. 22. Dorchester: Dorset Natural History and Archaeological Society, 214-224.

Williams, T.J.T., 2015. Landscape and warfare in Anglo-Saxon England and the Viking campaign of 1006. *Early Medieval Europe*, 23 (3), 329-359.

Williams, T.J.T., 2016c. The place of slaughter: Exploring the West Saxon battlescape. *In:* Lavelle, R. and Roffey, S., eds. *Danes in Wessex: The Scandinavian impact on southern England, c.800-c.1100.* Oxford: Oxbow Books, 56-69.

Willmott, H., Townend, P., Mahoney Swales, D., Poinar, H., Eaton, K., and Klunk, J., 2020. A black death mass grave at Thornton Abbey: the discovery and examination of a fourteenth-century rural catastrophe. *Antiquity*, 94 (373), 179-196.

Wilson, A. 2014, *Digitised diseases* [online]. Available from: http://www.digitiseddiseases.org/alpha/ [Accessed 20 November 2018].

Wilson, D.M., 1965. Some neglected late Anglo-Saxon swords. *Medieval archaeology,* 9 (1), 32-54.

Wilson, D.M., 2008. The earliest Vikings in Man. *In:* Wilson, D.M., ed. *The Vikings in the isle of man.* Aarhus: Aarhus University Press, 25-56*.*

Wilson, L.A.B., De Groote, I., and Humphrey, L.T., 2020. Sex differences in the patterning of age-related bone loss in the human hallucal metatarsal in rural and urban populations. *American Journal of Physical Anthropology,* 171 (4), 628-644.

Wolf, P.R., 1983. *Elements of photogrammetry*, 2nd Edition. Singapore: McGraw-Hill Book Company.

Wolf, P.R., and Dewitt, B.A., 2000. *Elements of photogrammetry with applications in GIS*, 3rd Edition. London: McGraw-Hill.

Wolf, P.R., Dewitt, B.A., and Wilkinson, B.A., 2014. *Elements of photogrammetry with applications in GIS* [online], 4th Edition. New York: McGraw-Hill.

Wong, J.Y., Oh, A.K., Ohta, E., Hunt, A.T., Rogers, G.F., Mulliken, J.B., and Deutsch, C.K., 2008. Validity and reliability of craniofacial anthropometric measurement of 3D digital photogrammetric images. *The Cleft Palate-Craniofacial Journal*, 45 (3), 232-239.

Wormald, P.C., 1982. Viking studies: whence and whither?. *In:* Farrell, R.T., ed. *The Vikings.* Chichester: Phillimore & Co. Ltd, 128-153.

Woźniak, K., Rzepecka-Woźniak, E., Moskała, A., Pohl, J., Latacz, K., and Dybała, B., 2012. Weapon identification using antemortem computer tomography with virtual 3D and rapid prototype modelling – A report in a case of blunt force head injury. *Forensic Science International,* 222, e29-e32.

Yastikli, N., 2007. Documentation of cultural heritage using digital photogrammetry and laser scanning. *Journal of Cultural Heritage*, 8, 423-427.

Yawen, T. and Jinxu, G., 2018. Research on vehicle detection technology based on SIFT feature. *In:* Institute of Electrical and Electronics Engineering (IEEE) ed. *2018 8th International Conference on Electronics Information and Emergency Communication (ICEIEC 2018).* Beijing 15-17 June 2018. Red Hook: Curran Associates, Inc, 274-278.

Yilmaz, H.M., Yakar, M., Gulec, S.A., and Dulgerler, O.N., 2007. Importance of digital close-range photogrammetry in documentation of cultural heritage. *Journal of Cultural Heritage*, 8, 428-433.

Yorke, B., 1995. *Wessex in the early middle ages.* London: Leicester University Press.

Yorke, B., 2013. Dorchester and the early shire centres of Wessex. *Proceedings of the Dorset natural history & archaeological society*, 134, 106-112.

Young, M., 1989. The pinhole camera: Imaging without lenses or mirrors. *The Physics Teacher,* 649-655.

Yravedra, J., García Vargas, E., Maté-González, M.Á., Palomeque-González, J.F., Vallés-Iriso, J., Matesanz-Vincente, J., González-Aguilara, D., and Domínguez-Rodrigo, M., 2017. The use of micro-photogrammetry and geometric morphometrics for identifying carnivore agency in bone assemblages. *Journal of Archaeological Science: Reports*, 14, 106-115.

Zawieska, D., Markiewocz., J., and Łuba, M., 2019. Macro photogrammetry in inventory of historic engravings at the royal castle in Warsaw. *In:* Cardaci, A., Fassi, F., and Remondino, F. eds. *The international archives of the photogrammetry, remote sensing & spatial information sciences volume XLII-2/W9, 8th international workshop 3D-ARCH "3D virtual reconstruction and visualization of complex architectures".* Bergamo 6-8 February 2019. 795-800.

Zejdlik, K., Nyárádi, Z., Gonciar, A., 2021. Evidence of horsemanship in two Szekler noblemen from the baroque period. *International Journal of Osteoarchaeology*, 31 (1), 66-76.

Zelazny, K.G., Sylvester, A.D., and Ruff, C.B., 2021. Bilateral asymmetry and developmental plasticity of the humerus in modern humans. *American Journal of Physical Anthropology,* 174 (3), 418-433.

Zoffman, K.Z., 1982 Az 1536-os Mohácsi csata 1976-ban feltárt tömegsírjainak embertani vizsgálata. Akadémiai Kiadó: Budapest.

# Abbreviations

| Abbreviation | Full Term |
|---|---|
| %ile | Percentile |
| (S/I) AF | Superior/inferior articular facet |
| [G]CP | [Ground] Control points |
| 1D | One dimensional |
| 2D | Two dimensional |
| 3D | Three dimensional |
| AD | Anno Domini |
| ALS | Aerial laser scanning |
| Ant | Anterior |
| *ASC* | Anglo-Saxon chronicle |
| BFT | Blunt force trauma |
| BI (cut) | Broken incised cutmark |
| CCD | Charge-coupled device |
| CC-O | Control Cradle-Object |
| cDPC | Cutmark dense point cloud |
| ChP | Check points |
| ClCo | CloudCompare |
| CMOS | Complementary metal-oxide semiconductor |
| CPR | Crude prevalence rate |
| CT | Computed tomography |
| CV | Cervical vertebra(e) |
| DEM | Digital elevation model |
| DFA | Discriminant function analysis |
| DOF | Depth of field |
| DP | Distal phalanx |
| DPC | Dense point cloud |
| DSLR | Digital single lens reflex |
| DSM | Digital surface model |
| DTM | Digital terrain model |
| EXIF | Exchangeable image file |
| *f* | Focal length |
| f/ | f-stop |
| fDPC | Full dense point cloud |
| FOV | Field of view |
| GMM | Geometric morphometrics |
| GNSS | Global navigation satellite system |
| GPA | General Procrustes analysis |
| HDR | High dynamic range |
| *i* | Distance between lens and image plane |
| I (cut) | Incised cutmark |
| IP | Intermediate phalanx |
| IQR | Interquartile range |
| ISO | International organisation for standards |
| JPEG | Joint photographic experts group |
| KP | Key points |
| LDA | Linear discriminant function |
| LiDAR | Light detection and ranging |
| MC | Metacarpal |
| MK2 | Second generation control cradle |
| MLNI | Most likely number of individuals |
| MNI | Minimum number of individuals |
| MVS | Multi-view stereo |
| NPTC | Not potential throat cuts |

| Abbreviation | Full Term |
| --- | --- |
| *o* | Distance between lens and object |
| OG | Original control cradle |
| PA | Projection accuracy |
| PC | Principal component |
| PCA | Principal component analysis |
| PETG | Polyethylene terephthalate glycol |
| PH | Second generation control cradle with central hole; designed for skulls |
| PLA | Polyactide |
| Post | Posterior |
| PP | Proximal phalanx |
| PRI | Point ruggedness index |
| PS | Pilot study |
| PTC | Potential throat cuts |
| px | Pixel |
| RAM | Random access memory |
| RE | Reprojection error |
| RED | Residual energy dispersal (fractures) |
| RGB | Colour (image); red, green, blue |
| RTI | Reflectance transformation imaging |
| RU | Reproduction uncertainty |
| S (cut) | Shaved cutmark |
| SBFT | Sharp-blunt force trauma |
| SCBA | Self-calibrating bundle adjustment |
| SD | Standard deviation |
| SE | Standard error (of mean) |
| SEM | Scanning electron microscope |
| SfM | Structure-from-motion |
| SFT | Sharp force trauma |
| SGM | Semi-global matching |
| SIFT | Scale-invariant feature transform |
| SK | Skeleton number |
| SLS | Structured light scanner |
| SP | Spinous process |
| SPC | Sparse point cloud |
| TIFF | Tag image file format |
| TLS | Terrestrial laser scanner |
| TP | Tie points |
| TPR | True prevalence rate |
| TRI | Terrain ruggedness index |
| TST | Total station theodolite |
| TV | Thoracic vertebra(e) |
| UAV | Uninhabited aerial vehicle |
| Unk | Unknown (cervical vertebrae) |
| μCT | Micro-computed tomography |

# Appendix A: Literature Review of Photogrammetric Studies

Table A-1: Selected examples of studies that have used photogrammetry across various disciplines (Section 2.5)

| Citation | Topic | Notes |
|---|---|---|
| Ashton et al. (2014) | Footprints | - Hominin footprints, United Kingdom |
| Barrand et al. (2009) | Ecology | - Glaciers |
| Bartzis (2017) | Archaeological site, archaeological object | - Choragic monument of Nicias, Greece |
| Bleed et al. (2017) | Artefacts/small items | - Lithics |
| Bryan and Chandler (2008) | Rock art | - Rock art, United Kingdom |
| Buck et al. (2013) | Forensic | - Crime scene |
| Buck et al. (2020) | Forensic | - Body<br>- Skin lesions or markings<br>- Sole of shoe |
| Cârlan and Dovleac (2017) | Archaeological site | - Arutela Roman Castrum, Romania |
| Chibunichev et al. (2018) | Archaeological site, archaeological object | - Excavation site, Russia<br>- Amphorae<br>- Statuette |
| Clini et al. (2016) | Artefacts/small items | - Statuette |
| Condorelli and Rinaudo (2018) | Historical images, cultural site | - Turin, Italy |
| De Reu et al. (2013) | Archaeological site, zooarchaeological remains | - Outbuilding at abbey site of Bourdelo, Belgium<br>- Well in Roman vicus of Harelbeke, Belgium<br>- Hopmarkt cellar, Belgium<br>- Horse skeletons |
| De Reu et al. (2014) | Archaeological site | - Outbuilding at abbey site of Bourdelo, Belgium<br>- |
| Dellepiane et al. (2013) | Archaeological site | - Uppåkra, Sweden |
| Douglass et al. (2017) | Artefacts/small items | - Native American objects |
| Earley et al. (2017) | Artefacts/small items | - Victorian era medical tools |
| Evgenikou and Georgopoulos (2015) | Artefacts/small items | - Assorted objects: brass, marble, plaster, mahogany, wax, wood, porcelain, bronze, plastic, metal, clay |
| Ferrari et al. (2021) | Ecology, marine ecology | - Coral reef |
| Ferriera et al. (2017) | Geomorphology | - Surface topography |
| Gallo et al. (2014) | Artefacts/small items | - Bronze broach<br>- Encrustations from marble statue |
| Gattet et al. (2015) | Archaeological site | - The Tholos, Greece |

| Citation | Topic | Notes |
|---|---|---|
| Giacomini et al. (2019) | Ecology, biology | - Bat skulls |
| Iglhaut et al. (2019) | Ecology | - Forests |
| James and Robson (2012) | Geomorphology | - Geomorphological features<br>- Rocks |
| Khalaf et al. (2018) | Archaeological site | - Abbasid alais, Baghdad |
| Koutsoudis et al. (2013) | Artefacts/small items | - Cycladic woman figurine |
| Koutsoudis et al. (2014) | Archaeological site | - Kioutouklou Baba Bekctashic Tekke Greece |
| Larsen et al. (2021) | Footprints, forensic | - Modern day footprints |
| Macheridis (2015) | Archaeological site, archaeological object | - Midden at Çatalhöyük, Turkey |
| Magnani (2014) | Artefacts/small items | - Lithics |
| Majid et al. (2017) | Rock art | - Cave paintings, Malaysia |
| Marchal et al. (2016) | Footprints, ecology | - Animal tracks and paws |
| McCarthy (2014) | Archaeological site, cultural site | - Rubha an Fhaing Dhuibh, United Kingdom<br>- Aberlady, United Kingdom<br>- Tetney Sands shipwreck, United Kingdom |
| Meijer (2015) | Rock art | - Aspeberget rock art, Sweden |
| Nicolae et al. (2014) | Artefacts/small items | - Marble statuette<br>- Bronze statuette<br>- Ceramic jug |
| Núñez et al. (2013) | Archaeological site | - Can Sadurní cave, Spain |
| Olson et al. (2013) | Archaeological site | - Tel Akko, Israel |
| Papworth et al. (2016) | Archaeological site | - Flower’s Barrow hillfort, United Kingdom<br>- Eggardon hillfort, United Kingdom |
| Peng et al. (2017) | Archaeological site, archaeological object | - Shuidonggou site complex, China |
| Plets et al. (2012) | Rock art | - Altai rock art, Russia |
| Remondino (2011) | Archaeological site, cultural site, archaeological object | - Various |
| Rossi et al. (2020) | Marine, ecology | - Coral reef |
| Sanger (2015) | Archaeological site | - Shell midden |
| Sapirstein (2016) | Archaeological site | - Hera Temple at Olympia, Greece |
| Sapirstein (2018) | Artefacts/small items | - Terracotta pot<br>- Deer statuette<br>- Small animal skull |
| Šedina et al. (2016) | Archaeological site | - Makhmur Al-Qadima, Iraq |
| Seitz et al. (2018) | Ecology | - Sediment core |
| Snavely et al. (2006) | Cultural site | - Multiple international culturally important sites (i.e. Great Wall of China, Trafalgar Square) |

| Citation | Topic | Notes |
| --- | --- | --- |
| Snavely et al. (2008) | Cultural site | - Multiple international culturally important sites (i.e. Great Wall of China, Trafalgar Square) |
| Urbanova et al. (2015) | Forensic | - Skin lesions or markings |
| Verhoeven et al. (2012) | Archaeological site | - Ancient quarry of Pitaranha, Portugal-Spain |
| Westoby et al. (2012) | Geomorphology | - Landscape features |
| Yastikli (2007) | Archaeological site, cultural site | - Tarabasi area facades, Turkey<br>- Fatih Mosque, Turkey<br>- Dolmabahçe, Turkey |
| Yilmaz et al. (2007) | Cultural site | - Historical building, Turkey |

# Appendix B: Further Historical Background

This appendix will begin with a discussion of the historical evidence used when studying the Vikings in Britain before providing further details about Wessex and the background of the Vikings (Sections 3.1 to 3.3).

## The Archaeological and Written Evidence

As with any historical study, it is important to address the sources that are used as they come with limitations (Wormald 1982). There are written records for events that took place over 1500 years ago which can be advantageous. There are enough overlapping pieces of information between sources, that large parts are thought to have occurred, but the circumstances in which they were written mean they need critical and cautious interpretation, especially where events cannot be corroborated by additional sources (Grimmer 2002; Abels 2008; Downham 2008; Dumville 2008; Fjalldal 2015; Hadley and Richards 2016; Williams 2016b). The main written sources at the time are various annals, laws, chronicles, and biographies, both insular and continental. All written contemporary evidence must be taken as potentially slightly inaccurate, and at the worst, fictitious (Yorke 1995; Williams 2016c). Depending on the writer of the works, events may have been embellished or altered to make a benefactor or ruler sound better. Who the author was and for what purpose it was written are important pieces of information to be able to put the creation of the source into context (Downham 2008; Williams 2016b). Unfortunately, there are some regions that are missing chronicles or annals entirely (Dumville 2008).

Parts of the *Anglo-Saxon Chronicle* (*ASC*) were written long after the events described, as it is generally accepted that it was not started until the late 9th century, long after the first recorded years (Cunliffe 1993; Dumville 2008; Williams 2016c). The constituent writings may be more concerned with “proving” a line of succession or reminding people of Wessex’s victories rather than the unbiased presentation of facts (Cunliffe 1993; Yorke 1995). There is also a notable case where there is a duplication of events, 19 years apart which leads to uncertain dating of early records (Harrison 1971; Yorke 1995). However, there is seen to be increasing reliability as time goes on, especially after the mid-7th century, therefore later events can be regarded with more confidence (Cunliffe 1993). Since the *ASC* began being recorded around the time that the Viking raids on England began, there is a higher chance of reliability with those events, although they may still contain biases. The version of the *ASC* used within the current thesis is Swanton’s (1996) translation and compilation. The Winchester (A) and Peterborough (E) manuscripts are primarily used.

The *Chronicle of Æthelred and Cnut* begins in 986 but seems to have been written sometime after 1016 and this hindsight is seen to augment negative opinions and attitudes towards the Vikings, the Anglo-Saxon ruler, and events in general (Dumville 2008). Although flaws in these sources do exist, the corroboration between various chronicles and annals both within Britain and overseas help give validity to their use as a source for historic documentation (Wormald 1982; Williams 2008; Hadley and Richards 2016).

Some of the sources of information about the Vikings encounter similar limitations. Many of the great sagas were only recorded in the 12th century and therefore inaccuracies may be present (Graham-Campbell 2001). Perhaps more critically, there is no record of the Viking perspective on any of these raids or invasions of the British Isles therefore the only written record is of the Vikings' victims (Wormald 1982; Yorke 1995; Richards 2000; Williams 2008; Ellis 2021). It is also worth noting that throughout much of the available sources, the Vikings were portrayed as brutal, ruthless warriors committing countless atrocities, although such views likely reflect a large degree of bias (Wormald 1982; Williams 2008; Fjalldal 2015; Ellis 2021). It was not until quite recently that there has been a shift in the general tone of historical treatments of early Medieval Scandinavians and there is now more impetus to look at their history and role in England that is more balanced and better grounded in the evidence (Fjalldal 2015). Additionally, the interpretation of evidence of warfare in the past must be done cautiously as there is the risk of projecting current frameworks for warfare onto past decisions (Williams 2015, 2016c). Things like battle locations must be considered in wider military networks of that time to have the best chance of accurate interpretation (Williams 2015).

There is generally very little archaeological evidence for the Viking raids themselves, but their presence in the country has left its mark (Richards 2000). Evidence for Viking settlement is found in artefacts, current DNA admixtures, and place names (Richards 2008; Fellows-Jensen 2008). Many artefacts have been found, demonstrating the presence of the Vikings in England (Richards 2000, 2008; Richards et al. 2004; Hadley and Richards 2016; Kershaw 2016). Items such as jewellery, combs, coins, hack-metal, Viking-style stone carvings, and Viking weaponry have been uncovered in excavations (Figure 110) (e.g. Biddle and Kjølbye-Biddle 2001; Leahy and Paterson 2001; Hadley and Richards 2016). Viking hoards are also sometimes found which usually contain items like hack-silver, ingots, and foreign coins, differentiating them from Anglo-Saxon hoards (Richards 2000). It must be noted though that the Vikings raiders and subsequent Scandinavian settlers integrated into the Anglo-Saxon population that was already present upon settling the land, so assuming that people of Scandinavian origin were only present where artefacts have been found may lead to erroneous conclusions (Hadley and Richards 2000).

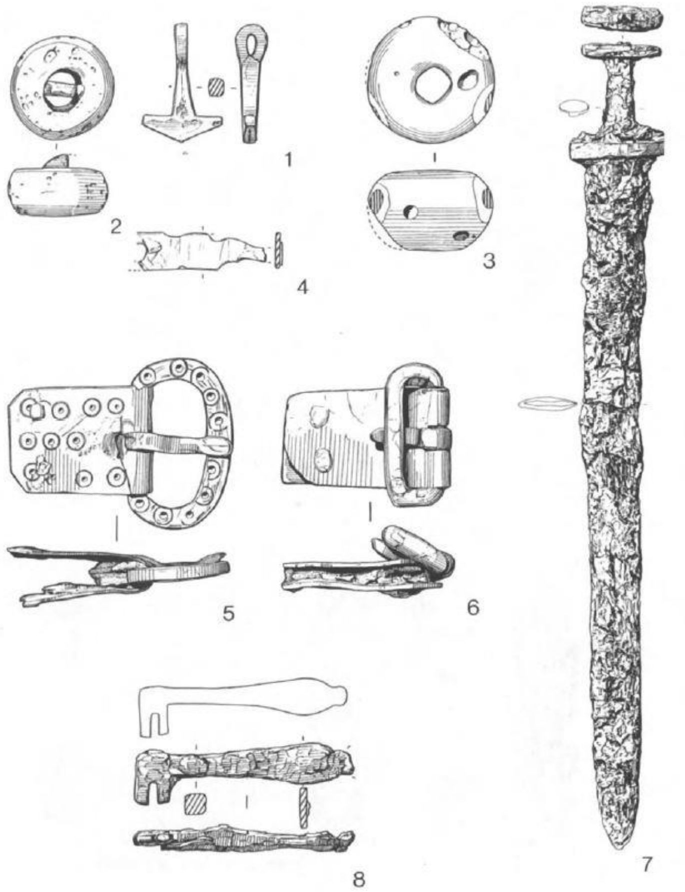


Figure 110: Assorted Viking metalwork from England (Biddle and Kjølbye-Biddle 2001, Fig. 4.14 “Repton: Grave 511. 1, silver Thor’s hammer; 2, 3, glass heads (2 with the loop of the Thor’s hammer in the hole); 4, copper-alloy ?fastener; 5, copper-alloy belt- or sword-strap buckly; 6, copper-alloy buckle from sword sheath; 7, iron sword; 8, iron key. (1-6, 1:1; 7, 1:6; 8, 1:2) Drawn by Judith Dobie”)

Place names and personal names in the Domesday Book can give indications as to the areas that were settled by Scandinavians (Richards 2000, 2002; Abrams 2012; Lewis 2016). A much higher concentrations of place names with Scandinavian markers, such as the endings *-by* and *-thorp(e)*, are found in the north east of England and the Scottish coasts since this is where the majority of the Vikings that settled took up residence (Richards 2000; Fellows-Jensen 2008). Studies have looked at current DNA admixtures in populations and compared the frequency of difference sequences to see whether areas within the *Danelaw* have proportions closer to Scandinavia or to Anglo-Saxon and Celtic areas (Helgason et al. 2001; Goodacre et al. 2005; McEvoy and Edwards 2005).

Overall, there is a paucity of osteological evidence for the Vikings in England (Richards 2000, 2002; Buckberry et al. 2014). It is thought that many of the burials of Scandinavian individuals may have taken place in Anglo-Saxon cemeteries without any traditional pagan evidence and thus are “invisible” within these cemeteries (Richards 2000; Buckberry et al. 2014). When inhumations or cremations are found, the preservation is often very poor, possibly also indicating that the chance of the survival of other Viking remains in those areas is low (Richards et al. 2004; Speed and Walton Rogers 2004). It is also possible that not everyone was given a grave (Price 2008).

There are some burials that have been found which contain grave goods of a Scandinavian origin or style (Richards 2002; Speed and Walton Rogers 2004; Wilson 2008). The most secure way of determining whether skeletons are possibly Scandinavian is through isotopic analysis (Budd et al. 2003; Speed and Walton Rogers 2004; Chenery et al. 2014; Loe et al. 2014b). Radiocarbon dating is also of use in conjunction with isotopic analysis, however it must be done carefully and accurately (Jarman et al. 2018, *cf* Biddle and Kjølbye-Biddle 2001).

There are two major instances of Viking ‘cemeteries’ being found and there is evidence that both may have been linked to the presences of the Great Viking Army (Richards et al. 2004). One is a cremation cemetery at Heath Wood, Ingleby (Derbys) (Richards 2002, 2008; Richards et al. 2004). There is evidence of cremations that were both burned in-situ, and those that were buried having been burned elsewhere. This possibly indicates that this was the final resting place for some members of the army who had died earlier in the campaign and whose ashes were brought along until a suitable burial place was found (Richards et al. 2004; Richards 2008). The other is a mixture of inhumations and charnel from the nearby Repton (Derbys), where the Great Viking Army was known to over-winter in the 870s (Biddle and Kjølbye-Biddle 1992, 2001; Richards 2002, 2008; Jarman et al. 2018). Two other mass graves of Vikings have been found in England, one at St. John’s College, Oxford (Oxon) and one along the Weymouth Ridgeway (Dorset) the latter of which is more extensively discussed in Chapter 5 (Pollard et al. 2012; Durrani 2013; Chenery et al. 2014; Loe et al. 2014b; Williams 2015).

## Kings of Wessex

A long line of kings of Wessex can be traced back to when the Saxons first arrived in England (Swanton 1996). Although some of the early links may be unclear and dubious, the later reigns are better recorded (Cunliffe 1993). Of import in this study are the kings during the Viking invasions. Alfred (871-899) was king when arguably the most critical parts of the first Viking attacks were taking place and Æthelred the Unready (978-1016) when the second wave occurred (Table B-1) (Cunliffe 1993; Swanton 1996). These kings likely had to deal with the beginnings of the second Viking invasions however Alfred and Æthelred are the kings who arguably had the most important dealings with the Vikings.

Table B-1: Kings reigning Wessex throughout the time period of Viking invasions under investigation in this study

| King | Years |
|---|---|
| Alfred | 871-899 |
| Edward the Elder | 899-924 |
| Athelstan | 924-939 |
| Edmund | 939-946 |
| Eadred | 946-955 |
| Eadwig | 955-959 |
| Edgar | 959-975 |
| Edward the Martyr | 975-978 |
| Æthelred the Unready | 978-1016 |
| Edmund Ironside | 1016 |
| Cnut | 1016-1035 |

Although many of the defensive actions taken by Alfred and Æthelred were similar, Alfred's biographer Asser was much more complimentary towards him than Æthelred's was and Wessex suffered more during the second wave of attacks, therefore history tends to look more favourably at Alfred's defence of Wessex (Yorke 1995; Abels 2008; Dumville 2008; Lavelle and Roffey 2016). Alfred's policies were a major part of the first wave of Viking attacks not successfully gaining control of the entirety of England: the construction of fortresses throughout Wessex, the reorganisation of the army, propaganda to unify his people, and treaties designed to divide his enemies (Downham 2008). Conversely, later chroniclers tend to pick apart Æthelred's reign and criticise policies and defences that they considered ineffective and inconsistent (Richards 2000).

## The Viking Migrations

The motivations for the Viking migrations are thought to be complex (Richards 2000). An overarching factor was possibly either a lack of silver in Scandinavia or an abundance elsewhere, though financial gain is not thought to be the sole cause (Ashby 2015). Portable wealth may have become more important and there were likely some raids that were specifically organised to gather more wealth and plunder the riches of others however, it is likely this was not always the primary motivation (Richards 2000; Graham-Campbell 2001; Williams 2008). Barrett (2008) notes that despite the Vikings initially targeting monasteries with portable wealth, if the sole motivation was for financial gain, then targeting urbanised regions that were shipping and trading areas may have made more sense.

Climatic changes have also been proposed as a possible factor (Barrett 2008). A warming during the final few centuries of the millennium may have increased the ability to settle in some location, but the timing of when the raids started does not fit with this being a primary factor (Barrett 2008). Arguments have been made that the development of maritime technology drove the raids, however, the Vikings previously had enough technological prowess to be able to make long journeys (Barrett 2008; Ashby 2015). Therefore, the maritime technology was necessary for the raids, but it was not the motivation (Richards 2000; Barrett 2008; Ashby 2015). Political factors have been considered and may provide some explanation, possibly for the timing of the second wave of Viking attacks on England, but more recently it has been argued that this is likely not the main cause (Brink 2008; Ashby 2015; Gore 2016). The external pull of weakness within nearby regions in combination with the internal push of the centralising power in Scandinavia may have been an influence (Barrett 2008).

Population pressures may have caused groups to seek new resources to exploit and new land to inhabit and cultivate (Wormald 1982; Graham-Campbell 2001). The coastal and inland areas to the north in Britain provided good opportunities to settle and tend land (Graham-Campbell 2001). There is evidence that some later returned with their families to settle. Others mixed with the native culture and took local wives. What is notable is that some of the Viking settlers came from previously conquered and settled lands, rather than from Scandinavia as might be expected with population pressure as the primary factor (Barrett 2008). Additionally, there are many years between the initial raids and any evidence of settlement in England which make these theories less likely (Barrett 2008).

One hypothesis that has recently been gaining support related to both demographic and financial causes; the search for '*bridewealth'* may have been a motivation (Barrett 2008; Ashby 2015). There was possibly an abundance of young men compared to women because of the increasing militarisation associated with the formation of states in Scandinavia (Barrett 2008). The "wealth" may not have just been portable wealth, but it may have been prestige and status that accompanied having gone on a raid (Ashby 2015). There is evidence that the Anglo-Saxon objects that were brought back were used, worn, or displayed, sometimes with modifications, but rarely were they melted down (Ashby 2015). This would indicate they were meant for public viewing which supports the idea of raiding for prestige. Scandinavian ideology may have played a factor in this as well, with honour and fatalism being major facets (Barrett 2008).

## The Viking Invasions of Britain and Wessex

The Vikings are mainly known for having settled in the north and east of Britain, in an area that would be termed the *Danelaw*. Despite this, they were present in the south of England, including Wessex (Loyn 1977). The Viking attacks on England can generally be thought of in two waves; those that occurred prior to 900 and those that occurred after 900 (Lavelle and Roffey 2016). The years following the Vikings arriving in Britain were tumultuous, with periods of calm interspersed with periods of warfare and raiding (Loyn

1977). The size of the Viking war bands and armies that came to England is debated (see Wormald 1982).

The initial attacks often targeted religious sites because they were both wealthy and poorly defended (Wormald 1982; Richards 2000; Williams 2008). The first recorded raid was at Lindisfarne off the coast of present-day Northumberland in 793 followed by another raid the subsequent year (Swanton 1996; Richards 2000; Graham-Campbell 2001; Downham 2008; Raffield 2020). These events are often considered the start of the Viking Age (Brink 2008).

Although not in the form of a raid, it is probable the Vikings were encountered prior to that in the south of England. There are records of three ships appearing near Weymouth or Portland (Dorset) in approximately 789 (Cunliffe 1993; Yorke 1995; Swanton 1996; Richards 2000; Graham-Campbell 2001; Downham 2008; Gore 2016). The crew of these ships killed the reeve from Dorchester (Dorset) who had come to greet them and ask them to come to the town, erroneously thinking they were traders (Cunliffe 1993; Richards 2000; Yorke 2013; Gore 2016; Lavelle 2016). There is also mention of Offa, King of Mercia making arrangements for the defence of Mercia against ‘pagan people’ though their origins are not mentioned and therefore it cannot be definitively stated that they were Vikings (Richards 2000). For almost half a decade after that, the *ASC* is silent in regards to Viking attacks (Downham 2008).

### Pre-AD 900

The attack on the southern coast did not start in earnest until the 830s (Gore 2016) (Figure 111). In 835, Sheppey (Kent), was attacked, starting nearly three decades of raids that came nearly annually (Swanton 1996; Graham-Campbell 2001; Downham 2008). Kent was subjected to the early attacks, but soon the whole south coast of England was targeted (Yorke 1995). Attacks came from both the Bristol Channel and the English Channel and there are probably some that go unrecorded (Yorke 1995). There were mixed fortunes in the fighting; Anglo-Saxon losses are noted in 838 and 844, however a Viking defeat is recorded in 851 (Downham 2008). From the mid-9$^{th}$ century, groups of Vikings periodically began to overwinter on the fringes of England, such as in Thanet (Kent) in 850 and Sheppey in 855 (Swanton 1996; Richards 2000; Buckberry et al. 2014; Hadley and Richards 2016). Hamwic ([Southampton], Hants) was raided, as well as Portland (Dorset); Winchester (Hants) was attacked in 860 but the shire armies in that area managed to push the raiders back (Yorke 1995; Swanton 1996; Roffey and Lavelle 2016).

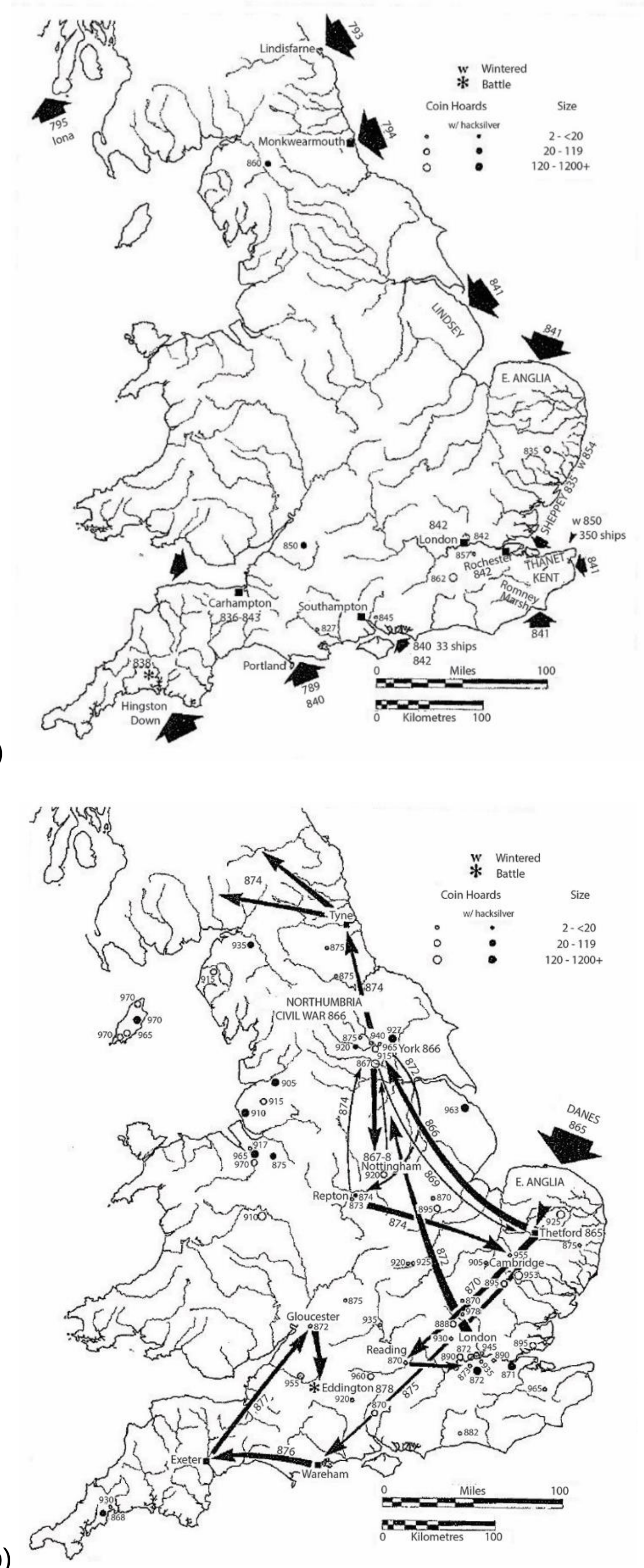


a)



b)

Figure 111: Maps showing the locations and paths of Viking raiders and armies in England a) 789-864 and b) 865-896 (amended from Richards 2000, Fig. 4 and 8, p.22 and 28)

After the overwintering of the Great Army, York (N Yorks) was taken in 866 much of the northern and eastern parts of England followed soon after (Swanton 1996). Northumbria and Mercia soon also fell under Viking control as the Vikings took advantage of internal feuds and warfare and by 870, the Great Army had set their sights on Wessex (Cunliffe 1993; Yorke 1995; Biddle and Kjølbye-Biddle 2001; Richards et al. 2004; Downham 2008; Gore 2016; Hadley and Richards 2016).

The Vikings used Reading (Berks) as a base and what followed was a series of battles and minor skirmishes in 871, such as the Battle of Ashdown, where the victory was traded back and forth and by end of which, it appears the Vikings had a slight advantage because they were paid to stop and leave Wessex alone (Cunliffe 1993; Yorke 1995; Richards et al. 2004; Roffey and Lavelle 2016; Gore 2016). There was a minor reprieve from the attacks, however, they did not stop (Yorke 1995). In the early 870s, other Viking forces came to join the campaign (Downham 2008). During this period, the Great Army is known to have overwintered in London in 870 and the Midlands (Hadley and Richards 2016). In the winter of 872-873 they stayed at Torksey (Lincs) where recent excavations have been turning up many Viking artefacts (Hadley and Richards 2016). The following year, there is both written and physical evidence that they overwintered at Repton (Biddle and Kjølbye-Biddle 1992, 2001; Richards 2008; Jarman et al. 2018). The nature of the army was often changing by this point with forces joining and leaving periodically. After the overwintering, the Great Army split and a portion of it, led by Guthrum amongst others, went to try to conquer Wessex.

In the later 870s, the Vikings would often use the tactic of targeting places in Wessex they could attack by both land and sea (Swanton 1996; Williams 2008). These were not always successful, with some of their fleets either being delayed or wrecked, such as in 876 at Wareham (Cunliffe 1993). After an exchange of hostages and an oath to leave Exeter (Devon) and Wessex in 877, Guthrum and the Great Army overwintered in Gloucester (Glos) (Gore 2016). In 878, the Vikings conquered Chippenham (Wilts) the Great Army made a third and final attempt to conquer Wessex (Yorke 1995; Gore 2016). Alfred, who had been king during the majority of these invasion of Wessex, re-gathered his troops after being forced to shelter in Somerset and won at Edington (Wilts) after a series of engagements (Yorke 1995; Swanton 1996; Richards 2000; Richards et al. 2004; Williams 2016c). Following this ,the Treaty of Alfred and Guthrum, was created outlining the '*Danelaw*', which included York, East Anglia, and the Five Boroughs; Derby, Nottingham, Stamford, Leicester, and Lincoln (Derbys, Notts, Lincs, Leic, and Lincs, respectively; Cunliffe 1993; Yorke 1995; Richards 2000, 2008; Graham-Campbell 2001; Abels 2008; Downham 2008; Hadley 2008; Loe et al. 2014b, Hadley and Richards 2016; Raffield 2020)

The number of Scandinavians settling in the *Danelaw* is unknown and the pattern in which they came, whether it be large numbers at one time or smaller numbers over a longer time, is debated (Richards 2008). It was a complex political and cultural landscape at the time and the focus of the written record is the raiding and political aspects rather than any settlement (Abrams 2012; Raffield 2020). Some signs of them are seen in the archaeological record, however, it appears there was some degree of assimilation with the native population.

Not all was entirely peaceful; after Guthrum's death in 890, different bands of Vikings began raiding on both side of the English Channel (Yorke 1995; Swanton 1996; Gore 2016). However, they were held off and by 896, the army had further split apart (Yorke 1995; Richards 2000; Graham-Campbell 2001; Downham 2008). Some of these Vikings also settled in the *Danelaw* or on the continent and some continued raiding elsewhere (Richards 2000; Downham 2008).

### Post-AD 900

Generally, after Alfred's death, the Viking invasions stopped for a while. In this time, the kings succeeding Alfred worked to gain control over lost territories. Mercia and Wessex were united through marriage and starting with London, control of the *Danelaw* was gradually retaken by the Anglo-Saxons (Richards 2000; Abels 2008; Downham 2008). Finally, in 954, the last Viking King of York, Erik Bloodaxe, was driven out (Richards 2000; Graham-Campbell 2001). Eventually, their conquest was successfully completed, with Edgar being the first king of both Wessex and Britain (Yorke 1995).

In the early 10$^{th}$ century, there are a couple recorded attacks by Vikings (Figure 112). The *ASC* is a bit sparse at that time, so smaller raids may not have been recorded (Yorke 1995). There are some theories that the political instability that came with Æthelred's reign was a factor in the renewed Viking invasions (Richards 2000; Foard 2003; Downham 2008; Dumville 2008). In 980, Southampton was attacked and many inhabitants either killed or enslaved (Cunliffe 1993). The same year, there was a Viking invasion at Thanet as well. Portland and London were both attacked two year later and Vikings from Ireland attacked the Devon, Cornwall, and north coast of Somerset (Cunliffe 1993; Yorke 1995; Loe et al. 2014b).

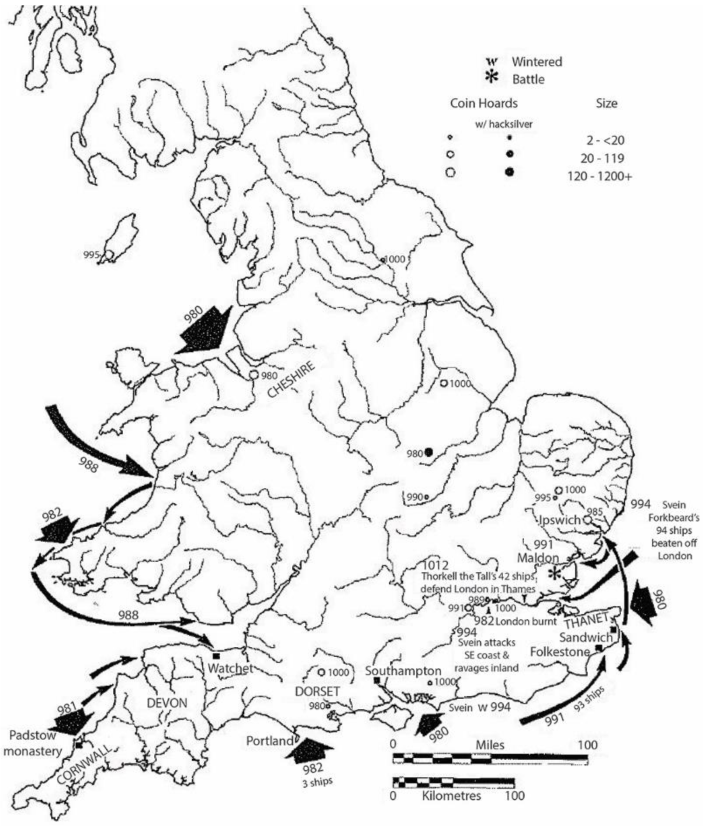


Figure 112: A map showing the locations and paths of Viking raiders and armies in England 980-1012 (amended from Richards 2000, Fig. 14, p.36)

On the east coast in 991, a large army, possibly led by Olaf Trygvasson, landed and subsequently fought the Battle of Maldon (Essex) against the Anglo-Saxons (Cunliffe 1993; Swanton 1996; Foard 2003; Downham 2008). This ended in a victory for the Vikings and a payment of *Danegeld*, which was money and gold given to the Vikings to leave Wessex alone. Not long after, the attacks on the south coast restarted and lasted for about 15 years (Cunliffe 1993). In 993 or 994, a treaty was made at Andover (Hampshire) between Olaf and an ealdorman on behalf of Wessex (Abels 2008; Lavelle 2016). Around the same time, a Viking army is known to have overwintered in Southampton (Loe et al. 2014b).

In 1002, Æthelred ordered all people of Danish origin to be killed likely either as retribution or a deterrent; this became known as the St Brice's Day Massacre, though the full extent is unknown (Section 3.3.2; Yorke 1995; Pollard et al. 2012; Loe et al. 2014b). This did not discourage the Vikings from returning. Between 994 and 1012, increasingly large *Danegeld* was demanded and paid by Wessex (Yorke 1995; Richards 2000; Graham-Campbell 2001). Parts of Wessex continued to be attacked and pillaged throughout this time, despite the payment of *Danegeld* (Williams 2015, 2016c). By 1012, nearly all of eastern and south-eastern England was under Viking control (Cunliffe 1993). There were instances of Viking bands becoming mercenaries for Anglo-Saxon rulers for enough money, as was the case with Thorkel the Tall (also written as Thurkil) who was recruited as a mercenary for Æthelred a couple years after leading an attack against England before returning to fight for the Vikings again (Williams 1986; Yorke 1995; Graham-Campbell 2001; Williams 2016b).

In 1013, Swein Forkbeard of Denmark (also written as Sveinn) landed at Sandwich (Kent), and then advanced to the Humber where he got the Five Boroughs to accept him as king (Figure 113) (Cunliffe 1993; Richards 2000; Graham-Campbell 2001). The army marched south, conquering Oxford, Winchester, Wallingford (Oxon), and Bath (Somerset) (Cunliffe 1993; Yorke 1995). An attempt was made to take London, but Æthelred's defences held strong. Æthelred fled to Normandy in 1013 and remained there until after Swein's death the following year (Yorke 1995; Richards 2000; Downham 2008).

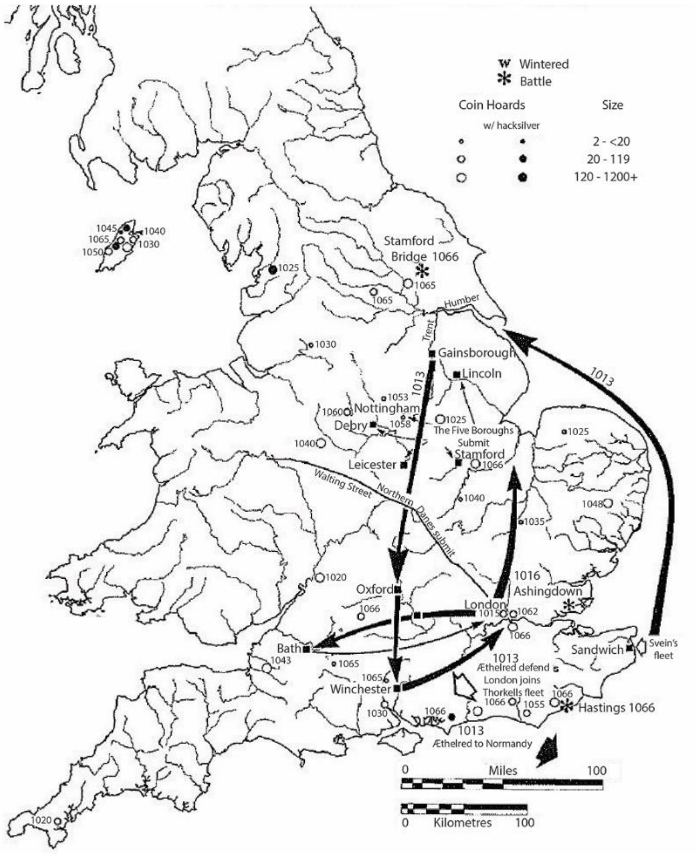


Figure 113: A map showing the locations and paths of Viking raiders and armies in England 1013-1066 (amended from Richards 2000, Fig. 16, p.38)

After Swein died in 1014, Æthelred was recalled to England to rule (Lund 2008). Swein's son Cnut (also written Knut or Knútr) gathered an army, repeatedly attacking England and, following Æthelred's death in 1016, was involved in a struggle for succession with his Anglo-Saxon half-brother and Æthelred's son, Edmund Ironside (Yorke 1995; Downham 2008; Loe et al. 2014b). After the Battle of Assandun, Cnut was crowded king of Mercia and Edmund king of Wessex (Yorke 1995; Roffey and Lavelle 2016). Edmund died shortly thereafter and Cnut became the king of all of England and ruled from Winchester (Yorke 1995; Richards 2000; Lund 2008). He divided England into four earldoms, roughly in-line with the Anglo-Saxon Kingdoms of over a century prior; Northumbria, East Anglia, Wessex, and Mercia; he kept Wessex for himself (Yorke 1995; Lund 2008; Williams 2016b).

## The Impact of the Viking Raids in Britain

The interactions of the Anglo-Saxons and the Vikings likely would have been very different regionally. Those who were directly affected by the raids may have had their livelihood destroyed and thus needed to entirely re-build their lives. Those who were not directly in the path of the Viking armies may not have noticed much difference. As alluded to earlier, the scale of the colonisation of England by the Vikings is debated (Richards 2000). There is evidence that the scale of immigration was larger during the first waves of raids compared to the second wave (Williams 1986). The land in the *Danelaw* was not unoccupied and it was not a free-for-all. Evidence suggests land was distributed by Viking leaders, who would then likely expect tribute. The Vikings who chose to settle in the *Danelaw* appear to have done so relatively peacefully and integrated into the native population there. They were not killed when Alfred’s successors re-took that area, but rather submitted to them along with the Anglo-Saxons (Richards 2000). Political intermarriages occurred during this time as well, with a sister of Æthelstan being married to the Viking king of York (Roffey and Lavelle 2016). Intermarriages at other levels of society have been noted too both in personal names and in DNA studies (Williams 1986; Goodacre et al. 2005; McEvoy and Edwards 2005; Helgason et al. 2011).

Relations between the factions were not always volatile. As a component of many of the treaties that were established, the Viking leaders would be asked to convert to Christianity with an Anglo-Saxon as his sponsor (Lavelle 2016). Although the treaties often broke down not long after they were established, this interaction been Anglo-Saxon nobles and Viking leaders seems to have been a rather peaceful part of their relationship. There are also known examples of Vikings becoming mercenaries and working for the Anglo-Saxon leaders. Probably the best-known example of this is Thorkell the Tall, who attacked England around the turn of the millennium before joining Æthelred in 1012 before going back and joining Cnut prior to when the latter came to rule all of England (Swanton 1996; Williams 2016b).

## Burghal Hidage and Alfred’s Defences

King Alfred set out an important plan for the defence of Wessex (Williams 2008). Although he did suffer some defeats and had to pay tribute in the form of *Danegeld*, he was overall successful in maintaining Wessex's independence. He initiated the idea of a standing peasant army in Wessex, half of which was at home and half of which was on active duty (Richards 2000). He also required bridges and ships to be built for the defence of the kingdom (Richards 2000; Williams 2008). One of his most enduring legacies was the formalised system of fortification to defend against the Vikings. This list of fortified towns, known as *burhs*, is called the *Burghal Hidage* (Cunliffe 1993; Yorke 1995; Richards 2008). It is a list of *burhs,* a tax assessment in hides for each, and a formula for calculation (Yorke 1995; Richards 2000). This allowed for the length of defences that needed to be maintained and manned could be calculated. It may have been started to a lesser extent before Alfred and continued after. It is an important source of how the population of Wessex responded to the initial wave of invasions but unfortunately the original manuscript does not survive (Yorke 1995). Iron Age earthworks and Roman fortifications were reused where they could be (Richards 2000; Williams 2016c). By 899, there were approximately 30 places on the list (Bettey 1986). Towns such as Wareham, Christchurch, Wilton, Bath, and Southampton, however there are a few interesting omissions of previously important towns such as Dorchester, Bristol, and Ilchester (Cunliffe 1993; Yorke 1995). Scholars have estimated that all parts of Wessex with within 20 miles of a *burh* (Richards 2000). The *burh* system was extended as *Danelaw* was reconquered (Richards 2000).

# Appendix C: aDNA Results

The following are the results from the Viking aDNA study by Margaryan et al. (2020) (Section 5.1.3.2). In all cases, petrous portion was sampled from the Weymouth Ridgeway Vikings and all were confirmed as male (Tables C-1 and C-2). The data was isolated from the supplementary tables in order to solely present information on the Weymouth Vikings. Any isotope data in this appendix is from Loe et al. (2014b) or Chenery et al. (2014). Full conclusions are available in the original paper, but overall, the Weymouth Vikings seem to have a mix of Northern European/Scandinavian genes with a relatively low Swedish-like contribution. These results support that they likely were Vikings, possibly from a wide geographic origin, and that gene flow was present in Viking-Age Scandinavia (Figure 114 and Table C-3). Unfortunately, those that were tested for isotopes prior to aDNA were all generally from the same origin so they aDNA of any of the isotopic outliers was not analysed.

Table C-1: The results of the aDNA study excluding haplogroups (Margaryan et al. 2020)

| Sample (SK) | AvgDepth (X) | Contam_ mtDNA | Damage (%) | DoC_X | Contam_X (%) | DoC mtDNA |
|---|---|---|---|---|---|---|
| VK256 (3722) | 1.362 | 0.27 | 23.36 | 0.70 | 1.29 | 167.8 |
| VK257 (3723) | 1.017 | 0.77 | 27.27 | 0.52 | 1.87 | 116.3 |
| VK258 (3733) | 1.022 | 2.23 | 23.88 | 0.52 | 1.66 | 112.1 |
| VK259 (3734) | 1.183 | 0.23 | 22.99 | 0.61 | 1.31 | 134.7 |
| VK260 (3735) | 0.904 | 0.15 | 27.08 | 0.46 | 1.93 | 96.0 |
| VK261 (3736) | 1.049 | 1.01 | 25.77 | 0.53 | 1.12 | 126.8 |
| VK262 (3739) | 1.220 | 0.57 | 23.10 | 0.63 | 2.10 | 133.6 |
| VK263 (3742) | 1.374 | 3.51 | 22.69 | 0.71 | 1.84 | 122.9 |
| VK264 (3744) | 0.991 | 1.40 | 25.89 | 0.51 | 1.96 | 125.7 |
| VK449 (3746) | 1.431 | 1.66 | 14.95 | 0.74 | 1.17 | 109.3 |

Table C-2: The results of the aDNA study highlighting the Y and mtDNA haplogroups (Margaryan et al. 2020)

| Sample (SK) | Y Haplogroup | mtDNA Haplogroups |
|---|---|---|
| VK256 (3722) | R1a1a1b1a3a1 | H1c7 |
| VK257 (3723) | I1a1 | H5a1c1a |
| VK258 (3733) | R1a1a1b1a3a | K1a4a1 |
| VK259 (3734) | R1b1a1b1a1a1b1a | I2 |
| VK260 (3735) | Q1b | H1e1a |
| VK261 (3736) | R1b1a1b1a1a2 | H52 |
| VK262 (3739) | I1a2a | J1c4 |
| VK263 (3742) | R1b1a1b1a1a2c1a2b2b | K1a4d |
| VK264 (3744) | R1a1a1b1a3a | N1a1a1a2 |
| VK449 (3746) | R1b1a1b1a1a1b | H6a2a |

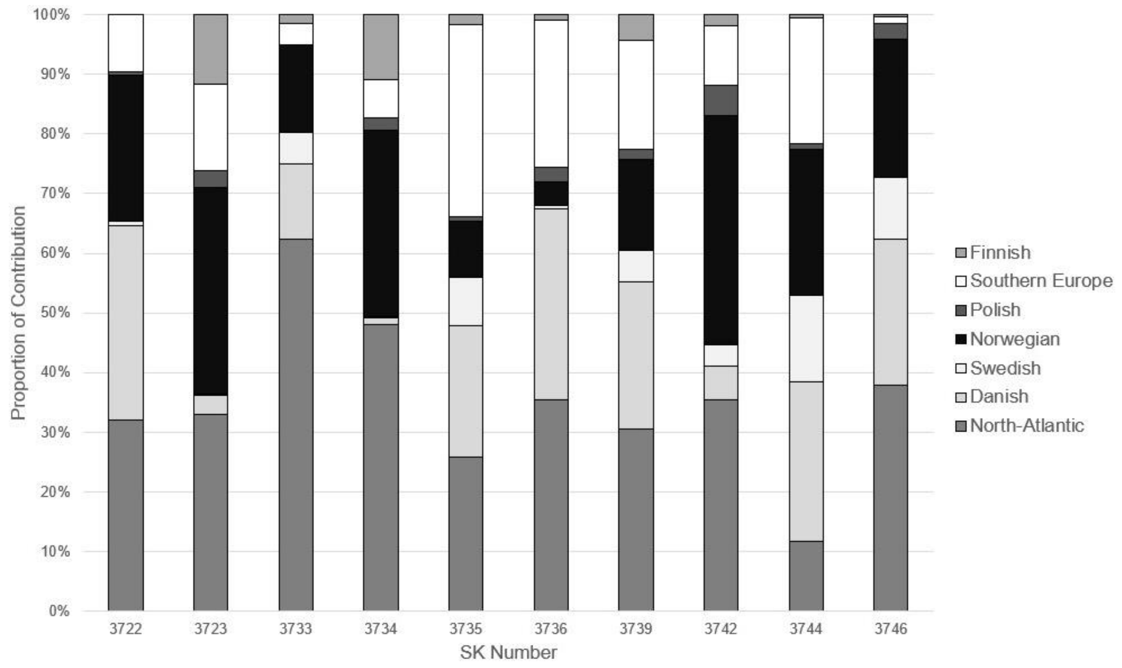


Figure 114: aDNA graph (data from Margaryan et al. 2020)

Table C-3: Bootstrapped mean ancestry estimates of the ancient samples with the highest two categories for each highlighted (data from Margaryan et al. 2020)

| Sample (SK) | British-like/North Atlantic | Danish-like | Swedish-like | Norwegian-like | Polish-like | Southern European-like | Finnish-like |
|---|---|---|---|---|---|---|---|
| VK256 (3722) | 0.321 | 0.324 | 0.008 | 0.244 | 0.007 | 0.095 | 0.000 |
| VK257 (3723) | 0.330 | 0.032 | 0.003 | 0.346 | 0.028 | 0.146 | 0.116 |
| VK258 (3733) | 0.625 | 0.126 | 0.052 | 0.147 | 0.001 | 0.035 | 0.015 |
| VK259 (3734) | 0.480 | 0.011 | 0.003 | 0.313 | 0.020 | 0.063 | 0.110 |
| VK260 (3735) | 0.258 | 0.221 | 0.080 | 0.094 | 0.009 | 0.322 | 0.016 |
| VK261 (3736) | 0.354 | 0.321 | 0.005 | 0.039 | 0.026 | 0.246 | 0.009 |
| VK262 (3739) | 0.305 | 0.246 | 0.054 | 0.151 | 0.017 | 0.183 | 0.043 |
| VK263 (3742) | 0.355 | 0.056 | 0.036 | 0.383 | 0.051 | 0.100 | 0.019 |
| VK264 (3744) | 0.117 | 0.267 | 0.146 | 0.244 | 0.010 | 0.210 | 0.006 |
| VK449 (3746) | 0.378 | 0.246 | 0.103 | 0.231 | 0.027 | 0.011 | 0.004 |

# Appendix D: Specifications, Settings, Workflow, and Code

All information within this appendix was originally introduced in Chapter 5.

## Software

### Table D-1: The software used for this project

| Software (Name in text if different) | Version | Uses | Developer or Maintainer (Citation) |
|---|---|---|---|
| Agisoft Photoscan Professional (Photoscan) | 1.4 | Creation of pilot study SfM-MVS models | Agisoft LLC (Agisoft LLC 2018b) |
| Agisoft Metashape Professional (Metashape) | 1.6.1 | Creation of full data collection SfM-MVS models | Agisoft LLC (Agisoft LLC 2020b) |
| CloudCompare (ClCo) | 2.10.2 Zephyrus | Measuring and analysing point clouds and extracting profiles | Daniel G.M. (CloudCompare 2019) |
| ImageJ (IJ) | 2.0.0 | Measuring the wall heights, opening angle, and width of the profiles for SfM-MVS models and Keyence Microscope models | Wayne Rasband, National Institute of Health (Rasband 2015) |
| R | 3.6.3 | Statistical analysis | The R Foundation for Statistical Computing (R Core Team 2020) |
| RStudio | 1.4.1103 | Statistical analysis | Rstudio, Inc (RStudio Team 2021) |
| *Momocs* | 1.3.2 | Shape analysis | Vincent Bonhomme (Bonhomme et al. 2014) |
| *Here* | 1.0.1 | Shape analysis | Kirill Müller (Müller 2017) |
| *Tidyverse* | 1.3.1 | All R processing; ggplot2 and dplyr are within | Hadley Wickham (Wickham et al. 2019) |
| Statistical Package for Social Sciences (SPSS) | 26 | Statistical analysis | IBM (IBM 2019) |
| QGIS | 3.16 Hannover | Surface roughness analysis | QGIS Development Team (QGIS.org 2021a) |
| Adobe Illustrator CC (Illustrator) | 2020 | Digitising outlines for shape analysis; patterning trauma; figures | Adobe (Adobe 2020) |
| Adobe Photoshop CC (Photoshop) | 19 | Conversion of RAW to TIFF | Adobe (Adobe 2018) |

## Specifications

Table D-2: The specifications of the two Nikon cameras used in this study (Nikon 2021a, 2021b)

| Specification | Camera | |
|---|---|---|
| | Nikon DX – D5300 | Nikon FX – D810 |
| Type | DSLR | DSLR |
| Effective view angle | Focal length equivalent to ~1.5x that of lens with FX format angle of view | -- |
| Effective pixels | 24.2 M | 36.3 M |
| Image sensor | 23.5 x 15.6mm | 35.9 x 24.0mm |
| Total pixels | 24.78 M | 37.09 M |
| Sensor type | CMOS | CMOS |
| Image size (not RAW) | L 6000 x 4000<br>M 4496 x 3000<br>S 2992 x 2000 | L 7360 x 4912<br>M 5520 x 33680<br>S 3680 x 2456 |
| RAW | NEF – 12 or 14 bit<br>Fine JPEG – 1:4 compression | NEF – 12 or 14 bit<br>TIFF<br>Fine JPEG – 1:4 compression |
| Frame coverage | ~95% horizontal and vertical | ~100% horizontal and vertical |
| Magnification | ~0.82x (50mm f/1.4 lens at infinity, -1.0 m-1) | ~0.7x (50mm f/1.4 lens at infinity, -1.0 m-1) |
| Eyepoint | 18mm (-1.0 m-1; from centre surface of viewfinder eyepiece lens) | 17mm (-1.0 m-1; from centre surface of viewfinder eyepiece lens) |
| Diopter Adjustment | -1.7 - +1.0 m-1 | -3 - +1.0 m-1 |
| Dimensions (WxHxD) | 125 x 98 x 76mm | 146 x 123 x 81.5mm |
| Weight | 530g (with battery and memory card) | 980g (with battery and memory card) |
| | 480g (body only) | 880g (body only) |

Table D-3: The specifications of the AF-S Micro NIKKOR 60mm f/2.8G ED lens used in this study (Nikon 2020b)

| Category | Details |
|---|---|
| Focal length | 60mm |
| Maximum aperture | f/2.8 |
| Minimum aperture | f/32 |
| Lens construction | 12 elements, 9 groups |
| Angle of view | FX Diagonal 39º40’<br>DX Diagonal 26º30’ |
| Minimum focus distance | 0.185m |
| Maximum reproduction ratio | 1x |
| No. of diaphragm blades | 9 (rounded) |
| Filter attachment size | 62mm |
| Diameter x length | 73 x 89mm |
| Weight | 425g |

## Settings and Workflow

Figure 115 presents the general workflow for the entire project with no sections specifically highlighted. It is referred to in text in Sections 5.2, 5.3, and 5.4. The detailed methodological workflow is Figure 64 and the iterative testing workflow is Figure 116.

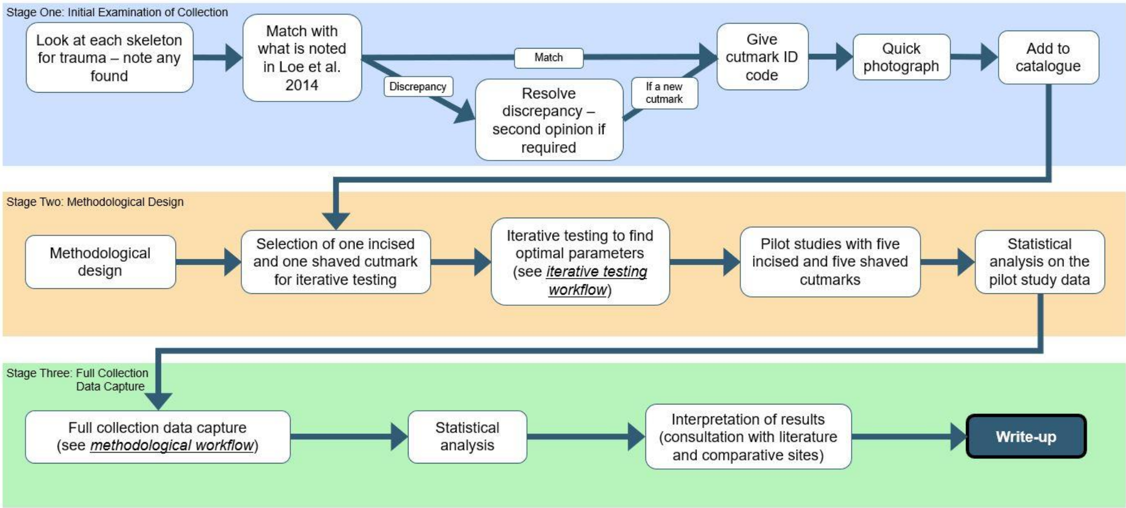


Figure 115: The full workflow for this research project

Table D-4: The settings used in Agisoft Photoscan 1.4 and Metashape 1.6

| Stage | Setting | Value | Notes |
|---|---|---|---|
| Alignment | KP | 40,000 | Default |
| | TP | 4,000 | Default |
| | Accuracy | High | If the model did not align, Highest was used<br>If Highest did not work, images were retaken |
| | Preselection | Generic | Reference Preselection not enabled |
| | Masks | None | Unless masking required due to background defect |
| Control Points | Accuracy | 0.0005 | Units automatically in m |
| | Camera optimisation | f, cx, cy, k1, k2, k3, p1, and p2 | Default<br>f – focal length in px<br>cx, cy – principal point coordinates<br>k1, k2, k3 – radial distortion coefficients<br>p1, p2 – tangential distortion coefficients |
| Model Editing | Reprojection Error | 0.1 | |
| | Reproduction Uncertainty | 50 | |
| | Projection Accuracy | 10 | |
| Dense Point Cloud | Quality | High | |
| | Depth filtering | Disabled | |
| | Calculate Point Colours | Enabled | Not required, but did not affect processing time for this project |
| | Calculate Point Confidence | Disabled | Function not present for large part of data processing |

## Code

The following is an example of the code used for the graphics in this research written in R (example is pilot study 1, length):

```
###Boxplot example for pilot study measurements###

library(ggplot2)
library(dplyr)

#Length with all four measurements; colour and then greyscale

a1 <- ggplot(subset (ps_boxplots, Measurement %in% c("Length")), aes(x=Method,
y=Value, fill=Test, colour=Test)) +
  geom_boxplot() +
  scale_color_manual(values=c("#FF9900", "#000099")) +
  scale_fill_manual(values=c("#FFCC33", "#3366FF")) +
  scale_y_continuous(labels = scales::number_format(accuracy = 0.01),
breaks=seq(-2, 30, 2), expand = c(0,3)) +
  theme(panel.grid.major=element_blank()) +
  ylab("Value (in mm)")

a1


a2 <- ggplot(subset (ps_boxplots, Measurement %in% c("Length")), aes(x=Method,
y=Value, fill=Test, colour=Test)) +
  geom_boxplot() +
  scale_color_manual(values=c("#666666", "#000000")) +
  scale_fill_manual(values=c("#999999", "#333333")) +
  scale_y_continuous(labels = scales::number_format(accuracy = 0.01),
breaks=seq(-2, 30, 2), expand = c(0,3)) +
  theme(panel.grid.major=element_blank()) +
  ylab("Value (in mm)")


a2
```

The following in an example of the code used to create the scatterplots for the control cradle tests written in R (example MK2, x):

```
###Scatterplot example for testing the error and values found with the control
cradles###

library(ggplot2)
library(dplyr)

greyscale <- c("#CCCCCC", "#999999", "#666666", "#333333", "#000000")

b1 <- ggplot(subset(MK2_scatters, Direction %in% c("x")), aes(x=Value,
y=Error, colour=Model)) +
  geom_point(shape=19, size=2) +
  ylab("Absolute Error (in mm)") +
  xlab("Value (in mm)") +
  scale_colour_manual(values=greyscale) +
  scale_y_continuous(labels = scales::number_format(accuracy = 0.001),
                     breaks=seq(0, 2, 0.025)) +
  scale_x_continuous(labels = scales::number_format(accuracy = 0.001)) +
  geom_hline(yintercept = 0) +
  geom_vline(xintercept = 0)

b1
```

The following is an example of the code used for shape analysis in this research written in R (example is full collection, weaponry and width). The script, including most of the notes, is originally from Hoggard 2020. Slight adaptations have been made for this project:

```
#Loading the packages
library(Momocs)
library(rio)
library(tidyverse)
library(here)
library(ggplot2)

'''
importing non-tps
'''

jpg.list <-
list.files(here("C:\\Users\\Heather\\Documents\\Academic\\PhD\\R\\Updated_Shap
e_Analysis\\img_half_no_angle"), full.names = T)

coo <- import_jpg(jpg.list)


#Out(coo)

#make sure database is imported and change anything to a factor if needed
#SAP_chart$location <- as.factor(SAP_chart$location)


shape_file <- Out(coo, fac = incised_data_not_angled)
shape_file



'''
data vis
'''

panel(shape_file, main = "All Extracted Outlines", fac = 'variable')
  #does not give a legend automatically

mosaic(shape_file, ~location, asp = 1, legend = FALSE)
  #will replace panel, can change legend to TRUE

coo_plot(shape_file[1], col = "grey", centroid = TRUE, main = "3861.01_A")
  #specifically for one item, based on indexing


'''
Outline normalisation
'''

#It is recommended to normalise (standardise) and align your shapes before the
`Momocs::efourier()` process.
#Rotation was considered prior outline digitisation, however rotation could
also be explored in Momocs through the `Momocs::coo_aligncalliper()` function
prior the `Momocs:efourier()` argument.
#Here we will perform three transformation processes: 1)
`Momocs::coo_center()`, 2) `Momocs::coo_scale()` and 3) `Momocs::coo_close()`.
#These three functions perform the following actions:
  #`Momocs::coo_center()`: This action centres coordinates on a common
origin/common centroid).
  #`Momocs::coo_scale()`: This action scales the coordinates by their 'scale'
if provided, or a given centroid size if 'scale is not provided.
  #`Momocs::coo_close()`: Closes unclosed shapes (precautionary).
```

```
shapenorm <- coo_center(shape_file)
shapenorm <- coo_scale(shapenorm)
shapenorm <- coo_close(shapenorm)


#stack the outlines after normalisation
#may need to rotate if not done prior
plot1 <- stack(shapenorm, title = "Stacked and Normalised Outlines")

#piping here to slide the landmark to the right - changing the starting point
of the landmarks to line up
shapenorm2 <- shapenorm %>% coo_slidedirection("right") %>% coo_untiltx()

plot2 <- stack(shapenorm2, title = "Stacked and Normalised Outlines with
'coo_slidedirection()' Used")

'''
Elliptic Fourier transform

'''
#too high a harmonic level = inroduce statistical noise
#When a level of harmonic power (shape complexity) is determined by the
researcher (95%, 99%, 99.9%, 99.99% shape approximation), a series of
procedures can be implemented to test how many harmonics are necessary:

  #`Momocs::calibrate_harmonicpower_efourier()': This function estimates the
number of harmonics required for the elliptic Fourier process (and all other
Fourier processes).
  #`Momocs::calibrate_reconstructions_efourier()`: This procedure calculates
reconstructed shapes for a series of harmonic numbers. This process best
demonstrates the harmonic process.
  #`Momocs::calibrate_deviations_efourier()': This procedure calculates
deviations from the original and reconstructed shapes for a series of harmonic
numbers.


calibrate_harmonicpower_efourier(shapenorm2, nb.h = 20, plot = FALSE)
  #will give you number of harmonics needed for each error level

calibrate_reconstructions_efourier(shapenorm2, range = 1:20)
  #will select a random one and show how the harmonics affect

calibrate_deviations_efourier(shapenorm2, id = 4)
  #calculates deviations from original and reconstructed shapes, along the
shape outline, for a range of harmonic numbers

efashape <- efourier(shapenorm2, nb.h = 9, smooth.it = 0, norm = TRUE)
  #gone with 17 here because that was 99.9% in this dataset
  #should be OutCoe object


#Technical note: certain artefact shapes may be prone to bad alignment among
the first ellipses and result in not-as-ideal homologous coefficients,
#and in certain instances upside-down (or 180 degrees rotated) shapes on the
morphospace (e.g. PCA plots) may occur.
#It is considered good practice to normalise outlines (as we have done here)
and performing the efourier function with `norm = FALSE`.

#Other normalisation procedures not performed here include the addition of
landmarks,
#in order to anchor your artefacts, or through `Momocs::fgProcrustes` through
your calliper length.

#`norm = TRUE`, and the use of a numerical alignment ("through the first
ellipse"), is also a suitable option following prior normalisation.
#The degree of prior normalisation is dependent on the complexity of artefact
shape and is thus the choice of the researcher.
```

```
'''
PCA
'''

#With our new elliptic Fourier coefficients we can begin the exploratory and
analytical procedure.
#We will start by exploring the main theoretical differences in shape through
a **Principal Component Analysis (PCA)**.
#Please refer to the first workshop for a detailed explanation of PCA, and the
second workshop for further examples.
#In the second workshop we needed to turn our LdkCoe() into a PCA class object
through the `Momocs::PCA()` function.
#Here we need to repeat the process (or as demonstrated previously we can
utilise the dplyr piping operators).


#use the newly created dataset from the efourier to run the PCA
pcashape <- PCA(efashape)

#look at scree table and then visualise using a scree plot to find what axes
account for the most variation
scree(pcashape)
scree_plot(pcashape, nax = 1:16)
  #first 15 used here

scree_results <- scree(pcashape)


#if wanted to visualise less of the PCs to see the contribution, use the
following
PCcontrib(pcashape, nax = 1:9)
PCcontrib(pcashape, nax = 1:3)
#faceted outline graph with the SD

pcashape$eig



'''
Weaponry with full notes
'''

#Now we know what each principal component represents, and their values to
overall shape variation within our analysis,
#we can plot our artefacts within a morphospace representative of these
components.
#Here we will use the highly-customisable `Momocs::plot_PCA()` function:

pca1 <- plot_PCA(pcashape,
         axes = c(1,2),
         ~throat_cut,
         morphospace_position = "full_axes",
         zoom = 2,
         chull = FALSE) %>% layer_points(cex = 1) %>% layer_ellipses()

pca2 <- plot_PCA(pcashape,
                     axes = c(1,3),
                     ~throat_cut,
                     morphospace_position = "full_axes",
                     zoom = 2,
                     chull = FALSE) %>% layer_points(cex = 1) %>%
layer_ellipses()

pca3 <- plot_PCA(pcashape,
                     axes = c(2,3),
                     ~throat_cut,
                     morphospace_position = "full_axes",
                     zoom = 2,
                     chull = FALSE) %>% layer_points(cex = 1) %>%
layer_ellipses()
```

```
#In this diagram we can observe the different distributions of each variable within the morphospace,
#and the relative clustering of each unit within this graph.
#Some clusters appear incredibly tight, while others are broad, meaning that the variable is represented by varying shapes, some seen in other variables.
#It's important to remember that this graph only represents the first two principal components, and we may wish to examine other sources of shape variation
#(some which may be of importance to the archaeological relevance and discriminatory  powerful of shapes).

#Note: pipes (%>%) are used here to processes multiple arguments at the same time.
#Momocs supports piping with the whole process able to be 'piped'.
#For teaching purposes we are doing the 'long way' of GMM (as previous).

#If we wish to examine the relationship between different principal components we can use the `axes` argument to change our graph configuration.
#For example, if we wish to examine differences in shape between PC1 and PC3 we can specify the `axes` argument in the following way:

#just shows where the artifact is in terms of those two components

#can play with visualisation
plot_PCA(pcashape,
         axes = c(1,2),
         ~location,
         palette = pal_div_PiYG,
         morphospace_position = "circle",
         zoom = 1.5,
         chull = FALSE) %>% layer_points(cex = 1) %>% layer_ellipses()

#can also visualise as a box plot for first 5 axes
boxplot(pcashape, ~throat_cut, nax = 1:3)

'''
Discriminant Analysis (LDA/DA/CVA)
'''

#Through a discriminant analysis we can examine differences in shape as based on their maximum group separation
#(between-group variation in contrast to within-group variation).
#In Momocs, we use the `Momocs::LDA()` function on either the elliptic Fourier coefficients or the PCA scores
#to produce our class accuracy, plots and correction scores.
#There is no correct answer as to which to use, it depends on the data you wish to examine e.g. the degree of dimension reductionality.
#In using the PCA scores it is possible to retain a number of components that are deemed important, this can be either:
  #1) the first nth components,
  #2) the number of components representing a certain level of shape variance (e.g. 95%, 99%, 99.9%), or
  #3) all principal components
#The coefficients, in contrast would encapsulate all shape data.
#choose based on number of samples and number of coefficients/PCs

#With greater levels of data you may include a higher degree of unintentional statistical importance,
#with smaller unimportant variables taking precedence, and so an optimal amount of data is necessary.

#Below:
  #1) the Fourier coefficients,
  #2) 95% cumulative shape variance as expressed in PC scores, and
  #3) 99% cumulative shape variance expressed in PC scores.

dashapefc <- LDA(efashape, ~throat_cut)
dashape95 <- LDA(pcashape, ~throat_cut, retain = 0.95)
dashape99 <- LDA(pcashape, ~throat_cut, retain = 0.99)
```

```
#correction percentages and classification error
dashapefc$CV.correct
dashapefc$CV.ce
dashape95$CV.correct
dashape95$CV.ce
dashape99$CV.correct
dashape99$CV.ce


#When we examine the Fourier coefficients, a Leave-one-out cross-validation
score of 24% (60/250) is obtained in this example
#These three discriminant analyses highlight the relative robustness of
certain groups, and the weakness of many others,
#irrespective of how much data is provided.

#More detailed metrics are included in the `Momocs::classification_metrics()`
function (not covered here).

#Alternatively, these data can be transformed and assessed through further
supervised and unsupervised classificatory techniques
#through tidy machine learning techniques (see the parsnip package for
example).

#If we wish to visualise our plot, as is common in exploratory procedures we
can use the `Momocs::plot_LDA()` function,
#using similar arguments to `Momocs::plot_PCA()`.
#For example, to visualise the discriminant analysis for the Fourier
coefficients:

plot_LDA(dashapefc,
         axes = c(1,2),
         zoom = 1.5,
         chull = FALSE) %>% layer_points(cex = 1) %>%
layer_morphospace_LDA(position = "circle")


plot_LDA(dashapefc,
         axes = c(1,3),
         zoom = 1.5,
         chull = FALSE) %>% layer_points(cex = 1) %>%
layer_morphospace_LDA(position = "circle")


plot_LDA(dashapefc,
         axes = c(2,3),
         zoom = 1.5,
         chull = FALSE) %>% layer_points(cex = 1) %>%
layer_morphospace_LDA(position = "circle")


plot_LDA(dashape95,
         axes = c(1,2),
         zoom = 1.5,
         chull = FALSE) %>% layer_points(cex = 1) %>%
layer_morphospace_LDA(position = "circle")

plot_LDA(dashape95,
         axes = c(1,3),
         zoom = 1.5,
         chull = FALSE) %>% layer_points(cex = 1) %>%
layer_morphospace_LDA(position = "circle")

plot_LDA(dashape95,
         axes = c(2,3),
         zoom = 1.5,
         chull = FALSE) %>% layer_points(cex = 1) %>%
layer_morphospace_LDA(position = "circle")

'''
```

```
Multivariate Analysis of Variance (MANOVA)
'''

#Now we can test, within an Null Hypothesis Significance Testing (NHST) framework,
#whether there is difference between the different archaeological units.
#Again, this can be conducted on the Outline data (Fourier Coefficients) or the PCA scores.

#Once we have chosen a desired alpha level as of marker of difference (that is to say the boundary with which we are able to reject the null hypothesis of same populations)
#e.g. 0.05 we can use the `Momocs::MANOVA()` function, noting "Archaeological_Unit" to be our factor which we want to consider.
#For example, through piping, and for the three different methods above:

efashape %>% MANOVA(~throat_cut)

pcashape %>% MANOVA(~throat_cut, retain = 0.95)

pcashape %>% MANOVA(~throat_cut, retain = 0.99)


#This, however, doesn't tell us where the differences lie. Only with PC scores

pcashape %>% MANOVA_PW(~throat_cut, retain = 0.95)

pcashape %>% MANOVA_PW(~throat_cut, retain = 0.99)

#This rather large amount of information provides the p values for each combination of archaeological units
#and depicts level of significance in star form.
#In terms of analysis this data highlights, as previously the degree to which specific archaeological units
#can be distinguished from others in terms of their two-dimensional outline shape.


'''
Hierarchical and K-Means Cluster Analysis
'''

#We can now use the elliptic Fourier coefficients and/or the PCA data to examine, irrespective of previous groupings,
#how similar objects relate to one another within the overall set of examples.
#The end-point here will be the construction a set of clusters,
#where each cluster is distinct from each other cluster,
#and the objects within each cluster are broadly similar in two-dimensional outline shape.

#This can be done through two different methods in Momocs:
  #Hierarchical Cluster Analysis, where the structure is provided, or
  #K-Means analysis which partitions the shapes into k groups.

#To perform a Hierarchical Cluster Analysis we can use the `Momocs::CLUST()` function,
#a wrapper of `stats::dist()` and `stats::hclust()`.
#We can specify what type of shape we wish for our tree to be using the `type` argument (horizontal as default),
#and the specific `hclust` (complete as default) and `dist_method` (euclidean as default).
#Again, we can use the number of PCA scores as we find applicable or use the elliptic Fourier coefficients.

CLUST(pcashape,
      ~throat_cut,
      dist_method = "euclidean",
      hclust_method = "complete",
      palette = pal_qual)
```

```
#if want certain number of groups
CLUST(pcashape,
      ~throat_cut,
      dist_method = "euclidean",
      hclust_method = "complete",
      palette = pal_qual,
      k=3)

#This tree can be further examined in the `ape` package and customised further
through tree-specific packages e.g. `ggtree`.

#Alternatively we can use the `Momocs::KMEANS()` function to derive four x
number of groups from the data.
#top down
#or example, if we wish for four groups:

KMEANS(pcashape, centers = 4)




###Condensed Code

'''
WIDTH
'''



pca_wid1 <- plot_PCA(pcashape,
                     axes = c(1,2),
                     ~width,
                     morphospace_position = "full_axes",
                     zoom = 2,
                     chull = FALSE) %>% layer_points(cex = 1) %>%
layer_ellipses()


pca_wid2 <- plot_PCA(pcashape,
                     axes = c(1,3),
                     ~width,
                     morphospace_position = "full_axes",
                     zoom = 2,
                     chull = FALSE) %>% layer_points(cex = 1) %>%
layer_ellipses()


pca_wid3 <- plot_PCA(pcashape,
                     axes = c(2,3),
                     ~width,
                     morphospace_position = "full_axes",
                     zoom = 2,
                     chull = FALSE) %>% layer_points(cex = 1) %>%
layer_ellipses()


boxplot(pcashape, ~width, nax = 1:3)


w_dashapefc <- LDA(efashape, ~width)
w_dashape95 <- LDA(pcashape, ~width, retain = 0.95)

#correction percentages and classification error
w_dashapefc$CV.correct
w_dashapefc$CV.ce
w_dashape95$CV.correct
w_dashape95$CV.ce


plot_LDA(w_dashapefc,
```

```
         axes = c(1,2),
         zoom = 1.5,
         chull = FALSE) %>% layer_points(cex = 1) %>%
layer_morphospace_LDA(position = "circle")

plot_LDA(w_dashapefc,
         axes = c(1,3),
         zoom = 1.5,
         chull = FALSE) %>% layer_points(cex = 1) %>%
layer_morphospace_LDA(position = "circle")

plot_LDA(w_dashapefc,
         axes = c(2,3),
         zoom = 1.5,
         chull = FALSE) %>% layer_points(cex = 1) %>%
layer_morphospace_LDA(position = "circle")



plot_LDA(w_dashape95,
         axes = c(1,2),
         zoom = 1.5,
         chull = FALSE) %>% layer_points(cex = 1) %>%
layer_morphospace_LDA(position = "circle")

plot_LDA(w_dashape95,
         axes = c(1,3),
         zoom = 1.5,
         chull = FALSE) %>% layer_points(cex = 1) %>%
layer_morphospace_LDA(position = "circle")

plot_LDA(w_dashape95,
         axes = c(2,3),
         zoom = 1.5,
         chull = FALSE) %>% layer_points(cex = 1) %>%
layer_morphospace_LDA(position = "circle")


efashape %>% MANOVA(~width)

pcashape %>% MANOVA(~width, retain = 0.95)


#This, however, doesn't tell us where the differences lie. Only with PC scores


pcashape %>% MANOVA_PW(~width, retain = 0.95)


CLUST(pcashape,
      ~width,
      dist_method = "euclidean",
      hclust_method = "complete",
      palette = pal_qual)

#if want certain number of groups
CLUST(pcashape,
      ~width,
      dist_method = "euclidean",
      hclust_method = "complete",
      palette = pal_qual,
      k=4)


KMEANS(pcashape, centers = 2)
```

The following is an example of the code used for grouped bar charts written in R (example is cranial):

```
###Grouped bar chart example for counts of individuals with each number of
blows###

library(ggplot2)
library(dplyr)

#fully assembled in one go

#cranial only, first colour, then greyscale
#expand affects how close to edges of graph

p1 <- ggplot(c_grouped_bar, aes(fill=Amount, colour=Amount, y=Count, x=Cuts))
+
  geom_bar(position="dodge", stat="identity") +
  scale_colour_manual(values=c("#FFCC33", "#3366FF")) +
  scale_fill_manual(values=c("#FFCC33", "#3366FF")) +
  scale_y_continuous(labels = scales::number_format(accuracy = 1),
breaks=seq(0, 10, 1), expand = c(0,0.1)) +
  scale_x_continuous(breaks=seq(0, 12, 1), expand = c(0,0.5)) +
  theme(panel.grid.minor=element_blank())

p1

p2 <- ggplot(c_grouped_bar, aes(fill=Amount, colour=Amount, y=Count, x=Cuts))
+
  geom_bar(position="dodge", stat="identity") +
  scale_colour_manual(values=c("#999999", "#333333")) +
  scale_fill_manual(values=c("#999999", "#333333")) +
  scale_y_continuous(labels = scales::number_format(accuracy = 1),
breaks=seq(0, 10, 1), expand = c(0,0.1)) +
  scale_x_continuous(breaks=seq(0, 12, 1), expand = c(0,0.5)) +
  theme(panel.grid.minor=element_blank())


p2
```

The following is the code version of the QGIS graphic modeller extracted in python:

```
"""
Model exported as python.
Name : s_r_test
Group : test
With QGIS : 31604
"""

from qgis.core import QgsProcessing
from qgis.core import QgsProcessingAlgorithm
from qgis.core import QgsProcessingMultiStepFeedback
from qgis.core import QgsProcessingParameterDistance
from qgis.core import QgsProcessingParameterVectorLayer
from qgis.core import QgsProcessingParameterFeatureSink
import processing


class S_r_test(QgsProcessingAlgorithm):

    def initAlgorithm(self, config=None):
        self.addParameter(QgsProcessingParameterDistance('BufferSize', 'Buffer
Size', parentParameterName='PointCloudFile', minValue=-1.79769e+308,
defaultValue=None))
        self.addParameter(QgsProcessingParameterVectorLayer('PointCloudFile',
'Point Cloud File', types=[QgsProcessing.TypeVectorPoint], defaultValue=None))
```

```
        self.addParameter(QgsProcessingParameterFeatureSink('CentroidOutput',
'Centroid Output', type=QgsProcessing.TypeVectorPoint, createByDefault=True,
supportsAppend=True, defaultValue=None))

    def processAlgorithm(self, parameters, context, model_feedback):
        # Use a multi-step feedback, so that individual child algorithm
progress reports are adjusted for the
        # overall progress through the model
        feedback = QgsProcessingMultiStepFeedback(5, model_feedback)
        results = {}
        outputs = {}

        # Buffer
        alg_params = {
            'DISSOLVE': False,
            'DISTANCE': parameters['BufferSize'],
            'END_CAP_STYLE': 0,
            'INPUT': parameters['PointCloudFile'],
            'JOIN_STYLE': 0,
            'MITER_LIMIT': 2,
            'SEGMENTS': 5,
            'OUTPUT': QgsProcessing.TEMPORARY_OUTPUT
        }
        outputs['Buffer'] = processing.run('native:buffer', alg_params,
context=context, feedback=feedback, is_child_algorithm=True)

        feedback.setCurrentStep(1)
        if feedback.isCanceled():
            return {}

        # Point Cloud Spatial Index
        alg_params = {
            'INPUT': parameters['PointCloudFile']
        }
        outputs['PointCloudSpatialIndex'] =
processing.run('native:createspatialindex', alg_params, context=context,
feedback=feedback, is_child_algorithm=True)

        feedback.setCurrentStep(2)
        if feedback.isCanceled():
            return {}

        # Buffer Spatial Index
        alg_params = {
            'INPUT': outputs['Buffer']['OUTPUT']
        }
        outputs['BufferSpatialIndex'] =
processing.run('native:createspatialindex', alg_params, context=context,
feedback=feedback, is_child_algorithm=True)

        feedback.setCurrentStep(3)
        if feedback.isCanceled():
            return {}

        # Join attributes by location (summary)
        alg_params = {
            'DISCARD_NONMATCHING': False,
            'INPUT': outputs['Buffer']['OUTPUT'],
            'JOIN': parameters['PointCloudFile'],
            'JOIN_FIELDS': ['Z'],
            'PREDICATE': [0],
            'SUMMARIES': [6,13],
            'OUTPUT': QgsProcessing.TEMPORARY_OUTPUT
        }
        outputs['JoinAttributesByLocationSummary'] =
processing.run('qgis:joinbylocationsummary', alg_params, context=context,
feedback=feedback, is_child_algorithm=True)

        feedback.setCurrentStep(4)
        if feedback.isCanceled():
```

```
                return {}

            # Centroids
            alg_params = {
                'ALL_PARTS': True,
                'INPUT': outputs['JoinAttributesByLocationSummary']['OUTPUT'],
                'OUTPUT': parameters['CentroidOutput']
            }
            outputs['Centroids'] = processing.run('native:centroids', alg_params,
    context=context, feedback=feedback, is_child_algorithm=True)
            results['CentroidOutput'] = outputs['Centroids']['OUTPUT']
            return results

        def name(self):
            return 's_r_test'

        def displayName(self):
            return 's_r_test'

        def group(self):
            return 'test'

        def groupId(self):
            return 'test'

        def createInstance(self):
            return S_r_test()
```

# Appendix E: Iterative Tests, Pilot Study Statistics, and Control Cradle Tests

## Iterative Tests

The following section contains the graphs and figures associated with the iterative testing processing used to choose some of the Agisoft Photoscan/Metashape settings. The full write-up is found in Section 5.3.4. Table E-1 displays the camera settings used for the iterative tests and Fig. 116 shows the testing process without the final variables.

Table E-1: The parameters in use for the pilot study image capture

| Parameter | Incised | Shaved |
|---|---|---|
| ISO | 100 | 100 |
| Aperture | f22 | f25 |
| Shutter Speed | 1/1.6 | 1.6 |

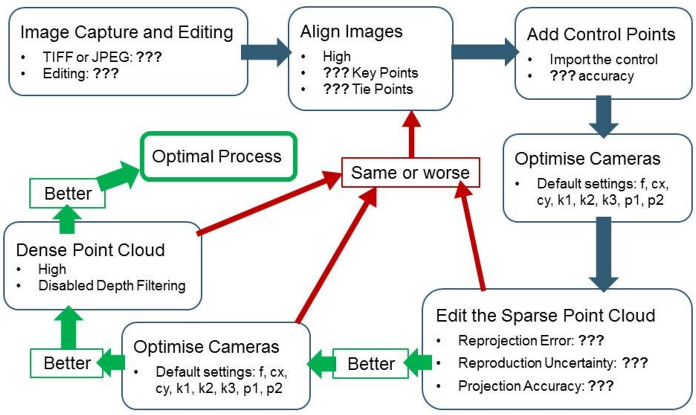


Figure 116: The iterative testing workflow used in this project

## Bit-Depth and Editing Trials

The following tables (E-2 through E-5) are associated with Section 5.3.4.1, pertaining to the initial testing of the file format and bit-depth.

Table E-2: Results of the bit-depth trials for both pilot studies

| | Edit | Bit depth | C/GS | SPC Full | Post-edit SPC | Errors (mm) | Errors (px) |
|---|---|---|---|---|---|---|---|
| PS1 | No | 8 | Greyscale | 13988 | 6455 | 0.105 | 3.994 |
| | | 16 | Greyscale | 13987 | 6451 | 0.090 | 2.921 |
| | | 24 | Colour | 13502 | 6977 | 0.091 | 2.385 |
| | | 48 | Colour | 13668 | 6186 | 0.101 | 3.349 |
| | Yes | 8 | Greyscale | 12659 | 7397 | 0.085 | 1.796 |
| | | 16 | Greyscale | 12865 | 8020 | 0.090 | 1.676 |
| | | 24 | Colour | 12156 | 6563 | 0.089 | 2.561 |
| | | 48 | Colour | 12498 | 5885 | 0.089 | 2.570 |
| | No | JPEG | Colour | 12456 | 6299 | 0.076 | 2.423 |
| PS2 | No | 8 | Greyscale | 15322 | 9801 | 0.090 | 0.756 |
| | | 16 | Greyscale | 15232 | 9569 | 0.094 | 0.633 |
| | | 24 | Colour | 15222 | 9792 | 0.099 | 0.663 |
| | | 48 | Colour | 15045 | 9548 | 0.090 | 0.706 |
| | Yes | 8 | Greyscale | 10658 | 6120 | 0.091 | 0.709 |
| | | 16 | Greyscale | 10590 | 6304 | 0.095 | 0.654 |
| | | 24 | Colour | 10708 | 6263 | 0.097 | 0.667 |
| | | 48 | Colour | 10701 | 6305 | 0.102 | 0.718 |
| | No | JPEG | Colour | 10544 | 6113 | 0.110 | 0.658 |

Table E-3: Results of the bit-depth trials with relative changes in the full DPC for both pilot studies with largest three changes that are also over 5% for each pilot study in bold

| | Edit | Bit depth | C/GS | File Size (kB) | Full DPC | Δ Points | % Δ Points* |
|---|---|---|---|---|---|---|---|
| PS1 | No | 8 | Greyscale | 389000 | 6320238 | 273999 | 4.5% |
| | | 16 | Greyscale | 778000 | 7087287 | 1041048 | 17.2% |
| | | 24 | Colour | 1130000 | 6017114 | -29125 | -0.5% |
| | | 48 | Colour | 2280000 | 7293272 | 1247033 | **20.6%** |
| | Yes | 8 | Greyscale | 389000 | 6611920 | 565681 | 9.4% |
| | | 16 | Greyscale | 778000 | 7295279 | 1249040 | **20.7%** |
| | | 24 | Colour | 1130000 | 7089718 | 1043479 | 17.3% |
| | | 48 | Colour | 2280000 | 7345176 | 1298937 | **21.5%** |
| | No | JPEG | Colour | 146000 | 6046239 | -- | -- |
| PS2 | No | 8 | Greyscale | 389000 | 10655610 | -498045 | -4.5% |
| | | 16 | Greyscale | 778000 | 11750810 | 597155 | **5.4%** |
| | | 24 | Colour | 1130000 | 11376233 | 222578 | 2.0% |
| | | 48 | Colour | 2280000 | 11916733 | 763078 | **6.8%** |
| | Yes | 8 | Greyscale | 389000 | 10333335 | -820320 | -7.4% |
| | | 16 | Greyscale | 778000 | 11044954 | -108701 | -1.0% |
| | | 24 | Colour | 1130000 | 11176819 | 23164 | 0.2% |
| | | 48 | Colour | 2270000 | 11895931 | 742276 | **6.7%** |
| | No | JPEG | Colour | 151000 | 11153655 | -- | -- |

*Relative to JPEG

Table E-4: Results of the bit-depth trials with relative changes in the cutmark DPC for both pilot studies with largest three changes that are also over 5% for each pilot study in bold

| | Edit | Bit depth | C/GS | File Size (kB) | Cut DPC | Δ kB | Δ Points | % Δ Points* |
|---|---|---|---|---|---|---|---|---|
| PS1 | No | 8 | Greyscale | 389000 | 277549 | 243000 | 18991 | **7.3%** |
| | | 16 | Greyscale | 778000 | 267849 | 632000 | 9291 | 3.6% |
| | | 24 | Colour | 1130000 | 272582 | 984000 | 14024 | 5.4% |
| | | 48 | Colour | 2280000 | 261788 | 2134000 | 3230 | 1.2% |
| | Yes | 8 | Greyscale | 389000 | 273037 | 243000 | 14479 | 5.6% |
| | | 16 | Greyscale | 778000 | 288462 | 632000 | 29904 | **11.6%** |
| | | 24 | Colour | 1130000 | 281984 | 984000 | 23426 | 9.1% |
| | | 48 | Colour | 2280000 | 301273 | 2134000 | 42715 | **16.5%** |
| | No | JPEG | Colour | 146000 | 258558 | 0 | 0 | -- |
| PS2 | No | 8 | Greyscale | 389000 | 2452641 | 238000 | -74517 | -2.9% |
| | | 16 | Greyscale | 778000 | 2533558 | 627000 | 6400 | 0.3% |
| | | 24 | Colour | 1130000 | 2540795 | 979000 | 13637 | 0.5% |
| | | 48 | Colour | 2280000 | 2560157 | 2129000 | 32999 | 1.3% |
| | Yes | 8 | Greyscale | 389000 | 2465276 | 238000 | -61882 | -2.4% |
| | | 16 | Greyscale | 778000 | 2492193 | 627000 | -34965 | -1.4% |
| | | 24 | Colour | 1130000 | 2539412 | 979000 | 12254 | 0.5% |
| | | 48 | Colour | 2270000 | 2558877 | 2119000 | 31719 | 1.3% |
| | No | JPEG | Colour | 151000 | 2527158 | 0 | 0 | -- |

*Relative to JPEG

Table E-5: The comparison of the edited and unedited images in both pilot studies at different bit-depths

| | | | DPC Cutmark | | | DPC Full | | |
|---|---|---|---|---|---|---|---|---|
| | Bit-depth | C/GS | Unedited Points | Edited Points | % Diff Uned. to Edited | Unedited Points | Edited Points | % Diff Uned. to Edited |
| PS1 | 8 | Greyscale | 18991 | 14479 | -1.6% | 6320238 | 6611920 | 4.6% |
| | 16 | Greyscale | 9291 | 29904 | 7.7% | 7087287 | 7295279 | 2.9% |
| | 24 | Colour | 14024 | 23426 | 3.4% | 6017114 | 7089718 | 17.8% |
| | 48 | Colour | 3230 | 42715 | 15.1% | 7293272 | 7345176 | 0.7% |
| PS2 | 8 | Greyscale | 2452641 | 2465276 | 0.5% | 10655610 | 10333335 | -3.0% |
| | 16 | Greyscale | 2533558 | 2492193 | -1.6% | 11750810 | 11044954 | -6.0% |
| | 24 | Colour | 2540795 | 2539412 | -0.1% | 11376233 | 11176819 | -1.8% |
| | 48 | Colour | 2560157 | 2558877 | 0.0% | 11916733 | 11895931 | -0.2% |

Overall, the findings suggested that the process is fairly robust to changes and all combinations produced a usable point cloud.

## Tie Point Trials

The following tables (E-6 through E-8) hold the results from the tie point (TP) trials for both pilot studies.

Table E-6: Points in the point clouds at different levels of TPs in both pilot studies

| | Trial | Key Points | Tie Points | Pre-Edit SPC | 0.2 Edit SPC | 0.2 DPC | 0.1 Edit SPC | 0.1 DPC |
|---|---|---|---|---|---|---|---|---|
| PS1 | 1 | 40000 | 4000 | 12798 | 7505 | 12363020 | 4246 | 12257773 |
| | 2 | 40000 | 8000 | 12859 | 7837 | 12216064 | 4375 | 12105090 |
| | 3 | 40000 | 12000 | 12875 | 8876 | 12233451 | 5408 | 12174008 |
| | 4 | 40000 | 16000 | 12864 | 7728 | 12245052 | 4543 | 12155021 |
| | 5 | 40000 | 20000 | 12847 | 7362 | 12192675 | 4285 | 12141837 |
| PS2 | 1 | 40000 | 4000 | 14749 | 9520 | 11677540 | 5071 | 11592658 |
| | 2 | 40000 | 8000 | 18310 | 12739 | 11733507 | 7136 | 11629085 |
| | 3 | 40000 | 12000 | 19838 | 14335 | 11726693 | 8489 | 11628260 |
| | 4 | 40000 | 16000 | 19857 | 14451 | 11674458 | 8361 | 11555997 |
| | 5 | 40000 | 20000 | 19804 | 14808 | 11648240 | 8709 | 11586711 |

Table E-7: The comparison of the RE levels in the full DPCs in both pilot studies at different TPs

| | Trial | Key Points | Tie Points | 0.2 Reprojection Error | | 0.1 Reprojection Error | | %Diff 0.2 to 0.1 |
|---|---|---|---|---|---|---|---|---|
| | | | | DPC Points | %Diff compared to default | DPC Points | %Diff compared to default | |
| PS1 | 1 | 40000 | 4000 | 12363020 | -- | 12257773 | -- | -0.9% |
| | 2 | 40000 | 8000 | 12216064 | -1.2% | 12105090 | -1.2% | -0.9% |
| | 3 | 40000 | 12000 | 12233451 | -1.0% | 12174008 | -0.7% | -0.5% |
| | 4 | 40000 | 16000 | 12245052 | -1.0% | 12155021 | -0.8% | -0.7% |
| | 5 | 40000 | 20000 | 12192675 | -1.4% | 12141837 | -0.9% | -0.4% |
| PS2 | 1 | 40000 | 4000 | 11677540 | -- | 11592658 | -- | 0.3% |
| | 2 | 40000 | 8000 | 11733507 | 0.7% | 11629085 | 0.3% | 0.0% |
| | 3 | 40000 | 12000 | 11726693 | 1.4% | 11628260 | 0.6% | -0.5% |
| | 4 | 40000 | 16000 | 11674458 | 0.1% | 11555997 | 0.0% | 0.2% |
| | 5 | 40000 | 20000 | 11648240 | 0.3% | 11586711 | 0.3% | 0.2% |

Table E-8: The comparison of the RE levels in the cutmark DPCs in both pilot studies at different TPs

| | Trial | Key Points | Tie Points | 0.2 Reprojection Error | | 0.1 Reprojection Error | | %Diff 0.2 to 0.1 |
|---|---|---|---|---|---|---|---|---|
| | | | | Cutmark Points | %Diff compared to default | Cutmark Points | %Diff compared to default | |
| PS1 | 1 | 40000 | 4000 | 228000 | -- | 241792 | -- | 6.0% |
| | 2 | 40000 | 8000 | 222445 | -2.4% | 236831 | -2.1% | 6.5% |
| | 3 | 40000 | 12000 | 213342 | -6.4% | 239338 | -1.0% | 12.2% |
| | 4 | 40000 | 16000 | 233854 | 2.6% | 241448 | -0.1% | 3.2% |
| | 5 | 40000 | 20000 | 221162 | -3.0% | 231057 | -4.4% | 4.5% |
| PS2 | 1 | 40000 | 4000 | 2518361 | -- | 2526331 | -- | -0.7% |
| | 2 | 40000 | 8000 | 2534942 | 0.5% | 2533780 | 0.3% | -0.9% |
| | 3 | 40000 | 12000 | 2552665 | 0.4% | 2540889 | 0.3% | -0.8% |
| | 4 | 40000 | 16000 | 2521146 | 0.0% | 2526557 | -0.3% | -1.0% |
| | 5 | 40000 | 20000 | 2527089 | -0.3% | 2532782 | -0.1% | -0.5% |

## Key Point Trials

The following tables (E-9 through E-11) show the results from the key point (KP) trials for both pilot studies.

Table E-9: Points in the point clouds at different levels of KPs in both pilot studies

| | Trial | Key Points | Tie Points | Pre-Edit SPC | 0.2 Edit SPC | 0.2 DPC | 0.1 Edit SPC | 0.1 DPC |
|---|---|---|---|---|---|---|---|---|
| PS1 | 1 | 50000 | 4000 | 15127 | 9695 | 12005752 | 5845 | 11969234 |
| | 2 | 40000 | 4000 | 12853 | 8183 | 12203672 | 5022 | 12127349 |
| | 3 | 30000 | 4000 | 10402 | 6762 | 12224376 | 4165 | 12141219 |
| | 4 | 20000 | 4000 | 7701 | 4887 | 12341071 | 2806 | 12240111 |
| | 5 | 10000 | 4000 | 4380 | 2965 | 12623629 | 1875 | 12524729 |
| PS2 | 1 | 50000 | 4000 | 16806 | 10600 | 11761191 | 5490 | 11689440 |
| | 2 | 40000 | 4000 | 15054 | 9943 | 11669846 | 5250 | 11592505 |
| | 3 | 30000 | 4000 | 9894 | 6239 | 11636498 | 3040 | 11496844 |
| | 4 | 20000 | 4000 | 9203 | 6521 | 11688462 | 3527 | 11529817 |
| | 5 | 10000 | 4000 | 5783 | 4371 | 11759031 | 2579 | 11665015 |

Table E-10: The comparison of the RE levels in the full DPCs in both pilot studies at different KPs

| | Trial | Key Points | Tie Points | 0.2 Reprojection Error DPC Points | 0.2 Reprojection Error %Diff compared to default | 0.1 Reprojection Error DPC Points | 0.1 Reprojection Error %Diff compared to default | %Diff 0.2 to 0.1 |
|---|---|---|---|---|---|---|---|---|
| PS1 | 1 | 50000 | 4000 | 12005752 | -1.6% | 11969234 | -1.3% | 0.3% |
| | 2 | 40000 | 4000 | 12203672 | -- | 12127349 | -- | 0.6% |
| | 3 | 30000 | 4000 | 12224376 | 0.2% | 12141219 | 0.1% | 0.7% |
| | 4 | 20000 | 4000 | 12341071 | 1.1% | 12240111 | 0.9% | 0.8% |
| | 5 | 10000 | 4000 | 12623629 | 3.4% | 12524729 | 3.3% | 0.8% |
| PS2 | 1 | 50000 | 4000 | 11761191 | 0.8% | 11689440 | 0.8% | -0.6% |
| | 2 | 40000 | 4000 | 11669846 | -- | 11592505 | -- | -0.7% |
| | 3 | 30000 | 4000 | 11636498 | -0.3% | 11496844 | -0.8% | -1.2% |
| | 4 | 20000 | 4000 | 11688462 | 0.2% | 11529817 | -0.5% | -1.4% |
| | 5 | 10000 | 4000 | 11759031 | 0.8% | 11665015 | 0.6% | -0.8% |

Table E-11: The comparison of the RE levels in the cutmark DPCs in both pilot studies at different KPs

| | Trial | Key Points | Tie Points | 0.2 Reprojection Error DPC Points | 0.2 Reprojection Error %Diff compared to default | 0.1 Reprojection Error DPC Points | 0.1 Reprojection Error %Diff compared to default | %Diff 0.2 to 0.1 |
|---|---|---|---|---|---|---|---|---|
| PS1 | 1 | 50000 | 4000 | 238926 | -6.5% | 270199 | 0.7% | 13.1% |
| | 2 | 40000 | 4000 | 255642 | -- | 268300 | -- | 5.0% |
| | 3 | 30000 | 4000 | 228961 | -10.4% | 254147 | -5.3% | 11.0% |
| | 4 | 20000 | 4000 | 232782 | -8.9% | 257924 | -3.9% | 10.8% |
| | 5 | 10000 | 4000 | 255736 | 0.0% | 268397 | 0.0% | 5.0% |
| PS2 | 1 | 50000 | 4000 | 2545235 | 0.6% | 2540861 | 0.3% | -0.2% |
| | 2 | 40000 | 4000 | 2530376 | -- | 2533646 | -- | 0.1% |
| | 3 | 30000 | 4000 | 2520341 | -0.4% | 2521235 | -0.5% | 0.0% |
| | 4 | 20000 | 4000 | 2499262 | -1.2% | 2465069 | -2.7% | -1.4% |
| | 5 | 10000 | 4000 | 2522046 | -0.3% | 2538610 | 0.2% | 0.7% |

## Control Accuracy Trials

The following tables (E-12 and E-13) show the results from the trials of different accuracy levels for both pilot studies.

Table E-12: The error values from the accuracy trials in both pilot studies

| | Trial | Accuracy (mm) | Error (mm) | Post-Edit Error (mm) | Error (px) | Post-Edit Error (px) |
|---|---|---|---|---|---|---|
| PS1 | 1 | 0.0005 | 0.065 | 0.065 | 1.825 | 1.856 |
| | 2 | 0.0010 | 0.071 | 0.071 | 1.577 | 1.594 |
| | 3 | 0.0050 | 0.084 | 0.084 | 1.407 | 1.405 |
| | 4 | 0.0100 | 0.085 | 0.085 | 1.406 | 1.403 |
| | 5 | 0.0500 | 0.086 | 0.086 | 1.406 | 1.403 |
| | 6 | 0.1000 | 0.086 | 0.086 | 1.406 | 1.403 |
| | 7 | 0.5000 | 0.086 | 0.086 | 1.406 | 1.403 |
| | 8 | 1.0000 | 0.086 | 0.086 | 1.406 | 1.403 |
| | 9 | 1.5000 | 0.086 | 0.086 | 1.406 | 1.403 |
| | 10 | 2.0000 | 0.086 | 0.086 | 1.406 | 1.403 |
| | 11 | 2.5000 | 0.086 | 0.086 | 1.406 | 1.403 |
| | 12 | 500.0000 | 0.086 | 0.086 | 1.406 | 1.403 |
| | 13 | 1000.0000 | 0.086 | 0.086 | 1.406 | 1.403 |
| PS2 | 1 | 0.0005 | 0.064 | 0.063 | 1.376 | 1.403 |
| | 2 | 0.0010 | 0.070 | 0.069 | 1.059 | 1.076 |
| | 3 | 0.0050 | 0.093 | 0.092 | 0.648 | 0.648 |
| | 4 | 0.0100 | 0.097 | 0.095 | 0.641 | 0.639 |
| | 5 | 0.0500 | 0.097 | 0.097 | 0.641 | 0.638 |
| | 6 | 0.1000 | 0.097 | 0.097 | 0.641 | 0.638 |
| | 7 | 0.5000 | 0.097 | 0.097 | 0.641 | 0.638 |
| | 8 | 1.0000 | 0.097 | 0.097 | 0.641 | 0.638 |
| | 9 | 1.5000 | 0.097 | 0.097 | 0.641 | 0.638 |
| | 10 | 2.0000 | 0.097 | 0.097 | 0.641 | 0.638 |
| | 11 | 2.5000 | 0.097 | 0.097 | 0.641 | 0.638 |
| | 12 | 500.0000 | 0.097 | 0.097 | 0.641 | 0.638 |
| | 13 | 1000.0000 | 0.097 | 0.097 | 0.641 | 0.638 |

Table E-13: The number of points in the full and cutmark DPC from the accuracy trials in both pilot studies

| | Trial | Accuracy (mm) | DPC Full | DPC Cutmark | %Diff Full | %Diff cutmark |
|---|---|---|---|---|---|---|
| PS1 | 1 | 0.0005 | 11895993 | 244286 | -1.3% | 2.3% |
| | 2 | 0.0010 | 11973733 | 237883 | -0.7% | -0.4% |
| | 3 | 0.0050 | 12058390 | 241752 | 0.0% | 1.3% |
| | 4 | 0.0100 | 12079877 | 241530 | 0.2% | 1.2% |
| | 5 | 0.0500 | 12055134 | 241678 | 0.0% | 1.2% |
| | 6 | 0.1000 | 12088655 | 238622 | 0.3% | 0.0% |
| | 7 | 0.5000 | 12087222 | 237331 | 0.3% | -0.6% |
| | 8 | 1.0000 | 12054696 | 240602 | 0.0% | 0.8% |
| | 9 | 1.5000 | 12052672 | 238739 | -- | -- |
| | 10 | 2.0000 | 12054057 | 241512 | 0.0% | 1.2% |
| | 11 | 2.5000 | 12086943 | 236286 | 0.3% | -1.0% |
| | 12 | 500.0000 | 12081725 | 240761 | 0.2% | 0.8% |
| | 13 | 1000.0000 | 12080257 | 241434 | 0.2% | 1.1% |
| PS2 | 1 | 0.0005 | 12202630 | 2604288 | 5.1% | 3.1% |
| | 2 | 0.0010 | 12016321 | 2720554 | 3.5% | 7.7% |
| | 3 | 0.0050 | 11606604 | 2528396 | -0.1% | 0.1% |
| | 4 | 0.0100 | 11608898 | 2529393 | 0.0% | 0.2% |
| | 5 | 0.0500 | 11618203 | 2518814 | 0.0% | -0.3% |
| | 6 | 0.1000 | 11605402 | 2526577 | -0.1% | 0.0% |
| | 7 | 0.5000 | 11602597 | 2536636 | -0.1% | 0.4% |
| | 8 | 1.0000 | 11604227 | 2530365 | -0.1% | 0.2% |
| | 9 | 1.5000 | 11612698 | 2525432 | -- | -- |
| | 10 | 2.0000 | 11599299 | 2533093 | -0.1% | 0.3% |
| | 11 | 2.5000 | 11611197 | 2525356 | 0.0% | 0.0% |
| | 12 | 500.0000 | 11606552 | 2528114 | -0.1% | 0.1% |
| | 13 | 1000.0000 | 11619827 | 2532148 | 0.1% | 0.3% |

## Pilot Study Statistics

The following are the additional graphs showing the intra-observer error and method comparison for the pilot study tests (Section 5.3.5, see Figures 71 to 73). Figures 117 to 119 present the additional measurements for pilot study 1. Pilot study 2 had no additional measurements.

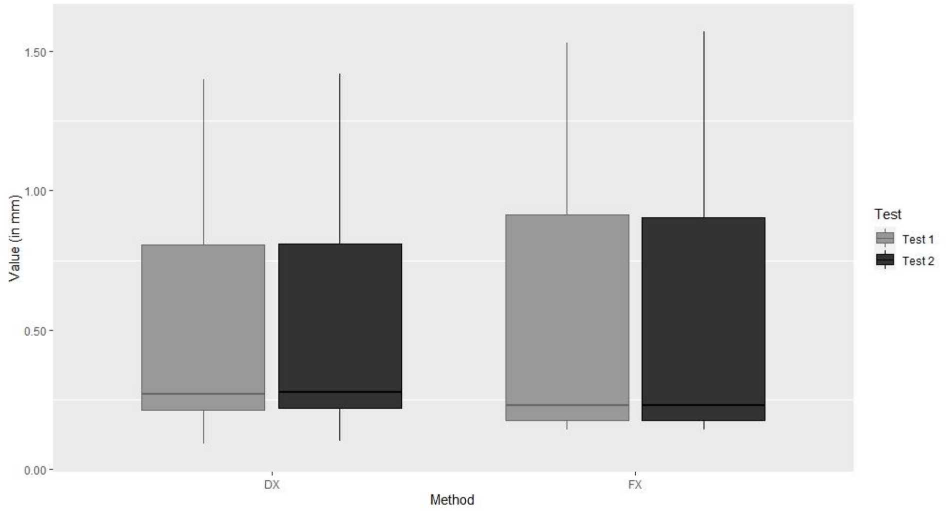


Figure 117: The intra-observer error and comparison of the DX and FX models for wall height 1 in pilot study 1

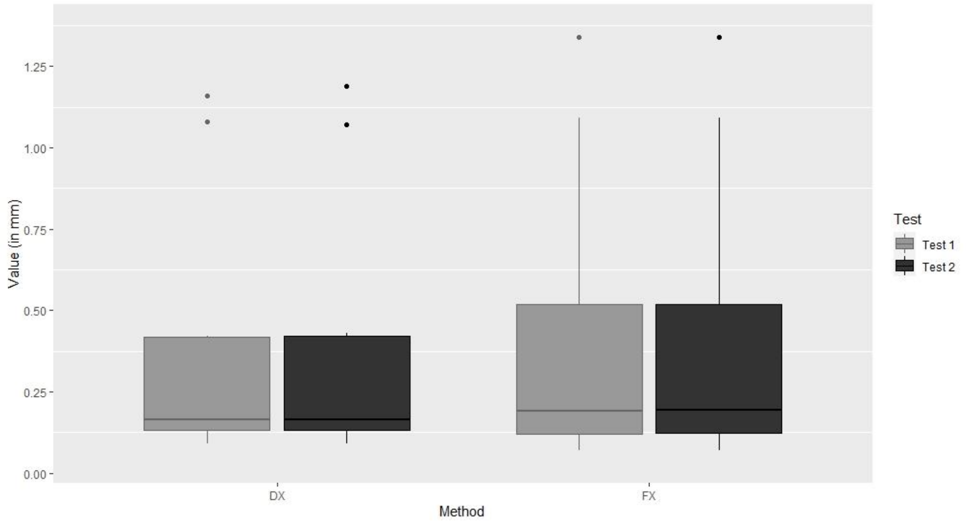


Figure 118: The intra-observer error and comparison of the DX and FX models for wall height 2 in pilot study 1

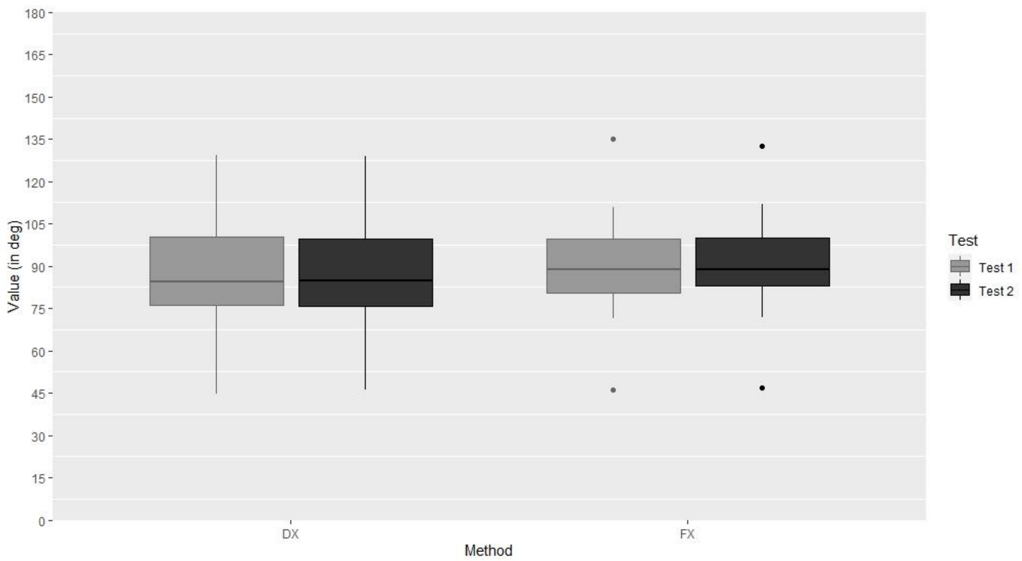


Figure 119: The intra-observer error and comparison of the DX and FX models for opening angle in pilot study 1

## Control Cradle Tests

The following are the additional graphs created when investigating the control cradles (Section 5.3.6).

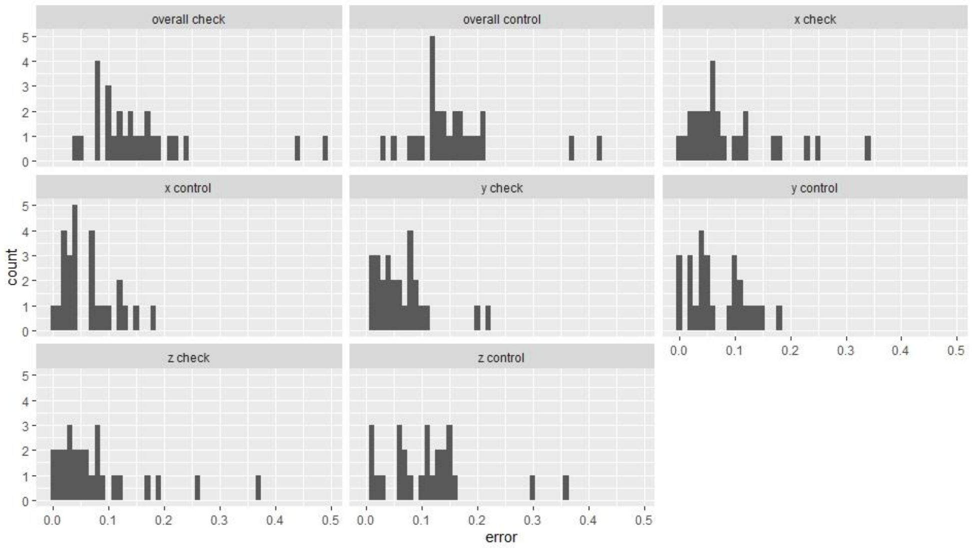


Figure 120: Histograms of the errors seen in MK2 to investigate normality (error in mm)

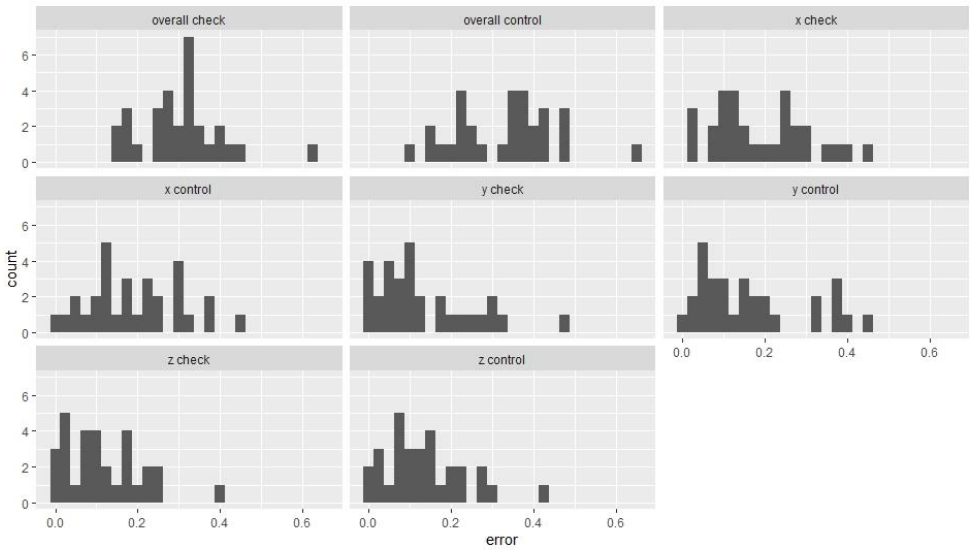


Figure 121: Histograms of the errors seen in PH to investigate normality (error in mm)

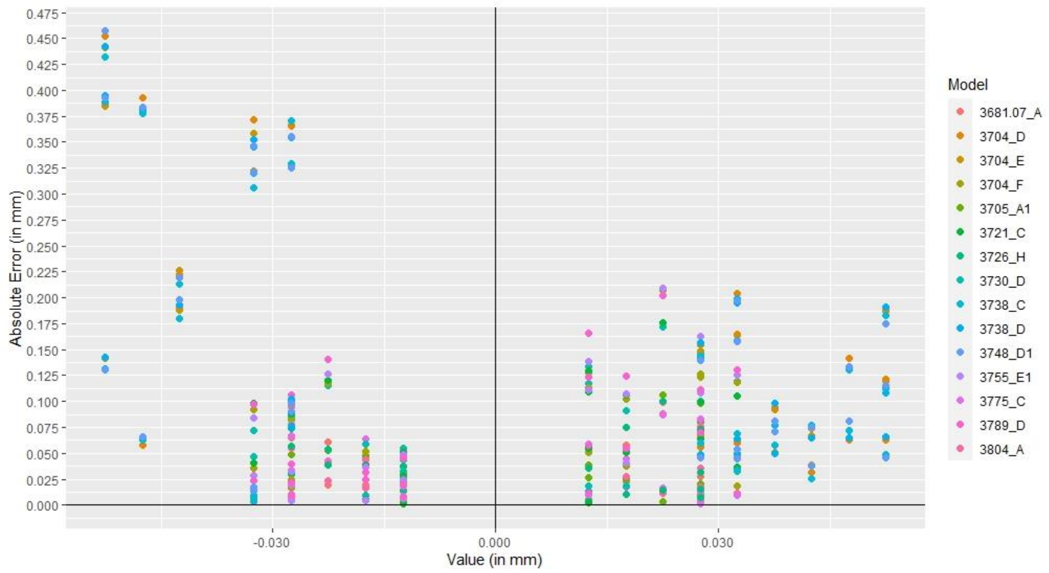


Figure 122: The y-value and y-error scatterplot for all cradles

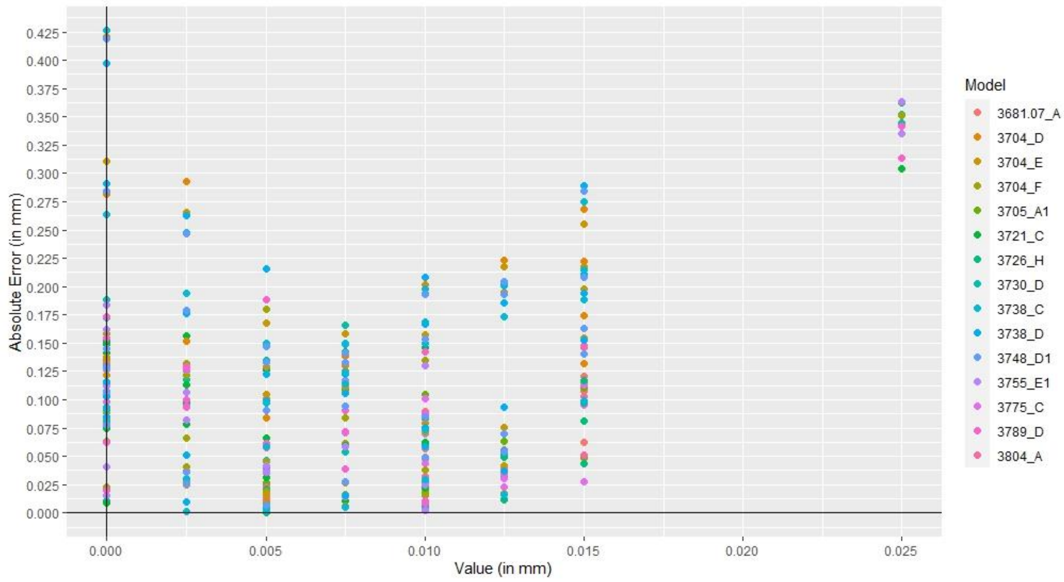


Figure 123: The z-value and z-error scatterplot for all cradles

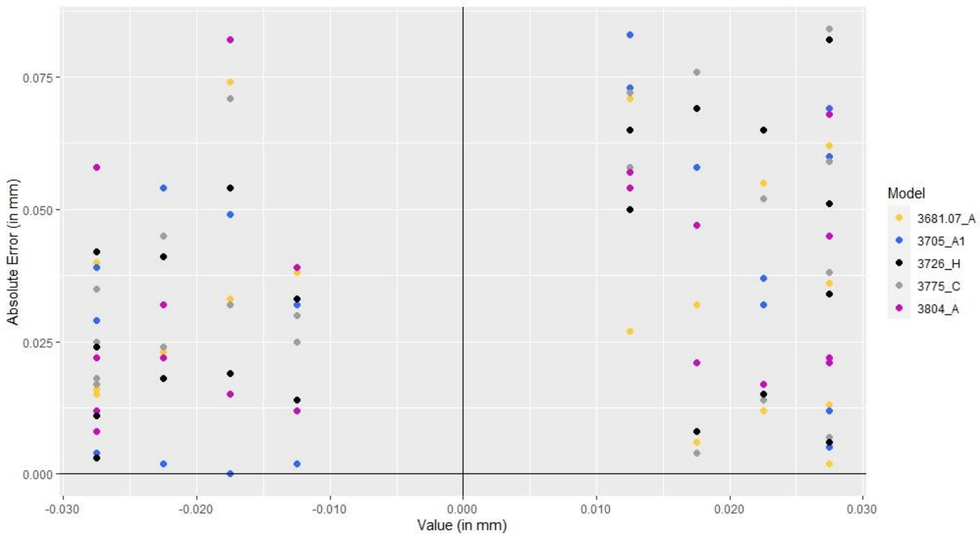


Figure 124: The x-value and x-error scatterplot for OG

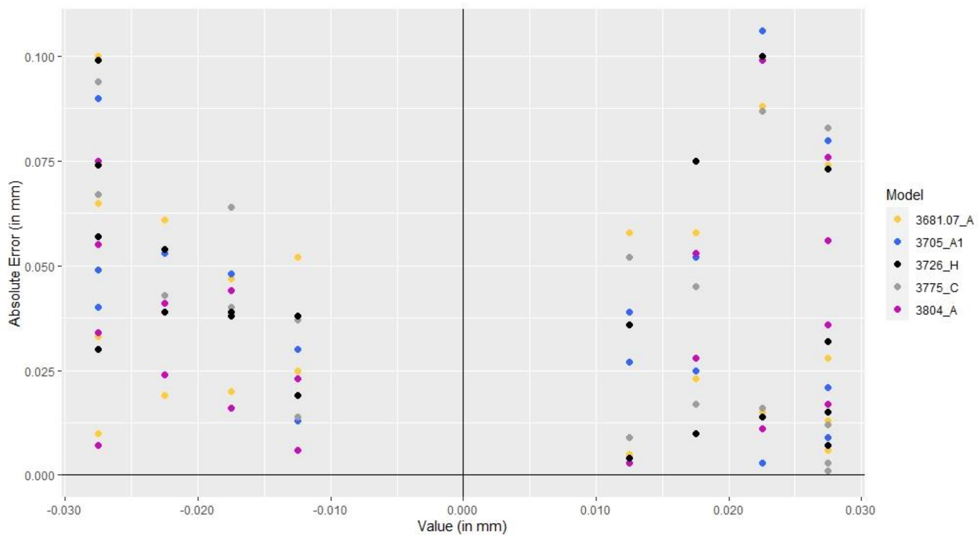


Figure 125: The y-value and y-error scatterplot for OG

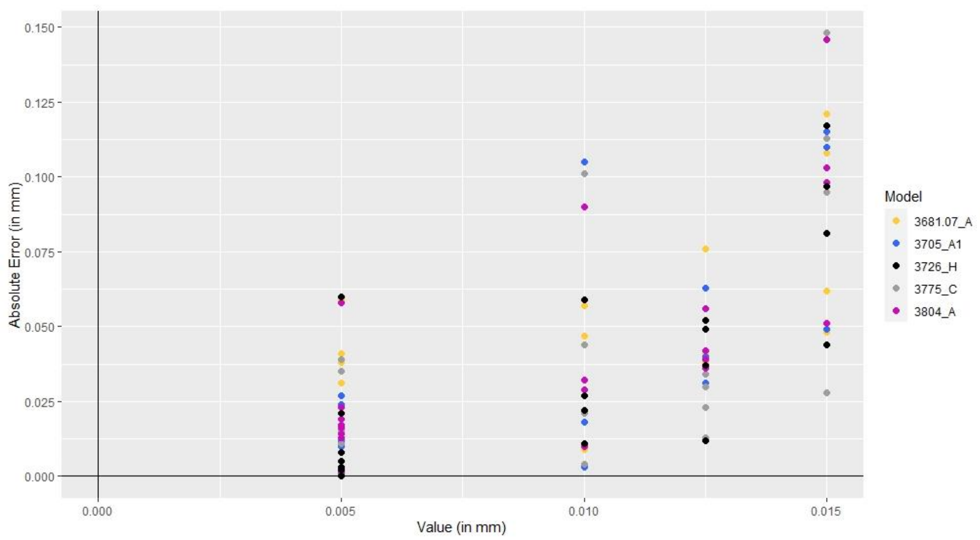


Figure 126: The z-value and z-error scatterplot for OG

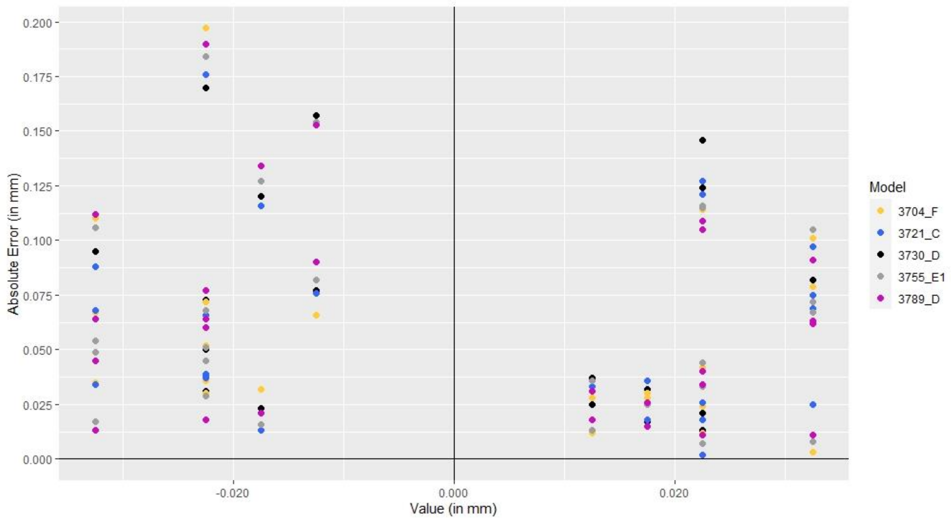


Figure 127: The x-value and x-error scatterplot for MK2

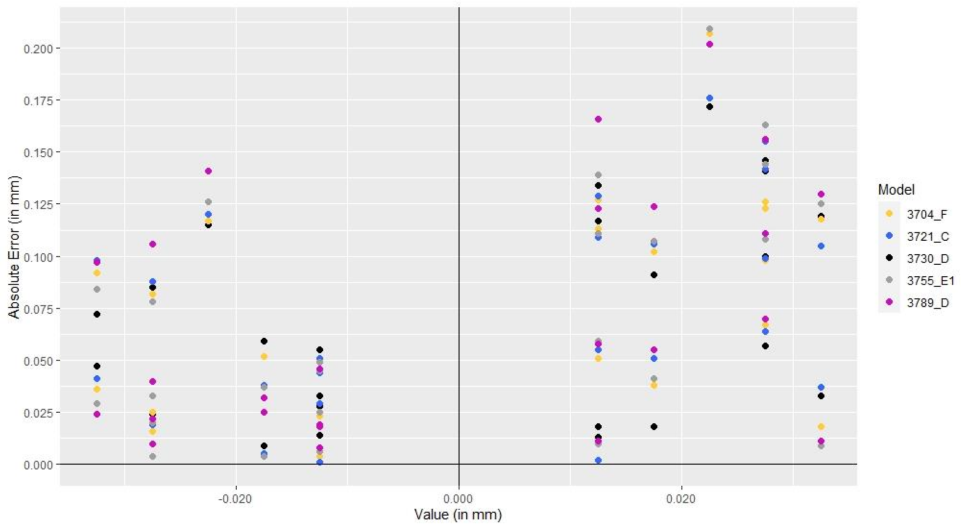


Figure 128: The y-value and y-error scatterplot for MK2

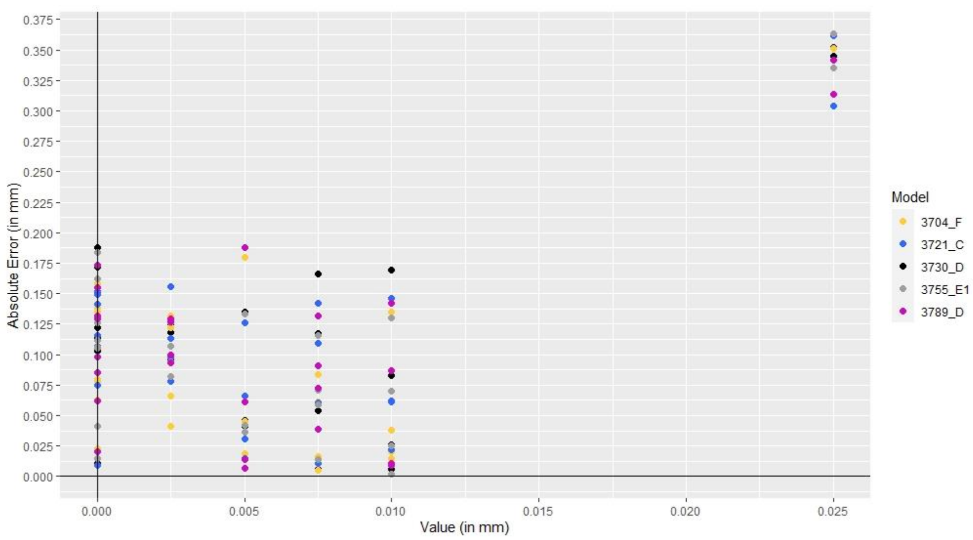


Figure 129: The z-value and z-error scatterplot for MK2

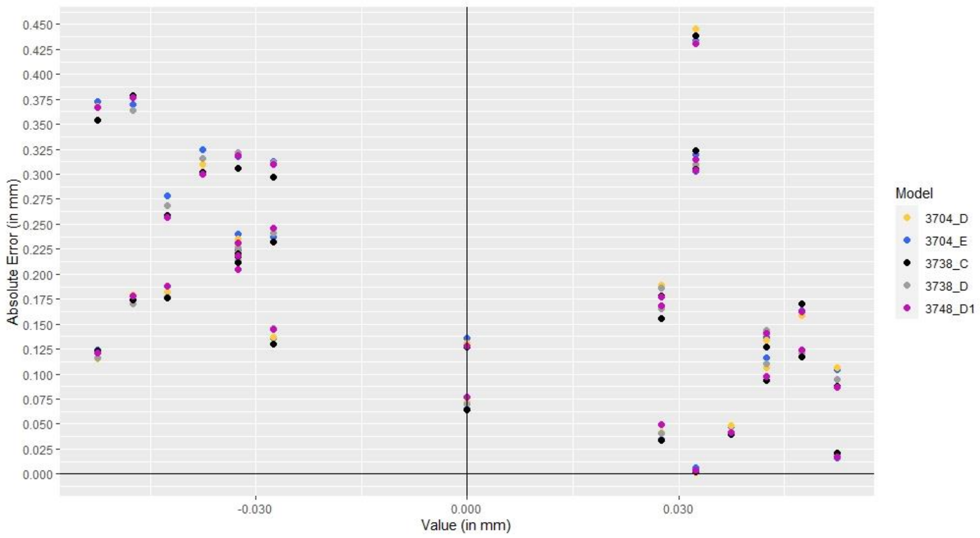


Figure 130: The x-value and x-error scatterplot for PH

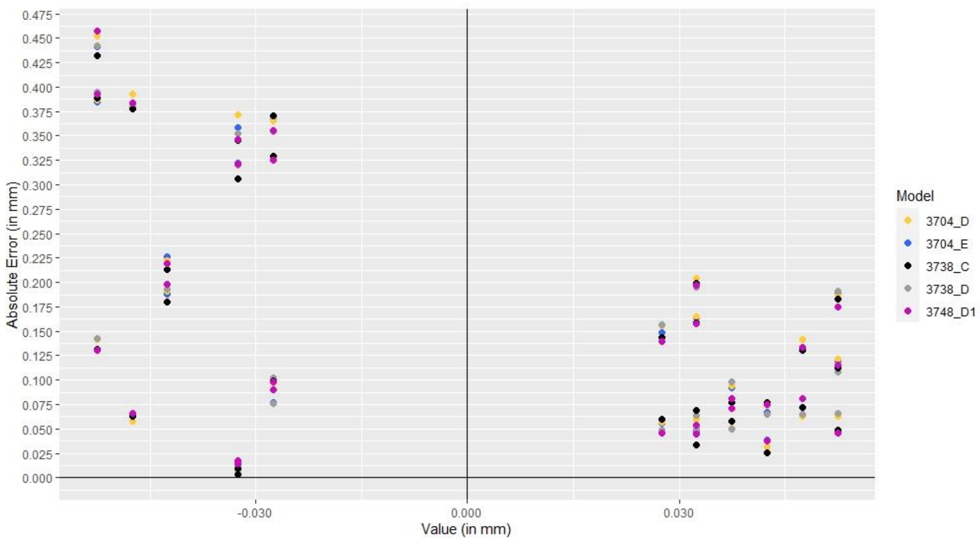


Figure 131: The y-value and y-error scatterplot for PH

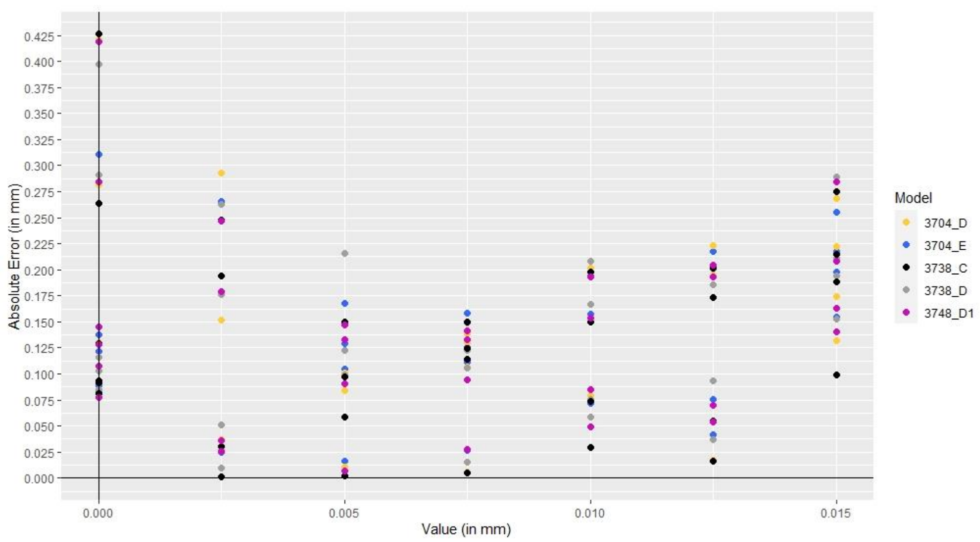


Figure 132: The z-value and z-error scatterplot for PH

# Appendix F: Sharp Force Trauma Catalogue of the Articulated Remains

Cutmark Coding:

**0000_A0**

Context Number
Cutmark ID
Segment of cutmark, if applicable

Italicised=Cranial
Non-Italicised=Postcranial

Key:

AF – Articular Facet (S – superior, I – inferior)
CV – Cervical Vertebrae
SP – Spinous Process
MC – Metacarpal
PP – Proximal Phalanx
IP – Intermediate Phalanx
DP – Distal Phalanx
DNE – Does not exist
I – Incised Cutmark
S – Shaved Cutmark
BI – Broken Incised
^ – Not in osteological report

Direction of blow:
→ Direction of entry known
– Direction of entry unknown
NEI Not Enough Information
(?) – Direction only known due to associations
n.b. all directions in relation to standard anatomical position

Associations levels of certainty:
Potential → Possible → Likely

Table F-1: The cutmark catalogue for the articulated remains (Section 7.1)

| ID # | Bone (Side) | Location | Cat* | Description | Associations | Direction of Blow // Angle of Cutmark *Based on anatomical position |
|---|---|---|---|---|---|---|
| ***3686_A1*** | Parietal (R) | Squama | BI ^ | Angled cut to posterior parietal<br>Cut runs: Superior/Anterior – Inferior/Posterior<br>Superior portion<br>Cut found after digitation complete | -- | Blow: Superior/Posterior → Inferior/Anterior |
| ***3686_A2*** | Parietal (R) | Squama | BI ^ | Angled cut to posterior parietal<br>Cut runs: Superior/Anterior – Inferior/Posterior<br>Inferior portion<br>Cut found after digitation complete | -- | Blow: Superior/Posterior → Inferior/Anterior |

| ID # | Bone (Side) | Location | Cat* | Description | Associations | Direction of Blow // Angle of Cutmark *Based on anatomical position |
|---|---|---|---|---|---|---|
| **3687** | -- | -- | -- | -- | -- | -- |
| **3688** | -- | -- | -- | -- | -- | -- |
| **3689_A** | CV 3 (R) | SAF | S | Only a small fragment left; top of R SAF removed by blow<br>Taphonomic damage | -- | Blow: Anterior/Right → Posterior/Left |
| **3689_B** | CV 7 (L) | Body | I ^ | Superior left body<br>Individual has supernumerary rib<br>Some taphonomic damage | -- | Blow: Left → Right<br>Oriented near vertical, possibly stabbing motion |
| **3689_C** | Capitate (L) | Medial dorsal part | S | Medial dorsal aspect removed<br>Some taphonomic damage | Likely 3689_D and 3689_E | Blow: Anterior/Right(Med) – Posterior/Left(Lat) |
| **3689_D** | MC 3 (L) | Lateral base | S | Lateral proximal part of the base removed | Likely 3689_C and E | Blow: Anterior – Posterior |
| **3689_E** | MC 2 (L) | Shaft | S | Potentially just resultant/RED fracturing<br>Fragmented | Likely 3689_C and D | Blow: Inferior/Left(Lat) – Superior/Right(Med) |
| ***3692*** | -- | -- | -- | -- | -- | -- |
| ***3693_A1*** | Frontal (L) | Squama, near coronal suture | I | PM cracking through the cutmark; superior portion<br>Cut runs from superior/medial/anterior on the frontal bone to inferior/lateral/posterior, nearing the coronal suture | -- | Blow: Superior/Left(Lat) → Inferior/Right(Med)<br>Nearly in coronal plane |
| ***3693_A2*** | Frontal (L) | Squama, near coronal suture | I | PM cracking through the cutmark; inferior portion<br>Cut runs from superior/medial/anterior on the frontal bone to inferior/lateral/posterior, nearing the coronal suture | -- | Blow: Superior/Left(Lat) → Inferior/Right(Med)<br>Nearly in coronal plane |
| ***3694_A1*** | CV 3 (R) | Body | S | Inferior right of the body removed<br>Some taphonomic damage | -- | Blow: Superior/Anterior/Right → Inferior/Posterior/Left |
| ***3694_A2*** | CV 3 (L) | IAF | S | Inferior part of IAF removed | -- | Blow: Superior/Anterior/Right → Inferior/Posterior/Left |

| ID # | Bone (Side) | Location | Cat* | Description | Associations | Direction of Blow // Angle of Cutmark *Based on anatomical position |
|---|---|---|---|---|---|---|
| ***3695_A*** | CV ?3 (L) | IAF and arch | S ^ | Only the inferior part of the lamina and IAF remain<br>PM damage to lateral side | Possibly 3695_B | Blow: Anterior/Left(Lat) → Posterior/Right(Med)<br>Nearly in transverse plane |
| ***3695_B*** | CV 2 (L) | Arch and SP | S ^ | Inferior portion of SP/arch removed<br>No damage visible on R side | Possibly 3695_A | Blow: ?Left → Right<br>Nearly in transverse plane |
| | | | | Possibly cut on L mandible but taphonomy too severe | | |
| ***3696*** | -- | -- | -- | -- | -- | -- |
| **3697** | -- | -- | -- | -- | -- | -- |
| **3698** | -- | -- | -- | -- | -- | -- |
| **3699** | -- | -- | -- | -- | -- | -- |
| **3700_A1** | CV 2 (R) | SAF | S | Odontoid removed and not present<br>Medial part of SAF<br>Taphonomic damage | -- | Blow: nearly in transverse plane |
| **3700_A2** | CV 2 (L) | SAF | S | Odontoid removed and not present<br>Medial part of SAF | -- | Blow: nearly in transverse plane |
| ***3704_A1*** | CV 2 | Body | S | Posterior/inferior left body removed | Potentially 3704_J<br>If neck flexed or mandible open, potentially 3704_H | Blow: Anterior/Right →Posterior/Left<br>Angled: Superior/Left – Inferior/Right<br>Nearly in transverse plane |
| ***3704_A2*** | CV 2 (L) | Arch and IAF | S | Inferior aspect of left arch and IAF removed<br>(RED) | Potentially 3704_J<br>If neck flexed or mandible open, potentially 3704_H | Blow: Anterior/Right →Posterior/Left<br>Angled: Superior/Left – Inferior/Right<br>Nearly in transverse plane |
| ***3704_C1*** | CV 2 (L) | Arch | S | Cut on the posterior left arch<br>Anterior part<br>Taphonomic damage | -- | Blow: Anterior/Left → Posterior/Right<br>Angle: Superior/Left(Lat) – Inferior/Right(Med) |

| ID # | Bone (Side) | Location | Cat* | Description | Associations | Direction of Blow // Angle of Cutmark *Based on anatomical position |
|---|---|---|---|---|---|---|
| ***3704_C2*** | CV 2 (L) | Arch | S | Cut on the posterior left arch<br>Posterior part<br>Taphonomic damage | -- | Blow: Anterior/Left → Posterior/Right<br>Angle: Superior/Left(Lat) – Inferior/Right(Med) |
| ***3704_D*** | Parietal (L) | Squama | I | Cut central on side of L parietal<br>Runs from anterior/medial aspect (aligned with bregma) to posterior/lateral<br>Anterior wall smoother | -- | Blow: Superior/Left(Lat) → Inferior/Right(Med)<br>Slight: Posterior → Anterior |
| ***3704_E*** | Parietal (R) | Posterior | I ^ | Cut in posterior portion of R parietal<br>Runs from posterior/medial aspect (aligned with lambda) to anterior/lateral<br>Anterior wall smoother | -- | Blow: Superior/Right(Lat) → Inferior/Left(Med)<br>Slight: Anterior → Posterior |
| ***3704_F*** | Mandible (R) | Corpus | BI | Large cut about halfway into the corpus before resultant fracturing<br>Posterior to 3704_G<br>No equivalent on L | -- | Blow: Inferior/Posterior → Superior/Anterior |
| ***3704_G*** | Mandible (R) | Corpus | BI ^ | Large cut about halfway into the corpus before resultant fracturing<br>Anterior to 3704_F<br>No equivalent on L | -- | Blow: Inferior/Posterior → Superior/Anterior |
| ***3704_H*** | Mandible (R) | Ascending Ramus | I | Posterior part; about halfway up<br>No equivalent on L | If neck flexed or mandible open, potentially 3704_As, and/or J, K | Blow: Inferior/Posterior → Superior/Anterior |
| ***3704_I1*** | Mandible (L) | Ascending Ramus | BI | On the lateral side of the mandible<br>Cut runs from superior/anterior to inferior/posterior<br>Possibly distinct from 3704_L which is just inferior to | -- | Blow: Superior/Left(Lat) → Inferior/Right(Med) |
| ***3704_I2*** | Mandible (L) | Ascending Ramus | S | On the lateral side of the mandible<br>Cut runs from superior/anterior to inferior/posterior<br>Anterior continuation | -- | Blow: Superior/Left(Lat) → Inferior/Right(Med) |

| ID # | Bone (Side) | Location | Cat* | Description | Associations | Direction of Blow // Angle of Cutmark *Based on anatomical position |
|---|---|---|---|---|---|---|
| ***3704_J*** | CV 2 (R) | IAF | I ^ | Distinct from and superior to 3704_K<br>End point visible in bone | Possibly 3704_As | Blow: Anterior/Right →Posterior/Left<br>Angled: Superior/Left – Inferior/Right<br>Nearly in transverse plane |
| ***3704_K*** | CV 2 (R) | IAF | BI ^ | Distinct from and inferior to 3704_J | -- | Nearly in transverse plane |
| ***3704_L*** | Mandible (L) | Ascending Ramus | I | On the lateral side of the mandible<br>Cut runs from superior/anterior to inferior/posterior<br>Inferior to and smaller than 3704_I | -- | Blow: Superior/Left (Lat) → Inferior/Right(Med) |
| ***3705_A1*** | CV 1 (L) | IAF | BI ^ | Part of the cut that is on the main remaining part of the CV 1<br>Opposite to 3705_A2 | -- | Blow: Superior/Posterior/Left → Inferior/Anterior/Right |
| ***3705_A2*** | CV 1 (L) | IAF | BI ^ | The IAF removed from the remaining part of CV 1<br>Opposite to 3705_A1 | -- | Blow: Superior/Posterior/Left → Inferior/Anterior/Right |
| ***3705_A3*** | CV 1 (R) | IAF and Pedicle | I | End point of 3705_A1 and 2<br>Cut runs Superior/Posterior – Inferior/Anterior | -- | Blow: Superior/Posterior/Left → Inferior/Anterior/Right |
| ***3705_A4*** | CV 1 (R) | Arch | I | Continuation of 3705_A3<br>Cut runs Superior/Posterior – Inferior/Anterior | -- | Blow: Superior/Posterior/Left → Inferior/Anterior/Right |
| ***3705_B*** | CV 1 (L) | Arch | I ^ | Cut on inferior part of the posterior arch | -- | Blow: Superior/Left → Inferior/Right |
| ***3705_C1*** | CV 2 | Dens | BI | The odontoid had been cut at an angle<br>Inferior portion<br>Superior to 3705_D1 and 2 | -- | Blow: Superior/Right – Inferior/Left |
| ***3705_C2*** | CV 2 | Dens | BI | Superior portion, tip of the odontoid<br>Superior to 3705_D1 and 2 | -- | Blow: Superior/Right – Inferior/Left |
| ***3705_D1*** | CV 2 | Body | BI ^ | Both sides present<br>Taphonomic damage<br>Inferior to 3705_C1 and 2 | Possibly 3705_Is and J | Blow: Superior/Right – Inferior/Left<br>Blow: ?Inferior/Left(Lat) → Superior/Right(Med) |
| ***3705_D2*** | CV 2 | Body | BI ^ | Both sides present<br>Taphonomic damage<br>Inferior to 3705_C1 and 2 | Possibly 3705_Is and J | Blow: Superior/Right – Inferior/Left<br>Blow: ?Inferior/Left(Lat) → Superior/Right(Med) |

| ID # | Bone (Side) | Location | Cat* | Description | Associations | Direction of Blow // Angle of Cutmark *Based on anatomical position |
|---|---|---|---|---|---|---|
| ***3705_E*** | CV 2 (R) | IAF | S ^ | Inferior portion of R IAF removed | Potentially 3705_L | Anterior → Posterior<br>Angled: Superior/Right – Inferior/Left |
| ***3705_F1*** | CV 3 (R) | IAF and arch | S | Inferior part of IAF removed | Likely 3705_M | Blow: Nearly in transverse plane |
| ***3705_F2*** | CV 3 (L) | IAF and arch | S ^ | Inferior part of IAF removed; debatable | Likely 3705_M | Blow: Nearly in transverse plane |
| ***3705_G*** | CV 1 (R) | Anterior arch | I ^ | Superior to 3705_H | -- | Blow: Anterior → Posterior<br>Nearly in transverse plane |
| ***3705_H*** | CV 1 (R) | Anterior arch | S ^ | Inferior to 3705_G<br>Only superior aspect of arch remains | -- | Blow: Inferior/Anterior → Superior/Posterior<br>Nearly in transverse plane |
| ***3705_I1*** | Mandible (R) | Ascending Ramus | I ^ | Cut into medial side of ascending ramus<br>End point of the cut | Possibly 3705_Ds<br>Likely 3705_J | Blow: Inferior/Left(Med) → Superior/Right(Lat) |
| ***3705_I2*** | Mandible (L) | Ascending Ramus | S ^ | Cut through ascending ramus about half way up | Possibly 3705_Ds<br>Likely 3705_J | Blow: Inferior/Left(Lat) → Superior/Right(Med) |
| ***3705_J*** | Maxilla (R) | Alveolar process | I ^ | Seen on the roots of R $M^1$ and $M^2$<br>Small part of cut in alveolar process | Possibly 3705_Ds<br>Likely 3705_Is | Blow: Inferior/Left(Med) → Superior/Right(Lat) |
| ***3705_K*** | CV 1 (L) | IAF | S ^ | Lateral tip of L IAF removed<br>On the fragment with cut 3705_A2 | | Blow: Superior/Posterior/Left → Inferior/Anterior/Right |
| ***3705_L*** | CV 3 (L) | SAF | S ^ | On the fragment with cut 3705_F2<br>Tip of SAF removed | Possibly 3705_E | Blow: Anterior/Left → Posterior/Right |
| ***3705_M*** | Mandible (L) | Ascending ramus | S | Large amounts of taphonomic overprinting | Likely 3705_Fs | Blow: Nearly horizontal |
| ***3706*** | -- | -- | -- | -- | -- | -- |
| ***3707_A1*** | CV1 | Arch | BI | Main part of CV, superior part of posterior arch removed | Possibly 3707_Fs, G, and Hs | Blow: Inferior/Posterior → Superior/Anterior |
| ***3707_A2*** | CV1 | Arch | BI | The posterior part of the arch that was removed | Possibly 3707_Fs, G, and Hs | Blow: Inferior/Posterior → Superior/Anterior |
| ***3707_B1*** | CV 2 | Body | S | Anterior inferior part of body removed | Likely 3707_D | Blow: Inferior/Left – Superior/Right |

| ID # | Bone (Side) | Location | Cat* | Description | Associations | Direction of Blow // Angle of Cutmark *Based on anatomical position |
|---|---|---|---|---|---|---|
| ***3707_B2*** | CV 2 | Body | S | Small part of L inferior, anterior part of body remaining | Likely 3707_D | Blow: Inferior/Left – Superior/Right |
| ***3707_C1*** | CV 2 (L) | IAF and arch | BI | Main body of the CV 2<br>L IAF and inferior arch removed | -- | Blow: Inferior/Posterior → Superior/Anterior<br>Angle: Superior/Left – Inferior/Right |
| ***3707_C2*** | CV 2 (L) | IAF | BI | The inferior part of the L IAF that was removed | -- | Blow: Inferior/Posterior → Superior/Anterior<br>Angle: Superior/Left – Inferior/Right |
| ***3707_C3*** | CV 2 (R) | Arch | I | Inferior arch<br>Possible ending point of the blade | -- | Blow: Inferior/Posterior → Superior/Anterior<br>Angle: Superior/Left – Inferior/Right |
| ***3707_D*** | CV 3 (L) | Body | I ^ | Cut on the superior anterior L edge of the body<br>Superior to 3707_E1, E2 | Likely 3707_Bs | Blow: Anterior → Posterior<br>In transverse plane |
| ***3707_E1*** | CV 3 (L) | Body | I ^ | Cut on anterior L body<br>Some taphonomic damage<br>Inferior to 3707_D | -- | Blow: Anterior → Posterior<br>Nearly in transverse plane Angled: slightly Inferior/Right – Superior/Left |
| ***3707_E2*** | CV 3 (L) | Anterior tubercle | I ^ | Cut on anterior part of L anterior tubercle<br>Taphonomic damage<br>Inferior to 3707_D | -- | Blow: Anterior → Posterior<br>Nearly in transverse plane Angled: slightly Inferior/Right – Superior/Left |
| ***3707_F1*** | Temporal (L) | Mastoid process | S | Will get more information from the mastoid itself | Likely 3707_Gs, H<br>Possibly 3707_As | Nearly in transverse plane |
| ***3707_F2*** | Temporal (L) | Mastoid process | S | The mastoid | Likely 3707_Gs, H<br>Possibly 3707_As | Nearly in transverse plane |
| ***3707_F3*** | Temporal (L) | Near lambdoid suture | S ^ | Just medial to the mastoid process | Likely 3707_Gs, H<br>Possibly 3707_As | Nearly in transverse plane |

| ID # | Bone (Side) | Location | Cat* | Description | Associations | Direction of Blow // Angle of Cutmark *Based on anatomical position |
|---|---|---|---|---|---|---|
| ***3707_G1*** | Occipital (L) | Near lambdoid suture | S ^ | Rearticulates with the temporal<br>Lines up with 3707_F3 | Likely 3707_Gs, H<br>Possibly 3707_As | Nearly in transverse plane |
| ***3707_G2*** | Occipital (L) | Base | S ^ | Rearticulates with the temporal<br>Medial | Likely 3707_Gs, H<br>Possibly 3707_As | Nearly in transverse plane |
| ***3707_G3*** | Occipital | Base | S ^ | Central occipital<br>Models demarcated as H, but fixed for the patterning | Likely 3707_Gs, H<br>Possibly 3707_As | Nearly in transverse plane |
| ***3707_I*** | Frontal (R) | Central | S ^ | Just superior to brow area<br>Runs approximately parallel to the coronal suture | -- | Blow: Superior/Right(Lat) → Inferior/Left(Med)<br>Nearly in coronal plane |
| ***3707_J1*** | Occipital | Central | S / BI | Multiple pieces remain<br>Changes into resultant fracturing inferiorly | -- | Blow: Superior/Posterior/Left(Med) → Inferior/Anterior/Right(Lat) |
| ***3707_J2*** | Occipital (R) | Central | S / BI | Multiple pieces remain, the lateral portion<br>Changes into resultant fracturing inferiorly | -- | Blow: Superior/Posterior/Left(Med) → Inferior/Anterior/Right(Lat) |
| ***3707_K*** | Maxilla (L) | Zygomatic process | S ^ | Possibly shaved surface of zygomatic process of L maxilla<br>May be mainly RED | -- | Blow: Superior/Right(Med) – Inferior/Left(Lat) |
| ***3707_L1*** | Mandible (L) | Corpus | S ^ | Central part of the inferior of the corpus | -- | Blow: Inferior/Left – Superior/Right |
| ***3707_L2*** | Mandible (R) | Corpus | S ^ | Central part of the inferior of the corpus<br>More significant than 3707_L1 | -- | Blow: Inferior/Left – Superior/Right |
| ***3707_N*** | CV 3 | Body | I ^ | The anterior body, inferior to 3707_E1 | -- | Blow: Anterior → Posterior<br>Nearly in transverse plane<br>Angled: slightly Inferior/Right – Superior/Left |

| ID # | Bone (Side) | Location | Cat* | Description | Associations | Direction of Blow // Angle of Cutmark *Based on anatomical position |
|---|---|---|---|---|---|---|
| ***3707_P*** | CV 2 (L) | Pedicle | I ^ | On the lateral aspect of the L pedicle just superior to the IAF<br>On fragment with 3707_C2 | -- | Blow: Posterior/Left → Anterior/Right |
| ***3708_A*** | CV 2 | SP | S | Inferior posterior part of SP removed | Likely 3708_B | Blow: Superior/Posterior – Inferior/Anterior<br>Blow: ?Superior/Posterior → Inferior/Anterior |
| ***3708_B*** | CV 3 | IAF | S | Only part of R remaining<br>Inferior of R IAF removed | Likely 3708_A | Blow: Superior/Posterior → Inferior/Anterior |
| ***3708_C*** | Clavicle (?) | Medial end | S ^ | Small fragment of medial clavicle remains | -- | NEI |
| ***3708_D*** | Hyoid (L) | Inner surface | I ^ | Cut perpendicular to longitudinal axis | -- | Blow: Posterior → Anterior |
| ***3708_E*** | Temporal (L) | Mastoid process | S | Inferior portion of mastoid removed<br>Heavy taphonomic damage | -- | Angle: ?Superior/Left(Lat) → Inferior/Right(Med) |
| ***3708_F1*** | Mandible (R) | Corpus | S | Mandible broken<br>Central and left portion<br>Inferior surface of corpus removed<br>Extensive RED | -- | Blow: Anterior/Right(Lat) → Posterior/Left(Med)<br>Nearly in transverse plane |
| ***3708_F2*** | Mandible (R) | Corpus | S | Mandible broken<br>Right portion<br>Inferior surface of corpus removed<br>Extensive RED | -- | Blow: Anterior/Right(Lat) → Posterior/Left(Med)<br>Nearly in transverse plane |
| ***3708_G*** | Mandible (R) | Condyle | S | Condyle removed, neck remains | -- | Nearly in transverse plane |
| ***3708_H*** | Occipital | | I ^ | Offset slightly to left<br>Near external occipital protuberance<br>Runs inferior left to superior right | -- | Blow: Inferior/Posterior → Superior/Anterior |
| ***3709_A*** | CV 1 (R) | IAF | S ^ | Posterior lateral tip of IAF removed | Likely 3709_B | Angle: Inferior/Anterior/Left – Superior/Posterior/Right |
| ***3709_B*** | CV 2 | Body | S | Most CV gone<br>Inferior body, arches gone | Likely 3709_A | Angle: Inferior/Anterior/Left – Superior/Posterior/Right |
| ***3709_C1*** | Mandible (R) | Corpus | | Cut into inferior corpus<br>Missing pieces, significant RED | -- | Blow: Left → Right<br>Nearly in transverse plane |

| ID # | Bone (Side) | Location | Cat* | Description | Associations | Direction of Blow // Angle of Cutmark *Based on anatomical position |
|---|---|---|---|---|---|---|
| ***3709_C2*** | Mandible (R) | Ascending ramus | I ^ | This originally called an intrusive in 3710<br>Cut on medial portion of lower ascending ramus | -- | Blow: Left → Right<br>Nearly in transverse plane |
| ***3709_D*** | Mandible (L) | Ascending ramus | I | Just superior to gonial angle | -- | Blow: Superior/Posterior → Inferior/Anterior |
| ***3709_E*** | Mandible (R) | Ascending ramus | I ^ | This originally called an intrusive in 3710<br>Cut on medial portion of lower ascending ramus<br>Inferior to 3709_C2 | -- | Blow: Left → Right<br>Nearly in transverse plane |
| ***3710_A*** | CV 2 | Odontoid process | BI | Cut into posterior superior odontoid process | Possibly 3710_B and C and Fs | Blow: Posterior → Anterior<br>Angled: Inferior/Left – Superior/Right<br>Nearly in transverse plane |
| ***3710_B*** | Occipital (R) | Lateralis | S ^ | Occipital condyle removed | Possibly 3710_A and C and Fs | Blow: ?Posterior → Anterior<br>Angled: Inferior/Left – Superior/Right<br>Nearly in transverse plane |
| ***3710_C*** | Temporal (R) | Mastoid | S ^ | Some PM warping likely, does not completely fit with other part of temporal | Possibly 3710_A and B and Fs | Blow: ?Posterior → Anterior<br>Angled: Inferior/Left – Superior/Right<br>Nearly in transverse plane |
| ***3710_D*** | Mandible (L) | Ascending ramus | BI | Cut small, mainly RED<br>On posterior edge | -- | Angled: Superior/Right – Inferior/Left |
| ***3710_E*** | Mandible (L) | Corpus | BI ^ | Entry point in anterior medial area of the left mandible<br>Extensive RED and fracturing | -- | Angled: Posterior/Left – Anterior/Right |
| ***3710_F1*** | Mandible (R) | Condyle | S | Condyle removed | Possibly 3710_A, B, and C | Blow: Posterior → Anterior<br>Angled: Inferior/Left – Superior/Right<br>Nearly in transverse plane |
| ***3710_F2*** | Mandible (R) | Condyle | S | Condyle removed<br>The disarticulated condyle | Possibly 3710_A, B, and C | Blow: Posterior → Anterior<br>Angled: Inferior/Left – Superior/Right<br>Nearly in transverse plane |
| ***3710_G1*** | Mandible (L) | Corpus | S ^ | Medial side of the mandible<br>Inferior portion of the cut | -- | Angled: Superior/Anterior – Inferior/Posterior |
| ***3710_G2*** | Mandible (L) | Corpus | S ^ | Medial side of the mandible<br>Superior portion of the cut | -- | Angled: Superior/Anterior – Inferior/Posterior |

| ID # | Bone (Side) | Location | Cat* | Description | Associations | Direction of Blow // Angle of Cutmark *Based on anatomical position |
|---|---|---|---|---|---|---|
| ***3710_H1*** | Occipital (R) | Squama | S ^ | Inferior portion of occipital | -- | Blow: Inferior/Posterior → Superior/Anterior |
| ***3710_H2*** | Occipital (R) | Squama | S ^ | Inferior portion of occipital | -- | Blow: Inferior/Posterior → Superior/Anterior |
| ***3711_A1*** | CV 2 | Body | BI | Superior part of body<br>Anterior part of body broken<br>Some taphonomic damage | -- | Blow: Posterior → Anterior<br>Angled: Superior/Posterior/Right – Inferior/Anterior/Left |
| ***3711_A2*** | CV 2 | Body | BI | Inferior part of body<br>Mainly RED<br>Some taphonomic damage | -- | Blow: Posterior → Anterior<br>Angled: Superior/Posterior/Right – Inferior/Anterior/Left |
| ***3711_B1*** | CV 3 (L) | IAF | S | Tip of facet removed | Potentially 3711_D | Blow: Right → Left<br>In transverse plane |
| ***3711_B2*** | CV 3 | Arch | S | Inferior part of posterior arch | Potentially 3711_D | Blow: Right → Left<br>In transverse plane |
| ***3711_B3*** | CV 3 (L) | Body | S | Part of inferior body removed | Potentially 3711_D | Blow: Right → Left<br>In transverse plane |
| ***3711_B4*** | CV 3 (L) | Body | S | The corresponding part of inferior body | Potentially 3711_D | Blow: Right → Left<br>In transverse plane |
| ***3711_C1*** | CV 4 (L) | Body | S | Inferior part of body missing | Possibly 3711_F | Nearly in transverse plane |
| ***3711_C2*** | CV 4 (R) | Body | S | Inferior part of body missing | Possibly 3711_F | Nearly in transverse plane |
| ***3711_C3*** | CV 4 (L) | IAF | S | Significant taphonomic damage | Possibly 3711_F | Nearly in transverse plane |
| ***3711_C4*** | CV 4 (R) | IAF | S | Small, much of it is RED | Possibly 3711_F | Nearly in transverse plane |
| ***3711_C5*** | CV 4 (L) | Arch | S | Inferior part of posterior arch | Possibly 3711_F | Nearly in transverse plane |

| ID # | Bone (Side) | Location | Cat* | Description | Associations | Direction of Blow // Angle of Cutmark<br>*Based on anatomical position |
|---|---|---|---|---|---|---|
| ***3711_D*** | Mandible (R) | Ascending ramus | I | Cut into posterior aspect of ascending ramus<br>Cut runs from superior right to inferior left | Possibly 3711_Bs<br>Or potentially 3711_As and G | Blow: Inferior/Posterior → Superior/Anterior |
| ***3711_E*** | Mandible (R) | Corpus | S | Medial part of corpus<br>Small amount evident as cut (sub-mm) turning into significant RED | -- | Blow: Left → Right<br>Nearly horizontal |
| ***3711_F*** | Mandible (L) | Corpus | S ^ | Inferior corpus on L side removed | Possibly 3711_C | Blow: Left → Right<br>Angled: Superior/Posterior/Left(Lat) – Inferior/Anterior/Right(Med) |
| ***3711_H*** | CV 2 (L) | Arch | S ^ | Slightly different angle to 3711_A | Small possibility 3711_As | Angle: Superior/Right – Inferior/Left |
| ***3711_I*** | CV (R) | SAF | S ^ | Only the R SAF remains | If head flexed or mandible open, potentially 3711_X<br>Depending on which #CV, potentially 3711_Cs | Nearly in transverse plane |
| ***3711_J1*** | CV 4 | Body | S ^ | On the L half piece of the body<br>Lateral | If head flexed or mandible open, potentially 3711_X | Blow: Superior/Left(Lat) → Inferior/Right(Med) |
| ***3711_J2*** | CV 4 | Body | S ^ | On the L half piece of the body<br>Medial | If head flexed or mandible open, potentially 3711_X | Blow: Superior/Left(Lat) → Inferior/Right(Med) |

| ID # | Bone (Side) | Location | Cat* | Description | Associations | Direction of Blow // Angle of Cutmark *Based on anatomical position |
|---|---|---|---|---|---|---|
| ***3711_X*** | Mandible (L) | Gonial angle | S ^ | Small flat part on the anterior aspect | If head flexed or mandible open, potentially 3711_Js Possibly 3711_J if open | Blow: Inferior → Superior<br>Nearly in coronal plane |
| ***3711_Y*** | Mandible (L) | Gonial angle | I ^ | Posterior part of inferior gonial angle<br>On the medial aspect | -- | Blow: Right → Left<br>Nearly in coronal plane |
| ***3712_A*** | CV 2 | Body | S | Inferior anterior body removed | | Blow: ?Right → Left<br>Angled: Superior/Anterior/Right – Inferior/Posterior/Left |
| ***3712_B*** | CV 4 (R) | Pedicle | I ^ | Cut into anterior R pedicle<br>Inferior to 3712_C, D | -- | Blow: Anterior → Posterior |
| ***3712_C*** | CV 4 (R) | Pedicle | I ^ | Cut into anterior lateral R pedicle<br>Inferior to 3712_ D, superior to 3712_B | -- | Blow: Anterior → Posterior<br>?Right → Left thrust (??) |
| ***3712_D*** | CV 4 (R) | Pedicle | I ^ | Cut into anterior R pedicle<br>Superior to 3712_B, C | -- | Blow: Anterior → Posterior<br>?Right → Left thrust (??) |
| ***3712_E*** | Mandible (R) | Ascending ramus | BI | Runs from anterior aspect of ascending ramus, inferiorly to the posterior border on the lateral side | Potentially 3712_F if head flexed | Blow: Right → Left |
| ***3712_F*** | CV 4 (R) | IAF | S | Inferior part of IAF removed | Potentially 3712_E if head flexed | Angled: Superior/Anterior/Right – Inferior/Posterior/Left |
| ***3712_G*** | Mandible (R) | Ascending ramus | S ^ | | -- | Angled: Superior/Left – Inferior/Right |
| **3713** | -- | -- | -- | -- | -- | -- |
| **3714** | -- | -- | -- | -- | -- | -- |
| **3715_A** | CV 1 (L) | SAF | S | Superior and lateral part of L SAF removed | Possibly 3715_C or potentially 3715_J | Blow: ?Inferior/Anterior → Superior/Posterior |

| ID # | Bone (Side) | Location | Cat* | Description | Associations | Direction of Blow // Angle of Cutmark<br>*Based on anatomical position |
|---|---|---|---|---|---|---|
| **3715_B** | CV 1 (L) | IAF | S | Inferior and posterior lateral part of L IAF removed<br>Some may be RED | Possibly 3715_D<br>Or K | Blow: ?Posterior → Anterior or ?Posterior/Left → Anterior/Right |
| **3715_C** | CV 2 | Odontoid process | S | Tip of odontoid process removed | Possibly 3715_A | Angled: Superior/Posterior – Inferior/Anterior |
| **3715_D** | CV 2 | Odontoid process | BI | Base of odontoid cut; removed due to RED fx | Possibly 3715_B<br>If only one odontoid cut, 3715_Ks | Blow: Superior/Posterior → Inferior/Anterior |
| **3715_E** | CV 2 (L) | Arch | BI | Only the end point is visible near the L SAF<br>Rest removed by subsequent inferior cutmark 3715_F | -- | Blow: Posterior → Anterior<br>Angled: Superior/Posterior/Left – Inferior/Anterior/Right |
| **3715_F** | CV 2 (L) | Arch | BI | Cut along L arch into L lamina<br>Removed most evidence of and inferior to 3715_E | -- | Blow: Posterior → Anterior<br>Angled: Superior/Posterior/Left – Inferior/Anterior/Right |
| **3715_G** | CV 3 (R) | Arch | S | Inferior portion of R arch removed<br>Turned to RED part way | -- | Blow: Superior/Posterior/Right → Inferior/Anterior/Left |
| **3715_H** | Clavicle (L) | Lateral end | S / BI | Cut through, likely affected scapula<br>Part way through turned to RED<br>Lateral end missing | --<br>Could be assoc with verte trauma if shoulder fully abducted | Angled: Posterior/Right(Med) → Anterior/Left(Lat) |
| **3715_I** | Clavicle (L) | Lateral end | I | Medial to 3715_H; cut into lateral end of L clavicle, did not fully penetrate | --<br>Could be assoc with verte trauma if shoulder fully abducted | Angled: Anterior/Right(Med) – Posterior/ Left(Lat) |
| **3715_J** | CV 2 | Odontoid process | S ^ | Tip of odontoid process removed<br>Different than 3715_C, more horizontal | Possibly 3715_A | Angled: Nearly in transverse plane |

| ID # | Bone (Side) | Location | Cat* | Description | Associations | Direction of Blow // Angle of Cutmark *Based on anatomical position |
|---|---|---|---|---|---|---|
| **3715_K1** | CV 2 (R) | SAF | S ^ | Medial part of SAF removed, curves up anteriorly | Possibly 3715_B<br>If only one odontoid cut, 3715_D | Blow: Inferior/Posterior → Superior/Anterior<br>Nearly in transverse plane |
| **3715_K2** | CV 2 (L) | SAF | S ^ | Medial part of SAF removed, curves up anteriorly | Possibly 3715_B<br>If only one odontoid cut, 3715_D | Blow: Inferior/Posterior → Superior/Anterior<br>Nearly in transverse plane |
| **3715_K3** | CV 2 | Odontoid process | BI ^ | Possible second cut in the odontoid process inferior to D | Possibly 3715_B<br>If only one odontoid cut, 3715_D | Blow: Inferior/Posterior → Superior/Anterior<br>Nearly in transverse plane |
| **3715_M** | CV 1 (L) | Pedicle | I | Posterior to the IAF<br>Posterior to 3715_N | If thin blade, possibly 3715_N | Blow: Inferior → Superior |
| **3715_N** | CV 1 (L) | Pedicle | I | Posterior to the IAF<br>Anterior to 3715_M | If thin blade, possibly 3715_M | Blow: Inferior/Posterior → Superior/Anterior |
| **3716** | -- | -- | -- | -- | -- | -- |
| **3719** | -- | -- | -- | -- | -- | -- |
| ***3720_A*** | CV 2 | Odontoid process | BI | Odontoid the only part left<br>Mainly RED<br>Likely CV1 involvement but obscured by taphonomy | -- | Blow: Anterior/Right → Posterior/Left → |
| ***3720_B1*** | Mandible (R) | Corpus | S ^ | R inferior corpus removed<br>Extensive RED and PM damage throughout mandible<br>Anterior to 3720_B2 | -- | Blow: Anterior/Left → Posterior/Right<br>Angled: Superior/Posterior/Right – Inferior/Anterior/Left<br>Nearly in transverse plane |

| ID # | Bone (Side) | Location | Cat* | Description | Associations | Direction of Blow // Angle of Cutmark *Based on anatomical position |
|---|---|---|---|---|---|---|
| ***3720_B2*** | Mandible (R) | Corpus | S ^ | R inferior corpus removed<br>Extensive RED and PM damage throughout mandible<br>Posterior to 3720_B1 | -- | Blow: Anterior/Left → Posterior/Right<br>Angled: Superior/Posterior/Right – Inferior/Anterior/Left<br>Nearly in transverse plane |
| ***3721_A*** | CV 2 | Odontoid process | S / BI | Odontoid the only part left<br>Small cut into RED | Likely 3721_C | Blow: Superior/Posterior → Inferior/Anterior |
| ***3721_B*** | CV 2 (L) | SP | S ^ | Inferior part of L SP and small bit of arch removed | Potentially 3721_D/E | Blow: Anterior/Left → Posterior/Right |
| ***3721_C*** | Mandible (R) | Ascending ramus | BI | Small cut into RED removing the gonial angle | Likely 3721_A | Superior/Posterior → Inferior/Anterior |
| ***3721_D*** | Mandible (L) | Corpus | S ^ | High levels of taphonomic overprinting on lateral side<br>Towards inferior portion | Potentially 3721_B | Nearly in transverse plane |
| ***3722_A1*** | CV 2 (L) | Arch | BI | Inferior L arch removed<br>End of cut visible in bone with associated fracturing of L SAF | Likely 3722_Ks | Blow: Inferior/Posterior → Superior/Anterior |
| ***3722_A2*** | CV 2 (L) | IAF | BI | Partial piece of L IAF<br>Same piece as 3722_B3 | Likely 3722_Ks | Blow: Inferior/Posterior → Superior/Anterior |
| ***3722_B1*** | CV 2 (L) | Arch and SP | S ^ | Inferior L aspect of SP and posterior L arch removed | Likely 3722_C<br>Potentially 3722_L | Blow: Posterior/Left → Anterior/Right<br>Nearly in transverse plane |
| ***3722_B2*** | CV 2 (R) | SP | S ^ | Inferior R aspect of SP removed | Likely 3722_C<br>Potentially 3722_L | Blow: Posterior/Left → Anterior/Right<br>Nearly in transverse plane |
| ***3722_B3*** | CV 2 (L) | IAF | S ^ | Inferior L aspect of IAF removed<br>Same piece as 3722_A2 | Likely 3722_C<br>Potentially 3722_L | Blow: Posterior/Left → Anterior/Right<br>Nearly in transverse plane |
| ***3722_B4*** | CV 2 | Body | S ^ | Inferior portion of L body removed | Possibly 3722_C<br>Potentially 3722_L | Blow: Posterior/Left → Anterior/Right<br>Nearly in transverse plane |

| ID # | Bone (Side) | Location | Cat* | Description | Associations | Direction of Blow // Angle of Cutmark<br>*Based on anatomical position |
|---|---|---|---|---|---|---|
| ***3722_C1*** | CV 3 | SP | S ^ | Superior part of SP removed | Likely 3722_Bs<br>Potentially 3722_L | Blow: ?Posterior/Left → Anterior/Right<br>Blow: Anterior/Superior – Inferior/Posterior |
| ***3722_C2*** | CV 3 | SAF | S ^ | SAF affected but there is taphonomic overprinting | Likely 3722_Bs<br>Potentially 3722_L | Blow: ?Posterior/Left → Anterior/Right<br>Blow: Anterior/Superior – Inferior/Posterior |
| ***3722_D*** | CV ?5 (L) | IAF | S | Only L arch and IAF present<br>Inferior IAF removed | Potentially 3722_N | Angled: Superior/Right – Inferior/Left<br>Nearly in transverse plane |
| ***3722_E1*** | CV ?4 (R) | IAF | S | Inferior IAF removed | -- | Blow: Posterior → Anterior<br>Angled: Superior/Anterior/Left – Inferior/Posterior/Right<br>Nearly in transverse plane |
| ***3722_E2*** | CV ?4 | Body | I | Small mark in posterior R body | -- | Blow: Posterior → Anterior<br>Angled: Superior/Anterior/Left – Inferior/Posterior/Right<br>Nearly in transverse plane |
| ***3722_H*** | CV ?5 (L) | SAF | I ^ | Cutmark in L SAF<br>Superior to 3722_D | -- | Blow: Anterior/Left → Posterior/Right<br>Angled: Nearly in transverse plane |
| ***3722_I*** | CV 2 | Body | S | Inferior anterior part of body removed<br>Changed from 3722_B3 | -- | Blow: Anterior/Superior – Inferior/Posterior<br>Nearly in transverse plane |
| ***3722_J*** | CV (R) | SAF | S | R SAF remains<br>Likely extraneous; size difference in the facet too great | -- | Angled: Nearly in transverse plane |
| ***3722_K1*** | Mandible (L) | Ascending Ramus | BI | Upper 1/3 of the posterior part of the mandible; upper half | Possibly 3722_A | Blow: Posterior → Anterior |
| ***3722_K2*** | Mandible (L) | Ascending Ramus | BI | Upper 1/3 of the posterior part of the mandible; lower half | Possibly 3722_A<br>Possibly 3722_D and E if is CV3 | Blow: Posterior → Anterior |

| ID # | Bone (Side) | Location | Cat* | Description | Associations | Direction of Blow // Angle of Cutmark *Based on anatomical position |
|---|---|---|---|---|---|---|
| ***3722_L1*** | Mandible (L) | Ascending Ramus | S | One cut through the lateral part of the ascending ramus<br>Likely before 3722_O to make it possible (if reconstructed properly) | Possibly 3722_Bs and Cs | Blow: Posterior/Left → Anterior/Right |
| ***3722_L2*** | Mandible (L) | Ascending Ramus | S | One cut through the lateral part of the ascending ramus<br>Likely before 3722_O to make it possible (if reconstructed properly)<br>The piece with the condyle | Possibly 3722_Bs and Cs | Blow: Posterior/Left → Anterior/Right |
| ***3722_L3*** | Mandible (L) | Ascending Ramus | S | One cut through the lateral part of the ascending ramus<br>Likely before 3722_O to make it possible (if reconstructed properly) | Possibly 3722_Bs and Cs | Blow: Posterior/Left → Anterior/Right |
| ***3722_L4*** | Mandible (L) | Ascending Ramus | I | One cut through the lateral part of the ascending ramus<br>Likely before 3722_O to make it possible (if reconstructed properly)<br>The piece with the teeth | Possibly 3722_Bs and Cs | Blow: Posterior/Left → Anterior/Right |
| ***3722_M*** | Mandible (L) | Ascending Ramus | I ^ | Thin cut<br>Inferior to 3722_Ks on the piece with 3722_L1 and K2 | -- | Blow: Posterior/Left(Lat) → Anterior/Right(Med) |
| ***3722_N1*** | Mandible (L) | Corpus | S ^ | Inferior corpus<br>On the piece that is denoted as a cut in the osteological report | Potentially 3722_D | Blow: Posterior → Anterior<br>Nearly in the transverse plane |
| ***3722_N2*** | Mandible (L) | Corpus | S ^ | Posterior to 3722_N<br>Unsure if continuation or different | Potentially 3722_D | Blow: Posterior → Anterior<br>Nearly in the transverse plane |
| ***3722_O*** | Mandible (L) | Ascending Ramus | BI ^ | Near teeth<br>Could only have happened if the 3722_Ls came first | -- | Inferior/Posterior → Superior/Anterior |
| ***3723_A*** | CV 2 (L) | Arch | S | Inferior portion of L arch removed<br>No evidence of in body or on R side<br>Some taphonomic damage | | Angled: Superior/Posterior/Left – Inferior/Anterior/Right<br>Nearly in transverse plane |
| ***3723_B1*** | CV 4 (L) | Arch and IAF | S | Inferior portion of IAF removed | -- | Blow: Posterior/Left → Anterior/Right<br>Nearly in transverse plane |

| ID # | Bone (Side) | Location | Cat* | Description | Associations | Direction of Blow // Angle of Cutmark *Based on anatomical position |
|---|---|---|---|---|---|---|
| ***3723_B2*** | CV 4 (L) | Body | I | Cut ends in body | -- | Blow: Posterior/Left → Anterior/Right<br>Nearly in transverse plane |
| ***3723_C*** | Temporal (R) | Mastoid process | S | Inferior portion of mastoid removed | Likely 3723_Ds and Fs | Blow: Superior/Posterior/Right(Lat) → Inferior/Anterior/Left(Med)<br>Angled: Superior/Posterior – Inferior/Anterior |
| ***3723_D1*** | Maxilla (R) | Alveolar processes | S ^ | Inferior portion of alveolar process removed<br>Teeth impacted as well<br>Anterior to 3723_D2 | Likely 3723_Cs and Fs | Blow: Superior/Posterior/Right(Lat) → Inferior/Anterior/Left(Med) |
| ***3723_D2*** | Maxilla (R) | Alveolar processes | S ^ | Inferior portion of alveolar process removed<br>Teeth impacted as well<br>Posterior to 3723_D1 | Likely 3723_Cs and Fs | Blow: Superior/Posterior/Right(Lat) → Inferior/Anterior/Left(Med) |
| ***3723_E1*** | Mandible (R) | Condylar neck | S ^ | Blow to the posterior neck of the R condyle | Possibly 3723_H | Blow: Superior/Posterior → Inferior/Anterior<br>Angled: Right(Lat) – Left(Med)<br>Nearly in transverse plane |
| ***3723_ E2*** | Mandible (L) | Condylar neck | S | Blow to the posterior neck of the L condyle<br>Model denoted as 3723_G | Possibly 3723_H | Blow: Superior/Posterior → Inferior/Anterior<br>Angled: Right(Lat) – Left(Med)<br>Nearly in transverse plane |
| ***3723_F1*** | Mandible (R) | Coronoid process | S | Coronoid process remains, inferior portion and ascending ramus removed<br>Anterior to 3723_F2 | Likely 3723_Cs and Ds | Blow: Superior/Posterior/Right(Lat) → Inferior/Anterior/Left(Med) |
| ***3723_F2*** | Mandible (R) | Condylar neck | S | Part of the condylar neck that has 3723_E, but related to 3723_F1 rather than 3723_E | Likely 3723_Cs and Ds | Blow: Superior/Posterior/Right(Lat) → Inferior/Anterior/Left(Med) |
| ***3723_H1*** | Occipital (R) | Condyle | S ^ | Inferior portion removed | Likely 3723_Es | Blow: Superior/Posterior → Inferior/Anterior<br>Angled: Lateral(R) – Medial(L)<br>Nearly in transverse plane |

| ID # | Bone (Side) | Location | Cat* | Description | Associations | Direction of Blow // Angle of Cutmark *Based on anatomical position |
|---|---|---|---|---|---|---|
| ***3723_H2*** | Occipital (L) | Condyle | S ^ | Inferior portion removed | Likely 3723_Es | Blow: Superior/Posterior → Inferior/Anterior<br>Angled: Lateral(R) – Medial(L)<br>Nearly in transverse plane |
| ***3724_X*** | Comm. Mandible (R) | Ascending ramus | BI | Majority of this is fracture | | Blow: Posterior/Inferior – Anterior/Superior<br>Nearly horizontal |
| ***3725*** | | | | Skeleton DNE | | |
| ***3726_A*** | CV 1 (L) | IAF | S | Only one small posterior part actually a cut<br>Much of the arch is RED | Likely 3726_B and H<br>Potentially 3726_Es | Blow: Superior/Posterior → Inferior/Anterior |
| ***3726_B*** | CV 2 | Odontoid | S | Only the tip of the odontoid remains | Likely 3726_A and H<br>Potentially 3726_Es | Angled: Superior/Left – Inferior/Right |
| ***3726_C1*** | CV 3 (L) | Body | S | Inferior part of L body removed | Likely 3726_D<br>Potentially 3726_F | Blow: Posterior/Inferior → Anterior/Superior |
| ***3726_C2*** | CV 3 (R) | Body | S | Smaller than 3726_C1<br>Some RED or taphonomic damage | Likely 3726_D<br>Potentially 3726_F | Blow: Posterior/Inferior → Anterior/Superior |
| ***3726_D*** | CV 4 (L) | SAF | S | Superior part of SAF removed | Likely 3726_Cs<br>Potentially 3726_F | Blow: Superior/Anterior/Right(Med) – Inferior/Posterior/Left(Lat) |
| ***3726_E1*** | Mandible (L) | Ascending Ramus | I | In mylohyoid line superior to $M_3$<br>Runs from anterior ascending ramus, inferiorly to posterior portion<br>Medial side of ascending ramus | Potentially 3726_A, B, and H | Blow: Right → Left |
| ***3726_E2*** | Mandible (L) | Ascending Ramus | I ^ | Runs from anterior ascending ramus, inferiorly to posterior portion<br>Medial side of ascending ramus<br>On edge of 3726_F | Potentially 3726_A, B, and H | Blow: Right → Left |

| ID # | Bone (Side) | Location | Cat* | Description | Associations | Direction of Blow // Angle of Cutmark *Based on anatomical position |
|---|---|---|---|---|---|---|
| ***3726_F*** | Mandible (L) | Ascending Ramus | BI | Curves into running in coronal plane and then becomes RED<br>Lots of chattering | Potentially 3726_Cs and D | Blow: Posterior → Anterior |
| ***3726_G*** | Mandible (L) | Ascending Ramus | I ^ | Inferior-most of the medial cuts<br>Runs from mylohyoid line under $M_3$, inferiorly to posterior portion and terminates at the edge of the RED from 3726_F | -- | Blow: Right → Left |
| ***3726_H*** | Mandible (R) | Ascending Ramus | S | Just inferior to condyle | Likely 3726_A and B<br>Potentially 3726_Es | Blow: Superior/Posterior → Inferior/Anterior<br>Angled: Superior/Left – Inferior/Right |
| ***3726_I*** | Maxilla (R) | Alveolar processes | S ^ | Near centre, affecting $I^1$ at the inferior-most part | -- | Angled: Inferior/Left(Med) – Superior/Right(Lat) |
| ***3726_J*** | Zygomatic (R) | | S ^ | Taphonomic overprinting<br>Inferior portion removed | -- | Angled: Superior/Anterior → Inferior/Posterior |
| ***3727*** | -- | -- | -- | -- | -- | -- |
| ***3728_A*** | CV (L) | SAF | S | Only SAF remains | Depending which #CV, potentially 3728_D or G | Angled: Nearly in transverse plane |
| ***3728_B*** | Temporal (R) | Mastoid | S | Mastoid present but taphonomically damaged | Likely 3728_E | Blow: Superior/Posterior/Right(Lat) → Inferior/Anterior/Left(Med) |
| ***3728_C1*** | Mandible (R) | Ascending ramus | I | Superior to 3728_D | -- | Blow: Right → Left |
| ***3728_C2*** | Mandible (R) | Ascending ramus | BI | Small posterior continuation | -- | Blow: Right → Left |
| ***3728_D*** | Mandible (R) | Ascending ramus | S ^ | Cut into the posterior of the ascending ramus | Depending which #CV, potentially 3728_A | Blow: Posterior → Anterior |
| ***3728_E*** | Mandible (R) | Condyle | S | Only the condyle remains | Likely 3728_B | Blow: Superior/Posterior/Right(Lat) → Inferior/Anterior/Left(Med) |

| ID # | Bone (Side) | Location | Cat* | Description | Associations | Direction of Blow // Angle of Cutmark<br>*Based on anatomical position |
|---|---|---|---|---|---|---|
| ***3728_F*** | CV 1 | IAF | S ^ | Only the IAF remains<br>Taphonomic overprinting<br>Could be RED | | Blow: Nearly in transverse plane |
| ***3729_A1*** | CV 5 (L) | IAF | S | Inferior portion of IAF removed | -- | Blow: ?Posterior → Anterior<br>Angled: Superior/Left – Inferior/Right<br>Nearly horizontal |
| ***3729_A2*** | CV 5 (L) | Body | S | Left inferior body removed | -- | Blow: ?Posterior → Anterior<br>Angled: Superior/Left – Inferior/Right<br>Nearly horizontal |
| ***3730_A1*** | CV 1 (L) | IAF | S | L IAF entirely removed<br>Posterior portion | Likely 3730_C, E, and G | Blow: (?) Superior/Left → Inferior/Right |
| ***3730_A2*** | CV 1 (L) | IAF | S | L IAF entirely removed<br>Anterior portion | Likely 3730_C, E, and G | Blow: (?) Superior/Left → Inferior/Right |
| ***3730_B*** | CV 2 | Body | S | Inferior part of left anterior body removed | Potentially 3730_F | Angled: Inferior/Right – Superior/Left |
| ***3730_C*** | CV 2 (L) | SAF | I ^ | Left neck of odontoid | Likely 3730_A, E, and G | Blow: Left → Right<br>Nearly in transverse plane |
| ***3730_D*** | Mandible (L) | Corpus | S | Inferior L corpus removed<br>Extensive RED and PM damage | -- | Blow: ?Posterior → Anterior<br>Angled: Superior/Left(Lat) – Inferior/Right(Med) |
| ***3730_E*** | Mandible (L) | Condylar neck | S | L condyle removed | Likely 3730_A, C, and G | Blow: Posterior/Left → Anterior/Right<br>Angled: Superior/Left(Lat) – Inferior/Right(Med) |
| ***3730_F*** | Mandible (L) | Ascending ramus | I | Superior to gonial angle | Potentially 3730_B | Blow: Superior/Posterior → Inferior/Anterior |
| ***3730_G*** | Temporal (L) | Mastoid process | S | Inferior portion of mastoid removed | Likely 3730_A, C, and E | Angled: Superior/Left(Lat) – Inferior/Right(Med) |
| ***3730_H1*** | Mandible (L) | Corpus | S ^ | Anterior of the mandible, superior to the RED from 3730_D<br>Left side of the fracture | -- | Blow: Superior/Left → Inferior/Right<br>Angled: Superior/Posterior/Left – Inferior/Anterior/Right |
| ***3730_H2*** | Mandible (L) | Corpus | S ^ | Anterior of the mandible, superior to the RED from 3730_D<br>Right side of the fracture | -- | Blow: Superior/Left → Inferior/Right<br>Angled: Superior/Posterior/Left – Inferior/Anterior/Right |

| ID # | Bone (Side) | Location | Cat* | Description | Associations | Direction of Blow // Angle of Cutmark *Based on anatomical position |
|---|---|---|---|---|---|---|
| ***3730_X*** | Mandible (L) | Coronoid Process | I ^ | Possible extraneous<br>Lateral side of coronoid hit | -- | Blow: Left → Right<br>Nearly in transverse plane |
| ***3731*** | -- | -- | -- | -- | -- | -- |
| ***3732*** | -- | -- | -- | -- | -- | -- |
| ***3733_A*** | CV 3? (L) | Body | S | The inferior and right parts of the body removed | -- | Blow: Left → Right<br>Nearly in transverse plane |
| ***3733_B1*** | CV 4? (L) | Body and SAF | BI | The superior part of the body and L SAF removed | -- | Blow: Inferior/Anterior/Left → Superior/Posterior/Right |
| ***3733_B2*** | CV 4? | Body | BI | The superior portion of the body | -- | Blow: Inferior/Anterior/Left → Superior/Posterior/Right |
| ***3734_A1*** | CV 2 (L) | Arch | I ^ | Superior and posterior part of the L arch<br>Cut runs superior/anterior to inferior posterior | Likely 3734_B | Blow: Left → Right |
| ***3734_A2*** | CV 2 (L) | Spinous process | I ^ | Posterior spinous process<br>Cut runs superior/anterior to inferior posterior | Likely 3734_B | Blow: Left → Right |
| ***3734_B*** | Mandible (L) | Neck | BI | Cut part way into ascending ramus/condylar neck of L mandible and rest RED | Likely 3734_As | Blow: Posterior/Left(Lat) → Anterior/Right(Med) |
| ***3734_C1*** | Parietal (L) | | S | Superior part of posterior parietal | -- | Angled: Anterior/Left – Posterior/Right |
| ***3734_C2*** | Parietal (L) | | S | Formerly 3735_X<br>Inferior part of posterior parietal | -- | Angled: Anterior/Left – Posterior/Right |
| ***3735_A1*** | Mandible (R) | Inferior corpus | S | Anterior to and continuation of 3735_A2<br>Inferior border removed | --<br>Depending on #CV possibly 3735_B | Blow: Posterior/Right → Anterior/Left<br>Nearly in transverse plane |
| ***3735_A2*** | Mandible (R) | Inferior corpus | S | Posterior to and continuation of 3735_A1<br>Inferior border removed | --<br>Depending on #CV possibly 3735_B | Blow: Posterior/Right → Anterior/Left |

| ID # | Bone (Side) | Location | Cat* | Description | Associations | Direction of Blow // Angle of Cutmark *Based on anatomical position |
|---|---|---|---|---|---|---|
| ***3735_A3*** | Mandible (L) | Inferior corpus | S ^ | Same cut as 3735_A1 and 3735_A2<br>Inferior border removed | --<br>Depending on #CV possibly 3735_B | Nearly in transverse plane |
| ***3735_B*** | CV (L) | SAF | S ^ | Very small fragment; only SAF remains<br>Likely CV 4/5 | --<br>Depending on #CV possibly 3735_As | Nearly in transverse plane |
| ***3736_A*** | CV 1 (R) | IAF | I ^ | Small cut with resultant RED fracturing<br>Cut running from Superior/Right(Lat) – Inferior/Left(Med) | Likely 3736_Bs<br>Potentially 3736_G depending on the individual's anatomy | Blow: Inferior/Posterior → Superior/Anterior |
| ***3736_B1*** | CV 2 | Odontoid | I | Base of odontoid | Likely 3736_A<br>Potentially 3736_G depending on the individual's anatomy | Blow: Superior/Posterior → Inferior/Anterior |
| ***3736_B2*** | CV 2 (L) | SAF | S ^ | Posterior part of SAF removed | Likely 3736_A<br>Potentially 3736_G depending on the individual's anatomy | Blow: Superior/Posterior → Inferior/Anterior |
| ***3736_B3*** | CV 2 (L) | SAF | S ^ | Posterior part of SAF removed<br>Posterior continuation of 3736_B2 | Likely 3736_A<br>Potentially 3736_G depending on the individual's anatomy | Blow: Superior/Posterior → Inferior/Anterior |

| ID # | Bone (Side) | Location | Cat* | Description | Associations | Direction of Blow // Angle of Cutmark *Based on anatomical position |
|---|---|---|---|---|---|---|
| ***3736_C*** | CV 6 | Body | S | Inferior portion of body removed | -- | Angled: Superior/Anterior/Right – Inferior/Posterior/Left |
| ***3736_D*** | CV 6 (R) | IAF | S ^ | Inferior portion of IAF removed | | Angled: Superior/Anterior/Left – Inferior/Posterior/Right |
| ***3736_E1*** | Frontal (L) | Squama | S | Runs nearly parallel to coronal sutures | -- | Blow: Superior → Inferior<br>Angled: Superior/Posterior – Inferior/Anterior |
| ***3736_E3*** | Frontal (L) | Squama | S | Runs nearly parallel to coronal sutures<br>3736_E2 omitted after reconsideration | -- | Blow: Superior → Inferior<br>Angled: Superior/Posterior – Inferior/Anterior |
| ***3736_F*** | Frontal (L) | Zygomatic process | S | Small cut near sutures | -- | Nearly in coronal plane |
| ***3736_G*** | Mandible (L) | Ascending Ramus | I | Small cut in inferior portion of ascending ramus; unilateral | Potentially 3736_A and Bs depending on the individual's anatomy | Blow: Inferior/Posterior → Superior/Anterior |
| ***3736_H*** | CV (R) | IAF | S ^ | Inferior portion of IAF removed<br>Possibly supernumerary | -- | Blow: Superior/Right – Inferior/Left<br>Nearly in transverse plane |
| ***3736_I*** | CV (R) | SAF and arch | S ^ | SAF bisected<br>Possibly supernumerary<br>Material missing from inferior portion between IAF and body | -- | Blow: ?Posterior → Anterior<br>Superior/Right(Lat) – Inferior/Left(Med) |
| ***3736_J*** | CV 6 (L) | IAF | S | Inferior portion of IAF removed | -- | Angled: Superior/Anterior/Right – Inferior/Posterior/Left |
| ***3737*** | -- | -- | -- | -- | | -- |
| ***3738_B1*** | CV 4 (R) | IAF | S | Inferior part of R IAF removed | -- | Angled: Inferior/Posterior/Right – Superior/Anterior/Left |
| ***3738_B2*** | CV 4 (R) | Body | S | Inferior part of body removed | -- | Angled: Inferior/Posterior/Right – Superior/Anterior/Left |

| ID # | Bone (Side) | Location | Cat* | Description | Associations | Direction of Blow // Angle of Cutmark<br>*Based on anatomical position |
|---|---|---|---|---|---|---|
| ***3738_C*** | Parietal (L) | Central | S / BI | Roundel removed, fully penetrating<br>Smooth upper edge | -- | Blow: Superior/Right(Med) → Inferior/Left(Lat)<br>Nearly in sagittal plane |
| ***3738_D*** | Parietal (R) | Superior central | I | Some flaking on superior side<br>Runs in sagittal plane<br>In close proximity and posterior to 3738_E | -- | Blow: ?Posterior/Right → Anterior/Left<br>Blow: Right → Left<br>Nearly in sagittal plane |
| ***3738_E*** | Parietal (R) | Superior central | I | Slight angle running from the anterior/right to posterior/left<br>In close proximity and anterior to 3738_F | -- | Angled: Superior/Right → Inferior/Left |
| ***3738_F*** | Parietal (R) | Central | S | Roundel removed, not into diploe<br>Two raised lines, possible blade defects | -- | Blow: Superior/Posterior → Inferior/Anterior |
| ***3738_G*** | Mandible (R) | Corpus | BI ^ | Small cut, quickly into RED fracturing | -- | Blow: Inferior/Posterior → Superior/Anterior<br>Nearly in coronal plane |
| ***3738_Xi*** | CV 1 (R) | SAF | S | Majority of R SAF removed<br>Supernumerary | -- | Blow: Nearly in transverse plane |
| ***3738_Xii*** | CV 1 (R) | IAF | S ^ | Inferior R IAF and R arch removed<br>Some RED medially<br>Supernumerary | -- | Blow: Nearly in transverse plane |
| ***3739_A*** | Mandible (L) | Ascending ramus | BI ^ | Cut into posterior part of L ramus<br>Some taphonomic overprinting | -- | Blow: Superior/Posterior → Inferior/Anterior |
| ***3739_B1*** | Mandible (L) | Inferior corpus | BI | Anterior<br>Portion of the inferior part of the mandibular corpus removed<br>Masking tape holds the mandible together | -- | Blow: Posterior → Anterior<br>Angled: Superior/Left(Lat) – Inferior/ Right(Med)<br>Nearly in the transverse plane |
| ***3739_B2*** | Mandible (L) | Inferior corpus | BI | Posterior<br>Portion of the inferior part of the mandibular corpus removed<br>Masking tape holds the mandible together | -- | Blow: Posterior → Anterior<br>Angled: Superior/Left(Lat) – Inferior/ Right(Med)<br>Nearly in the transverse plane |

| ID # | Bone (Side) | Location | Cat* | Description | Associations | Direction of Blow // Angle of Cutmark *Based on anatomical position |
|---|---|---|---|---|---|---|
| ***3740*** | -- | -- | -- | Skull missing since excavation | -- | -- |
| ***3741_A*** | CV 3 (L) | Pedicle | BI ^ | Cut is small, and on pedicle<br>Rest is RED fracturing<br>Much of the vertebrae is missing | -- | Angled: Nearly in transverse plane |
| ***3741_B*** | CV 2 (R) | IAF | S ^ | Inferior portion of R IAF removed | -- | Angled: Nearly in transverse plane |
| ***3742_A*** | CV 1 (L) | Inferior to condylar fossa | I ^ | Inferior to the L condylar fossa but superior to the arch | Likely 3742_G Potentially 3742_Bs | Blow: Posterior/Superior → Anterior/Inferior<br>Angled: Inferior/Left – Superior/Right |
| ***3742_B1*** | CV 2 | SAFs and posterior body | I | Blow across posterior of body<br>Superior to 3742_C1, C2, D1, D2 | Potentially 3742_A and G | Blow: Posterior → Anterior<br>Angled: Nearly in transverse plane |
| ***3742_B2*** | CV 2 (L) | Arch | S ^ | Most lateral of the cutmarks on the arch | Potentially 3742_A and G | Blow: Posterior → Anterior<br>Angled: Nearly in transverse plane |
| ***3742_C1*** | CV 2 (L) | SAF and posterior body | BI | Blow across posterior of body and removal of part of L SAFs<br>Superior to 3742_ D1, D2<br>Inferior to 3742_B | -- | Blow: Posterior → Anterior<br>Angled: Superior/Left – Inferior/Right |
| ***3742_C2*** | CV 2 (R) | SAF and arch | I | Blow across superior R arch and removal of part of R SAFs<br>Superior to 3742_ D1, D2<br>Inferior to 3742_B | -- | Blow: Posterior → Anterior<br>Angled: Superior/Left – Inferior/Right |
| ***3742_C3*** | CV 2 (L) | Arch | S ^ | The middle cutmarks on the arch | -- | Blow: Posterior → Anterior<br>Angled: Superior/Left – Inferior/Right |
| ***3742_D1*** | CV 2 (L) | Arch | BI | The most medial removal of superior part of L arch<br>Inferior to 3742_A, C1, C2 | -- | Blow: Posterior → Anterior<br>Angled: Superior/Left – Inferior/Right |
| ***3742_D2*** | CV 2 | SP | BI ^ | SP removed from CV 2 partly by blow (R side) and partly breakage (L side)<br>Inferior to 3742_A, C1, C2 | -- | Blow: Posterior → Anterior<br>Angled: Superior/Left – Inferior/Right |
| ***3742_E1*** | CV 3 (L) | IAF and arch | S | Inferior part of L arch and IAF removed<br>Right side damaged through taphonomy | If head flexed or mandible open, potentially 3742_F | Angled: Nearly in transverse plane |

| ID # | Bone (Side) | Location | Cat* | Description | Associations | Direction of Blow // Angle of Cutmark *Based on anatomical position |
|---|---|---|---|---|---|---|
| ***3742_E2*** | CV 3 (L) | Body | S | Inferior part of posterior body removed | If head flexed or mandible open, potentially 3742_F | Angled: Nearly in transverse plane |
| ***3742_F*** | Mandible (L) | Ascending ramus | S | Extensive RED and taphonomic fracturing/loss | If head flexed or mandible open, potentially 3742_Es | Blow: Posterior → Anterior<br>Inferior/Posterior/Left(Lat) – Superior/Anterior/Right(Med) |
| ***3742_G*** | Occipital (R) | Lateralis portion | S ^ | Just superior to foramen magnum; likely the same blow as 3742_A and one of the CV 2 cuts<br>Not in the book | Likely 3742_A<br>Potentially 3742_Bs | Inferior/Anterior/Left – Superior/Posterior/Right |
| ***3743*** | -- | -- | -- | Missing | -- | -- |
| ***3744_A1*** | CV 2 | Odontoid process | S | All of odontoid process removed | Potentially 3744_D | Angled: Superior/Left – Inferior/Right |
| ***3744_A2*** | CV 2 (R) | SAF | S | Lateral part of R SAF removed | Potentially 3744_D | Angled: Superior/Left – Inferior/Right |
| ***3744_A3*** | CV 2 | Odontoid process | S | The tip of the odontoid process | Potentially 3744_D | Angled: Superior/Left – Inferior/Right |
| ***3744_B*** | CV 3 (R) | SAF and arch | S | Superior part of R SAF and R arch removed | -- | Blow: Right → Left<br>Angled: Inferior/Posterior/Left – Superior/Anterior/Right |
| ***3744_C*** | Mandible (R) | Ascending ramus | BI | Cut part way through the ascending ramus; does not reach the anterior part; extensive RED fracturing | -- | Blow: Right/Posterior → Left/Anterior<br>Nearly horizontal |
| ***3744_D*** | Occipital (R) | Condyle | S ^ | Small medial portion of condyle removed | Potentially 3744_As | |
| ***3744_E*** | Loose frag | | I ^ | Unidentified fragment, possibly vertebrae<br>Not patterned | -- | |

| ID # | Bone (Side) | Location | Cat* | Description | Associations | Direction of Blow // Angle of Cutmark *Based on anatomical position |
|---|---|---|---|---|---|---|
| ***3745_A1*** | CV | Body | S ^ | Individual not in book<br>Inferior portion of posterior body removed | -- | Angled: Superior/Posterior/Left – Inferior/Anterior/Right |
| ***3745_A2*** | CV (R) | IAF and arch | S ^ | Individual not in book<br>Inferior portion of arch and IAF removed | -- | Angled: Superior/Posterior/Left – Inferior/Anterior/Right |
| ***3745_B*** | CV | Body | S ^ | Individual not in book<br>Inferior portion of anterior body removed | -- | Angled: Superior/Anterior/Right – Inferior/Posterior/Left |
| ***3746_A*** | CV2 (L) | IAF | S / BI^ | Inferior tip of IAF removed | -- | Blow: Posterior → Anterior<br>Nearly horizontal |
| ***3746_B1*** | CV 4 (R) | IAF and arch | S | Inferior R IAF and arch removed<br>Body unaffected | -- | Angled: Superior/Anterior/Right – Inferior/Posterior/Left |
| ***3746_B2*** | CV 4 (L) | Transverse process | S | Inferior transverse process removed | -- | Angled: Superior/Right – Inferior/Left |
| ***3746_C*** | CV 5 (L) | Body and SAF | S | Inferior body and IAF removed | -- | Angled: Nearly in transverse plane |
| ***3747_A1*** | CV 6 | Body | S | Inferior body cut off<br>Very fragmented and not all present | -- | Angled: Superior/Left – Inferior/Right |
| ***3747_A2*** | CV 6 (R) | IAF | S | Inferior portion of IAF removed | -- | Angled: Superior/Left – Inferior/Right |
| ***3747_B*** | CV 6 | Body | S | Posterior part of inferior body removed | -- | Angled: Nearly in transverse plane |
| ***3748_A1*** | CV 2 (R) | SP | S ^ | Inferior portion of R SP missing<br>3748_A2 connected to A1 on reconsideration | -- | Angle: Inferior/Right – Superior/Left<br>Nearly in transverse plane |
| ***3748_A3*** | CV 2 (R) | Body | S | Inferior right portion of body missing | -- | Angle: Inferior/Right – Superior/Left<br>Nearly in transverse plane |
| ***3748_A4*** | CV 2 | Body | S | Anterior inferior portion of body missing | -- | Angle: Inferior/Right – Superior/Left<br>Nearly in transverse plane |
| ***3748_B1*** | Mandible (L) | Corpus | S | Inferior corpus removed but present<br>Extensive RED<br>Posterior portion | -- | Blow: Posterior → Anterior<br>Angled: Nearly in transverse plane |
| ***3748_B2*** | Mandible (L) | Corpus | S | Anterior portion of corpus | -- | Blow: Posterior → Anterior<br>Angled: Nearly in transverse plane |

| ID # | Bone (Side) | Location | Cat* | Description | Associations | Direction of Blow // Angle of Cutmark *Based on anatomical position |
|---|---|---|---|---|---|---|
| ***3748_C*** | Mandible (L) | Gonial angle | I ^ | Small cut<br>Gonial angle missing from other side, unable to tell if bilateral although evidence of RED on R side | -- | Blow: Inferior/Left(Lat) → Superior/Right(Med)<br>Angled: Nearly in coronal plane |
| ***3748_D1*** | Occipital (L) | Squama | S | Cut through inferior to nuchal crest<br>Discontinuous from 3748_D5 due to taphonomy | Likely 3748_Es and F | Blow: Posterior → Anterior<br>Angled: Nearly in transverse plane |
| ***3748_D2*** | Occipital (L) | Squama | S | Can be reassoc with 3748_D1 | Likely 3748_Es and F | Blow: Posterior → Anterior<br>Angled: Nearly in transverse plane |
| ***3748_D3*** | Occipital (L) | Basilaris | I ^ | Superior to condyles | Likely 3748_Es and F | Blow: Posterior → Anterior<br>Angled: Nearly in transverse plane |
| ***3748_D4*** | Occipital(R) | Basilaris | S ^ | Superior to condyles | Likely 3748_Es and F | Blow: Posterior → Anterior<br>Angled: Nearly in transverse plane |
| ***3748_D5*** | Occipital (R) | Squama | S | Cut through inferior to nuchal crest<br>Discontinuous from 3748_D1 due to taphonomy | Likely 3748_Es and F | Blow: Posterior → Anterior<br>Angled: Nearly in transverse plane |
| ***3748_E1*** | Temporal (L) | Petrous portion | S | Inferior aspect of petrous portion removed | Likely 3748_Ds and F | Blow: Posterior → Anterior<br>Angled: Nearly in transverse plane |
| ***3748_E2*** | Temporal (L) | Petrous portion | S | Inferior aspect of petrous portion removed | Likely 3748_Ds and Es | Blow: Posterior → Anterior<br>Angled: Nearly in transverse plane |
| ***3748_F*** | Temporal (R) | Petrous portion | S | Inferior aspect of petrous portion removed | Likely 3748_Ds and F | Blow: Posterior → Anterior<br>Angled: Nearly in transverse plane |
| ***3749_A1*** | CV 3 (L) | Body | S | Body broken in half<br>Inferior part removed | -- | Angled: Inferior/Posterior/Left – Superior/Anterior/Right |
| ***3749_A2*** | CV 3 (R) | Body | S | Body broken in half<br>Inferior part removed | -- | Angled: Inferior/Posterior/Left – Superior/Anterior/Right |

| ID # | Bone (Side) | Location | Cat* | Description | Associations | Direction of Blow // Angle of Cutmark *Based on anatomical position |
|---|---|---|---|---|---|---|
| ***3750_A*** | CV 2 (L) | IAF and arch | S ^ | Inferior/left surface of L arch and L IAF removed<br>Taphonomic overprinting | Likely 3750_B | Blow: Superior/Left → Inferior/Right |
| ***3750_B*** | CV 3 (L) | Body and pedicle | S | Left inferior side removed | Likely 3750_A | Blow: Superior/Left → Inferior/Right |
| ***3750_C1*** | Mandible (R) | Inferior corpus | BI | Blow turns into RED as it goes back and up through the ascending ramus | -- | Blow: Inferior/Anterior → Superior/Posterior |
| ***3750_C2*** | Mandible (L) | Inferior corpus | BI | Blow turns into RED as it goes back and up through the ascending ramus | -- | Blow: Inferior/Anterior → Superior/Posterior |
| ***3750_D*** | Mandible (R) | Ascending ramus | I ^ | In the RED resulting from 3750_Cs on the ascending ramus | -- | Blow: Inferior/Posterior → Superior/Anterior |
| ***3750_E1*** | Occipital (R) | Squama | BI ^ | Cut running superior left to inferior right | -- | Blow: Posterior → Anterior |
| ***3750_E2*** | Occipital (R) | Squama | BI ^ | Cut running superior left to inferior right | -- | Blow: Posterior → Anterior |
| ***3751*** | -- | -- | -- | Skeleton DNE | -- | -- |
| ***3752_A*** | CV 1 (R) | SAF | S ^ | Top of R SAF removed<br>Taphonomic overprinting | Likely 3752_B<br>Potentially 3752_C | Angled: Nearly in transverse plane |
| ***3752_B*** | Occipital (R) | Condyle | S ^ | Inferior surface of R condyle removed | Likely 3752_A<br>Potentially 3752_C | Angled: Nearly in transverse plane |
| ***3752_C*** | Mandible (R) | Ascending ramus | I | Cut into posterior aspect of R ascending ramus<br>About 1/3 of the way from the condyle | Potentially 3752_A and B | Blow: Inferior/Posterior → Superior/Anterior |
| ***3752_D1*** | Mandible (L) | Inferior corpus | BI | Inferior border of L anterior mandible<br>Initially a cut, turns to RED<br>Mandible broken centrally | -- | Blow: Right → Left<br>Angled: Nearly in transverse plane |
| ***3752_D2*** | Mandible (R) | Inferior corpus | S | Inferior border of R anterior mandible<br>Likely the initial point of contact<br>Mandible broken centrally | -- | Blow: Right → Left<br>Angled: Nearly in transverse plane |

| ID # | Bone (Side) | Location | Cat* | Description | Associations | Direction of Blow // Angle of Cutmark *Based on anatomical position |
|---|---|---|---|---|---|---|
| ***3752_E*** | Mandible (L) | Neck | BI | Just below condyle<br>Part way before RED<br>Cut runs Superior/Left(Lat) – Inferior/Right(Med) | -- | Blow: Posterior → Anterior |
| **3753_A1** | CV 6 (L) | Body | S | Superior aspect of left body missing | -- | Angled: Nearly in transverse plane |
| **3753_A2** | CV 6 (R) | Body | S | Superior aspect of right body missing | -- | Angled: Nearly in transverse plane |
| **3753_B2** | CV 6 (L) | SAF | S | Top of SAF missing | -- | Angled: Superior/Right – Inferior/Left<br>Nearly in transverse plane |
| **3753_B1** | CV 6 (R) | SAF | S ^ | Top of SAF missing | -- | Angled: Superior/Right – Inferior/Left<br>Nearly in transverse plane |
| **3753_C** | MC 3 (R) | Head | I ^ | Palmar surface of MC<br>Cut runs from distal/medial – proximal/lateral across entire head | 3753_D | Blow: Anterior → Posterior |
| **3753_D** | MC 2 (R) | Head | I ^ | Palmar surface of MC<br>Cut runs from distal/medial – proximal/lateral at proximal end of head | 3753_C | Blow: Anterior → Posterior |
| **3754** | -- | -- | -- | -- | -- | -- |
| **3755_A** | CV 3 (R) | Inferior arch | S ^ | Removed the inferior portion of the R arch | -- | Nearly in transverse plane |
| **3755_B** | CV 3 (R) | Superior arch | S | Removed part of the superior portion of the R arch | Likely 3755_Cs | Angled: Inferior/Anterior – Superior/Posterior<br>Nearly in transverse plane |
| **3755_C1** | CV 4 (L) | SAF | S ^ | Superior tip of the L SAF removed | Likely 3755_B | Angled: Inferior/Anterior – Superior/Posterior<br>Nearly in transverse plane |
| **3755_C2** | CV 4 (R) | SAF | S ^ | Superior tip of the R SAF removed | Likely 3755_B | Angled: Inferior/Anterior – Superior/Posterior<br>Nearly in transverse plane |
| **3755_D1** | Scapula (L) | Acromion process | BI | Medial portion of the acromion<br>Smoother surface<br>Cut runs Posterior/Right(Med) – Anterior/Left(Lat) | 3755_Es | Blow: Superior/Posterior → Inferior/Anterior<br>Nearly in sagittal plane |

| ID # | Bone (Side) | Location | Cat* | Description | Associations | Direction of Blow // Angle of Cutmark *Based on anatomical position |
|---|---|---|---|---|---|---|
| **3755_D2** | Scapula (L) | Acromion process | BI | Lateral portion of the acromion<br>More flaking<br>Cut runs Posterior/Right(Med) – Anterior/Left(Lat) | 3755_Es | Blow: Superior/Posterior → Inferior/Anterior<br>Nearly in sagittal plane |
| **3755_E1** | Clavicle (L) | Lateral end | BI | Medial portion of the clavicle<br>Smoother surface<br>Lateral portion too taphonomically damaged<br>Cut runs Posterior/Right(Med) – Anterior/Left(Lat) | 3755_Ds | Blow: Superior/Posterior → Inferior/Anterior<br>Nearly in sagittal plane |
| **3756_A1** | CV 5 (L) | SAF | S ^ | Superior portion of L SAF removed | -- | Blow: Superior/Anterior/Left – Inferior/Posterior/Right |
| **3756_A2** | CV 5 (R) | SAF | S ^ | Most of R SAF removed<br>Some taphonomic damage | -- | Blow: Superior/Anterior/Left – Inferior/Posterior/Right |
| ***3757_A1*** | CV 3 (R) | Body | I / BI | Cut into the R side of the body | Likely 3757_C | Blow: Right/Anterior → Left/Posterior<br>Nearly in transverse plane |
| ***3757_A2*** | CV 3 (R) | Body | I / BI | Cut into the R side of the body | Likely 3757_C | Blow: Right/Anterior → Left/Posterior<br>Nearly in transverse plane |
| ***3757_B1*** | CV 4 (R) | SP | S | Inferior part of SP removed | Possibly 3757_Ds or 3757_Es if head flexed down | Blow: ?Right → ?Left OR ?Posterior/Right → Anterior/Left<br>Angled: Superior/Right – Inferior/Left<br>Nearly in transverse plane |
| ***3757_B2*** | CV 4 (R) | IAF | S | Inferior part of R IAF removed | Possibly 3757_Ds | Blow: ?Right → ?Left OR ?Posterior/Right → Anterior/Left<br>Angled: Superior/Right – Inferior/Left<br>Nearly in transverse plane |
| ***3757_B3*** | CV 4 | Posterior body | S | Inferior part of posterior body removed | Possibly 3757_Ds | Blow: ?Right → ?Left OR ?Posterior/Right → Anterior/Left<br>Angled: Superior/Right – Inferior/Left<br>Nearly in transverse plane |

| ID # | Bone (Side) | Location | Cat* | Description | Associations | Direction of Blow // Angle of Cutmark *Based on anatomical position |
|---|---|---|---|---|---|---|
| ***3757_B4*** | CV 4 | Anterior body | S | Inferior part of anterior body removed; full extent confounded by taphonomy | Possibly 3757_Ds | Blow: ?Right → ?Left OR ?Posterior/Right → Anterior/Left<br>Angled: Superior/Right – Inferior/Left<br>Nearly in transverse plane |
| ***3757_C*** | CV 4 (R) | SAF | S | Superior part of R SAF removed<br>Entire facet removed | Likely 3757_A | Angled: Inferior/Posterior/Right – Superior/Anterior/Left |
| ***3757_D1*** | Mandible (R) | Gonial angle | S | Cut near R gonial angle, extends width of ascending ramus before turning to RED<br>L side unaffected<br>Posterior part of cut on the gonial fragment<br>Blue-tack and tape on the mandible | Possibly 3757_Bs | Blow: Posterior/Right(Lat) → Anterior/Left(Med)<br>Nearly in transverse plane |
| ***3757_D2*** | Mandible (R) | Gonial angle | S | Cut near R gonial angle, extends width of ascending ramus before turning to RED<br>L side unaffected<br>Anterior part, very small | Possibly 3757_Bs | Blow: Posterior/Right(Lat) → Anterior/Left(Med)<br>Nearly in transverse plane |
| ***3757_E1*** | Mandible (R) | Body | BI ^ | Cut upwards from below<br>Likely before 3757_D in sequence<br>Medial part – denoted separately because of fracturing | | Blow: Inferior/Posterior → Superior/Anterior |
| ***3757_E2*** | Mandible (R) | Body | BI ^ | Cut upwards from below<br>Likely before 3757_D in sequence<br>Lateral part – denoted separately because of fracturing | | Blow: Inferior/Posterior → Superior/Anterior |
| ***3758_A*** | CV 2 (R) | IAF and arch | S | Inferior portion of R IAF and arch removed<br>Different angle to 3758_B | Likely 3758_Ds | Blow: Inferior/Posterior/Left → Superior/Anterior/Right<br>Nearly in the transverse plane Angled: Superior/Right(Lat)/Posterior – Inferior/Left(Med)/Anterior |

| ID # | Bone (Side) | Location | Cat* | Description | Associations | Direction of Blow // Angle of Cutmark *Based on anatomical position |
|---|---|---|---|---|---|---|
| ***3758_B*** | CV 2 | SP | S ^ | Inferior/posterior portion of the SP removed<br>Different angle to 3758_A | Possibly 3758_Cs and 3758_F<br>Or Possibly 3758_Es | Angled: Superior/Posterior – Inferior/Anterior |
| ***3758_C1*** | CV 3 (L) | IAF | S | Inferior portion of L IAF removed | Likely 3758_F<br>Possibly 3758_B | Blow: Superior/Posterior → Inferior/Anterior |
| ***3758_C2*** | CV 3 | Inferior body | S | Inferior portion of posterior body removed; may be related to | Likely 3758_F<br>Possibly 3758_B | Blow: Superior/Posterior → Inferior/Anterior |
| ***3758_C3*** | CV 3 (R) | IAF | S | Inferior portion of R IAF removed | Likely 3758_F<br>Possibly 3758_B | Blow: Superior/Posterior → Inferior/Anterior |
| ***3758_D1*** | CV 3 | Superior body | S ^ | Superior portion of L posterior body removed | Likely 3758_A | Blow: Inferior/Posterior/Left → Superior/Anterior/Right<br>Nearly in the transverse plane |
| ***3758_D2*** | CV 3 (R) | Superior body | BI / S ^ | Superior portion of R posterior body removed | Likely 3758_A | Blow: Inferior/Posterior/Left → Superior/Anterior/Right<br>Nearly in the transverse plane |
| ***3758_D3*** | CV 3 (R) | SAF | S ^ | Top portion of R SAF removed | Likely 3758_A | Blow: Inferior/Posterior/Left → Superior/Anterior/Right<br>Nearly in the transverse plane |
| ***3758_D4*** | CV 3 (R) | Uncinate process | I ^ | Blade end point in posterior part of anterior uncinate process | Likely 3758_A | Blow: Inferior/Posterior/Left → Superior/Anterior/Right<br>Nearly in the transverse plane |
| ***3758_D5*** | CV 3 (L) | SAF | S ^ | Top medial portion of L SAF removed | Likely 3758_A | Blow: Inferior/Posterior/Left → Superior/Anterior/Right<br>Nearly in the transverse plane |
| ***3758_E1*** | CV4 (L) | IAF | S | Inferior portion of L IAF removed | Possibly 3758_B | Angled: Nearly in transverse plane |
| ***3758_E2*** | CV4 | Inferior body | S | Inferior portion of posterior body removed | Possibly 3758_B | Angled: Nearly in transverse plane |

| ID # | Bone (Side) | Location | Cat* | Description | Associations | Direction of Blow // Angle of Cutmark *Based on anatomical position |
|---|---|---|---|---|---|---|
| ***3758_E3*** | CV4(R) | IAF | S | Inferior portion of R IAF removed | Possibly 3758_B | Angled: Nearly in transverse plane |
| ***3758_F*** | CV4 (R) | Superior body | BI ^ | Anterior superior part of R body removed<br>Begins as cut and turns to RED | Likely 3758_Cs<br>Possibly 3758_B | Angled: Superior/Posterior – Inferior/Anterior |
| ***3758_G*** | CV4 (R) | IAF and arch | S ^ | Different angle to and posterior to 3758_E<br>Inferior portion of IAF and arch removed | | Angled: Superior/Posterior – Inferior/Anterior |
| ***3759_A1*** | CV 1 (L) | Arch | BI | No damage to any processes<br>Inferior portion of the posterior arch removed<br>R side of arch RED fracturing | Possibly 3759_B | Blow: Posterior/Left → Anterior/Right<br>Angled: Inferior/Left – Superior/Right |
| ***3759_A2*** | CV 1 (L) | Arch | BI | The inferior fragment of the arch | Possibly 3759_B | Blow: Posterior/Left → Anterior/Right<br>Angled: Inferior/Left – Superior/Right |
| ***3759_B*** | CV 2 (L) | SAF | BI / S ^ | Damage confined to posterior L SAF<br>No damage to the R SAF | Possibly 3759_A | Blow: Posterior/Left → Anterior/Right<br>Angled: Inferior/Left – Superior/Right |
| ***3759_C*** | CV 3 | Inferior body | S | Anterior portion of inferior body removed<br>No damage posterior to this cut | -- | Blow: Anterior → Posterior<br>Nearly in transverse plane |
| ***3759_D*** | Mandible (R) | Gonial angle | BI | Removed the gonial angle; the lateral margin is cut, RED by the medial margin | -- | Blow: Superior/Right(Lat)/Posterior → Inferior/Left(Med)/Anterior |
| ***3759_E*** | Parietal (R) | Inferior and posterior aspect | BI | Defect shaved part way into parietal and then broken/RED<br>Incomplete, part missing inferiorly | -- | Blow: Superior/Anterior → Inferior/Posterior<br>Nearly in sagittal plane |
| ***3759_F*** | Parietal (R) | Superior and posterior aspect | I ^ | Superior and posterior to 3759_E<br>Cut runs from superior/anterior/left to inferior/posterior/right | -- | Blow: Superior/Right → Inferior/Left<br>Superior/Medial(L) – Inferior/Lateral(R) |
| ***3760_A1*** | CV 3 (L) | IAF | S | Inferior part of L IAF removed | -- | Blow: Inferior/Posterior/Left → Superior/Anterior/Right<br>Nearly in transverse plane |

| ID # | Bone (Side) | Location | Cat* | Description | Associations | Direction of Blow // Angle of Cutmark *Based on anatomical position |
|---|---|---|---|---|---|---|
| ***3760_A2*** | CV 3 | Inferior body | S | Posterior/right part of inferior body removed | -- | Blow: Inferior/Posterior/Left → Superior/Anterior/Right<br>Nearly in transverse plane |
| ***3760_A3*** | CV 3 (R) | IAF and pedicle | BI / S | Inferior part of pedicle and R IAF removed<br>Transition into RED | -- | Blow: Inferior/Posterior/Left → Superior/Anterior/Right<br>Nearly in transverse plane |
| ***3760_A4*** | CV 3 | Inferior body | S | Anterior/right part of inferior body removed | -- | Blow: Inferior/Posterior/Left → Superior/Anterior/Right<br>Nearly in transverse plane |
| ***3760_B*** | Hyoid (L) | Greater horn | I ^ | Cut mark on the internal surface of part of the hyoid<br>Cut runs Superior/Left – Inferior/Right | -- | Blow: Posterior/Right → Anterior/Left |
| ***3761_A1*** | CV 2 (L) | Inferior arch and IAF | S | Opposite side not damaged | -- | Blow: Posterior → Anterior<br>Angled: Superior/Left – Inferior/Right |
| ***3761_A2*** | CV 2 (R) | Transverse process | S | More damaged posteriorly | -- | Blow: Posterior → Anterior<br>Angled: Superior/Left – Inferior/Right |
| ***3761_A3*** | CV 2 (L) | Transverse process | BI | Transverse process more damaged posteriorly<br>Most of the body has been fractured by the force | -- | Blow: Posterior → Anterior<br>Angled: Superior/Left – Inferior/Right |
| ***3761_B*** | Mandible (R) | Inferior corpus | BI / S | Posterior to 3761_C<br>Extensive RED | -- | Blow: Superior/Anterior/Right(Lat) → Inferior/Posterior/Left(Med)<br>Nearly in transverse plane |
| ***3761_C*** | Mandible (R) | Inferior corpus | I ^ | Possibly a skip mark or related to the CV2 trauma<br>Anterior to 3761_B | -- | Blow: Inferior/Anterior/Left(Med) → Superior/Posterior/Right(Lat) |
| **3762** | -- | -- | -- | -- | -- | -- |
| **3763_A1** | CV 4 (R) | SAF | S | Removal of superior part of R SAF | -- | Blow: Posterior → Anterior<br>Angled: Superior/Right – Inferior/Left |
| **3763_A2** | CV 4 (L) | Lamina | I | Cut through superior surface of L lamina and into the bone just below the L SAF | -- | Blow: Posterior → Anterior<br>Angled: Superior/Right – Inferior/Left |
| **3763_B** | CV 4 (R) | IAF | S | Inferior edge of R IAF cut off<br>Some taphonomic damage | Likely 3763_C | Blow: Posterior → Anterior<br>Nearly in transverse plane |

| ID # | Bone (Side) | Location | Cat* | Description | Associations | Direction of Blow // Angle of Cutmark *Based on anatomical position |
|---|---|---|---|---|---|---|
| **3763_C** | CV 5 (R) | SAF | I | Cut into R SAF | Likely 3763_B | Blow: Posterior → Anterior<br>Nearly in transverse plane |
| **3763_D** | Clavicle (L) | Sternal end | BI | Cut into anterior/superior surface of sternal clavicle<br>Cutmark itself is small, RED fracture propagation laterally | -- | Blow: Superior/Right(Med) → Inferior/Left(Lat) |
| **3763_E** | Clavicle (R) | Sternal end | I | Cut into the anterior part of the sternal end running from superior/left to inferior/right<br>Resultant fracturing<br>Possibly from the tip of the blade | -- | Blow: Anterior → Posterior |
| **3763_F** | CV 4 (L) | SAF | S | Removal of superior part of L SAF | -- | Blow: Posterior → Anterior<br>Angled: Superior/Right – Inferior/Left |
| **3764_A** | CV 4 | Anterior body | I | Cut runs from superior/right to inferior/left | -- | Blow: Anterior → Posterior<br>Slice: Superior/Right – Inferior/Left |
| **3764_B** | CV 4 | Anterior body | I ^ | Cut runs from superior/right to inferior/left<br>Superior portion in same track as 3764_A, diverges inferiorly | -- | Blow: Anterior → Posterior<br>Slice: Superior/Right – Inferior/Left |
| **3766** | -- | -- | -- | -- | -- | -- |
| **3767** | -- | -- | -- | -- | -- | -- |
| **3768** | -- | -- | -- | -- | -- | -- |
| **3769** | -- | -- | -- | -- | -- | -- |
| **3770** | -- | -- | -- | -- | -- | -- |
| **3771_A1** | Radius (R) | Distal shaft | S | Posterior aspect of distal end Large shaved defect, two grooves running vertically possibly reflecting defects in the blade<br>Distal epiphysis not affected<br>*Broken since original osteo report | -- | Angled: Superior – Inferior<br>Nearly in coronal plane |

| ID # | Bone (Side) | Location | Cat* | Description | Associations | Direction of Blow // Angle of Cutmark *Based on anatomical position |
|---|---|---|---|---|---|---|
| **3771_A2** | Radius (R) | Distal shaft | S | Posterior aspect of distal end Large shaved defect, two grooves running vertically possibly reflecting defects in the blade<br>Distal epiphysis not affected<br>*Broken since original osteo report | -- | Angled: Superior – Inferior<br>Nearly in coronal plane |
| **3771_A3** | Radius (R) | Distal shaft | S | Posterior aspect of distal end Large shaved defect, two grooves running vertically possibly reflecting defects in the blade<br>Distal epiphysis not affected<br>*Broken since original osteo report | -- | Angled: Superior – Inferior<br>Nearly in coronal plane |
| **3772** | -- | -- | -- | -- | -- | -- |
| **3773** | -- | -- | -- | -- | -- | -- |
| **3774** | -- | -- | -- | -- | -- | -- |
| **3775_A** | CV (L) | L SAF | S | Superior/left side of SAF removed | -- | Blow: Superior/Anterior/Left – Inferior/Posterior/Right |
| **3775_B** | Hamate (R) | Posterior lateral side | S | Anterior lateral side removed | -- | Nearly in coronal plane |
| **3775_C** | MC 2 (L) | Dorsal base | S | Dorsal surface of the base removed | Likely 3775_D, E, and F | Angled: nearly in coronal plane |
| **3775_D** | MC 3 (L) | Dorsal base | S | Dorsal surface of the base removed | Likely 3775_C, E, and F | Angled: nearly in coronal plane |
| **3775_E** | Capitate (L) | Head | S | Dorsal surface of head removed | Likely 3775_C, D, and F | Angled: nearly in coronal plane |
| **3775_F** | Trapezoid (L) | Base | S | Dorsal surface of base removed | Likely 3775_C, D, and E | Angled: nearly in coronal plane |
| **3775_G** | Lunate (L) | Dorsal | I | Cut ends | Possibly 3775_H | Blow: Posterior → Anterior (?)<br>Angled: nearly in coronal plane |
| **3775_H** | Scaphoid (L) | Distal side | S | Dorsal surface removed<br>Palmar surface missing due to taphonomy | Possibly 3775_G | Angled: nearly in coronal plane |

| ID # | Bone (Side) | Location | Cat* | Description | Associations | Direction of Blow // Angle of Cutmark *Based on anatomical position |
|---|---|---|---|---|---|---|
| **3775_I** | CV (L) | SAF | S | Superior tip of L SAF removed | -- | In transverse plane |
| **3777_A1** | CV 3 | Body | S | Superior R side removed<br>L undamaged | -- | Blow: Right → Left OR Anterior/Right → Posterior/Left<br>Nearly in transverse plane |
| **3777_A2** | CV 3 (R) | SAF | S | Superior portion removed<br>Some taphonomic damage | -- | Blow: Right → Left OR Anterior/Right → Posterior/Left<br>Nearly in transverse plane |
| **3777_B** | PP 1 (L) | Head | S | Medial part of head removed | Likely 3777_Cs<br>Possibly 3777_N and Q | Angled: Inferior/Left(Lat) – Superior/Right(Med)<br>Nearly in sagittal plane |
| **3777_C1** | DP 1 (L) | Entire (lateral) | BI | Two halves, split along sagittal plane | Likely 3777_B<br>Possibly 3777_N and Q | In sagittal plane |
| **3777_C2** | DP 1 (L) | Entire (medial) | BI | Two halves, split along sagittal plane<br>Missing distal part | Likely 3777_B<br>Possibly 3777_N and Q | In sagittal plane |
| **3777_D** | MC 3 (L) | Head | S | Medial/anterior side of head removed | Possibly 3777_O<br>Or Possibly 3777_E and H | Angled: Superior/Left(Lat) – Inferior/Right(Med) |
| **3777_E** | MC 3 (L) | Base | I ^ | Small shaved cut progressing into incised on lateral/anterior side of base | Possibly 3777_D<br>Or Possibly 3777_H | Blow: Inferior → Superior<br>Angled: Superior/Left(Lat) – Inferior/Right(Med) |
| **3777_F** | MC 3 (L) | Base | I | Proximal anterior/medial shaft with a shaved into an incised | -- | Angled: Superior/Left(Lat) – Inferior/Right(Med) |
| **3777_G** | MC 4 (L) | Head | S | Posterior/lateral part of the head removed | Potentially 3777_S if flexed | Angled: Superior/Left(Lat) – Inferior/Right(Med) |
| **3777_H** | MC 4 (L) | Base | S | Posterior/lateral part of base | Possibly 3777_D and E | Angled: Superior/Left(Lat) – Inferior/Right(Med) |

| ID # | Bone (Side) | Location | Cat* | Description | Associations | Direction of Blow // Angle of Cutmark *Based on anatomical position |
|---|---|---|---|---|---|---|
| **3777_I** | MC 4 (L) | Head | I | Anterior surface running from Superior/Medial to Inferior/Lateral<br>Some taphonomic damage | -- | Blow: Anterior → Posterior |
| **3777_J** | MC 5 (L) | Head | S | Posterior/lateral corner removed<br>Taphonomic damage | Potentially 3777_S | Angled: Superior/Left(Lat) – Inferior/Right(Med) |
| **3777_K** | PP 4? (L) | Shaft | BI | Posterior surface cut into about half way and then broken | -- | Blow: Posterior → Anterior<br>Inferior/Left(Lat) – Superior/Right(Med) |
| **3777_L** | IP | Base | S | Only proximal portion remains | -- | Angled: Inferior/Right – Superior/Left |
| **3777_M** | Scaphoid (L) | | S | Medial aspect removed | -- | Angled: Inferior/Lateral – Superior/Medial<br>Nearly in sagittal plane |
| **3777_N** | Trapezium (L) | | S | Nearly in sagittal plane | Possibly 3777_B, Cs, and Q | Angled: Inferior/Lateral – Superior/Medial<br>Nearly in sagittal plane |
| **3777_O** | Trapezoid (L) | Palmar surface | S | Palmar surface removed | Possibly 3777_D | Blow: Left → Right<br>Nearly in coronal plane |
| **3777_Q** | MC 1 (L) | Base | S ^ | Medial/posterior part of base removed<br>Taphonomic damage | Possibly 3777_B, C1s, and N | Nearly in sagittal plane<br>Taphonomic damage makes it challenging to tell |
| **3777_R** | PP ? | Distal portion | S | Posterior surface cut into, broken beyond a point | -- | Blow: Left → Right<br>Angled: Inferior/Right – Superior/Left |
| **3777_S** | PP ? | Base | S | Same fragment as 3777_R | Potentially 3777_G or J | Blow: Posterior/Right – Anterior/Left |
| **3778_A** | CV | Inferior body | S ^ | Body the only portion left; same vertebrae as 3778_B | -- | Angled: Nearly in transverse plane |
| **3778_B** | CV | Superior body | S ^ | Body the only portion left; same vertebrae as 3778_A | -- | Angled: Nearly in transverse plane |
| **3778_C** | Clavicle (R) | Superior shaft | BI | Begins as cut, rest is RED<br>Cut runs Anterior/Right(Lat)–Posterior/Left(Med)<br>Lateral to 3778_M | -- | Blow: Superior → Inferior |

| ID # | Bone (Side) | Location | Cat* | Description | Associations | Direction of Blow // Angle of Cutmark<br>*Based on anatomical position |
|---|---|---|---|---|---|---|
| **3778_D** | Ulna (R) | Distal shaft | I | Posterior aspect of distal shaft<br>Curves, convex facing laterally<br>Cut runs Superior – Inferior | Possibly 3778_E | Blow: Posterior → Anterior |
| **3778_E** | Radius (R) | Distal shaft | I | Posterior aspect of distal shaft<br>Cut runs Superior/Right(Lat) – Inferior/Left(Med)<br>Potential additional cut distally but taphonomic damage makes it unclear | Possibly 3778_D | Blow: Posterior → Anterior |
| **3778_F** | Trapezium (R) | Medial edge | S | Medial edge removed<br>Cut down between ray 1 and 2 | | Angled: Nearly in sagittal plane |
| **3778_G** | Capitate (R) | Palmar edge | S | Palmar edge removed | Potentially 3778_H and I | Angled: Nearly in coronal plane |
| **3778_H** | Scaphoid (R) | Dorsal side | S | Medial half of dorsal side removed | Potentially 3778_G and I | Angled: Nearly in coronal plane |
| **3778_I** | Hamate (R) | Dorsal side | S | Dorsal side removed | Potentially 3778_G and H | Angled: Nearly in coronal plane |
| **3778_J1** | MC 5 (R) | Head | S | Medial edge removed | Possibly 3778_K and L | Angled: Anterior/Lateral – Posterior/Medial |
| **3778_J2** | MC 5 (R) | Base | S | Medial edge removed | Possibly 3778_K and L | Angled: Anterior/Lateral – Posterior/Medial |
| **3778_K** | PP ?4 (R) | Mid-shaft | S | Only the distal portion remains; proximal portion removed | Possibly 3778_J and L | Blow: Inferior/Posterior → Superior/Anterior<br>Angled: Superior/Right – Inferior/Left |
| **3778_L** | PP ?3 (R) | Mid-shaft | S | Only the proximal portion remains; distal portion removed | Possibly 3778_J and K | Blow: Inferior/Posterior → Superior/Anterior<br>Angled: Superior/Right – Inferior/Left |
| **3778_M** | Clavicle (R) | Superior shaft | BI | Just medial to 3778_C | -- | Blow: Superior → Inferior<br>Angled: Anterior/Right(Lat) – Posterior/Left(Med) |
| **3778_N** | Radius (R) | Distal shaft | I | Posterior aspect of distal shaft, inferior to 3778_E<br>Cut runs Superior/Right(Lat) – Inferior/Left(Med) | -- | Blow: Posterior → Anterior |

| ID # | Bone (Side) | Location | Cat* | Description | Associations | Direction of Blow // Angle of Cutmark<br>*Based on anatomical position |
|---|---|---|---|---|---|---|
| **3779** | -- | -- | -- | -- | -- | -- |
| **3780** | -- | -- | -- | -- | -- | -- |
| **3781_A** | CV 4 (L) | IAF | S | Only a sliver remains<br>Superior to 3781_B<br>Cut through articular surface | | Angled: Superior/Anterior – Inferior/Posterior |
| **3781_B** | CV 4 (L) | IAF | S | Only a sliver remains<br>Inferior to 3781_A | Likely 3781_C | Angled: Superior/Anterior – Inferior/Posterior |
| **3781_C** | CV 5 (L) | SAF | S | Superior part of L SAF removed | Likely 3781_B | Angled: Superior/Right – Inferior/Left |
| **3782** | -- | -- | -- | Possible BFT to fib | | -- |
| **3783_A** | CV 3 (L) | IAF | S | Only remaining fragment<br>Superior part removed | Possibly 3783_B | Angled: Superior/Right – Inferior/Left<br>Nearly in transverse plane |
| **3783_B** | CV 4 (R) | Arch and IAF | S | Superior part of R arch and entire SAF removed<br>Fracturing anteriorly | Possibly 3783_A | Blow: Posterior/Right → Anterior/Left<br>Angled: Superior/Right – Inferior/Left<br>Nearly in transverse plane |
| **3783_C** | CV 5 (L) | SAF | S | Superior portion of L SAF removed | -- | Angled: Superior/Right – Inferior/Left |
| **3784** | -- | -- | -- | -- | -- | -- |
| **3785_A** | PP1 (R) | Mid-shaft | S | Only the distal half remains | -- | Blow: Inferior/Medial(L) → Superior/Lateral(R) |
| **3785_B** | IP | Mid-shaft, dorsal | I ^ | Shave on dorsal surface<br>Wide-angle incised | -- | Superior/Posterior → Inferior/Anterior |
| **3785_C** | IP | Head, dorsal | S ^ | Cut partly into head of IP | -- | Inferior → Superior |
| **3786_A1** | CV 5 | Superior body | S | Bisected obliquely through the body<br>Taphonomic damage to left, no processes on R damaged<br>Pieces do not fit perfectly | Possibly 3786_Ds or C | Blow: ?Posterior → Anterior OR ?Left → Right<br>Angled: Superior/Left – Inferior/Right<br>More likely L if assoc with D or C |
| **3786_A2** | CV 5 | Inferior body | S | Bisected obliquely through the body<br>Taphonomic damage to left, no processes on R damaged<br>Pieces do not fit perfectly | Possibly 3786_Ds or C | Blow: ?Posterior → Anterior OR ?Left → Right<br>Angled: Superior/Left – Inferior/Right |
| **3786_B** | CV 6 (L) | IAF | S | Inferior of L IAF removed<br>Only part of the body and the L AFs survive<br>Body unaffected | -- | Blow: ?Posterior → Anterior OR ?Left → Right<br>Angled: Superior/Left – Inferior/Right |

| ID # | Bone (Side) | Location | Cat* | Description | Associations | Direction of Blow // Angle of Cutmark<br>*Based on anatomical position |
|---|---|---|---|---|---|---|
| **3786_C** | Clavicle (R) | Acromial end | I | Superior/anterior surface of lateral end<br>Running anterior/right – posterior/left<br>Lateral to 3786_D | Possibly 3786_As | Blow: Superior/Left(Med) → Inferior/Right(Lat) |
| **3786_D1** | Clavicle (R) | Acromial end | BI | Partially penetrating before fracturing<br>Superior/anterior surface of lateral end<br>Medial side, smoother<br>Medial to 3786_C | Possibly 3786_As | Blow: Superior/Left(Med) → Inferior/Right(Lat) |
| **3786_D2** | Clavicle (R) | Acromial end | BI | Partially penetrating before fracturing<br>Superior/anterior surface of lateral end<br>Lateral side, more ragged<br>Medial to 3786_C | Possibly 3786_As | Blow: Superior/Left(Med) → Inferior/Right(Lat) |
| **3787_A1** | CV 3 | Superior body | S | Superior surface of body on R side removed<br>Cut ends leading into R SAF | -- | Angled: Inferior/Anterior – Superior/Posterior |
| **3787_A2** | CV 3 | Superior body | S | Anterior superior body, on the left side of the vertical crack | -- | Angled: Inferior/Anterior – Superior/Posterior |
| **3787_B1** | CV 3 | Inferior body | S ^ | Anterior inferior portion of the body removed | -- | Angled: Superior/Anterior/Left – Inferior/Posterior/Right |
| **3787_B2** | CV 3 | Inferior body | S ^ | Anterior inferior portion of the body removed<br>On the right side of the vertical crack | -- | Angled: Superior/Anterior/Left – Inferior/Posterior/Right |
| **3788_A1** | CV 4 (R) | Lamina and arch | S | Superior R lamina removed | -- | Angled: Superior/Anterior – Inferior/Posterior<br>Nearly in transverse plane |
| **3788_A2** | CV 4 | Superior body | S | Posterior part of superior body removed | -- | Angled: Superior/Anterior – Inferior/Posterior<br>Nearly in transverse plane |
| **3789_A** | CV | Arch | BI ^ | Small fragment<br>Only part is a cut, the rest is RED | -- | Blow: ?Anterior → Posterior<br>Angled: Superior/Anterior – Inferior/Posterior<br>Nearly in transverse plane |

| ID # | Bone (Side) | Location | Cat* | Description | Associations | Direction of Blow // Angle of Cutmark *Based on anatomical position |
|---|---|---|---|---|---|---|
| **3789_B** | Scapula (R) | Coracoid process | I ^ | Anterior, superior aspect<br>Cut runs medial to lateral | Possibly 3789_Es | Blow: Anterior/Left → Posterior/Right<br>Nearly in transverse plane |
| **3789_C** | Clavicle (L) | Acromial end | I | Inferior side of acromial end<br>Hard to access, possibly a stabbing motion | -- | Blow: Inferior/Right(Med) → Superior/Left(Lat)<br>Nearly in transverse plane |
| **3789_D** | Clavicle (R) | Acromial end | I | Superior surface<br>Significant flaking on lateral side | -- | Blow: Superior/Anterior/Left(Med) → Inferior/Posterior/Right(Lat) |
| **3789_E1** | Clavicle (R) | Acromial end | S | Medial to and same angle as 3789_D<br>Lateral side<br>Completely transects the clavicle | Possibly 3789_B | Blow: Superior/Anterior/Left(Med) → Inferior/Posterior/Right(Lat) |
| **3789_E2** | Clavicle (R) | Acromial end | S | Medial to and same angle as 3789_D<br>Medial side<br>Completely transects the clavicle | Possibly 3789_B | Blow: Superior/Anterior/Left(Med) → Inferior/Posterior/Right(Lat) |
| **3789_F** | Clavicle (R) | Shaft | BI | Inferior lateral surface<br>Inferior and medial to 3789_E | -- | Blow: Inferior/Right(Lat) → Superior/Left(Med)<br>Nearly in transverse plane |
| **3789_G** | Clavicle (R) | Shaft | BI | Inferior lateral surface<br>Slightly inferior to 3789_F, only the end point in the bone is still evident | -- | Blow: Inferior/Right(Lat) → Superior/Left(Med)<br>Nearly in transverse plane |
| **3790** | -- | -- | -- | -- | -- | -- |
| **3791** | -- | -- | -- | -- | -- | -- |
| **3792** | -- | -- | -- | -- | -- | -- |
| **3793** | -- | -- | -- | -- | -- | -- |
| **3794** | -- | -- | -- | Missing CV 3 with trauma | -- | -- |
| **3795** | -- | -- | -- | -- | -- | -- |
| **3796_A1** | CV 5 (R) | SAF | S | Superior R SAF removed cleanly | -- | Blow: Posterior → Anterior<br>Angled: Superior/Right – Anterior/Left |
| **3796_A2** | CV 5 (L) | SAF | S | Superior L SAF removed, less cleanly than R counterpart | -- | Blow: Posterior → Anterior<br>Angled: Superior/Right – Anterior/Left |
| **3796_B** | Radius (L) | Shaft | I | Posterior lateral portion of shaft<br>More proximal<br>Cut runs from superior/posterior to inferior/anterior | -- | Blow: Superior/Posterior → Inferior/Anterior |

| ID # | Bone (Side) | Location | Cat* | Description | Associations | Direction of Blow // Angle of Cutmark *Based on anatomical position |
|---|---|---|---|---|---|---|
| **3796_C** | Radius (L) | Shaft | I | Posterior lateral portion of shaft<br>More distal<br>Cut runs from superior/posterior to inferior/anterior<br>Deeper than 3796_B | -- | Blow: Superior/Posterior → Inferior/Anterior |
| **3797** | -- | -- | -- | -- | -- | -- |
| **3798** | -- | -- | -- | -- | -- | -- |
| **3799** | -- | -- | -- | Noted in book CV2 – RED | -- | -- |
| **3800_A1** | CV 2 (R) | SAF | S | Body present as separate piece<br>Superior part of posterior R SAF removed | -- | Blow: Inferior/Posterior → Superior/Anterior<br>Nearly in transverse plane |
| **3800_A2** | CV 2 (L) | SAF | S | Body present as separate piece<br>Superior part of medial posterior L SAF removed | -- | Blow: Inferior/Posterior → Superior/Anterior<br>Nearly in transverse plane |
| **3800_A3** | CV 2 (R) | SAF | S | Arch present as separate piece<br>Small, anterior medial continuation of 3800_A1 | -- | Blow: Inferior/Posterior → Superior/Anterior<br>Nearly in transverse plane |
| **3800_A4** | CV 2 (L) | SAF | S | Arch present as separate piece Anterior medial continuation of 3800_A2 | -- | Blow: Inferior/Posterior → Superior/Anterior<br>Nearly in transverse plane |
| **3801** | -- | -- | -- | -- | -- | -- |
| **3802** | -- | -- | -- | -- | -- | -- |
| **3803_A1** | CV 5 (L) | Body | S ^ | Body broken in half, unrelated to cut | Likely 3803_B | Nearly in transverse plane |
| **3803_A2** | CV 5 (R) | Body | S ^ | Body broken in half, unrelated to cut | Likely 3803_B | Nearly in transverse plane |
| **3803_B** | CV 6 (R) | SAF | S | Tip of R SAF removed<br>Some taphonomic damage | Likely 3803_As | Nearly in transverse plane |
| **3804_A** | CV 6 (R) | SAF | S | Superior part of R SAF removed<br>L SAF undamaged<br>Some taphonomic damage to SP | Likely 3804_B | Angled: Superior/Anterior – Inferior/Posterior |
| **3804_B** | CV 7 | SP | S | Superior posterior tip of SP removed | Likely 3804_A | Angled: Superior/Anterior – Inferior/Posterior |
| **3805_A** | CV (?R) | IAF | S | Very small fragment left | -- | N.E.I. |
| **3805_B** | CV (?L) | IAF | S | Small fragment | -- | N.E.I. |

| ID # | Bone (Side) | Location | Cat* | Description | Associations | Direction of Blow // Angle of Cutmark *Based on anatomical position |
|---|---|---|---|---|---|---|
| **3805_C** | CV (L) | IAF | S | Only the L IAF remains | -- | Nearly in transverse plane |
| **3806** | -- | -- | -- | -- | -- | -- |
| **3809_A1** | CV 3 (L) | IAF | S | Inferior portion of IAF removed<br>RED damage to R superior arch likely caused by this blow | -- | Blow: Posterior → Anterior<br>Angled: Inferior/Left – Superior/Right |
| **3809_A2** | CV 3 | Posterior body | I | Cut into posterior body running inferior left to superior right | -- | Blow: Posterior → Anterior |
| **3809_B1** | CV 5 (L) | Superior body | S | Removal of the superior anterior body on the left side | -- | Angled: Inferior/Anterior/Left – Superior/Posterior/Right |
| **3809_B2** | CV 5 (R) | Superior body | S | Removal of the superior anterior body on the right side | -- | Angled: Inferior/Anterior/Left – Superior/Posterior/Right |
| **3809_B3** | CV 5 (L) | SAF | S | Removal of the superior anterior SAF<br>Glued together previously, re-broke | -- | Angled: Inferior/Anterior/Left – Superior/Posterior/Right |
| **3809_C** | CV 3 (L) | Superior body | S ^ | Superior aspect of left body removed | -- | Nearly in transverse plane |
| **3810_A1** | CV 3 (L) | Pedicle | I | Between inferior pedicle and uncinate process<br>Anterior body damage is PM | Likely 3810_C | Blow: Inferior/Posterior → Superior/Anterior<br>Nearly in coronal plane |
| **3810_A2** | CV 3 (R) | Pedicle and IAF | I | Between inferior pedicle and uncinate process, IAF also damaged<br>Anterior body damage is PM | Likely 3810_C | Blow: Inferior/Posterior → Superior/Anterior<br>Nearly in coronal plane |
| **3810_B1** | CV 4 (R) | Pedicle | I | Between inferior pedicle and uncinate process<br>Assoc with 3810_B2 and 3 | Likely 3810_D | Blow: Inferior/Anterior → Superior/Posterior |
| **3810_B2** | CV 4 | Body | S | Inferior portion of the body removed<br>Think what is remaining is the superior body | Likely 3810_D | Blow: Inferior/Anterior → Superior/Posterior |
| **3810_B3** | CV 4 (L) | Pedicle | I | Between inferior pedicle and uncinate process | Likely 3810_D | Blow: Inferior/Anterior → Superior/Posterior |
| **3810_C** | CV 4 (L) | Pedicle | S | Anterior portion of L pedicle removed<br>Superior to 3810_B3 | Likely 3810_As | Blow: Inferior/Posterior → Superior/Anterior<br>Nearly in coronal plane |

| ID # | Bone (Side) | Location | Cat* | Description | Associations | Direction of Blow // Angle of Cutmark *Based on anatomical position |
|---|---|---|---|---|---|---|
| **3810_D** | CV 5 (R) | Body | S | Anterior portion of the right superior body removed<br>Superior anterior part of body taphonomically damaged | Likely 3810_Bs | Blow: Inferior/Anterior → Superior/Posterior |
| **3810_E1** | CV 6 | Body | S | Inferior portion of body removed<br>Taphonomic overprinting | Likely 3810_Fs | Blow: Anterior → Posterior<br>Angled: Superior/Left – Inferior/Right<br>Nearly in transverse plane |
| **3810_E2** | CV 6 (L) | IAF | S | Inferior portion of IAF removed<br>Taphonomic overprinting | Likely 3810_Fs | Blow: Anterior → Posterior<br>Angled: Superior/Left – Inferior/Right<br>Nearly in transverse plane |
| **3810_E3** | CV 6 (R) | Spinous Process | I | Anterior portion of the inferior right SP<br>Cut runs inferior right to superior left, nearly in transverse plane | Likely 3810_Fs | Blow: Anterior → Posterior<br>Angled: Superior/Left – Inferior/Right<br>Nearly in transverse plane |
| **3810_E4** | CV 6 (L) | Spinous Process | I | Anterior portion of the inferior left SP<br>Cut runs inferior right to superior left, nearly in transverse plane | Likely 3810_Fs | Blow: Anterior → Posterior<br>Angled: Superior/Left – Inferior/Right<br>Nearly in transverse plane |
| **3810_F1** | CV 7 (L) | SAF | S | Superior tip of left SAF removed | Likely 3810_Es | Blow: Anterior → Posterior (?)<br>Angled: Superior/Left – Inferior/Right<br>Nearly in transverse plane |
| **3810_F2** | CV 7 (R) | SAF | S | Superior tip of right SAF removed | Likely 3810_Es | Blow: Anterior → Posterior (?)<br>Angled: Superior/Left – Inferior/Right<br>Nearly in transverse plane |
| **3810_G** | Clavicle (R) | Acromial end | I | Superior acromial end<br>Potentially related to a neck cut (none of the angles make sense in anatomical position) | -- | Blow: Superior/Left(Med) → Inferior/Right(Lat) |
| **3810_H** | MC 2 (L) | Shaft | BI | Posterior medial edge of shaft | Possibly 3810_I | Angle: Anterior/Right – Posterior/Left |
| **3810_I** | PP 2 (L) | Head | S ^ | Posterior medial portion of head removed<br>Taphonomic damage | Possibly 3810_H | Angle: Anterior/Right – Posterior/Left |
| **3810_J** | PP 3 (L) | Head | S | Anterior medial portion of head removed | Possibly 3810_L | Angled: Anterior/Left – Posterior/Right |

| ID # | Bone (Side) | Location | Cat* | Description | Associations | Direction of Blow // Angle of Cutmark *Based on anatomical position |
|---|---|---|---|---|---|---|
| **3810_K** | CV 5 | Body | I ^ | On inferior portion of body<br>Fine cut, resembling a fracture<br>Running from right to left, terminating about halfway through the body | -- | Blow: Inferior/Anterior → Superior/Posterior |
| **3810_L** | IP (L) | Shaft | I ^ | Medial side of IP has an angled cut<br>Running Superior/Right(Med) – Inferior/Left(Lat) | Possibly 3810_J | |
| **3811_A** | CV 5 (R) | SAF | S | Top of R SAF removed | -- | Angled: Superior/Right – Inferior/Left<br>Nearly in transverse plane |
| **3811_B** | Radius (L) | Shaft | I | Posterior lateral portion of shaft<br>Towards the distal end (1/3 from) | -- | Blow: Superior/Left(Lat) → Inferior/Right(Med)<br>Nearly in transverse plane |
| **3812** | -- | -- | -- | -- | -- | -- |

*I = incised cutmark; S = shaved cutmark; BI = broken incised

# Appendix G: Sharp Force Trauma Catalogue of the Disarticulated Remains

Cutmark Coding:

**0000.00_A0**

Context Number
Discrete piece of bone
Cutmark ID
Segment of cutmark, if applicable

Key:

AF – Articular Facet (S – superior, I – inferior)
CV – Cervical Vertebrae
SP – Spinous Process
DNE – Does not exist
I – incised cutmark
S – shaved cutmark
BI – broken incised
^ – Not in osteological report

Direction of blow:
→ Direction of entry known
– Direction of entry unknown
NEI Not Enough Information
n.b. all directions in relation to standard anatomical position

Table G-1: The catalogue of cutmarks for the disarticulated remains (Section 7.1)

| ID # | Bone (Side) | Location | Cat* | Description | Direction of Blow // Angle of Cutmark *Based on anatomical position |
|---|---|---|---|---|---|
| **3681.01_A** | Radius (R) | Posterior shaft | I ^ | Trauma to posterior portion of the mid-shaft | Blow: Superior(Proximal) → Inferior(Distal) |
| **3681.02_B** | Clavicle (R) | Lateral end | I | Cut on superior anterior surface of lateral R clavicle; lateral to 3681.02_C | Blow: Superior/Left(Med) → Inferior/Right(Lat) |
| **3681.02_C** | Clavicle (R) | Lateral end | I | Cut on superior anterior surface of lateral R clavicle; medial to 3681.02_B | Blow: Superior/Left(Med) → Inferior/Right(Lat) |
| **3681.03_D** | ?Radius (?) | Fragment | I ^ | Longitudinal cut in bone, not fully penetrating | NEI |
| **3681.04_E** | Proximal phalanx 1 | Head | S ^ | Cut to the dorsal aspect of the head of a PP 1<br>Some taphonomic damage | Angle: Anterior/Left – Posterior/Right |
| **3681.05_F1** | CV (R) | SAF | S ^ | Superior part of R SAF removed<br>Some taphonomic damage | Nearly in transverse plane |
| **3681.05_F2** | CV (R) | Body | S ^ | Superior part of R body removed<br>Some taphonomic damage | Nearly in transverse plane |

| ID # | Bone (Side) | Location | Cat* | Description | Direction of Blow // Angle of Cutmark<br>*Based on anatomical position |
|---|---|---|---|---|---|
| **3681.05_F3** | CV (L) | Body | S ^ | Superior part of L body removed<br>Some taphonomic damage | Nearly in transverse plane |
| **3681.06_G** | Radius (L) | Shaft | S ^ | Cut in distal posterior shaft running from distal/left(med) to proximal/right(lat)<br>Broken in two pieces likely due to cut, only one has evidence of a cut on it; good fit | Blow: Superior → Inferior |
| **3681.07_H1** | CV | Body | S | Superior portion of body removed<br>Slight curve to cut | Blow: Superior/Posterior – Inferior/Anterior |
| **3681.07_H2** | CV (R) | SAF | S | Superior portion of R SAF removed | Blow: Superior/Posterior – Inferior/Anterior |
| **3681.07_I1** | CV | Body | S | Inferior portion of body removed | Nearly in transverse plane |
| **3681.07_I2** | CV (R) | IAF | S | Inferior portion of R IAF removed | Nearly in transverse plane |
| **3681.08_J** | Radius or Ulna (?) | Shaft | I ^ | Fragment; uncertain<br>Some taphonomic damage | NEI |
| **3681.01_N** | Radius (R) | Posterior shaft | I ^ | Small cut into the edge of 3681.01_A on the posterior portion of the mid-shaft | Blow: Superior → Inferior |
| **3685.01_A** | Scapula (L) | Acromion process | I | Cut into acromion process of L scapula; not fully penetrating<br>Same fragment as 3685.01_N | Blow: Superior/Medial → Inferior/Lateral |
| **3685.02_B** | Metacarpal 2 (L) | Shaft | S | Longitudinal cut through the shaft<br>Some taphonomic damage | Angled: Proximal/Left – Distal/Right |
| **3685.03_C** | Proximal phalanx | Proximal end | S | Longitudinally cut | Blow: In sagittal plane |
| **3685.04_D** | Proximal phalanx | Proximal end | S | Longitudinally cut | Blow: In sagittal plane |
| **3685.05_E** | Mandible (R) | Ascending ramus | S | Superior to lingula | Blow: ?Posterior → Anterior<br>Nearly in transverse plane |
| **3685.05_F** | Mandible (R) | Ascending ramus | S | Inferior to lingula | Blow: Superior/Posterior – Inferior/Anterior<br>Nearly in transverse plane |
| **3685.06_G** | Mandible (?L) | Condyle | S ^ | Small cut, most is RED | Blow: Posterior/Superior → Anterior/Inferior |
| **3685.07_H** | CV 1 (L) | SAF | S | L SAF missing, no damage to R (only taphonomy)<br>Some taphonomic damage | Nearly in transverse plane |

| ID # | Bone (Side) | Location | Cat* | Description | Direction of Blow // Angle of Cutmark *Based on anatomical position |
|---|---|---|---|---|---|
| **3685.08_I** | CV (R) | Inferior surface | S | Inferior surface of CV removed | Blow: Posterior/Superior/Right – Anterior/Inferior/Left |
| **3685.09_J1** | CV 2 | Posterior body | I | Cut into body below odontoid process<br>Runs from superior/left at the L SAF to inferior/right to under R SAF<br>Middle segment | Blow: Posterior/Left → Anterior/Right |
| **3685.09_J2** | CV 2 (R) | SAF | I | Continuation of 3685.09_J1 in posterior R SAF<br>Runs from superior/left at the L SAF to inferior/right to under R SAF<br>Segment under at the R SAF | Blow: Posterior/Left → Anterior/Right |
| **3685.09_J3** | CV 2 (L) | SAF | I | Partial shave of superior L SAF; continuation of 3685.09_J1<br>Runs from superior/left at the L SAF to inferior/right to under R SAF | Blow: Posterior/Left → Anterior/Right |
| **3685.10_K** | CV 2 | Posterior body | I | Cut into body below odontoid process | Blow: Posterior → Anterior<br>Nearly in transverse plane |
| **3685.10_L** | CV 2 | Odontoid process | S | Tip of odontoid cut off | Blow: Superior/Anterior – Inferior/Posterior |
| **3685.11_M** | CV2 | Inferior body | S | Inferior/anterior body removed<br>Some taphonomic damage | Blow: Superior/Anterior/Left – Inferior/Posterior/Right |
| **3685.01_N** | Scapula (L) | Acromion process | S ^ | Cut into acromion process of L scapula; not fully penetrating<br>Same fragment as 3685.01_A | Angled: Superior/Anterior – Inferior/Posterior |
| **3685.05_O** | Mandible (R) | Ascending ramus | S ^ | Just superior to 3685.05_F | Blow: Posterior → Anterior<br>Nearly in transverse plane |
| **3685.05_P** | Mandible (R) | Ascending ramus | I ^ | On the medial side of the ascending ramus<br>Just superior to 3685.05_O | Blow: Left → Right<br>Nearly in transverse plane |
| **10369_A** | Mandible (R) | Posterior condyle | S | Cut to posterior condyle | Blow: Posterior → Anterior |
| **10372_A** | Mandible (?L) | Condyle | S | Cut to posterior condyle | Blow: Posterior → Anterior<br>In transverse plane |
| **10420_A1** | Mandible (L) | Condyle | S | Removed condyle and coronoid process | Blow: Superior/Left – Inferior/Right |

| ID # | Bone (Side) | Location | Cat* | Description | Direction of Blow // Angle of Cutmark *Based on anatomical position |
|---|---|---|---|---|---|
| **10420_A2** | Mandible (L) | Coronoid | S | Removed condyle and coronoid process | Blow: Superior/Left – Inferior/Right |
| **10420_B** | Mandible (L) | Ascending ramus | I | Anterior/medial side of ascending ramus<br>Cut runs from superior/anterior to inferior/posterior | Blow: Right → Left |
| **10420_C1** | Mandible (L) | Ascending ramus and body | I | Posterior/medial side of ascending ramus; discontinuous<br>Cut runs from $M_3$ to posterior ascending ramus | Blow: Right → Left<br>In transverse plane |
| **10420_C2** | Mandible (L) | Ascending ramus and body | I | Posterior/medial side of alveolar processes of L teeth; discontinuous<br>Cut runs from $M_3$ to posterior ascending ramus | Blow: Right → Left<br>In transverse plane |
| **10420_D1** | Mandible (L) | Alveolar processes | I | Posterior to 10420_D2<br>Cut along superior, medial aspect of alveolar process | Blow: Right → Left<br>In transverse plane |
| **10420_D2** | Mandible (L) | Alveolar processes | I | Anterior to 10420_D1<br>Cut along superior, medial aspect of alveolar process | Blow: Right → Left<br>In transverse plane |
| **10421_A** | Mandible (R) | Anterior corpus | S | One side of cut missing; superior to 10421_B | Blow: ?Posterior/Right → Anterior/Left<br>Nearly in transverse plane |
| **10421_B** | Mandible (L) | Anterior corpus | S | Superior surface smoother; inferior to 10421_A | Blow: ?Posterior/Left → Anterior/Right<br>Nearly in transverse plane |

All others noted as SFT in osteological report were re-classified as RED

# Appendix H: Illustrator Drawings

The following are the illustrations that were done to examine the patterning of the cutmarks (Sections 7.1 and 7.6, Chapter 9). The Illustrator files are provided separately where each bone/skeleton can be examined individually and the regions that are missing or taphonomically damaged can also be seen.

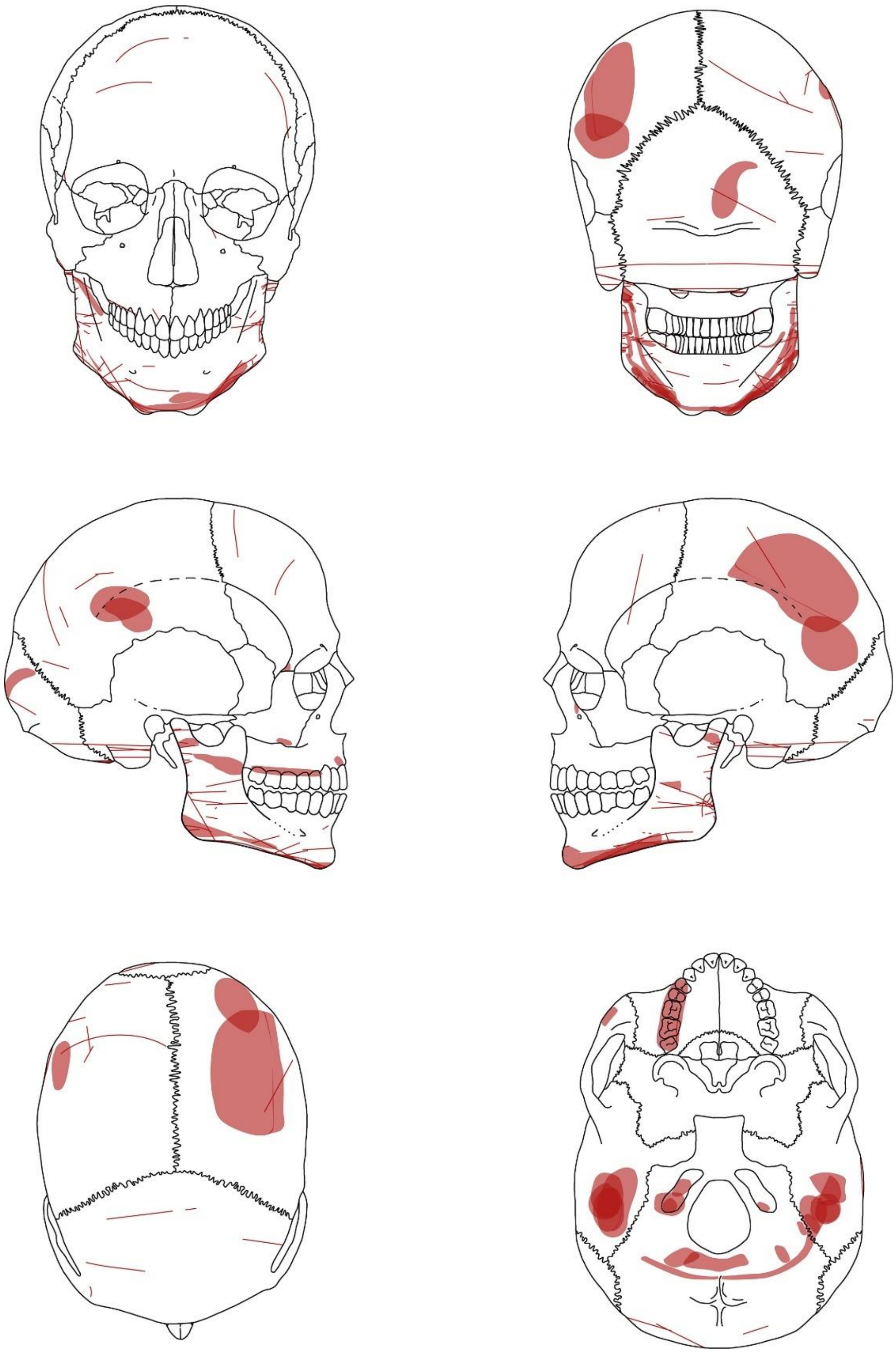

Figure 133: The skull in multiple orientation, from left to right and top to bottom; anterior, posterior, right, left, superior, and inferior

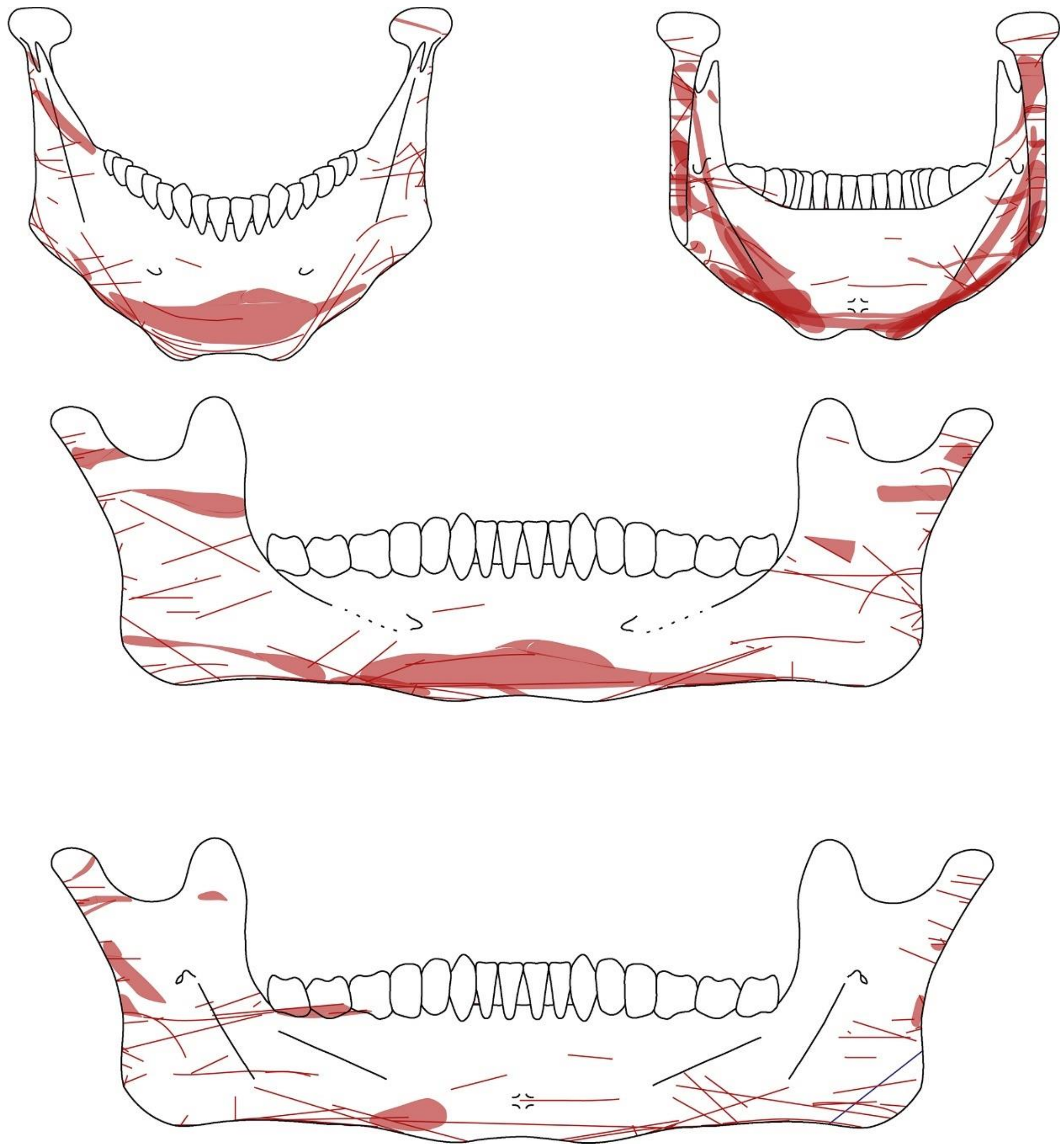

Figure 134: The mandible in multiple orientations, from left to right and top to bottom; anterior, posterior, buccal, and lingual

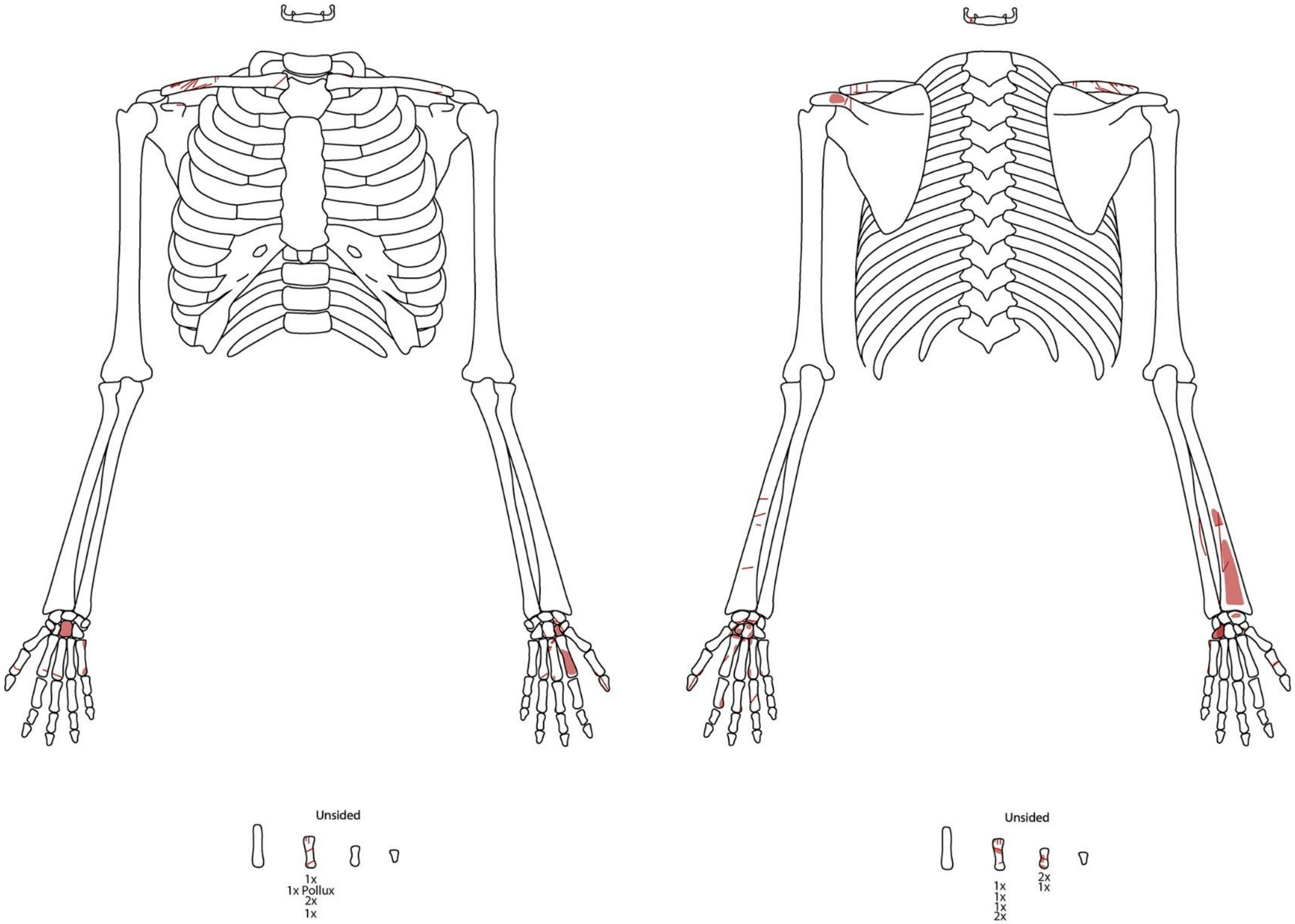


Figure 135: The upper body in multiple orientations, from left to right; anterior and posterior

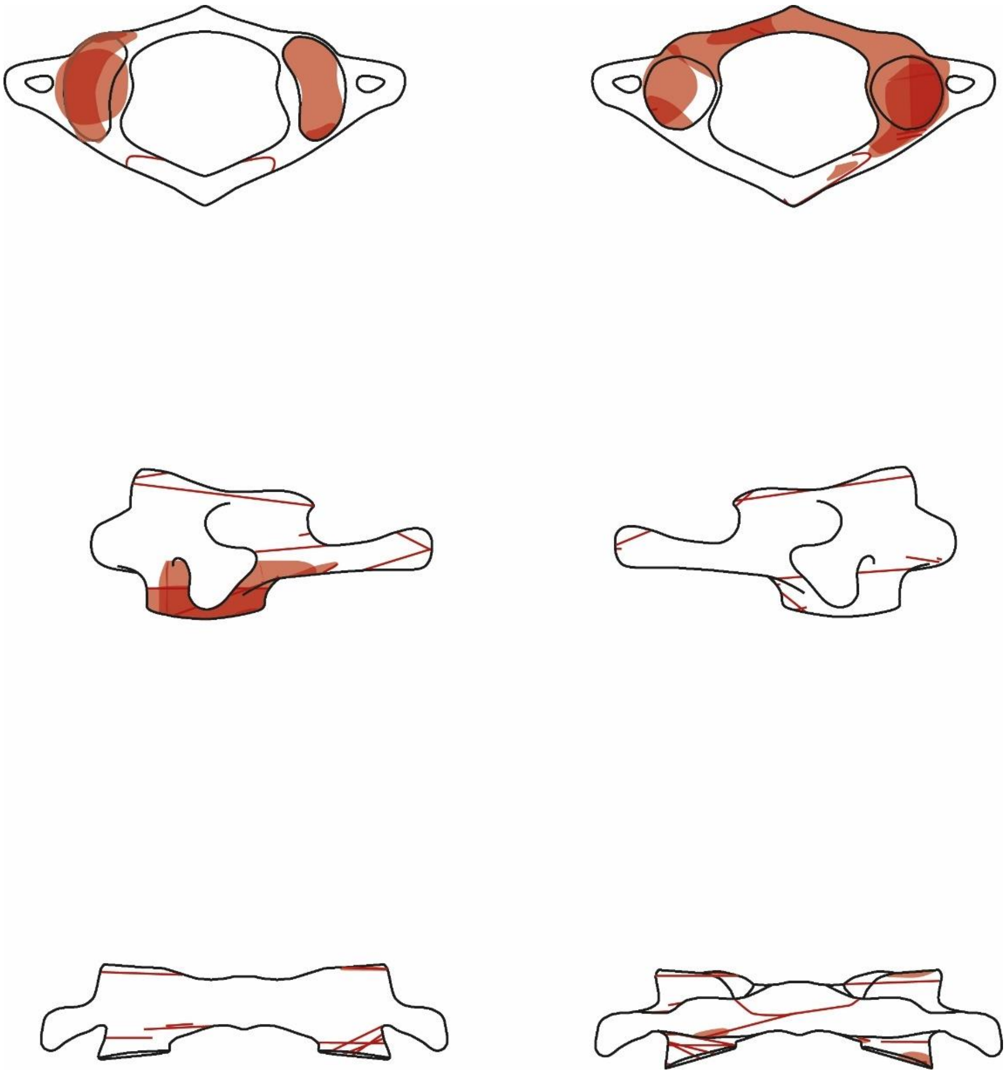

Figure 136: CV1 in multiple orientations, from left to right and top to bottom; superior, inferior, left, right, anterior, and posterior

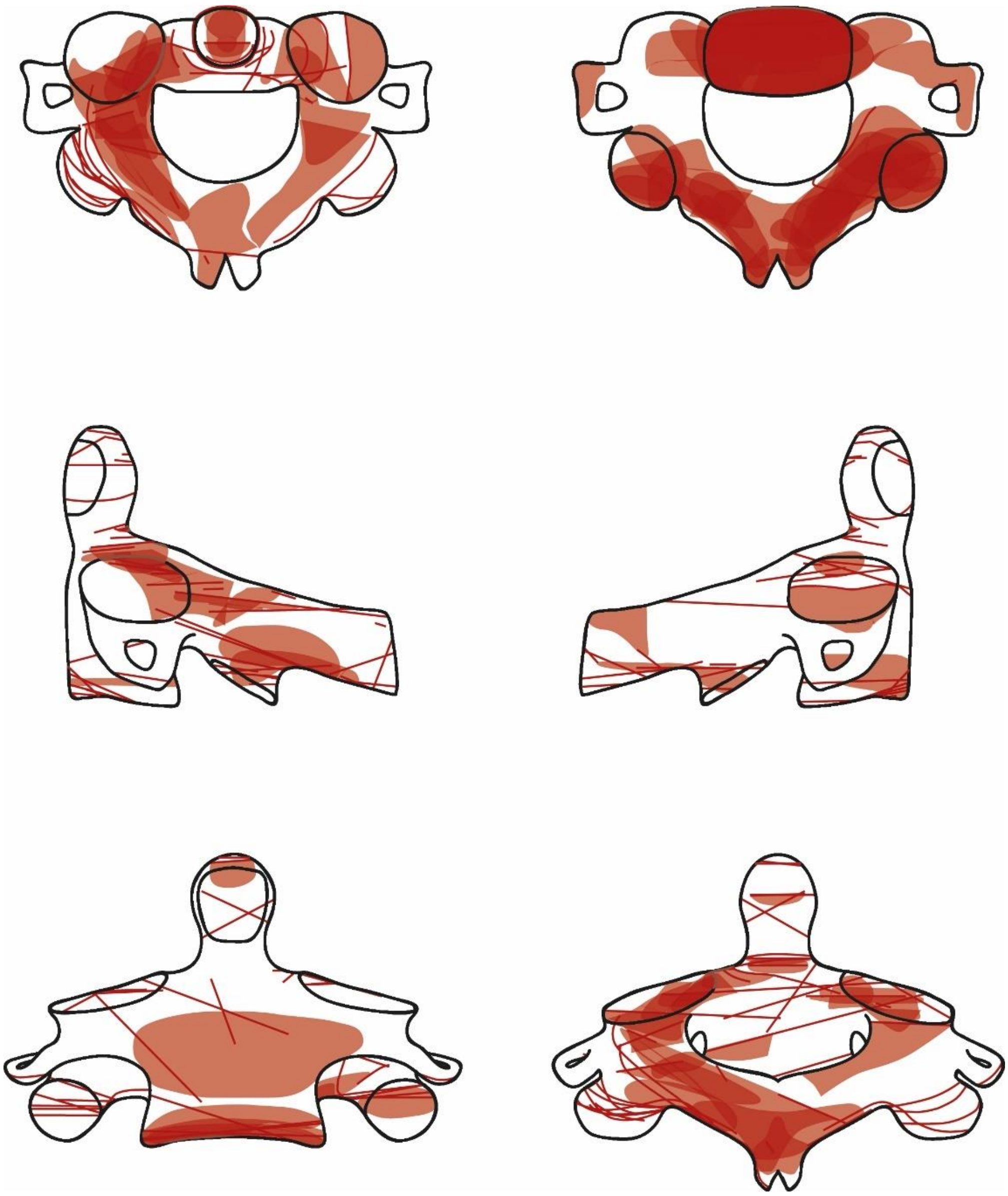

Figure 137: CV2 in multiple orientations, from left to right and top to bottom; superior, inferior, left, right, anterior, and posterior

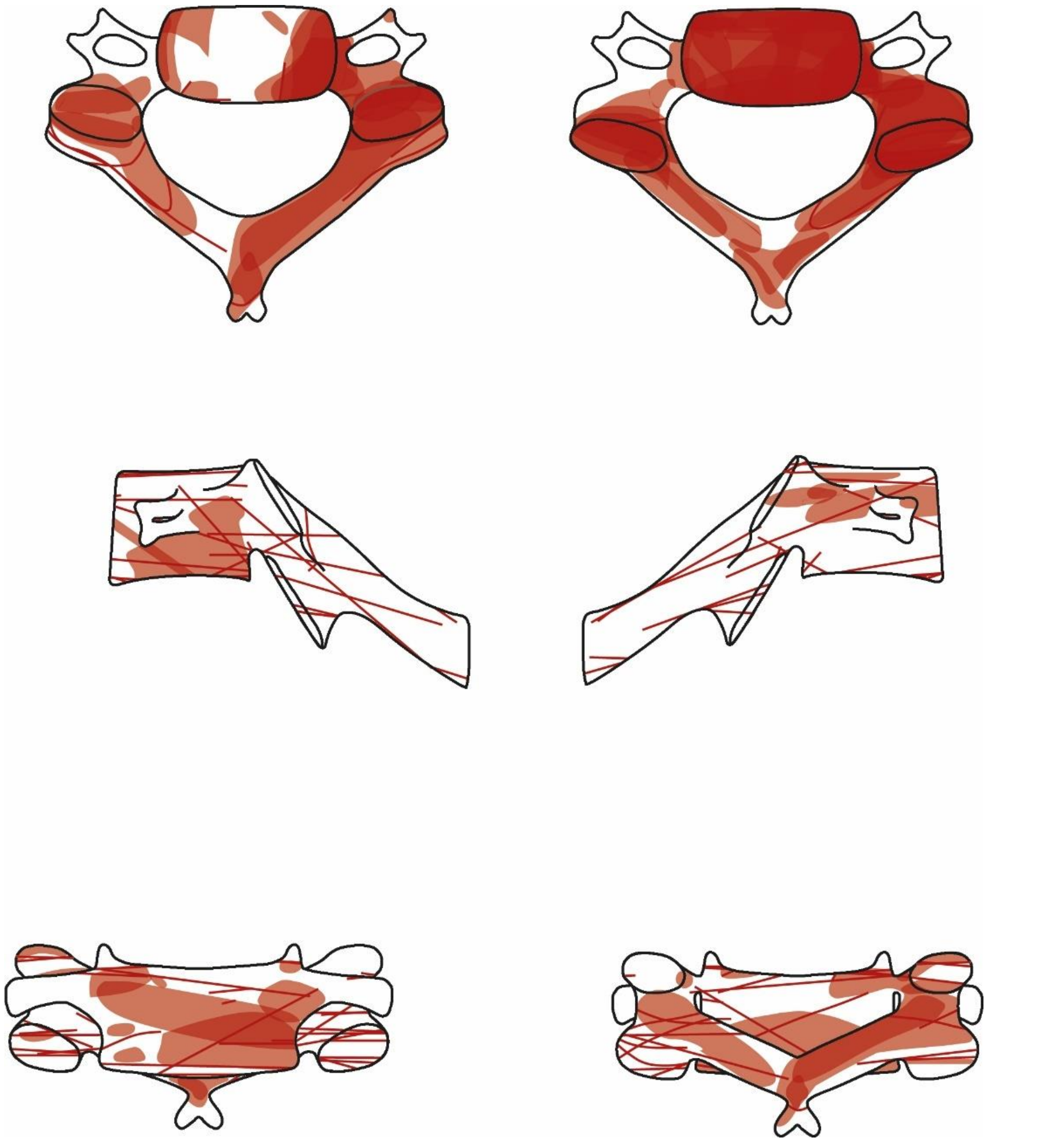

Figure 138: CV3 in multiple orientations, from left to right and top to bottom; superior, inferior, left, right, anterior, and posterior

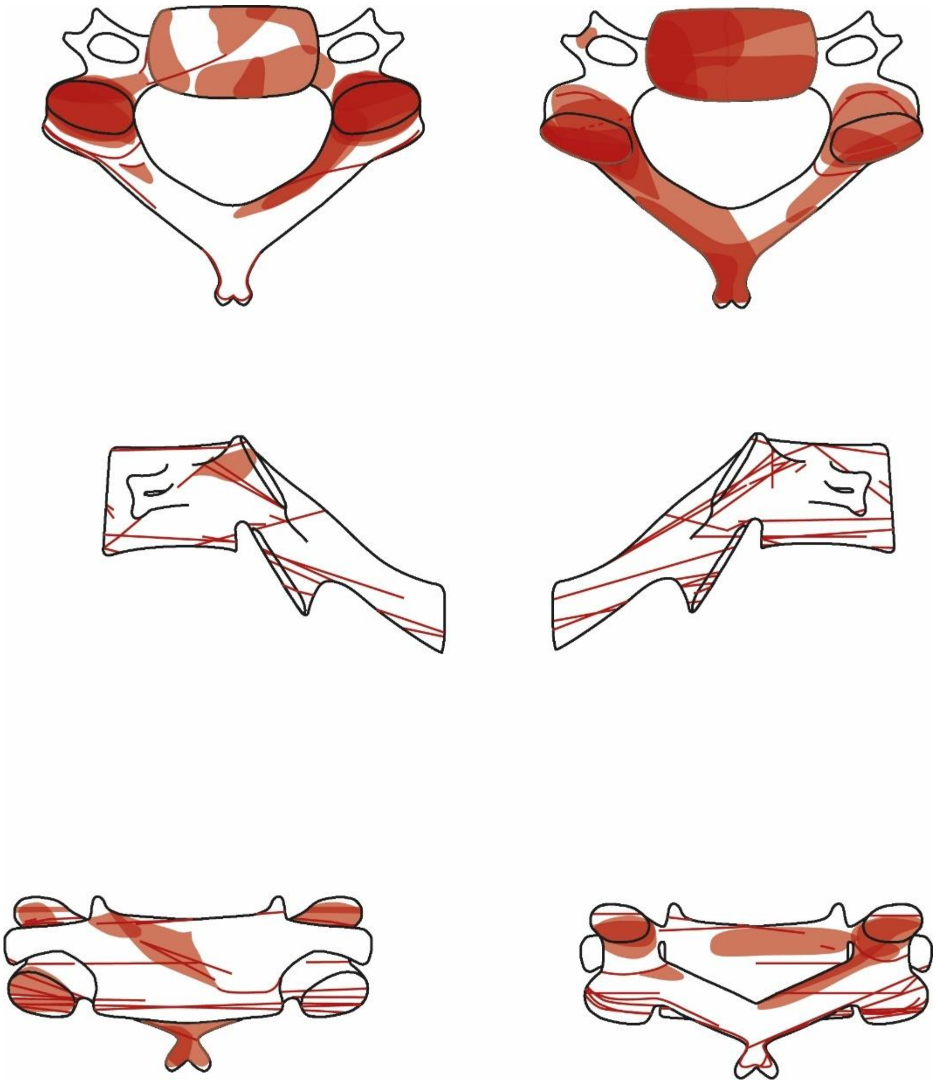

Figure 139: CV4 in multiple orientations, from left to right and top to bottom; superior, inferior, left, right, anterior, and posterior

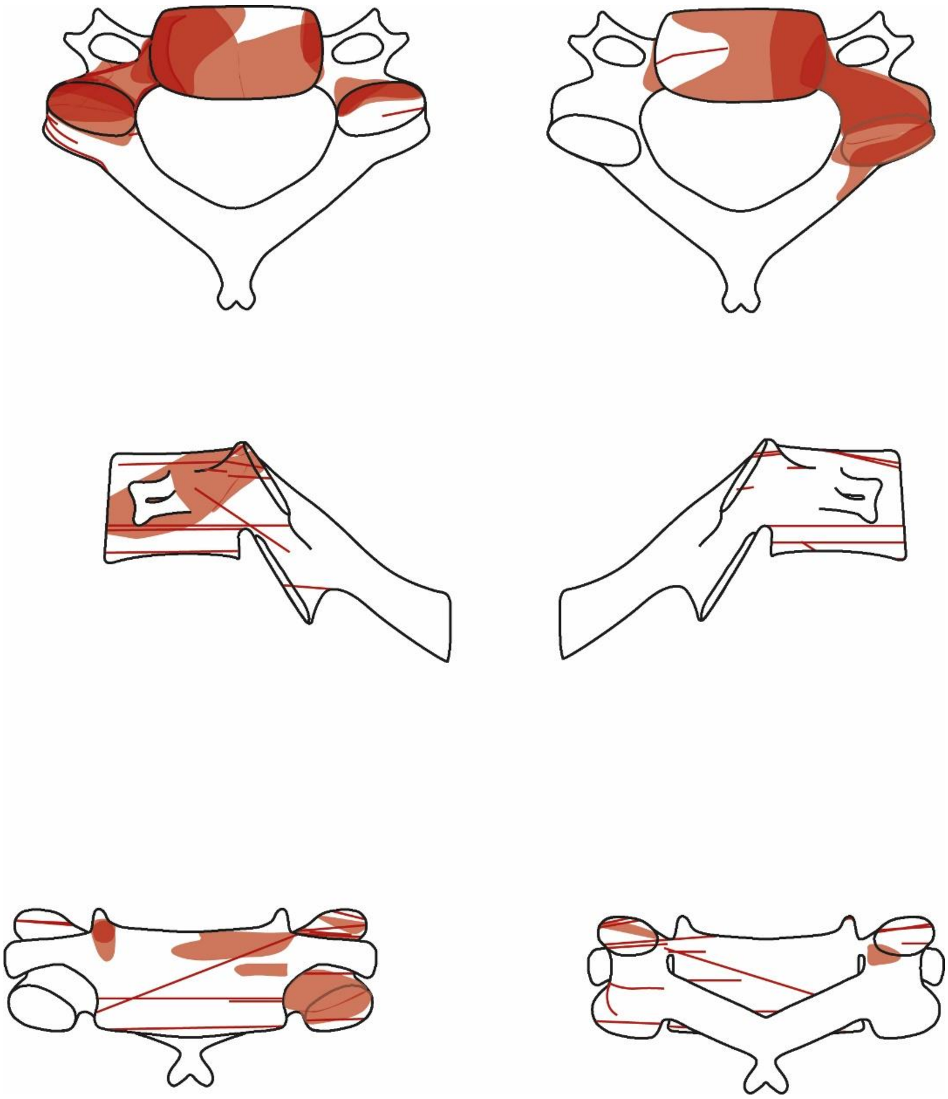

Figure 140: CV5 in multiple orientations, from left to right and top to bottom; superior, inferior, left, right, anterior, and posterior

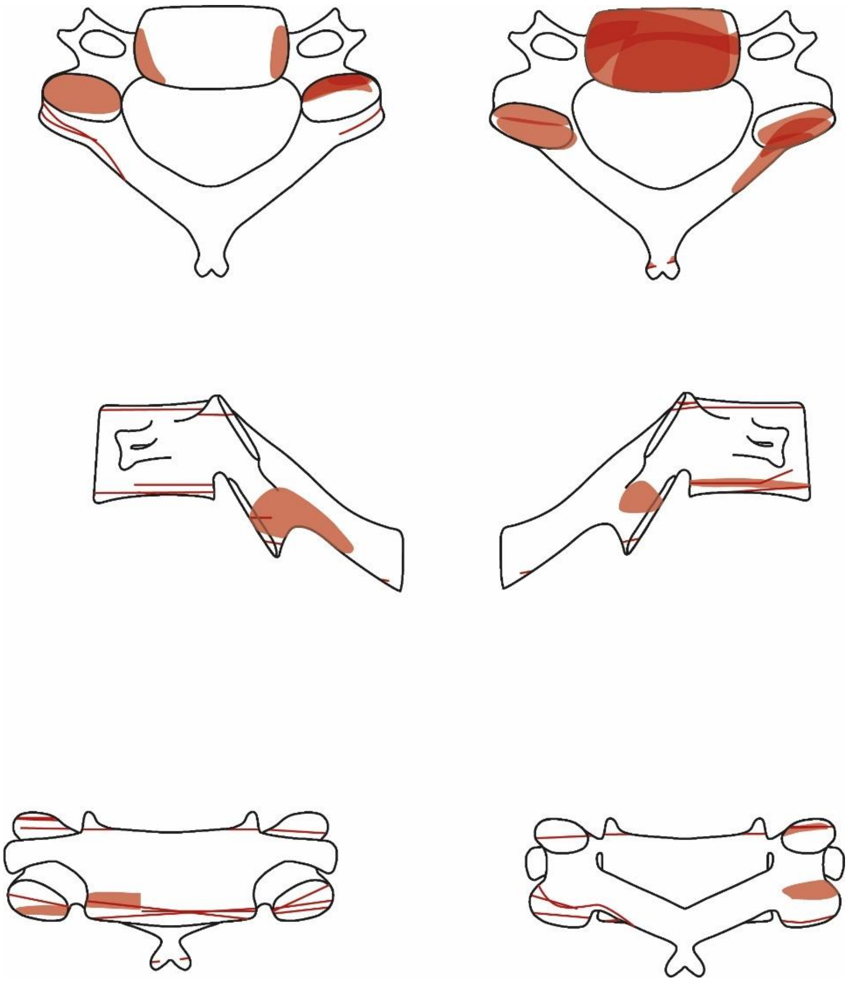

Figure 141: CV6 in multiple orientations, from left to right and top to bottom; superior, inferior, left, right, anterior, and posterior

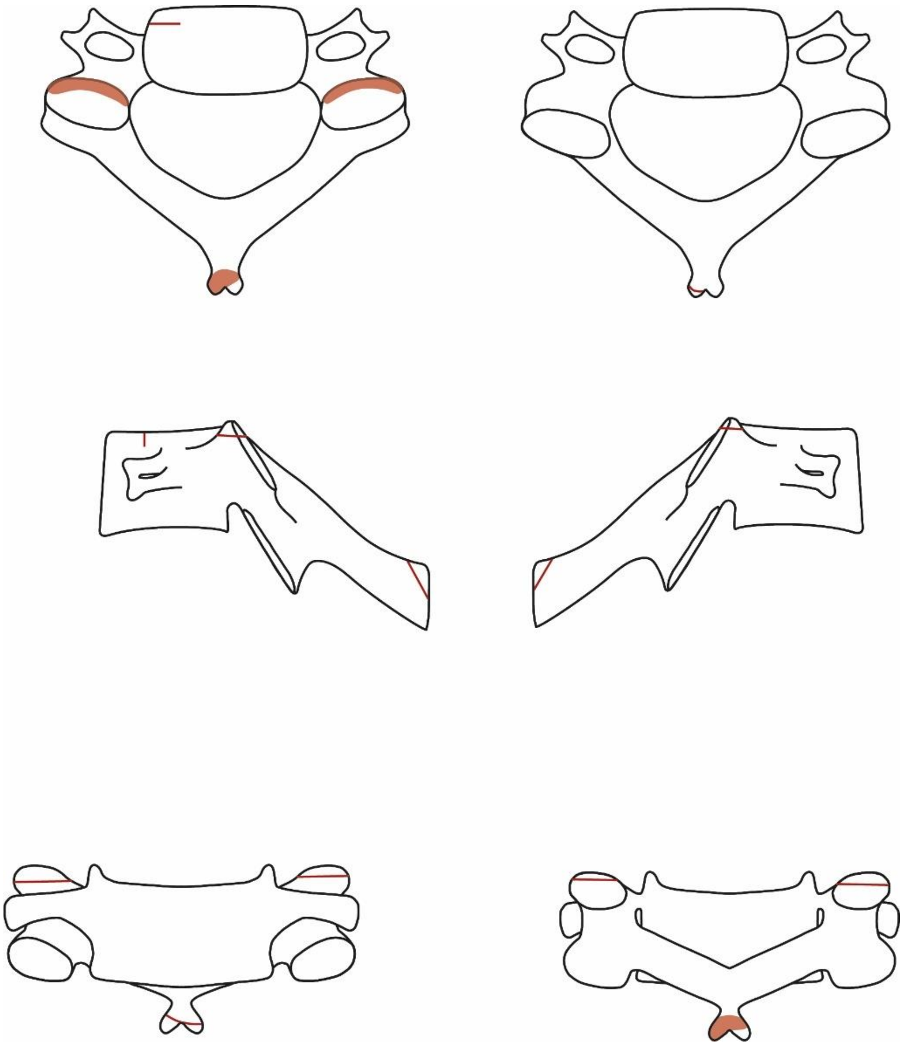

Figure 142: CV7 in multiple orientations, from left to right and top to bottom; superior, inferior, left, right, anterior, and posterior

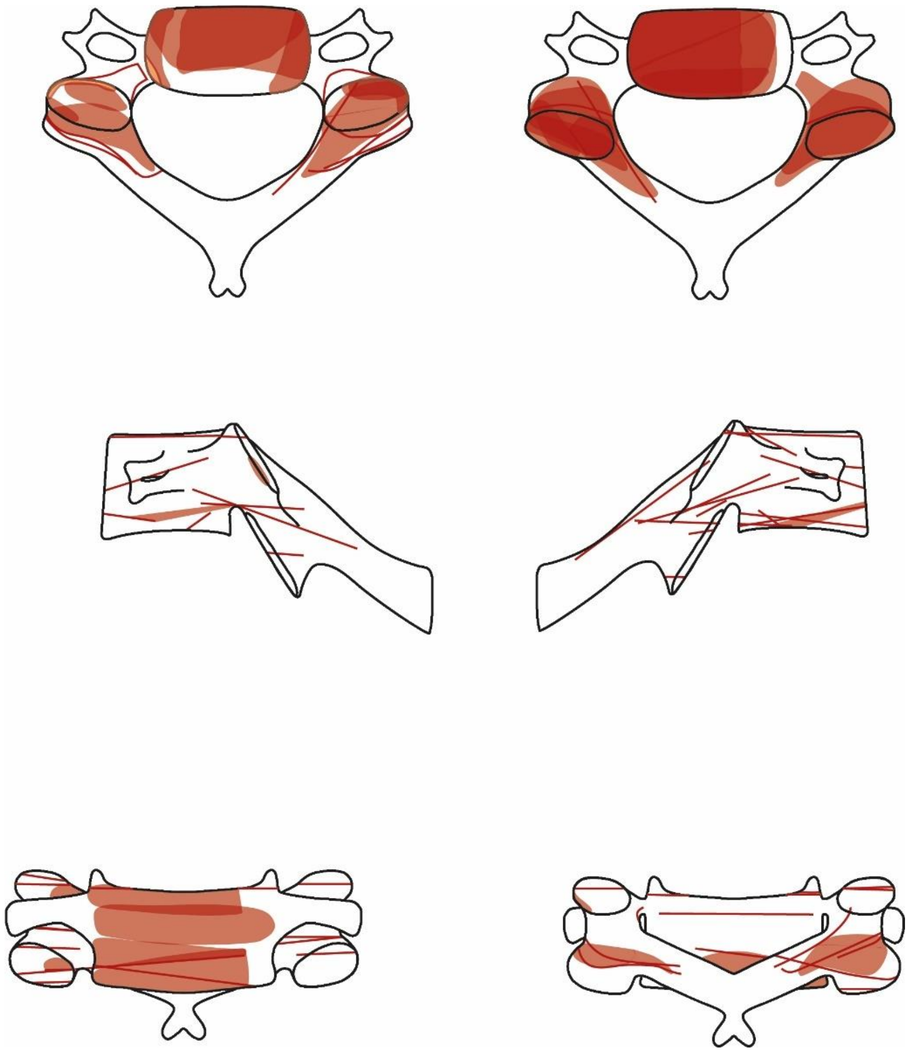

Figure 143: CVUnk in multiple orientations, from left to right and top to bottom; superior, inferior, left, right, anterior, and posterior

# Appendix I: Shape Analysis and Surface Roughness

The following are the graphical outputs from the shape analysis discussed in Section 7.2. The boxplots overlaid on PC contributions and additional PCA and LDA plots can be found in TamminenSupplementary_Shape Analysis_Compat.ai for easier comparison.

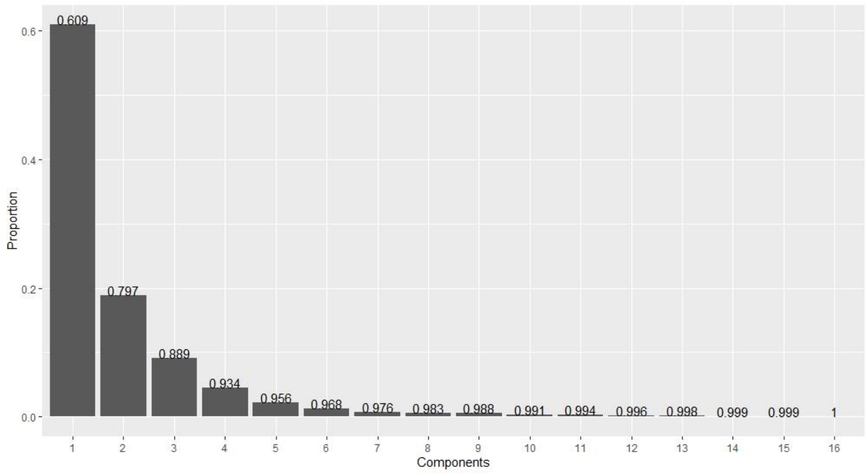


Figure 144: The scree plot for the PCA of the full collection

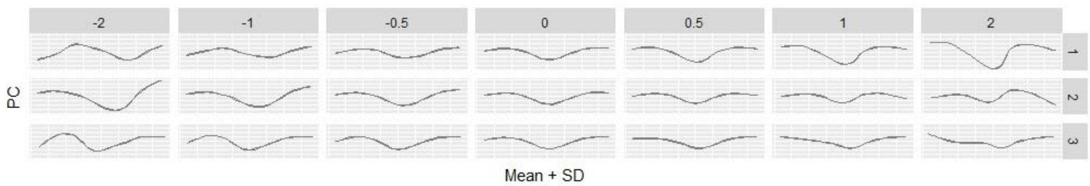


Figure 145: The PC contributions of only the angled collection

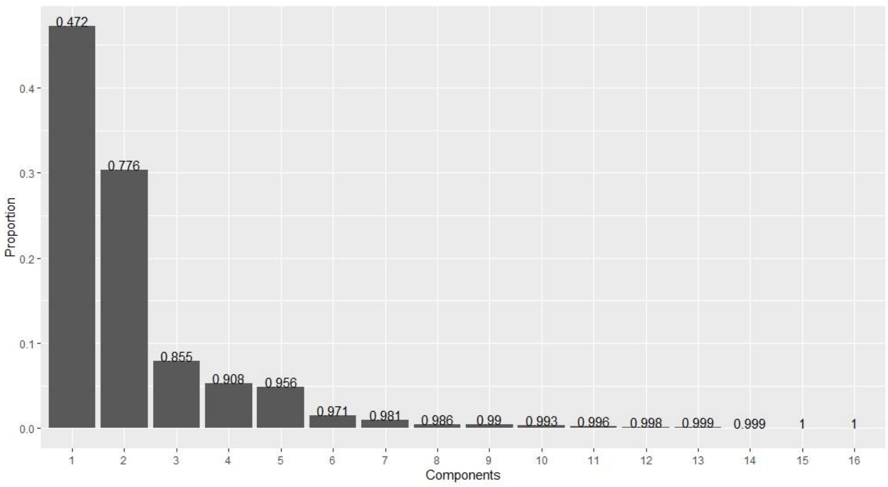


Figure 146: The scree plot for the PCA of the angled collection

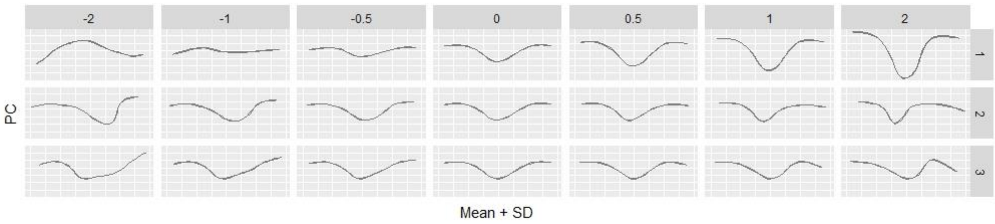


Figure 147: The PC contributions of only the non-angled collection

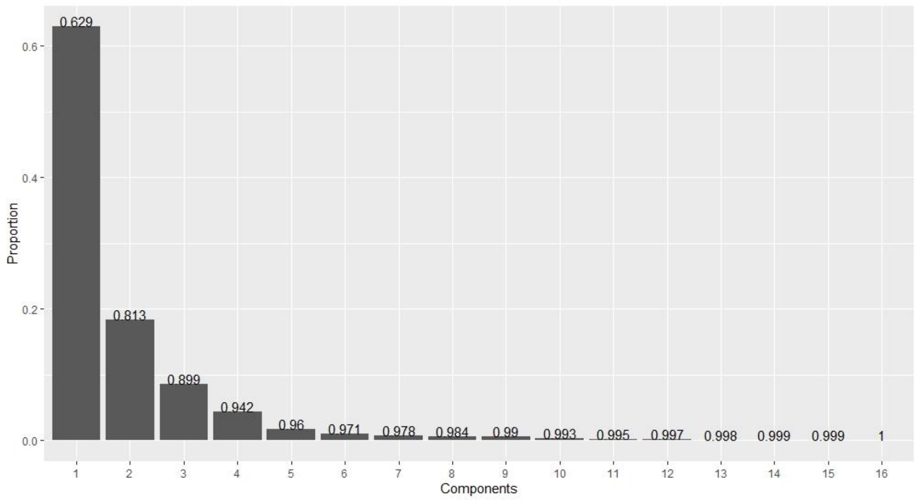


Figure 148: The scree plot for the PCA of non-angled collection

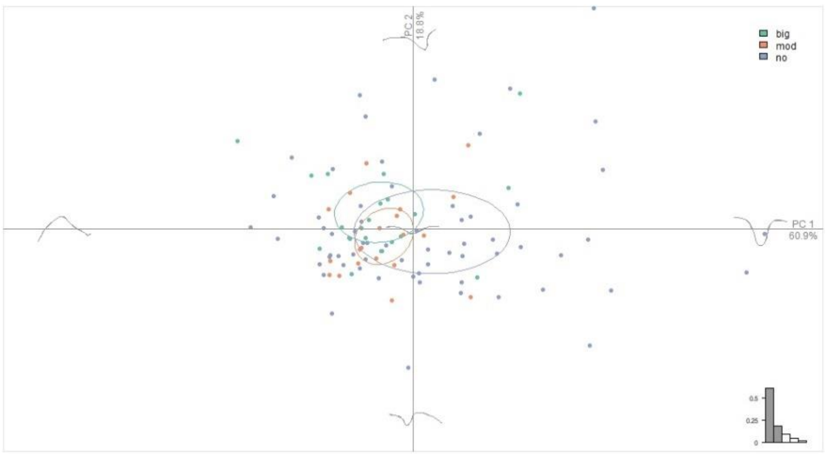


Figure 149: The PCA plot of the variable 'angle' showing PC1 and 2

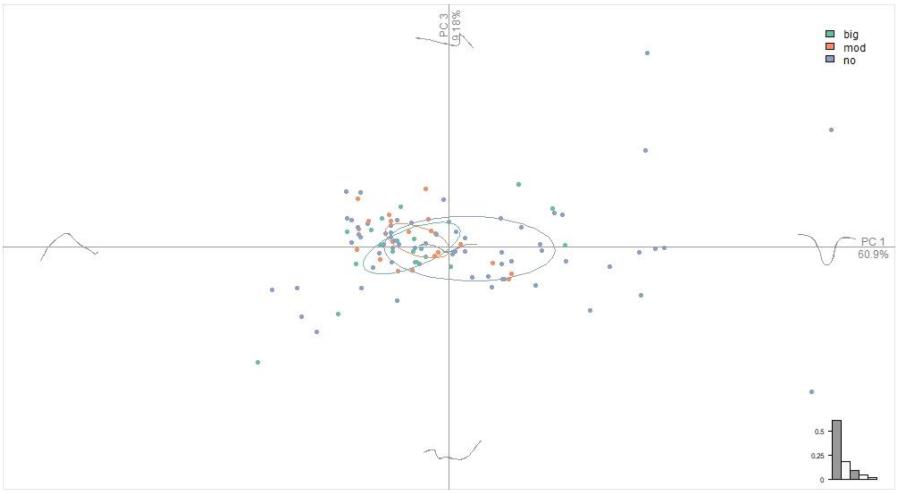


Figure 150:The PCA plot of the variable 'angle' showing PC1 and 3

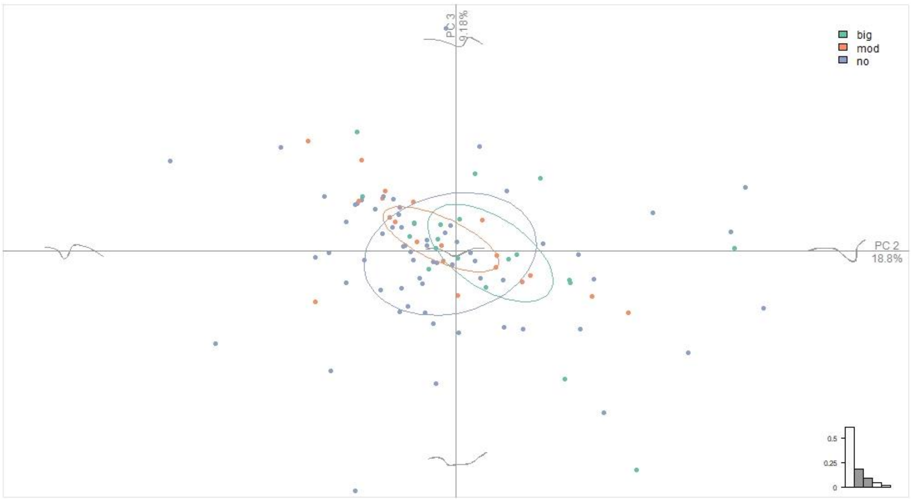


Figure 151: The PCA plot of the variable 'angle' showing PC2 and 3

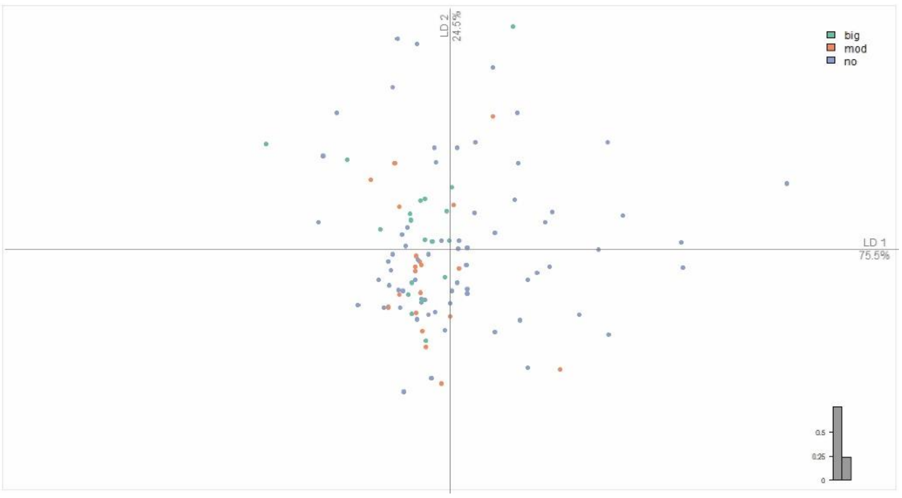


Figure 152: The 95%LDA plot for the variable 'angle' showing LD1 and 2

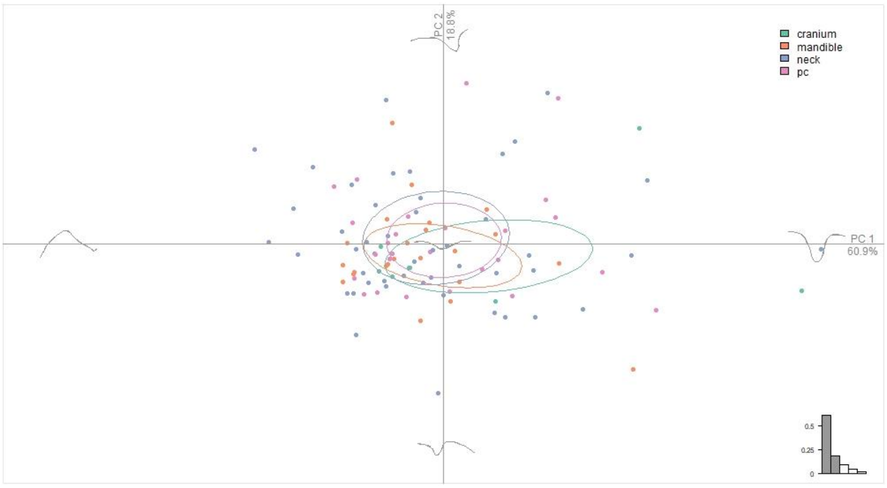


Figure 153: The PCA plot of the variable 'location' showing PC1 and 2

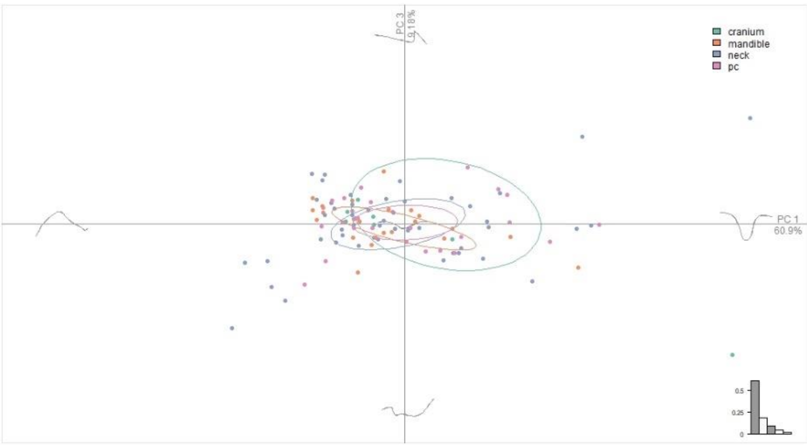


Figure 154: The PCA plot of the variable 'location' showing PC1 and 3

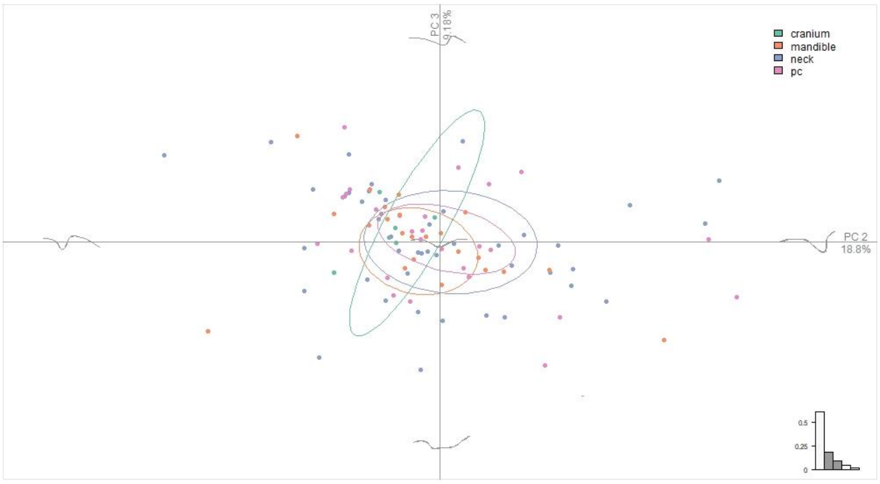


Figure 155: The PCA plot of the variable 'location' showing PC2 and 3

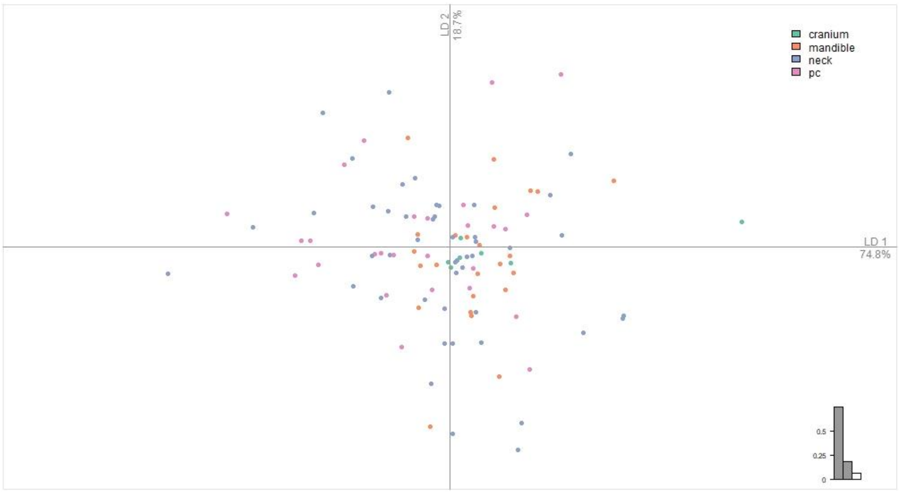


Figure 156: The 95%LDA plot of the variable 'location' showing LD1 and 2

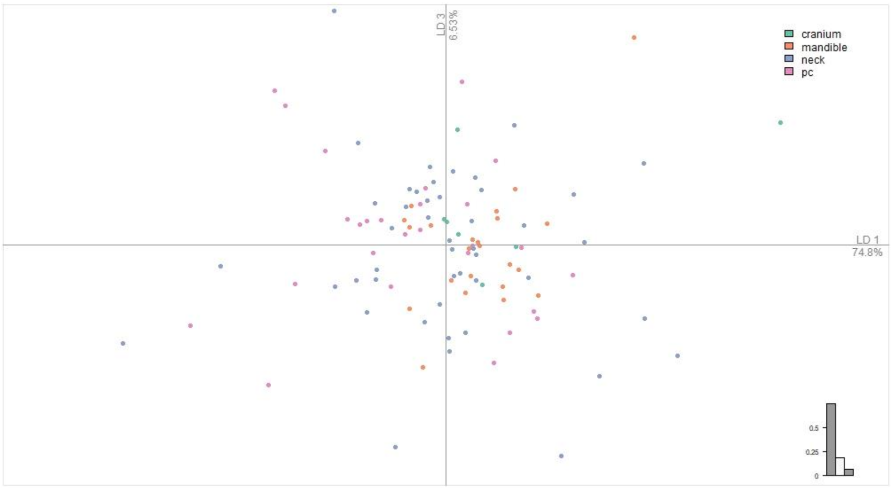


Figure 157: The 95%LDA plot of the variable 'location' showing LD1 and 3

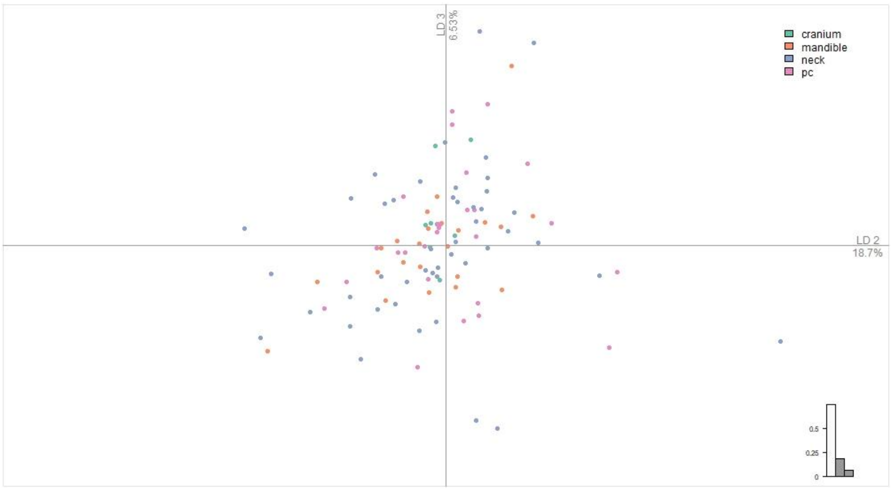


Figure 158: The 95%LDA plot of the variable 'location' showing LD2 and 3

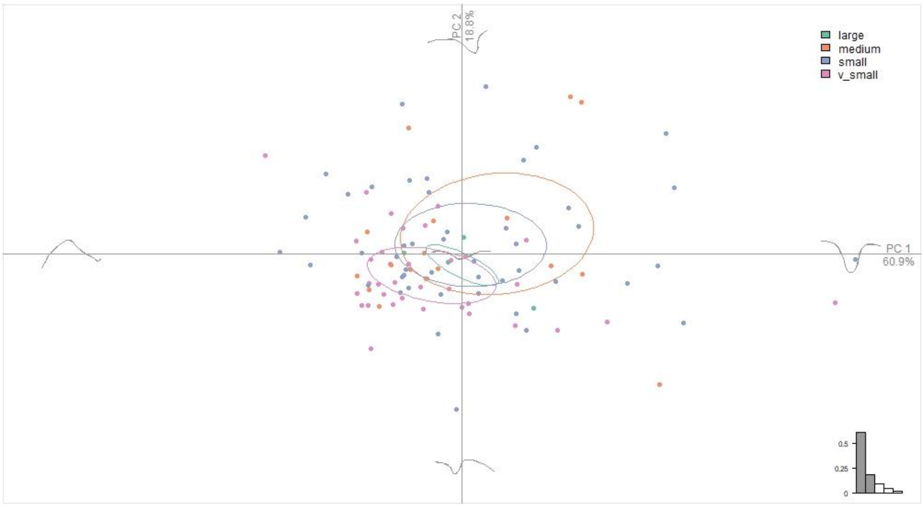


Figure 159: The PCA plot of the variable 'width' showing PC1 and 2

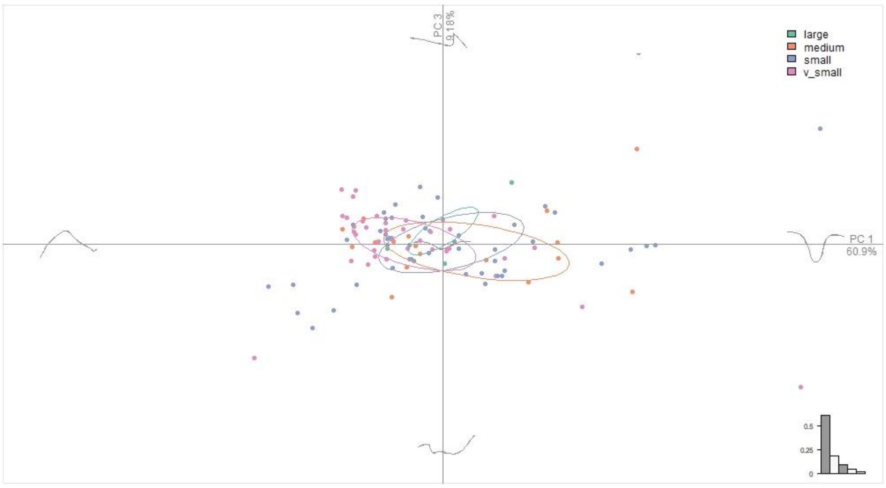


Figure 160: The PCA plot of the variable 'width' showing PC1 and 3

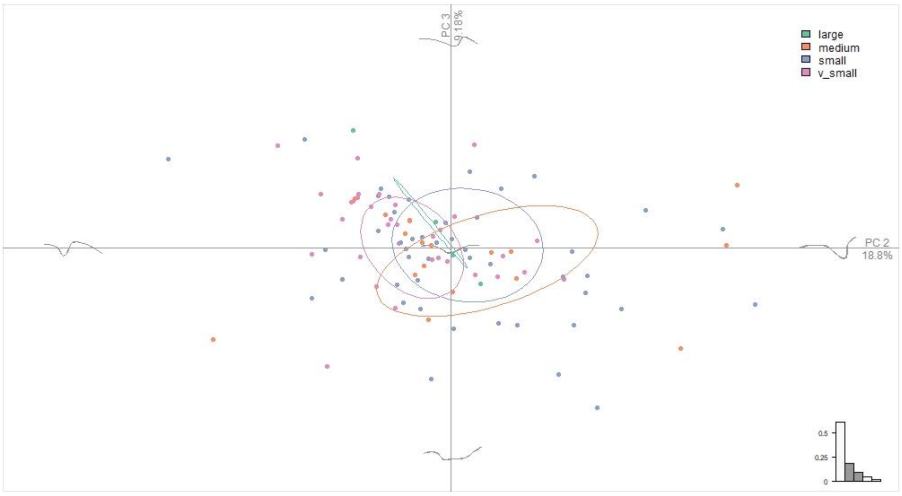


Figure 161: The PCA plot of the variable 'width' showing PC2 and 3

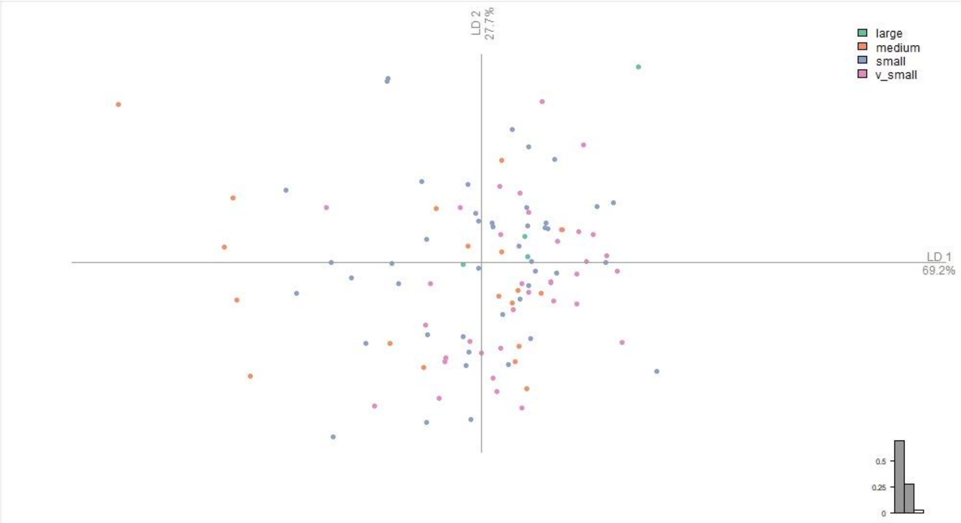


Figure 162: The 95%LDA plot of the variable 'width' showing LD1 and 2

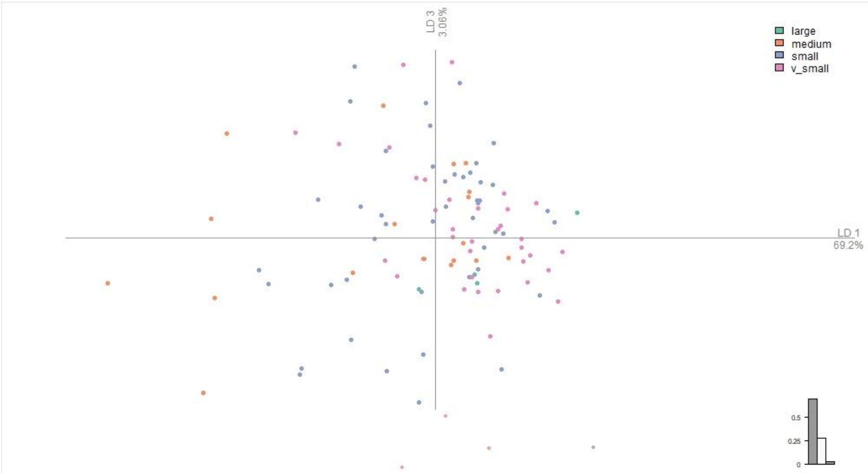


Figure 163: The 95%LDA plot of the variable 'width' showing LD1 and 3

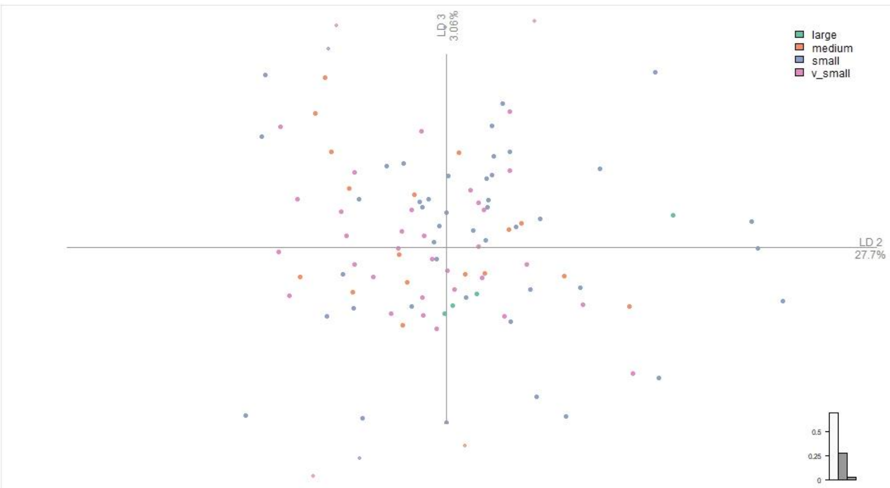


Figure 164: The 95%LDA plot of the variable 'width' showing LD2 and 3

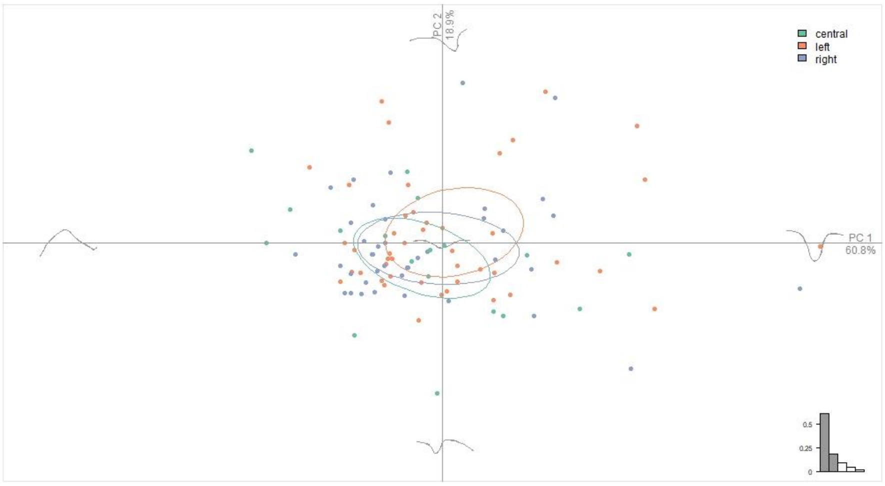


Figure 165: The PCA plot of the variable 'side' showing PC1 and 2

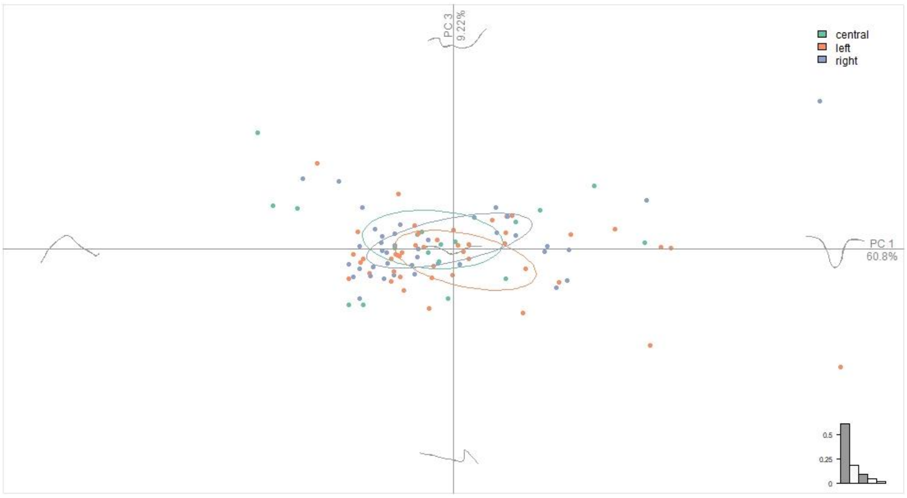


Figure 166: The PCA plot of the variable 'side' showing PC1 and 3

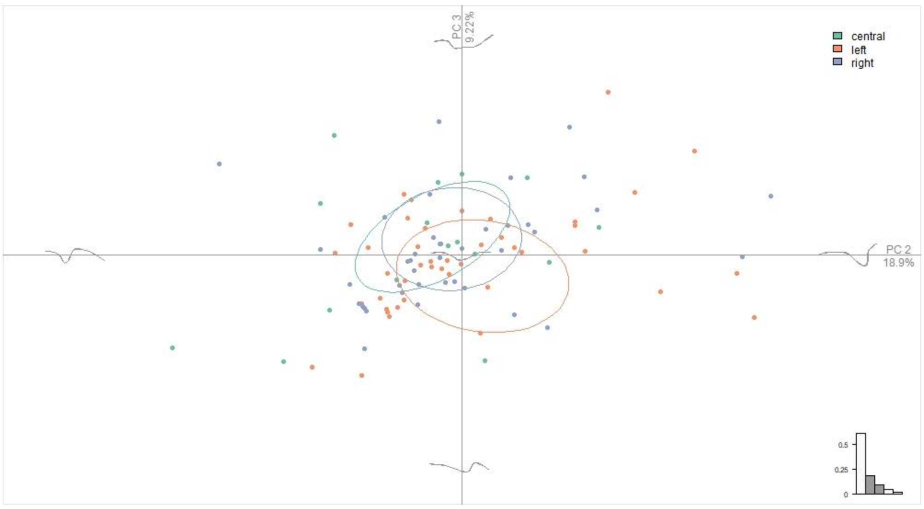


Figure 167: The PCA plot of the variable 'side' showing PC2 and 3

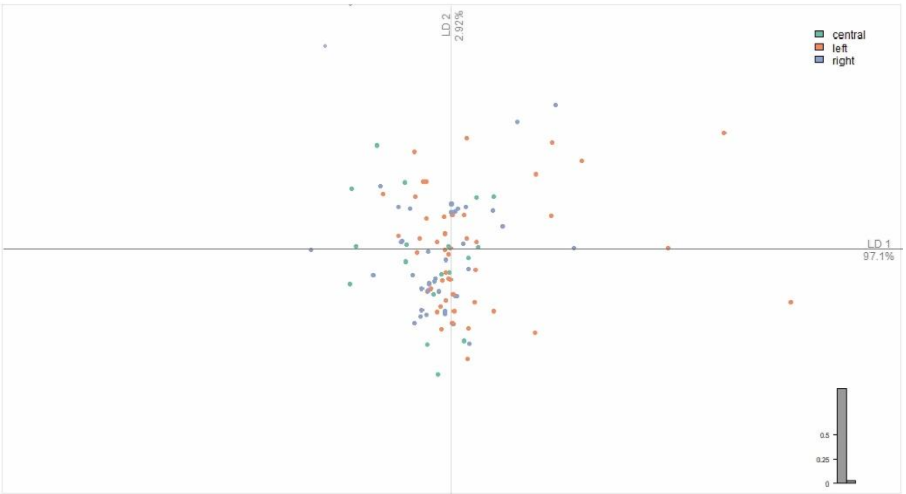


Figure 168: The 95%LDA plot of the variable 'side' showing LD1 and 2

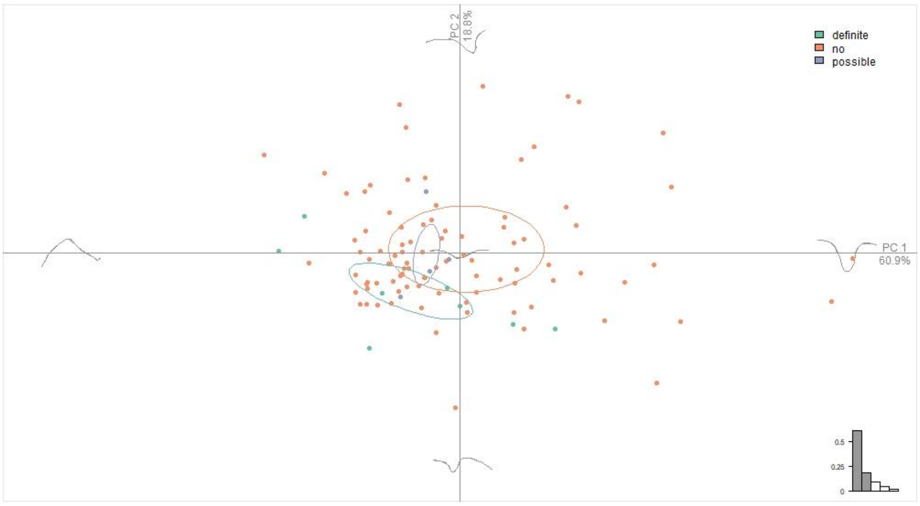


Figure 169: The PCA plot of the variable 'weaponry' showing PC1 and 2

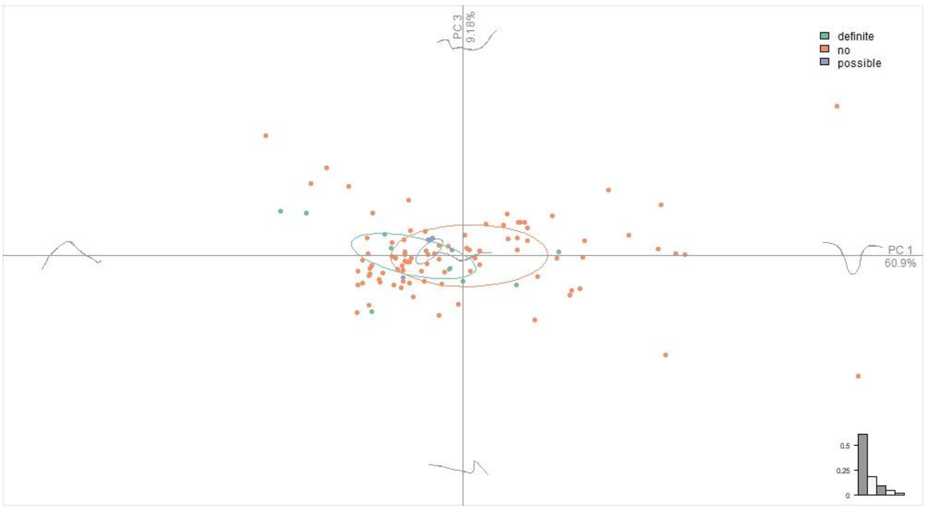


Figure 170: The PCA plot of the variable 'weaponry' showing PC1 and 3

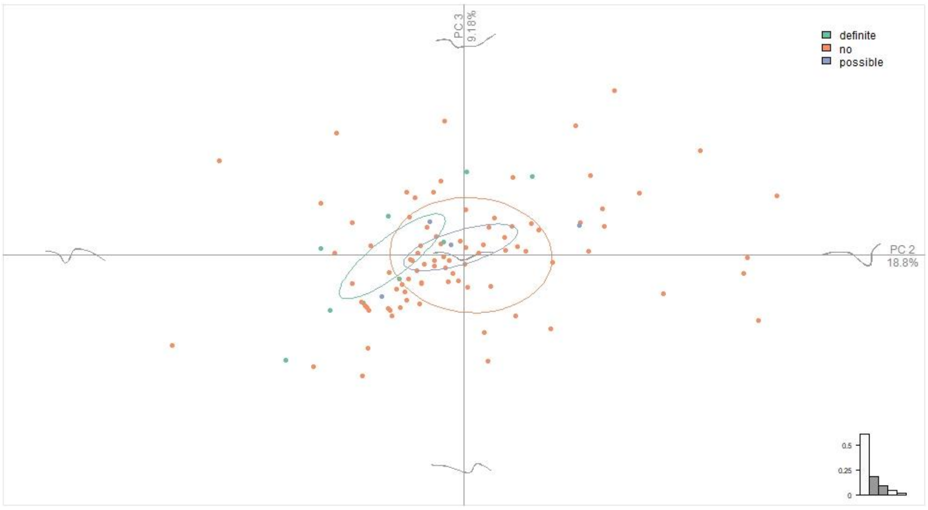


Figure 171: The PCA plot of the variable 'weaponry' showing PC2 and 3

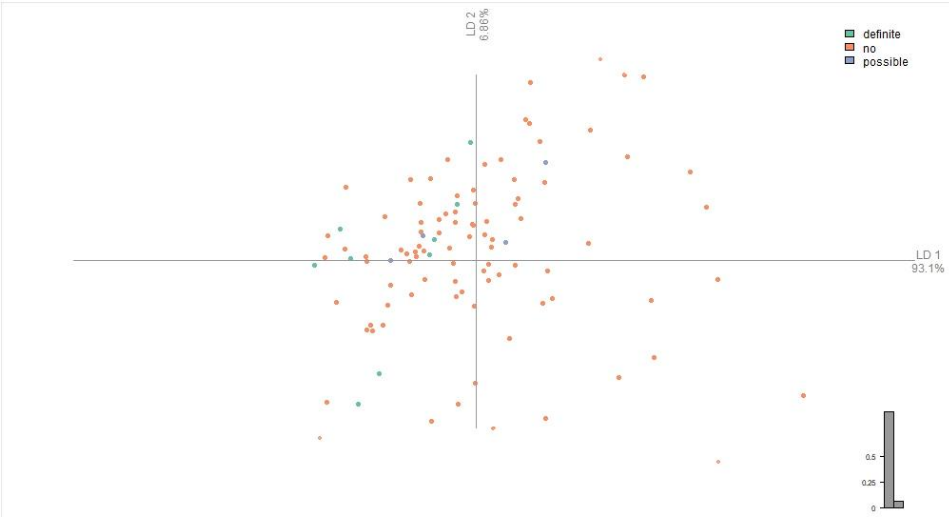


Figure 172: The 95%LDA plot of the variable 'weaponry' showing LD1 and 2

The following are the surface roughness outputs with both equal classes and equal breaks for the ten shaved cutmarks that were investigated in Section 6.3.

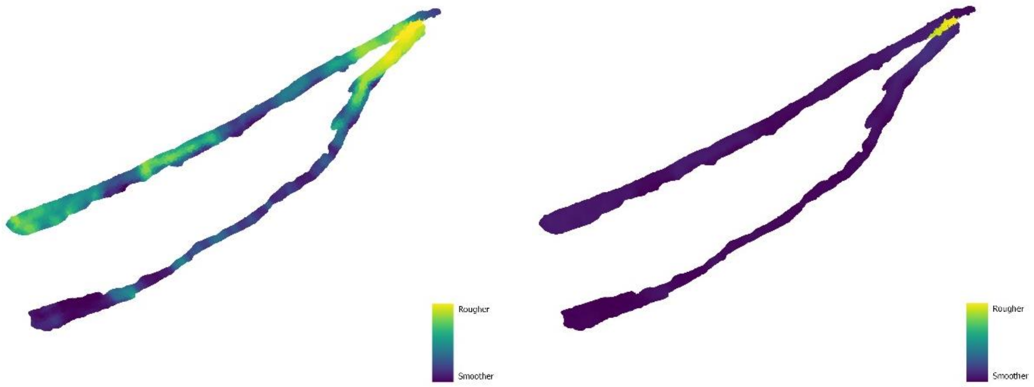


a) b)

Figure 173: The surface roughness outputs for 3708_F2 with a) equal counts and b) equal intervals

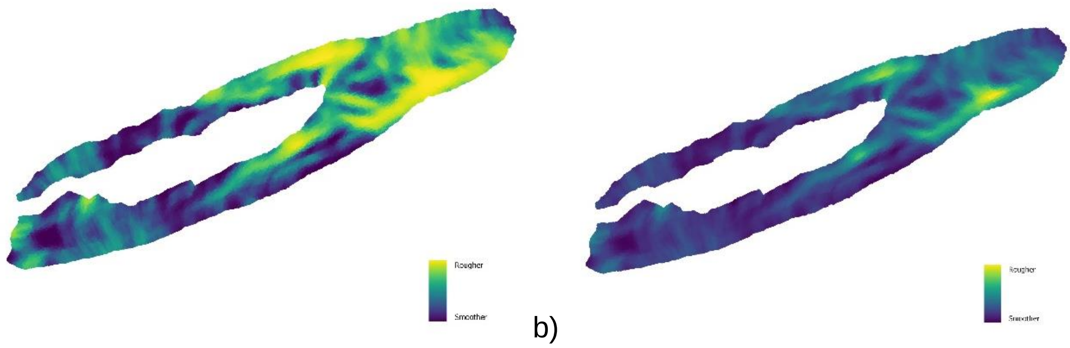


a) b)

Figure 174: The surface roughness outputs for 3711_F with a) equal counts and b) equal intervals

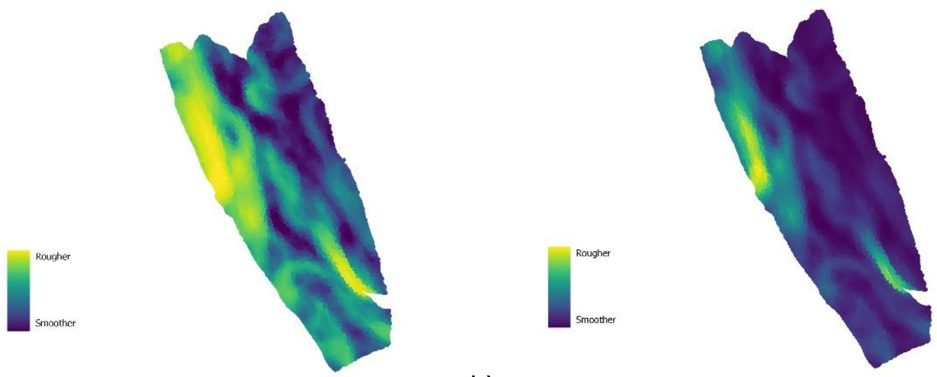


a) b)

Figure 175: The surface roughness outputs for 3720_B2 with a) equal counts and b) equal intervals

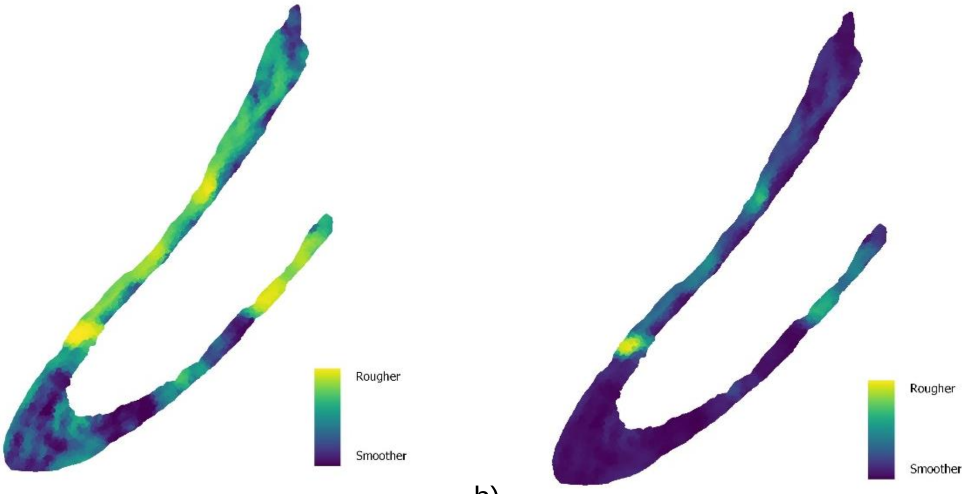


a) b)

Figure 176: The surface roughness outputs for 3730_D with a) equal counts and b) equal intervals

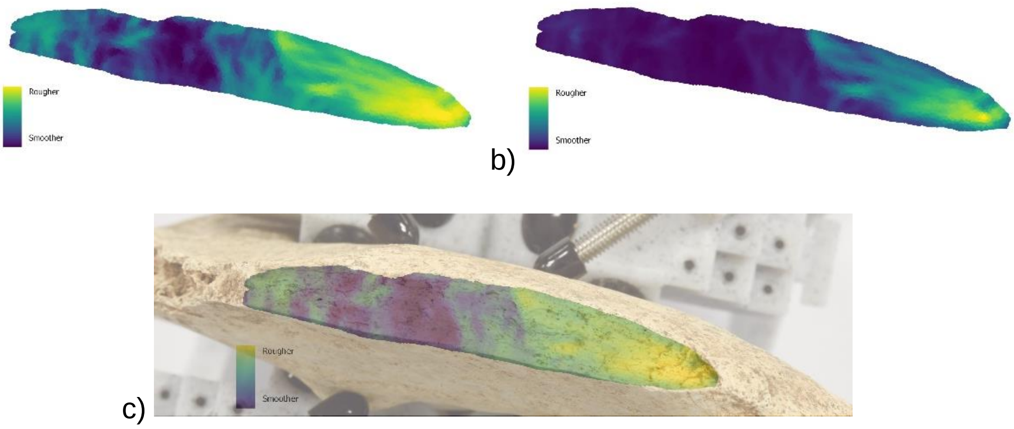


a) b) c)

Figure 177: The surface roughness outputs for 3735_A1 with a) equal counts, b) equal intervals, and c) the overlay on the vertical image

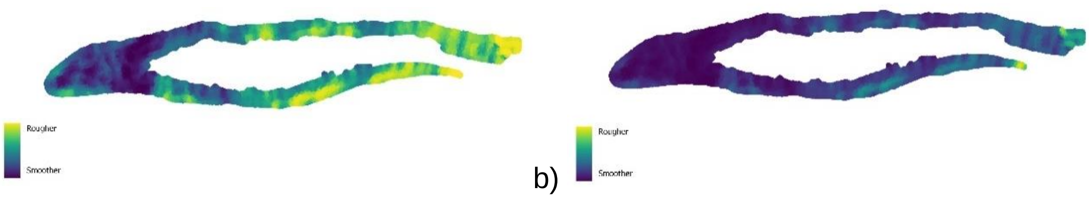


a) b)

Figure 178: The surface roughness outputs for 3750_C2 with a) equal counts and b) equal intervals

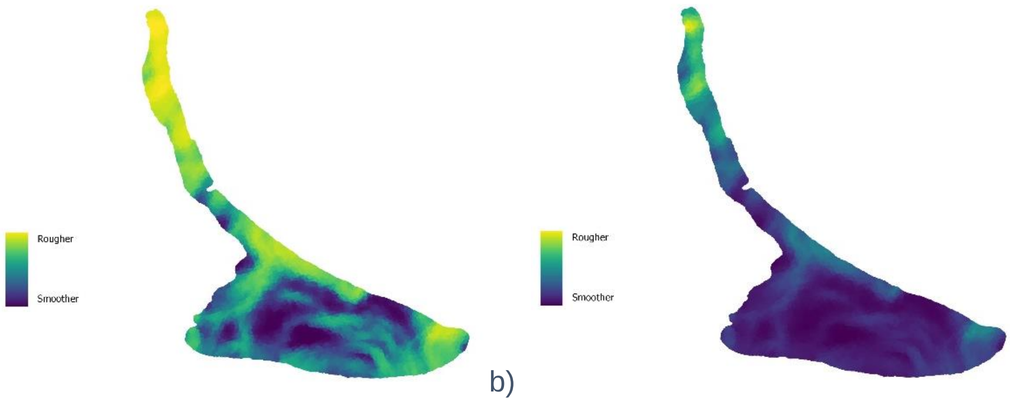


a) b)

Figure 179: The surface roughness outputs for 3752_D2 with a) equal counts and b) equal intervals

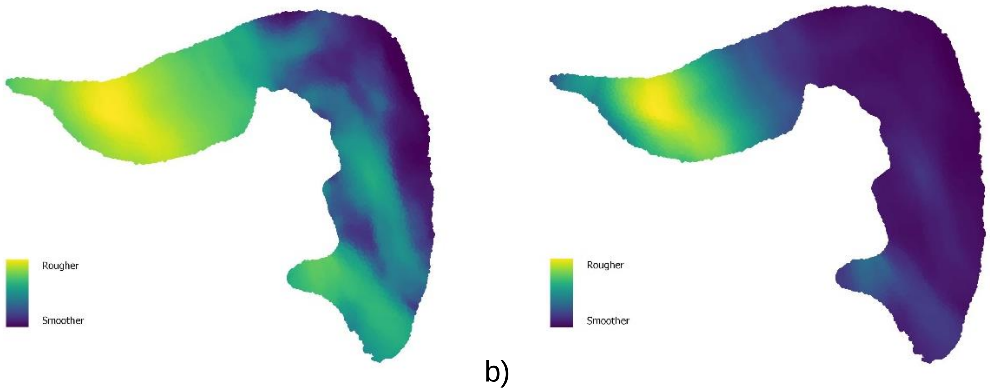


a) b)

Figure 180: The surface roughness outputs for 3752_E with a) equal counts and b) equal intervals

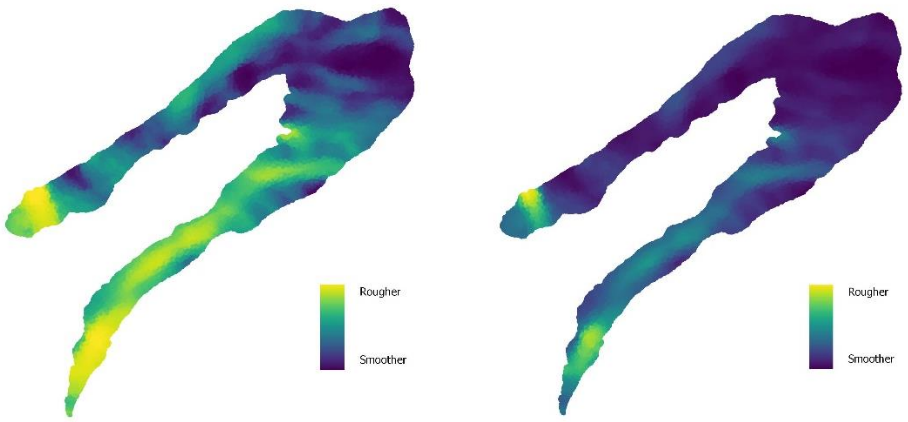


a) b)

Figure 181: The surface roughness outputs for 3763_D with a) equal counts and b) equal intervals

# Appendix J: Recent Studies Involving Manual Measurements

Table J-1: A selection of papers from 2020-2021 from the American Journal of Physical Anthropology, the International Journal of Osteoarchaeology, and Forensic Science International involving the calliper measurements of human remains evidencing the frequency with which manual measurements are taken (Section 10.1)

| Authors (Year) | Aspects Measured | Purpose | Notes |
|---|---|---|---|
| Alberto-Barroso et al. (2021) | Multiple bones | Perinatal burials | |
| Anastopoulou et al. (2020) | Upper extremities | Reassociation | Commingled remains |
| Anzellini and Toyne (2020) | Multiple bones | Stature | |
| Chevalier and Tignères (2020) | Fibulae | Age estimation; bone structure | Used CT for CSA |
| Díaz-Navarro (2021) | Crania | Trepanation and scalping | Case study |
| Dorado et al. (2021) | Hand bones | Brachymetacarpia | Case study |
| Hlad et al. (2021) | Multiple bones | Sex estimation | Thermally-altered; supervised learning |
| Laffranchi et al. (2020) | Dentition | Physiological stress | |
| Liebenberg and Krüger (2020) | Multiple bones | Osteometry | |
| Lorentz and Casa (2020) | MC1 | Trauma | |
| Maijanen et al. (2021) | Multiple bones | Sex estimation; stature | Used CT for CSA |
| McFarlane et al. (2021) | Mandibular canines | Dental wear | Teeth donated from living individuals |
| Navitainuck et al (2021) | Multiple bones | Sex estimation | |
| Osipov et al. (2020) | Multiple bones | Physiological stress | |
| Palamenghi et al. (2020) | Humeri | Non-metric trait | |
| Praxmarer et al. (2020) | Pelvis | Pelvic scarring | |
| Rathmann et al. (2021) | Crania and dentition | Intra-site comparison | Case study |
| Rozendaal et al. (2020) | Cervical vertebrae | Sex estimation | |
| Smith et al. (2021) | Crania and mandibles | Age estimation | |
| Viciano et al. (2021) | Dentition | Sex estimation | |
| Wilson et al. (2020) | MT1 | Age-related bone loss | Used CT for CSA |
| Zejdlik et al. (2020) | Lower extremities | Activity | Case study |
| Zelazny et al. (2021) | Humeri | Bilateral asymmetry; bone structure | Used CT for CSA |